Universität Trier

Pre-Shape Calculus

a Unified Framework for Mesh Quality and Shape Optimization

DISSERTATION

zur Erlangung des akademischen Grades eines
Doktors der Naturwissenschaften (Dr. rer. nat.)

vorgelegt am Fachbereich IV - Mathematik
der Universität Trier von

Daniel Luft

im September 2021

Gutachter: Prof. Dr. Volker H. Schulz
Prof. Dr. Michael Hintermüller

Abstract

In common shape optimization routines, deformations of the computational mesh usually suffer from decrease of mesh quality or even destruction of the mesh.

To mitigate this, we propose a theoretical framework using so-called pre-shape spaces. This gives an opportunity for a unified theory of shape optimization, and of problems related to parameterization and mesh quality. With this, we stay in the free-form approach of shape optimization, in contrast to parameterized approaches that limit possible shapes. The concept of pre-shape derivatives is defined, and according structure and calculus theorems are derived, which generalize classical shape optimization and its calculus. Tangential and normal directions are featured in pre-shape derivatives, in contrast to classical shape derivatives featuring only normal directions on shapes. Techniques from classical shape optimization and calculus are shown to carry over to this framework, and are collected in generality for future reference.

A pre-shape parameterization tracking problem class for mesh quality is introduced, which is solvable by use of pre-shape derivatives. This class allows for non-uniform user prescribed adaptations of the shape and hold-all domain meshes. It acts as a regularizer for classical shape objectives. Existence of regularized solutions is guaranteed, and corresponding optimal pre-shapes are shown to correspond to optimal shapes of the original problem, which additionally achieve the user prescribed parameterization.

We present shape gradient system modifications, which allow simultaneous numerical shape optimization with mesh quality improvement. Further, consistency of modified pre-shape gradient systems is established. The computational burden of our approach is limited, since additional solution of possibly larger (non-)linear systems for regularized shape gradients is not necessary. We implement and compare these pre-shape gradient regularization approaches for a 2D problem, which is prone to mesh degeneration. As our approach does not depend on the choice of forms to represent shape gradients, we employ and compare weak linear elasticity and weak quasilinear p-Laplacian pre-shape gradient representations.

We also introduce a Quasi-Newton-ADM inspired algorithm for mesh quality, which guarantees sufficient adaption of meshes to user specification during the routines. It is applicable in addition to simultaneous mesh regularization techniques.

Unrelated to mesh regularization techniques, we consider shape optimization problems constrained by elliptic variational inequalities of the first kind, so-called obstacle-type problems. In general, standard necessary optimality conditions cannot be formulated in a straightforward manner for such semi-smooth shape optimization problems. Under appropriate assumptions, we prove existence and convergence of adjoints for smooth regularizations of the VI-constraint. Moreover, we derive shape derivatives for the regularized problem and prove convergence to a limit object. Based on this analysis, an efficient optimization algorithm is devised and tested numerically.

All previous pre-shape regularization techniques are applied to a variational inequality constrained shape optimization problem, where we also create customized targets for increased mesh adaptation of changing embedded shapes and active set boundaries of the constraining variational inequality.

Zusammenfassung

Übliche Formoptimierungsverfahren basieren häufig auf Verformungen des Berechnungsnetzes, welche in der Regel zu einer Verringerung der Netzqualität oder sogar zu dessen Zerstörung führen.

Wir formulieren einen geeigneten theoretischen Rahmen mittels sogenannter Präformräume, um das Auftreten solcher Komplikationen zu vermeiden. Dies ermöglicht eine einheitliche Theorie der Formoptimierung und von Problemen im Zusammenhang mit der Parametrisierung und Netzqualität. Damit verfolgen wir einen Freiform-Ansatz zur Formoptimierung, im Gegensatz zu parametrischen Ansätzen, die mögliche Formen einschränken. Wir definieren das Konzept der Präformableitungen, und leiten zugehörige Struktur- und Kalkültheoreme her, welche die klassische Formoptimierung und das zugehörige Formkalkül verallgemeinern. Tangentiale und Normalenrichtungen fließen beide in Präformableitungen mit ein, im Gegensatz zu klassischen Formableitungen, welche ausschließlich Normalenrichtungen auf Formen beinhalten. Techniken der klassischen Formoptimierung und das zugehörige Formkalkül lassen sich in diese Theorie übertragen, und sind in allgemeiner Formulierung für zukünftige Referenz zusammengetragen.

Eine Problemklasse zur Sicherstellung der Netzqualität wird eingeführt, welche durch Verwendung der Präformableitungen lösbar ist. Diese Problemklasse erlaubt eine nichtuniforme Adaptierung des Form- und des gesamten Rechennetzes, welche durch den Nutzer spezifizierbar ist. Sie kann als Regularisierung zur simultanen Optimierung klassischer Formoptimierungsgrößen und der Netzqualität dienen. Existenz regularisierter Lösungen wird garantiert, und es wird gezeigt, dass zugehörige optimale Präformen den optimalen Formen des ursprünglichen Formoptimierungsproblems entsprechen, wobei diese zusätzlich die durch den Nutzer vorgeschriebene Parameterisierung erfüllen.

Wir präsentieren Modifizierungen von Formgradientensystemen, welche ein simultanes numerisches Optimieren von Formen bei gleichzeitiger Verbesserung der Netzqualität bewerkstelligen. Weiterhin wird die Konsistenz der modifizierten Gradientensysteme sichergestellt. Der numerische Rechenaufwand unserer Techniken ist begrenzt, da kein zusätzliches Lösen möglicherweise größerer (nicht-)linearer Systeme für regularisierte Formgradienten nötig wird. Wir implementieren und vergleichen diese Regularisierungen der Präformgradienten für ein 2D-Problem, welches anfällig für Zerstörung des Netzes ist. Da unser Zugang nicht von der Art abhängt, mit der Formgradienten dargestellt werden, verwenden und vergleichen wir Darstellungen von Präformgradienten mittels schwacher linearer Elastizitäts- und schwacher quasilinearer p-Laplace-Gleichungen.

Weiterhin führen wir einen Quasi-Newton-ADM inspirierten Algorithmus für Netzqualität ein, welcher hinreichende nutzerspezifizierte Adaptierung des Netzes gewährleistet. Dieser ist zusätzlich zu den Techniken der simultanen Netzregularisierung anwendbar.

Unabhängig von den Techniken zur Netzregularisierung, betrachten wir Formoptimierungsprobleme, welche durch elliptische variationelle Ungleichungen erster Ordnung beschränkt sind, d.h. sogenannte Hürden-Probleme. Im Allgemeinen lassen sich keine üblichen notwendigen Optimalitätsbedingungen für solche semi-glatten Formoptimierungsprobleme formulieren. Unter geeigneten Annahmen beweisen wir Existenz und Konvergenz von Adjungierten, welche zu glatten Regularisierungen der variationellen Ungleichungsbeschränkung gehören. Außerdem leiten wir Formableitungen für das regularisierte Problem her, und beweisen deren Konvergenz zu einem Grenzobjekt. Basierend auf dieser Analyse, entwickeln wir einen effizienten Optimierungsalgorithmus, welchen wir numerisch testen.

Alle vorhergehenden Techniken der Präformregularisierung werden an einem beispielhaften Formoptimierungsproblem getestet, welches durch eine variationelle Ungleichung beschränkt ist. Hierbei entwerfen wir passende Zielgrößen zur verbesserten Netzadaptierung an sich verändernde eingebettete Formen, und zur Adaptierung an Ränder der zur variationellen Ungleichungsbeschränkung gehörigen aktiven Menge.

to Emil Luft

Acknowledgements

I am very thankful to Volker Schulz (Trier University), who has shown his trust by providing me with the freedom to express my creativity, and for always taking his time to have friendly discussions. I also thank Michael Hintermüller (Humboldt University Berlin, Weierstraß-Institute) for showing interest in this work, and for taking his time to review it. The working group of Volker Schulz was a friendly environment, providing a good spirit to fuel my research pursuits. Many thanks go to the members of the GivEn research group, especially Johanna Schultes and Jan Backhaus. They were always keen to help, and were great companions during our seemingly endless remote programming adventures in the times of Corona. I would like to thank Leonhard Frerick (Trier University) and Jochen Wengenroth (Trier University) for helpful and interesting discussions about differentiability and convergence in infinite dimensions. Furthermore, this work profited from remarks on variational inequalities by Gerd Wachsmuth (Brandenburg University of Technology).
I am very grateful for the warmth and support provided by my parents, Alexander and Marina Luft, and my beloved brother Andreas.
Perhaps the greatest debt is owed to Kingkanok Chanog, who has never let me down in this journey. Words cannot describe how thankful I am to you.
This work has been partly supported by the German Research Foundation (DFG) within the priority program "Non-smooth and Complementarity-based Distributed Parameter Systems: Simulation and Hierarchical Optimization" SPP 1962/1 under contract number Schu804/15-1, by the DFG research training group 2126 on Algorithmic Optimization, and by the BMBF (Bundesministerium für Bildung und Forschung) within the collaborative project GivEn (FKZ: 05M18UTA).

Preface

The following four publications were written as part of this dissertation.
A selection of the material from [7] is presented in section 3.2. For this publication, the contribution from the author of this work is given by [7, Sec. 2.1.2], and corresponding numerical implementations and figures described and found therein.
Findings of [122] are given in chapter 8. They are adapted to fit the more general context of this work, with more detailed discussions at appropriate places.
The material of [120] is found in chapter 4, section 5.1, section 5.3, and section 5.4. However, the respective theorems and discussions of [120] are significantly extended in this work, and are put in a more general mathematical framework.
The material of [121] is found in chapter 6, section 7.1, and section 7.2. Results and discussions of [121] are also stated in more general and detailed manner in this work. In particular, shapes in this work are allowed to have boundaries themselves.
Both [120] and [121] are accepted for publication in the journal Control and Cybernetics 2021.
All figures, tables and numerical implementations presented in this work, including those which are also found in the works [7, 122, 120, 121], are made by the author of this work.

Glossary of Spaces and Object Collections

$B_e(M, \mathbb{R}^{n+1})$	Space of smooth shapes, abbreviated by B_e^n
$C^0(M)$	Space of continuous functions
$C^\infty(M)$	Space of smooth functions
$C^\infty(M, \bigwedge^n T^*M)$	Space of smooth volume forms on M
$C^\infty_{0,\varphi(M)}(\mathbb{D}, \mathbb{R}^{n+1})$	Space of smooth vector fields vanishing on $\varphi(M) \cup \partial\mathbb{D}$
$C^k(M)$	Space of k-times differentiable functions with continuous k'th derivative
$C^{0,1}(M)$	Space of Lipschitz functions
$C^{k,\alpha}(M)$	Space of k-times differentiable functions with k'th continuous derivative having Hölder coefficient α
$C^\infty_0(M)$	Space of smooth functions vanishing at ∂M
$C^\infty_c(M)$	Space of smooth functions with compact support
$H^s(\mathbb{D}, \mathbb{R}^{n+1})$	Space of s-times weakly differentiable vector fields with square-integrable weak derivatives
$H^s_0(\mathbb{D}, \mathbb{R}^{n+1})$	Space of s-times weakly differentiable vector fields vanishing on $\partial\mathbb{D}$ with square-integrable weak derivatives
$H^s_{0,\varphi(M)}(\mathbb{D}, \mathbb{R}^{n+1})$	Space of s-times weakly differentiable vector fields vanishing on $\varphi \cup \partial\mathbb{D}$ with square-integrable weak derivatives
$L^\infty(\mathbb{D})$	Space of essentially bounded functions
$L^p(\mathbb{D})$	Space of p-integrable functions
$T_\rho \operatorname{Diff}(\varphi(M))$	Tangent space of fiber at ρ, vertical bundle component of $T_\varphi \operatorname{Emb}(M, \mathbb{R}^{n+1})$
$T_\varphi \operatorname{Emb}(M, \mathbb{R}^{n+1})$	Tangent space of pre-shape space at $\varphi \in \operatorname{Emb}(M, \mathbb{R}^{n+1})$
$T_{\pi(\varphi)} B_e^n$	Tangent space of shape space at $\pi(\varphi)$, horizontal bundle component of $T_\varphi \operatorname{Emb}(M, \mathbb{R}^{n+1})$
$W^{k,p}(\mathbb{D})$	Space of k-times weakly differentiable functions with weak derivatives in $L^p(\mathbb{D})$
$\mathbb{D}$	$n+1$-dimensional open hold-all domain, usually a subset of $\mathbb{R}^{n+1}$
M	n-dimensional manifold, perhaps with boundary ∂M
$\mathbb{N}$	Natural numbers
$\mathcal{N}$	Space of normal vector fields, horizontal bundle representation
$\mathbb{R}$	Real numbers
$\mathcal{A}$	Set of admissible shapes as sets, a subset of $\mathcal{P}(\mathbb{R}^{n+1})$
$\mathcal{T}$	Space of tangential vector fields parallel to boundaries, vertical bundle representation
$\mathbb{H}^n$	Half-space of $\mathbb{R}^n$
$\mathcal{P}(\mathbb{R}^{n+1})$	Power set, collection of all subsets of $\mathbb{R}^{n+1}$
$\operatorname{Diff}(M)$	Group of smooth diffeomorphisms of M
$\operatorname{Diff}^0(M)$	Group of homeomorphisms of M

$\mathrm{Diff}^s(M)$	Group of H^s-Sobolev diffeomorphisms of M
$\mathrm{Diff}^s_\omega(M)$	Group of H^s-diffeomorphisms of M preserving volume form ω
$\mathrm{Diff}_+(M)$	Group of orientation preserving smooth diffeomorphisms of M
$\mathrm{Diff}_\omega(M)$	Group of smooth diffeomorphisms of M preserving volume form ω
$\mathrm{Diff}_{\varphi(M)}(\mathbb{D})$	Group of smooth diffeomorphisms of $\mathbb{D}$, which leave $\varphi(M) \cup \partial\mathbb{D}$ pointwise invariant
$\mathrm{Emb}(M, \mathbb{R}^{n+1})$	Pre-shape space, collection of smooth embeddings
$\mathrm{Emb}_{\partial M}(M, \mathbb{R}^{n+1})$	Pre-shape space with invariant boundary, collection of smooth embeddings which leave ∂M pointwise invariant
$\mathrm{Gr}(M, \mathbb{R}^{n+1})$	Nonlinear Grassmannian, collection of all submanifolds of $\mathbb{R}^{n+1}$ of diffeomorphism class M
$\mathrm{int}(\mathbb{D})$	Interior of $\mathbb{D}$
$\mathrm{vol}^+_\omega(M)$	Space of smooth volume forms on M with same orientation and total volume as ω
$\overline{\mathbb{D}}$	Closure of $\mathbb{D}$
$\overline{\mathbb{R}}^n_+$	Nonnegative first orthant of $\mathbb{R}^n$
$\partial\mathbb{D}$	Boundary of $\mathbb{D}$

Glossary of Objects

$D\phi$	Jacobian matrix of ϕ
$D^\tau\varphi$	Covariant derivative of φ
$D_\Gamma\phi$	Tangential derivative of ϕ on a subset
T_t	Domain perturbation
U	(Pre-)shape gradient, or open subset of a base space
V, W	Vector fields
$\mathfrak{a}(\cdot,\cdot)$	Form for (pre-)shape gradient representations
$a(\cdot,\cdot)$	Bilinear form featured in state equations
γ	Curve
Δf	Laplacian of f
ρ	Diffeomorphism
κ	Mean curvature
n	Outer unit normal vector field, or dimension
n_M	Outward pointing unit normal vector field for manifolds with boundary ∂M
ψ	Obstacle
$\mathfrak{D}\mathfrak{J}$	Pre-shape derivative of $\mathfrak{J}$
$\mathfrak{D}^2\mathfrak{J}$	Pre-shape Hessian of $\mathfrak{J}$
$\mathfrak{D}_m\mathfrak{J}$	Pre-shape material derivative of $\mathfrak{J}$
π	Fiber bundle projection
r	Right-hand side of state equations
$q, q^{\mathbb{D}}$	Externally defined parameterization tracking targets
Γ	Shape
φ	Pre-shape
φ^*	Pullback of differential forms via φ
$\mathcal{D}\mathcal{J}$	Shape derivative of $\mathcal{J}$
$\mathcal{D}_m\mathcal{J}$	Shape material derivative of $\mathcal{J}$
τ	Tangent unit vector field
$\mathfrak{J}$	Pre-shape functional
$\mathfrak{J}^M, \mathfrak{J}^{\mathbb{D}}$	Pre-shape parameterization tracking functionals
$\mathcal{J}$	Shape functional
ϕ	Pre-shape for the hold-all domain $\mathbb{D}$
$\mathrm{d}f$	Differential of pushforward of tangent vectors via f
$\dot{\gamma}$	Tangential vector via velocity of γ
$\mathbb{1}_A$	Indicator function of A
$\mathcal{L}$	Lagrangian function
$\mathcal{L}_V\omega$	Lie derivative of ω in direction V
$\nabla_\Gamma f$	Tangential gradient of f on a subset
∇f	Gradient of f
ω	Volume form
$\mathrm{Pr}_{H^1_{0,\varphi(M)}}$	Projection operator mapping $H^1(\mathbb{D},\mathbb{R}^{n+1}) \to H^1_{0,\varphi(M)}(\mathbb{D},\mathbb{R}^{n+1})$

Tr_X	Trace operator for functions onto X
$\det D^\tau\varphi$	Jacobian determinant of $D^\tau\varphi$
$\mathrm{div}(V)$	Divergence of V
$\mathrm{div}_\Gamma(V)$	Tangential divergence of V on a subset
$\mathrm{div}_\omega(V)$	Divergence of V with respect to volume form ω
$\mathrm{div}_{f,\Gamma}(V)$	Tangential f-divergence of V on a subset
$\max(0,\alpha)$	Maximum function of 0 and α
$\max_\gamma(\alpha)$	Smoothed version of maximum function $\max(0,\alpha)$ with smoothing parameter γ
$\mathrm{sign}(\alpha)$	Derivative of $\max_\gamma(\alpha)$
$\mathrm{sign}(\alpha)$	Heaviside step function
$\mathrm{supp}\, V$	Support of V
$\mathrm{tr}(A)$	Trace of matrix A
$\mathrm{vol}(\mathbb{D})$	Lebesgue measure of $\mathbb{D}$
$f, f^{\mathbb{D}}$	Pre-shape parameterization tracking target densities
$g^M, g^{\mathbb{D}}$	Initial densities for parameterization tracking
$g^{\mathcal{N}}$	Normal pre-shape derivative component
$g^{\mathcal{T}}$	Tangential pre-shape derivative component

Contents

Glossary of Spaces and Object Collections **x**

Glossary of Objects **xii**

Contents **xiv**

1 Introduction **1**
1.1 Literature Review 4

2 Background Material **9**

3 Introduction to Shape Optimization and Shape Calculus **15**
3.1 Shape Calculus 15
3.2 Industrial Application of Steklov-Poincaré Metrics 20

4 General Theory of Pre-Shape Calculus **24**
4.1 Shape and Pre-Shape Spaces 25
4.2 Pre-Shape Calculus 34

5 The Pre-Shape Parameterization Tracking Problem **49**
5.1 Introduction and Existence of Solutions to Parameterization Tracking 50
5.2 Properties of the Pre-Shape Parameterization Tracking Problem . . 59
5.2.1 Pre-Shape Parameterization Tracking and Finite Point Sets . 59
5.2.2 Characterization of Solutions by Diffeomorphism Groups and Euler Flows 63
5.3 Pre-Shape Derivative and Optimality Conditions of Parameterization Tracking 77
5.4 Numerical Tests of Parameterization Tracking Involving Pre-Shape Derivatives 87
5.5 The Pre-Shape Hessian of Parameterization Tracking Problems . . . 92

6 Regularizing Shape Optimization Problems by Parameterization Tracking **99**
6.1 Simultaneous Shape Mesh Quality and Shape Optimization 100
6.2 Simultaneous Volume Mesh Quality and Shape Optimization 105
6.2.1 Volume Parameterization Tracking Problem with Invariant Shapes 105
6.2.2 Simultaneous Shape and Volume Mesh Regularization for Shape Optimization 111

7 Implementation of Shape and Volume Mesh Quality Regularizations 116
7.1 Model Problem and Application of Pre-Shape Mesh Quality Regularization . . . 117
7.1.1 Model Problem Formulation and Regularization . . . 117
7.1.2 Construction of Initial and Target Node Densities . . . 118
7.1.3 Pre-Shape Gradient Systems . . . 121
7.2 Numerical Results and Comparison of Algorithms . . . 125
7.3 Shape Mesh Regularization via Full and Tangential Pre-Shape Derivatives . . . 135
7.4 Comparing Direct and Shape Invariant Volume Parameterization Tracking . . . 138

8 Shape Optimization Problems Constrained by First Order Variational Inequalities 141
8.1 First Order VI-Constrained Tracking Type Shape Optimization Problems . . . 142
8.2 Regularized State and Adjoint Equations . . . 143
8.3 Shape Derivatives of Regularized VI-Constrained Problems . . . 150
8.4 Algorithmic and Numerical Aspects of VI-Constrained Tracking Type Problems . . . 162

9 Custom Pre-Shape Regularization for VI-Constrained Shape Optimization 171
9.1 Constructing a VI-Specific Cell Volume Target . . . 172
9.2 A Quasi-Newton-ADM Approach for Mesh Quality and Shape Optimization . . . 176
9.3 Implementation and Results . . . 180

10 Conclusion and Outlook 191

List of Figures 194

List of Tables 195

List of Algorithms 196

Bibliography 196

Chapter 1

Introduction

Shape optimization is an active research area at the border of theoretical and applied mathematics. Not only is it a subject concerned with spaces and objects of astounding structural richness, but also a key tool for industrial applications. To give some examples, shape optimization is used in the design of turbomachinery (cf. [7, 8, 66]), superconductors (cf. [109]), wing configurations of aircrafts (cf. [97, 153, 156]), acoustic devices (cf. [157]), pharmaceutical applications (cf. [165, 140]), electrical motors (cf. [59]) and for electrical impedance tomography (cf. [48, 107]).

In most practical scenarios of shape optimization, it is inevitable to use numerical techniques to construct desired optimal shape solutions. The quality of solutions is strongly linked to the representation of shapes and computational domains. A large family of shape optimization methods is based on discretization of shapes and hold-all domains by meshes, similar to those found in finite element computations. It is common to pursue a design process, in which the coordinates of the domain and shapes are updated in each iteration. These techniques are sometimes denoted as mesh-morphing algorithms. In particular, they permit application of shape derivative based techniques, such as shape gradient descents in various styles, or shape quasi-Newton methods.

A fundamental, perhaps unavoidable, problem of mesh-morphing routines is the possible degeneration or destruction of the computational mesh after sufficiently many or large deformations. This particularly affects many shape optimization problems of interest, which have a constraint, such as a partial differential equation or a variational inequality. A key component of reliable solutions to these is the quality of the computational mesh. For example, it is well-known that poor quality of elements affect the stability, convergence, and accuracy of finite element and other solvers due to poorly conditioned stiffness matrices (cf. [163]). Therefore, an accurate solution of underlying model problems on degenerated meshes, and thus of the entire shape optimization problem, is hard or next to impossible.

Goals of This Work A main goal of this work is to design shape optimization techniques, which ensure desired mesh quality. These should come with little additional numerical cost, be compatible with other different shape optimization techniques found in the literature, and not interfere with the original problem. The techniques we develop do not involve changes in mesh topologies, and particularly avoid remeshing or mesh refinements.

To handle this task, we propose an abstract framework for shape optimization using so-called pre-shape spaces. This setting is suitable to formalize two seemingly unrelated classes of problems. For one, pre-shape spaces are suitable to state shape optimization problems. On the other hand, they can also be used to pose parameterization or mesh quality problems. The novelty of our approach is to simultaneously

situate both shape optimization, and mesh quality optimization in a single unified framework. For these spaces, we can derive a pre-shape calculus, generalizing classical shape calculus. Pre-shape spaces are suitable to state a class of so-called pre-shape parameterization tracking problems, which can act as regularizers for shape optimization problems. These problems are used to achieve specified, perhaps non-uniform, cell volume distributions of the hold-all domain and the shape mesh. Shapes are permitted to have boundaries, and can have arbitrary integer codimension with respect to their ambient space. In specialized cases, this problem class yields numerical algorithms similar to so-called deformation methods, which reallocate nodes of numerical meshes according to target element volumes. With their pre-shape derivatives, we formulate efficient routines for shape optimization problems, which at the same time optimize quality of the surface mesh representing the shape, and of the volume mesh representing the hold-all domain.

These regularizations are implementable in existing numerical routines solely by adding additional pre-shape derivative terms on the right-hand sides of shape gradient representations. This ensures that shape gradient systems neither increase in size, nor become nonlinear. Also, our approach does not depend on the left-hand side, which can be any sufficient bi- or nonlinear form. The user is free to choose his preferred shape gradient representation, with our mesh quality regularization approach employable in addition. Pre-shape techniques presented in this work are applicable to general problems, and do not interfere with the original shape optimization problem.

We also design a second, complementary mesh quality routine inspired by the alternating directions method (ADM). This routine can be applied on top of the regularized shape gradient systems, and permits application of efficient optimization techniques, such as (quasi-)Newton methods. With these techniques, desired surface and surrounding volume mesh quality are ensured during shape optimization with mesh morphing, while optimal shapes stay invariant.

Further, we examine tracking type shape optimization problems constrained by elliptic variational inequalities of first kind. The results concerning their regularizations, shape derivatives, and convergence behaviors can stand on their own, and are not necessarily linked to pre-shape techniques. However, to highlight the applicability and flexibility of our pre-shape techniques, we design a mesh quality regularization technique tailored for the application to shape optimization under variational inequalities. These methods adapt the mesh for higher resolution of areas with interesting features of the constraint, and are not just applicable for VI-constrained shape optimization problems, but adaptable for general shape optimization.

Structure of This Work The outline of this work is as follows. Selected parts of this work are found in [122, 120, 121, 7], and are published or accepted for publication at the time writing.

First, we give a literature overview of related works in the remainder of this introduction. In **chapter 2**, we collect theoretical background material not related to shape optimization. Then, in **chapter 3**, we give a brief introduction to selected aspects of shape optimization. In particular, we highlight our application of so-called Steklov-Poincaré metrics for optimization of turbomachinery in the context of BMBF project GivEn.

Chapter 4 is divided into two parts. In section 4.1, we give an introduction to shape and pre-shape spaces in the context of infinite dimensional differential geometry, relate their tangent bundles, and give some notes on topology. Thereafter, the remainder of this work consists of our own results. Section 4.2 begins with definitions of pre-shape functionals and corresponding pre-shape derivatives. We show that shape differentiable functionals are pre-shape differentiable, and derive a

structure theorem for pre-shape derivatives in style of the Hadamard-Zolésio theorem. Corresponding pre-shape calculus rules, in particular using pre-shape material derivatives, are collected, and also hold in the specialized case of shape calculus.

After establishing the general theory of pre-shape calculus, we study the pre-shape parameterization tracking problem class in **chapter 5**. We show existence of solutions for each shape, perhaps with boundary, in the pre-shape space in section 5.1, and give a discussion on generalizations for shapes of arbitrary codimension, embedded in nonlinear ambient spaces. Following this, we show some general properties of the parameterization tracking problem concerning finite point sets in section 5.2.1. Then, we focus on the non-uniqueness of solutions in section 5.2.2, and characterize locally neighboring solutions by use of f-divergences and Euler-Arnold flows induced by L^2-metrics on the fibers of pre-shape spaces. The pre-shape derivative of the parameterization tracking problem is derived and analyzed in section 5.3. We harness the pre-shape derivative structure to show that a weaker notion of vanishing pre-shape derivative is in fact a sufficient condition for global optimality of parameterization tracking. Building on this, we present a first numerical implementation in section 5.4, which shows how the parameterization tracking problem can be used to achieve desired mesh qualities. After this numerical intermezzo, we derive a closed expression for its pre-shape Hessian in section 5.5, and discuss its properties in solutions.

In **chapter 6**, we build the theory for simultaneous shape and mesh quality optimization using pre-shapes. Particularly, we start with regularization of meshes representing the shapes in section 6.1. Then, we propose a modified parameterization tracking problem for hold-all domains in section 6.2.1, which permits invariance of embedded shapes. We prove existence of solutions, and formulate a shape and volume mesh regularized bilevel version of shape optimization problems. An existence result for the regularized bilevel problem is provided in section 6.2.2, consistency of pre-shape gradient systems is guaranteed, and invariance of solutions to the underlying original shape optimization problem is shown.

Numerical implementations of these mesh quality regularization techniques are shown in **chapter 7**. We pose a model problem in section 7.1, and describe how point densities and their pre-shape material derivatives for pre-shape parameterization tracking are constructed. The various pre-shape gradient systems for mesh quality regularization are discussed in section 7.1.3. In particular, we highlight the flexibility of our approach by applying it to linear elasticity and quasilinear p-Laplacian shape gradient representations. Several unregularized and regularized shape optimization procedures are implemented, and the comparative results are illustrated and discussed in section 7.2. Also, the pitfalls of more direct approaches for pre-shape regularizations are numerically highlighted in section 7.3 and section 7.4, and compared to our proposed methods.

In **chapter 8**, we take a slight detour from pre-shape calculus techniques, and focus on a tracking type shape optimization problem class constrained by elliptic variational inequalities (VI) of first kind. Regularization techniques are shown, which permit existence results for adjoints and shape derivatives. Convergence of these objects is shown for vanishing regularizations, and are put into numerical practice.

Finally, we combine all previous results in **chapter 9**, and provide a customized pre-shape regularization target for VI-constrained shape optimization problems. An ADM inspired pre-shape regularization algorithm featuring L-BFGS methods for mesh quality is proposed in section 9.2, which is also applicable outside the frame of VI-constrained shape optimization, and can be combined with all previous techniques. We numerically compare our approaches for the VI-constrained shape optimization problem in section 9.3.

An outlook on potential topics for further research is presented in chapter 10.

1.1 Literature Review

In this section, we collect literature on techniques and subjects related to this work. This list is by no means exhaustive, but should make it easier for the reader to contextualize this work, and to evaluate its significance. For the pre-shape regularization techniques for mesh quality, we consider two categories of literature. First non-shape optimization results, with techniques for mesh adaptation having relations to our approach, or being special cases of our approach. And second, shape optimization techniques for mesh quality, which try to achieve similar goals as our strategies, but are different in their way of achieving this. Then we also consider literature related to our approach for shape optimization under variational inequalities.

The techniques for pre-shape parameterization tracking we introduce in section 5.1 have their roots in a result by Moser [134] from 1965. Essentially, Moser's theorem guarantees existence of diffeomorphisms on manifolds, which give rise to specified volume forms via pullbacks. This results was extended to Riemannian manifolds with boundary by Banyaga in [10], and then refined in [39] by Dacorogna and Moser. In [39], several different analytical techniques guarantee existence and regularity for PDEs involving the Jacobian determinant. Also, Moser's existence theorem is extended to manifolds with corners by Bruveris, Michor et al. in [28], which includes the cases of simplicial complexes and polyhedric meshes. These existence theorems lay the foundation of so-called mesh deformation methods, and also play a role for some results of this work. Deformation methods redistribute mesh vertices, such that a target cell volume is achieved, while preventing mesh tangling. This method was pioneered in [112] by Liao and Anderson. It is a special case of our results, in the sense, that it correspond to uniform cell volume allocations.

In [19], Bochev, Liao and dela Pena introduce a deformation method by looking at Euler-Lagrange equations of several different functionals, in order to track for element volume distributions. A divergence equation is formulated, and an additional curl condition is imposed to provide existence and uniqueness of deformation directions for the case of Lipschitz domains without reentrant corners in 2 and 3 dimensions. The generated vector fields are used to implement an ODE, which gives a mesh deformation with desired volume allocation properties for a fixed mesh. These results also apply to non-uniform cell volume allocations. In [114], Liao et al. apply the deformation method developed in [19] to steady state Euler equations to adapt meshes for better resolution of interfaces and shocks. The authors of [31] look at a deformation law to achieve volume concentrations of cells measured by Jacobians, which is given by advection flows generated via minimization of a least squares functional. [29] extend these methods to time dependent problems by looking at a least-squares formulation for deformations to track the element volume distribution of meshes at various points in time. These techniques can be related to the pre-shape parameterization tracking problem in section 5.1 for the special case of invariant Euclidean domains, i.e. mesh quality optimization of codimension zero shapes, which are left fixed, and where no shape optimization takes place.

The techniques in [112, 19, 114, 29] are not directly suitable for simultaneous shape optimization, because they do not guarantee invariance of optimal shapes, since the mesh nodes are unrestricted in their movement to achieve desired cell volumes. Moreover, they need to solve an additional PDE and ODE to generate the mesh deformation for a fixed mesh. Also, they are not stated for manifolds, i.e. are not directly applicable to the regularization of surface meshes arising in shape optimization. The regularizations with the pre-shape parameterization tracking in chapter 5 and chapter 6 do not suffer from these drawbacks. In particular, we do not rely on solution of additional (non-)linear systems, PDEs or ODEs. Instead, we modify right-hand sides of shape gradient systems, such that the underlying mesh is simul-

taneously increasing quality and reducing the shape optimization objective. The non-uniqueness characterization of solutions to pre-shape parameterization tracking via L^2-metrics on diffeomorphism groups and Euler flows in section 5.2.2 can be related to the curl condition in [19] for the special case of uniform targets, no shape optimization taking place, and Euclidean domains.

Mesh deformation methods are also encountered in mesh generation, as in [185], where a higher order element mesh generation algorithm is derived by combining a local refinement technique with the deformation method on variable domains. It uses a div-curl system and techniques similar to [19, 29].

In [43], Delzanno and Finn propose a framework for mesh deformation methods by using a tracking type objective functional with additional terms. They show connections to L^p-Monge-Kantorovich and L^p-Monge-Ampère problems. Also, an L^p-fluid dynamic formulation, in which a density obeying a continuity equation is advected, is shown to be equivalent to L^p-Monge-Kantorovich deformation methods. These results are not posed in the context of shape optimization, and as such are not immediately suitable for the same reasons just discussed for [19, 114, 29]. However, they are interesting, since we also recover connections of our techniques to optimal transport on manifolds at the end of section 5.1.

In [180, 68, 69], Turek et al. employ deformations methods originating in [19] to design moving mesh strategies for solution of differential equations. The authors of [180] show how alternating solution of flow equations by a multigrid fictitious boundary method, and application of a deformation method similar to [112], yields an efficient algorithm for simulation of particle flows. In [68], a deformation method is proposed, which generalizes techniques from [112] by introducing a function g capturing the volume distribution of the initial mesh. Then, a divergence equation with additional constraint is solved, giving a vector field used to assemble an ODE. Solving this ODE results in the desired mesh deformation at final time.

On Euclidean domains and the special case of optimization in so-called fibers of pre-shape spaces, our method computes mesh deformations related to those in [68], but with methods of pre-shape calculus. In contrast to [68], this does not require alternating solutions of ODEs for mesh deformations. Instead, we can apply our techniques on gradient systems, which could be interpreted as a deformation method working simultaneously with shape optimization descents. Also, techniques of [180, 68, 69] are not directly suitable to optimization of manifold meshes.

The work [69] builds on [68] by introducing a multigrid approach to speed up calculation of mesh deformations, which has a runtime growing only linearly with the problems size. In chapter 9, we take a different route, because our mesh quality problem is posed in the context of pre-shape spaces. This permits application of shape quasi-Newton methods for mesh quality increase.

[60] use optimization methods based on condition numbers and reference Jacobians of elements on non-planar surface meshes as criteria to increase mesh quality. [123] design an optimization method using a gradient descent for penalty functions based on Jacobians of mesh elements in order to improve mesh quality, while checking for validity of node placements.

There are also techniques for mesh quality, which are not related to Moser's theorem and the resulting deformation methods previously discussed. For example, [53] explores the use of Laplacian smoothing combined with local Delaunay retriangulation to improve mesh quality. [54] develops various algorithms to increase mesh quality by combining local Laplacian smoothing together with optimization of mesh quality criteria, such as dihedral angles or aspect ratios, in different ways. In [164], mesh warping algorithms for unstructured tetrahedric meshes are enhanced by determining weights for a deformation using an interior point method. Based on the new locations and previous weights, a linear system is solved to determine final nodal positions, which in total mimics effects of locally weighted Laplacian smooth-

ing. The authors of [184] use a combination of smoothing based and geometric flow optimization to improve quality of quadrilateral and hexahedral manifold meshes, while preserving geometric features. In particular, it is based on diffusions on the shape modeled by the Laplace-Beltrami operator.

These approaches differ considerably from our approach, since they are not directly applicable to shape optimization due to possible deformation of embedded shapes. Further, the use of mesh smoothing techniques does not allow for specified mesh quality targets, which is possible with the techniques explored in section 5.1 and further chapters.
We explicitly emphasize, that our methods are not related to mesh untangling and -relaxation, edge swapping or remeshing strategies such as [54, 55, 2, 98]. By their nature, these type of methods are based on a discrete setting, as opposed to our methods based on a continuous framework.

The following literature falls under the category of shape optimization techniques to achieve better mesh quality, or are related to these.

In [145], Onyshkevych and Siebenborn develop a method for shape optimization, which modifies gradient representations of shape derivatives. The boundary formulation of the shape derivative is used as a Neumann condition on the shape to assemble a system incorporating a nonlinear advection term to represent a shape gradient in volume formulation. This formulation advects nodes of the volume mesh in order to mitigate element degeneration, and requires solution of a nonlinear system to construct the shape gradient. Advection parameters have to be chosen a priori.
In [75], Haubner, Siebenborn and Ulbrich develop an approach to shape optimization using the method of mappings to guarantee non-degenerate deformations of meshes is presented. For this, the shape optimization problem is regarded as an optimization in function spaces. A penalty term for the Jacobian determinants of deformations is added, which leads to a non-smooth optimality system. Deformations computed by solving this system have less tendency to degenerate volumes of cells.
In the work [49], Etling, Herzog, Loayza-Romero and Wachsmuth enhance mesh morphing routines for shape optimization by correcting the invalidity of the Hadamard theorem due to discretization of the problem. The correction for degenerate steps requires a restriction of deformation directions based on normal fields of shapes, which leads to larger linear systems for shape gradients due to the additional constraints.
In [155], Schmidt applies mesh smoothing inspired by centroidal Voronoi reparameterization to construct a tangential vector field to correct degenerate surface mesh cells. For correction of volume mesh cell degeneration, a shape gradient representation featuring a nonlinear advection term is used, where the integrand of the shape derivative in boundary formulation acts as a Neumann condition on the shape. Construction of the advection term relies on solution of an Eikonal equation with respect to the shape.

In contrast to techniques proposed in this work, no node or target cell volume allocation are possible with the approaches found in [145, 75, 155, 49]. User specified gradient representations are also not valid in general, or require modification of techniques. Numerical costs are higher in comparison, since the modification of left-hand sides of shape gradient representations in [145] and [155] result in nonlinear systems. Corrected discrete shape gradient representations in [49] result in significantly larger linear systems compared to standard shape gradient representations. Our techniques have approximately the same numerical expense as the chosen shape gradient representation, since only right-hand sides of gradient systems are modified.

In order to mitigate roughness of shape gradients and resulting degeneration of

meshes, Schulz, Siebenborn and Welker construct shape gradient representations by use of Steklov-Poincaré metrics in [161, 159]. As an example, they propose the weak linear elasticity metric, giving a more regular shape gradient representation by solution of a linear system with volume formulations of shape derivatives.

In [40], Deckelnick, Herbert and Hinze employ shape descent directions in the $W^{1,\infty}$-topology, which are related to shape gradient representations with the ∞-Laplacian. Numerical results show enhanced convergence properties for a shape optimization problem on star-shaped domains, especially enhancing resolution of corners. The authors of [135] build on [40], and propose shape gradient representations using the strong formulation of the nonlinear p-Laplacian equation. The system is solved via Picard iterations, and numerical results in the context of fluid dynamics suggest better suitability of p-Laplacian represented shape gradients for large deformations, particularly for optimal shapes with corners.

Our approaches are compatible with those of [161, 159, 135], and can in fact be used in addition to any type of shape gradient representation. To highlight this, we use pre-shape gradient representations similar to those of [161, 159, 135] in numerical applications of our techniques found in section 5.4, chapter 7 and section 9.3.

In [84], Hiptmair and Paganini view shape optimization as optimization over an admissible set of vector fields with sufficiently small norms, which represent diffeomorphisms of the shape and domain by a perturbation of identity approach. This results in a method that uses nested trial spaces to represent shapes via B-splines, and does not rely on a moving mesh approach. The framework of this approach is related to our work, since we situate shape optimization in the context of pre-shape spaces, which have the diffeomorphism groups of domains discussed in [84] as special cases.

In [78], Herzog and Loayza-Romero construct a Riemannian metric for the manifold of planar triangular meshes with given fixed connectivity, which makes the space geodesically complete. They propose a mesh morphing routine by geodesic flows, which uses the Hamiltonian formulation of the geodesic equation solved with symplectic numerical integrators. Numerical experiments in [78] suggest that cell aspect ratios are bounded away from zero, and thus avoid mesh degradation during deformations.

Outside the context of shape optimization, Laurain and Walker [108] design a method for shape/mesh morphing by approximating a given flow of shapes with mean-curvature flows respecting volume-preservation.

As we propose regularization techniques for elliptic VI-constrained shape optimization problems in chapter 8, we give a selected literature overview on this and related topics.

By usage of tools of modern analysis, such as monotone operators in Banach spaces, significant results on properties of solution operators of variational inequalities have been achieved since the 1960s by Brézis, Stampacchia and Lions [26, 27, 113]. Bonnans and Tiba [22] deal with control problems of variational inequalities governed by semilinear elliptic operators. Optimality conditions are derived via smoothing methods, and convergence of the regularized state and control for vanishing smoothing are shown. Liu and Rubio [115, 116] present existence results for shape optimization problems which can be reformulated as optimal control problems. In [104], Kocvara and Outrata study shape optimization of 2D elastoplastic bodies, where the shape is simplified to a graph such that one dimension can be written as a function of the other. The non-trivial existence of solutions of VI-constrained shape optimization problems is discussed in [41, 168]. For example, in [168, Ch. 4], shape derivatives of elliptic variational inequality constrained problems are presented in the form of solutions to again variational inequalities. Ito and Kunisch [93] discuss optimality conditions for optimal control problems constrained by elliptic variational inequalities via a primal-dual penalty approach.

Under sufficient assumptions, existence of Lagrange multipliers and convergence of solutions of the penalized problems to the original problem are shown, and a primal-dual active set strategy is devised. In [79], Hintermüller considers least-squares problems constrained by variational inequalities in bilevel formulations. Primal-dual penalization techniques from [93] are extended, and so-called complementarity functions are used to allow formulation of optimality systems in form of equalities. In [138, 139], Myśliński proposes and applies level-set methods to graph-like two-dimensional contact problems. Hintermüller [80] extends [79] by building on the concept of C-stationarity to avoid problems from low regularity multipliers. With this, an active-set method with feasibility restoration is developed. Instead of using penalty techniques, Hintermüller and Kopacka [81] relax complementarity constraints of VI-constrained optimal control problems. Then, Moreau-Yosida type regularizations are applied, and a semi-smooth Newton method is proposed to solve the regularized subproblems. In [83], Hintermüller and Surowiec avoid the use of penalization or relaxations techniques as found in [81, 79], and directly derive optimality conditions to VI-constrained optimal control problems by use of variational analysis. Hintermüller and Laurain [82] present a regularization approach to the computation of shape and topological derivatives in the context of elliptic variational inequalities, circumventing the numerical problems in [168, Ch. 4]. Schiela and Wachsmuth [152] look at optimal control problems constrained by elliptic VI, which are regularized and smoothed to give semilinear elliptic PDE. Sharp convergence estimates and optimality conditions of regularized solutions are derived. In [35], Christof, Clason, Meyer and Walther analyze optimal control problems constrained by semilinear and semi-smooth elliptic equations, which similarly arise for variational inequalities of first kind. They give descriptions of subdifferentials, and of necessary optimality conditions via smoothing techniques. In [76], Heinemann and Sturm perform a sensitivity analysis for a class of semilinear variational inequalities, a strong convergence property is shown for the material derivative, and state-shape derivatives are established under regularity assumptions. Brett, Elliott, Hintermüller and Löbhard [25] consider adaptive mesh refinement techniques for tracking type optimal control problems constrained by elliptic variational inequalities. These are based on a refinement indicators constructed via error of the regularized and unregularized objective functional and mismatch in complementarity of primal variables and their multipliers. In [109], Laurain, Winckler and Yousept examine shape optimization of superconductors, with physics governed by curl-curl variational inequalities of second kind with L^1-nonlinearities. State equations are regularized, and existence and closed formulations of respective shape derivatives are provided. In [57], Führ, Schulz and Welker devise a shape optimization method based on an ad-hoc smoothing of a variational inequality of first kind based on [94]. The authors of [57] observed that the performance of this algorithm strongly depends on the tightness of the obstacle. This problem does no longer arise with the strategy developed in chapter 8. The solution algorithm gets even faster, the more degrees of freedom are constrained by the obstacle.

Chapter 2

Background Material

Before we delve into the theory of pre-shape calculus and its application to mesh quality optimization during shape optimization, we collect some preliminary results from various areas of mathematics in this chapter. Of course, we cannot give a complete overview of all definitions and techniques we employ throughout this work, so we limit ourselves to a selection of these. We begin by defining so-called Fréchet spaces. For an introduction to Banach, Hilbert and Sobolev spaces, we refer the reader to [147, 175, 50]. Essentially, Fréchet spaces are metrizable, complete, locally convex vector spaces (cf. [175, App. A.3]).

Definition 1 (Fréchet Spaces)**.** *Let F be a vector space, perhaps infinite dimensional. Consider a countable family $|\cdot|_s \colon F \to [0,\infty)$ of semi-norms, i.e.*

(i) $|\alpha \cdot f|_s = |\alpha| \cdot |f|_s$ *for all* $f \in F$, $\alpha \in \mathbb{R}$

(ii) $|f+g|_s \leq |f|_s + |g|_s$ *for all* $f, g \in F$.

Additionally assume

$$f \neq 0 \implies |f|_s \neq 0 \quad \text{for some } s \in \mathbb{N}.$$

Then F is a metric space with distance function

$$d(f,g) = \sum_{s=0}^{\infty} 2^{-s} \frac{|f-g|_s}{1+|f-g|_s}. \tag{2.1}$$

We say (F,d) is a Fréchet space*, if it is complete with respect to the distance function defined in equation* (2.1)*. Further, convergence with respect to $d(\cdot,\cdot)$ is equivalent to*

$$|f_n - f|_s \to 0 \quad \text{for } n \to \infty \quad \text{for all} \quad |\cdot|_s.$$

The most important examples of Fréchet spaces in this work are the spaces of smooth functions $C^\infty(M)$ on compact manifolds M. The discussion of topologies on these spaces is postponed to section 4.1. In the following, we define maps which preserve the smooth structure of Fréchet spaces. This definition is a special case, where a more general definition for so-called convenient vector spaces holds (cf. [105, Ch. 1.1.13]).

Definition 2 (Diffeomorphisms of Fréchet Spaces)**.** *Let F be a Fréchet space, and $U, V \subset F$ be open subsets. Consider a map $\rho \colon U \to V$.*

We call ρ a C^k-diffeomorphism *of U and V, if ρ is k-times Fréchet-differentiable and bijective with k-times Fréchet-differentiable inverse ρ^{-1}. If this property holds for $k = \infty$, we say ρ is a smooth or C^∞-diffeomorphism of U and V.*

The next definition describes structure preserving maps for topological spaces (cf. [111, App. A]).

Definition 3 (Homeomorphisms of Topological Spaces)**.** *Let X and Y be topological spaces. Consider a map $\rho\colon X \to Y$.*

Then we say ρ is a homeomorphism*, if it is continuous and bijective with continuous inverse ρ^{-1}.*

In the following definition, we give a description of the nonlinear spaces we consider in this work. The definition of topological and smooth manifolds, perhaps with boundary or corners, is found in [111, Ch. 1, Ch. 16], whereas the infinite dimensional definitions are found in [71, Ch. 2.1].

Definition 4 (Manifolds)**.** *Let M be a topological space. Then we say M is an n-dimensional* topological manifold*, if*

(i) M is a Hausdorff space*, i.e. for every pair of distinct points $p, q \in M$, there are disjoint open sets $U, V \subset M$, such that $p \in U$ and $q \in V$*

(ii) M is second countable*, i.e. its topology has a countable basis*

(iii) M is locally Euclidean *or* modeled on $\mathbb{R}^n$*, i.e. for all $p \in M$, we can find open $U \subset M$ and $V \subset \mathbb{R}^n$, and a homeomorphism $\rho\colon U \to V$.*

We call such a homeomorphism ρ for $p \in M$ a chart centered in p*. A collection of charts with domains U covering M is called an* atlas for M*. Two charts ρ_1 and ρ_2 with domains U_1 and U_2 are* smoothly compatible of C^k-regularity*, if either $U_1 \cap U_2 = \varnothing$, or $\rho_1 \circ \rho_2\colon U_1 \cap U_2 \to U_1 \cap U_2$ is a C^k-map.*

A topological manifold M is said to be C^k-regular*, if there exists an atlas for M, consisting of smoothly compatible charts of C^k-regularity. For $k = \infty$, we say M is a* smooth or C^∞-manifold*.*

We say M is a

- manifold with boundary*, if $\mathbb{R}^n$ in (iii) is replaced by the half-space $\mathbb{H}^n := \{(x_1, \dots, x_n) \in \mathbb{R}^n : x_n \geq 0\}$*
- manifold with corners*, if $\mathbb{R}^n$ in (iii) is replaced by the nonnegative orthant $\overline{\mathbb{R}}^n_+ := \{(x_1, \dots, x_n) \in \mathbb{R}^n : x_1 \geq 0, \dots, x_n \geq 0\}$*
- Hilbert manifold*, if $\mathbb{R}^n$ in (iii) is replaced by a Hilbert space H with its underlying topology*
- Banach manifold*, if $\mathbb{R}^n$ in (iii) is replaced by a Banach space B with its underlying topology*
- Fréchet manifold*, if $\mathbb{R}^n$ in (iii) is replaced by a Fréchet space F with its underlying topology*
- Sobolev manifold*, if $\mathbb{R}^n$ in (iii) is replaced by a Sobolev space W with its underlying topology.*

For the case of manifolds with boundary or corners, open subsets of the modeling spaces $\mathbb{H}^n \subset \mathbb{R}^n$ and $\overline{\mathbb{R}}^n_+ \subset \mathbb{R}^n$ are elements of the relative topology. We mention this, because by definition, open subsets of manifolds M with boundaries or corners can have boundaries themselves. An example is the relative open half ball $B_1(0) \cap \mathbb{H}^n$. Also notice, that connected finite-dimensional topological manifolds are automatically path-connected (cf. [111, Prop. 1.11]). Further, for infinite-dimensional manifolds M, the choice of topology on the modeling space is non-trivial. Topologies in the context of Fréchet spaces are discussed in section 4.1.

We also remind the reader, that a map $f\colon M \to N$ is $C^k(M,N)$, if its local representations via charts is C^k for appropriate modeling vector spaces.

Next, we describe a certain class of manifolds, the so-called fiber bundles. These are of great importance in this work, as infinite dimensional pre-shape spaces carry a natural fiber bundle structure. This structure is also reflected in the pre-shape calculus we develop in later chapters. Put simply, fiber bundles are manifolds, which locally look like product manifolds. The following definition is found in [105, Ch. 37] and [111, Ch. 10.37].

Definition 5 (Fiber Bundles)**.** *Let E, F and B be smooth manifolds. We say E is a* smooth fiber bundle over B with standard fiber F*, if there is a surjective smooth map $\pi\colon E \to B$, with the property that for every $x \in B$, there exists a neighborhood $U \subset B$ of x, and a diffeomorphism $\Phi\colon \pi^{-1}(U) \to B \times F$, such that*

$$\begin{array}{ccc} \pi^{-1}(U) \subset E & \xrightarrow{\quad\Phi\quad} & U \times S \subset B \times F \\ & {\scriptstyle \pi^{-1}} \nwarrow \quad \nearrow {\scriptstyle \pi_1} & \\ & U \subset B & \end{array} \tag{2.2}$$

commutes. Here, $\pi_1\colon B \times F \to B$ is the projection onto the first component. We call the spaces E total space*, B* base space *and F* standard fiber*. Also, we call $\pi\colon E \to B$* canonical projection*, and a pair (U, Φ)* fiber chart *or* local trivialization*.*

In order to derive a sufficient calculus for shape and pre-shape spaces, we provide a concept for directions on manifolds M. At the same time, these can serve as a local linearization of M (cf. [111, Ch. 3]).

Definition 6 (Tangent Spaces and Tangent Bundles)**.** *Let M be a smooth manifold, perhaps with smooth boundary. For $p \in M$ and an interval $I \subset \mathbb{R}$ containing 0, consider smooth curves $\gamma_1, \gamma_2\colon I \to M$ with $\gamma_1(0) = p = \gamma_2(0)$. Define an equivalence relation of curves by*

$$\gamma_1 \sim \gamma_2 \;:\Leftrightarrow\; \frac{\mathrm{d}}{\mathrm{d}t}_{|t=0}\big(f \circ \gamma_1\big)(0) = \frac{\mathrm{d}}{\mathrm{d}t}_{|t=0}\big(f \circ \gamma_2\big)(0) \qquad \forall f \in C^\infty(M, \mathbb{R}). \tag{2.3}$$

An equivalence class $[\gamma]$ for p is called a tangent vector at p*, and the collection of equivalence classes T_pM is called* tangent space at p*. It has a vector space structure, and its elements $\dot\gamma \in T_pM$ act as derivations on functions $f \in C^\infty(M, \mathbb{R})$ by*

$$\dot\gamma(f)(p) := \frac{\mathrm{d}}{\mathrm{d}t}_{|t=0}(f \circ \gamma)(0). \tag{2.4}$$

The collection of tangent spaces $TM := \bigsqcup_{p \in M} T_pM$ forms a smooth fiber bundle over the base space M with standard fiber T_pM, and a smooth canonical projection $\pi\colon TM \to M$ mapping $\dot\gamma \in T_pM \mapsto p$.

The linearization of maps between manifolds is called *differential*. In the literature, it is often denoted as the *pushforward* of a map, as it permits to transfer tangential vectors from one manifold to another. It also contains information about the well-behavedness of maps between manifolds. The following definition is found in [111, Ch. 3, Prop. 3.6].

Definition 7 (Differential of Manifold Maps)**.** *Consider two smooth manifolds M and N, perhaps with smooth boundaries. Let $F\colon M \to N$ be a smooth map.*

Then its differential *in $p \in M$ is the map*

$$\mathrm{d}F_p\colon T_pM \to T_{F(p)}N \tag{2.5}$$

defined by its action on tangential directions $\dot{\gamma} \in T_pM$ and functions $f \in C^\infty(N, \mathbb{R})$ via

$$\mathrm{d}F_p\big(\dot{\gamma}\big)(f) = \dot{\gamma}\big(f \circ F\big)(p). \tag{2.6}$$

It is linear and satisfies the chain rule.

With this collection of differential geometric concepts, we slightly shift our focus, and collect some results from functional analysis, which are used in our study of shape optimization constrained by variational inequalities. The next definitions are found in [148, Ch. 3.1.1, App. A, Lem. 10.4] and [50, Ch. 6.2.1].

Definition 8 (Monotone and Coercive Operators)**.** *Let B be a real, reflexive Banach space, and denote by $\langle \cdot, \cdot \rangle_B$ its duality product. Consider an operator $A\colon B \to B^*$, possibly nonlinear. We say A is* monotone*, if*

$$\langle Ax - Ay, x - y \rangle_B \geq 0 \qquad \forall x, y \in B. \tag{2.7}$$

The operator A is strictly monotone*, if inequality (2.7) is a strict inequality for all $x \neq y$. We say A is* coercive*, if*

$$\lim_{\|x\|_B \to \infty} \frac{\langle Ax, x \rangle_B}{\|x\|_B} = \infty \qquad \forall x \in B. \tag{2.8}$$

For a real Hilbert space H, a bilinear form $a\colon H \times H \to \mathbb{R}$ is called coercive*, or* elliptic*, if there exists a constant $K > 0$, such that*

$$a(x, x) \geq K \cdot \|x\|_H^2 \qquad \forall x \in H. \tag{2.9}$$

With these properties of operators on function spaces, we can give two existence theorems. The first result is the lemma of Lax-Milgram, which is of interest for linear elliptic equations, and is found in [148, App. A, Lem. 10.4] and [50, Ch. 6.2, Thm. 1].

Theorem 1 (Lemma of Lax-Milgram)**.** *Let H be a real Hilbert space with a coercive, bounded, possibly non-symmetric, bilinear form $[\cdot, \cdot]\colon H \times H \to \mathbb{R}$. Then for every bounded functional $f \in H^*$, there exists a unique $u \in H$, such that*

$$[u, v] = f(v) \qquad \forall v \in H. \tag{2.10}$$

The second existence result is the Browder-Minty theorem. It considers semilinear equations, where the nonlinearity stems from a monotone operator. We state a specialized case, the general case for so-called hemicontinuous operators is found in [148, Ch. 3.1.1, Thm. 1.5].

Theorem 2 (Browder-Minty Theorem)**.** *Let X be a separable, reflexive and real Banach space with its dual space X^*. Consider a coercive, monotone and continuous operator $A\colon X \to X^*$. Then for all $b \in X^*$, the solution set to*

$$Ax = b \tag{2.11}$$

is nonempty, closed, bounded and convex. Further, if A is strictly monotone, then the solution $x \in X$ is unique.

These existence results will serve us in our study on variational inequalities. For a class of so-called pre-shape parameterization tracking problems, we rely on different, perhaps lesser known existence results of so-called pull-back equations. An extensive treatise on pull-back equations is given in [38]. The origin of the following collection of theorems is found in [134] due to Moser from 1965. It affirmatively answers the question, whether there exist diffeomorphisms, such that a prescribed volume form on a manifold can be constructed via pull-back of another given volume form. We rely on several different versions of this theorem, and begin by stating its nonlinear PDE version from [38, Thm. 10.1].

Theorem 3 (Dacorogna-Moser Theorem I)**.** *Let $\Omega \subset \mathbb{R}^{n+1}$ be a bounded, connected and open domain. For $k \geq 0$ and $\alpha \in (0,1)$, let $\partial\Omega$ have $C^{k+2,\alpha}$-Hölder regularity. Let $f\colon \overline{\Omega} \to (0,\infty)$, $g\colon \overline{\Omega} \to (0,\infty)$ be $C^{k,\alpha}(\overline{\Omega})$-regular functions.*

Then there exists a diffeomorphism $\rho\colon \overline{\Omega} \to \overline{\Omega}$ with $C^{k+1,\alpha}(\overline{\Omega})$-regularity, such that

$$\begin{aligned} g\big(\rho(x)\big) \cdot \det D\rho(x) &= \lambda \cdot f(x) \qquad && \forall x \in \Omega \\ \rho(x) &= x && \forall x \in \partial\Omega, \end{aligned} \tag{2.12}$$

where $\lambda = \int_\Omega g / \int_\Omega f$.

Notice that due to occurrence of the Jacobi determinant, equation (2.12) is a nonlinear partial differential equation. Also, the Dacorogna-Moser theorem does not provide uniqueness of solutions. In fact, non-trivial cases of equation (2.12) always possess multiple solutions.

The next version is due to Bruveris, Michor et al. [28], and generalizes Moser's theorem to manifolds with corners. This includes the important case of simplicial complexes, and thus holds for most meshes used in numerical computations. In the following, we say a point $x \in M$ is a corner of codimension $q > 0$, if x lies in the intersection of q distinct coordinate hyperplanes. We denote by $\partial^q M$ the set of all corners of codimension q. Notice that by this definition, the boundary ∂M of a manifold with corners is not necessarily a manifold with corners itself. A counterexample is $M = [0,1]^3$, which is problematic at the corners. The following result also holds for non-orientable manifolds, if volume forms are replaced by densities. Also, we abuse notation by using the same symbols for volume forms and their local coefficient functions. For an introduction to differential volume forms and integration on manifolds, we refer the reader to [111, Ch. 14-16].

Theorem 4 (Dacorogna-Moser Theorem for Manifolds with Corners)**.** *Let M be a compact, connected, smooth, oriented, n-dimensional manifold with corners. Let f and g be smooth and positive volume forms on M with $\int_M f = \int_M g$.*

Then there exists a diffeomorphism $\rho\colon M \to M$, such that its pull-back satisfies $\rho^*(g) = f$. Locally, this means

$$g\big((\rho(x)\big) \cdot \det D\rho(x) \cdot \mathrm{d}x_1 \wedge \cdots \wedge \mathrm{d}x_n = f(x) \cdot \mathrm{d}x_1 \wedge \cdots \wedge \mathrm{d}x_n. \tag{2.13}$$

Moreover, ρ can be chosen as the identity on ∂M if and only if $f = g$ on $\partial^q M$ for all $q \geq 2$.

The demanded equality $f = g$ on $\partial^q M$ for all $q \geq 2$ is natural, since corners are invariant under diffeomorphisms (cf. [111, Prop. 16.20]). We provide another version of the Dacorogna-Moser theorem, which holds on more general domains. This version gives explicit knowledge of where the solution ρ acts as the identity. However, to achieve this, it sacrifices additional regularity gain of solutions ρ found in theorem 3. The following version is a special case of [39, Thm. 7]. It is important, that it also holds for domains with lower dimensional boundaries, where isolated points can be added or removed, and even cusps are permitted ([39, Appendix and Remarks on Condition (H_k)]). In the following, $\mathrm{Diff}^k(\Omega)$ denotes the set of C^k-diffeomorphisms of Ω, with the special case of homeomorphisms for $k = 0$ (cf. definition 2, definition 3).

Theorem 5 (Dacorogna-Moser Theorem II)**.** *Let $\Omega \subset \mathbb{R}^{n+1}$ be a connected, bounded and open Lipschitz domain. For $k \geq 0$, consider $f, g \in C^k(\Omega, (0,\infty))$, such that $f + \frac{1}{f}$, $g + \frac{1}{g}$ are bounded. Further assume*

$$\int_\Omega f \,\mathrm{d}x = \int_\Omega g \,\mathrm{d}x. \tag{2.14}$$

Then there exists a $\rho \in \mathrm{Diff}^k(\Omega) \cap \mathrm{Diff}^0(\overline{\Omega})$*, such that for every open subset* $E \subset \Omega$ *the equality*

$$\int_{\rho(E)} g \, \mathrm{d}x = \int_E f \, \mathrm{d}x \tag{2.15}$$

holds, with $\rho(x) = x$ *for all* $x \in \partial\Omega$*. Moreover, if* $\mathrm{supp}(f - g) \subset \Omega$*, then* $\mathrm{supp}(\rho - \mathrm{id}_{\overline{\Omega}}) \subset \Omega$*.*

Notice that the functions f and g only need to have C^k-regularity on the open set Ω, and not on its closure $\overline{\Omega}$. Also, the general case of continuous f and g is permitted. The solution $\rho \in \mathrm{Diff}^k(\Omega) \cap \mathrm{Diff}^0(\overline{\Omega})$ is differentiable on the interior, but extends only continuously to a homeomorphism on the boundary $\partial\Omega$. We remind the reader, that equation (2.15) holds for all open subsets $E \subset \Omega$, and is a weaker version of equation (2.12). This weak formulation is necessary, since f and g are not necessarily differentiable, which is mandatory to formulate the strong problem in equation (2.12). However, if f and g have at least C^1-regularity in Ω, then equation (2.15) for all open subsets $E \subset \Omega$ is equivalent to equation (2.12) with $\rho \in \mathrm{Diff}^k(\Omega) \cap \mathrm{Diff}^0(\overline{\Omega})$ and $\lambda = 1$. This can be seen by application of the transformation formula to equation (2.15), which gives

$$\int_E g\big(\rho(x)\big) \cdot \det D\rho(x) \, \mathrm{d}x = \int_E f \, \mathrm{d}x \tag{2.16}$$

for all open subsets $E \subset \Omega$.

We leave the area of existence results for equations, and give the so-called Jacobi formula for determinants of derivatives (cf. [175, p. 7, p. 29]). It is a practical tool in matrix analysis, but we also apply it for calculation of a pre-shape derivatives in section 5.3.

Proposition 1 (Jacobi's Formula for Determinants of Derivatives)**.** *Let* $A(t) \in \mathbb{R}^{n\times n}$ *be a differentiable curve of* $n \times n$*-matrices. Then*

$$\frac{\mathrm{d}}{\mathrm{d}t} \det\big(A(t)\big) = \mathrm{tr}\left(\mathrm{Adju}\big(A(t)\big) \frac{\mathrm{d}}{\mathrm{d}t} A(t)\right), \tag{2.17}$$

where $\mathrm{Adju}\big(A(t)\big)$ *is the adjugate matrix of* $A(t)$*, and* $\mathrm{tr}(\cdot)$ *is the trace operator for matrices.*

Lastly, we cover the celebrated Jordan-Brouwer theorem, which describes the topology of Euclidean spaces separated by manifolds (cf. [70, p. 89]). We emphasize the crucial property of M to have no boundary.

Theorem 6 (Jordan-Brouwer Theorem)**.** *Let* $M \subset \mathbb{R}^{n+1}$ *be a compact, connected* n*-dimensional manifold without boundary.*

Then its complement in $\mathbb{R}^{n+1}$ *consists of two connected open sets* $\mathbb{D}^{in}$ *and* $\mathbb{D}^{out}$*. Moreover,* $\overline{\mathbb{D}^{in}}$ *is a compact manifold with boundary* $\partial\overline{\mathbb{D}^{in}} = M$*.*

We finished our collective endeavor on general results from various areas, and start with the introduction of shape optimization.

Chapter 3

Introduction to Shape Optimization and Shape Calculus

Shape optimization is the discipline of mathematical optimization concerned with the control of geometric quantities under given conditions. This should not be confused with topological optimization, which deals with the control of topological properties, such as the number and placement of holes in a given geometrical object (cf. [167, 16] and the references therein). Topological optimization is not the focus of this work. Instead, we use an approach, which fixes a prototype manifold M, such that shapes which arise in optimization are from the same homeomorphism class. This means that all shapes from a (pre-)shape space share the same topological properties as M. In particular, number of holes and connectedness are fixed a priori.

3.1 Shape Calculus

In this section, we accumulate some basics on shape optimization and its calculus. We also highlight, how some recent developments in shape optimization are incorporated in modern industrial applications. These results were provided by the author during his involvement in the BMBF project GivEn, in cooperation with Siemens Power and Gas/Corporate Technology, the German Aero Space Center (DLR) and the University of Wuppertal. The results are partly published in [7, Ch. 2.1], and presented in this work for other GivEn members to reference.

Before we can pursue shape optimization, it is necessary to specify, what we mean by a 'shape'. There are several theories, which precisely formulate the notion of shapes. For the introduction of general shape calculus, we use the framework of [42] by Delfour and Zolésio. From this perspective, shapes are simply seen as subsets of a specified ambient space. The corresponding definition of shape functionals, which serve as objectives in shape optimization problems, is found in [42, Ch. 4.3, Def. 4.1]. We use a specialized version, which looks at shape functionals as maps into $\mathbb{R}$, instead of considering general topological vector spaces as image spaces.

Definition 9 (Shape Functionals via Sets)**.** *Consider a nonempty hold-all domain* $\mathbb{D} \subset \mathbb{R}^{n+1}$*, and its power set* $\mathcal{P}(\mathbb{D}) := \{ \Gamma : \Gamma \subset \mathbb{D} \}$.

Then, for an admissible set of shapes $\mathcal{A} \subset \mathcal{P}(\mathbb{D})$*, the function*

$$\mathcal{J} : \mathcal{A} \to \mathbb{R} \tag{3.1}$$

is called set-theoretic shape functional over the admissible set $\mathcal{A}$.

Due to its generality, such a formalization of shape functionals has to rely on techniques with general applicability, such as those from geometric measure theory. Even in this case, the set of admissible shapes has to be restricted. Otherwise, highly pathological shapes, such as sets with non-integer Hausdorff dimension, or even non-Lebesgue measurable sets are permitted. Therefore, we specialize this framework in chapter 4 by choosing specific sets of admissible shapes $\mathcal{A}$. This specialization allows us to use techniques from differential geometry, which we then use to extend shape calculus to pre-shape calculus.

In the general setting of definition 9, a prototypical shape optimization problem is of the form

$$\min_{\Gamma \in \mathcal{A}} \mathcal{J}(\Gamma). \tag{3.2}$$

There are multiple ways to tackle these problems. A large number of shape optimization algorithms utilize derivatives to achieve this. However, since shapes $\Gamma \in \mathcal{A} \subset \mathcal{P}(\mathbb{D})$ are in general just sets, their collection does not possess a vector space structure. There is no canonical addition or scalar multiplication available, which in particular prohibits direct formulation of difference quotients. Hence, the common definitions for Gâteaux or Fréchet derivatives from functional analysis are not applicable. A possible way to circumvent this issue is the introduction of domain perturbations and so-called shape derivatives. Throughout this work, we adopt this perspective, and frame our algorithms in light of domain-derivative based methods. Methods to construct domain perturbations include the perturbation of identity approach, and velocity methods, both found in [42, Ch. 4.3.2]. With shape functionals at hand, we can define shape derivatives via the perturbation of identity as in [42, Ch. 4.3.2] and [161, Ch. 2.1].

Definition 10 (Shape Derivatives)**.** *Let $\mathcal{J}$ be a shape functional with admissible set $\mathcal{A} \subset \mathcal{P}(\mathbb{R}^{n+1})$. Consider a set $\Gamma_0 \in \mathcal{A}$ and a direction $V \in C^k(\mathbb{R}^{n+1}, \mathbb{R}^{n+1})$. The* perturbation of identity *of Γ_0 in direction V is defined as*

$$\Gamma_t := \left\{ x + t \cdot V(x) : \ x \in \Gamma_0 \right\} \tag{3.3}$$

for $t \in [0, \tau]$ and some $\tau > 0$. If the limit

$$\mathcal{D}\mathcal{J}(\Gamma_0)[V] := \lim_{t \to 0} \frac{\mathcal{J}(\Gamma_t) - \mathcal{J}(\Gamma_0)}{t}. \tag{3.4}$$

exists, and is linear and bounded as a function of V, then we call it shape derivative *for $\mathcal{J}$ at Γ_0 in direction V.*

A structural description of shape derivatives is given by the Hadamard-Zolésio theorem. Its key insight is, that only perturbations of the shape in its normal directions influence the value of the shape derivative. According to [42, Ch. 9, Rem. 3.2], in the year 1907, Hadamard used displacements along the normal to the boundary of a C^∞-domain to compute the derivative of the first eigenvalue of a clamped plate. The structure theorem for shape functionals on open domains with a C^{k+1}-boundary is due to Zolésio [186] in 1979. Its version in [42, Ch. 9.3.4, Thm. 3.6] deals with shape derivatives of general open or closed sets $\Omega \subset \mathbb{R}^{n+1}$, which is a significantly larger class of shapes compared to smooth ones. In the following, we state the case for shapes $\Gamma \in \mathcal{A}$, which are compact, sufficiently smooth, and which can be interpreted as boundaries of open domains. This suffices, since we assume similar regularity in later chapters of our studies. The following theorem is found in [42, Ch. 9.3.4, Cor. 1].

Theorem 7 (Hadamard-Zolésio Structure Theorem)**.** *Let $\Omega \subset \mathbb{R}^{n+1}$ be an open set, such that its boundary Γ is compact and has C^{k+1}-regularity. Denote by $n \in C^k(\Gamma, \mathbb{R}^{n+1})$ its unique outer unit normal vector field. Consider a shape differentiable shape functional $\mathcal{J}$.*

Then there exists a scalar valued distribution $g^{\mathcal{N}} \in C^k(\Gamma, \mathbb{R})^*$, such that

$$\mathcal{DJ}(\Gamma)[V] = \left\langle g^{\mathcal{N}}, \left\langle n, \mathrm{Tr}_\Gamma(V) \right\rangle_2 \right\rangle_{C^k(\Gamma,\mathbb{R})^*} \qquad \forall V \in C^k(\mathbb{R}^{n+1}, \mathbb{R}^{n+1}), \tag{3.5}$$

where $\mathrm{Tr}_\Gamma \colon C^k(\mathbb{R}^{n+1}, \mathbb{R}^{n+1}) \to C^k(\Gamma, \mathbb{R}^{n+1})$ is a trace operator. Further, if $g^{\mathcal{N}}$ is representable as a function in $L^1(\Gamma, \mathbb{R})$, then $\mathcal{DJ}$ has the boundary formulation

$$\mathcal{DJ}(\Gamma)[V] = \int_\Gamma g^{\mathcal{N}} \cdot \left\langle n, \mathrm{Tr}_\Gamma(V) \right\rangle_2 \mathrm{d}s \qquad \forall V \in C^k(\mathbb{R}^{n+1}, \mathbb{R}^{n+1}). \tag{3.6}$$

We emphasize, that the Hadamard-Zolésio theorem is a result concerning the support of shape derivatives. Since the shape derivative is a general linear and continuous functional acting on directions $V \in C^k(\mathbb{R}^{n+1}, \mathbb{R}^{n+1})$, it is in general only representable as a distribution $g^{\mathcal{N}}$. Only in special cases, which consist of many applications in practice, the distribution $g^{\mathcal{N}}$ can be represented as a classical function in style of a Riesz representative. If this is the case, the duality product from equation (3.5) can be written as a boundary integral with participating normal components of V as seen in equation (3.6). In such a scenario, the function representative of $g^{\mathcal{N}}$ is often called the shape gradient of $\mathcal{DJ}$ (cf. [159]). Hence, under the mentioned conditions, the representation of shape derivatives $\mathcal{DJ}$ by use of boundary integrals as in equation (3.6) is termed *boundary formulation*. In contrast to this, it is often easier to derive a so-called *volume representation*, where the shape derivative $\mathcal{DJ}$ is represented as a volume integral on the hold-all domain, or codimension zero subsets thereof.

There are multiple approaches to guarantee shape differentiability of shape functionals $\mathcal{J}$. Among them, there is the material derivative approach (cf. [17]). We develop a related, more general calculus for so-called pre-shapes in chapter 4. To avoid redundancy, we postpone the introduction of shape calculus rules featuring material derivatives to chapter 4, where they occur as a special case. Another method to guarantee existence of shape derivatives is the *averaged adjoint approach* found in [172, Ch. 7, Thm. 7.1], which is an extension of the Corea-Seeger theorem from [37]. Since we apply the averaged adjoint theorem in chapter 8, we state it in a version suiting our situation in the following.

For PDE-constrained shape optimization problems, a common technique to derive optimality conditions or shape derivatives is by use of the *Lagrangian* (cf. [160]). Let us consider a constrained shape optimization problem with objective $\mathcal{J} \colon E \times \mathcal{A} \to \mathbb{R}$, i.e.

$$\begin{aligned} &\min_{\Gamma \in \mathcal{A}} \ \mathcal{J}(y, \Gamma) \\ &\quad \text{s.t. } e(\Gamma, y) = 0, \end{aligned} \tag{3.7}$$

where E is a Banach space and $e \colon \mathcal{A} \times E \to \mathbb{R}$ is an equality constraint. The associated Lagrangian function is given by

$$\mathcal{L} \colon \mathcal{A} \times E \times F \to \mathbb{R}, \ \ (\Gamma, y, p) \mapsto \mathcal{J}(y, \Gamma) + \left\langle p, e(\Gamma, y) \right\rangle_F, \tag{3.8}$$

where F is the dual space to E, and $\langle \cdot, \cdot \rangle_F$ its duality pairing. Differentiation with respect to y gives the so-called *adjoint equation*, whereas differentiation with respect to shape Γ results in an expression for the shape derivative.

The averaged adjoint theorem from [172, Ch. 7, Thm. 7.1] is stated with respect to a retracted version of the Lagrangian in equation (3.8). For a direction V with sufficient regularity, transformations

$$T_t \colon \mathbb{D} \to \mathbb{D}, \;\; x \mapsto x + t \cdot V(x) \tag{3.9}$$

are bijective mappings of the hold-all domain $\mathbb{D} \subset \mathbb{R}^{n+1}$ for sufficiently small $\tau \geq t \geq 0$. Then for a $\Gamma \in \mathcal{A}$, the *shape Lagrangian* is given for some $\tau > 0$ as

$$G \colon [0,\tau] \times E \times F \to \mathbb{R}, \;\; (t,y,p) \mapsto G(t,y,p) := \mathcal{L}\big(\Gamma_t, y \circ T_t^{-1}, p \circ T_t^{-1}\big), \tag{3.10}$$

where Γ_t is a perturbed shape, and T_t^{-1} the corresponding retraction to the reference domain $\mathbb{D}$. The shape Lagrangian serves as a tool to guarantee existence of shape derivatives by the following theorem (cf. [172, Ch. 7, Thm. 7.1]). An exemplary application can be found in [109, Ch. 4].

Theorem 8 (Averaged Adjoint Theorem)**.** *Consider a constrained shape optimization problem* (3.7)*. Fix a shape $\Gamma \in \mathcal{A} \subset \mathcal{P}(\mathbb{D})$ in the hold-all domain $\mathbb{D} \subset \mathbb{R}^{n+1}$. Let $G \colon [0,\tau] \times E \times F \to \mathbb{R}$ be the corresponding shape Lagrangian. Denote by*

$$X(t) := \left\{ y \in E : \; \frac{\partial}{\partial p} G(t,y,0;\tilde{p}) = 0 \quad \forall \tilde{p} \in F \right\} \tag{3.11}$$

the set of retracted state solutions for perturbed domains and shapes at time $t \in [0,\tau]$. For $y^t \in X(t)$ and $y^0 \in X(0)$, introduce the set of averaged adjoints

$$Y(t,y^t,y^0) := \left\{ q \in F : \; \int_0^1 \frac{\partial}{\partial y} G\big(t, sy^t + (1-s)y^0, q; \tilde{y}\big) \, \mathrm{d}s = 0 \quad \forall \tilde{y} \in E \right\}. \tag{3.12}$$

Let the following assumptions hold

(H0) $X(t)$ is single valued for all $t \in [0,\tau]$, and the map

$$s \mapsto G\big(t, sy^t + (1-s)y^0, p\big) \tag{3.13}$$

is absolutely continuous and

$$s \mapsto \frac{\partial}{\partial y} G\big(t, sy^t + (1-s)y^0, p; \tilde{y}\big) \tag{3.14}$$

is well-defined and belongs to $L^1(0,1)$

(H1) for all $t \in [0,\tau]$ and all $(y,p) \in E \times F$, the derivative $\frac{\partial}{\partial t} G(t,y,p)$ exists

(H2) for all $t \in [0,\tau]$, the set $Y(t,y^t,y^0)$ is nonempty and $Y(t,y^0,y^0)$ is single-valued

(H3) for $p^0 \in F$ and any sequence $\{t_n\}_{n\in\mathbb{N}}$ of non-negative natural numbers converging to zero, there is a subsequence $\{t_{n_k}\}_{k\in\mathbb{N}}$ and $p^{t_{n_k}} \in Y(t_{n_k}, y^{t_{n_k}}, y^0)$, such that

$$\lim_{\substack{k\to\infty \\ t\searrow 0}} \frac{\partial}{\partial t} G\big(t, y^0, p^{t_{n_k}}\big) = \frac{\partial}{\partial t} G\big(0, y^0, p^0\big). \tag{3.15}$$

Then $\mathcal{J}$ is shape differentiable with shape derivative given by

$$\mathcal{D}\mathcal{J}\big(y^0,\Gamma\big)[V] = \frac{\mathrm{d}}{\mathrm{d}t}_{|t=0} G\big(t, y^t, p\big) = \frac{\partial}{\partial t} G\big(0, y^0, p^0\big), \tag{3.16}$$

for all $p \in F$ and the solution to the adjoint equation $p^0 \in Y(0,y^0,y^0)$.

In chapter 8, we also make use of identity

$$D\big(f \circ T_t\big)W = Df\big(T_t\big)DT_tW = \nabla f\big(T_t\big)^T DT_tW = \Big(DT_t^T \nabla f\big(T_t\big)\Big)^T W, \quad (3.17)$$

for functions $f\colon \mathbb{D} \to \mathbb{R}$ used in [172]. It implies

$$(\nabla f) \circ T_t = DT_t^{-T} \nabla\big(f \circ T_t\big). \quad (3.18)$$

Let us assume we have a shape derivative in closed form, or one derived by automatic differentiation. The question arises, how to apply it in order to solve a shape optimization problems as in equation (3.2) or equation (3.7). A straightforward, and perhaps naive approach would be to use the degrees of freedom of a finite element representation of $\mathcal{DJ}$, or $g^{\mathcal{N}}$, as directions for a deformation. However, we have seen in theorem 7, that the shape derivative $\mathcal{DJ}$ or its boundary representation via $g^{\mathcal{N}}$ can have distributional character. This means shape derivatives are numerically not suitable for direct application as descent directions, as roughness of the deformation could lead to destruction of the mesh. An example for such roughness of an L^2-representation of shape derivatives in an industrial application is seen in figure 3.1 (b) and (d) of the next section.

A possible remedy for this situation is the introduction of so-called *Steklov-Poincaré type metrics* as pioneered in [161]. One key idea is to use a bilinear form $\mathfrak{a}(\cdot,\cdot)$ in order to represent the shape derivative $\mathcal{DJ}$ as a gradient vector field on the hold-all domain, while gaining additional regularity of the gradient, such as higher smoothness. In light of theorem 7, the authors of [161] define a metric on the space of normal vector fields on a shape Γ in the Sobolev setting, which is motivated by a Neumann-to-Dirichlet map. This comes from the observation, that the distributional representation $g^{\mathcal{N}}$ of a shape derivative $\mathcal{DJ}(\Gamma)$ with support solely on normal vector fields can serve as a Neumann boundary condition on Γ. Let us assume bounded shapes Γ with C^1-regularity, and $g^{\mathcal{N}} \in H^{-\frac{1}{2}}(\Gamma, \mathbb{R})$. Consider a symmetric and coercive bilinear form

$$\mathfrak{a}(\cdot,\cdot)\colon H^1\big(\mathbb{R}^{n+1}, \mathbb{R}^{n+1}\big) \times H^1\big(\mathbb{R}^{n+1}, \mathbb{R}^{n+1}\big) \to \mathbb{R}, \quad (3.19)$$

the outer unit normal vector field n on Γ, and the Sobolev trace operator (cf. [50, Ch. 5.5])

$$\mathrm{Tr}_{|\Gamma}\colon H^1\big(\mathbb{R}^{n+1}, \mathbb{R}^{n+1}\big) \to H^{\frac{1}{2}}\big(\Gamma, \mathbb{R}^{n+1}\big). \quad (3.20)$$

Then the solution vector field $U \in H^1(\mathbb{R}^{n+1}, \mathbb{R}^{n+1})$ of the variational problem

$$\mathfrak{a}(U,V) = g^{\mathcal{N}}\Big(\big\langle n, \mathrm{Tr}_{|\Gamma}(V)\big\rangle_2\Big) \qquad \forall V \in H_0^1\big(\mathbb{R}^{n+1}, \mathbb{R}^{n+1}\big) \quad (3.21)$$

is called *shape gradient representation* of $\mathcal{DJ}(\Gamma)$ by $\mathfrak{a}(\cdot,\cdot)$. The projected Neumann-to-Dirichlet map from [161, Ch. 3.2] with respect to $\mathfrak{a}(\cdot,\cdot)$ is then given by

$$S^p\colon H^{-\frac{1}{2}}(\Gamma, \mathbb{R}) \to H^{\frac{1}{2}}(\Gamma, \mathbb{R}), \;\; g^{\mathcal{N}} \mapsto \big\langle n, \mathrm{Tr}_{|\Gamma}(U)\big\rangle_2, \quad (3.22)$$

where U is the solution of equation (3.21). The projected Neumann-to-Dirichlet map can be used to define Steklov-Poincaré metrics on the tangent bundle of certain spaces of shapes. However, we do not go into details, as the techniques of this work do not rely on the choice of specific Riemannian metrics on shape or pre-shape spaces. We postpone the introduction of shape spaces and their respective tangent bundles to chapter 4. This allows to have a clearer derivation without redundancies, since they are naturally connected to the construction of pre-shape spaces and their tangent bundles.

A key property of the shape gradient representation via bilinear forms $\mathfrak{a}(\cdot,\cdot)$ is the additional gain of regularity. Under the mentioned assumptions, it amounts to

represent the distribution $g^{\mathcal{N}} \in H^{-\frac{1}{2}}(\Gamma, \mathbb{R})$ of $\mathcal{DJ}$ as a vector field $U \in H^1(\mathbb{R}^{n+1}, \mathbb{R})$ via the primal space. Thus the shape gradient representation U is more suitable for mesh morphing based descent algorithms than the shape derivative $\mathcal{DJ}(\Gamma)$. The choice of Steklov-Poincaré metrics is flexible, in the sense, that metrics do not need to have an immediate connection to the state equations of PDE-constrained shape optimization problems at hand (cf. [135, 145]). Further, such a procedure can be used, even when there is no available boundary formulation of $\mathcal{DJ}$ as in equation (3.6). Assuming enough regularity, we can see this with the Hadamard-Zolésio theorem 7 via

$$\mathfrak{a}(U,V) = g^{\mathcal{N}}\Big(\big\langle n, \mathrm{Tr}_{|\Gamma}(V)\big\rangle_2\Big) = \mathcal{DJ}(\Gamma)[V] \qquad \forall V \in H_0^1\big(\mathbb{R}^{n+1}, \mathbb{R}^{n+1}\big). \tag{3.23}$$

Compared to boundary formulations, the volume formulation is also advantageous in the context of finite element representations. This was studied for an elliptic problem by Hiptmair et al. in [85]. Using piecewise linear Lagrangian finite element approximations to state and adjoint variables, they find that the approximation error of the shape derivative by a discrete volume formulation scales $\mathcal{O}(h^2)$ in mesh width h, whereas the error scales only $\mathcal{O}(h)$ for boundary formulations.

3.2 Industrial Application of Steklov-Poincaré Metrics

During his participation in the BMBF project GivEn (Shape Optimization for Gas Turbines in Volatile Energy Networks, FKZ: 05M18UTA), the author of this work developed the software package TRASOR (TRACE Shape Optimization Routine) for non-parametric shape optimization of turbo-machinery using Steklov-Poincaré metrics. This was done in cooperation with the University of Wuppertal, the German Aerospace Center (DLR), and Siemens Power and Gas/ Corporate Technology. BMBF project GivEn pursues research on the multi-objective and multi-physics free-form optimization of turbo geometries. The following results are published in [7, Ch. 2.1].

TRASOR features are tested on a Q3D model of the low-pressure turbine cascade T106A designed by MTU Aero Engines (cf. [88]). The state equations consist of multiple systems of coupled equations. The exterior flow around the blade is governed by a compressible and Reynolds averaged Navier-Stokes equation (RANS) in a rotational frame of reference. The equations are Favre averaged and the result closed by means of turbulence models. On the turbine blade itself, thermal and mechanical stresses are present, which influence the longevity of the material. The mechanical part is described by a linear elasticity equation on the turbine blade, together with a Laplace equation for the thermic component. Also, a cooling channel is incorporated in the geometry, whose role is to increase life expectancy by mitigation of stresses induced by extensive heating of the blade (cf. [7, Ch. 2.2]). The heat flow is modeled as a one-dimensional flow with parametric models for friction and heat transfer, similar to the work in [127] and [174]. The thermo-mechanic equations are coupled to the exterior Navier-Stokes flow via Robin boundary conditions of the pressure and temperature (cf. [7, Ch. 2.3.2]). For a more detailed discussion of the modeling approach, see [7].

For the T106A and the described multi-physics model, the TRASOR tool allows the user to freely choose from a multitude of objective functionals for (multi-criterial) shape optimization. They include quantities of the Navier-Stokes flow, such as pressure ratios of in- and outlet, coefficients for entropy rise, discharge angle at the tip of the blade, and more. For an exhaustive list, we refer the reader to [62]. An important ambition of GivEn is the incorporation of the life expectancy of

the turbine blade. This feature is described by the so-called *low cycle fatigue* (LCF). Essentially, the LCF objective functional used in GivEn gives a quantification of life expectancy of the turbine blade under load. Damage mechanisms surrounding the low cycle fatigue, and their probabilistic relation to shape optimization can be found in [141, 52, 169] and [66, 18, 21, 20]. The LCF objective value is derived as an integral quantity of the local deterministic numbers of life cycles over the turbine blade, depending on displacements of the ceramic material coming from the linear elasticity equation (cf. [66, 67, 124, 65]).

The software package TRASOR is built on several solver bundles connected by an interface in Python 2.7 and 3.5. One major package is TRACE 9.2, provided by the German Aerospace Center (DLR). It permits simulation of interior flows in turbomachinery. Assuming stationarity of the Navier-Stokes equations, which are spatially discretized using the finite volume method, a steady state solution method is obtained in TRACE by pseudo-time marching. The TRASOR software provides shape gradient representations using Steklov-Poincaré metrics based on shape sensitivities derived by the DLR software package adjointTRACE. The package adjointTRACE itself uses automatic differentiation of Lagrangians associated to the respective objectives chosen by the user (cf. [149, 8, 15]). Associated discrete adjoints require a solution of linearized problems backward in time.

TRASOR interfaces with FEniCS 2017.2.0 [4, 117], which is a Python based finite element software for solution of differential equations based on weak formulations. It utilizes the Unified Form Language (UFL, [3]), Automated Finite Element Computing (DOLFIN, [118, 119]) and the Portable, Extensible Toolkit for Scientific Computation (PETSc, [9]) as a linear algebra backend. Various solver options, including CG, GMRES, PETCs's built in LU solver and preconditioning using incomplete LU and Cholesky, SOR or algebraic multigrid methods are available in FEniCS, and thus applicable in TRASOR. FEniCS/PETSc also offer the possibility to parallelize finite element solving, making the Steklov-Poincaré gradient calculation scalable in processor number. For the user specified objectives, the TRACE generated or Steklov-Poincaré represented gradients are then applicable for a steepest descent algorithm for optimization of the T106A via mesh morphing.

In order to calculate shape gradients represented by Steklov-Poincaré metrics via FEniCS, we created a mesh conversion pipeline from structured quadrilateral meshes in CGNS format prescribed by TRACE to unstructured meshes in HDF5 format feasible for FEniCS. As FEniCS 2017.2.0 used at this time was not fully capable of supporting hexahedral and quadrilateral elements , hexahedral and quadrilateral elements used in TRACE are partitioned to conforming tetrahedral and triangular elements respecting the structured TRACE mesh. The conversion process from TRACE to FEniCS mesh, including the data formats, is given by the following steps and tools (cf. [154, 119])

$$\begin{aligned} \text{TRACE.cgns} \overset{\text{POST}}{\longrightarrow} \text{TRACE.dat} \overset{\text{TRASOR}}{\longrightarrow} \text{FEniCS.msh} \ \ldots \\ \ldots \overset{\text{meshio}}{\longrightarrow} \text{FEniCS.xdmf/-.h5} \overset{\text{DOLFIN}}{\longrightarrow} \text{FEniCS mesh.} \end{aligned} \tag{3.24}$$

To represent the discrete TRACE generated mesh sensitivities $\mathcal{D}_{\mathrm{ad}}\mathcal{J}_{\mathrm{discr}}$ as a Steklov-Poincaré gradient, a sufficient metric $\mathfrak{a}(\cdot,\cdot)$ has to be chosen. In light of [161], the linear elasticity model in weak formulation is employed in TRASOR. Additional regularity for the resulting gradients is given by increasing smoothness

through solution of the system

$$\begin{aligned}\int_{\mathbb{D}_{\text{ext}}} \sigma\big(U\big) : \epsilon(V)\,\mathrm{d}x &= \mathcal{D}_{\text{ad}}\mathcal{J}_{\text{discr}}(\Gamma)[V] \qquad \forall\, V \in H_0^1\big(\mathbb{D}_{\text{ext}}, \mathbb{R}^{n+1}\big)\\ U &= 0 \qquad \text{on } \Gamma_{\text{Inlet/Outlet}}\\ \sigma(U) &= \lambda\,\mathrm{Tr}\big(\epsilon(U)\big)I + 2\mu\epsilon(U)\\ \epsilon(V) &= \frac{1}{2}\big(\nabla V + \nabla V^T\big),\end{aligned} \tag{3.25}$$

where $\lambda \in \mathbb{R}$, $\mu \in \mathbb{R}_+$ are the so called Lamé parameters. This is an explicit example of the abstract system seen in equation (3.23). If $\mathbb{D}$ is the entire duct including the shape of the turbine blade Γ, then $\mathbb{D}_{\text{ext}} = \mathbb{D} \setminus \Gamma$ is the external computational domain where the fluid dynamics takes place. The inlet and outlet of the cascade are given as $\Gamma_{\text{Inlet/Outlet}}$, and are forced to stay invariant. Continuous Galerkin type elements of order one are used for target and test spaces in the FEniCS subroutine conducting the shape gradient calculation. Algorithm 3.1 shows the prototypical version of the steepest descent implemented in TRASOR, including the Steklov-Poincaré gradient representation. For the objectives entropy rise and low-cycle-

```
1  Set flow parameters in TRACE.cgns, optimization parameters and targets in
     TRASOR.py
2  Build TRASOR file architecture
3  Assemble and load FEniCS data from TRACE.cgns
4  while ‖U_k‖ > ε_shape do:
5      Flow simulation and (AD) checkpoint creation using TRACE
6      Calculate mesh sensitivities by automatic differentiation using
         adjointTRACE
7      Pass mesh sensitivities to FEniCS setup
8      Generate Steklov-Poincaré gradient in FEniCS:
9          Calculate Lamé-Parameters
10         Solve linear elasticity problem (3.25) for U_k
11     Extract target and flow values to update protocols and .pvd/.vtu files
12     Deform FEniCS mesh using FEniCS Steklov-Poincaré gradient and
         Arbitrary Lagrangian-Eulerian (ALE)
13     Create TRACE_deformation.dat files from FEniCS Steklov-Poincaré
         gradient
14     Deform TRACE mesh using PREP
```

Algorithm 3.1: TRASOR algorithm using Steklov-Poincaré metrics.

fatigue (LCF), an exemplary comparison between TRACE and Steklov-Poincaré gradients generated via TRASOR is shown in figure 3.1. For the LCF objective, several linear interpolation steps are used to transport data from the FEniCS and TRACE CFD meshes to the non-consistent thermo-mechanic mesh of the blade and its interior, and vice versa. The TRACE gradient is generated by solving a linear elasticity mesh smoothing system with Dirichlet boundaries being the lattice sensitivities $\mathcal{D}_{\text{ad}}\mathcal{J}(\Omega_{\text{ext}})$, whereas the Steklov-Poincaré gradient is calculated by solving a linear elasticity system in weak formulation (3.25) with Lamé parameters $\lambda = 0$ and constant $\mu > 0$. We clearly see the roughness of TRACE generated gradients in figure 3.1 (b) and (d), highlighting their distributional character. On the other hand, their linear elasticity representations in figure 3.1 (a), (c), (e) and (f) admit increased smoothness, both on the turbine blade and the volume mesh.

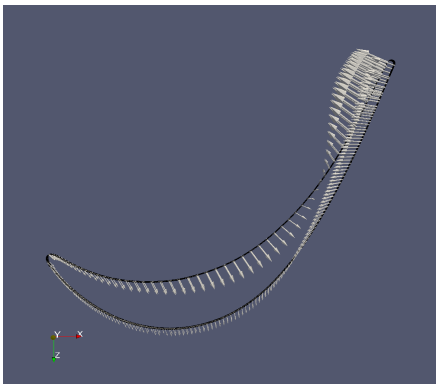

(a) Steklov-Poincaré gradient CoefEntropyRise

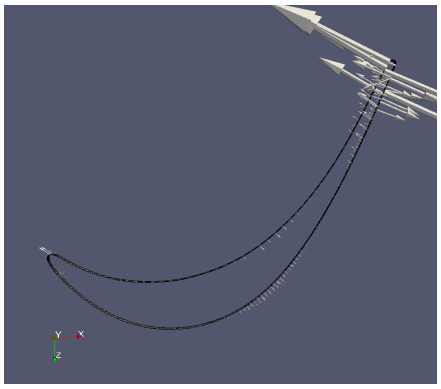

(b) TRACE sensitivity CoefEntropyRise

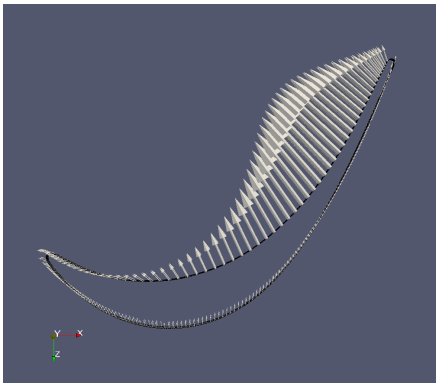

(c) Steklov-Poincaré gradient LCF

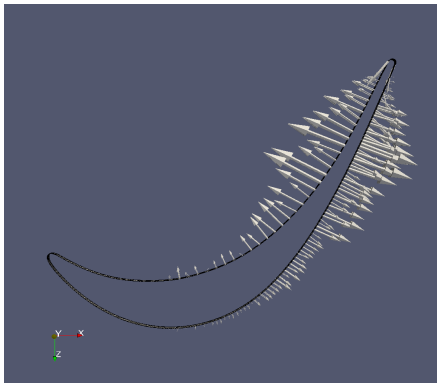

(d) TRACE sensitivity LCF

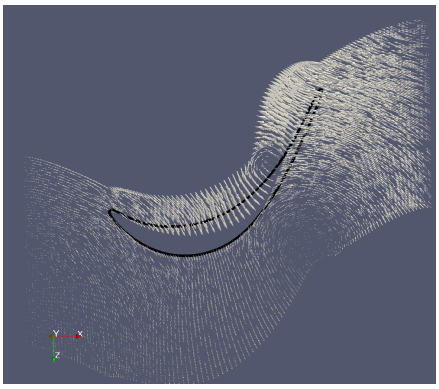

(e) Volume Steklov-Poincaré gradient CoefEntropyRise

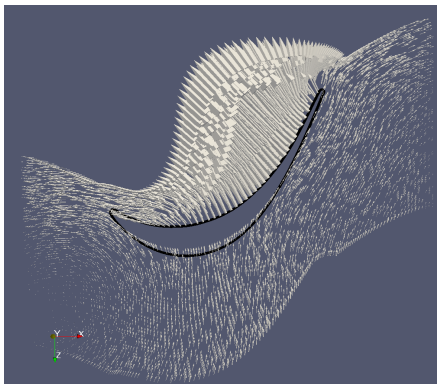

(f) Volume Steklov-Poincaré gradient LCF

Figure 3.1: Several gradients on the surface and volume mesh of the T106A with various representations and objective functionals. (a) Steklov-Poincaré gradient CoefEntropyRise scaled by $2 \cdot 10^9$. (b) TRACE sensitivity CoefEntropyRise scaled by $5 \cdot 10^6$. (c) Steklov-Poincaré gradient LCF scaled by $-1 \cdot 10^{13}$. (d) TRACE sensitivity LCF scaled by $-2.5 \cdot 10^{11}$. (e) Volume Steklov-Poincaré gradient CoefEntropyRise scaled by $2.5 \cdot 10^9$. (f) Volume Steklov-Poincaré gradient LCF scaled by $-1 \cdot 10^{13}$.

Chapter 4

General Theory of Pre-Shape Calculus

So far, we have regarded shape optimization as optimization over a specified collection of admissible sets $\mathcal{A} \subset \mathcal{P}(\mathbb{D})$. The generality of viewing shapes only as sets is restrictive. Working in this scenario requires use of techniques, which hold in respective generality, for example those of geometric measure theory. From an applicational point of view, PDE-constrained shape optimization is also not easily situated in this general shape framework. Existence and regularity theory become increasingly difficult for pathological shapes, if possible at all. Hence, in this chapter, we restrict the admissible set of shapes $\mathcal{A} \subset \mathcal{P}(\mathbb{D})$ to those, which satisfy enough regularity to form specific classes of shape spaces. We stay in this framework for the rest of this work.

The shape space approach permits applicability of various tools from infinite dimensional differential geometry. An attractive consequence of this approach is, that it naturally permits to regard shapes with their parameterizations at the same time. In this continuous framework, we associate the information contained in embeddings simultaneously to shapes and their parameterizations. After discretization, the continuous embedding serves as a descriptor for the mesh configuration representing the shape. Such a framework serves as the key to derive an extension of shape calculus, which captures variation in both shapes and their parameterizations. This *pre-shape calculus* is the basis to modify numerical routines in such a way, that they optimize mesh quality, without interfering with the shape optimization taking place. We pursue a first optimize, then discretize approach. For an excellent overview of shape spaces we refer to [12], from which we borrow several definitions and results for shape spaces in the following. A more recent introduction can be found in [130].

This chapter is split into two major parts. First, in section 4.1, we collect relevant material on shape and pre-shape spaces, their tangential bundles, and some notes on topology. Then, in section 4.2, we begin with our own contribution by introducing a calculus on pre-shape spaces. In particular, we define pre-shape derivatives, highlight their structure and relation to shape derivatives as introduced in background chapter 3, and collect respective calculus identities. This serves as a foundation for later chapters, where we put pre-shape calculus for mesh quality control into practice.

For the rest of this chapter, let $M \subset \mathbb{R}^{n+1}$ be an n-dimensional, oriented, connected and compact C^∞-submanifold, perhaps with smooth boundary, if not stated otherwise. In this chapter we work with the Euclidean ambient space $\mathbb{R}^{n+1}$. However, the results of this chapter are valid, when $\mathbb{R}^{n+1}$ is replaced by a bounded, connected and open domain $\mathbb{D} \subset \mathbb{R}^{n+1}$ with smooth boundary.

4.1 Shape and Pre-Shape Spaces

There are many types of shapes spaces with different geometric properties. Examples include the spaces B_i and $B_{i,f}$ of immersed and freely immersed shapes. These spaces form so called Riemannian orbifolds with and without singular points (cf. [34, 13], [12, Ch. 3.1]). We do not rely on these large spaces in this work, as self-intersecting shapes are included in B_i and $B_{i,f}$. Another shape space is $B^{1/2}$, consisting of continuous $H^{1/2}$-shapes of Sobolev regularity. Due to low regularity of the shapes, this space is not a manifold, but has a more general diffeological structure (cf. [182]). Moreover, there is the possibility to use finite dimensional parameterizations of shapes, such as B-spline representations found in [24]. This specializes shape optimization to the case of finite dimensional optimization in a parameter space. However, the price to be paid for such an approach is a limitation of achievable shapes. For this work, we choose to rely on the space B_e, which we introduce in this section (cf. [12, Ch. 3.1], [131, 130, 61]). This approach can be seen as a compromise between the set theoretic approach introduced in section 3.1, and the finite dimensional parametric approach. It permits enough structure to derive a feasible theory for parameterized shapes, while still staying in the context of free-form optimization, without severe restriction of permissible shapes.

Two main classes of objects in this work are embeddings and diffeomorphisms of manifolds. With these, we can formalize the notion of parameterized shapes. They are also instrumental in the construction of the shape space B_e. An introduction to these classes of mappings in a differential geometric context is found in [111, Ch. 4]

Definition 11 (Embeddings and Diffeomorphisms of Manifolds)**.** *Let M be a smooth manifold, perhaps with boundary. We say $\varphi\colon M \to \mathbb{R}^{n+1}$ is a C^∞-*embedding*, if φ is smooth and injective, has an injective differential for all $p \in M$, and is a homeomorphism onto its image. The collection of C^∞-embeddings is denoted by*

$$\operatorname{Emb}\left(M, \mathbb{R}^{n+1}\right) := \left\{ \varphi \in C^\infty\left(M, \mathbb{R}^{n+1}\right) : \varphi \text{ is a } C^\infty\text{-embedding} \right\}. \tag{4.1}$$

*Further, we say $\rho\colon M \to M$ is a C^∞-*diffeomorphism *of M, if ρ is bijective and smooth, and has a smooth inverse ρ^{-1}. The collection of C^∞-diffeomorphisms is denoted by*

$$\operatorname{Diff}(M) := \left\{ \rho \in C^\infty\left(M, M\right) : \rho \text{ is a } C^\infty\text{-diffeomorphism} \right\}. \tag{4.2}$$

Notice that for compact manifolds M, a smooth and injective $\varphi\colon M \to \mathbb{R}^{n+1}$ with injective differential for all $p \in M$ is necessarily a homeomorphism onto its image (cf. [111, Prop. 4.22 (c)]). Since we only study shapes represented as compact manifolds, the last demanded property is in fact automatically fulfilled, and thus redundant to the definition of embeddings. Also, if M has a non-trivial boundary ∂M, an embedding φ necessarily maps its boundary onto the boundary of the image, i.e. $\varphi(\partial M) = \partial(\varphi(M))$.

Topologies for $C^\infty(M, N)$ For the introduction of the manifold of shapes B_e, we have to stick with C^∞-regularity. However, notice that the pre-shape calculus we introduce is valid for the Hölder-regularity setting. We model shape and pre-shape spaces based on infinite dimensional spaces of smooth functions. Hence there are several different choices to equip them with topologies. Let us consider a smooth manifold N, which acts as the ambient space, where $\mathbb{R}^{n+1}$ can serve as a special example. Usually, the chosen topology depends on the task at hand. The following topologies are examples from coarse to increasingly fine. There is the compact-open C^∞-topology, whose basis is formed by the union of topologies induced by inclusion

operators $i_k \colon C^\infty(M,N) \to C^k(M,N)$, where $C^k(M,N)$ are equipped with their compact-open/weak C^k-topologies. This topology is also called weak C^∞-topology in the literature. If the Banach spaces $C^k(M,N)$ are equipped with their strong C^k-topologies, i.e. those induced by their respective norms, the topology resulting from the above construction is called the strong C^∞-topology. Confusingly, terms for this topology vary in the literature. Depending on the author, this is denoted as the Whitney C^∞-topology or Mather C^∞-topology (cf. discussion in [92]). The basis of the strong C^∞-topology distinguishes smooth functions up to derivatives of bounded order. A refinement of the strong C^∞-topology (cf. [92]) gives the so-called very strong C^∞-topology. It is in some sense a natural topology for the C^∞-framework, since its basis captures information of derivatives of functions up to unbounded order. In [129], Michor introduces a further refinement of the very strong C^∞-topology, which is sometimes called the fine very strong C^∞-topology. It permits a manifold structure on $C^\infty(M,N)$ for possibly non-compact M. We want to mention, that in [71] Omori uses the term ILH-C^∞-topology (inverse limit of Hilbert C^∞-topology) for the topology on $C^\infty(M,N)$ induced by the inverse limit of the chain of $C^k(M,N)$. This topology is the initial topology with respect to inclusions, i.e. the coarsest topology making $i_k \colon C^\infty(M,N) \to C^k(M,N)$ continuous embeddings. Thus it depends on the topologies chosen on $C^k(M,N)$.

For this work it is important to notice, that all previously mentioned topologies coincide for the case of compact manifolds M. Hence, we can denote the topology on the spaces of embeddings and diffeomorphisms simply by C^∞-topology (cf. [86, Ch. 2]). If still more descriptive names are used, we do so to emphasis the topology used in the source of the argument or technique at hand. We refer the interested reader to [87] for a brief, and [86, Ch. 2] and [105] for in-depth introductions to this topic.

The C^∞-framework also affects the topological group structure of $\mathrm{Diff}(M)$. It might be tempting to work in the more special setting of Hilbert or Banach spaces. However, notice the following. For H^s-diffeomorphisms of Sobolev regularity with $s > \frac{\dim(M)}{2} + 1$, the space $\mathrm{Diff}^s(M)$ is a Hilbert manifold, so in some sense nicer than the Fréchet manifolds $\mathrm{Diff}(M)$ and $\mathrm{Emb}(M, \mathbb{R}^{n+1})$. As a drawback $\mathrm{Diff}^s(M)$, are only topological groups, not having Lie structure. This is rooted in the fact that the composition operator from the left fails to be smooth, while composition from the right is smooth (cf. α- and ω-lemmas [166, Ch. 2], [47, Ch. 2]). On a more general note, the Banach space setting for modeling parameterization groups of compact manifolds as Lie groups is too restrictive. In 1978, Omori showed that every Banach-Lie group acting effectively, transitively and smoothly on a compact manifold must be a finite dimensional Lie group (cf. [144, Thm. B]). This reduces modeling possibilities when Lie structure is desired. For $\mathrm{Diff}(M)$, this is not the case. It is indeed a Lie group in the sense of Omori, since C^∞-regularity holds for group actions. We emphasize, that constructions of shape spaces B_e^n with C^k-, $C^{k,\alpha}$ or H^s-regularity do not yield manifold structures, which is only the case for C^∞-regularity. Instead, resulting spaces only possess a diffeological structure, which can be viewed as a generalization of manifold structures (cf. [182]). This means that there is a trade-off when choosing regularity. Either Banach/Hilbert manifold structure or Lie group structure are achieved for the diffeomorphism groups. Still, there is enough structure on $\mathrm{Diff}(M)$ to carry over some techniques from Hilbert spaces, as it can be constructed as an inverse limit of Hilbert manifolds $\mathrm{Diff}^s(M)$ of Sobolev regularity $s > \dim(M) + 5$. Hence $\mathrm{Diff}(M)$ is called an ILH-Lie group by Omori ([71]). In particular, a generalized formulation of the implicit function theorem holds in this setting (cf. [71, Ch. 1.6]). We employ some of these techniques in section 5.2.2. For an overview and discussion of infinite dimensional diffeomorphism groups, the reader might refer to [166, Ch. 2] and [71].

Shape and Pre-Shape Spaces via Fiber Bundles With the collection of embeddings $\mathrm{Emb}(M, \mathbb{R}^{n+1})$ at hand, we can define the space B_e of unparameterized C^∞-shapes in $\mathbb{R}^{n+1}$ (cf. [61, 105, 12, 132]). The following definition is in fact a theorem, whose proof demands sophisticated techniques of differential geometry in infinite dimensions. The proof for the case of compact M without boundary can be found in [105, Thm. 44.1], while the non-trivial boundary case was first proved in [61, Thm. 2.2]. Notice, that the following definition and its assertions require the C^∞-framework.

Definition 12 (Shape Space $B_e(M, \mathbb{R}^{n+1})$)**.** *Let M be an n-dimensional compact, connected and oriented C^∞-submanifold of $\mathbb{R}^{n+1}$, perhaps with smooth boundary. Then the* shape space $B_e(M, \mathbb{R}^{n+1})$ *is defined as the quotient*

$$B_e\big(M, \mathbb{R}^{n+1}\big) := \mathrm{Emb}\left(M, \mathbb{R}^{n+1}\right) / \mathrm{Diff}(M), \tag{4.3}$$

where the group of C^∞-diffeomorphisms $\mathrm{Diff}(M)$ *acts on the right. The associated projection is called* canonical projection π*, and is given by*

$$\pi(\varphi) := \left\{ \psi \in \mathrm{Emb}\left(M, \mathbb{R}^{n+1}\right) : \ \exists \rho \in \mathrm{Diff}(M) \ \textit{s.t.}\ \varphi = \psi \circ \rho \right\} \in B_e^n. \tag{4.4}$$

The shape space $B_e(M, \mathbb{R}^{n+1})$ is a smooth Fréchet manifold.

Depending on the context, the resulting space $B_e(M, \mathbb{R}^{n+1})$ is also called *nonlinear Grassmannian* (cf. [61]) or *differentiable Chow-variety* (cf. [128]). Its elements can be regarded as unparameterized shapes of $\mathbb{R}^{n+1}$ of diffeomorphism class M (cf. [61, Thm. 2.2]). The term nonlinear Grassmannian is motivated by the fact, that there is a bijection

$$\beta \colon B_e\big(M, \mathbb{R}^{n+1}\big) \to \mathrm{Gr}\left(M, \mathbb{R}^{n+1}\right), \ \ [\varphi] \mapsto \varphi(M) \subset \mathbb{R}^{n+1}, \tag{4.5}$$

where $\mathrm{Gr}(M, \mathbb{R}^{n+1})$ is the set of all smooth submanifolds $\Gamma \subset \mathbb{R}^{n+1}$ that are C^∞-diffeomorphic to M. This means we have two different interpretations of shapes $\Gamma \in B_e(M, \mathbb{R}^{n+1})$. The first views $\Gamma = [\varphi]$ as an *equivalence class of embeddings* with the same image, while the second sees $\Gamma \subset \mathbb{R}^{n+1}$ as a *set with submanifold structure* diffeomorphic to M. For our work it is important to distinguish between these interpretations. Hence we denote the collection of embeddings with identical image manifold by $\pi(\varphi) \in B_e(M, \mathbb{R}^{n+1})$ as in equation (4.4). We write $\varphi(M) \subset \mathbb{R}^{n+1}$, when we mean the set interpretation of a shape.

In the following, we abbreviate $B_e(M, \mathbb{R}^{n+1})$ by B_e^n, still having the implicit relation to the manifold M and its dimension in mind. To acquire intuition about B_e^n, a graphical visualization is given in figure 4.1. This space can be equipped with various metrics, which means shape optimization can be regarded as optimization on an infinite dimensional Riemannian manifold (cf. [158]). For an exemplary collection of metrics on shape spaces, we refer the reader to [132, 12]. Questions regarding different choices of metrics on shape spaces and diffeomorphism groups is still an active area of research. There are phenomena apparent in infinite dimensional Riemannian geometry, which are not present in finite dimensions. For example, equipping B_e^n with an L^2-metric induces vanishing geodesics. In [131], Michor and Mumford give a vivid description of this situation:

> 'The picture that emerges for these infinite dimensional manifolds is quite interesting: there are simple expressions for the Christoffel symbols and curvature tensor, the geodesic equations are simple and of hyperbolic type and, at least in the case of plane curves, the geodesic spray exists locally. But the curvature is positive and unbounded in some high frequency directions, so these spaces wrap up on themselves arbitrarily tightly, allowing the infimum of path lengths between two given points [, i.e. shapes,] to be zero.'

Cases for other metrics and spaces are discussed in [11] and [14]. In this work, we do not rely on the specific choice of a Riemannian metric on shape and pre-shape spaces.

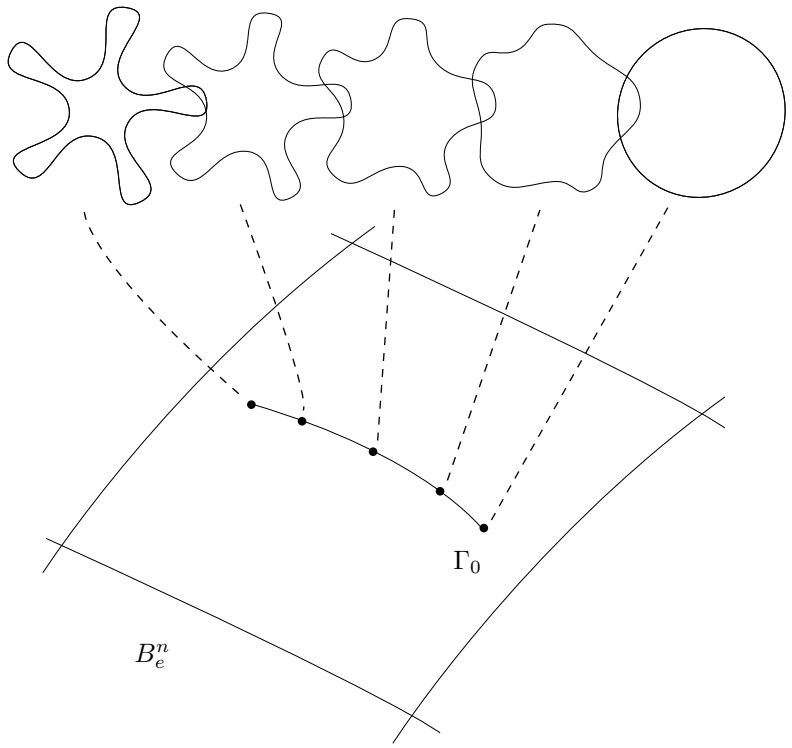

Figure 4.1: Illustration of a path in the shape space B_e^n for $M = S^1$.

For our purposes it is not enough to view shape optimization as optimization in B_e^n. Instead, we base our framework on optimization in $\mathrm{Emb}(M, \mathbb{R}^{n+1})$. This permits us to exploit additional structures induced by the action of $\mathrm{Diff}(M)$. The authors of [12, Ch. 1.1] call $\mathrm{Emb}(M, \mathbb{R}^{n+1})$ a *pre-shape space*, an expression we use for the techniques we derive in this work. We give a definition of pre-shape spaces and summarize several of their properties. A graphical sketch of a pre-shape space can be seen in figure 4.2.

Definition 13 (Pre-Shape Space $\mathrm{Emb}(M, \mathbb{R}^{n+1})$ as a Fiber Bundle)**.** *Let $M \subset \mathbb{R}^{n+1}$ be an n-dimensional compact, connected and oriented C^∞-submanifold, perhaps with smooth boundary.*

Then we call $\mathrm{Emb}(M, \mathbb{R}^{n+1})$ *a* pre-shape space*. The space* $\mathrm{Emb}(M, \mathbb{R}^{n+1})$ *is a smooth Fréchet manifold and an open subset of $C^\infty(M, \mathbb{R}^{n+1})$. It forms a smooth fiber bundle with base space $B_e(M, \mathbb{R}^{n+1})$ and standard fiber* $\mathrm{Diff}(M)$ *(cf. definition 5). The canonical projection π from equation* (4.4) *acts as the bundle projection.*

As with the definition of B_e^n, the definition of pre-shape spaces is actually a theorem, whose proof for the empty boundary case can be found in [105, Thm. 44.1]. A proof that $\mathrm{Emb}(M, \mathbb{R}^{n+1})$ is an open Fréchet-submanifold of $C^\infty(M, \mathbb{R}^{n+1})$ is found in [129, Prop. 5.3]. The formation of fiber bundle structure in the nonempty boundary case is a main result of [61, Thm. 2.2]. Notice that the term pre-shape space is used differently depending on the literature. For example, the authors of

[101] use this term for the space of labeled landmarks which are equivalent under translation and scaling.

Elements $\varphi \in \mathrm{Emb}(M, \mathbb{R}^{n+1})$ can be interpreted as parameterized shapes in the ambient space $\mathbb{R}^{n+1}$, whereas elements of $\mathrm{Diff}(M)$ acting on the right can be seen as reparameterizations. The standard fiber $\mathrm{Diff}(M)$ acts as a prototype for parameterizations of shapes $\varphi(M)$, which can be seen via the isomorphism

$$\mathrm{Diff}(M) \cong \mathrm{Diff}\big(\varphi(M)\big) \quad \text{by} \quad i_\varphi \colon \rho \mapsto \varphi \circ \rho \circ \varphi^{-1} \qquad \forall \varphi \in \mathrm{Emb}\big(M, \mathbb{R}^{n+1}\big). \tag{4.6}$$

Therefore the application of bundle projection π from equation (4.4) to a parameterized shape $\varphi \in \mathrm{Emb}(M, \mathbb{R}^{n+1})$ gives the collection $\pi(\varphi)$ of all C^∞-parameterizations corresponding to the shape $\varphi(M)$ in $\mathbb{R}^{n+1}$.

We remind the reader, that a fiber bundle is a manifold, which locally looks like a product space $U \times S$, where U corresponds to the base space, and S corresponds to the standard fiber (cf. definition 5). In our context, this means the pre-shape space $\mathrm{Emb}(M, \mathbb{R}^{n+1})$ is the collection of parameterized shapes, which locally looks like a product 'Shape'×'Parameterization'. However, this relationship holds only locally, and the global structure of the pre-shape space $\mathrm{Emb}(M, \mathbb{R}^{n+1})$ is much more complex. The situation is graphically sketched in figure 4.2.

These fibers permit us to not just view the shape itself, but also to distinguish various types of discretizations and associated numerical meshes. We make use of this by formulating objective functionals for mesh quality, such that desired parameterizations of shapes are minimizers in their corresponding fibers. Even further, the concept of pre-shape spaces provides a framework to control the parameterization of hold-all domains, i.e. volume meshes, during shape optimization.

Remark 1 (Shapes and Pre-Shapes in Non-Euclidean Spaces)**.** *We want the reader to notice the generality, under which our framework holds. In definition 12 and definition 13, we demanded M to be a submanifold of $\mathbb{R}^{n+1}$ with codimension 1. The sole purpose of this restriction is to suit our numerical applications in shape optimization. Definitions and properties guaranteed in definition 12 and definition 13 are also valid for embeddings $\mathrm{Emb}(M, N)$, where N is a finite dimensional C^∞-manifold without boundary, and M is a compact C^∞-manifold of dimension $\dim(N) \geq \dim(M)$, perhaps with smooth boundary (cf. [61, Thm. 2.2]). Notice that connectedness and orientability are not necessary. Corresponding shape spaces B_e then consist of shapes embedded in the manifold N.*

Even more general, definitions and properties of $\mathrm{Emb}(M, N)$ and $B_e(M, N)$ are still true for M being a so called compact Whitney manifold germ and N being a smooth manifold of dimension $\dim(N) > \dim(M)$ (cf. [130, Ch. 7.2]). In particular, this encompasses manifolds M with corners and closed subsets $M \subset \mathbb{R}^{n+1}$ with dense interiors and Lipschitz boundaries (cf. [130, Ch. 4.3]). However, in this generality, Fréchet spaces and manifolds have to be replaced by Frölicher spaces and manifolds. These are spaces, whose smooth structure is essentially determined by compatibility conditions for given sets of smooth curves and real functions (cf. [105, Ch. V.23]). The pre-shape calculus developed in this work can be extended to these more general ambient spaces N and model manifolds M.

Remark 2 (Manifold M as an Initial Shape in Optimization)**.** *From numerical perspective, the model manifold $M \subset \mathbb{R}^{n+1}$ can be regarded as an initial or starting iterate for a shape optimization routine. In this situation, there is a canonical reference element $\varphi_{id} \in \mathrm{Emb}(M, \mathbb{R}^{n+1})$, which is the identity operator embedding M into $\mathbb{R}^{n+1}$. Choosing the initial shape M fixes the pre-shape space $\mathrm{Emb}(M, \mathbb{R}^{n+1})$, and therefore determines the topological properties of feasible shapes. The fiber $\pi(\varphi_{id})$ corresponds to the possible choices of parameterizing M. In the discrete setting,*

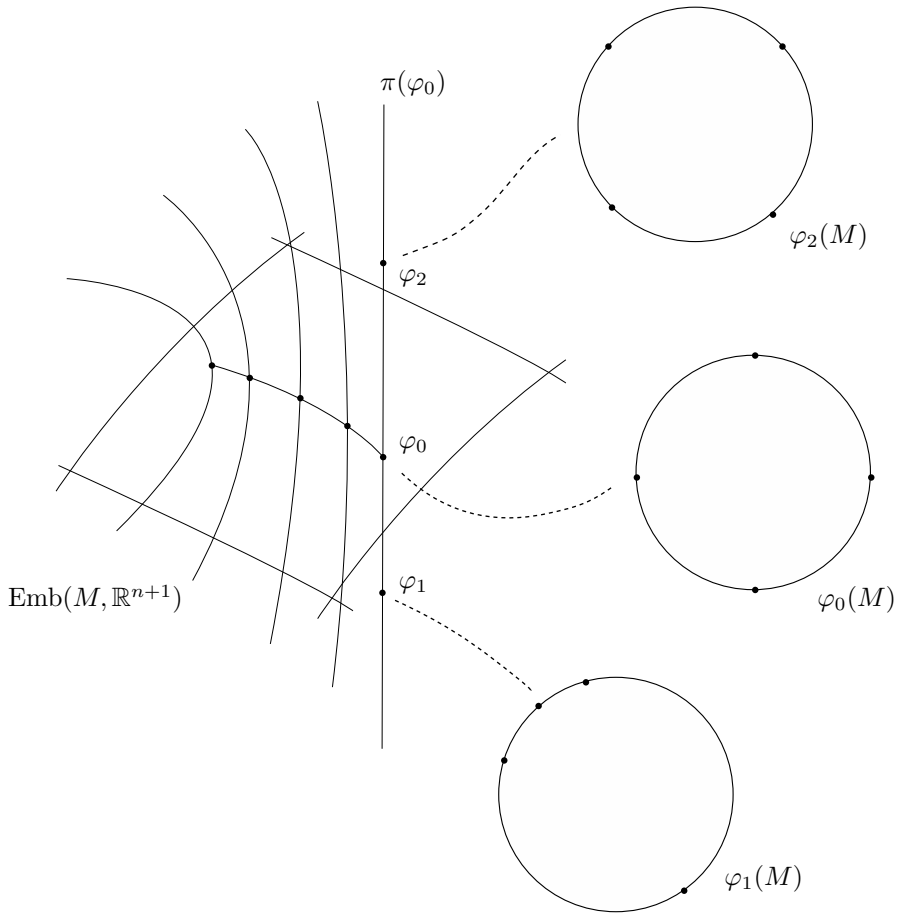

Figure 4.2: Depiction of the pre-shape space $\mathrm{Emb}(M, \mathbb{R}^{n+1})$ for $M = S^1$. To illustrate the parameterization interpretation of fibers $\pi(\varphi)$, the same four points are mapped from M to $\varphi_i(M)$.

this amounts to possible discretizations of the continuous initial shape. Thinking this way, shape optimization and change of parameterizations take place relative to the fixed chosen reference shape with parameterization φ_{id}.

The Tangential Bundles TB_e^n and $T\,\mathrm{Emb}(M, \mathbb{R}^{n+1})$ As we want to formulate an analogue of shape calculus in $\mathrm{Emb}(M, \mathbb{R}^{n+1})$, a characterization of the tangential bundles $T\,\mathrm{Emb}(M, \mathbb{R}^{n+1})$ and TB_e^n and their relations is required. A brief introduction to these is found in [61, Ch. 2.2.3], and a detailed discussion in [105].

Before we turn to the bundles TB_e^n and $T\,\mathrm{Emb}(M, \mathbb{R}^{n+1})$, let us first consider vector bundles for finite dimensional submanifolds $M \subset \mathbb{R}^{n+1}$ with boundary. In the nonempty boundary case, the tangent spaces T_pM and the tangent bundle TM are defined identically as in the empty boundary case (cf. definition 6). As M is a submanifold of $\mathbb{R}^{n+1}$, the inclusion map $i_M \colon M \to \mathbb{R}^{n+1}$ gives a natural partition of the tangential bundle $T\mathbb{R}^{n+1}$ (cf. [111, Lem. 10.34, Cor. 10.35]). We call the vector bundle $TM^\perp$ *normal bundle* of M with respect to $\mathbb{R}^{n+1}$, where the normal vector spaces are defined as quotients of tangent spaces

$$T_pM^\perp := T_p\mathbb{R}^{n+1}/T_pM \qquad \forall p \in M. \tag{4.7}$$

On $M \subset \mathbb{R}^{n+1}$, the tangential bundle of the ambient space $T\mathbb{R}^{n+1}$ splits into the

normal bundle $TM^\perp$ and the tangential bundle TM, i.e.

$$T_p\mathbb{R}^{n+1} \cong T_pM \oplus T_pM^\perp \qquad \forall p \in M. \tag{4.8}$$

In Euclidean space, this corresponds to the fact that vectors on M split into two orthogonal components with respect to the Euclidean scalar product. In the interior of M, the first component is parallel, i.e. tangential to M, while the second component is normal to M. However, notice that for n-dimensional manifolds M with boundary, all tangent spaces T_pM for all $p \in M$ are of dimension n (cf. [111, Prop. 3.12]). This includes the tangent spaces at the boundary T_pM for $p \in \partial M$. To grasp the situation on ∂M, we further refine the splitting. The same procedure as before can be performed for the boundary ∂M, which itself is a submanifold of M. This yields

$$T_pM \cong T_p\partial M \oplus T_p\partial M^\perp \qquad \forall p \in \partial M. \tag{4.9}$$

Notice that this decomposition is intrinsic to M, meaning that the normal bundle $T\partial M^\perp$ consists of vectors, which are orthogonal to ∂M and tangential to M. In particular, $T_p\partial M^\perp$ is of dimension 1. We can now rewrite the decomposition of $T\mathbb{R}^{n+1}$ on the submanifold M as

$$T_p\mathbb{R}^{n+1} \cong T_pM^\parallel \oplus T_p\partial M^\perp \oplus T_pM^\perp \qquad \forall p \in M, \tag{4.10}$$

where $T_pM^\parallel$ denotes the space of vectors tangential to M for p in the interior and tangential to ∂M and M for $p \in \partial M$. Notice that $T_p\partial M^\perp$ is non-trivial only for $p \in \partial M$. In the following, we refer to vectors from $TM^\parallel$ as tangential vectors that are parallel to M. Decomposition (4.10) tells us that the spaces of normal vectors on M are one-dimensional in the interior, and two-dimensional on the boundary ∂M.

This decomposition carries over to the infinite dimensional tangential bundles TB_e^n and $T\operatorname{Emb}(M,\mathbb{R}^{n+1})$. Since we assume M to be compact, [105, Thm. 42.17, comment above Lemma 42.5] gives us a characterization of the tangent bundle of $C^\infty(M,\mathbb{R}^{n+1})$ by

$$TC^\infty\big(M,\mathbb{R}^{n+1}\big) \cong C_c^\infty\big(M,T\mathbb{R}^{n+1}\big). \tag{4.11}$$

As mentioned in definition 13, the pre-shape space $\operatorname{Emb}(M,\mathbb{R}^{n+1})$ is an open subset of $C^\infty(M,\mathbb{R}^{n+1})$. Therefore relation (4.11) also characterizes the tangential bundle $T\operatorname{Emb}(M,\mathbb{R}^{n+1})$. In particular, for the respective tangent spaces we have

$$T_\varphi \operatorname{Emb}\big(M,\mathbb{R}^{n+1}\big) \cong C_c^\infty\big(\varphi(M),\mathbb{R}^{n+1}\big) \qquad \forall \varphi \in \operatorname{Emb}\big(M,\mathbb{R}^{n+1}\big). \tag{4.12}$$

The fiber bundle structure of $\operatorname{Emb}(M,\mathbb{R}^{n+1})$ canonically extends to its tangential bundle (cf. [105, Ch. 37.2.f], [61, Ch. 2.2.3]). This happens by use of the pushforward of the bundle projection

$$T\pi\colon T\operatorname{Emb}\big(M,\mathbb{R}^{n+1}\big) \to TB_e^n,\ \ V \mapsto \mathrm{d}\pi(V). \tag{4.13}$$

It is surjective by construction of B_e^n as a quotient manifold, meaning that π is a submersion. This leads to a decomposition of the tangent bundle of the total space $T\operatorname{Emb}(M,\mathbb{R}^{n+1})$ into the so called *vertical bundle*, which is defined as $\ker T\pi \subset T\operatorname{Emb}(M,\mathbb{R}^{n+1})$, and the *horizontal bundle* (cf. [105, 29.9.], [12, Ch. 2.2], [61, Ch. 2.2.3]). Thus we obtain

$$T_\varphi \operatorname{Emb}\big(M,\mathbb{R}^{n+1}\big) \cong T_{\pi(\varphi)}B_e^n \oplus T_\rho \operatorname{Diff}\big(\varphi(M)\big) \qquad \forall \varphi \in \operatorname{Emb}\big(M,\mathbb{R}^{n+1}\big), \tag{4.14}$$

for every $\rho \in \operatorname{Diff}(\varphi(M))$. Here, the tangential bundle of the base space TB_e^n associates to the horizontal bundle, whereas the tangential bundle of fibers represents the vertical bundle.

Since we only deal with compact and orientable n-dimensional submanifolds M, the existence of smooth outer unit normal vector-fields n on $\varphi(M) \subset \mathbb{R}^{n+1}$ is guaranteed. Also, let us denote the outward facing unit normal vector field orthogonal to n on $\partial\varphi(M)$ by $n_{\varphi(M)}$. In the following, let $\langle\cdot,\cdot\rangle_2$ denote the L^2-scalar products on $\partial\varphi(M)$ or $\varphi(M)$. We can associate the spaces of the horizontal bundle via

$$T_{\pi(\varphi)}B_e^n \cong \mathcal{N}_{\partial\varphi(M)} \oplus \mathcal{N}_{\varphi(M)}, \tag{4.15}$$

where the *space of outward facing normal vector fields on* $\partial\varphi(M)$ is given by

$$\mathcal{N}_{\partial\varphi(M)} := \Big\{ h \in C^\infty\big(\partial\varphi(M), \mathbb{R}^{n+1}\big) : \; h = \alpha \cdot n_{\varphi(M)},\; \alpha \in C^\infty\big(\partial\varphi(M), \mathbb{R}\big) \Big\}, \tag{4.16}$$

and *space of outer normal vector fields on* $\varphi(M)$

$$\mathcal{N}_{\varphi(M)} := \Big\{ h \in C^\infty\big(\varphi(M), \mathbb{R}^{n+1}\big) : \; h = \alpha \cdot n,\; \alpha \in C^\infty\big(\varphi(M), \mathbb{R}\big) \Big\}. \tag{4.17}$$

This is the characterization of tangential bundles of the shape spaces B_e^n by normal vector fields. Notice that the first component of relation (4.15) vanishes if M has no boundary. The spaces associated to the vertical bundle can be described by

$$T_\rho \operatorname{Diff}\big(\varphi(M)\big) \cong \mathcal{T}_{\varphi(M)}, \tag{4.18}$$

where the *space of tangential vector fields parallel to* $\partial\varphi(M)$ is defined as

$$\mathcal{T}_{\varphi(M)} := \Big\{ h \in C^\infty\big(\varphi(M), \mathbb{R}^{n+1}\big) : \; \langle n, h\rangle_2 = 0 \;\text{ on } \varphi(M) \text{ and } \langle n_{\varphi(M)}, h\rangle_2 = 0 \;\text{ on } \partial\varphi(M) \Big\}. \tag{4.19}$$

These tangential vector fields are elements of the vertical bundle, whereas the normal vector fields constitute the horizontal bundle part. We visualize the situation for tangential bundles in figure 4.3 and figure 4.4.

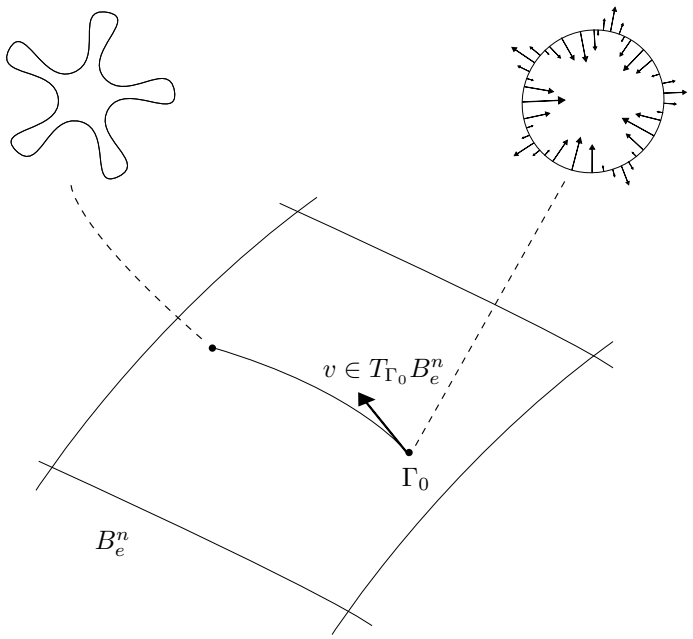

Figure 4.3: Illustration of a tangential vector from TB_e^n for $M = S^1$.

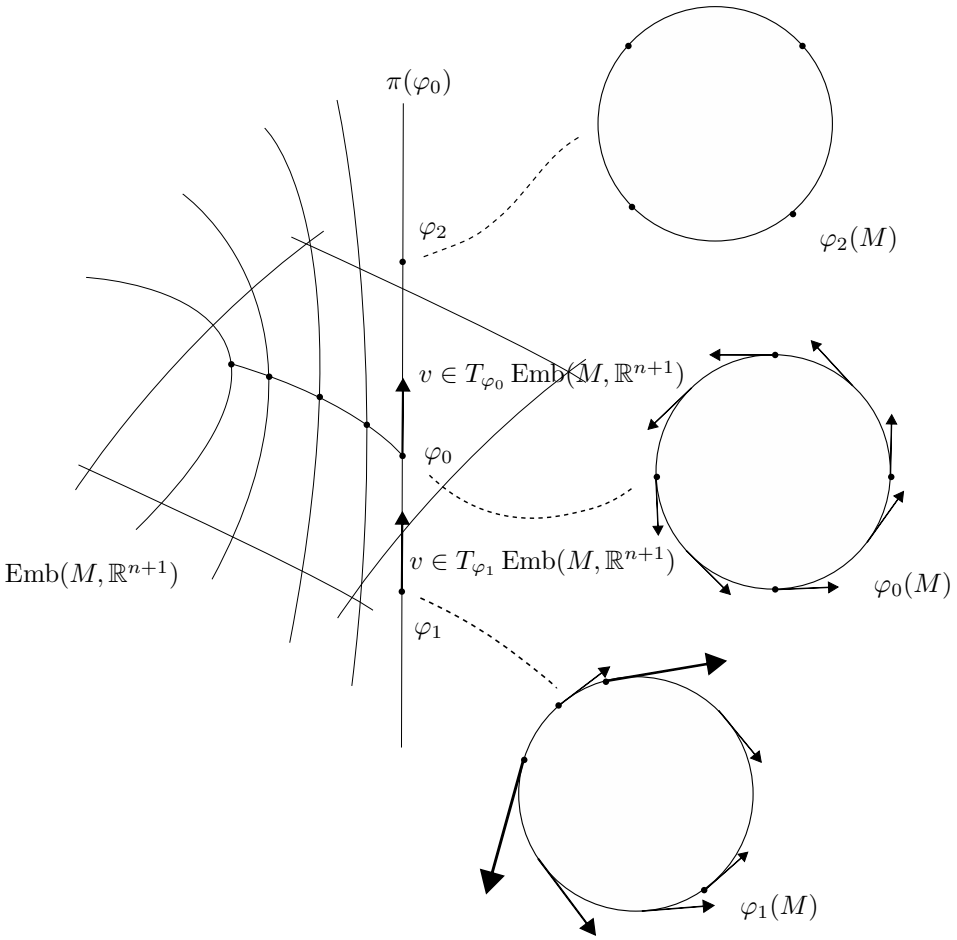

Figure 4.4: Illustration of tangential vectors from $T \operatorname{Emb}(M, \mathbb{R}^{n+1})$ with pure vertical components for $M = S^1$. Note that four points are added to illustrate the parameterization interpretation of fibers $\pi(\varphi)$.

4.2 Pre-Shape Calculus

Now we are in possession of a formalized definition of shapes and their corresponding parameterizations in form of embeddings. In this section, we begin with the introduction of our own results by deriving a suitable calculus for pre-shapes. We are inspired by shape derivative formulations presented in chapter 3, where directions act as perturbations of domains. The *pre-shape derivatives* we define in this section are based on families of pre-shapes via perturbation of the image space. Their relation to classical shape derivatives is highlighted. In particular, we give a structure theorem generalizing the Hadamard-Zolésio theorem 7. Shape calculus and sensitivity analysis of classical shape optimization (cf. [96, Ch. 3], [17]) carries over to pre-shape spaces naturally.

With definition 9, we have a set-theoretic version of shape functionals $\mathcal{J}\colon \mathcal{A} \subset \mathcal{P}(\mathbb{R}^{n+1}) \to \mathbb{R}$. Throughout the rest of this work, we restrict the admissible set of shapes to

$$\mathcal{A} = \mathrm{Gr}\left(M, \mathbb{R}^{n+1}\right) = \beta\Big(B_e\big(M, \mathbb{R}^{n+1}\big)\Big), \tag{4.20}$$

where $\mathrm{Gr}(M, \mathbb{R}^{n+1})$ is the nonlinear Grassmannian as described after definition 12, and $\beta\colon B_e(M, \mathbb{R}^{n+1}) \to \mathrm{Gr}(M, \mathbb{R}^{n+1})$ is the bijection from equation (4.5). We can canonically associate every equivalence class $\pi(\varphi) \in B_e^n$ with its set interpretation $\varphi(M) \in \mathrm{Gr}(M, \mathbb{R}^{n+1})$ of the nonlinear Grassmannian, which motivates the following definition.

Definition 14 (Shape Functionals via Shape Spaces and Pre-Shape Functionals)**.** *Let $M \subset \mathbb{R}^{n+1}$ be an n-dimensional, compact, connected and oriented C^∞-submanifold, perhaps with smooth boundary. Consider the shape space B_e^n and the pre-shape space* $\mathrm{Emb}(M, \mathbb{R}^{n+1})$*.*

Then a function

$$\mathcal{J}\colon B_e^n \to \mathbb{R} \tag{4.21}$$

is called shape functional*. A function*

$$\mathfrak{J}\colon \mathrm{Emb}\left(M, \mathbb{R}^{n+1}\right) \to \mathbb{R} \tag{4.22}$$

is called pre-shape functional*.*

Since we rely on functions $\mathcal{J}\colon B_e^n \to \mathbb{R}$ throughout the rest of this work, we use the short term 'shape functional' for them. On the other hand, the more general functions $\mathcal{J}\colon \mathcal{A} \subset \mathcal{P}(\mathbb{R}^{n+1}) \to \mathbb{R}$ are termed 'set-theoretic shape functionals'. The nomenclature pre-shape functional for functions as in (4.22) is motivated by regarding $\mathrm{Emb}(M, \mathbb{R}^{n+1})$ as a pre-shape space, e.g. as done by Michor et al. in [12, Ch. 1.1]. Since optimization is classically taking place in shape spaces, as opposed to pre-shape spaces, we have to investigate their correspondences and relations. For this, the following definition comes in handy. It is motivated by the construction of the shape space B_e^n in definition 12.

Definition 15 (Shape Functionality)**.** *Let $\mathfrak{J}$ be a pre-shape functional and let $\varphi \in \mathrm{Emb}(M, \mathbb{R}^{n+1})$. We say $\mathfrak{J}$ has* shape functionality in φ*, if it is consistent with the fiber projection, i.e.*

$$\mathfrak{J}(\varphi \circ \rho) = \mathfrak{J}(\varphi) \qquad \forall \rho \in \mathrm{Diff}(M). \tag{4.23}$$

If $\mathfrak{J}$ has shape functionality for all $\varphi \in \mathrm{Emb}(M, \mathbb{R}^{n+1})$, we say $\mathfrak{J}$ has shape functionality*.*

In order to give optimality criteria for the pre-shape optimization problems, and to formulate according optimization algorithms, we introduce a domain derivative for $\mathrm{Emb}(M, \mathbb{R}^{n+1})$. It is desirable that such a pre-shape derivative is compatible

with the classical Eulerian shape derivative from definition 10. Hence, we do not choose a standard Fréchet or Gâteaux derivative formulation on $C^\infty(M, \mathbb{R}^{n+1})$ for this endeavor, as directions for which we differentiate would correspond to tangential vectors of the space $\mathrm{Emb}(M, \mathbb{R}^{n+1})$ only. Instead, we want directions on the whole ambient space $V \in C^\infty(\mathbb{R}^{n+1}, \mathbb{R}^{n+1})$ to be permissible, which is natural in numerical shape optimization by deformation of the hold-all domain.

Definition 16 (Perturbation of Identity and Pre-Shape Derivatives)**.** *Consider a pre-shape functional $\mathfrak{J}$, not necessarily having shape functionality. Let $\varphi \in \mathrm{Emb}(M, \mathbb{R}^{n+1})$ and $V \in C^\infty(\mathbb{R}^{n+1}, \mathbb{R}^{n+1})$. Then the family of functions*

$$\varphi_t := \varphi + t \cdot V \circ \varphi \tag{4.24}$$

is called perturbation of identity of φ in direction V *for $t \in [0, \tau]$ and some $\tau > 0$. The limit*

$$\mathfrak{D}\mathfrak{J}(\varphi)[V] := \lim_{t \to 0} \frac{\mathfrak{J}(\varphi_t) - \mathfrak{J}(\varphi)}{t} \tag{4.25}$$

is called pre-shape derivative *of $\mathfrak{J}$ at $\varphi \in \mathrm{Emb}(M, \mathbb{R}^{n+1})$ in direction V, if it exists and is linear and bounded in V.*

We want to remind the reader, that C^∞-regularity for pre-shapes is not necessary to introduce the concept of pre-shape derivatives. Instead, the same definition can be adapted for embeddings φ of Sobolev- or Hölder-regularity. In these cases, test functions and directions V need to have according regularity.

We also emphasize that pre-shape derivatives are distinctively different to classical shape derivatives as in definition 10, and should not be confused with each other. The difference quotients employed for their definitions use completely different types of objects. Recall that the perturbation of identity for shapes at $\Gamma_0 \subset \mathbb{R}^{n+1}$ in direction $V \in C^\infty(\mathbb{R}^{n+1}, \mathbb{R}^{n+1})$ is defined via equation (3.3). It gives a curve of sets, in contrast to the perturbation of identity for pre-shapes in equation (4.24), which is a curve of functions in $\mathrm{Emb}(M, \mathbb{R}^{n+1})$.

Despite their difference, the perturbation of identity for pre-shapes (4.24) is naturally related to the perturbation of identity for shapes $\pi(\varphi) \in B_e^n$. This can be seen by the following reasoning. For arbitrary $V \in C^\infty(\mathbb{R}^{n+1}, \mathbb{R}^{n+1})$, the mapping φ_t as in (4.24) is in $C^\infty(M, \mathbb{R}^{n+1})$. Since $\mathrm{Emb}(M, \mathbb{R}^{n+1})$ is an open submanifold of $C^\infty(M, \mathbb{R}^{n+1})$ with respect to the C^∞-topology (cf. [105, Thm. 44.1] and p. 25), φ_t is an element of $\mathrm{Emb}(M, \mathbb{R}^{n+1})$ for $t \in [0, \tilde{\tau}]$ with $\tilde{\tau} > 0$ small enough. For such small perturbations, the bundle projection $\pi \colon \mathrm{Emb}(M, \mathbb{R}^{n+1}) \to B_e^n$ is applicable. The resulting curve of equivalence classes can then be associated with a curve of shapes in the nonlinear Grassmannian via β as in (4.5). Formally, this means

$$\varphi_t(M) = (\beta \circ \pi)(\varphi_t) = \varphi(M)_t \tag{4.26}$$

for all $t \in [0, \tilde{\tau}]$ with $\tilde{\tau} > 0$ small enough. We emphasize that $\varphi_t(M)$ are the application of the pre-shape perturbations of identity to M, while $\varphi(M)_t$ is the shape perturbation of identity of the shape $\varphi(M)$ as in definition 10.

Remark 3 (Pre-Shape Derivatives as Differentials)**.** *The pre-shape derivative from equation (4.25) can be understood as a differential for $\mathfrak{J}$ at $\varphi \in \mathrm{Emb}(M, \mathbb{R}^{n+1})$ on the open submanifold $\mathrm{Emb}(M, \mathbb{R}^{n+1})$ in $C^\infty(M, \mathbb{R}^{n+1})$ (cf. [105, Ch. 28.15]). This stems from the assumed linearity and boundedness of the pre-shape derivative in addition to their existence. In other words, for each $V \in C^\infty(\mathbb{R}^{n+1}, \mathbb{R}^{n+1})$ there exist $\tilde{V} \in T_\varphi \mathrm{Emb}(M, \mathbb{R}^{n+1})$, such that the pre-shape derivative can be seen as the application of a corresponding tangent vector $\tilde{V}$ to $\mathfrak{J}$, i.e.*

$$\mathfrak{D}\mathfrak{J}(\varphi)[V] = \mathrm{d}\mathfrak{J}(\varphi)\big[\tilde{V}\big]. \tag{4.27}$$

This is true, since the perturbation of identity from equation (4.24) *defines a representative curve in the equivalence class of the tangent vector* $\tilde{V}$*. Of course, the correspondence of* V *and* $\tilde{V}$ *is not unique, which is made precise in structure theorem 9 (i).*

Remark 4 (General Perturbations of Pre-Shapes)**.** *For the definition of pre-shape derivatives via equation* (4.25)*, we are not limited to families of perturbed embeddings* $\varphi_t \in \mathrm{Emb}(M, \mathbb{R}^{n+1})$ *given by the perturbation of identity as in equation* (4.24)*. Instead, any sufficiently regular flow given by operators*

$$G_t \colon \mathrm{Emb}\left(M, \mathbb{R}^{n+1}\right) \to \mathrm{Emb}\left(M, \mathbb{R}^{n+1}\right),\ G_0 = \mathrm{id}_{\mathrm{Emb}(M,\mathbb{R}^{n+1})} \tag{4.28}$$

gives rise to similar families of embeddings $\varphi_t := G_t(\varphi)$*. We emphasize that* G_t *define a flow in the space of pre-shapes* $\mathrm{Emb}(M, \mathbb{R}^{n+1})$*, which should not to be confused with diffeomorphisms or flows of the image space* $\mathbb{R}^{n+1}$*.*

The flow on $\mathrm{Emb}(M, \mathbb{R}^{n+1})$ *generated by the velocity method can serve as an example here. If the according semiderivative in equation* (4.25) *is demanded to exist and to be independent of choice of velocities that are identical at* $t = 0$*, we get a pre-shape derivative analogue of the Hadamard semiderivatives as found in [42, Ch. 4, Def. 3.2 and comments therein]. Such a notion of (pre-)shape derivatives is stronger than the one based on perturbations of identity, as it demands that the limit in equation* (4.25) *does not depend on the way* φ_t *approaches* φ *for* $t \to 0$*. Notice that this depends on the topology of the pre-shape spaces. If the limits in equation* (4.25) *are linear and bounded, then the Hadamard derivative satisfies the chain rule, whereas the derivative based on perturbations of identity as in definition 16 does not in general.*

The next proposition shows the relationship of classical shape- and pre-shape differentiability.

Proposition 2 (Shape Differentiability Implies Pre-Shape Differentiability)**.** *Let* $\mathcal{J} \colon B_e^n \to \mathbb{R}$ *be a shape functional.*

Then it has a canonical extension to a pre-shape functional

$$\mathfrak{J} \colon \mathrm{Emb}\left(M, \mathbb{R}^{n+1}\right) \to \mathbb{R},\ \ \varphi \mapsto \mathcal{J}\big(\pi(\varphi)\big), \tag{4.29}$$

where π *is the bundle projection from definition 13. Further, there is a one-to-one correspondence of shape functionals* $\mathcal{J}$ *and pre-shape functionals* $\mathfrak{J}$ *with shape functionality.*

Additionally, if $\mathcal{J}$ *is shape differentiable in the sense of definition 10, then its extension* $\mathfrak{J}$ *is pre-shape differentiable.*

Proof. One-to-one correspondence of pre-shape functionals with the property of shape functionality as in definition 15 and classical shape functionals as in (4.21) comes from the following. On the one hand, every canonical extension $\mathfrak{J}$ of a classical shape functional $\mathcal{J}$ as in (4.29) has shape functionality by definition (4.4) of π. On the other hand, every pre-shape functional $\tilde{\mathfrak{J}}$ with shape functionality gives rise to a well-defined shape functional $\mathcal{J}$ fulfilling (4.29). This holds, since the fibers $\pi(\varphi)$ are the disjoint orbits of φ by $\mathrm{Diff}(M)$ acting from the right, which makes $\tilde{\mathfrak{J}}$ constant on fibers by the definition 15 of shape functionality.

Next, we prove that shape differentiability implies pre-shape differentiability of the pre-shape extension. For this, assume that $\mathcal{J}$ is shape differentiable. Let us fix a $\varphi \in \mathrm{Emb}(M, \mathbb{R}^{n+1})$. Now we can use a case analysis for directions $V \in C^\infty(\mathbb{R}^{n+1}, \mathbb{R}^{n+1})$ either being tangential or normal at $\varphi(M)$. With this, we show existence of the pre-shape derivative $\mathfrak{D}(\mathcal{J} \circ \pi)(\varphi) \colon C^\infty(\mathbb{R}^{n+1}, \mathbb{R}^{n+1}) \to \mathbb{R}$ as in (4.25) for all $V \in C^\infty(\mathbb{R}^{n+1}, \mathbb{R}^{n+1})$, as well as its linearity and boundedness.

We recur that the fiber bundle projection π naturally defines a fiber bundle projection on the tangent bundle $T\pi$ as in (4.13), which is linear and bounded. This lets us use decomposition (4.14) of the tangent bundle $T\operatorname{Emb}(M,\mathbb{R}^{n+1})$ into horizontal and vertical component. Every tangent vector of $\operatorname{Emb}(M,\mathbb{R}^{n+1})$ is uniquely representable as a sum of both parts. Hence it is sufficient to show existence of equation (4.25) for tangent vectors in $T_\rho\operatorname{Diff}(\varphi(M))$ and $T_\varphi B_e^n$ separately. This enables us to use that $\mathcal{J}\circ\pi$ is constant on fibers.

For the first case, let $V\in C^\infty(\mathbb{R}^{n+1},\mathbb{R}^{n+1})$ be such that $V\circ\varphi\in\mathcal{T}_{\varphi(M)}$. By definition of the pre-shape derivative with the perturbation of identity as in equation (4.24), we have

$$\mathfrak{D}(\mathcal{J}\circ\pi)(\varphi)[V]=\frac{\mathrm{d}}{\mathrm{d}t}_{|t=0}(\mathcal{J}\circ\pi)(\varphi_t)=\dot{\varphi}_0\,(\mathcal{J}\circ\pi)\,, \tag{4.30}$$

with $\dot{\varphi}_0\in T\operatorname{Emb}(M,\mathbb{R}^{n+1})$ being the tangent vector representing $V\circ\varphi\in\mathcal{T}_{\varphi(M)}$. The perturbed curves φ_t are generally not running in fibers, i.e. there is a $t>0$ such that $\pi(\varphi_t)\neq\pi(\varphi)$ in any open neighborhood of φ. Instead, we can choose a different representative curve $\tilde{\varphi}_t$ for $\dot{\varphi}_0$, such that $\tilde{\varphi}_0=\varphi$, $\dot{\tilde{\varphi}_0}=\dot{\varphi}_0$ and $\pi(\tilde{\varphi}_t)=\pi(\varphi)$ in an open neighborhood of φ. This means $\tilde{\varphi}_t$ is running through the same fiber as φ. Such a choice can be made, since $\operatorname{Emb}(M,\mathbb{R}^{n+1})$ is open and locally trivializable, as it is a fiber bundle (cf. definition 13 and definition 5). Thus we find an open set $U\subset B_e^n$, such that $W:=\pi^{-1}(U)\subset\operatorname{Emb}(M,\mathbb{R}^{n+1})$ is an open neighborhood of φ_0 with a diffeomorphism $\operatorname{triv}_U\colon W\to U\times S$. The set U corresponds to the base space and S to the standard fiber $\operatorname{Diff}(M)$. For sufficiently small $t>0$, we can write

$$\operatorname{triv}_U(\varphi_t)=(u_t,s_t) \tag{4.31}$$

for some $u_t\in U$ and $s_t\in S$. Now we construct the desired curve by setting

$$\tilde{\varphi}_t:=\operatorname{triv}^{-1}\big(u_0,s_t\big). \tag{4.32}$$

By construction, the desired properties are verified, in particular $\dot{\tilde{\varphi}_0}=\dot{\varphi}_0$ due to equation (4.14) and $\pi(\tilde{\varphi}_t)=\pi(\varphi_0)$ for all $t\in[0,\tau]$ small enough. This shows that $\tilde{\varphi}_t$ stays in the same fiber as φ_0 in an open neighborhood W of φ_0. This proves the first case via

$$\begin{aligned}\mathfrak{D}(\mathcal{J}\circ\pi)(\varphi)[V]&=\dot{\varphi}_0(\mathcal{J}\circ\pi)\\&=\dot{\tilde{\varphi}_0}(\mathcal{J}\circ\pi)\\&=\frac{\mathrm{d}}{\mathrm{d}t}_{|t=0}(\mathcal{J}\circ\pi)(\tilde{\varphi}_t)\\&=\frac{\mathrm{d}}{\mathrm{d}t}_{|t=0}\mathcal{J}\big(\pi(\tilde{\varphi}_0)\big)\\&=0.\end{aligned} \tag{4.33}$$

For the second case, we consider the horizontal bundle. It splits into spaces of normal vectors on ∂M and M according to relation (4.15). The following argument is applicable to both components separately, which then gives the result for all vector fields corresponding to the horizontal bundle. Let $V\in C^\infty(\mathbb{R}^{n+1},\mathbb{R}^{n+1})$ be such that $V\circ\varphi\in\mathcal{N}_{\varphi(M)}$ and $V\circ\varphi$ is non-trivial. If a curve of embeddings φ_t runs along a fiber, i.e. $\pi(\varphi_t)=\pi(\varphi_0)$ for all $t>0$, then $\dot{\varphi}$ is in the vertical bundle part of $T\operatorname{Emb}(M,\mathbb{R}^{n+1})$ by its definition as $\ker T\pi$. By choosing a representing curve $\tilde{\varphi}_t$ for $V\circ\varphi$, combined with non-triviality of $V\circ\varphi$, we see that $\pi(\tilde{\varphi}_t)$ cannot be constant around a sufficiently small open neighborhood of φ. Since π is continuous,

$\tilde{\varphi}_t$ defines a non-constant curve $\pi(\tilde{\varphi}_t)$ in B_e^n. Thus

$$\begin{aligned}\mathfrak{D}(\mathcal{J}\circ\pi)(\varphi)[V] &= \dot{\tilde{\varphi}_0}(\mathcal{J}\circ\pi)\\ &= \frac{\mathrm{d}}{\mathrm{d}t}_{|t=0}\mathcal{J}\big(\pi(\tilde{\varphi}_t)\big)\\ &= \mathcal{D}\mathcal{J}\big(\pi(\varphi_0)\big)[V].\end{aligned} \tag{4.34}$$

The pre-shape derivative in equation (4.34) is well defined, because existence of the last term in equation (4.34) is guaranteed by the assumption of shape differentiability of $\mathcal{J}\colon B_e^n \to \mathbb{R}$.

For a general $V \in C^\infty(\mathbb{R}^{n+1},\mathbb{R}^{n+1})$, we combine this case study with decomposition (4.14), to get

$$\begin{aligned}\mathfrak{D}(\mathcal{J}\circ\pi)(\varphi)[V] &= \dot{\varphi}_0(\mathcal{J}\circ\pi)\\ &= \Big(\dot{\varphi}_0^{\mathcal{N}} + \dot{\varphi}_0^{\mathcal{T}}\Big)(\mathcal{J}\circ\pi)\\ &= \dot{\varphi}_0^{\mathcal{N}}(\mathcal{J}\circ\pi) + \dot{\varphi}_0^{\mathcal{T}}(\mathcal{J}\circ\pi)\\ &= \mathcal{D}\mathcal{J}\big(\pi(\varphi)\big)[V] + 0,\end{aligned}$$

where $\dot{\varphi}_0^{\mathcal{N}} \in T_\varphi \operatorname{Emb}(M,\mathbb{R}^{n+1})$ is the horizontal, and $\dot{\varphi}_0^{\mathcal{T}} \in T_\varphi \operatorname{Emb}(M,\mathbb{R}^{n+1})$ the vertical component of the tangent vector associated to $V\circ\varphi$. Therefore, the pre-shape derivative $\mathfrak{D}(\mathcal{J}\circ\pi)(\varphi)[V]$ exists for all $\varphi \in \operatorname{Emb}(M,\mathbb{R}^{n+1})$ and all $V \in C^\infty(\mathbb{R}^{n+1},\mathbb{R}^{n+1})$. Linearity and boundedness of $\mathfrak{D}(\mathcal{J}\circ\pi)(\varphi)[V]$ in V is seen due to $\mathcal{J}\circ\pi$ being constant on fibers, and linearity and boundedness of the shape derivative $\mathcal{D}\mathcal{J}$ by assumption and definition 10. □

With proposition 2, we can situate classical shape optimization problems in the context of optimization in pre-shape spaces $\operatorname{Emb}(M,\mathbb{R}^{n+1})$ for suitable manifolds M. But first, we observe that a unique solution $\varphi(M)$ of a shape optimization problem has multiple parameterizations in general. For shape optimization problems posed in the pre-shape space $\operatorname{Emb}(M,\mathbb{R}^{n+1})$, this leads to non-uniqueness of solutions, which at first might seem like a disadvantage. However, due to non-uniqueness up to elements in the solution fiber $\pi(\varphi)$, it is possible to demand additional properties for the pre-shape solution. This gives several opportunities to enhance numerical shape optimization routines, while at the same time narrowing down the amount of non-uniqueness of pre-shape solutions to a reasonable level. We exploit this idea in later chapters. For example, increasing mesh quality while not changing the shape at hand can be viewed as a condition posed on a shape optimization problem selecting a pre-shape in a given fiber.

Proposition 2 also offers a possibility to transfer results concerning shape differentiability of classical shape functionals to the pre-shape setting, without the need for new proofs. In particular, existence of stationary points in B_e^n is carried over to $\operatorname{Emb}(M,\mathbb{R}^{n+1})$ as existence of stationary fibers. Hence, proposition 2 shows that pre-shape optimization is in some sense a canonical generalization of classical shape optimization.

In the following, we give a characterization of the pre-shape derivative in the style of the Hadamard-Zolésio theorem 7. For introductions and facts concerning the use of distributions, the reader can consult [147, Rem. 6.2, Def. 6.22, Def. 6.34, Thm. 7.10, Ex. 7.12] and [89, Ch. 2]. A slight difference of our formulation compared to theorem 7 is, that we use distributions supported on vector fields, instead of a distribution on scalar valued functions. This is a necessity in the pre-shape setting, since multiple linearly independent tangential directions on shapes $\varphi(M)$ can exist. For the classical Hadamard-Zolésio theorem 7, it suffices to consider only

the coefficients of the single outer unit normal direction of vector fields on a hypersurface. In the following, we denote by $C_c^\infty(\mathbb{R}^{n+1},\mathbb{R}^{n+1})$ the space of smooth vector fields on $\mathbb{R}^{n+1}$ with compact support and assume the strong C^∞-topology. Also, we abbreviate $\langle g^{\mathcal{N}}, V\rangle_{C^\infty(\mathbb{R}^{n+1},\mathbb{R}^{n+1})^*}$ by $\langle g, V\rangle$ for readability, being aware of the duality product suiting the distribution $g \in C^\infty(\mathbb{R}^{n+1},\mathbb{R}^{n+1})^*$ (cf. remark 7). We use trace operators to indicate restrictions, which is overkill for smooth functions, but acts as a hint for generalization to the Sobolev setting.

Theorem 9 (Structure Theorem for Pre-Shape Derivatives)**.** *Let $M \subset \mathbb{R}^{n+1}$ be a compact, connected and oriented n-dimensional C^∞-submanifold, perhaps with smooth boundary. Consider a pre-shape differentiable pre-shape functional $\mathfrak{J}\colon \operatorname{Emb}(M,\mathbb{R}^{n+1}) \to \mathbb{R}$, not necessarily having shape functionality. Let $\varphi \in \operatorname{Emb}(M,\mathbb{R}^{n+1})$. Denote by n the outer unit normal vector field of the shape $\varphi(M)$, and by $n_{\varphi(M)}$ the outward pointing unit normal vector field with respect to $\partial\varphi(M)$.*

Then the following holds:

(i) The support of $\mathfrak{D}\mathfrak{J}(\varphi)$ is given by

$$\operatorname{supp}\mathfrak{D}\mathfrak{J}(\varphi) \subseteq \Big\{ V \in C^\infty\big(\mathbb{R}^{n+1},\mathbb{R}^{n+1}\big) :\ \varphi(M) \cap \operatorname{supp} V \neq \varnothing \Big\}. \tag{4.35}$$

(ii) There exist continuous linear functionals $g^{\mathcal{N}}\colon C^\infty(\mathbb{R}^{n+1},\mathbb{R}^{n+1}) \to \mathbb{R}$ and $g^{\mathcal{T}}\colon C^\infty(\mathbb{R}^{n+1},\mathbb{R}^{n+1}) \to \mathbb{R}$ depending on φ, which are distributions with compact support on $\varphi(M)$, such that

$$\mathfrak{D}\mathfrak{J}(\varphi)[V] = \big\langle g^{\mathcal{N}}, V\big\rangle + \big\langle g^{\mathcal{T}}, V\big\rangle \qquad \forall V \in C^\infty\big(\mathbb{R}^{n+1},\mathbb{R}^{n+1}\big). \tag{4.36}$$

Moreover,

$$\operatorname{supp} g^{\mathcal{N}} \subseteq \operatorname{supp}\mathfrak{D}\mathfrak{J}(\varphi) \cap \Big\{ V \in C^\infty\big(\mathbb{R}^{n+1},\mathbb{R}^{n+1}\big) :\ \operatorname{Tr}_{|\varphi(M)}[V] \in \mathcal{N}_{\varphi(M)} \text{ or } \operatorname{Tr}_{|\partial\varphi(M)}[V] \in \mathcal{N}_{\partial\varphi(M)} \Big\} \tag{4.37}$$

and

$$\operatorname{supp} g^{\mathcal{T}} \subseteq \operatorname{supp}\mathfrak{D}\mathfrak{J}(\varphi) \cap \Big\{ V \in C^\infty\big(\mathbb{R}^{n+1},\mathbb{R}^{n+1}\big) :\ \operatorname{Tr}_{|\varphi(M)}[V] \in \mathcal{T}_{\varphi(M)} \Big\}, \tag{4.38}$$

where $\operatorname{Tr}_{|\varphi(M)}\colon C^\infty(\mathbb{R}^{n+1},\mathbb{R}^{n+1}) \to C^\infty(\varphi(M),\mathbb{R}^{n+1})$ is a trace operator, $\mathcal{N}_{\varphi(M)}$ and $\mathcal{N}_{\partial\varphi(M)}$ are normal spaces as in equation (4.17) and equation (4.16), and $\mathcal{T}_{\varphi(M)}$ is the tangential space as in equation (4.19).

(iii) If $\mathfrak{J}$ has shape functionality, then for all $\varphi \in \operatorname{Emb}(M,\mathbb{R}^{n+1})$, we have $g^{\mathcal{T}} = 0$ and

$$\mathfrak{D}\mathfrak{J}(\varphi)[V] = \mathcal{D}\mathcal{J}\big(\pi(\varphi)\big)[V] \qquad \forall V \in C^\infty\big(\mathbb{R}^{n+1},\mathbb{R}^{n+1}\big), \tag{4.39}$$

where $\mathcal{J}\colon B_e^n \to \mathbb{R}$ is the natural shape functional corresponding to $\mathfrak{J}$ by $\mathcal{J}\circ\pi = \mathfrak{J}$. In particular, $g^{\mathcal{N}}$ corresponds to the distribution of the classical Hadamard-Zolésio theorem 7.

(iv) If for all $\varphi \in \operatorname{Emb}(M,\mathbb{R}^{n+1})$ the pre-shape derivative vanishes in tangential directions on $\varphi(M)$ parallel to $\partial\varphi(M)$, i.e.

$$\mathfrak{D}\mathfrak{J}(\varphi)[V] = 0 \quad \forall V \in C^\infty\big(\mathbb{R}^{n+1},\mathbb{R}^{n+1}\big) \text{ with } \operatorname{Tr}_{|\varphi(M)}[V] \in \mathcal{T}_{\varphi(M)}, \tag{4.40}$$

then $\mathfrak{J}$ is locally constant on each fiber in $\operatorname{Emb}(M,\mathbb{R}^{n+1})$. If additionally $\mathfrak{J}$ is constant under change of orientation and $M \in \{S^1, S^2, S^3\}$, then $\mathfrak{J}$ has shape functionality.

Proof. Let $\mathcal{J}\colon \mathrm{Emb}(M,\mathbb{R}^{n+1}) \to \mathbb{R}$ be a pre-shape differentiable pre-shape functional and fix a $\varphi \in \mathrm{Emb}(M,\mathbb{R}^{n+1})$ for the rest of this proof.

For (i), let $V \in C^\infty(\mathbb{R}^{n+1},\mathbb{R}^{n+1})$ be such that $\varphi(M) \cap \operatorname{supp} V = \varnothing$. Consider the perturbation of identity φ_t for V of φ as in equation (4.24). By $\varphi(M) \cap \operatorname{supp} V = \varnothing$, we have $V \circ \varphi = 0$, resulting in $\varphi_t = \varphi$ being constant in t. This yields $\mathfrak{D}\mathfrak{J}(\varphi)[V] = 0$ via the difference quotient in equation (4.25), which immediately gives us (i).

Now let us consider assertion (ii). We follow reasoning of [42, Ch. 9.3.4, Cor. 1] to some extent, where Banach spaces $C^k(\mathbb{R}^{n+1},\mathbb{R}^{n+1})$ are considered. By (i), the pre-shape derivative $\mathfrak{D}\mathfrak{J}(\varphi)\colon C^\infty(\mathbb{R}^{n+1},\mathbb{R}^{n+1}) \to \mathbb{R}$ is a linear functional with compact support as in relation (4.35). Hence we do not lose information by restricting the space of permissible test functions V to $C_c^\infty(\mathbb{R}^{n+1},\mathbb{R}^{n+1})$. This gives a distribution $g \in \mathcal{D}'(\mathbb{R}^{n+1},\mathbb{R}^{n+1})$ with compact support in the sense of [89, Def. 2.1.1], such that

$$\mathfrak{D}\mathfrak{J}(\varphi)[V] = \langle g, V\rangle_{\mathcal{D}'(\mathbb{R}^{n+1},\mathbb{R}^{n+1})} \qquad \forall V \in C_c^\infty\big(\mathbb{R}^{n+1},\mathbb{R}^{n+1}\big). \tag{4.41}$$

Since we found the support of $\mathfrak{D}\mathfrak{J}(\varphi)$ in (i), we also have that the support of g is on $\varphi(M)$. By [89, Thm. 2.3.1], and as continuity is demanded for $\mathfrak{D}\mathfrak{J}(\varphi)$ by definition, we see that the pre-shape derivative is also a distribution with compact support on the domain $C^\infty(\mathbb{R}^{n+1},\mathbb{R}^{n+1})$.

We can define $\tilde{g}^{\mathcal{T}}$ and $\tilde{g}^{\mathcal{N}}$ as the restriction of g to either vertical or horizontal directions of $C^\infty(\varphi(M),\mathbb{R}^{n+1})$, recurring on decomposition (4.14) of the tangent bundle in horizontal and vertical components. These are again distributions with compact support (cf. [89, Ch. 2.2]). By use of [89, Thm. 2.2.5] via compactness of $\varphi(M)$, we can uniquely extend the distributions $\tilde{g}^{\mathcal{T}}$ and $\tilde{g}^{\mathcal{N}}$ by zero to the entire domain $C^\infty(\mathbb{R}^{n+1},\mathbb{R}^{n+1})$. Denote the extended distributions by $g^{\mathcal{T}}$ and $g^{\mathcal{N}}$ respectively. By construction, we see that both distributions are supported on compact $\varphi(M)$, with relation (4.38) and (4.37) satisfied. Due to their unique extension by zero, and values of $\tilde{g}^{\mathcal{T}}$ and $\tilde{g}^{\mathcal{N}}$ coming from restrictions of $\mathfrak{D}\mathfrak{J}(\varphi)$ to vertical and horizontal components, we see that equation (4.36) is also satisfied by construction, giving us (ii).

For (iii), let $\mathfrak{J}$ have shape functionality. Let us consider an arbitrary direction $V \in C^\infty(\mathbb{R}^{n+1},\mathbb{R}^{n+1})$ parallel to $\varphi(M)$, i.e. $\mathrm{Tr}_{|\varphi(M)}[V] \in \mathcal{T}_{\varphi(M)}$. We can follow analogous arguments as in the proof of proposition 2, giving us a curve φ_t in the fiber $\pi(\varphi)$ generating $\mathfrak{D}\mathfrak{J}(\varphi)[V]$ for a given φ. As φ_t is running on the fiber of φ, and since $\mathfrak{J}$ has shape functionality (cf. definition 15) in φ by assumption, $\mathfrak{J}(\varphi_t)$ is constant for all t. By definition of the pre-shape derivative in equation (4.25), we have $\mathfrak{D}\mathfrak{J}(\varphi)[V] = 0$. This holds for all directions $V \in C^\infty(\mathbb{R}^{n+1},\mathbb{R}^{n+1})$ parallel to $\varphi(M)$. Hence by decomposition equation (4.36), together with support relations (4.37) and (4.38) , we have $g^{\mathcal{T}} = 0$.

Further, vanishing of $g^{\mathcal{T}}$ implies that equation (4.36) reduces to

$$\mathfrak{D}\mathfrak{J}(\varphi)[V] = \big\langle g^{\mathcal{N}}, V\big\rangle \qquad \forall V \in C^\infty(\mathbb{R}^{n+1},\mathbb{R}^{n+1}). \tag{4.42}$$

We can use proposition 2, and see that shape functionality of $\mathfrak{J}$ leads to a well defined shape differentiable shape functional $\mathcal{J}\colon B_e^n \to \mathbb{R}$ with $\mathcal{J} \circ \pi = \mathfrak{J}$. As the vertical part of V has no impact on $\mathfrak{D}\mathfrak{J}(\varphi)[V]$, we can find a horizontal curve φ_t generating $\mathfrak{D}\mathfrak{J}(\varphi)[V]$. The representative φ_t either creates a trivial curve $\pi(\varphi_t)$ in B_e^n, which leads to equation (4.39) being 0 on both sides, or a non-trivial curve $\pi(\varphi_t)$ in B_e^n. If $\pi(\varphi_t)$ is non trivial, we have

$$\mathcal{D}\mathcal{J}\big(\pi(\varphi)\big)[V] = \frac{\mathrm{d}}{\mathrm{d}t}_{|t=0} \mathcal{J}\big(\pi(\varphi_t)\big) = \frac{\mathrm{d}}{\mathrm{d}t}_{|t=0} \mathfrak{J}(\varphi_t) = \mathfrak{D}\mathfrak{J}(\varphi)[V] \tag{4.43}$$

for the shape derivative $\mathcal{D}\mathcal{J}(\pi(\varphi))$ and pre-shape derivative $\mathfrak{D}\mathfrak{J}(\varphi)$, resulting in equation (4.39). Together with equation (4.42), and by association of $\varphi(M)$ with

$\pi(\varphi) \in B_e^n$, this also shows that $g^{\mathcal{N}}$ corresponds to the distribution taking coefficients of normal components from the Hadamard-Zolésio theorem 7, giving us (iii).

It remains to proof (iv), so let us assume equation (4.40) to be true. We show that $\mathfrak{J}$ is locally constant on each fiber. Let us fix a $\varphi \in \mathrm{Emb}(M, \mathbb{R}^{n+1})$ and define

$$G_\varphi \colon \mathrm{Diff}(M) \to \mathrm{Emb}(M, \mathbb{R}^{n+1}),\ \rho \to \varphi \circ \rho, \tag{4.44}$$

the action of $\mathrm{Diff}(M)$ from the right on the fixed element φ. As $\mathrm{Diff}(M) = \mathrm{Emb}(M, M)$, the structure group $\mathrm{Diff}(M)$ itself is an open manifold of the vector space $C^\infty(M, M)$ equipped with the fine very strong C^∞-topology (cf. [105, Thm. 43.1], p. 25). This makes it possible to apply the concept of differentials for G_φ. Thus, for local constancy of $\mathfrak{J}$ in each fiber, it is sufficient to show that the differential $\mathrm{d}(\mathfrak{J} \circ G_\varphi)(\rho)$ is zero for all $\rho \in \mathrm{Diff}(M)$, where

$$\mathfrak{J} \circ G_\varphi \colon \mathrm{Diff}(M) \to \mathrm{Emb}(M, \mathbb{R}^{n+1}) \to \mathbb{R} \tag{4.45}$$

This is true, since we have that $\mathfrak{D}\mathfrak{J}(\varphi)$ is linear and continuous for all $\varphi \in \mathrm{Emb}(M, \mathbb{R}^{n+1})$, as G_φ describes the action of the regular Lie group $\mathrm{Diff}(M)$. This in turn allows for an application of the mean value theorem to give local constancy.

For this, we see that

$$0 \to T_\rho \mathrm{Diff}(M) \overset{\mathrm{d}G_\varphi}{\to} T_{G_\varphi(\rho)} \mathrm{Emb}(M, \mathbb{R}^{n+1}) \overset{\mathrm{d}\pi}{\to} T_{\pi(G_\varphi(\rho))} B_e^n \to 0 \tag{4.46}$$

is a short exact sequence, i.e. $\mathrm{Im}(\mathrm{d}G_\varphi) = \ker(\mathrm{d}\pi)$. This is true by the following argumentation. For the differential we have $\mathrm{d}G_\varphi(\rho) = D\varphi \circ \rho$ for all $\rho \in \mathrm{Diff}(M)$, and for directions $\tilde{V} \in T_\rho \mathrm{Diff}(M)$ the chain rule yields

$$\mathrm{d}G_\varphi(\rho)\big[\tilde{V}\big] = \frac{\mathrm{d}}{\mathrm{d}t}_{|t=0}(\varphi \circ \rho_t) = D\varphi(\rho_0)\frac{\mathrm{d}}{\mathrm{d}t}_{|t=0}\rho_t = (D\varphi \circ \rho)\tilde{V}, \tag{4.47}$$

with a curve ρ_t on $\mathrm{Diff}(M)$ representing $\tilde{V}$. This in turn makes G_φ an immersion, since $D\varphi$ is injective by φ being an embedding. Since G_φ defines an immersion of $\mathrm{Diff}(M)$ onto a fiber of $\mathrm{Emb}(M, \mathbb{R}^{n+1})$, it makes $\mathrm{d}G_\varphi$ an isomorphism of $T_\rho \mathrm{Diff}(M)$ and its image $\mathrm{Im}(\mathrm{d}G_\varphi(\rho)) \cong \mathcal{T}_{\varphi(M)}$. Also, $\mathrm{d}\pi_{G_\varphi(\rho)} = T\pi_{|T_{G_\varphi(\rho)}\mathrm{Emb}(M,\mathbb{R}^{n+1})}$ is linear, and sends the vertical space to zero. We therefore have $\mathrm{Im}(\mathrm{d}G_\varphi) = \ker(\mathrm{d}\pi)$ by definition of the vertical space (cf. equation (4.13)). This gives the exactness of the short sequence (4.46). Hence we get

$$T\pi(\mathrm{d}G_\varphi(\rho)) = \mathrm{d}\pi \circ \mathrm{d}G_\varphi(\rho) = 0, \tag{4.48}$$

which means that $\mathrm{d}G_\varphi(\rho)[\tilde{V}]$ can be associated to an element of the vertical space $\ker(T\pi_\varphi) \cong \mathcal{T}_{\varphi(M)}$ for all directions $\tilde{V} \in T_\rho \mathrm{Diff}(M)$ via (4.14) and (4.18). By interpreting the pre-shape derivative as a differential (cf. equation (4.27)), we differentiate with respect to ρ and use the chain rule for differentials to arrive at

$$\begin{aligned}
\mathrm{d}\big(\mathfrak{J} \circ G_\varphi\big)(\rho)\big[\tilde{V}\big] &= \mathrm{d}\mathfrak{J}(\varphi \circ \rho)\Big[\mathrm{d}G_\varphi(\rho)\big[\tilde{V}\big]\Big] \\
&= \mathfrak{D}\mathfrak{J}(\varphi \circ \rho)\big[V^{\mathcal{T}}\big] \\
&= 0,
\end{aligned}$$

where $V^{\mathcal{T}} \in C^\infty(\mathbb{R}^{n+1}, \mathbb{R}^{n+1})$ is a vector field associated to $\mathrm{d}G_\varphi(\rho)[\tilde{V}]$ according to equation (4.27). Assumption (4.40) then gives the last equality to zero.

This true for all $\varphi \in \mathrm{Emb}(M, \mathbb{R}^{n+1})$, all $\rho \in \mathrm{Diff}(M)$ and all $\tilde{V} \in T_\rho \mathrm{Diff}(M)$. Therefore $\mathfrak{J}$ is locally constant on each fiber in $\mathrm{Emb}(M, \mathbb{R}^{n+1})$, which is the first part

of (iv). Additionally, if $M \in \{S^1, S^2, S^3\}$, then several topological results partly proved and conjectured by Smale (cf. [166, Thm. 13.14f]) tell us that $\mathrm{Diff}(M)$ has homotopy type of the orthogonal group $\mathrm{O}(n)$, $n \in \{2, 3, 4\}$ accordingly. The orthogonal group $\mathrm{O}(n)$ itself has two connected components, one consisting of elements with determinant 1, corresponding to $\mathrm{SL}(n)$, and one for element with determinant -1. Hence $\mathrm{Diff}(M)$ also has two connected components, corresponding to orientation preserving and reversing diffeomorphisms. If $\mathfrak{J}$ is assumed to be invariant under change of orientation on each fiber, we have that local constants on each connected component are equal. In this case $\mathfrak{J}$ is constant on each fiber, which implies that $\mathfrak{J}$ has shape functionality, finally concluding the proof. □

Theorem 9 gives an intuitive way to understand the pre-shape derivative from definition 16 and the relation of shape functionals and pre-shape functionals. Part (i) of theorem 9 has the same meaning as in the classical Hadamard-Zolésio structure theorem for shape derivatives. Namely, deformations of the hold-all domain only influence the pre-shape functional if they deform the shape $\varphi(M)$.

The difference to classical shape derivatives is illustrated in equation (4.36), where the effect of deformations on the objective is split into normal and tangential components. The normal part $g^{\mathcal{N}}$ can be understood as the shape optimization part of $\mathfrak{D}\mathfrak{J}$, i.e. $\mathfrak{J}$ depending on the change of interface $\varphi(M)$. This is also reflected by the structure of its support given in relation (4.37), which states that only directions deforming $\varphi(M)$ in normal direction have an effect on $g^{\mathcal{N}}$. Notice that on points of the boundary $\partial\varphi(M)$, there is one more degree of freedom for normal directions compared to the interior of $\varphi(M)$. On the other hand, $g^{\mathcal{T}}$ is interpretable as the part of $\mathfrak{D}\mathfrak{J}$ sensitive to reparameterizations of the shape $\varphi(M)$, which is shown by the structure of its support in relation (4.38). Only vector fields that are parallel to $\varphi(M)$ play a role, i.e. vector fields tangential to $\varphi(M)$ and $\partial\varphi(M)$. In classical shape optimization, tangential vectors are always in the kernel of the shape derivative. But in the more general pre-shape case, both normal and tangential components can have a combined non-trivial effect.

The influence of tangential and normal directions on $\mathfrak{J}$ is also reflected in theorem 9 (iii) and (iv). Pre-shape functionals $\mathfrak{J}$ with shape functionality have vanishing tangential part $g^{\mathcal{T}}$ of the pre-shape derivative $\mathfrak{D}\mathfrak{J}$, meaning that they are only supported by normal components of the deformation field $V \in C^\infty(\mathbb{R}^{n+1}, \mathbb{R}^{n+1})$. This coincides with classical shape optimization theory. On the other hand, if 'shape derivatives' are not found to vanish in tangential directions, the 'shape functional' at hand is actually a true pre-shape functional. Such behavior is the case for pre-shape functionals for mesh quality optimization we develop in the next chapters.

Remark 5 (Structure Theorem for Arbitrary Codimension Shapes in Euclidean Space)**.** *In the proof of theorem 9, we did not rely on the specific codimension of shapes $\varphi(M) \subset \mathbb{R}^{n+1}$, except in decomposition* (4.14)*, where tangential vectors of the pre-shape space are decomposed into horizontal and vertical components. In fact, decomposition* (4.14) *into vertical and horizontal bundles and their respective descriptions are valid for model manifolds M of dimension $\dim(M) \leq n+1$ (cf. [61, Thm. 2.2]). Therefore the proof for theorem 9 applies to pre-shape spaces $\mathrm{Emb}(M, \mathbb{R}^{n+1})$ with model manifolds of dimension $\dim(M) \leq n+1$, where smooth boundaries ∂M are also permitted. Normal spaces $\mathcal{N}_{\varphi(M)}$ and tangential spaces $\mathcal{T}_{\varphi(M)}$ as in* (4.17) *and* (4.19) *have to be adjusted for the number of linearly independent normal and tangent vectors. If for example $\mathrm{Emb}([0,1], \mathbb{R}^3)$ is considered, the space $\mathcal{N}_{\varphi(M)}$ contains normal vector fields on embedded lines, where there are at least two linearly independent normal vectors for each point on $\varphi([0,1])$. On the other hand, $\mathcal{T}_{\varphi(M)}$ consists of vector fields tangential to the curve $\varphi([0,1])$, which vanish on its end points $\partial\varphi([0,1]) = \{\varphi(0), \varphi(1)\}$.*

The classical Hadamard-Zolésio theorem 7 is generalized in [173, Thm. 5.5] for shapes being bounded and topologically closed C^{k+1}-submanifolds of $\mathbb{R}^{n+1}$ with nonempty interior. For the case of C^∞-shapes and an objective $\mathfrak{J}$ with shape functionality, i.e. vanishing tangential component of the pre-shape derivative as by theorem 9, the results of [173, Cor. 4.2] coincide with theorem 9.

Remark 6 (Shape Functionality and Vanishing Tangential Pre-Shape Derivative Component are not Equivalent)**.** *In theorem 9 (iii) we see, that shape functionality implies that the pre-shape and shape derivatives coincide. Perhaps surprisingly, the opposite is not true in general. Vanishing tangential component of pre-shape derivatives do not imply shape functionality of pre-shape functionals $\mathfrak{J}$. Only the slightly weaker notion of locally constant pre-shape functionals $\mathfrak{J}$ described in theorem 9 (iv) holds. The issue stems from the peculiar fact, that orientable, connected manifolds M can give rise to multiple connected components of $\mathrm{Diff}(M)$. For the cases $M \in \{S^1, S^2, S^3\}$, these correspond to orientation preserving and reversing diffeomorphisms of M (cf. [111, Ch. 15]), which we have used at the end of the proof for theorem 9 (iv). The existence of multiple connected components in $\mathrm{Diff}(M)$ makes fibers in $\mathrm{Emb}(M, \mathbb{R}^{n+1})$ non-connected. For $n = 1$ and M without boundary, the only permitted case is S^1 (cf. [58]), for which the last assertion of theorem 9 (iv) holds.*

The more general case is way more complex, and multiple connected components can indeed arise. Even for orientable, connected, compact surfaces the situation regarding their diffeomorphism group $\mathrm{Diff}(M)$ is non-trivial and needs sophisticated techniques, such as mapping class groups and the Nielsen-Thurston-Classification theorem (cf. [51]). The situation for diffeomorphism groups of manifolds with dimension greater two is still not completely understood, and subject of extensive research at the time writing this work. Also, for dimensions $n \geq 3$ there are cases of closed and orientable M, where no orientation reversing diffeomorphisms exist (cf. [136]). This makes the situation for $\mathrm{Diff}(M)$ even more obscure. However, this phenomenon does not occur in dimensions $n \leq 2$.

The peculiarity regarding connected components of $\mathrm{Diff}(M)$, and thus of fibers in $\mathrm{Emb}(M, \mathbb{R}^{n+1})$, plays a role in the design of numerical techniques. Non-appropriate construction of $\mathfrak{J}$ or initialization of pre-shape optimization routines leads to mesh iterates, which leave the starting component of their fibers in $\mathrm{Emb}(M, \mathbb{R}^{n+1}) \subset \mathrm{Imm}(M, \mathbb{R}^{n+1})$ to reach optimality. For example, this happens when covariant derivatives are assembled without care for coherent orientation of local tangential orthonormal bases. The pre-shapes thus become true immersions, which at the discrete level materializes in self intersections of the mesh. This can finally lead to destruction of the mesh, rendering it useless for further computations.

In numerical applications, we give remedy to this by staying on the connected component of the identity. As M is considered a subset of the hold-all domain, the initial mesh of the starting shape can be interpreted as the trivial embedding (cf. remark 2). Therefore, by choosing small step sizes for mesh morphing and prohibiting self-intersecting mesh configurations, it is guaranteed that we stay on the connected component of the identity.

Remark 7 (Impact of the C^∞-Setting)**.** *The general version of the Hadamard-Zolésio theorem 7 is formulated in the context of C^k-regularity for shapes and according C^{k+1}-vector fields V on the hold-all domain (cf. [42, Ch. 9.3.4]). Since $C^{k+1}(\mathbb{R}^{n+1}, \mathbb{R}^{n+1})$ are Banach spaces, working with their continuous duals is convenient, as the authors of [42] display. Their resulting structure theorem states existence of distributions of certain finite order (cf. [42, Ch. 9.3.4, Rem. 3.1]). Hence a version of the pre-shape derivative structure theorem 9 (i) and (ii) for directions from the Banach spaces $C^k(\mathbb{R}^{n+1}, \mathbb{R}^{n+1})$ holds with an analogous proof, with adaptation of definition 16 to respective directions.*

The formulations used in the pre-shape derivative structure equation (4.36) *are partly owed to the unbounded domain* $\mathbb{R}^{n+1}$ *for vector fields* V *in the* C^∞*-setting. The continuous and linear functional* $\mathfrak{DJ}(\varphi)$ *takes arguments from the Fréchet space* $C^\infty(\mathbb{R}^{n+1},\mathbb{R}^{n+1})$ *equipped with the topology induced by the semi-norms of* $C^k(\mathbb{R}^{n+1},\mathbb{R}^{n+1})$*. From the discussion in [89, Thm. 2.3.1], we know that the set of distributions with compact support* $\mathcal{D}'(\mathbb{R}^{n+1},\mathbb{R}^{n+1})$ *is identical to the continuous dual space of* $C^\infty(\mathbb{R}^{n+1},\mathbb{R}^{n+1})$ *with the strong topology defined by the respective semi-norms. The first part of the proof of (ii) justifies to call* $\mathfrak{DJ}$ *a distribution in the sense of Hörmander [89, Def. 2.1.1]. It is permissible, since* $\mathfrak{DJ}$ *can be restricted to* $C_c^\infty(\mathbb{R}^{n+1},\mathbb{R}^{n+1})$ *due to its compact support on the shape* $\varphi(M)$ *proved in relation* (4.35) *of (i). To sharpen cautiousness of the reader, we emphasize that the continuous dual of* $C^\infty(\mathbb{R}^{n+1},\mathbb{R}^{n+1})$ *has no dual norm analogue as in Banach spaces, does neither form a Banach space, nor a Fréchet space with its weak*-topology, and is not metrizable. In general, the pre-shape derivative* $\mathfrak{DJ}(\varphi)$ *cannot be represented via integrals on* $\varphi(M)$ *similar to the boundary formulation equation* (3.6)*.*

The combined use of material and shape derivatives found in classical shape optimization and structural sensitivity analysis literature (cf. [17, Def. 1, Def. 2], [96, Ch. 3.3.1]) showed useful for practical calculations. In particular, through the application of material derivatives, it is often straightforward to derive closed expressions for shape derivatives of integral quantities. Our next task is to extend the notion of material derivatives from the classical context to pre-shapes, and to formulate calculus rules which harness their benefits.

Definition 17 (Pre-Shape Material Derivative)**.** *Let* $M \subset \mathbb{R}^{n+1}$ *be a compact, connected and oriented* n*-dimensional* C^∞*-manifold. Consider a family of functions* $\{f_\varphi\colon \mathbb{R}^{n+1} \to \mathbb{R}\}_{\varphi\in\mathrm{Emb}(M,\mathbb{R}^{n+1})}$*. For a direction* $V \in C^\infty(\mathbb{R}^{n+1},\mathbb{R}^{n+1})$*, we define the* pre-shape material derivative *in* $x_0 \in \mathbb{R}^{n+1}$ *by*

$$\mathfrak{D}_m f(\varphi)[V](x_0) := \frac{\mathrm{d}}{\mathrm{d}t}_{|t=0} f_{\varphi_t}(x_t), \tag{4.49}$$

if the limit exists. Here, φ_t *is the perturbation of identity for pre-shapes (cf. equation* (4.24)*), and* $x_t = x_0 + t\cdot V(x_0)$ *is a perturbed point.*

The careful reader might notice the similarity of classical shape and pre-shape material derivatives. However, the main difference is a possible dependence of functions f on parameterizations of shapes and domains they are defined for. This is expressed by the larger index class for the family $\{f_\varphi\}_{\varphi\in\mathrm{Emb}(M,\mathbb{R}^{n+1})}$. In contrast, only families with smaller index classes $\{f_\Gamma\}_{\Gamma\in B_e^n}$ are permitted for classical material derivatives. Still, both notions coincide if the pre-shape functional has shape functionality, as we see in the upcoming corollary 1 resulting from structure theorem 9.

Remark 8 (Pre-Shape Material Derivatives under Weaker Assumptions)**.** *The definition of the material derivative can be generalized to functions and domains of weaker regularity, such as Sobolev functions and open subset* $\Omega \subset \mathbb{R}^{n+1}$ *with Lipschitz boundaries. A necessity for this comes from the fact, that state solutions from PDE-constrained shape optimization problems need a well-defined material derivative for sensitivity analysis to be applicable. This can be done in the same manner as with the classical shape material derivative (cf. [96, p. 111]). Also, the family* $\{f_\varphi\colon \mathbb{R}^{n+1} \to \mathbb{R}\}_{\varphi\in\mathrm{Emb}(M,\mathbb{R}^{n+1})}$ *does not need to be defined for all* $\varphi \in \mathrm{Emb}(M,\mathbb{R}^{n+1})$*, but only in an open neighborhood of a* φ_0*. The neighborhood solely needs to contain the set of all perturbations* φ_t *of* φ_0 *generated by* $V \in C^\infty(\mathbb{R}^{n+1},\mathbb{R}^{n+1})$ *for sufficiently small* $t > 0$*, for which the material derivative is taken.*

Remark 9 (Relating Pre-Shape Material and Pre-Shape Derivatives)**.** *It is important that the family* $\{f_\varphi \colon \mathbb{R}^{n+1} \to \mathbb{R}\}_{\varphi \in \mathrm{Emb}(M,\mathbb{R}^{n+1})}$ *can be seen as a function* $f \colon \mathrm{Emb}(M,\mathbb{R}^{n+1}) \times \mathbb{R}^{n+1} \to \mathbb{R}$*. Thus the pre-shape material derivative defined in equation* (4.49) *is the total derivative of the one parameter family* $f(\varphi_t, x_t)$*. In the first component, the perturbation of identity for pre-shapes comes into play, which differs from the classical shape material derivative. By application of the chain rule, this leads to the decomposition of pre-shape material derivatives*

$$\mathfrak{D}_m f(\varphi)[V] = \mathfrak{D} f(\varphi)[V] + \nabla f_\varphi^T V, \tag{4.50}$$

where $\mathfrak{D} f(\varphi)[V]$ *is the pre-shape derivative of* f *in* φ *in direction* V*. It is an extension of the classical material derivative formula, for example given by Haslinger and Mäkinen in [96, p. 111, (3.39)].*

Before we examine some exemplary pre-shape derivatives and their decompositions, we formulate a simple corollary, which connects classical material derivatives to their pre-shape versions.

Corollary 1 (Decomposition of Pre-Shape Material Derivatives)**.**
Let $f \colon \mathrm{Emb}(M,\mathbb{R}^{n+1}) \times \mathbb{R}^{n+1} \to \mathbb{R}$ *be pre-shape differentiable in the first and smooth in the second argument. Fix* $\varphi \in \mathrm{Emb}(M,\mathbb{R}^{n+1})$ *and* $V \in C^\infty(\mathbb{R}^{n+1},\mathbb{R}^{n+1})$*. Then the pre-shape material derivative decomposes to*

$$\mathfrak{D}_m f(\varphi)[V] = \langle g^{\mathcal{N}}, V \rangle + \langle g^{\mathcal{T}}, V \rangle + \nabla f_\varphi^T V, \tag{4.51}$$

where $g^{\mathcal{N}}$ *and* $g^{\mathcal{T}}$ *are distributions with supports as in relation* (4.37) *and* (4.38)*. If* f *has shape functionality, then the corresponding shape dependent function* $\tilde{f} \colon B_e \times \mathbb{R}^{n+1} \to \mathbb{R}$ *satisfies*

$$\mathfrak{D}_m f(\varphi)[V] = \mathcal{D}_m \tilde{f}\big(\pi(\varphi)\big)[V] \tag{4.52}$$

for all $\varphi \in \mathrm{Emb}(M,\mathbb{R}^{n+1})$*. In this case, the pre-shape and classical material derivative coincide.*

Lastly, suppose $\tilde{f} \colon B_e \times \mathbb{R}^{n+1} \to \mathbb{R}$ *is shape differentiable in the first argument. Then it is also pre-shape differentiable, and its pre-shape material derivative is equivalent to its classical material derivative.*

Proof. To get equation (4.51), we simply use formula (4.50) and apply decomposition (4.36) from the structure theorem 9 to the occurring pre-shape derivatives for fixed $x_0 \in \mathbb{R}^{n+1}$.

Assume f has shape functionality in the first argument (cf. definition 15). Its corresponding shape function is given by $\tilde{f} \colon B_e^n \times \mathbb{R}^{n+1} \to \mathbb{R}$ with $f(\cdot,\cdot) = \tilde{f}(\pi(\cdot),\cdot)$. We can now apply part (iii) of theorem 9 to decomposition equation (4.51) and see

$$\mathfrak{D}_m f(\varphi)[V] = \langle g^{\mathcal{N}}, V \rangle + \nabla f_\varphi^T V. \tag{4.53}$$

Since $g^{\mathcal{N}}$ corresponds to the distribution from the classical Hadamard theorem, the right-hand side of equation (4.53) equals the classical material derivative $\mathcal{D}_m \tilde{f}(\pi(\varphi))[V]$.

For the last part, assume $\tilde{f} \colon B_e^n \times \mathbb{R}^{n+1} \to \mathbb{R}$ is shape differentiable. From proposition 2 we know that the pre-shape extension $\tilde{f}(\pi(\cdot),\cdot)$ is indeed pre-shape differentiable. Also, $\tilde{f}(\pi(\cdot),\cdot)$ has shape functionality by construction. So we can apply the previous arguments to see equation (4.52), which shows the last assertion. □

Structure theorem 9, proposition 2 and corollary 1 guarantee validity of classical shape calculus formulae and results in the context of pre-shapes. Pre-shape calculus can be applied to objects from shape optimization, if they are associated with their

corresponding pre-shape counterparts. This leads to the same derivatives, and thus optimization methods. Even further, it is possible to apply pre-shape calculus to mixed shape and pre-shape problems, where the shape part is treated just as if shape calculus was applied. The key difference is, that a pre-shape component would otherwise be non-accessible. In the following, we show some simple examples. Technically more involved applications follow in chapter 5 and thereafter.

Example 1 For a fixed target pre-shape $\bar{\varphi} \in \mathrm{Emb}(S^1, \mathbb{R}^2)$, let us define a pre-shape optimization problem by

$$\min_{\varphi \in \mathrm{Emb}(S^1,\mathbb{R}^2)} \frac{1}{2} \int_{S^1} |\varphi(s) - \bar{\varphi}(s)|^2 \, \mathrm{d}s \;=: \mathfrak{J}(\varphi). \tag{4.54}$$

The pre-shape functional $\mathfrak{J}$ measures the difference of a target $\bar{\varphi}$ to another parameterized shape φ.

Its pre-shape derivative can be calculated for directions $V \in C^\infty(\mathbb{R}^2, \mathbb{R}^2)$ by elementary techniques

$$\begin{aligned} \mathfrak{D}\mathfrak{J}(\varphi)[V] &= \frac{\mathrm{d}}{\mathrm{d}t}_{|t=0} \frac{1}{2} \int_{S^1} |\varphi_t - \bar{\varphi}|^2 \, \mathrm{d}s \\ &= \frac{1}{2} \int_{S^1} \frac{\mathrm{d}}{\mathrm{d}t}_{|t=0} \langle \varphi + t \cdot V \circ \varphi - \bar{\varphi}, \varphi + t \cdot V \circ \varphi - \bar{\varphi} \rangle_2 \, \mathrm{d}s \\ &= \int_{S^1} \langle \varphi - \bar{\varphi}, V \circ \varphi \rangle_2 \, \mathrm{d}s. \end{aligned} \tag{4.55}$$

We can choose S^1 with canonical parameterization as a starting pre-shape by considering

$$\varphi_{id} \colon S^1 \subset \mathbb{R}^2 \to \mathbb{R}^2, \;\; \begin{pmatrix} x_1 \\ x_2 \end{pmatrix} \mapsto \begin{pmatrix} x_1 \\ x_2 \end{pmatrix}. \tag{4.56}$$

In order to formulate the decomposition as in equation (4.36) of the structure theorem, we need the outer unit normal vector field and an oriented unit tangential vector field, which for S^1 are given by

$$n \colon S^1 \to \mathbb{R}^2, \;\; \begin{pmatrix} x_1 \\ x_2 \end{pmatrix} \mapsto \begin{pmatrix} x_1 \\ x_2 \end{pmatrix}, \qquad \tau \colon S^1 \to \mathbb{R}^2, \;\; \begin{pmatrix} x_1 \\ x_2 \end{pmatrix} \mapsto \begin{pmatrix} -x_2 \\ x_1 \end{pmatrix}. \tag{4.57}$$

Now we can examine the problem for several different parameterized target shapes $\bar{\varphi} \in \mathrm{Emb}(S^1, \mathbb{R}^2)$. First, we can consider rescaling by a factor $\alpha \in (0, \infty)$, which lets S^1 contract or expand. The according target is given by

$$\bar{\varphi} \colon S^1 \to \mathbb{R}^2, \;\; \begin{pmatrix} x_1 \\ x_2 \end{pmatrix} \mapsto \alpha \cdot \begin{pmatrix} x_1 \\ x_2 \end{pmatrix}. \tag{4.58}$$

Using equation (4.55), the pre-shape derivative at the identity becomes

$$\mathfrak{D}\mathfrak{J}(\varphi_{id})[V] = \int_{S^1} (1 - \alpha) \cdot \langle n, V \rangle_2 \, \mathrm{d}s. \tag{4.59}$$

This shows that rescaling of S^1 has vanishing parameterization part $g^{\mathcal{T}} = 0$, whereas the remaining shape component $g^{\mathcal{N}}$ is in the style of the classical Hadamard-Zolésio representation given above. In particular, only vector fields V acting in normal direction are supported.

Next, let us consider a rotation of the circle. For this, we let $\alpha \in [0, 2\pi)$ and consider target rotations

$$\bar{\varphi} \colon S^1 \to \mathbb{R}^2, \;\; \begin{pmatrix} x_1 \\ x_2 \end{pmatrix} \mapsto \begin{pmatrix} \cos(\alpha) & -\sin(\alpha) \\ \sin(\alpha) & \cos(\alpha) \end{pmatrix} \begin{pmatrix} x_1 \\ x_2 \end{pmatrix}. \tag{4.60}$$

Plugging this into equation (4.55) and doing some reformulations, the according decomposition becomes

$$\mathfrak{DJ}(\varphi_{id})[V] = \int_{S^1} \big(1 - \cos(\alpha)\big) \cdot \langle n, V\rangle_2 \, \mathrm{d}s + \int_{S^1} \sin(\alpha) \cdot \langle \tau, V\rangle_2 \, \mathrm{d}s. \tag{4.61}$$

Here we see both components of the pre-shape derivative decomposition. The first corresponds to the horizontal part $g^{\mathcal{N}}$, and the second to the vertical part $g^{\mathcal{T}}$. Notice that the horizontal component vanishes exactly for trivial rotations, whereas the vertical one also vanishes for the reflection at origin in case $\alpha = \pi$.

Finally, we can translate S^1 by some fixed $z \in \mathbb{R}^2$, which gives a target

$$\bar{\varphi}\colon S^1 \to \mathbb{R}^2, \ \begin{pmatrix} x_1 \\ x_2 \end{pmatrix} \mapsto \begin{pmatrix} x_1 \\ x_2 \end{pmatrix} + z. \tag{4.62}$$

The decomposition of the pre-shape derivative at the identity becomes

$$\mathfrak{DJ}(\varphi_{id})[V] = \int_{S^1} \langle n, z\rangle_2 \cdot \langle n, V\rangle_2 \, \mathrm{d}s + \int_{S^1} \langle \tau, z\rangle_2 \cdot \langle \tau, V\rangle_2 \, \mathrm{d}s, \tag{4.63}$$

where the decomposition into $g^{\mathcal{N}}$ and $g^{\mathcal{T}}$ depends on normal and tangential components of z on S^1.

Remark 10 (Pre-Shape Material Derivatives on Moving Boundaries)**.** *The use of pre-shape material derivatives makes sense for families of differentiable functions on varying domains $\{f_\varphi\colon \varphi(M) \to \mathbb{R}\}_{\varphi \in \mathrm{Emb}(M,\mathbb{R}^{n+1})}$ depending smoothly on φ. This works, since the term $f_{\varphi_t}(x_t)$ involved in the limit $\mathfrak{D}_m f(\varphi)[V]$ is well-defined. For an $x_0 \in \varphi(M)$, an easy check with definition 16 of the perturbation of identity for pre-shapes shows*

$$x_t = x_0 + t \cdot V(x_0) = \varphi\big(\varphi^{-1}(x_0)\big) + t \cdot V \circ \varphi\big(\varphi^{-1}(x_0)\big) = \varphi_t\big(\varphi^{-1}(x_0)\big) \in \varphi_t(M). \tag{4.64}$$

However, in this case there is no decomposition for $\mathfrak{D}_m f(\varphi)$ as in equation (4.50), since $x_t \notin \varphi(M)$ and $x_0 \notin \varphi_t(M)$ in general. Nevertheless, it remains possible to derive closed formulae for these types of material derivatives in some cases, which we achieve in section 5.3.

Next, we give a summary of several useful pre-shape calculus rules. For this, we remind the reader that the tangential divergence for an n-dimensional smooth submanifold $M \subset \mathbb{R}^{n+1}$ is defined as (cf. [42, Ch. 9.5.2])

$$\mathrm{div}_\Gamma\colon C^\infty(\mathbb{R}^{n+1}, \mathbb{R}^{n+1}) \to C^\infty(M, \mathbb{R}), \ V \mapsto \mathrm{div}(V)_{|M} - \langle DVn, n\rangle_2, \tag{4.65}$$

where n is the outer unit normal vector field on M. Due to proposition 2 and corollary 1, the following rules are also true for shape derivatives and shape functionals.

Corollary 2 (Pre-Shape Calculus Rules)**.** *Let $f, g\colon \mathrm{Emb}(M, \mathbb{R}^{n+1}) \times \mathbb{R}^{n+1} \to \mathbb{R}$ be pre-shape differentiable in the first and smooth in the second argument, and let $h\colon \mathbb{R} \to \mathbb{R}$ be smooth. Let $\Omega \subseteq \mathbb{R}^{n+1}$ be an open, bounded domain with Lipschitz boundary, and let Γ be an n-dimensional C^∞-submanifold of $\mathbb{R}^{n+1}$. Consider $\varphi \in \mathrm{Emb}(M, \mathbb{R}^{n+1})$ and $V \in C^\infty(\mathbb{R}^{n+1}, \mathbb{R}^{n+1})$. Then the following rules for pre-shape*

and material derivatives apply

$$
\begin{aligned}
&(i) && \mathfrak{D}_m f(\varphi)[V] && = \mathfrak{D} f(\varphi)[V] + \nabla f_\varphi^T V \\
&(ii) && \mathfrak{D}_m (f \cdot g)(\varphi)[V] && = \mathfrak{D}_m f(\varphi)[V] \cdot g_\varphi + f_\varphi \cdot \mathfrak{D}_m g(\varphi)[V] \\
&(iii) && \mathfrak{D}_m (h \circ f)(\varphi)[V] && = Dh(f_\varphi) \mathfrak{D}_m f(\varphi)[V] \\
&(iv) && \mathfrak{D}\left(\int_\Omega f_\varphi \, \mathrm{d}x \right)[V] && = \int_\Omega \mathfrak{D}_m f(\varphi)[V] + \operatorname{div}(V) \cdot f_\varphi \, \mathrm{d}x \\
& && && = \int_\Omega \mathfrak{D} f(\varphi)[V] \, \mathrm{d}x + \int_{\partial\Omega} f_\varphi \cdot \langle n, V \rangle_2 \, \mathrm{d}s \\
&(v) && \mathfrak{D}\left(\int_\Gamma f_\varphi \, \mathrm{d}s \right)[V] && = \int_\Gamma \mathfrak{D}_m f(\varphi)[V] + \operatorname{div}_\Gamma(V) \cdot f_\varphi \, \mathrm{d}s \\
&(vi) && \mathfrak{D}_m \big(\nabla f_\varphi \big)[V] && = \nabla \Big(\mathfrak{D}_m f(\varphi)[V] \Big) - \nabla V^T \nabla f_\varphi
\end{aligned}
$$

with $\operatorname{div}_\Gamma(V)$ *being the tangential divergence of* V *on* Γ.

Proof. Let the assumptions stated above hold. Identity (i) was already discussed in corollary 1.

The product and chain rule (ii) and (iii) are simple consequences of the definition of the pre-shape material derivative in equation (4.49).

For (iv), the conditions for [77, Thm. 5.2.2] apply by considering $f_{\varphi_t}(x_t)$ as a function of $t \geq 0$. Alternatively, since we assumed Lipschitz boundary for Ω, the change of variable formula is applicable, and the standard proof found in [96, p. 112, Lem. 3.3] can be used as well.

For (v), computations as in [77, Thm. 5.4.17] or [42, Ch. 9.4, Thm. 4.3] can be made.

For (vi), the calculations for [17, Ch. 4, Eq. 2.14] give the desired equality. □

Remark 11 (Weakening Assumptions for Pre-Shape Calculus Rules)**.** *The formulae provided in corollary 2 hold in greater generality.*

In particular, the chain rule (iii) can be stated for Fréchet differentiable operators h on Banach spaces of continuous functions with help of [42, Ch. 9, Thm. 2.5]. However, care must be taken if structure theorems and resulting calculus rules are derived (cf. remark 7).

The first equality of formula (iv) for volume integrals can be stated for Ω which are merely measurable, and pre-shape differentiable families of class $\{f_\varphi \in W^{1,1}(\mathbb{R}^{n+1}, \mathbb{R})\}_{\varphi \in \mathrm{Emb}(M, \mathbb{R}^{n+1})}$ by use of [77, Thm. 5.2.2]. However, the second equality in (iv) requires Ω to be an open set with Lipschitz boundary (cf. [77, Ch. 5.3.2, Rmk.]).

Formula (v) for boundary integrals can be generalized to compact submanifolds $\Gamma \subset \mathbb{R}^{n+1}$ of C^1-regularity and pre-shape differentiable families of class $\{f_\varphi \in W^{1,1}(\mathbb{R}^{n+1}, \mathbb{R})\}_{\varphi \in \mathrm{Emb}(M, \mathbb{R}^{n+1})}$ by use of [77, Thm. 5.4.17].

Finally, (vi) also applies to functions f_φ of Sobolev-regularity. For this, the definition of the pre-shape material derivative needs to be adapted, e.g. as in [96, p. 111]. Notice that in this generality, it is additionally necessary that pre-shape material derivatives have weak derivatives, e.g. by requiring $\mathfrak{D}_m(f_\varphi)[V] \in W^{1,1}(\mathbb{R}^{n+1}, \mathbb{R})$.

So far, we have considered first order pre-shape derivatives. It is of course possible to extend this concept to higher order pre-shape derivatives. In particular, we introduce and derive a pre-shape Hessian for an elaborate example in section 5.5.

Chapter 5

The Pre-Shape Parameterization Tracking Problem

Our completed general study of pre-shape spaces and their calculus in chapter 4 provides us with the necessary tools to discuss the main model problem class of this work. The aim of this chapter is to introduce and study the so-called class of *pre-shape parameterization tracking problems* posed in $\mathrm{Emb}(M, \mathbb{R}^{n+1})$. This problem class enables us to adapt the overall cell volume distribution of meshes representing various shapes and hold-all domains. The target cell volumes are allowed to be non-uniform, and are specifiable via functions f. Throughout this chapter, we study the parameterization tracking problem class without combined application to shape optimization problems. Later chapters build on this, and apply the parameterization tracking problem to simultaneously optimize mesh quality, while solving shape optimization problems in pre-shape spaces. We emphasize, that the techniques we develop do not involve changes in mesh topologies, and particularly avoid remeshing or mesh refinements. However, they can be combined with refinement and remeshing approaches.

We motivate the problem class in the special case of 1-dimensional shapes, then we state the general version of the *pre-shape parameterization tracking functional* in the ambient space $\mathbb{R}^{n+1}$. An existence result is formulated, where non-unique solutions to parameterization tracking can be found in every fiber of $\mathrm{Emb}(M, \mathbb{R}^{n+1})$. We also discuss a generalization for arbitrary codimension shapes in nonlinear ambient spaces. The characterization of solutions is deepened in section 5.2.2, where we relate non-unique optimal parameterizations of a fixed shape by use of flows obeying Euler-Arnold equations on the shape. As a necessary pre-requisite for this characterization, we provide additional decompositions of pre-shape spaces $\mathrm{Emb}(M, \mathbb{R}^{n+1})$ and their tangential bundle structures. Once this is done, we start using our pre-shape calculus tools developed in chapter 4. We derive the pre-shape derivative of the parameterization tracking problem in section 5.3, which turns out to provide sufficient conditions for global optimality. This also serves as an example of a non-trivial problem, whose pre-shape derivative is not a classical shape derivative, and thus not tractable by shape calculus. The pre-shape derivative decomposition in light of structure theorem 9 is given, and connection of its components to deformation methods and minimal surfaces is discussed. Some first numerical implementations of parameterization tracking without application to shape optimization problems are highlighted in section 5.4. Going one step further in section 5.5, we give a closed form of the pre-shape Hessian, particularly in solutions.

5.1 Introduction and Existence of Solutions to Parameterization Tracking

In this section we define the pre-shape parameterization tracking problem, and give sufficient conditions for existence of solutions in each fiber of the pre-shape space. A main goal of this work is to construct regularizations for shape optimization routines, which enable us to control the quality of meshes involved. Hence we want to achieve generality of the classes of pre-shapes for which our techniques apply. In particular, existence of boundaries, dimensions of meshes, i.e. applicability to volume or surface manifolds, should be no limitations. At the end of this section, we discuss a possible generalization of parameterization tracking for shapes with arbitrary codimension and boundaries embedded in open manifolds as ambient spaces.

Before proposing a pre-shape parameterization tracking problem in $\mathbb{R}^{n+1}$, we introduce an equivalent problem for the special case $\mathrm{Emb}(S^1, \mathbb{R}^2)$ of the unit circle embedded in the plane $\mathbb{R}^2$ and the associated space of shapes B_e^1. We then introduce necessary structures to generalize this problem for embeddings of n-dimensional, orientable, connected and compact manifolds $M \subset \mathbb{R}^{n+1}$, possibly with nonempty boundary ∂M.

Our approach for the simple case $\mathrm{Emb}(S^1, \mathbb{R}^2)$ is motivated by several studies on shape analysis for curves in Euclidean spaces (cf. [170, 177, 99]). The authors of [170] construct metrics and corresponding geodesics on spaces of open and closed curves in $\mathbb{R}^{n+1}$. They rely on the so-called square-root velocity representation $\dot\gamma/\sqrt{|\dot\gamma|}$ of a given curve $\gamma\colon I \to \mathbb{R}^{n+1}$ on a parameter interval $I \subset \mathbb{R}$. The motivational insight for this technique is that γ is defined up to translation by its unit speed vector $\dot\gamma/|\dot\gamma|$ and speed $|\dot\gamma|$ (cf. [170, Ch. III. A.], [110, Def. 4.3]). Both quantities uniquely determine $\dot\gamma$.

At first glance, it might seem appropriate to track parameterizations directly, e.g. as in example 1 of section 4.2. It turns out not to be feasible to directly track a parameterization. Instead, we focus on $|\dot\gamma|$ as a proxy for parameterizations, since do not want to change the associated shape. If we specify a family of target speeds or elastic parts $f_\gamma \in C^\infty(S^1, (0,\infty))$, which we let depend on the parameterized shape γ, an according tracking type problem takes the form

$$\min_{\gamma \in \mathrm{Emb}(S^1,\mathbb{R}^2)} \frac{1}{2} \int_{S^1} \Big(|\dot\gamma(s)| - f_\gamma(s) \Big)^2 \,\mathrm{d}s. \tag{5.1}$$

If f_γ is chosen fixed for each fiber, i.e. to be given for each shape a priori, the underlying shape of γ is not relevant for minimizing problem (5.1). This comes from the observation that only scaling of the speed direction $\dot\gamma$ is mandatory to match f_γ. The direction modulo scaling is determined by the shape of $\gamma(S^1)$, which we want to remain invariant. In general, the objective of problem (5.1) does not possess shape functionality. Also, it has optimal values for each possible shape $\gamma(S^1)$ represented as $\pi(\gamma) \in B_e^1$. These are desirable properties for combining problem (5.1) with classical shape optimization objectives, because solving problem (5.1) can give a pre-shape in the fiber of the optimal shape of the classical shape objective.

Before we further elaborate on this, we introduce necessary vocabulary and notation to generalize problem (5.1) to $\mathrm{Emb}(M, \mathbb{R}^{n+1})$ for more general M.

First, we introduce the concept of *local frames*, which are local orthonormal bases of tangential vectors on M (cf. [111, Ch. 8]). For an open subset $U \subseteq M$, a smooth local frame is a tuple of $\dim(M)$ tangential vector fields $\tau := (\tau_1, \dots, \tau_n)$, such that for each $p \in U$, the tangential vectors $\tau_i(p) \in T_pM$ are linearly independent. In case of manifold M with boundary, the subset U is relatively open, and a chart takes it diffeomorphically to the upper half space $\mathbb{H}^n \subset \mathbb{R}^n$. If we have a Riemannian metric on M, e.g. a metric induced by the Euclidean metric of the ambient space for

submanifolds $M \subset \mathbb{R}^{n+1}$, then we can additionally demand $\tau(p) = (\tau_1(p), \dots, \tau_n(p))$ to be orthonormal with respect to the Riemannian metric for all $p \in U$. In this case we call the frame $(\tau_1, \dots, \tau_n)$ a *local orthonormal frame*. Note that local orthonormal frames always exist, by application of the Gram-Schmidt algorithm in tangential spaces (cf. [111, Lem. 8.13]).

To achieve a natural and numerically tractable formulation of the pre-shape parameterization tracking problem, we also introduce the *covariant derivative*. For this, we use similar definitions as in [42, Ch. 9.5.6], which we modify to our situation using local orthonormal frames. Given a $\varphi \in \mathrm{Emb}(M, \mathbb{R}^{n+1})$, let $\tau \colon U \to (TM)^n$ be a smooth local orthonormal frame on $U \subseteq M$, and let $\tau^\varphi \colon V \to (T\varphi(M))^n$ be a local orthonormal frame on $V \subseteq \varphi(M)$. Without loss of generality, we can assume $V = \varphi(U)$, since we can choose $V \cap \varphi(U)$. Then we define the local covariant derivative representation for φ in $p \in U$ under choice of frames τ and τ^φ by

$$D^\tau \varphi_{|U}(p) := \begin{pmatrix} \left\langle D\varphi\tau_1(p), \tau_1^\varphi\big(\varphi(p)\big)\right\rangle_2 & \dots & \left\langle D\varphi\tau_n(p), \tau_1^\varphi\big(\varphi(p)\big)\right\rangle_2 \\ \vdots & \ddots & \vdots \\ \left\langle D\varphi\tau_1(p), \tau_n^\varphi\big(\varphi(p)\big)\right\rangle_2 & \dots & \left\langle D\varphi\tau_n(p), \tau_n^\varphi\big(\varphi(p)\big)\right\rangle_2 \end{pmatrix}, \tag{5.2}$$

where $D\varphi$ is the Jacobian matrix of φ and $\langle \cdot, \cdot \rangle_2$ the Euclidean scalar product of $\mathbb{R}^{n+1}$. For $p \in \partial M$, we remind the reader that the tangential space T_pM is $\dim(M)$ dimensional, and not $\dim(M) - 1$ dimensional (cf. [111, Prop. 10.4]). This is simply due to the definition of tangential vectors via curves on M, which in particular means that the outward pointing normal vector $n_M(p)$ is in T_pM for $p \in \partial M$. Note that such a $n_M(p)$ always exists and is unique (cf. [111, Prop. 15.33]). Hence a local orthonormal basis of a frame in vicinity of ∂M may look like $(\tau_1(p), \dots, \tau_{n-1}(p), n_M(p))$ if evaluated in $p \in \partial M$.

We also want to make clear that the covariant derivative $D^\tau\varphi$ should not be mistaken for the tangential derivative $D_\Gamma\varphi$, which is given via outer unit normal vector fields n^M on M as (cf. [42, Ch. 9.5.2])

$$D_\Gamma\varphi = D\varphi - D\varphi n^M \big(n^M\big)^T. \tag{5.3}$$

In elementary terms, the covariant derivative $D^\tau\varphi$ of a map $\varphi \colon M \subset \mathbb{R}^{n+1} \to \mathbb{R}^{n+1}$ can be locally derived by changing bases representing the Jacobian $D\varphi$ to $(\tau_1, \dots, \tau_n, n^M)$ and $(\tau_1^\varphi, \dots, \tau_n^\varphi, n^{\varphi(M)})$, and then crossing out row $n+1$ and column $n+1$. Here, n^M and $n^{\varphi(M)}$ are outer unit normal vector fields with respect to M and $\varphi(M)$, which must not be confused with outward pointing normal vectors n_M and $n_{\varphi(M)}$ on boundaries ∂M and $\partial\varphi(M)$.

Using the introduced notation, we can now reformulate tangential speed tracking problem (5.1). It is useful to associate parameterizations of a $\gamma \in \mathrm{Emb}(S^1, \mathbb{R}^2)$ to its velocity vector field in direction of a unit tangential vector field $\tau \in C^\infty(S^1, TS^1)$ with appropriate sign via

$$\dot\gamma(s) = D\gamma(s)\tau(s) \quad \forall s \in S^1. \tag{5.4}$$

The choice of a smooth section of unit tangents is not unique, and essentially corresponds to the choice of an orientation for the curve $\Gamma(\gamma)$. For higher dimensional shapes, the situation regarding choice of unit tangential vector fields is further complicated, see remark 6. Since determinants act trivially in dimension 1, we can rephrase the functional from problem (5.1) by using equation (5.4) and the local representation of covariant derivatives (5.2) with orthonormal frames, to get

$$\int_{S^1} \Big(|\dot\gamma(s)| - f_\gamma(s)\Big)^2 \,\mathrm{d}s = \int_{S^1} \Big(|\det D^\tau\gamma(s)| - f_\gamma(s)\Big)^2 \,\mathrm{d}s. \tag{5.5}$$

Dropping the absolute value for the determinant, this offers a possibility to generalize problem (5.1) to higher dimensional manifolds by using volume forms instead of speed as a proxy to parameterization. For general manifolds, this takes the form of

$$\min_{\varphi\in\mathrm{Emb}(M,\mathbb{R}^{n+1})} \int_M \left(\det D^\tau\varphi(s) - f_\varphi(s)\right)^2 \mathrm{d}s. \tag{5.6}$$

Such a formulation does not resort to perhaps unnatural constructions using multiple speed functions to mimic problem (5.1). Here $f_\varphi\colon M \to \mathbb{R}$ is the coefficient function of the target volume form, which might explicitly depend on $\varphi \in \mathrm{Emb}(M,\mathbb{R}^{n+1})$. Due to the quadratic nature of the objective function in problem (5.6), it is clear that a sufficient condition for optimality is given by

$$\det D^\tau\varphi = f_\varphi. \tag{5.7}$$

Notice, that this can be interpreted as an equality of smooth volume forms as in Moser's theorem 4. For a thorough introduction to differential and volume forms, we refer the reader to [111, Ch. 14-16].

Having numerical implementations in mind, we are also interested in the case where boundaries of shapes ∂M are left pointwise invariant. We define the pre-shape space of embeddings suitable for this as

$$\mathrm{Emb}_{\partial M}\left(M,\mathbb{R}^{n+1}\right) := \left\{ \varphi \in \mathrm{Emb}\left(M,\mathbb{R}^{n+1}\right) :\ \varphi(p) = p \quad \forall p \in \partial M \right\}. \tag{5.8}$$

For numerical routines, this means that a specified boundary ∂M of the starting shape is left fixed, i.e. prohibiting change of the boundary shape and parameterization. The interior of the shape is still allowed to be deformed and to change its parameterization. Vector spaces and tangent bundles appropriate for $\mathrm{Emb}_{\partial M}(M,\mathbb{R}^{n+1})$ consist of vector fields which vanish on the boundary ∂M.

The following reformulation of problem (5.6) is tweaked by two alterations, while still preserving globally optimal solutions analogously. First, we incorporate a positive function $g^M\colon M \to (0,\infty)$, which in practice represents the cell volume distribution of the initial mesh of M. The second alteration formulates the objective functional on shapes $\varphi(M)$ instead of M, which is realized by using pullbacks of inverses φ^{-1}. These act as pushforwards of volume forms from M to $\varphi(M)$. This reformulation makes numerical implementation more convenient, since integrals and pre-shape derivatives can be evaluated on current mesh iterates. The next theorem gives the definition, well-definedness and existence of solutions of the pre-shape parameterization tracking problem.

Theorem 10 (Pre-Shape Parameterization Tracking Problem and Existence Theorem)**.** *Let $M \subset \mathbb{R}^{n+1}$ be an n-dimensional, oriented, connected and compact C^∞-submanifold, possibly with nonempty boundary ∂M of C^∞-regularity. Further, let $g^M\colon M \to (0,\infty)$ and $f_\varphi\colon \varphi(M) \to (0,\infty)$ be C^∞-functions. Let f have shape functionality. Additionally, let*

$$\int_{\varphi(M)} f_\varphi(s)\,\mathrm{d}s = \int_M g^M(s)\,\mathrm{d}s \qquad \forall\varphi \in \mathrm{Emb}\left(M,\mathbb{R}^{n+1}\right). \tag{5.9}$$

Then the optimization problem

$$\min_{\varphi\in\mathrm{Emb}(M,\mathbb{R}^{n+1})} \frac{1}{2}\int_{\varphi(M)} \left(g^M\circ\varphi^{-1}(s)\cdot\det D^\tau\varphi^{-1}(s) - f_\varphi(s)\right)^2 \mathrm{d}s \tag{5.10}$$

is called pre-shape parameterization tracking problem. *It is well-defined and independent of choice of local orthonormal frames τ on M and τ^φ on $\varphi(M)$. There exists a global C^∞-solution to problem* (5.10) *in each fiber $\pi(\varphi)$. For a fixed fiber $\pi(\varphi)$ and a given global solution $\tilde\varphi \in \pi(\varphi)$, the following assertions are equivalent*

(i) $\hat{\varphi} \in \pi(\varphi)$ *is a global solution to* (5.10)

(ii) relations

$$\left(g^M \circ \tilde{\varphi}^{-1}\right) \cdot \det D^\tau \tilde{\varphi}^{-1} = f_\varphi = \left(g^M \circ \hat{\varphi}^{-1}\right) \cdot \det D^\tau \hat{\varphi}^{-1} \quad \text{on } \varphi(M)$$

are fulfilled

(iii) there is a $\rho \in \mathrm{Diff}(\varphi(M))$*, preserving the volume coefficient function* $f_{\tilde{\varphi}}$ *on* $\varphi(M)$*, such that* $\hat{\varphi} = \rho \circ \tilde{\varphi}$ *is a global solution.*

If ∂M *is non-trivial, then for every* $\varphi \in \mathrm{Emb}(M, \mathbb{R}^{n+1})$ *there is a global solution* $\hat{\varphi} \in \pi(\varphi)$*, such that* $\hat{\varphi}_{|\partial M} = \varphi_{|\partial M}$*. In particular, if problem* (5.10) *is stated over the space of embeddings* $\mathrm{Emb}_{\partial M}(M, \mathbb{R}^{n+1})$ *leaving* ∂M *pointwise invariant, all previous statements remain valid.*

Proof. The main ingredient of the existence proof is the Dacorogna-Moser theorem 4, which guarantees existence of solution for equations of pullback-type on manifolds involving volume forms.

Let $M \subset \mathbb{R}^{n+1}$ be an n-dimensional, orientable, connected and compact C^∞-submanifold, possibly with nonempty boundary ∂M of C^∞-regularity. Fix an orientation for M and let $\varphi \in \mathrm{Emb}(M, \mathbb{R}^{n+1})$. Consider local orthonormal frames τ and τ^φ on M and $\varphi(M)$ with respect to the Riemannian metric induced by the Euclidean ambient space. We see that the integrand in problem (5.10) is well-defined. This is due to the embedding property of φ. It is in particular an immersion, which makes $D^\tau \varphi \in \mathrm{GL}(n, \mathbb{R})$ and thus $\det D^\tau \varphi^{-1}$ non-trivial. Independence of choice of orientated local orthonormal bases inducing the covariant derivative is also clear (cf. equation (5.2)), since an orientation preserving change of orthonormal base can be realized by multiplications with orthogonal matrices $\tilde{B}, B \in \mathrm{SO}(n)$. By the determinant product rule, the Jacobian determinant $\det D^\tau \varphi$ remains invariant under such a change of base. Further, if no global orthonormal frame exists, we can use a partition of unity, which covers $\varphi(M)$ with open domains for local orthonormal frames. Then linearity of integrals lets us apply the previous argument about the change of orthonormal bases, which guarantees well-definedness and independence of choice of local orthonormal frames of problem (5.10).

Next, we come to existence of solutions to the pre-shape parameterization problem (5.10) in each fiber $\pi(\varphi)$. Let us fix an arbitrary $\varphi \in \mathrm{Emb}(M, \mathbb{R}^{n+1})$. Since each fiber $\pi(\varphi)$ is isomorphic to the standard fiber $\mathrm{Diff}(M)$, we can without loss of generality assume $\varphi \in \pi(\varphi)$ to be orientation preserving, since we otherwise pick an orientation preserving representative from the connected component of the identity of the same fiber (cf. remark 6). In the following, we construct a global solution $\tilde{\varphi} \in \pi(\varphi)$.

To apply the Dacorogna-Moser theorem 4, we define an equation of pullback-type with volume forms on $\varphi(M)$ represented by their local coefficient functions. More specifically, we look for a $\tilde{\rho} \in \mathrm{Diff}(\varphi(M))$ solving

$$f_\varphi \circ \tilde{\rho} \cdot \det D^\tau \tilde{\rho} = g^M \circ \varphi^{-1} \cdot \det D^\tau \varphi^{-1} \quad \text{on } \varphi(M). \tag{5.11}$$

Due to normalization assumption (5.9), an application of the transformation formula reveals

$$\int_{\varphi(M)} g^M \circ \varphi^{-1} \cdot \det D^\tau \varphi^{-1} \, \mathrm{d}s = \int_M g^M \, \mathrm{d}s = \int_{\varphi(M)} f_\varphi \, \mathrm{d}s. \tag{5.12}$$

Hence to the rule for determinants of inverses, and $D^\tau \varphi$ having full rank by $\varphi \in \mathrm{Emb}(M, \mathbb{R}^{n+1})$, we see that $\det D^\tau \varphi^{-1}$ is non-vanishing. Moreover, Jacobian determinants can be locally expressed as a polynomials, which ensures that the right-hand side is C^∞-regular due to C^∞-regularity of φ^{-1} and g^M. Since M is a connected and compact C^∞-manifold, the shape $\varphi(M)$ has these properties as well.

Because f_φ and g^M are strictly positive by assumption, and since the inverse Jacobian determinant is strictly positive due to the inverse determinant formula, and $\varphi \in \mathrm{Emb}(M, \mathbb{R}^{n+1})$ being an orientation preserving embedding, the coefficient functions in equation (5.11) are all strictly positive. This means we have checked the necessary prerequisites to apply the Dacorogna-Moser theorem 4. Existence of an orientation preserving $\tilde{\rho} \in \mathrm{Diff}(\varphi(M))$ solving equation (5.11) is guaranteed. Pointwise invariance of $\partial\varphi(M)$ is also guaranteed due to $\partial^q M = \varnothing$ for $q \geq 2$, since M is a manifold with boundary by assumption.

Now we construct a solution for problem (5.10) by setting $\tilde{\varphi} := \tilde{\rho} \circ \varphi \in \mathrm{Emb}(M, \mathbb{R}^{n+1})$. First, we see that $\rho := \varphi^{-1} \circ \tilde{\varphi}$ defines a C^∞-diffeomorphism on M. Since $\tilde{\varphi} = \varphi \circ \rho$ by construction, we know by definition of the equivalence relations of fibers (4.4) that $\tilde{\varphi} \in \pi(\varphi)$. By equivalent reformulation of the defining pullback equation (5.11) for $\tilde{\rho}$ via the formula for inverse determinants, and use of the product rule for determinants, we check

$$\begin{aligned} g^M \circ \tilde{\varphi}^{-1} \cdot \det D^\tau \tilde{\varphi}^{-1} &= g^M \circ (\tilde{\rho} \circ \varphi)^{-1} \cdot \det D^\tau (\tilde{\rho} \circ \varphi)^{-1} \\ &= g^M \circ \varphi^{-1} \circ \tilde{\rho}^{-1} \cdot \det D^\tau \varphi^{-1} \circ \tilde{\rho}^{-1} \cdot \det D^\tau \tilde{\rho}^{-1} \\ &= \left(g^M \circ \varphi^{-1} \cdot \det D^\tau \varphi^{-1}\right) \circ \tilde{\rho}^{-1} \cdot \det D^\tau \tilde{\rho}^{-1} \\ &= f_\varphi. \end{aligned} \tag{5.13}$$

Since the objective functional of problem (5.10) is of quadratic nature, and $\tilde{\varphi} \in \pi(\varphi)$ with f_φ having shape functionality, this indeed shows that $\tilde{\varphi}$ is a global minimizer. As the construction of $\tilde{\rho}$ did not rely on explicit choice of the fiber, we can analogously construct global solutions for φ coming from any fiber of $\mathrm{Emb}(M, \mathbb{R}^{n+1})$.

Next we show the three equivalences characterizing the solutions in each fiber $\pi(\varphi)$. For this, let $\tilde{\varphi}, \hat{\varphi} \in \pi(\varphi)$ be global solutions to problem (5.10). Since for each fiber there is a global solution satisfying equation (5.13) as previously shown, both $\tilde{\varphi}$ and $\hat{\varphi}$ satisfy

$$g^M \circ \tilde{\varphi}^{-1} \cdot \det D^\tau \tilde{\varphi}^{-1} = f_{\tilde{\varphi}} = f_{\hat{\varphi}} = g^M \circ \hat{\varphi}^{-1} \cdot \det D^\tau \hat{\varphi}^{-1} \quad \text{on } \varphi(M), \tag{5.14}$$

where the second equality holds by the shape functionality assumption of f_φ. This gives the equivalence of (i) and (ii).

For the last equivalence we set $\rho := \hat{\varphi} \circ \tilde{\varphi}^{-1}$, and see that this defines a diffeomorphism $\rho \in \mathrm{Diff}(\varphi(M))$ with $\rho \circ \tilde{\varphi} = \hat{\varphi}$. The diffeomorphism ρ indeed preserves the volume form $f_\varphi \cdot \mathrm{d}s$, due to

$$\begin{aligned} f_\varphi \circ \rho \cdot \det D^\tau \rho &= f_\varphi \circ \hat{\varphi} \circ \tilde{\varphi}^{-1} \cdot \det D^\tau \left(\hat{\varphi} \circ \tilde{\varphi}^{-1}\right) \\ &= \left(g^M \circ \hat{\varphi}^{-1} \cdot \det D^\tau \hat{\varphi}^{-1}\right) \circ \hat{\varphi} \circ \tilde{\varphi}^{-1} \cdot \det D^\tau \hat{\varphi} \circ \tilde{\varphi}^{-1} \cdot \det D^\tau \tilde{\varphi}^{-1} \\ &= g^M \circ \tilde{\varphi}^{-1} \cdot \frac{1}{\det D^\tau \hat{\varphi} \circ \tilde{\varphi}^{-1}} \cdot \det D^\tau \hat{\varphi} \circ \tilde{\varphi}^{-1} \cdot \det D^\tau \tilde{\varphi}^{-1} \\ &= g^M \circ \tilde{\varphi}^{-1} \cdot \det D^\tau \tilde{\varphi}^{-1} \\ &= f_\varphi. \end{aligned}$$

Here we used the rule for inverses of determinants, shape functionality of f_φ, and that $\tilde{\varphi}$ and $\hat{\varphi}$ are global solutions in the same fiber, which therefore satisfy equation (5.14). Analogous arguments can be used to show that for a global solution $\tilde{\varphi}$, an f_φ-volume preserving diffeomorphism $\rho \in \mathrm{Diff}(\varphi(M))$ gives another global solution $\hat{\varphi} := \rho \circ \tilde{\varphi}$ in the same fiber. This establishes equivalence of (i) and (ii) and (iii).

The last two assertions of theorem 10 only concern the case of nonempty boundary ∂M. We take a look at the solution construction of $\tilde{\varphi} := \tilde{\rho} \circ \varphi$ with $\tilde{\rho}$ coming from the Dacorogna-Moser theorem 4 applied to equation (5.11). It guarantees

pointwise invariance of the boundary $\tilde{\rho}_{|\partial\varphi(M)} = \mathrm{id}_{\partial\varphi(M)}$, because we have no higher order corners, i.e. $\partial^q M = \varnothing$ for $q \geq 2$ by assumption. So by construction, our solutions already satisfy the desired movement of the boundary

$$\tilde{\varphi}_{|\partial M} = \tilde{\rho}_{|\partial\varphi(M)} \circ \varphi_{|\partial M} = \varphi_{|\partial M}.$$

This also shows the last assertion concerning solutions which leave ∂M invariant. Namely, such a construction of global solutions in particular applies to the special case of $\varphi \in \mathrm{Emb}_{\partial M}(M, \mathbb{R}^{n+1}) \subset \mathrm{Emb}(M, \mathbb{R}^{n+1})$, which concludes the proof. □

Remark 12 (Case of Open Domains with Hölder Regularity)**.** *Existence and well-definedness results from theorem 10 also hold in the general context of bounded and connected open domains M with $C^{k,\alpha}$-Hölder regularity. For given $k \in \mathbb{N}$ and $\alpha \in (0,1)$, if M and f_φ and g^M have $C^{k,\alpha}$-regularity, and ∂M has $C^{k+2,\alpha}$-regularity, then solutions φ with $C^{k+1,\alpha}$-regularity exist in each fiber. For this, we can apply the Dacorogna-Moser theorem 3. This includes those cases of Sobolev-regularity, which satisfy necessary requirements for embedding theorems into Hölder spaces.*

Remark 13 (Existence Result for Arbitrary Codimension Manifolds M with Corners)**.** *Existence theorem 10 of solutions to the pre-shape parameterization tracking problem is stated for manifolds M with or without boundaries. The Dacorogna-Moser theorem 4 by Bruveris, Michor et al. also holds for the case of manifolds M with corners, not restricted by their dimension. As Moser's theorem is the central ingredient for the proof of theorem 10, its generalization stated in theorem 4 is suitable to extend the statements of theorem 10 to arbitrary codimension manifolds with corners.*

For this, an additional assumption is needed. Namely, for all $q \geq 2$, we need the pointwise equality

$$f_\varphi(x) = g^M\big(\varphi^{-1}(x)\big) \cdot \det D^\tau \varphi^{-1}(x) \qquad \forall x \in \partial^q \varphi(M). \tag{5.15}$$

This means f_φ and g^M have to be consistent on boundaries with codimension $q \geq 2$ of embedded shapes $\varphi(M)$. If this is guaranteed, then the proof of theorem 10 carries over to manifolds with corners. In practice, when continuous Galerkin representations are used, this can be achieved by constructing the target f_φ, such that its degrees of freedom on boundaries with codimension $q \geq 2$ are set according to equation (5.15)*. Notice that g^M is not a free parameter, in the sense, that it is already determined by the initial mesh configuration. Hence, the target f_φ is also predetermined on corners by choice of the initial mesh and the mesh configuration of current shape optimization iteration.*

Remark 14 (Normalization Condition is no Obstruction for Targets f_φ)**.** *Assumption* (5.9) *is simply a normalization requirement on f_φ. From practical perspective, f_φ can be defined using a given integrable function $\tilde{f}_\varphi \colon \varphi(M) \to (0, \infty)$ via*

$$f_\varphi := \frac{\int_M g^M \,\mathrm{d}s}{\int_{\varphi(M)} \tilde{f}_\varphi \,\mathrm{d}s} \cdot \tilde{f}_\varphi, \tag{5.16}$$

trivially fulfilling assumption (5.9)*.*

If the target f_φ is chosen such that the normalization condition (5.9) *is not fulfilled, solutions to problem* (5.10) *might still exist. However, the property that solutions exist in each fiber, and thus existence of optimal parameterizations for each given shape $\varphi(M)$, are lost in general. Using a more heuristic point of view, depending on whether $\int_M g^M$ is greater or smaller $\int_{\varphi(M)} f_\varphi$, a gradient flow generated by solving problem* (5.10) *locally shrinks or blows up the shape $\varphi(M)$ in*

normal direction to compensate for the difference. This changes the shape, and the fiber $\pi(\varphi)$ of $\varphi(M)$ is left in the process. In section 7.3, we capture a related effect in numerical implementations using steepest descents involving the normal components of the pre-shape derivative to the parameterization tracking problem (5.10).

We have introduced the pre-shape parameterization tracking by looking at a low-dimensional special case inspired by shape analysis of elastic curves. It is also possible to give an alternative motivation for the pre-shape parameterization problem related to methods for time dependent PDE found in [29, 31, 68]. In these articles, the authors introduce so-called mesh deformation methods, which track for a specified target cell volume f by changing coordinates of nodes. These methods are part of the family of moving mesh strategies for adaptive solution of time dependent PDEs. From this point of view, we can interpret the pre-shape parameterization tracking problem (5.10) as a least-squares formulation of the deformation method for element volume optimization on manifolds. As we took a slight twist to formulate problem (5.10) using inverse Jacobians, we have a different interpretation of optimal φ and targets f_φ compared to mentioned deformation methods for PDE. In our case, f_φ describes the desired local density of mesh vertices, and the positive function $g^M \colon M \to (0, \infty)$ acts as the node distribution of the initial mesh. On the other hand, the authors of [29, 31, 68] use targets f to describe the local cell volume. For this reason, the aforementioned authors incorporate reciprocals of f in their formulas, instead of reciprocals of Jacobians. Still, both formulations are related by inverting the solutions, Jacobians and targets.

Pre-Shape Parameterization Tracking for Shapes with Arbitrary Codimensions in Nonlinear Ambient Spaces, and Relation to Pullback Equations and Optimal Transport

To formulate the pre-shape parameterization problem (5.10), we have restricted ourselves to the setting of $M \subset \mathbb{R}^{n+1}$ being an n-dimensional submanifold. This is perhaps the most common case in practice, which does not rely on more advanced differential geometric techniques for numerical implementations, such as retractions or exponential maps. In light of remark 1, we can generalize pre-shape parameterization tracking problem (5.10) to pre-shape spaces $\mathrm{Emb}(M, N)$ with ambient spaces N, which are general C^∞-manifolds of finite dimension without boundary. Then for compact, connected and oriented C^∞-manifolds M of any dimension $\dim(M) \leq \dim N$, perhaps with smooth boundary ∂M, the pre-shape space $\mathrm{Emb}(M, N)$ is a Fréchet-fiber bundle over the base space $B_e(M, N)$ as described in definition 5 (cf. [61, Thm. 2.2]). Hence, by appropriate use of differential geometric concepts, we can state parameterization tracking problem (5.10) in this more general setting.

For this, the concept of differential forms is suitable, since determinants and coefficient functions featured in equation (5.10) can be naturally interpreted in terms of volume forms and pullbacks. An excellent introduction to this topic is found in [111]. In the following, we reiterate some facts on volume forms for manifolds M of dimension m. Let $C^\infty(M, \bigwedge^m T^*(M))$ denote the space of all smooth m-forms, i.e. smooth sections of the bundle of m'th exterior powers $\bigwedge^m (T_p^* M)$ with base space M. As m is the dimension of M, these smooth differential forms are called top-forms and correspond to *smooth volume forms* on M. A side effect of using volume forms for integration on manifolds is the occurrence of negative volume, which depends on the chosen orientation of M. To remedy this, either the concept of densities on manifolds (cf. [111, Ch. 16]) can be regarded or, as we do, by restricting ourselves to embeddings leaving a chosen orientation invariant. The latter is natural in the context of numerical implementation, since it is an automatic consequence of mesh morphing with sufficiently small step sizes. This corresponds to staying on the

identity component of fibers (cf. remark 2 and remark 6). Hence we remind the reader that, if necessary, the concept of density and volume forms can be swapped.

There is only a limited freedom of choice for volume forms on manifolds, since $\bigwedge^m(T_p^*M)$ is one-dimensional (cf. [111, Ch. 14]). This makes the space of smooth volume forms $C^\infty\big(M, \bigwedge^m T^*(M)\big)$ isomorphic to $C^\infty(M,\mathbb{R})$. In local coordinates, this means every volume form $\omega \in C^\infty\big(M, \bigwedge^m T^*(M)\big)$ can be rewritten with a local coefficient function $f \in C^\infty(M)$ to give

$$\omega = f \cdot \mathrm{d}x_1 \wedge \cdots \wedge \mathrm{d}x_m. \tag{5.17}$$

Next, we introduce *pullbacks of volume forms*, which are related to the transformation formula in $\mathbb{R}^{n+1}$ (cf. [111, Prop. 14.20]). As we are only interested in volume forms, we do not introduce pullbacks for general differential forms. Suppose that P and Q are smooth m-dimensional manifolds for a moment, and that we have a smooth mapping $F\colon P \to Q$. The pullback of a volume form $\omega \in C^\infty\big(Q, \bigwedge^m T^*(Q)\big)$ locally represented as $\omega = f \cdot \mathrm{d}y_1 \wedge \cdots \wedge \mathrm{d}y_m$ is then given by

$$F^*(\omega) = f \circ F \cdot \det DF \cdot \mathrm{d}x_1 \wedge \cdots \wedge \mathrm{d}x_m, \tag{5.18}$$

where $\det DF$ is the Jacobian determinant of F represented in respective local coordinates. If an oriented manifold M exhibits a Riemannian metric $\langle\cdot,\cdot\rangle^M$, then there is a canonical volume form for $\langle\cdot,\cdot\rangle^M$ corresponding to the chosen orientation (cf. [111, Prop. 16.45, Ex. 16.46]). In particular, this is the case for m-dimensional, oriented submanifolds of $\mathbb{R}^{n+1}$ with the metric $i^*(\langle\cdot,\cdot\rangle^{\mathbb{R}^{n+1}})$ induced by the Euclidean scalar product via pullback of the inclusion $i\colon M \to \mathbb{R}^{n+1}$. Since we assumed $M \subset \mathbb{R}^{n+1}$ in theorem 10, the formulation of pre-shape parameterization tracking problem (5.10) is implicitly stated with respect to the induced Riemannian metric $i^*(\langle\cdot,\cdot\rangle^{\mathbb{R}^{n+1}})$ and its corresponding volume form.

Let us substitute the Euclidean ambient space $\mathbb{R}^{n+1}$ with a general finite dimensional C^∞-manifold N without boundary equipped with a Riemannian metric $\langle\cdot,\cdot\rangle^N$. We equivalently reformulate problem (5.10) using pullbacks in the following. The reader is reminded of the more general dimensionality assumption $\dim(M) \leq \dim(N)$ for $M \subset N$ made in the beginning of this paragraph, permitting general codimensions. What we get is an abstract pre-shape parameterization tracking-type problem for volume forms

$$\min_{\varphi\in\mathrm{Emb}(M,N)} \frac{1}{2}\Big\|\big(\varphi^{-1}\big)^*\Big(g^M \cdot i_M^*\big(\omega_{\langle\cdot,\cdot\rangle^N}\big)\Big) - f_\varphi \cdot i_{\varphi(M)}^*\big(\omega_{\langle\cdot,\cdot\rangle^N}\big)\Big\|^2_{L^2(\varphi(M),\bigwedge^m T^*(\varphi(M)))}, \tag{5.19}$$

where $i_M\colon M \to N$ and $i_{\varphi(M)}\colon \varphi(M) \to N$ represent inclusions, and $\omega_{\langle\cdot,\cdot\rangle^N}$ is the volume form on N induced by the Riemannian metric $\langle\cdot,\cdot\rangle^N$. Here, $\|\cdot\|_{L^2(\varphi(M),\bigwedge^m T^*(\varphi(M)))}$ is the norm for square integrable volume forms on $\varphi(M)$, which is defined in analogy to the L^2-norm. In this context, the choice of $g^M\colon M \to (0,\infty)$ is equivalent to the choice of a positive volume form $\omega_M = g^M \cdot i_M^*(\omega_{\langle\cdot,\cdot\rangle^N})$ on M. This means $(\varphi^{-1})^*\big(g^M \cdot i_M^*\big(\omega_{\langle\cdot,\cdot\rangle^N}\big)\big)$ is the volume form on $\varphi(M)$, which is created by pushing the initial volume form $g^M \cdot i_M^*\big(\omega_{\langle\cdot,\cdot\rangle^N}\big)$ of M forward to $\varphi(M)$ by using the pullback of the inverse $(\varphi^{-1})^*$. The necessary normalization condition (5.9) is then restated as

$$\int_{\varphi(M)} f_\varphi \cdot i_{\varphi(M)}^*\big(\omega_{\langle\cdot,\cdot\rangle^N}\big) = \int_M g^M \cdot i_M^*\big(\omega_{\langle\cdot,\cdot\rangle^N}\big) \qquad \forall\varphi \in \mathrm{Emb}(M,N). \tag{5.20}$$

It demands that the weighted total volumes on $\varphi(M)$ and M, which are both induced by the Riemannian metric of the surrounding space N, coincide. In practice,

the normalization condition (5.20) can be achieved simply by proceeding as in remark 14.

Following this line of thought, it is possible to show an analogue of theorem 10 for the abstract problem (5.19). Arguments made in the proof of theorem 10 can be followed one by one, when objects introduced in this paragraph are used. In particular, computations regarding coefficient functions and Jacobian determinants are replaced by direct computations with volume forms and their pullbacks. The crucial ingredient is again the general Dacorogna-Moser theorem 4 formulated for volume forms.

A sufficient condition for global optimality for the abstract problem (5.19) is given by

$$\varphi^*\Big(f_\varphi \cdot i^*_{\varphi(M)}\big(\omega_{\langle\cdot,\cdot\rangle^N}\big)\Big) = g^M \cdot i^*_M\big(\omega_{\langle\cdot,\cdot\rangle^N}\big). \tag{5.21}$$

Notice that f_φ occurs on the left-hand side, since we have used φ^{-1} in the formulation of problem (5.19). Condition (5.21) demands that, if the volume form induced by the ambient space $i^*_{\varphi(M)}\big(\omega_{\langle\cdot,\cdot\rangle^N}\big)$ on an embedded shape $\varphi(M) \subset N$ weighted by f_φ is pulled back to M, then it should coincide with the initial volume form $g^M \cdot i^*_M\big(\omega_{\langle\cdot,\cdot\rangle^N}\big)$ on M. Equivalently, the pushforward $(\varphi^{-1})^*$ of the initial volume $g^M \cdot i^*_M\big(\omega_{\langle\cdot,\cdot\rangle^N}\big)$ on M redistributes the volume induced by the ambient space on $\varphi(M)$ according to the target weight f_φ. This more abstract framework also shows, why equation (5.11) from the proof of theorem 10 is termed an equation of pullback-type. Since we have existence of globally optimal solutions to equation (5.19), such solutions necessarily satisfy optimality criterion (5.21). Thus, solving the pre-shape parameterization tracking problem essentially constructs a solution to the pullback equation (5.21). Put differently, pre-shape calculus and optimization techniques can be used to solve differential equations of general pullback-type. As far as the author is aware, such an approach is not found in the current literature. We refer the interested reader to [38] for a thorough introduction to these large classes of nonlinear problems.

Another different perspective on pre-shape parameterization tracking becomes apparent, when expressions of volume forms are interpreted as measures on manifolds M. In particular, integration with respect to the induced Riemannian volume of submanifolds $M \subset \mathbb{R}^{n+1}$ coincides with integration using the m-dimensional Lebesgue and Hausdorff measures on M, as can be seen by using a partition of unity and [111, Prop. 16.5, Prop. 16.8] with isometries as chart mappings. With the measure interpretation, the formulation of the abstract parameterization tracking problem (5.19) restricted to a fiber $\pi(\varphi) \subset \mathrm{Emb}(M,N)$ can be viewed as an optimal transport problem in Monge formulation with constant cost function. The measures $\mu^{\varphi(M)}$ and μ^M are associated with $f_\varphi \cdot i^*_{\varphi(M)}(\omega_{\langle\cdot,\cdot\rangle^N})$ and $g^M \cdot i^*_M(\omega_{\langle\cdot,\cdot\rangle^N})$. Formally, the corresponding optimal transport problem in Monge formulation on M over the fiber $\pi(\varphi_0)$ then reads (cf. [150, Problem 1.1])

$$\begin{aligned} \min_{\varphi\in\pi(\varphi_0)} \int_M c_{\pi(\varphi_0)}\big(x,\varphi(x)\big)\,\mathrm{d}\mu^M \\ \text{s.t. } \varphi_*\big(\mu^M\big) = \mu^{\varphi(M)}, \end{aligned} \tag{5.22}$$

with cost function $c_{\pi(\varphi_0)}(x,y) = 1$ for all $x \in M$ and $y \in \varphi(M)$. Here, the pushforward of measures φ_* can be associated to the pullback of volume forms of the inverse $(\varphi^{-1})^*$. We see that in this context, the normalization condition in equation (5.20) simply means that both measures can be interpreted as probability measures after appropriate rescaling with the same factor. This problem is in some sense a degenerate optimal transport, since it only amounts to the selection of a feasible mapping φ, i.e. that its pushforward of $g^M \cdot i^*_M(\omega_{\langle\cdot,\cdot\rangle^N})$ results in $f_\varphi \cdot i^*_{\varphi(M)}\big(\omega_{\langle\cdot,\cdot\rangle^N}\big)$. There is no further restriction to the non-unique embeddings which satisfy such a property.

This point of view offers the possibility to extend the pre-shape parameterization tracking problem (5.19), such that a specific $\varphi \in \pi(\varphi_0)$ amongst those with the correct volume redistribution is selected. Criteria for selection can be implemented as cost functions $c_{\pi(\varphi_0)} \colon M \times \varphi(M) \to (0, \infty)$ for problem (5.22). This collection of optimal transport problems for each fiber can be stated over the fiber bundle $\mathrm{Emb}(M, N)$ to yield a generalized pre-shape parameterization tracking problem. Even further, different versions of such optimal transport problems for pre-shapes, such as their L^p-Monge-Ampère or L^p-Monge-Kantorovich formulations in light of [43] or [72], can be stated. A comparison of resulting pre-shape derivatives and numerical routines for mesh quality could certainly be of interest. Exploring this is beyond the scope of this work, but opens possibilities for further research.

5.2 Properties of the Pre-Shape Parameterization Tracking Problem

5.2.1 Pre-Shape Parameterization Tracking and Finite Point Sets

Before we pursue the application of pre-shape calculus to the parameterization tracking problem (5.10), we derive some of its properties using different methods. The insights are of a more general type, and in part result in enhanced theoretical understanding of techniques we apply in the numerical sections. The next proposition shows that there is a sufficiently large amount of possibilities to model movement of mesh nodes by choice of the target f_φ for the parameterization tracking problem.

Proposition 3 (Mesh N-Transitivity for Parameterization Tracking Problems)**.** *Let $M \subset \mathbb{R}^{n+1}$ be a compact, connected, oriented C^∞-submanifold of dimension $n \geq 2$ without boundary, and let $g^M \colon M \to (0, \infty)$ be smooth. Let $N \in \mathbb{N}$ and $P_M = (x_1, \dots, x_N) \subset M$ be an ordered collection of distinct points. Further denote by*

$$\mathcal{A}^P := \left\{ P_{\pi(\varphi)} = (y_1, \dots, y_N) \subset \varphi(M) \subset \mathbb{R}^{n+1} : \ \pi(\varphi) \in B_e^n \right\} \tag{5.23}$$

a family of distinct and ordered N-point collections for all shapes $\varphi(M)$ arising in $B_e^n(M)$.

Then there exists a family of C^∞-functions $f_\varphi \colon \varphi(M) \to (0, \infty)$ satisfying the assumptions of theorem 10, and global solutions $\hat{\varphi} \in \pi(\varphi)$ to problem (5.10) *in each fiber $\pi(\varphi) \in B_e^n$, such that*

$$\hat{\varphi}\big(P_M\big) = P_{\pi(\varphi)}. \tag{5.24}$$

Proof. The proof is essentially a consequence of the N-transitivity property of the group of smooth diffeomorphisms with compact support $\mathrm{Diff}_c(M)$ (cf. [133]). This property states that for given ordered sets of points $(x_1, \dots, x_N), (\tilde{p}_1, \dots, \tilde{p}_N) \subset M$, there is a $\rho \in \mathrm{Diff}_c(M)$, such that $\rho(x_i) = \tilde{p}_i$ for each i. By assumption, M is a compact, connected C^∞-manifold with $\dim(M) \geq 2$, so we have $\mathrm{Diff}_c(M) = \mathrm{Diff}(M)$ and N-transitivity for each $N \in \mathbb{N}$.

Let $N \in \mathbb{N}$ be fixed. Consider ordered point collections for all shapes $\mathcal{A}^P$ as in equation (5.23), and a given initial point collection $P_M = (x_1, \dots, x_N) \subset M$. Fix a shape $\pi(\varphi) \in B_e^n$ and a corresponding point collection $P_{\pi(\varphi)} = (y_1, \dots, y_N) \in \mathcal{A}^P$. We choose an arbitrary embedding $\varphi \in \pi(\varphi)$ in the fiber of the fixed shape. By the embedding property, our assumptions on the manifold M also hold for $\varphi(M)$. Since $\mathrm{Diff}(M) \cong \mathrm{Diff}(\varphi(M))$ are isomorphic (cf. relation (4.6)), we also have that $\mathrm{Diff}(\varphi(M))$ acts N-transitively on $\varphi(M)$.

We apply $\varphi\colon M \to \varphi(M)$ to $(x_1, \dots, x_N)$, which results in ordered vertices $(\varphi(x_1), \dots, \varphi(x_N)) \subset \varphi(M)$. Now we are in the position to use N-transitivity of $\mathrm{Diff}(\varphi(M))$, which gives existence of a $\rho \in \mathrm{Diff}(\varphi(M))$ with

$$\Big(\rho\big(\varphi(x_1)\big), \dots, \rho\big(\varphi(x_N)\big)\Big) = \big(y_1, \dots, y_N\big) = P_{\pi(\varphi)} \subset \varphi(M). \tag{5.25}$$

We define the possible solution candidate as $\hat{\varphi} := \rho \circ \varphi$, and see that $\hat{\varphi} \in \mathrm{Emb}(M, \mathbb{R}^{n+1})$. As we work with submanifolds of $\mathbb{R}^{n+1}$, we can set the target for parameterization tracking as $f_\varphi := g^M \circ \hat{\varphi}^{-1} \cdot \det D^\tau \hat{\varphi}^{-1}$ for all $\varphi \in \pi(\hat{\varphi})$, where $g^M\colon M \to (0, \infty)$ is given initially.

We now check the necessary assumptions made on f_φ in theorem 10. Since M is orientable, we can choose suitable orientations of local orthonormal frames, which gives $f_\varphi \geq 0$. This is strengthened to $f_\varphi > 0$, because we have $g^M > 0$ and $\hat{\varphi} \in \mathrm{Emb}(M, \mathbb{R}^{n+1})$. The latter also guarantees $f_\varphi \in C^\infty(M)$, as Jacobian determinants of smooth functions are smooth. Normalization assumption (5.9) is checked by application of the transformation formula. The arguments and constructions do not depend on the choice of fiber $\varphi(M)$, and hence can be carried out to construct f_φ for all fibers and point collections in $\mathcal{A}^P$. We also have shape functionality for f_φ, as we have set f_φ to the same function for all embeddings in their respective fibers $\pi(\varphi)$. This shows all necessary assumptions to use f_φ as a target for problem (5.10). Since we can plug f_φ into relation (ii) of theorem 10, we also verify that $\hat{\varphi}$ are global minimizers by construction, concluding the proof. □

In the following discussion, we associate meshes with collections of ordered point sets. Proposition 3 shows, that the selection of a target f_φ for pre-shape parameterization tracking provides enough modeling possibilities to achieve desired mesh configurations without changing the discretized shapes. Of course, in practice this holds only up to discretization errors. Let us say that, for a given starting shape Γ_0 of a shape optimization procedure, we have a corresponding mesh P_{Γ_0} representing Γ_0. Now, a user specifies desired discretizations for all shapes that could possibly arise during the optimization procedure. He does so by collecting the corresponding mesh node coordinates in $P_{\varphi(M)}$. Proposition 3 guarantees that for each shape, there is a target f_φ, such that the desired nodal coordinates are achieved by a solution φ of the parameterization tracking problem (5.10). We reiterate that the desired parameterizations φ exist in all fibers of shapes. This is a necessary property for construction of numerical algorithms that do not interfere with the shape optimization procedures. Here, the only assumption made on the target meshes $P_{\varphi(M)}$ is to have a fixed number of vertices N, and that the mesh topologies are consistent with the starting mesh. If mesh morphing is applied to realize the shape optimization routine, these assumptions are automatically valid, since number of nodes and mesh topology do not change under valid mesh deformations. Techniques such as remeshing or edge swapping in general result in inconsistent node numbers or mesh topologies. However, beware that proposition 3 is a purely theoretical existence result, and does not offer a constructive way to find target functions f_φ, such that desired shape discretizations are realized.

We also notice that, although an appropriate f_φ exists for any given shape discretization $P_{\varphi(M)}$, the pre-shape solution corresponding to the discretization $P_{\varphi(M)}$ is in general not the only global optimum in the fiber of $\varphi(M)$. Instead, there are multiple global solutions in each fiber, which give rise to different meshes for the same shape. In particular, this means we have no guarantee that a pre-shape $\tilde{\varphi}$, which realizes the specified target mesh coordinates, is selected during a pre-shape optimization routine for parameterization tracking problem (5.10). Still, the connection of pre-shape parameterization tracking to optimal transport (cf. p. 56) might offer an opportunity to select such specified parameterizations $\tilde{\varphi}$ by imposing additional constraints via the transport cost c_φ.

Remark 15 (N-Transitivity in Dimension 1)**.** *The case* $\dim(M) = 1$ *is not treated in proposition 3, since* N*-transitivity for diffeomorphism groups only holds for* $\dim(M) \geq 2$*. However, every compact, connected* C^∞*-manifold* M *of dimension* 1 *is either diffeomorphic to the circle* S^1 *or a closed interval of* $\mathbb{R}$ *(cf. [58]). Thus, if the orderings of point collections* P_M *and* $P_{\varphi(M)}$ *are assumed to agree, the same result as in proposition 3 holds for the one dimensional case. In practice, this corresponds to consistent node connectivities of the initial and desired meshes.*

The next proposition describes a property of pre-shape parameterization tracking, which is reflective of its behavior for meshes with different resolutions. In some sense, this can be viewed as an analogue of approximate mesh independence for solutions, and thus for numerical techniques we propose in later chapters.

Proposition 4 (Weak*-Convergence of Point Sets under Solutions of Pre-Shape Parameterization Tracking)**.** *Assume the setting of theorem 10. Further, let* g^M *and* f_φ *be normalized to one, i.e.*

$$\int_{\varphi(M)} f_\varphi(s)\,\mathrm{d}s = 1 = \int_M g^M(s)\,\mathrm{d}s \qquad \forall \varphi \in \mathrm{Emb}\left(M, \mathbb{R}^{n+1}\right). \tag{5.26}$$

Let $\{V_N^M\}_{N\in\mathbb{N}}$ *be a sequence of point collections, such that* $V_N^M \subset M$ *and* $|V_N^M| = N$*. Further, let*

$$\frac{1}{N}\sum_{x\in V_N^M} \delta_x \overset{weak^*}{\to} g^M\,\mathrm{d}s \quad \text{for } N \to \infty, \tag{5.27}$$

where δ_x *are Dirac measures in* x*.*

Then, for every fiber $\pi(\varphi) \subset \mathrm{Emb}(M, \mathbb{R}^{n+1})$ *and every global solution* $\hat{\varphi} \in \pi(\varphi)$ *to the parameterization tracking problem* (5.10)*, the point collections* $\{V_N^M\}_{N\in\mathbb{N}}$ *are weak***-convergent to the target* f_φ*, i.e.*

$$\frac{1}{N}\sum_{x\in V_N^M} \delta_{\hat{\varphi}(x)} \overset{weak^*}{\to} f_\varphi\,\mathrm{d}s \quad \text{for } N \to \infty. \tag{5.28}$$

Proof. Let all the assumptions stated in proposition 4 hold. We fix a fiber $\pi(\varphi)$. By assumption, the conditions to apply theorem 10 are met. This guarantees existence of global solutions to (5.10) in each fiber of $\mathrm{Emb}(M, \mathbb{R}^{n+1})$. Let $\hat{\varphi} \in \pi(\varphi)$ be such a global solution.

We use equation (5.26) to show that weak*-convergence is preserved while pushing the measures of concern forward by diffeomorphisms. For this, note that the pushforward of a Dirac measure by a measurable bijection $\Phi\colon X \to Y$ is given by

$$\left(\Phi^{-1}\right)^*\left(\delta_x\right)\left(\{y\}\right) = \delta_x\left(\Phi^{-1}(y)\right) = \delta_{\Phi(x)}\left(\{y\}\right). \tag{5.29}$$

Let $h \in C^0(\varphi(M))$ be an arbitrary continuous function on $\varphi(M)$. Then

$$\begin{aligned}
\int_{\varphi(M)} h\,\mathrm{d}\left(\frac{1}{N}\sum_{x\in V_N^M}\delta_{\hat{\varphi}(x)}\right) &= \int_{\varphi(M)} h\circ\hat{\varphi}\circ\hat{\varphi}^{-1}\,\mathrm{d}\left(\hat{\varphi}^{-1}\right)^*\left(\frac{1}{N}\sum_{x\in V_N^M}\delta_x\right)\\
&= \int_M h\circ\hat{\varphi}\,\mathrm{d}\left(\frac{1}{N}\sum_{x\in V_N^M}\delta_x\right)\\
&\to \int_M \left(h\circ\hat{\varphi}\right)\cdot g^M\,\mathrm{d}s \qquad \text{for } N\to\infty,
\end{aligned}$$

where we also used continuity of $h \circ \hat{\varphi}$ and assumption (5.27). On the other hand, we can use normalization condition (5.9) to see

$$\begin{aligned}\int_M \left(h \circ \hat{\varphi}\right) \cdot g^M \,\mathrm{d}s &= \int_{\varphi(M)} \left(\hat{\varphi}^{-1}\right)^* \left(h \circ \hat{\varphi} \cdot g^M \,\mathrm{d}s\right) \\ &= \int_{\varphi(M)} h \left(\hat{\varphi}^{-1}\right)^* \left(g^M \,\mathrm{d}s\right) \\ &= \int_{\varphi(M)} h \cdot \left(g^M \circ \hat{\varphi}^{-1}\right) \cdot \det D^\tau \hat{\varphi}^{-1} \,\mathrm{d}s \\ &= \int_{\varphi(M)} h \cdot f_\varphi \,\mathrm{d}s,\end{aligned}$$

where we used that $\hat{\varphi}$ is a global solution to (5.10) characterized by theorem 10 (ii). Since $h \in C^0(\varphi(M))$ was arbitrary, this results in the desired weak*-convergence (5.28). □

Before we interpret proposition 4, we emphasize that normalization condition (5.26) is not more restrictive than the normalization condition (5.9) found in theorem 10. In fact, we can rescale both g^M and f_φ by the same scalar without changing underlying solutions to the optimization problem (5.10). Hence, if condition (5.9) holds, we can assume normalization of g^M and f_φ to 1 without restriction of generality. A normalization to 1 lets g^M and f_φ act as densities of probability measures on M and $\varphi(M)$. Hence, these densities can be interpreted as the local vertex count relative to the total number of mesh vertices.

To give an interpretation of weak*-convergences (5.27) and (5.28), we can use the following analogy. Let us assume we start a (pre-)shape optimization routine in a shape corresponding to the manifold M, which is discretized by a mesh using N vertices. We associate this mesh with the normed sum of Dirac measures featured in proposition 4. Then, let us pretend that we use a mesh adaptation strategy, which gives increased local refinement of the underlying mesh. As the resolution of discrete representations of M increases for $N \to \infty$, the vertices start to locally accumulate. In the limit, the normalized local vertex count is converging to a density function, which shows how many vertices arise during refinement in different areas of M. Such a mesh limiting process is illustrated in figure 5.1. From this perspective, f_φ can be seen as the refinement rule for meshes discretizing shapes $\varphi(M)$. Analogously, g^M is the initial point density, which describes a discretization rule by which we choose the location of new vertices on the initial mesh of M, if we were to refine. Therefore, proposition 4 tells us that minimizing (5.10) redistributes the vertices of discretized shapes according to a target vertex distribution approximately independent of the number of vertices, for sufficiently fine meshes.

Since the number of mesh vertices is constant during standard shape optimization routines with mesh morphing, no convergence of point densities to g^M can be witnessed. Hence a discrete representation of g^M has to be estimated via the mesh discretization used in applications. For this, special care must be taken, since the outcome of the redistribution of vertices is crucially influenced by the choice of g^M. We address a possible choice for g^M regarding numerical implementation in section 5.4.

The growing amount of possibilities to locate N labeled points according to a prescribed distribution is the cause of non-unique solutions of problem (5.10). As N grows to infinity, characterization (iii) from theorem 10 shows that global solutions in each fiber are obtained by letting the $(f_\varphi \,\mathrm{d}s)$-volume-invariant diffeomorphisms act on a fixed global solution $\hat{\varphi} \in \pi(\varphi)$. In the discretized setting, this particularly means that the parameterization tracking problem (5.10) does neither recognize

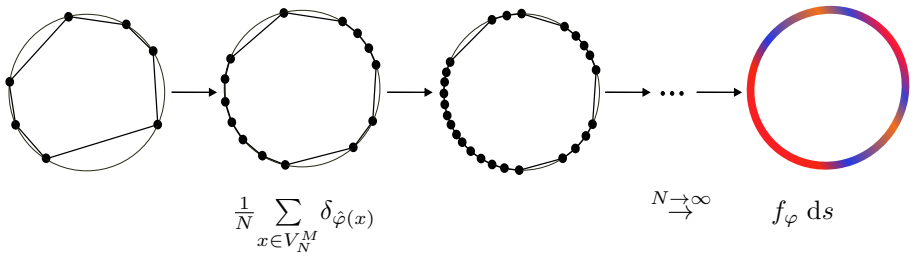

Figure 5.1: Illustration of normed Dirac distributions weak*-converging towards a limiting measure for growing N. The normed Dirac distributions can be interpreted as meshes with according vertices, while growing N increases their refinement, resulting in convergence to an infinitesimal mesh analogue $f_\varphi \, \mathrm{d}s$.

labeled mesh vertices, nor mesh topology or connectivities. Rather, its minimizers consist of parameterizations, which result in meshes of specified relative local resolution according to f_φ. This means the collection of volume-preserving diffeomorphisms can be interpreted as a symmetry group of each shape $\varphi(M)$, which leaves configuration of point distributions prescribed by f_φ invariant. We explore this in the next subsection, where we relate global solutions in fibers by L^2-metrics on volume-preserving diffeomorphism groups and Euler flows.

5.2.2 Characterization of Solutions by Diffeomorphism Groups and Euler Flows

In section 5.1, we have established an existence result for embeddings, which solve the pre-shape parameterization tracking problem (5.10) globally. It is perhaps unsatisfactory, that no result for uniqueness in each fiber is given in theorem 10. In this subsection, we study how these non-unique global solutions relate to each other. Also, we see how L^2-metrics on fibers of pre-shape spaces can serve as a tool to further understand the general structure of pre-shape spaces. Our approach is motivated from the following observation. As a consequence of the divergence theorem, we know that the divergence operator for vector fields on manifolds measures the local volume change of their induced flows (cf. [111, Prop. 16.33]). In particular, divergence-free vector fields induce flows which preserve the volume. From our abstraction of the parameterization tracking problem in (5.19), we know that its global solutions induce volume forms on manifolds according to a prescribed target density f_φ. It is then natural to ask, under which condition the target volume form is preserved by induced flows of vector fields. An answer can be given by considering general divergences, defined using Lie-derivatives with respect to volume forms. In this subsection, we give associated definitions. For submanifolds of $\mathbb{R}^{n+1}$, we relate these volume form specific divergences to so-called *tangential f-divergences*. Then we see, that vector fields with vanishing tangential f_φ-divergence induce flows that preserve the optimality of the parameterization tracking problem. In particular, this gives a local relationship of non-unique solutions in a given fiber. Put differently, with a suitable L^2-metric on fibers of the pre-shape space depending on f_φ, we find that corresponding geodesics leave the parameterization tracking problem (5.10) minimal in f-divergence free directions. Note that other authors, e.g. as in [47], use the term H_0-metric in this context.

To make this rigorous, and to fit the context of pre-shape spaces, we use techniques involving infinite dimensional diffeomorphism groups of manifolds originating from geometric mechanics. First results of this branch of mathematics were made

in the sixties by Russian mathematician Vladimir Arnold (cf. [6]), who related motions of incompressible ideal fluids to geodesics in the groups of volume-preserving diffeomorphisms. In the early seventies, this theory was developed further, with important contributions made by David Ebin and Jerrold Marsden (cf. [47]), and Hideki Omori (cf. [142, 143, 71]). The main result of this subsection states, that for a given global solution $\tilde{\varphi}$ to (5.10), all neighboring global solutions in its fiber $\pi(\tilde{\varphi})$ can be constructed via flows on the corresponding shape $\tilde{\varphi}(M)$ satisfying the incompressible Euler equations with zero force and tangential f-divergence free initial velocity. In this subsection, we stay in the C^∞-context. Still, notice that following results and formulations are true in the Hölder and Sobolev setting, and for nonlinear ambient spaces. We give remarks at suitable places indicating such modifications.

Relating Different Concepts of Divergences The notion of divergence with respect to volume forms builds on Lie derivatives, which are defined as follows (cf. [175, p. 77]).

Definition 18 (Lie Derivative of k-Forms)**.** *Let M be a smooth manifold and $\omega \in C^\infty(M, \bigwedge^k T^*M)$ a smooth k-form on M. For a smooth vector field $V \in C^\infty(M, TM)$, the* Lie derivative of ω in direction V *is given by*

$$\mathcal{L}_V \omega_p := \frac{\mathrm{d}}{\mathrm{d}t}_{|t=0} \Phi_t^* \big(\omega_{\Phi_t(p)}\big) \qquad \forall p \in M, \tag{5.30}$$

where Φ_t^* is the pullback of the flow $\Phi_t \colon M \to M$ generated by V satisfying

$$\dot{\Phi}_t(p) = V\big(\Phi_t(p)\big) \quad \textit{with} \quad \Phi_0(p) = p \tag{5.31}$$

for all $p \in M$.

Notice that this definition of a Lie derivative does not rely on the introduction of a Riemannian metric, or even a connection on the manifold M. For this reason, the following definition of divergence suits our purposes, since it is only based on a given volume form ω on M (cf. [166, Ch. 3.3], [111, Ch. 9], [175, Ch. 2.2], [47, p. 123]).

Definition 19 (Divergence on Manifolds by Volume Forms)**.** *Let M be a smooth, n-dimensional manifold. Consider a smooth volume form $\omega \in C^\infty(M, \bigwedge^n T^*M)$ and let $V \in C^\infty(M, TM)$ be a smooth tangential vector field. Then the* ω-divergence of V *is the unique smooth function* $\operatorname{div}_\omega(V) \colon M \to \mathbb{R}$ *defined by the relation*

$$\mathcal{L}_V \omega = \operatorname{div}_\omega(V) \cdot \omega. \tag{5.32}$$

We have introduced different concepts for divergences on manifolds , namely the tangential definition (4.65) , and the more abstract definition 19. For the next main result, we use the more abstract definition, as they involve volume forms. Still, to let these results carry over to the computationally feasible setting, we relate these notions to the numerically more practical tangential definitions.

Consider $M \subset \mathbb{R}^{n+1}$ to be a smooth, compact, n-dimensional submanifold of $\mathbb{R}^{n+1}$. Let us equip $\mathbb{R}^{n+1}$ with the Euclidean metric $\langle \cdot, \cdot \rangle^{\mathbb{R}^{n+1}}$. Now define a metric on M via the pullback of the inclusion map $i_M \colon M \subset \mathbb{R}^{n+1} \to \mathbb{R}^{n+1}$. For $V, W \in T_pM$, choose a local orthonormal frame of the form $(\tau_1, \dots, \tau_n, n)$ at $p \in M \subset \mathbb{R}^{n+1}$ with respect to $\langle \cdot, \cdot \rangle^{\mathbb{R}^{n+1}}$, where n is the outer unit normal vector field on M. Then the metric is locally represented as

$$i_M^* \Big(\langle \cdot, \cdot \rangle^{\mathbb{R}^{n+1}} \Big)(V, W) = \big\langle \mathrm{d}i_M(V), \mathrm{d}i_M(W) \big\rangle^{\mathbb{R}^{n+1}} \tag{5.33}$$

It induces a Riemannian volume form, which we denote by $\omega^M := i_M^*(\omega_{\langle\cdot,\cdot\rangle^{\mathbb{R}^{n+1}}})$. Due to injectivity of the inclusion map, we can define an inverse on its image, the restriction map denoted by i_M^{-1} with abuse of notation. The differentials of both maps have local representation as $(n+1)\times n$, respectively $n\times(n+1)$-matrices

$$\mathrm{d}i_M = \begin{pmatrix} 1 & \dots & 0 \\ \vdots & \ddots & \vdots \\ 0 & \dots & 1 \\ 0 & \dots & 0 \end{pmatrix}, \quad \mathrm{d}i_M^{-1} = \begin{pmatrix} 1 & \dots & 0 & 0 \\ \vdots & \ddots & \vdots & \vdots \\ 0 & \dots & 1 & 0 \end{pmatrix} \tag{5.34}$$

with respect to the orthonormal frames $(\tau_1,\dots,\tau_n) \subset (TM)^n$ and $(\tau_1,\dots,\tau_n,n) \subset (T\mathbb{R}^{n+1})^{n+1}$. We can now locally relate the tangential divergence $\mathrm{div}_\Gamma\colon C^\infty(\mathbb{R}^{n+1},\mathbb{R}^{n+1}) \to C^\infty(M,\mathbb{R})$ and the divergence $\mathrm{div}_{\omega^M}\colon C^\infty(M,TM) \to C^\infty(M,\mathbb{R})$ on M defined by the Euclidean induced volume ω^M (cf. definition 19). For $V \in C^\infty(\mathbb{R}^{n+1},\mathbb{R}^{n+1})$ and $W \in C^\infty(M,TM)$, the formal expressions involved are

$$\mathrm{div}_\Gamma(V) = \mathrm{div}_{\omega^M}\left(\mathrm{d}i_M^{-1}V\right) \qquad \text{and} \qquad \mathrm{div}_{\omega^M}(W) = \mathrm{div}_\Gamma\left(\mathrm{d}i_M W\right). \tag{5.35}$$

Hence, from the numerical perspective, the tangential divergence is the divergence on M with respect to the volume form induced by the Euclidean metric of $\mathbb{R}^{n+1}$. Notice that $\mathrm{d}i_M W$ can be smoothly extended in normal directions on tubular neighborhoods of the compact and C^∞-regular $M \subset \mathbb{R}^{n+1}$, which makes application of $\mathrm{div}_\Gamma\colon C^\infty(\mathbb{R}^{n+1},\mathbb{R}^{n+1}) \to C^\infty(M,\mathbb{R})$ well-defined. The theoretical justification for this is, that tangential and orthogonal bundles can be embedded in Euclidean spaces, and that for every embedded submanifold in Euclidean space, we have existence of tubular neighborhoods (cf. [111, Thm. 6.24]). Then, as a consequence of the Tietze-Urysohn extension theorem (cf. [137, Thm. 35.1]) and the Whitney approximation theorem (cf. [111, Thm. 6.26, Cor. 6.27]), we have guaranteed smooth extendability in normal directions.

Next, we give a conversion formula for the tangential definitions of divergences under arbitrary volume forms on shapes, which are feasible for numerical computations. Since we could not find such a derivation in the literature, we give one ourselves. For this, let us consider a smooth, orientable, compact n-dimensional submanifold $M \subset \mathbb{R}^{n+1}$. The next calculations are valid, if the prototype manifold M is replaced by shapes $\varphi(M)$ with $\varphi \in \mathrm{Emb}(M,\mathbb{R}^{n+1})$. After we choose an orientation on M, we can express all orientation respecting and non-vanishing volume forms $\omega \in C^\infty(M,\bigwedge^n T^*M)$ as $f\cdot\omega^M$, with positive coefficient functions $f \in C^\infty(M,(0,\infty))$. As discussed for generalization of parameterization tracking in section 5.1, these correspond to the choice of targets f_φ in theorem 10 for each fiber of $\mathrm{Emb}(M,\mathbb{R}^{n+1})$. In following, we need Cartan's formula for Lie derivatives from exterior calculus ([111, Thm. 14.35], [175, Ch. 1, Prop. 13.1]), which is given by

$$\mathcal{L}_V\omega = \mathrm{d}\big(i_V\omega\big) + i_V\big(\mathrm{d}\omega\big), \tag{5.36}$$

where i_V denotes the operator inserting V, also known as the interior product. With definition 19 of divergences on manifolds via Lie derivatives of volume forms,

we get a conversion formula for $\operatorname{div}_{f\cdot\omega^M}$ and $\operatorname{div}_{\omega^M}$ by

$$\begin{aligned}\operatorname{div}_{f\cdot\omega^M}(V)\cdot\big(f\cdot\omega^M\big) &= \mathcal{L}_V\big(f\cdot\omega^M\big)\\ &= \mathrm{d}\Big(i_V\big(f\cdot\omega^M\big)\Big) + i_V\Big(\mathrm{d}\big(f\cdot\omega^M\big)\Big)\\ &= \mathrm{d}\Big(i_V\big(f\cdot\omega^M\big)\Big) + 0\\ &= \mathrm{d}\Big(i_{f\cdot V}\big(\omega^M\big)\Big) \quad + i_{f\cdot V}\Big(\mathrm{d}\big(\omega^M\big)\Big)\\ &= \mathcal{L}_{f\cdot V}\big(\omega^M\big)\\ &= \operatorname{div}_{\omega^M}(f\cdot V)\cdot\omega^M,\end{aligned} \tag{5.37}$$

for all $V \in C^\infty(M, TM)$. Here, we used Cartan's formula for equalities two and five, and that exterior derivatives vanish for volume forms at equalities three and four. Notice that this computation does not rely on the choice of metric on M.

This conversion formula serves as a motivation to define a so-called *tangential f-divergence* via the standard tangential divergence for $f \in C^\infty(M, (0,\infty))$ by setting

$$\operatorname{div}_{f,\Gamma}(V) := \frac{1}{f}\cdot\operatorname{div}_\Gamma(f\cdot V) \qquad \forall V \in C^\infty\big(\mathbb{R}^{n+1}, \mathbb{R}^{n+1}\big). \tag{5.38}$$

We can now express divergences in the tangential calculus framework, which are not induced by the Euclidean metric of the ambient space. At the same time, tangential f-divergences are compatible with the intrinsically defined divergences via Lie derivatives from definition 19. In particular, for constant f, we recover the standard tangential divergence $\operatorname{div}_\Gamma$. Since f is non-vanishing, we get the relationship

$$V \text{ is tangential } f\text{-divergence free} \Leftrightarrow f\cdot V \text{ is tangential divergence free.} \tag{5.39}$$

Further, the definition of tangential f-divergence does not depend on the scaling of $f \in C^\infty(M, (0,\infty))$. More formally, for all $c > 0$, it holds

$$\operatorname{div}_{f,\Gamma}(V) = \operatorname{div}_{c\cdot f,\Gamma}(V) \quad \forall V \in C^\infty\big(\mathbb{R}^{n+1}, \mathbb{R}^{n+1}\big). \tag{5.40}$$

A graphical visualization of a divergence and f-divergence free vector field is shown in figure 5.2.

Splitting of Diffeomorphism Groups and Pre-Shape Spaces by Volume Forms With the definition of tangential f-divergence, we have a characterization of vector fields that leave a volume form $f\cdot\omega^M$ invariant. Next, we select several results made by Ebin and Marsden from their seminal paper [47] concerning Euler flows via diffeomorphism groups and volume forms. For excellent sources about infinite dimensional Lie group theory, we refer the reader to the compilations by Omori [71] and Smolentsev [166].

In their celebrated 1970 paper, Ebin and Marsden (cf. [47, Thm. 5.1, Thm. 8.6], [105, Thm. 43.7], [71, Ch. 8, Thm. 1.2]) extended a homeomorphism result of Omori (cf. [142]), which deals with the structure of diffeomorphism groups $\operatorname{Diff}(M)$, to a diffeomorphism one by use of Moser's theorem. Particularly, they showed that for a given compact, oriented C^∞-manifold M, perhaps with smooth boundary, and a given fixed volume form $\omega \in C^\infty(M, \bigwedge^n T^*M)$, the group $\operatorname{Diff}_+(M)$ of orientation preserving diffeomorphisms splits diffeomorphically to

$$\operatorname{Diff}_+(M) \cong \operatorname{Diff}_\omega(M) \times \operatorname{vol}^+_\omega(M). \tag{5.41}$$

Here,

$$\operatorname{Diff}_\omega(M) = \Big\{\, \rho \in \operatorname{Diff}(M) :\ \rho^*(\omega) = \omega \,\Big\} \tag{5.42}$$

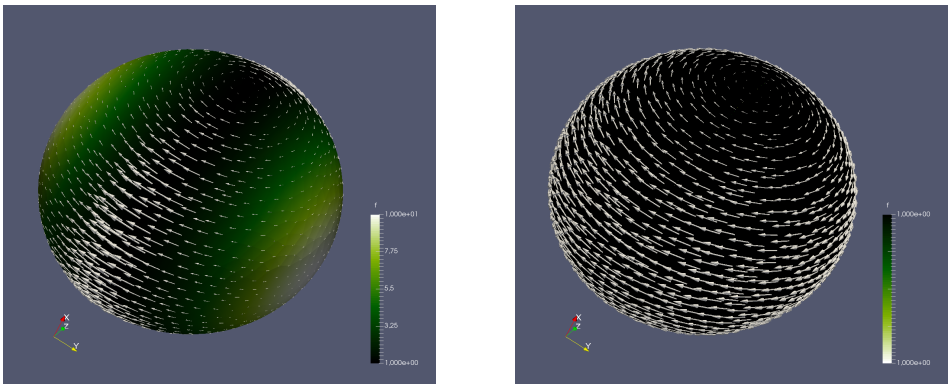

(a) Tangential f-divergence free V (b) Tangential divergence free V

Figure 5.2: Divergence free vector fields on a sphere with radius 0.3 and center $(0.5, 0.5, 0.5)$. Picture (a) uses a coefficient of volume form $f = 10(x - 0.5)^2 + 1$, while (b) uses $f = 1$, both depicted in green color. Since f is constant for (b), its color axis is reversed for visibility.

is the *group of ω-preserving diffeomorphisms of M*, and

$$\mathrm{vol}_\omega^+(M) = \left\{ \tilde{\omega} \in C^\infty\Big(M, \bigwedge^n T^*M\Big) : \ \tilde{\omega} > 0 \text{ and } \int_M \tilde{\omega} = \int_M \omega \right\} \tag{5.43}$$

is the *set of smooth volume forms with the same orientation and total volume as ω*. The choice of volume form ω is arbitrary. Thus, this splitting result gives a whole variety of possible ways to represent $\mathrm{Diff}_+(M)$. As argued in [61, Ch. 4], this result also holds for the group $\mathrm{Diff}(M)$, when $\mathrm{vol}_\omega^+(M)$ is replaced by the set of volume forms $\mathrm{vol}_\omega(M)$ with the same total integral as ω up to a difference in sign.

To fit our situation, ω can be chosen as

$$f_\varphi \cdot \omega^{\varphi(M)} = f_\varphi \cdot i^*_{\varphi(M)}\big(\omega_{\langle\cdot,\cdot\rangle^{\mathbb{R}^{n+1}}}\big),$$

which is the Euclidean induced volume form on $\varphi(M)$ weighted by a density f_φ already encountered in abstract problem (5.19). With the characterization of solutions to the parameterization tracking problem from theorem 10, we see that optimization in a fiber is essentially taking place for the components of φ in $\mathrm{vol}^+_{f_\varphi \cdot \omega^{\varphi(M)}}(\varphi(M))$. The non-uniqueness in each fibers is created by the remaining structure $\mathrm{Diff}_{f_\varphi \cdot \omega^{\varphi(M)}}(\varphi(M))$, which is reflected exactly by characterization (ii) and (iii) of equivalent solutions from theorem 10.

We know that fibers satisfy the isomorphism $\pi(\varphi) \cong \mathrm{Diff}(\varphi(M))$ (cf. definition 13, isomorphism (4.6)). Also, we are aware that $\mathrm{Diff}(\varphi(M))$ decomposes into multiple disjoint connected components. Two such collections of components are the orientation preserving diffeomorphisms $\mathrm{Diff}_+(\varphi(M))$, and potentially orientation reversing ones $\mathrm{Diff}_-(\varphi(M))$. To fulfill characterization theorem 10 (ii) of solutions to (5.10), global minimizers have to be orientation preserving embeddings, since otherwise negative Jacobians would conflict equality due to $g^M > 0$ and $f_\varphi > 0$. Given a global solution $\tilde{\varphi} \in \pi(\varphi)$ to the pre-shape parameterization tracking problem (5.10), we state the set of solutions in the fiber using diffeomorphism groups. With characterization (iii) of theorem 10, the space of solutions in the fiber $\pi(\varphi)$ is given by

$$\mathrm{Diff}_{f_\varphi \cdot \omega^{\varphi(M)}}\big(\varphi(M)\big) \circ \tilde{\varphi} := \Big\{ \rho \circ \tilde{\varphi} : \ \rho \in \mathrm{Diff}_{f_\varphi \cdot \omega^{\varphi(M)}}\big(\varphi(M)\big) \Big\} \subset \pi(\varphi) \subset \mathrm{Emb}\big(M, \mathbb{R}^{n+1}\big). \tag{5.44}$$

Before we can state the main result of this subsection, we need to clear the situation concerning Riemannian metrics on diffeomorphism groups. A main result of Ebin and Marsden made in [47, Ch. 9, Ch. 10, Ch. 14] is, that for a given Riemannian metric $\langle\cdot,\cdot\rangle^M$ on a sufficiently smooth, compact and finite-dimensional manifold M, perhaps with boundary, flows which obey the Euler equations on M for a perfect fluid can be constructed using geodesics on the group of ω-volume preserving diffeomorphisms of $\mathrm{Diff}_{\omega_{\langle\cdot,\cdot\rangle^M}}(M)$. In this framework, the flow equations are often referred to as *Euler-Arnold equations*. The authors of [47] work in the context of weakly differentiable diffeomorphisms in Hilbert manifolds $\mathrm{Diff}^s_{\omega_{\langle\cdot,\cdot\rangle^M}}(M)$ of order $s > \frac{\dim(M)}{2} + 1$ (cf. [47, Thm. 9.1, Thm. 9.6]), which is owed to the Sobolev embedding theorems. These spaces are completions of $\mathrm{Diff}_{\omega_{\langle\cdot,\cdot\rangle^M}}(M)$ with respect to Sobolev norms $\|\cdot\|_{H^s}$, and thus enlargements of it. Also, they do not form groups of Lie-type (see discussion in remark 7 and p. 25). For these groups, the H^0- or L^2-metric at $\rho \in \mathrm{Diff}^s_{\omega_{\langle\cdot,\cdot\rangle^M}}(M)$ is defined as

$$\big\langle V, W\big\rangle^{H_0}_{\rho} := \int_M \big\langle V(x), W(x)\big\rangle^M_{\rho(x)} \omega_{\langle\cdot,\cdot\rangle^M,x} \tag{5.45}$$

for $V, W \in T_\rho \mathrm{Diff}^s_{\omega_{\langle\cdot,\cdot\rangle^M}}(M) = \{\, V \in H^s(M, \mathbb{R}^{n+1}) :\ \pi_{\mathrm{Diff}^s(M)} \circ V = \rho\}$. In [47, Thm. 9.1, Thm. 9.6, Ch. 9 Important Remark], Ebin and Marsden show that this indeed defines a weak Riemannian metric. By weak Riemannian metric, we mean that the metric is injective as a map from the tangent bundle to the cotangent bundle, but not necessarily surjective (cf. [132]). It gives a well-defined Riemannian exponential map on a neighborhood of the zero section of $T\,\mathrm{Diff}^s_{\omega_{\langle\cdot,\cdot\rangle^M}}(M)$, whose geodesics are flows of Euler-Arnold equations (cf. [47, Problem 15.1 and following]). In this setting, uniqueness of solutions to Euler-Arnold equations is guaranteed for $s > \frac{\dim(M)}{2} + 1$ (cf. [47, Thm. 15.2]). The Riemannian exponential must not be mistaken with the group exponentials of $\mathrm{Diff}^s_{\omega_{\langle\cdot,\cdot\rangle^M}}(M)$, which are not surjective in a neighborhood of the identity. Due to this infinite dimensional phenomenon, it does not connect all local pairs of diffeomorphisms in general (cf. [47, Ch. 9 Important Remark]). For our situation, this means the group exponentials of $\mathrm{Diff}^s_{\omega_{\langle\cdot,\cdot\rangle^M}}(\varphi(M))$ are not suitable to locally connect solutions of (5.10) in a fiber $\pi(\varphi)$.

For the following theorem and proof, notice that $\varphi \in \mathrm{Emb}(M, \mathbb{R}^{n+1})$ denotes a global solution, and takes the role of $\tilde{\varphi}$ from theorem 10 for readability. Also, we denote by $\nabla_u u$ the covariant derivative of u in direction u with respect to a Riemannian metric, i.e. its Levi-Civita connection, and by 'grad' the gradient defined with respect to a Riemannian metric.

Theorem 11 (Characterization of Equivalent Solutions to Shape Parameterization Tracking by Euler Flows)**.** *Assume the setting of theorem 10. Let φ be a global solution to the pre-shape parameterization tracking problem* (5.10) *and $\varphi(M)$ its corresponding shape.*

Then there exists a Riemannian metric $\langle\cdot,\cdot\rangle^{\varphi(M),f}$ with corresponding volume form $\omega^{\varphi(M),f}$ on $\varphi(M)$, such that for every vector field $V \in C^\infty(\mathbb{R}^{n+1}, \mathbb{R}^{n+1})$ parallel to the boundary $\partial\varphi(M)$ with vanishing tangential f_φ-divergence

$$\mathrm{div}_{f_\varphi,\Gamma}(V) = 0, \tag{5.46}$$

there exists a $\tau > 0$ and a unique time-dependent tangential vector field $u(t,x)\colon (-\tau,\tau) \times \varphi(M) \to T\varphi(M)$, parallel to $\partial\varphi(M)$ and smooth in $\mathrm{int}(\varphi(M))$*, and $p(t,x)\colon (-\tau,\tau) \times \varphi(M) \to \mathbb{R}$, such that the* incompressible Euler equations on

$\varphi(M)$ without external force

$$\begin{aligned} \frac{\partial u_t}{\partial t} + \nabla^{\varphi(M),f}_{u_t}(u_t) &= \operatorname{grad}^{\varphi(M),f}(p_t) \\ \operatorname{div}_{\omega^{\varphi(M),f}}(u_t) &= 0 \\ u_0 &= \mathrm{d}i^{-1}_{\varphi(M)} V_{|\varphi(M)} \\ u_t &\text{ parallel to } \partial\varphi(M) \end{aligned} \tag{5.47}$$

are satisfied (cf. equation (5.38)*). Further, u_t defines a flow $\Phi_t \colon \varphi(M) \to \varphi(M)$, such that for all $t \in (-\tau, \tau)$, the embeddings $(\Phi_t \circ \varphi) \in \pi(\varphi)$ are global solutions to* (5.10) *in the fiber of $\varphi(M)$.*

For the converse, let $s > \frac{\dim(M)}{2} + 1$. Then there exists an open neighborhood U of φ in the space of all solutions in the same fiber $\operatorname{Diff}_{f_\varphi \cdot \omega^{\varphi(M)}}(\varphi(M)) \circ \varphi$ endowed with the C^∞-topology (cf. p. 25), such that the following property holds. For every $\hat{\varphi} \in U$, we can find a direction $V \in H^s(\mathbb{R}^{n+1}, \mathbb{R}^{n+1})$, tangential to $\varphi(M)$ and parallel to $\partial\varphi(M)$, satisfying vanishing f-divergence equation (5.46)*, and unique H^s-solutions u_t and p_t to the Euler equations* (5.47)*, such that $\Phi_1 \circ \varphi = \hat{\varphi}$ is a global C^∞-solution to* (5.10) *with the flow Φ_t in $\operatorname{Diff}^s_{f_\varphi \cdot \omega^{\varphi(M)}}(\varphi(M))$ generated by u_t. The restrictions of such directions $V_{|\varphi(M)}$ all correspond to a unique direction $\tilde{V} \in H^s(\varphi(M), T\varphi(M))$.*

If ∂M is empty, then the unique initial velocity $\tilde{V}$ is smooth, i.e. $\tilde{V} \in C^\infty(\varphi(M), T\varphi(M))$ and the flow Φ_t is in $\operatorname{Diff}_{f_\varphi \cdot \omega^{\varphi(M)}}(\varphi(M))$.

Proof. For the proof we proceed in multiple steps. First, let us assume the setting of theorem 10 and fix a global solution φ to the pre-shape parameterization tracking problem (5.10), which exists by theorem 10. We explicitly construct a Riemannian metric on the shape $\varphi(M)$ using solution φ, which corresponds to the target volume form $f_\varphi \cdot \omega^{\varphi(M)}$. Then, we use techniques by Ebin and Marsden [47] to define a Riemannian metric on the space of solutions in the fiber $\pi(\varphi)$, with geodesics of regularity corresponding to Euler flows on $\varphi(M)$. These give us local C^∞-diffeomorphisms on the solution space by the exponential map of the weak Riemannian metric, which we use to connect a given local pair of global minimizers. For the last part of the second assertion, owed to the C^∞-regularity setting, we use techniques developed by Omori in [71].

Let us first construct an appropriate volume form on $\varphi(M)$. Since M is assumed to be a submanifold of $\mathbb{R}^{n+1}$, we can equip M with a Riemannian metric $\langle \cdot, \cdot \rangle^M$ induced via pullback of the Euclidean metric, which itself induces a corresponding volume form we denote by ω^M. Now we use global solution characterization (ii) of theorem 10, and rearrange it by use of pullbacks and $g^M > 0$ to get

$$g^M \circ \varphi^{-1} \cdot \left(\varphi^{-1}\right)^* \left(\omega^M\right) = f_\varphi \cdot \omega^{\varphi(M)} \quad \text{on } \varphi(M) \tag{5.48}$$

as an equality of volume forms. This motivates the definition of a map

$$\langle \cdot, \cdot \rangle^{\varphi(M),f} := \left(g^M \circ \varphi^{-1}\right)^2 \cdot \left(\varphi^{-1}\right)^* \left(\langle \cdot, \cdot \rangle^M\right) \colon T\varphi(M) \times T\varphi(M) \to \mathbb{R}. \tag{5.49}$$

We see that $\langle \cdot, \cdot \rangle^{\varphi(M),f}$ indeed defines a Riemannian metric for $\varphi(M)$, as $\left(g^M \circ \varphi^{-1}\right)^2$ is positive, non-vanishing and φ^{-1} is a diffeomorphism when restricted to $\varphi(M)$. Next, we show that the volume form $\omega^{\varphi(M),f}$ coincides with $f_\varphi \cdot \omega^{\varphi(M)}$. We can see this by the following two identities. First, we can characterize coefficients

$(g_{ij}^{\varphi(M),f})_{i,j=1,\dots,n}$ corresponding to $\langle\cdot,\cdot\rangle^{\varphi(M),f}$ by use of local coordinates

$$\begin{aligned}\left(g_{ij}^{\varphi(M),f}\right)_{i,j=1,\dots,n} &= \left(g^M\circ\varphi^{-1}\right)^2\cdot\left((\varphi^{-1})^*\left(\langle\cdot,\cdot\rangle^M\right)\left[\frac{\partial}{\partial x_i},\frac{\partial}{\partial x_j}\right]\right)_{i,j=1,\dots,n}\\ &= \left(g^M\circ\varphi^{-1}\right)^2\cdot\left(\left\langle \mathrm{d}\varphi^{-1}\frac{\partial}{\partial x_i},\mathrm{d}\varphi^{-1}\frac{\partial}{\partial x_j}\right\rangle^M\right)_{i,j=1,\dots,n}\\ &= \left(g^M\circ\varphi^{-1}\right)^2\cdot D\varphi^{-T}\left(g_{ij}^M\right)_{i,j=1,\dots,n}D\varphi^{-1},\end{aligned}\tag{5.50}$$

where $D\varphi^{-1}$ is the local representation of $\mathrm{d}\varphi^{-1}$ by a Jacobian matrix, and $(g_{ij}^M)_{i,j=1,\dots,n}$ a local coefficient matrix of $\langle\cdot,\cdot\rangle^M$. Next, by using the formula for pullbacks [111, Prop. 14.20] and description of volume forms induced by Riemannian metrics in local coordinates [111, Prop. 15.31], we get

$$\begin{aligned}\omega^{\varphi(M),f} &= \sqrt{\det\left((g_{ij}^{\varphi(M),f})_{i,j=1,\dots,n}\right)}\cdot\mathrm{d}x_1\wedge\dots\wedge\mathrm{d}x_n\\ &= \sqrt{\det\left(\left(g^M\circ\varphi^{-1}\right)^2\cdot D\varphi^{-T}\left(g_{ij}^M\right)_{i,j=1,\dots,n}D\varphi^{-1}\right)}\cdot\mathrm{d}x_1\wedge\dots\wedge\mathrm{d}x_n\\ &= g^M\circ\varphi^{-1}\cdot\left(\det\left(D\varphi^{-1}\right)\cdot\sqrt{\det\left(g_{ij}^M\right)_{i,j=1,\dots,n}}\cdot\mathrm{d}x_1\wedge\dots\wedge\mathrm{d}x_n\right)\\ &= g^M\circ\varphi^{-1}\cdot(\varphi^{-1})^*(\omega^M)\\ &= f_\varphi\cdot\omega^{\varphi(M)},\end{aligned}\tag{5.51}$$

where we also used rules for determinants of transposes and products for the third equality, and motivating equation (5.48) for the last equality.

With a sufficient metric on $\varphi(M)$, we can formulate the Euler equations (5.47). Next, we focus on constructing parameterization tracking solutions by use of Euler flows. The authors of [47] work in the context of Hilbert manifolds $\mathrm{Diff}^s(\varphi(M))$. Hence we cannot simply reuse their results, but have to make modifications to suit our C^∞-context.

With the Riemannian metric from equation (5.49) on $\varphi(M)$, we can define a Riemannian metric on $\mathrm{Diff}^s_{f_\varphi\cdot\omega^{\varphi(M)}}(\varphi(M))$ for $s>\frac{\dim(M)}{2}+1$. The according bilinear form is

$$\left\langle V,W\right\rangle_\rho^{H_0}:=\int_{\varphi(M)}\left\langle V(x),W(x)\right\rangle_{\rho(x)}^{\varphi(M),f}\cdot\omega_x^{\varphi(M),f}\tag{5.52}$$

for $V,W\in T_\rho\,\mathrm{Diff}^s_{\omega^{\varphi(M),f}}(\varphi(M))$. From a technical perspective, if $\partial\varphi(M)$ is nonempty and vectors in outward normal direction are regarded, it is necessary to work with the tangent bundle of the double of $\varphi(M)$ (cf. [111, Ex. 9.32]). However, we are only interested in directions parallel to $\partial\varphi(M)$, and can hence avoid this. Since $\mathrm{Diff}_{\omega^{\varphi(M),f}}(\varphi(M))\subset\mathrm{Diff}^s_{\omega^{\varphi(M),f}}(\varphi(M))$, equation (5.52) also defines an identical bilinear form on $\mathrm{Diff}_{\omega^{\varphi(M),f}}(\varphi(M))$. With [47, Thm. 10.2], we see that this is indeed a weak Riemannian metric with an exponential map defined on a neighborhood of the zero section of $T\,\mathrm{Diff}_{\omega^{\varphi(M),f}}(\varphi(M))$, since the authors of [47] first proof necessary properties for C^∞-regular vector fields, and then apply a density argument to get the results for H^s-regular ones. In this context, the neighborhood is an element of the H_0-topology, which is the one induced by the distance function to equation (5.52), and is coarser than the C^∞-topology (cf. [166, Ch. 5.1]).

Let us consider a $V\in C^\infty(\mathbb{R}^{n+1},\mathbb{R}^{n+1})$ tangential to $\varphi(M)$ and parallel to the boundary $\partial\varphi(M)$, which fulfills equation (5.46) of vanishing tangential f_φ-divergence. By condition (5.46), we see that $V_{|\varphi(M)}$ corresponds to a unique

element $\tilde{V} \in T_{\mathrm{id}_{\varphi(M)}} \mathrm{Diff}_{\omega^{\varphi(M),f}}(\varphi(M))$. This is true, since $\mathrm{Diff}_+(\varphi(M))$ splits as in relation (5.41), and thus also induces a splitting of its tangential bundle $T\,\mathrm{Diff}_+(\varphi(M))$. The factor corresponding to $T_{\mathrm{id}_{\varphi(M)}} \mathrm{Diff}_{\omega^{\varphi(M),f}}(\varphi(M))$ consists exactly of f_φ-divergence free tangential vector fields on $\varphi(M)$ parallel to $\partial\varphi(M)$, because these form the Lie algebra of $\mathrm{Diff}_{\omega^{\varphi(M),f}}(\varphi(M))$ (cf. [47, Thm. 4.2], [166, Thm. 3.20]).

Since $\varphi(M)$ is compact, this gives a geodesic $\Phi\colon (-\tau,\tau) \to \mathrm{Diff}_{\omega^{\varphi(M),f}}(\varphi(M))$ to metric (5.52) in direction $\tilde{V}$ for some $\tau > 0$,. Its existence is guaranteed by [47, Thm. 10.2]. Also, this construction works for all V satisfying equation (5.46) by a rescaling argument for $\tilde{V}$ inserted in the exponential, since the corresponding exponential map is defined on a neighborhood of the zero section of $T\,\mathrm{Diff}_{\omega^{\varphi(M),f}}(\varphi(M))$. This defines a solution to the incompressible Euler equations (5.47) (cf. [47, Thm. 14.4, Remarks below Problem 15.1 and Remark 15.3]), in the sense, that the geodesic Φ_t is the flow to the solution velocity field u_t. Existence of solutions u_t and p_t of the incompressible Euler equations (5.47) on compact manifolds $\varphi(M)$, with u_t parallel to $\partial\varphi(M)$, associated to Φ_t is guaranteed by [47, Thm. 15.2].

Since the weak Riemannian metric (5.52) is constructed on Hilbert manifolds for $s > \frac{\dim(M)}{2} + 1$, the geodesic Φ_t might only consist of H^s-diffeomorphisms of $\varphi(M)$. However, the solutions φ of (5.10) have C^∞-regularity. Since $\varphi(M)$ is smooth and compact, and zero force is used, we can use the last assertion of regularity result [47, Thm. 15.2(i)] for all $s > \frac{\dim(M)}{2} + 1$. This gives C^∞-regularity of Φ_t for all $t \in (-\tau,\tau)$. The same holds on the interior $\mathrm{int}(\varphi(M))$ for solution u_t of the Euler equations (5.47) (cf. [47, Thm. 15.2(iii)]), which is special to the C^∞-situation, and perhaps not true for H^s-regularity. Summing up, the geodesic Φ_t is a curve of C^∞-diffeomorphisms in $\mathrm{Diff}_{\omega^{\varphi(M),f}}(\varphi(M))$. Therefore, a composition with the given global solution yields C^∞-embeddings in the same fiber $(\Phi_t \circ \varphi) \in \pi(\varphi)$. Since Φ_t is smooth and a curve of $\omega^{\varphi(M),f}$-preserving diffeomorphisms, all embeddings crossed by $(\Phi_t \circ \varphi)$ are also solutions to (5.10) by equation (5.51) and theorem 10 (iii). This gives us the first set of assertions of theorem 11.

For the second part of theorem 11, we construct a neighborhood of φ in the space of solutions, such that for every solution therein we can find a unique $\omega^{\varphi(M),f}$-divergence free $\tilde{V}$, for which the solution can be reached via the flow corresponding to the solution of the Euler equations (5.47). Let $s > \frac{\dim(M)}{2} + 1$, and ∂M perhaps nonempty. By the covering theorem in [47, Thm. 15.2 (vii)], we have existence of an open neighborhood $\tilde{U} \subset \mathrm{Diff}_{\omega^{\varphi(M),f}}(\varphi(M))$ of the identity, such that for every $\rho \in \tilde{U}$, we can find unique initial conditions $\tilde{V} \in H^s(\varphi(M), T(M))$ for the Euler equations (5.47), with the associated flow to the solution u_t achieving $\Phi_1 = \rho$.

Now we turn to the solution space. In [166, Ch. 2], the ILH-C^∞-topology on $\mathrm{Diff}(M)$ is defined as the minimal topology, such that all embeddings $\mathrm{Diff}_{\omega^{\varphi(M),f}}(M) \to \mathrm{Diff}^s_{\omega^{\varphi(M),f}}(M)$ are continuous. This means that the H^s-topologies are coarser than the C^∞-topology on $\mathrm{Diff}_{\omega^{\varphi(M),f}}(M)$. By using the bijection $(\rho \mapsto \rho \circ \varphi)$, we map $\mathrm{Diff}_{\omega^{\varphi(M),f}}(\varphi(M))$ onto the solution space of the fiber $\pi(\varphi)$. This induces a C^∞-topology on the solution space $\mathrm{Diff}_{\omega^{\varphi(M),f}}(\varphi(M)) \circ \varphi$. Since $\tilde{U}$ is a neighborhood of the identity $\mathrm{id}_{\varphi(M)}$, this gives a C^∞-neighborhood of the given solution φ

$$U := \Big(\tilde{U} \cap \mathrm{Diff}_{\omega^{\varphi(M),f}}\big(\varphi(M)\big)\Big) \circ \varphi \subset \mathrm{Diff}_{\omega^{\varphi(M),f}}\big(\varphi(M)\big) \circ \varphi.$$

By construction, for every $\hat{\varphi} \in U$, we get a unique $\rho = \hat{\varphi} \circ \varphi^{-1} \in \tilde{U}$ and unique $\tilde{V} \in T_{\mathrm{id}_{\varphi(M)}} \mathrm{Diff}_{\omega^{\varphi(M),f}}(\varphi(M))$, such that

$$\Phi_1 \circ \varphi = \exp_{\mathrm{id}_{\varphi(M)}}(\tilde{V}) \circ \varphi = \rho \circ \varphi = \hat{\varphi} \tag{5.53}$$

for the geodesic Φ_t on $\mathrm{Diff}^s_{\omega^{\varphi(M)},f}(\varphi(M))$ to the H_0-metric (5.52) with initial values $\dot{\Phi}_0 = \tilde{V}$ and $\Phi_0 = \mathrm{id}_{\varphi(M)}$. With previous arguments, the geodesic flow Φ_t corresponds to the flow of u_t, which is the unique velocity solution of Euler system (5.47). Any vector field $V \in C^\infty(\mathbb{R}^{n+1}, \mathbb{R}^{n+1})$, which is tangential to $\varphi(M)$ and parallel to $\partial\varphi(M)$, and whose restriction $V_{|\varphi(M)}$ corresponds to $\tilde{V}$, gives the same solution to the Euler system (5.47). In particular, such $V \in C^\infty(\mathbb{R}^{n+1}, \mathbb{R}^{n+1})$ necessarily fulfills f_φ-divergence condition (5.46). This proves the first part of the second assertion of theorem 11 for given global solution φ.

For the last part of the second assertion of theorem 11, we assume M to have empty boundary ∂M. We apply techniques from [71] by Omori. Consider $\mathrm{Diff}_{f_\varphi \cdot \omega^{\varphi(M)}}(\varphi(M))$ as an ILH-Lie group endowed with the ILH-C^∞-topology of the chain of Sobolev spaces

$$\Big\{ \mathrm{Diff}^s_{f_\varphi \cdot \omega^{\varphi(M)}}\big(\varphi(M)\big) : \; s \in \mathbb{N}, s > \frac{\dim(M)}{2} + 1 \Big\}.$$

We can do this with results summarized in [166, Ch. 2.2, Thm. 3.6]. Since $\varphi(M)$ has empty boundary, we have that the first and second order differentials of the Riemannian exponential map defined by equation (5.52) satisfy a linear estimate (cf. [71, Ch. 6.1, Eq. (L.Γ), Ch. 16 Thm. 1.2]). This permits the use of regularity result [71, Ch. 6.1, Thm. 1.4] for the Riemannian exponential map on the ILH-group $\mathrm{Diff}(\varphi(M))$ corresponding to equation (5.52). With this, the exponential map to equation (5.52) is a local C^∞-diffeomorphism of $T_{\mathrm{id}_{\varphi(M)}} \mathrm{Diff}_{\omega^{\varphi(M)},f}(\varphi(M))$ and $\mathrm{Diff}_{\omega^{\varphi(M)},f}(\varphi(M))$. In particular, we find a C^∞-neighborhood $\tilde{U} \subset \mathrm{Diff}_{\omega^{\varphi(M)},f}(\varphi(M))$ of the identity, such that for every $\rho \in \tilde{U}$, we can find a unique $\tilde{V} \in T_{\mathrm{id}_{\varphi(M)}} \mathrm{Diff}_{\omega^{\varphi(M)},f}(\varphi(M))$ with $\exp_{\mathrm{id}_{\varphi(M)}}(\tilde{V}) = \rho$. Since we can identify $T_{\mathrm{id}_{\varphi(M)}} \mathrm{Diff}_{\omega^{\varphi(M)},f}(\varphi(M))$ with the space of smooth f_φ-divergence-free vector fields, which are tangential on $\varphi(M)$ and parallel to $\partial\varphi(M)$ (cf. [47, Thm. 4.2]), we get C^∞-regularity of sufficient initial velocities $V \in C^\infty(\mathbb{R}^{n+1}, \mathbb{R}^{n+1})$ fulfilling f_φ-divergence freeness condition (5.46). The first part of theorem 11 guarantees that the associated flow Φ_t is in $\mathrm{Diff}_{\omega^{\varphi(M)},f}$.

Finally, all previous arguments did not depend on the specific choice of global solution $\varphi \in \mathrm{Emb}(M, \mathbb{R}^{n+1})$, nor on the structure of corresponding fibers $\pi(\varphi)$, and therefore hold for all global solutions in $\mathrm{Emb}(M, \mathbb{R}^{n+1})$. □

Remark 16 (Validity for Hölder and Sobolev Settings, and General Nonlinear Ambient Spaces)**.** *The results of the Euler characterization theorem 11 for locally similar solutions remains valid for $C^{k,\alpha}$-Hölder regular embeddings with $k \geq 1$ and $\alpha \in (0, \infty)$ (cf. [47, Rem. 12.2, Rem. 15.3]). The assertions are also true for Sobolev embeddings of H^s-regularity with $s > \frac{\dim(M)}{2} + 1$. However, if boundaries are non-trivial, they have to satisfy C^∞-regularity for similar results to hold in Hölder and Sobolev settings. Also notice that the flows Φ_t are only guaranteed to have C^1-regularity in time t, even for the C^∞-setting (cf. [47, Thm. 15.2]).*

Further, for the proof of theorem 11, we used abstract differential geometric techniques. The proof does neither rely on the ambient space to be $\mathbb{R}^{n+1}$, nor to have shapes of codimension one. Hence theorem 11 holds analogously for the abstract formulation (5.19) *of the pre-shape parameterization tracking problem, with corresponding assumptions made at p. 56 and following.*

At first, we discuss some elements of the proof to theorem 11, and then give interpretations and its implications to solution of parameterization tracking in the paragraphs thereafter.

The second assertion of the Euler characterization theorem states that there is a local one to one correspondence of initial velocities for Euler flows without force and solutions of the parameterization tracking problem in each fiber. The

key element of the proof is, that Euler flows correspond to geodesics of the H_0-metric (5.45) defined on the volume preserving diffeomorphisms $\mathrm{Diff}_{f_\varphi \cdot \omega^{\varphi(M)}}(\varphi(M))$ on shapes. In this framework, the second assertion becomes the property of the associated H_0-exponential map to be a local diffeomorphism. It is the C^∞-regularity of diffeomorphisms and pre-shapes, which makes the second part of theorem 11 rather delicate.

This stems from the fact, that Ebin and Marsden [47] use results for geodesic sprays to prove the local diffeomorphism property of the exponential map on Banach manifolds $\mathrm{Diff}^s_{f_\varphi \cdot \omega^{\varphi(M)}}(\varphi(M))$ for $s > \frac{\dim(M)}{2} + 1$. They rely on the inverse function theorem as used in [106, Ch. 4, Thm. 4.1]. However, the inverse function theorem is no longer valid in general Fréchet spaces, and thus also not for manifolds modeled by these. In particular, it does not apply for the group of C^∞-diffeomorphisms, even for compact manifolds. Hence mimicking the proof in [47, Thm. 12.1] to prove necessary properties in theorem 11 fails at this point of argument.

It is not straightforward to use regularity results of Euler flows from [47, Thm. 15.2] to prove the second assertion of theorem 11. Since we have zero force in the Euler equations (5.47), it is tempting to apply the covering property [47, Thm. 15.2 (vii)] for H^s-regular solutions. For each $s > \frac{\dim(M)}{2} + 1$, the covering property gives an open ε_s-ball of the identity in $\mathrm{Diff}^s_{\omega^{\varphi(M,f)}}(\varphi(M))$, such that there is a unique starting condition $\tilde{V}$ with H^s-regularity connecting the identity and every $\rho \in \mathrm{Diff}^s_{\omega^{\varphi(M,f)}}(\varphi(M))$ in the ε-ball by the H^s-flow to the velocity solving the Euler equations. Even by choosing a ρ with C^∞-regularity in such a ball, we only get H^s-regularity of the flow for $s < \infty$, since $\inf\{\varepsilon_s : \ s > \frac{\dim(M)}{2} + 1\} > 0$ is not guaranteed in general. Hence different arguments are needed.

There are two alternatives to the inverse function theorem in the context of Fréchet spaces, namely the Nash-Moser theorem and ILH-/ILB-normal inverse function theorems. The Nash-Moser theorem was rigorously elaborated by Hamilton in [73]. It offers a possibility to apply an inverse function theorem on so-called tamed Fréchet spaces, which includes the case of our interest. However, to apply the Nash-Moser theorem, invertibility of the differential of the exponential map at the identity is not enough. Instead, it is necessary to provide invertibility on a neighborhood of the identity, which seems rather tedious, considered that we are dealing with the differential of the exponential map of the weak Riemannian metric (5.52). Hence we choose to use results from Omori [71], which uses the technical setting of inverse limit Hilbert/Banach spaces. As we are naturally situated in this setting, we use calculations for local invertibility of the H_0-exponential map provided by Omori. The key argument of Omori is an inverse function theorem for so-called ILH-normal mappings applied at the identity element of $\mathrm{Diff}_{\omega^{\varphi(M),f}}(\varphi(M))$ and the corresponding zero section of the tangential bundle ([71, Ch. 1, Thm. 6.5]). Omori's version of the inverse function theorem of Fréchet spaces generated as inverse limits offers the attractive feature, that only invertibility of the differential at the point of interest is needed, much in line with the inverse function theorem in Banach spaces. As a caveat, it is not suited to deal with the situation of loss of derivatives, which does not happen in the C^∞-framework. When loss of derivatives occurs, the approach via tamed spaces by Hamilton is favorable.

We emphasize, that the result [71, Ch. 16, Thm. 1.2] from Omori is provided only for the case of empty boundary $\partial\varphi(M)$. Hence, theorem 11 has two parts for the second assertion, which differentiate between the nonempty and empty boundary cases. Also notice, that for the case with nonempty boundary $\partial\varphi(M)$, the second part of theorem 11 does not provide a direction, for which $\Phi_t \circ \varphi$ are solutions for all t. We cannot apply the first part from theorem 11 to achieve this, since C^∞-regularity of the unique initial velocity V is not guaranteed. Provided such a regularity results holds, the last part of theorem 11 can be extended to the nonempty boundary case.

Remark 17 (Different Metrics on $\mathrm{Diff}(\varphi(M))$)**.** *The proof of theorem 11 employs an H_0-metric on $\mathrm{Diff}_{\omega^{\varphi(M)},f}(\varphi(M))$ in style of [47]. However, the choice of an H_0-metric is rather arbitrary, and was made solely because the resulting geodesic equations correspond to Euler flows, which have a well-established regularity theory. Weak Riemannian metrics on $\mathrm{Diff}_{\omega^{\varphi(M)},f}(\varphi(M))$ for similar results as in theorem 11 need two crucial properties. The weak metric needs to induce an exponential map that gives a local diffeomorphism of a neighborhood of zero in $T\,\mathrm{Diff}_{\omega^{\varphi(M)},f}(\varphi(M))$ and a neighborhood of the identity in $\mathrm{Diff}_{\omega^{\varphi(M)},f}(\varphi(M))$. Also, the associated geodesic equations need to leave the target volume form $f_\varphi \cdot \omega^{\varphi(M)}$ invariant. The corresponding geodesic flows can be of different type, but still locally connect solutions of the parameterization tracking problems by the arguments made in the proof of theorem 11. Many weak Riemannian metrics on shape spaces and preshape fibers naturally satisfy these properties. For example, choosing an H^1_α-metric on certain subgroups of $\mathrm{Diff}_{\omega^{\varphi(M)},f}(\varphi(M))$ gives the so-called Lagrangian averaged Euler equations (LAE-equations) without external force (cf. [166, Ch. 7.4], [125]). For the special case of bounded, open domains $\varphi(M) \subset \mathbb{R}^{n+1}$ with smooth boundary, a divergence-free initial velocity V and volume-preserving diffeomorphisms leaving the boundary $\partial\varphi(M)$ pointwise fixed, these equations take the form*

$$\begin{aligned} \frac{\partial}{\partial t}\big(1-\alpha^2\cdot\Delta\big)u_t + \big(u_t\cdot\nabla\big)\big(1-\alpha^2\cdot\Delta\big)u_t + \alpha^2\cdot\big(\nabla u_t\big)^T\Delta u_t &= \nabla p_t \\ \operatorname{div}\big(u_t\big) &= 0 \\ u_0 &= V \\ u_t &= 0 \text{ on } \partial\varphi(M), \end{aligned} \tag{5.54}$$

where Δ denotes the Laplace operator.

Numerical Construction of Equivalent Solutions Next, we discuss some aspects concerning numerical simulations of equivalent solutions in light of theorem 11. In order to construct equivalent solutions, an explicit solution $\tilde{\varphi}$ of parameterization tracking problem (5.10) needs to be computed. With this solution, and $g^M\colon M \to (0,\infty)$ chosen a priori, the metric to theorem 11 can be constructed explicitly by the bilinear form

$$\langle\cdot,\cdot\rangle^\Gamma = \big(g^M\circ\tilde{\varphi}^{-1}\big)^2\cdot D^\tau\big(\tilde{\varphi}^{-1}\big)^T D^\tau\big(\tilde{\varphi}^{-1}\big), \tag{5.55}$$

where $D^\tau\tilde{\varphi}^{-1}$ have to be computed according to equation (5.2). Note that an inversion of $D^\tau\varphi$ is not necessary, as φ^{-1} is readily available by storing the vertex coordinates of starting and last iteration meshes. The differential operators $\mathrm{div}_{\omega^{f,\bar{\varphi}(M)}}$ and $\nabla^{f,\bar{\varphi}(M)}$ can be computed using Christoffel symbols from the local coefficients of the Riemannian metric (cf. [110, Ch. 13.1]). This makes the Euler equations (5.47) implementable, and in turn equivalent solutions to the numerically achieved optimal $\tilde{\varphi}$ constructible by using resulting flows as described in theorem 11.

If equivalent meshes are the only interest, it is easier to use relationship (5.39) to numerically construct equivalent solutions of the parameterization tracking problem. By this, we can avoid the use of the Riemannian metric constructed in the proof of theorem 11. Since the target f_φ is known a priori, we can transform solutions of Euler equations with respect to the metric of the ambient space, and construct solutions thereby.

Given a tangential divergence free vector field V parallel to $\partial\varphi(M)$, we can solve

the Euler equations

$$\begin{aligned} \frac{\partial}{\partial t} u_t + \big(u_t \cdot \nabla_\Gamma\big)(u_t) &= \nabla_\Gamma p_t \\ \operatorname{div}_\Gamma\big(u_t\big) &= 0 \\ u_0 &= V_{|\varphi(M)} \\ u_t &\text{ parallel to } \partial\varphi(M). \end{aligned} \tag{5.56}$$

The involved differential operators are readily available, and need neither knowledge of a solution $\tilde{\varphi}$ to the parameterization tracking problem, nor calculations via Christoffel symbols. This makes the formulation with respect to the Euclidean induced metric in system (5.56) more feasible than system (5.47). Local existence and regularity of solutions are guaranteed by [47, Thm. 15.2]. Since $\operatorname{div}_\Gamma(u_t) = 0$ for all $t \in [0, \tau)$ and some $\tau > 0$, we set

$$u_t^f := \frac{1}{f_\varphi} \cdot u_t. \tag{5.57}$$

By construction, u_t^f is tangentially f_φ-divergence free. The flow $\Phi_t^f : \varphi(M) \to \varphi(M)$ associated to u_t^f can be used to construct solutions in the fiber $\pi(\varphi)$. Indeed, given a solution $\tilde{\varphi} \in \pi(\varphi)$, we see that $\Phi_t^f \circ \tilde{\varphi}$ are global solutions to parameterization tracking, as they preserve the target volume form $f_\varphi \cdot \omega^{\varphi(M)}$ (cf. theorem 10, definition 19). Nevertheless, it is still necessary to have a solution $\tilde{\varphi} \in \pi(\varphi)$ to construct equivalent neighboring solutions in a fiber.

Interpretation with Regard to Solution of Parameterization Tracking In this paragraph, we discuss some intuitive interpretations of theorem 11. For this, let us assume the setting of discretized shapes. The discretization is usually realized by representing the underlying manifold by a mesh, i.e. a simplicial complex. Then a solution to the pre-shape parameterization tracking problem (5.10) in the discretized setting is a mesh with target configuration described by f_φ.

We can solve the incompressible Euler equations (5.47) for some given initial velocity V on an optimal mesh configuration. This gives a time dependent velocity field u_t, which in turn can be used to generate a flow on the shape. Now let the mesh vertices act as particles in the Euler flow, while still leaving the mesh connections and its topology intact. By such a flow of mesh vertices, a new mesh is generated at every point in time t for which the Euler flow exists. The first assertion of theorem 11 guarantees that, up to discretization error, all resulting meshes achieve the desired cell volume target f_φ. Also up to discretization error, the underlying shape remains invariant in time, as the resulting pre-shapes stay in the fiber of the corresponding shape.

The second part of theorem 11 strengthens this characterization, because all locally similar meshes with optimal cell volume features can be constructed via such flows. Interestingly, this means the degrees of freedom to design an optimal mesh with respect to f_φ for any given shape are in local one-to-one correspondence with tangential $f_\varphi \cdot \omega^{\varphi(M)}$-divergence-free vector fields $V \in C^\infty(\tilde{\varphi}(M), T\tilde{\varphi}(M))$, if discretization error is neglected.

The structural descriptions of pre-shape spaces $\operatorname{Emb}(M, \mathbb{R}^{n+1})$ used in the proof of theorem 11 also transfer to the tangent bundle $T\operatorname{Emb}(M, \mathbb{R}^{n+1})$. As described in [47, Thm. 4.2], the Lie algebra corresponding to $\operatorname{Diff}_{\omega^M}(\varphi(M))$ consists of ω^M-divergence free tangential vector fields on $\varphi(M)$ parallel to the boundary ∂M. If we also consider the decomposition (4.14) of $T\operatorname{Emb}(M, \mathbb{R}^{n+1})$ into horizontal and vertical parts, we get a decomposition of vector fields $V \in T_\varphi \operatorname{Emb}(M, \mathbb{R}^{n+1})$. With

slight abuse of notation, it is given as

$$V = \alpha \cdot n + W + X, \tag{5.58}$$

for a unique $\alpha \in C^\infty(\varphi(M), \mathbb{R})$ and the outer unit normal vector field n on $\varphi(M)$, a tangential $f_\varphi \cdot \omega^{\varphi(M)}$-divergence free vector field $W \in C^\infty(\varphi(M), T\varphi(M))$ parallel to $\partial\varphi(M)$, and a conservative tangential vector field $X \in C^\infty(\varphi(M), T\varphi(M))$, which can be described by a potential. Essentially, this decomposition is a combination of the orthogonal decomposition into normal and tangential components , and an additional Hodge-Helmholtz decomposition of the tangential part (cf. [162], [179, Thm. 5.2], [175, Ch. 5, Prop. 8.2]), neglecting the harmonic component (cf. [47, Cor. 7.3]).

If decomposition equation (5.58) is applied to the pre-shape gradient of the parameterization tracking problem, then each component has a different effect for the optimization. The normal component corresponds to the shape optimization part of the gradient, in line with the pre-shape derivative structure theorem 9. The exact part X is a tangential vector field from $T \operatorname{vol}_{f_\varphi \cdot \omega^{\varphi(M)}}(\varphi(M))$. This means it amounts to compression and expansion of local volume measured in comparison to f_φ. In a discrete setting, such components change local relative refinement of a mesh by reallocation of vertices. In view of the Euler characterization of solutions theorem 11, we see this component as the only relevant part of the gradient for minimization of the pre-shape parameterization tracking functional (5.10). The component W is the tangential f_φ-divergence free part of V. By examining equation (5.46) of the Euler flow characterization, we recognize that W can act as an initial condition to the incompressible Euler equations (5.47) to generate equivalent solutions in the solution space in a fiber of $\varphi(M)$ (cf. equation (5.44)). This in turn means, that vector fields from $T \operatorname{Diff}_{f_\varphi \cdot \omega^{\varphi(M)}}(\varphi(M))$ do not participate in the gradient descents for the pre-shape parameterization tracking problem. In section 5.5, we discover that the pre-shape Hessian to the parameterization tracking problem is positive semidefinite in solutions. The directions amounting to the indefiniteness are exactly the f_φ-divergence free vector fields. Hence, without use of pre-shape calculus techniques, the findings of this subsection show that weak L^2-metrics on the fibers of pre-shape spaces respect the structure of parameterization tracking problems and its higher order pre-shape derivatives.

We also emphasize that the presented decomposition involves vector fields from $C^\infty(\varphi(M), \mathbb{R}^{n+1})$, but it can be extended to vector fields on the ambient space or hold-all domain $C^\infty(\mathbb{R}^{n+1}, \mathbb{R}^{n+1})$ by taking equivalence classes of traces on $\varphi(M) \subset \mathbb{R}^{n+1}$ with regard to equation (5.58). This can serve as an initial idea for numerical methods to enforce uniqueness of the optimal parameterization in each fiber for a given starting shape with parameterization φ_0. By using descent directions and subtracting their $\operatorname{div}_{f_\varphi,\Gamma}$-free components on $\varphi(M)$, together with applying sufficiently small steps, convergence to a fiberwise unique global minimum depending on the initial data φ_0 could be achieved. Such techniques can be seen as a generalization of div-curl systems employed for deformation methods [185, 19, 29] in the special framework of Euclidean domains in 2 or 3 dimensions and uniform targets f. They can also be related to enforcement of irrotationality in mesh node advections via minimization of quadratic penalty terms found in [31]. If seen in the context of the abstract parameterization tracking formulation (5.19) and its connection to optimal transport problems, relations explored in this subsection can also be related to curl and divergence extraction techniques from [72], where optimal transport problems in Monge-Kantorovich formulation are solved for image registration and warping. However, exploring these techniques and connections, particularly to higher order methods, is beyond the scope of this work, and is left for future research.

5.3 Pre-Shape Derivative and Optimality Conditions of Parameterization Tracking

So far, we gained insight into properties of the pre-shape parameterization tracking problem (5.10) without use of pre-shape calculus. In this section, we turn our attention to its pre-shape derivative. This serves several different purposes. For one, it is of numerical interest, since a goal of this work is to construct effective algorithms for improvement of mesh quality in shape optimization routines. The results of proposition 3 and proposition 4 encourage us, as they guarantee sufficiently rich modeling possibilities of desired mesh configurations. At the same time, the parameterization tracking problem (5.10) serves as a non-trivial example to illustrate the application of pre-shape calculus techniques developed in chapter 4. In particular, we observe that its pre-shape derivative is not accessible via classical shape calculus techniques. And lastly, we give sufficient global optimality conditions for parameterization tracking via its decomposed pre-shape derivative.

In the following theorem, we leave the target functions f_φ general and only assume enough regularity for existence of the pre-shape derivative. Later in this section, we give an explicit construction of f_φ, while also ensuring existence of its pre-shape material derivatives with a closed form (cf. equation (5.84)). In section 9.1, we give another construction of f_φ tailored to shape optimization problems constrained by variational inequalities.

Theorem 12 (Pre-Shape Derivative of the Parameterization Tracking Problem)**.** *Let the assumptions of theorem 10 hold and denote by $\mathfrak{J}^M$ the objective functional of the pre-shape parameterization tracking problem* (5.10)*. Also, assume enough regularity for f_φ, such that pre-shape material derivatives exist.*

Then, for fixed $\varphi \in \mathrm{Emb}(M, \mathbb{R}^{n+1})$ and $V \in C^\infty(\mathbb{R}^{n+1}, \mathbb{R}^{n+1})$, the pre-shape derivative to problem (5.10) *is given by*

$$\begin{aligned}\mathfrak{D}\mathfrak{J}^M(\varphi)[V] = -\int_{\varphi(M)} \frac{1}{2}\cdot\Big(\big(g^M\circ\varphi^{-1}\cdot\det D^\tau\varphi^{-1}\big)^2 - f_\varphi^2\Big)\cdot\mathrm{div}_\Gamma(V)\\ + \Big(g^M\circ\varphi^{-1}\cdot\det D^\tau\varphi^{-1} - f_\varphi\Big)\cdot\mathfrak{D}_m\big(f_\varphi\big)[V]\,\mathrm{d}s,\end{aligned} \tag{5.59}$$

where $\mathfrak{D}_m(f_\varphi)$ is the pre-shape material derivative of f_φ, and div_Γ is the tangential divergence on $\varphi(M)$. The pre-shape derivative does not depend on the choice of oriented local orthonormal frames τ and τ^φ representing the covariant derivative D^τ.

Proof. For the proof we rely on pre-shape calculus rules established in chapter 4. In particular, we make use of formulae found in corollary 2. Let the assumptions made in theorem 10 hold. Fix a $\varphi \in \mathrm{Emb}(M, \mathbb{R}^{n+1})$ and let $V \in C^\infty(\mathbb{R}^{n+1}, \mathbb{R}^{n+1})$.

We begin by noticing, that the pre-shape material derivatives are well-defined for families of differentiable functions on varying domains $\{f_\varphi\colon \varphi(M) \to \mathbb{R}\}_{\varphi\in\mathrm{Emb}(M,\mathbb{R}^{n+1})}$ depending smoothly on φ (cf. remark 10). With this in mind, we can apply corollary 2 (v) and the formula for inverse determinants to get

$$\begin{aligned}\mathfrak{D}\mathfrak{J}^M(\varphi)[V] = \int_{\varphi(M)} \mathfrak{D}_m\left(\frac{1}{2}\Big(g^M\circ\varphi^{-1}\cdot\frac{1}{\det D^\tau\varphi}\circ\varphi^{-1} - f_\varphi\Big)^2\right)[V]\\ +\frac{1}{2}\,\mathrm{div}_\Gamma(V)\Big(g^M\circ\varphi^{-1}\cdot\frac{1}{\det D^\tau\varphi}\circ\varphi^{-1} - f_\varphi\Big)^2\,\mathrm{d}s.\end{aligned} \tag{5.60}$$

For simplification of the material derivative of the integrand, we employ our assumption on existence of material derivatives $\mathfrak{D}_m(f_\varphi)$, together with the chain and

product rule for material derivatives (cf. corollary 2)

$$\begin{aligned}
&\mathfrak{D}_m\left(\frac{1}{2}\Big(g^M\circ\varphi^{-1}\cdot\frac{1}{\det D^\tau\varphi}\circ\varphi^{-1}-f_\varphi\Big)^2\right)[V]\\
&=\Big(g^M\circ\varphi^{-1}\cdot\frac{1}{\det D^\tau\varphi}\circ\varphi^{-1}-f_\varphi\Big)\cdot\left(\mathfrak{D}_m\big(g^M\circ\varphi^{-1}\big)[V]\cdot\frac{1}{\det D^\tau\varphi}\circ\varphi^{-1}\right.\\
&\qquad\left.-\Big(g^M\circ\varphi^{-1}\cdot\frac{1}{(\det D^\tau\varphi)^2}\circ\varphi^{-1}\Big)\cdot\mathfrak{D}_m\big(\det D^\tau\varphi\circ\varphi^{-1}\big)[V]-\mathfrak{D}_m\big(f_\varphi\big)[V]\right).
\end{aligned}\tag{5.61}$$

In the following, we examine the remaining material derivatives of equation (5.61), except for $\mathfrak{D}_m(f_\varphi)[V]$, as we let f_φ remain general. To avoid confusion, we remind the reader that we are confronted with mappings h taking two arguments, one explicitly being a pre-shape, making them operators of the form

$$h\colon\ \mathrm{Emb}(M,\mathbb{R}^{n+1})\times M\to\mathbb{R},\ \ (\varphi,p)\mapsto h_\varphi(p).\tag{5.62}$$

We have the following relationship of embeddings and the domain perturbation T_t as in equation (3.9)

$$\varphi_t(p)=\big(T_t\circ\varphi\big)(p)\quad\forall p\in M\quad\Leftrightarrow\quad\big(\varphi_t^{-1}\circ T_t\big)(q)=\varphi^{-1}(q)\quad\forall q\in\varphi(M),\tag{5.63}$$

where φ_t is the perturbation of identity for pre-shapes for sufficiently small $t>0$ (cf. definition 16). If material derivatives of h are assumed to exist, equation (5.63) leads to the following elementary but interesting identity

$$\mathfrak{D}_m\big(h_\varphi\circ\varphi^{-1}\big)[V]=\frac{\mathrm{d}}{\mathrm{d}t}_{|t=0}h\big(\varphi_t,\varphi_t^{-1}\circ T_t\big)=\frac{\mathrm{d}}{\mathrm{d}t}_{|t=0}h\big(\varphi_t,\varphi^{-1}\big)=\mathfrak{D}\big(h_\varphi\big)[V]\circ\varphi^{-1}.\tag{5.64}$$

Applying this to the first remaining material derivative in equation (5.61), we get

$$\mathfrak{D}_m\big(g^M\circ\varphi^{-1}\big)[V]=\mathfrak{D}\big(g^M\big)[V]\circ\varphi^{-1}=0,\tag{5.65}$$

since g^M is does not depend on choice of $\varphi\in\mathrm{Emb}(M,\mathbb{R}^{n+1})$.

We apply analogous techniques to the second material derivative. Hence, for calculation of the material derivative of $\det D^\tau\varphi\circ\varphi^{-1}$, it is sufficient to calculate its pre-shape derivative. Since the flow $(\varphi_t)_{t\in[0,\tau]}$ given by the perturbation of identity in direction V is differentiable in t (cf. equation (4.24)), we can employ Jacobi's formula from proposition 1 for the derivative of the determinant at $t_0=0$

$$\begin{aligned}
\mathfrak{D}_m\big(\det D^\tau\varphi\circ\varphi^{-1}\big)[V]&=\left(\frac{\mathrm{d}}{\mathrm{d}t}_{|t=t_0}\det D^\tau\varphi_t\right)\circ\varphi^{-1}\\
&=\mathrm{tr}\left(\mathrm{Adju}\left(D^\tau\varphi_{t_0}\right)\frac{\mathrm{d}}{\mathrm{d}t}_{|t=t_0}D^\tau\varphi_t\right)\circ\varphi^{-1}\\
&\overset{t_0=0}{=}\mathrm{tr}\Big(\mathrm{Adju}\left(D^\tau\varphi\right)D^\tau(V\circ\varphi)\Big)\circ\varphi^{-1},
\end{aligned}\tag{5.66}$$

where $\mathrm{Adju}(\cdot)$ is the adjugate matrix and $\mathrm{tr}(\cdot)$ is the trace operator for matrices.

Knowing $D^\tau\varphi$ is invertible for all $p\in M$ due to $\varphi\in\mathrm{Emb}(M,\mathbb{R}^{n+1})$, we can use Cramer's rule to express the adjugate in terms of inverses. We additionally

use invariance of the trace operator under permutations of multiplicative order of matrices, giving us

$$\begin{aligned}\operatorname{tr}\Big(\operatorname{Adju}\big(D^\tau\varphi\big)D^\tau(V\circ\varphi)\Big)\circ\varphi^{-1} &= \operatorname{tr}\Big(\big(\det D^\tau\varphi\big)\cdot D^\tau\varphi^{-1}D^\tau(V\circ\varphi)\Big)\circ\varphi^{-1}\\ &= \big(\det D^\tau\varphi\big)\circ\varphi^{-1}\cdot\operatorname{tr}\Big(\big(D^\tau\varphi\big)^{-1}D^\tau V(\varphi)D^\tau\varphi\Big)\circ\varphi^{-1}\\ &= \big(\det D^\tau\varphi\big)\circ\varphi^{-1}\cdot\operatorname{tr}\Big(D^\tau V(\varphi)\Big)\circ\varphi^{-1}\\ &= \big(\det D^\tau\varphi\big)\circ\varphi^{-1}\cdot\operatorname{div}_\Gamma(V).\end{aligned} \tag{5.67}$$

Using equation (5.65) and equation (5.67) in equation (5.61), and plugging the resulting material derivative into equation (5.60), we arrive at

$$\begin{aligned}\mathfrak{D}\mathfrak{J}^M(\varphi)[V] &= \int_{\varphi(M)}\Big(g^M\circ\varphi^{-1}\cdot\frac{1}{\det D^\tau\varphi}\circ\varphi^{-1}-f_\varphi\Big)\\ &\qquad\cdot\Big(-g^M\circ\varphi^{-1}\cdot\frac{1}{\det D^\tau\varphi}\circ\varphi^{-1}\cdot\operatorname{div}_\Gamma(V)-\mathfrak{D}_m\big(f_\varphi\big)[V]\Big)\\ &\qquad+\frac{1}{2}\operatorname{div}_\Gamma(V)\Big(g^M\circ\varphi^{-1}\cdot\frac{1}{\det D^\tau\varphi}\circ\varphi^{-1}-f_\varphi\Big)^2\,\mathrm{d}s\\ &= -\int_{\varphi(M)}\Big(g^M\circ\varphi^{-1}\cdot\frac{1}{\det D^\tau\varphi}\circ\varphi^{-1}-f_\varphi\Big)\\ &\qquad\cdot\left(\frac{1}{2}\Big(g^M\circ\varphi^{-1}\cdot\frac{1}{\det D^\tau\varphi}\circ\varphi^{-1}+f_\varphi\Big)\cdot\operatorname{div}_\Gamma(V)+\mathfrak{D}_m\big(f_\varphi\big)[V]\right)\mathrm{d}s\\ &= -\int_{\varphi(M)}\frac{1}{2}\cdot\left(\Big(g^M\circ\varphi^{-1}\cdot\frac{1}{\det D^\tau\varphi}\circ\varphi^{-1}\Big)^2-f_\varphi^2\right)\cdot\operatorname{div}_\Gamma(V)\\ &\qquad+\Big(g^M\circ\varphi^{-1}\cdot\frac{1}{\det D^\tau\varphi}\circ\varphi^{-1}-f_\varphi\Big)\cdot\mathfrak{D}_m\big(f_\varphi\big)[V]\,\mathrm{d}s.\end{aligned} \tag{5.68}$$

After application of the inverse determinant formula, this is the desired pre-shape derivative (5.59). The covariant derivative $D^\tau\varphi$, and hence also the pre-shape derivative (5.59), is independent of choice of orthonormal frames by similar reasoning as in the first part of the proof to theorem 10. □

Notice that the pre-shape derivative formula (5.59) applies to the case of shapes with non-trivial boundary ∂M. Since no integration by parts, or Stokes and Gauss theorems were used in its derivation, there is no occurring boundary integral over $\partial\varphi(M)$. We emphasize that the pre-shape derivative (5.59) is represented by an integral over shapes $\varphi(M)$. Therefore it is a boundary formulation in style of equation (3.6), and not a volume formulation. This is also the case, if the modeling manifold $M\subset\mathbb{R}^{n+1}$ is of dimension $n+1$, e.g. for the parameterization tracking of hold-all domains we pursue in later chapters. In such a scenario, the pre-shape derivative equation (5.59) is represented as a volume integral, but is formally still in boundary formulation.

We observe that $\mathfrak{D}\mathfrak{J}^M(\varphi)[V]$ is non-vanishing for vector fields V tangential to $\varphi(M)$ in general. By structure theorem 9, vanishing pre-shape derivatives for tangential directions indicate a functional which is almost of classical shape type. If we take the form of pre-shape derivative (5.59) into account, this clearly means the parameterization tracking problem (5.10) can neither be formulated as a shape optimization problem, nor is it tractable by classical shape calculus.

Decomposing the Pre-Shape Derivative In light of the structure theorem 9 for pre-shape derivatives, we can further refine the representation in equation (5.59) by decomposition into normal and tangential components. Perhaps surprisingly, if the user wants to optimize for mesh quality by using pre-shape derivative based parameterization tracking, it is not recommendable to use the full pre-shape derivative found in equation (5.59). Instead, after decomposing the pre-shape derivative, it turns out that the tangential component is sufficient to reach global optimality. We further substantiate this observation with upcoming theorem 13 and in numerical section 7.3. If a special case of the pre-shape derivative's normal component is used for descent algorithms, we recover numerical methods solving Plateau's problem by constructing minimal surfaces (cf. [45, 146, 46]). In some sense orthogonal to this, the use of tangential components gives algorithms resembling the deformation method for optimization of mesh quality (cf. [112, 19, 68, 31]).

To derive this decomposition, we employ the following informal relationship between the tangential divergence and the mean curvature κ for hypersurfaces for $V \in C^\infty(\mathbb{R}^{n+1}, \mathbb{R}^{n+1})$ (cf. [110, Def. 4.23]). Orthogonality of tangential gradients $\nabla_\Gamma(\langle n, V\rangle_2)$ and the outer unit normal vector field n yield

$$\operatorname{div}_\Gamma\left(\langle n, V\rangle_2 \cdot n\right) = \left(\nabla_\Gamma \langle n, V\rangle_2\right)^T n + \langle n, V\rangle_2 \cdot \operatorname{div}_\Gamma(n) = \dim(M) \cdot \langle n, V\rangle_2 \cdot \kappa. \quad (5.69)$$

Let us briefly assume $f_\varphi \colon \mathbb{R}^{n+1} \to \mathbb{R}$ to map from the whole ambient space, which simplifies using normal derivatives of f_φ for the decomposition. With this, and the assumption of f_φ to have shape functionality, we can refine equation (5.59) to

$$\mathfrak{D}\mathfrak{J}^M(\varphi)[V] = \left\langle g_\varphi^{\mathcal{N}}, V\right\rangle + \left\langle g_\varphi^{\mathcal{T}}, V\right\rangle \qquad \forall V \in C^\infty(\mathbb{R}^{n+1}, \mathbb{R}^{n+1}), \quad (5.70)$$

with shape component

$$\begin{aligned}\left\langle g_\varphi^{\mathcal{N}}, V\right\rangle = -\int_{\varphi(M)} \frac{\dim(M)}{2} \cdot \Big(\left(g^M \circ \varphi^{-1} \cdot \det D^\tau \varphi^{-1}\right)^2 - f_\varphi^2\Big) \cdot \kappa \cdot \langle n, V\rangle_2 \\ + \Big(g^M \circ \varphi^{-1} \cdot \det D^\tau \varphi^{-1} - f_\varphi\Big) \cdot \left(\frac{\partial f_\varphi}{\partial n} \cdot \langle n, V\rangle_2 + \mathcal{D}\big(f_\varphi\big)[V]\right) \mathrm{d}s\end{aligned} \quad (5.71)$$

and parameterization component

$$\begin{aligned}\left\langle g_\varphi^{\mathcal{T}}, V\right\rangle = -\int_{\varphi(M)} \frac{1}{2} \cdot \Big(\left(g^M \circ \varphi^{-1} \cdot \det D^\tau \varphi^{-1}\right)^2 - f_\varphi^2\Big) \cdot \operatorname{div}_\Gamma\left(V - \langle n, V\rangle_2 \cdot n\right) \\ + \Big(g^M \circ \varphi^{-1} \cdot \det D^\tau \varphi^{-1} - f_\varphi\Big) \cdot \nabla_\Gamma f_\varphi^T V \, \mathrm{d}s.\end{aligned} \quad (5.72)$$

Here, $\mathcal{D}(f_\varphi)$ is the classical shape derivative of f_φ. The first integral corresponds to the classical shape derivative component $g^{\mathcal{N}}$ of the pre-shape derivative decomposition (4.36). It acts solely on directions normal on $\varphi(M)$. The second integral acts on tangential directions, and therefore corresponds to the parameterization part $g^{\mathcal{T}}$ from structure equation (4.36). Notice that we abuse notation, since technically $V - \langle n, V\rangle_2 \cdot n$ is not necessarily a smooth function. Nevertheless, its trace on $\varphi(M)$ can be arbitrarily extended in normal directions to evaluate tangential divergences, as these do not depend on normal directions. For a target $f_\varphi(x, y, z) = \frac{1}{\int_{\varphi(M)} 1 \, \mathrm{d}s} \cdot x$ and a sphere centered at $(0.5, 0.5, 0.5)$, a graphical visualization of a pre-shape gradient for the parameterization tracking problem (5.10) and its decomposition is shown in figure 5.3.

If $\partial\varphi(M)$ is nonempty, the normal part in equation (5.71) is not the complete shape component $g^{\mathcal{N}}$ from theorem 9, as it solely acts on vector fields in outer

normal direction n. To be complete, it also needs to take directions V into account, which point into outward normal direction $n_{\varphi(M)}$ on $\partial\varphi(M)$. While it is possible to extract a boundary integral on $\partial\varphi(M)$ by applying Stokes theorem to equation (5.72), the remaining integral over $\varphi(M)$ still acts on outward normal directions. Hence a further decomposition using function representations of distributions is not straightforward, if possible at all, since decompositions of V need to have enough smoothness for respective differential operators to be applicable. However, we point out that the tangential component (5.72) involves the complete parameterization part $g^{\mathcal{T}}$ from structure theorem 9, even for non-trivial boundaries ∂M. While equation (5.71) vanishes for all V tangential to $\varphi(M)$ and parallel to $\partial\varphi(M)$, we see that $g_{\varphi}^{\mathcal{T}}$ from equation (5.72) is left to act on these vector fields.

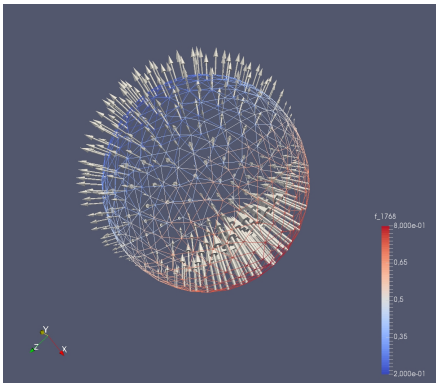

(a) Normal component representing the classical shape part

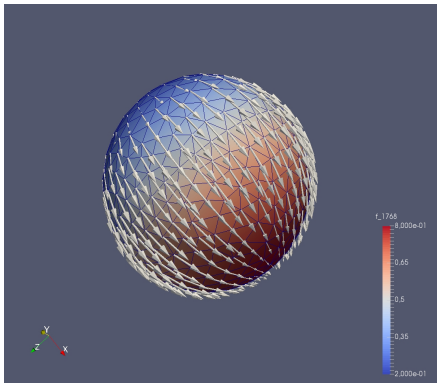

(b) Tangential component representing the parameterization part

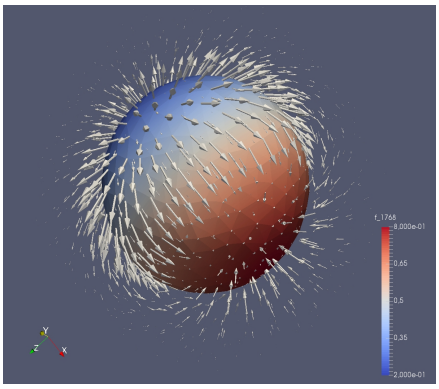

(c) Complete pre-shape gradient in volume mesh representation

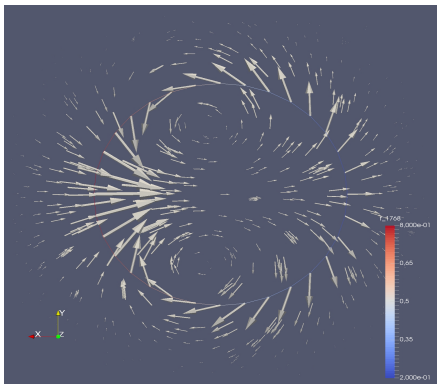

(d) Slice through xy-plane at center of complete volume pre-shape gradient

Figure 5.3: Negative pre-shape gradient of $\mathfrak{J}^M$ on a sphere scaled by 0.02. The target vertex density $f_\varphi(x,y,z) = \frac{1}{\int_{\varphi(M)} 1 \,\mathrm{ds}} \cdot x$ is depicted in color. Color shifting towards red means higher vertex allocation is desired. Gradient are represented by a weak linear elasticity equation.

The Normal Component and Minimal Surfaces For illustration, let us deviate from normalization condition (5.9), and choose a degenerate target $f_\varphi = 0$ and constant $g^M = 1$. Let us assume the setting, where we leave boundaries ∂M invariant, i.e. $\varphi \in \mathrm{Emb}_{\partial M}(M, \mathbb{R}^{n+1})$. Corresponding vector fields V acting as directions are restricted to those, which vanish on ∂M.

In this situation the classical shape derivative component of $\mathfrak{D}\mathfrak{J}^M(\varphi)$ is given by

$$\left\langle g_\varphi^{\mathcal{N}}, V \right\rangle = -\frac{\dim(M)}{2} \cdot \int_{\varphi(M)} \left(\det D^\tau \varphi^{-1}(s) \right)^2 \cdot \kappa(s) \cdot \left\langle V(s), n(s) \right\rangle_2 \mathrm{d}s. \quad (5.73)$$

Since φ is an embedding, and M is compact, according Jacobians are bounded and non-vanishing. In our special situation, this means the horizontal component of the pre-shape derivative in equation (5.73) vanishes exactly for shapes with vanishing mean curvature κ. Put differently, the pre-shapes of minimal surfaces and their higher dimensional analogues are exactly the stationary points for this horizontal component.

By this observation, a gradient ascend using normal component (5.73) resembles an algorithm for evolutionary surfaces proposed by Dziuk. In [45], Dziuk solves Plateau's problem by approximating a mean curvature flow. Note that an ascend is necessary, since our formulation of the pre-shape parameterization tracking problem involves inverse Jacobians, which is connected to Plateau's problem by

$$\max_{\varphi \in \mathrm{Emb}_{\partial M}(M, \mathbb{R}^{n+1})} \int_{\varphi(M)} \left(\det D^\tau \varphi^{-1}(s) \right)^2 \mathrm{d}s \Leftrightarrow \min_{\varphi \in \mathrm{Emb}_{\partial M}(M, \mathbb{R}^{n+1})} \int_M |\det D^\tau \varphi(s)| \, \mathrm{d}s. \quad (5.74)$$

With the connection to Plateau's problem, we gain insight into qualitative properties of a steepest descent using the complete pre-shape derivative. Briefly stated, if less vertices are desired at a location, the gradient descent in normal direction tends to blow up the shape, increasing distances of neighboring vertices. If more vertices are desired it tends to locally flatten the shape, driving the nodes together. This shows that, in general, parameterization tracking with its full pre-shape derivative distorts a shape in normal direction. Hence it is not directly suitable for regularization of shape optimization routines, as it might interfere by changing optimal shapes of the underlying shape optimization problem.

Use of the tangential pre-shape derivative component from equation (5.72) leads to algorithms similar to the mesh deformation methods from [112, 68, 31]. We use it to construct various regularization methods for shape optimization problems, but postpone their discussion to chapter 6 and chapter 7. Also, the just described effect of normal components is captured in the numerical comparison study of parameterization tracking with the full pre-shape derivative and its tangential component in section 7.3.

Optimality Conditions via Pre-Shape Derivatives Now that we have a closed pre-shape derivative formula available, we can use it to derive additional important properties of the parameterization tracking problem. The next result shows that stationary points in each fiber are already global solutions. In other words, necessary optimality conditions for parameterization tracking are in fact already sufficient.

Theorem 13 (Characterization of Global Solutions by Fiber Stationarity)**.** *Let assumptions of theorem 12 be satisfied. Then the following statements are equivalent:*

(i) $\varphi \in \mathrm{Emb}(M, \mathbb{R}^{n+1})$ *is a* fiber stationary point *of problem* (5.10)*, i.e.*

$$\mathfrak{D}\mathfrak{J}^M(\varphi)[V] = 0 \qquad \forall V \in C^\infty\left(\mathbb{R}^{n+1}, \mathbb{R}^{n+1}\right) \text{ with } \mathrm{Tr}_{|\varphi(M)}[V] \in \mathcal{T}_{\varphi(M)}, \quad (5.75)$$

where $\mathcal{T}_{\varphi(M)}$ *is the space of tangential vector fields on* $\varphi(M)$ *parallel to* $\partial\varphi(M)$ *(cf. equation* (4.19)*).*

(ii) φ is a global solution to equation (5.10)*, and in particular it satisfies*

$$g^M \circ \varphi^{-1} \cdot \det D^\tau \varphi^{-1} = f_\varphi \qquad \text{on } \varphi(M). \tag{5.76}$$

(iii) the complete pre-shape derivative of $\mathfrak{J}^M$ vanishes in φ, i.e.

$$\mathfrak{D}\mathfrak{J}^M(\varphi)[V] = 0 \qquad \forall V \in C^\infty\big(\mathbb{R}^{n+1}, \mathbb{R}^{n+1}\big). \tag{5.77}$$

Additionally, its normal component $g_\varphi^{\mathcal{N}}$ vanishes in φ.

The necessary first order condition regarding only directions V tangential to $\varphi(M)$ and parallel to $\partial\varphi(M)$ is already a sufficient condition for a global minimum to $\mathfrak{J}^M$.

Proof. Let us assume the setting of theorem 12. We show equivalence of all assertions by a circular argument '$(i) \implies (ii) \implies (iii) \implies (i)$'.

As a start, we prove '$(i) \implies (ii)$'. Let us assume (i) by fixing a $\varphi \in \operatorname{Emb}(M, \mathbb{R}^{n+1})$ satisfying fiber stationarity equation (5.75). With the pre-shape derivative formula from theorem 12, we apply an integration by parts on manifolds (cf. [175, Ch. 2.2, Prop. 2.3]) for a direction $V \in C^\infty(\mathbb{R}^{n+1}, \mathbb{R}^{n+1})$ with $\operatorname{Tr}_{|\varphi(M)}[V] \in \mathcal{T}_{\varphi(M)}$, and shape functionality of f_φ, to get

$$\begin{aligned}
&\mathfrak{D}\mathfrak{J}^M(\varphi)[V] \\
&= -\int_{\varphi(M)} \frac{1}{2} \cdot \Big(\big(g^M \circ \varphi^{-1} \cdot \det D^\tau \varphi^{-1}\big)^2 - f_\varphi^2 \Big) \cdot \operatorname{div}_\Gamma(V) \\
&\qquad + \Big(g^M \circ \varphi^{-1} \cdot \det D^\tau \varphi^{-1} - f_\varphi \Big) \cdot \mathfrak{D}_m\big(f_\varphi\big)[V] \, \mathrm{d}s \\
&= \int_{\varphi(M)} \frac{1}{2} \cdot \nabla_\Gamma \Big(\big(g^M \circ \varphi^{-1} \cdot \det D^\tau \varphi^{-1}\big)^2 - f_\varphi^2 \Big)^T V \\
&\qquad - \Big(g^M \circ \varphi^{-1} \cdot \det D^\tau \varphi^{-1} - f_\varphi \Big) \cdot \nabla_\Gamma f_\varphi^T V \, \mathrm{d}s \\
&= \int_{\varphi(M)} \Big(\big(g^M \circ \varphi^{-1} \cdot \det D^\tau \varphi^{-1}\big) \cdot \nabla_\Gamma \big(g^M \circ \varphi^{-1} \cdot \det D^\tau \varphi^{-1}\big) - f_\varphi \cdot \nabla_\Gamma f_\varphi \Big)^T V \\
&\qquad - \Big(\big(g^M \circ \varphi^{-1} \cdot \det D^\tau \varphi^{-1}\big) \cdot \nabla_\Gamma f_\varphi - f_\varphi \cdot \nabla_\Gamma f_\varphi \Big)^T V \, \mathrm{d}s \\
&= \int_{\varphi(M)} \left(\big(g^M \circ \varphi^{-1} \cdot \det D^\tau \varphi^{-1}\big) \cdot \Big(\nabla_\Gamma \big(g^M \circ \varphi^{-1} \cdot \det D^\tau \varphi^{-1}\big) - \nabla_\Gamma f_\varphi \Big) \right)^T V \, \mathrm{d}s.
\end{aligned} \tag{5.78}$$

Due to assumption (5.75) of fiber stationarity, we know equation (5.78) equals zero for all $V \in C^\infty(\mathbb{R}^{n+1}, \mathbb{R}^{n+1})$ tangential on $\varphi(M)$ and parallel to the boundary $\partial\varphi(M)$, so we get

$$\big(g^M \circ \varphi^{-1} \cdot \det D^\tau \varphi^{-1}\big) \cdot \Big(\nabla_\Gamma \big(g^M \circ \varphi^{-1} \cdot \det D^\tau \varphi^{-1}\big) - \nabla_\Gamma f_\varphi \Big) = 0 \qquad \text{in } \operatorname{int} \varphi(M). \tag{5.79}$$

We have $g^M > 0$ by assumption, which together with non-vanishing determinant by $\varphi \in \operatorname{Emb}(M, \mathbb{R}^{n+1})$ implies

$$\nabla_\Gamma (g^M \circ \varphi^{-1} \cdot \det D^\tau \varphi^{-1} - f_\varphi) = 0 \qquad \text{in } \operatorname{int} \varphi(M). \tag{5.80}$$

Since involved functions have continuous derivatives, and as theorem 13 assumes M to be smooth and connected, we can derive constancy of the involved term, i.e. there exists a $c \in \mathbb{R}$, such that

$$g^M \circ \varphi^{-1} \cdot \det D^\tau \varphi^{-1} = f_\varphi + c \qquad \text{on } \varphi(M). \tag{5.81}$$

Using normalization assumption (5.9) in combination with the transformation formula, we see that the discussed constant is 0. As we have the assumptions of theorem 10, we can apply the first equivalence from its characterization of global solutions in fibers, which proves assertion (ii).

Next, we show implication '$(ii) \implies (iii)$'. Assuming (ii), we can use the explicit pre-shape derivative formula from theorem 12. We see that the two integrands of $\mathfrak{D}\mathfrak{J}^M(\varphi)[V]$ in equation (5.59) featuring $g^M \circ \varphi^{-1} \cdot \det D^\tau \varphi^{-1}$ and f_φ are zero for all directions $V \in C^\infty(\mathbb{R}^{n+1}, \mathbb{R}^{n+1})$. This gives equation (5.77). The same argument applies for the tangential component $g_\varphi^{\mathcal{T}}$ involved in equation (5.72), which therefore vanishes. For shapes with non-trivial boundary, continuity of the pre-shape derivative and a sequence of vector fields tangential to $\varphi(M)$, which are fixed in outward normal direction and progressively vanishing on the interior, yields vanishing of the normal component $g_\varphi^{\mathcal{N}}$ as well. Hence we achieve (iii).

Lastly, we immediately see that '$(iii) \implies (i)$'. The complete vanishing of the pre-shape derivative in equation (5.77) particularly implies its vanishing for directions V tangential to $\varphi(M)$ and parallel to $\partial\varphi(M)$. This is fiber stationarity (5.75) for φ, concluding the proof. □

Theorem 13 essentially states, that there are no stationary points other than global solutions to the pre-shape parameterization tracking problem (5.10). In fact, we have a sufficient optimality criterion via the tangential component of its pre-shape derivative. This strongly resembles the situation for convex optimization problems, which usually involves optimization in a vector space. Clearly, this is not the case for parameterization tracking, as optimization for this problem is situated on the infinite dimensional manifold $\mathrm{Emb}(M, \mathbb{R}^{n+1})$. There also exist notions of convex functions on Riemannian manifolds, such as those found in [178, Ch. 3]. However, these notions depend on geodesics, and as such require the choice of a Riemannian metric. If not stated otherwise, the proofs of our results do not involve a Riemannian metric on $\mathrm{Emb}(M, \mathbb{R}^{n+1})$, so we abstain from calling the parameterization tracking problem (5.10) a convex problem, despite having certain characteristic features of one.

Notice that theorem 13 also guarantees existence of stationary points φ with respect to the pre-shape derivative in each fiber of $\mathrm{Emb}(M, \mathbb{R}^{n+1})$. Since stationary points are global solutions, we can simply use existence theorem 10 for this. Additionally, theorem 13 shows that optimization with the tangential component $g_\varphi^{\mathcal{T}}$ of pre-shape derivative (5.59) can be sufficient to reach a globally optimal solution for (5.10). And perhaps surprisingly, the normal component of the pre-shape derivative vanishes automatically, when the tangential component is zero. This feature permits design of regularizations for shape optimization problems, with the property to leave optimal shapes invariant, while at the same time finding an optimal parameterization of respective shapes.

A Class of Externally Defined Targets f_φ As we have left the target f_φ unspecified during derivation of the pre-shape derivative (5.59), we now give an constructive example, which can be implemented in numerical routines. By its specification, non-uniform target cell volumes can be achieved by minimizing the parameterization tracking objective. In [56], local sensitivities for minimization of the approximation error of linear elliptic second order PDE are derived and used to refine computational meshes. Also, [30] studies various target functions for mesh deformation methods in 2D by using elliptic and eigenvalue methods, e.g. to ensure certain coordinate lines of the mesh. Amongst other examples, this shows possible demand for non-uniform adaptation of computational meshes.

To construct sufficient targets f_φ, we have to satisfy normalization condition (5.9) for guaranteed existence of solutions. One way to accomplish this, is

by defining f_φ using a given globally defined function $q\colon \mathbb{R}^{n+1} \to (0,\infty)$. By assuming H^2-regularity for q, existence of pre-shape derivatives and their closed form as in equation (5.59) is guaranteed. The according target vertex density on a shape $\varphi(M)$ is then given by

$$f_\varphi := \frac{\int_M g^M \,\mathrm{d}s}{\int_{\varphi(M)} q_{|\varphi(M)} \,\mathrm{d}s} \cdot q_{|\varphi(M)}, \tag{5.82}$$

which is well-defined due to the trace theorem for Sobolev functions (cf. [50, Ch. 5.5]).

Next, we calculate $\mathfrak{D}_m(f_\varphi)[V]$ for a given $V \in C^\infty(\mathbb{R}^{n+1},\mathbb{R}^{n+1})$, which exists, since we have $q_{|\varphi(M)} \in H^1\big(\varphi(M)\big)$. For this, we apply pre-shape calculus rules established in corollary 2. Since the function $q\colon \mathbb{R}^{n+1} \to (0,\infty)$ is defined on the entire ambient space, we can make direct use of structure corollary 1 for pre-shape material derivatives. In the following calculation, we avoid to explicitly write restrictions for readability. Together with the fact that q and g^M do not depend on φ, this gives

$$\begin{aligned}
&\mathfrak{D}_m\big(f_\varphi\big)[V] \\
&= \mathfrak{D}_m\left(\frac{\int_M g^M \,\mathrm{d}s}{\int_{\varphi(M)} q \,\mathrm{d}s} \cdot q\right)[V] \\
&= -\frac{\int_M g^M \,\mathrm{d}s}{\big(\int_{\varphi(M)} q \,\mathrm{d}s\big)^2} \cdot \mathfrak{D}\left(\int_{\varphi(M)} q \,\mathrm{d}s\right)[V] \cdot q + \frac{\int_M g^M \,\mathrm{d}s}{\int_{\varphi(M)} q \,\mathrm{d}s} \cdot \mathfrak{D}_m(q)[V] \\
&= -\frac{\int_M g^M \,\mathrm{d}s}{\big(\int_{\varphi(M)} q \,\mathrm{d}s\big)^2} \cdot \int_{\varphi(M)} \Big(\mathfrak{D}_m(q)[V] + \mathrm{div}_\Gamma(V) \cdot q\Big) \,\mathrm{d}s \cdot q \\
&\quad + \frac{\int_M g^M \,\mathrm{d}s}{\int_{\varphi(M)} q \,\mathrm{d}s} \cdot \Big(\mathfrak{D}(q)[V] + \nabla q^T V\Big) \\
&= -\frac{\int_M g^M \,\mathrm{d}s}{\big(\int_{\varphi(M)} q \,\mathrm{d}s\big)^2} \cdot \int_{\varphi(M)} \Bigg(\nabla q^T V + \Big(\mathrm{div}_\Gamma\big(\langle n, V\rangle_2 \cdot n\big) \\
&\qquad\qquad + \mathrm{div}_\Gamma\big(V - \langle n, V\rangle_2 \cdot n\big)\Big) \cdot q\Bigg) \,\mathrm{d}s \cdot q + \frac{\int_M g^M \,\mathrm{d}s}{\int_{\varphi(M)} q \,\mathrm{d}s} \cdot \nabla q^T V \\
&= -\frac{\int_M g^M \,\mathrm{d}s}{\big(\int_{\varphi(M)} q \,\mathrm{d}s\big)^2} \cdot \Bigg(\int_{\varphi(M)} \frac{\partial q}{\partial n} \cdot \langle n, V\rangle_2 + \mathrm{div}_\Gamma\big(\langle n, V\rangle_2 \cdot n\big) \cdot q \,\mathrm{d}s \\
&\qquad\qquad + \int_{\varphi(M)} \mathrm{div}_\Gamma(q \cdot V) \,\mathrm{d}s\Bigg) \cdot q + \frac{\int_M g^M \,\mathrm{d}s}{\int_{\varphi(M)} q \,\mathrm{d}s} \cdot \nabla q^T V \\
&= -\frac{\int_M g^M \,\mathrm{d}s}{\big(\int_{\varphi(M)} q \,\mathrm{d}s\big)^2} \cdot \Bigg(\int_{\varphi(M)} \Big(\frac{\partial q}{\partial n} + \dim(M) \cdot \kappa \cdot q\Big) \cdot \langle n, V\rangle_2 \,\mathrm{d}s \\
&\qquad\qquad + \int_{\partial\varphi(M)} q \cdot \big\langle n_{\varphi(M)}, V\big\rangle_2 \,\mathrm{d}s\Bigg) \cdot q + \frac{\int_M g^M \,\mathrm{d}s}{\int_{\varphi(M)} q \,\mathrm{d}s} \cdot \nabla q^T V,
\end{aligned} \tag{5.83}$$

where the last equality comes from an application of the divergence theorem with outward pointing normal $n_{\varphi(M)}$ on $\partial\varphi(M)$ (cf. [175, Ch. 2.2, Thm. 2.1]), and orthogonality of tangential gradients and outer normal vectors. Note that we slightly abuse notation for normal and tangential components of V using $\langle n, V\rangle_2 \cdot n$ and $V - \langle n, V\rangle_2 \cdot n$. Here, κ is the mean curvature for hypersurfaces as in equation (5.69).

We summarize the calculation, and restate the pre-shape material derivative identity for future reference

$$\mathfrak{D}_m\big(f_\varphi\big)[V] = -\frac{\int_M g^M \,\mathrm{d}s}{\big(\int_{\varphi(M)} q \,\mathrm{d}s\big)^2} \cdot \Bigg(\int_{\varphi(M)} \Big(\frac{\partial q}{\partial n} + \dim(M)\cdot\kappa\cdot q\Big)\cdot\langle n, V\rangle_2 \,\mathrm{d}s + \int_{\partial\varphi(M)} q\cdot\big\langle n_{\varphi(M)}, V\big\rangle_2 \,\mathrm{d}s\Bigg)\cdot q + \frac{\int_M g^M \,\mathrm{d}s}{\int_{\varphi(M)} q \,\mathrm{d}s}\cdot\nabla q^T V. \tag{5.84}$$

For constant $q\colon \mathbb{R}^{n+1} \to (0,\infty)$, not necessarily equal to 1, the pre-shape material derivative (5.84) simplifies to

$$\mathfrak{D}_m\big(f_\varphi\big)[V] = -\frac{\int_M g^M \,\mathrm{d}s}{\big(\int_{\varphi(M)} 1 \,\mathrm{d}s\big)^2} \cdot \Bigg(\dim(M)\cdot\int_{\varphi(M)} \kappa\cdot\langle n, V\rangle_2 \,\mathrm{d}s + \int_{\partial\varphi(M)} \big\langle n_{\varphi(M)}, V\big\rangle_2 \,\mathrm{d}s\Bigg). \tag{5.85}$$

This highlights the role of the boundary integrals on $\varphi(M)$ and $\partial\varphi(M)$ in light of the horizontal bundle directions from equation (4.15). They capture the influence of the normalization operator in equation (5.82), when the shape $\varphi(M)$ is deformed. If we deform $\varphi(M)$ in outer normal direction n, then the sign of the pre-shape material derivative depends on the scalar curvature. Essentially, if we locally blow-up or flatten $\varphi(M)$, then the total volume of the resulting shape becomes larger, or smaller respectively. Thus the normalization in equation (5.82) decreases the global values of f_φ for enlargement, or increases them for the case of flattening. The second way to deform the shape, is to stretch or contract it in outward pointing normal direction. If V points in direction $n_{\varphi(M)}$, we stretch the shape in outward normal direction, and the pre-shape material derivative has negative sign. Again, this makes sense, since the value of f_φ has to decrease by normalization on a shape with higher total volume.

For directions V tangential on $\varphi(M)$ and parallel to $\partial\varphi(M)$, the pre-shape material derivative (5.84) simplifies to

$$\mathfrak{D}_m\big(f_\varphi\big)[V] = \frac{1}{\int_{\varphi(M)} q \,\mathrm{d}s}\cdot\nabla_\Gamma q^T V. \tag{5.86}$$

This reflects, that movement of points on a shape in tangential directions parallel to boundaries leaves the shape unchanged, and thus the normalization factor stays the same as well. Since targets defined by external functions as in equation (5.82) satisfy shape functionality, only the tangential gradient of $f_\varphi\colon \varphi(M) \to \mathbb{R}$ participates in the pre-shape material derivative for tangential directions parallel to boundaries.

Remark 18 (Preserving Initial Node Distributions)**.** *A target f_φ as defined in equation* (5.82) *prescribes a node distribution for meshes of shapes only depending on the shape itself and its location in the ambient space. Thus $q\colon \mathbb{R}^{n+1} \to (0,\infty)$ defines the shape parameterization through extrinsic factors, which could stem from PDEs or other external influences, and can be modeled according to these. In contrast to this, it also might be beneficial to make the prescribed vertex distribution of meshes for shapes dependent on intrinsic features. The shape optimization procedure might depend on material parameters located at the vertices of a discretized shape $\varphi(M)$ at hand. Lamé parameters of linear elastic equations or diffusion coefficients from heat equations solved on the shape $\varphi(M)$ can serve as examples. For such problems, material parameters change during mesh morphing depending on the shape.*

Hence it might be desired to either let an initially given mesh vertex configuration be preserved, or to reach a prescribed one depending on the desired distribution of intrinsic material properties of the modeled shape.

One way to preserve an initial vertex configuration, is to model a target point distribution $\tilde{f}_\varphi$ by

$$\tilde{f}_\varphi := f^M \circ \varphi^{-1} \qquad \forall \varphi \in \mathrm{Emb}(M, \mathbb{R}^{n+1}), \tag{5.87}$$

where we use $f^M \colon M \to (0, \infty)$ as a given intrinsic target point distribution in the starting mesh for M (cf. remark 2). Then, equation (5.87) preserves the point distributions of different meshes arising during optimization relative to f^M chosen at the beginning. When looking at the existence theorem 10 for the parameterization tracking problem, this might seem like a case not covered. This objection comes from observing, that $\tilde{f}_\varphi$ varies in the fiber of a fixed shape, since the point distributions are modeled on intrinsic features of the mesh. However, we can modify the initial point distribution g^M by replacing it with

$$\tilde{g}^M := \frac{g^M}{f^M}. \tag{5.88}$$

With this substitution, and by choosing f_φ to be constant, we remain in the framework of existence theorem 10. This guarantees existence for solutions to parameterization tracking, and existence of pre-shape derivatives given in theorem 12, while achieving the goal of intrinsic modeling of vertex allocation. The special case of $\tilde{g}^M = 1$ then leads to an algorithms, which tries to preserve the relative initial mesh node distribution.

5.4 Numerical Tests of Parameterization Tracking Involving Pre-Shape Derivatives

With the pre-shape derivative formula for parameterization tracking and its decomposition, we can implement some first numerical examples. In this intermezzo, we take a look at solo applications of parameterization tracking, i.e. no underlying shape optimization problem is regularized. The more involved cases of simultaneous shape optimization and mesh quality regularization are discussed in chapter 6, chapter 7 and chapter 9.

In order to test parameterization tracking, we present three implementations of pre-shape gradient descent methods. For this, we use the open-source finite-element software FEniCS (cf. [117, 4]). Construction of meshes is done via the free meshing software Gmsh (cf. [63]). We use a single core of an Intel(R) Core(Tm) i3-8100 CPU at 3.60 GHz featuring 16GB RAM. The single core runs at 800 MHz while the code is executed on a virtual machine.

The following three implementations solve the parameterization tracking problem (5.10) by using the tangential component of the pre-shape derivative seen in decomposition equation (5.70). The solution process features a simple backtracking line search, which scales the initial gradient of the current iteration U_i according to a given factor c, and rescales it by 0.5 if no sufficient decrease in $\mathfrak{J}^M$ is apparent. In the following, we denote the open and bounded computational hold-all domain by $\mathbb{D}$. In order to apply a descent algorithm, we are in need of pre-shape gradients. As discussed in chapter 3, there is a multitude of non-equivalent choices to represent derivatives as gradients in infinite dimensions. We choose a bilinear form inspired by the weak formulation of the linear elasticity as proposed in [161], which gives us H^1-regularity of pre-shape gradients. Additionally, we add a zero order term, and only use the shear component of the linear elasticity featuring the second Lamé

parameter μ_{elas}. For weights $\alpha_{\text{LE}}, \alpha_{L^2} > 0$, the pre-shape gradient U is calculated by solving its representing system

$$\begin{aligned} \alpha_{\text{LE}} \cdot \int_{\mathbb{D}} \mu_{\text{elas}} \cdot \epsilon(U) : \epsilon(V) \,\mathrm{d}x + \alpha_{L^2} \cdot (U,V)_{L^2(\mathbb{D},\mathbb{R}^{n+1})} &= \langle g_\varphi^{\mathcal{T}}, V \rangle \qquad \forall V \in H_0^1\big(\mathbb{D}, \mathbb{R}^{n+1}\big) \\ \epsilon(U) &= \frac{1}{2}\big(\nabla U^T + \nabla U\big) \\ \epsilon(V) &= \frac{1}{2}\big(\nabla V^T + \nabla V\big) \\ U &= 0 \qquad \text{on } \partial\mathbb{D}, \end{aligned} \tag{5.89}$$

where $g_\varphi^{\mathcal{T}}$ is the tangential pre-shape derivative component of $\mathfrak{D}\mathfrak{J}^M(\varphi)$ given as in equation (5.72). For $\mu_{\max}, \mu_{\min} > 0$, the second Lamé parameter μ_{elas} is chosen as the solution of the Laplace problem

$$\begin{aligned} -\Delta\mu_{\text{elas}} &= 0 && \text{in } \mathbb{D} \\ \mu_{\text{elas}} &= \mu_{\max} && \text{on } \varphi(M) \\ \mu_{\text{elas}} &= \mu_{\min} && \text{on } \partial\mathbb{D}. \end{aligned} \tag{5.90}$$

Solving equation (5.89) on the entire hold-all domain $\mathbb{D}$ gives us a volume representation U of the tangential pre-shape derivative component $g_\varphi^{\mathcal{T}}$. The pre-shape gradient system (5.89) is assembled in FEniCS and solved with a sparse LU method from PETSc used as a linear algebra backend.

The first example shows an application of the parameterization tracking problem to improve the quality of a given hold-all domain $\overline{\mathbb{D}} = [0,1]^2 \subset \mathbb{R}^2$. This is realized by using an unstructured 2D volume mesh created via Gmsh featuring 4262 triangular cells and 2212 nodes. We distort the mesh quality of this unstructured mesh by applying

$$\varphi_0 \begin{pmatrix} x \\ y \end{pmatrix} = \begin{pmatrix} 0.025 \cdot \sin(25.5 \cdot x) \\ 0 \end{pmatrix} \tag{5.91}$$

as a deformation to the interior $\mathbb{D}$, leaving the boundary $\partial\mathbb{D}$ fixed. The deformed initial mesh $\varphi_0(\overline{\mathbb{D}})$ is depicted in figure 5.4 (a). Notice that in this scenario, the initial model M is given by the hold-all domain $\overline{\mathbb{D}} = [0,1]^2$ with non-trivial boundary $\partial\mathbb{D}$ itself. We enforce invariance of the hold-all boundary $\partial\mathbb{D}$. Hence, there is no normal component of the pre-shape derivative in this case, as the codimension of $\mathbb{D} \subset \mathbb{R}^2$ is zero.

To formulate the parameterization tracking problem (5.10), we need to specify an initial point distribution g^M and target f_φ. For the first example, we choose a constant target

$$f_\varphi = \frac{1}{\int_{\mathbb{D}} 1 \,\mathrm{d}x}. \tag{5.92}$$

This makes a uniform cell volume distribution of the hold-all domain the target. The initial point distribution g^M is represented by using a continuous Galerkin Ansatz with linear elements. Degrees of freedom are situated at the mesh vertices, and set to the average of inverses of surrounding cell volumes, i.e.

$$g^M(p_i) = \frac{1}{|\mathcal{C}_i|} \cdot \sum_{C \in \mathcal{C}_i} \frac{1}{\int_C 1 \,\mathrm{d}x}. \tag{5.93}$$

Here, p_i is a mesh vertex and $\mathcal{C}_i$ is the set of its neighboring cells C. The resulting function is normed to satisfy the demanded normalization condition (5.9) of the parameterization tracking problem. The initial point distribution estimated by this procedure is shown in figure 5.4 (a).

With both g^M and f_φ specified, the target $\mathfrak{J}^M$ and its tangential pre-shape derivative component $g_\varphi^{\mathcal{T}}$ can be assembled. For the gradient representation, we use weights $\alpha_{\mathrm{LE}} = 0.02$ and $\alpha_{L^2} = 1$. Lamé parameters are $\mu_{\max} = \mu_{\min} = 1$, resulting in constant $\mu_{\mathrm{elas}} = 1$. An initial scaling factor of $c = 0.01$ for the negative gradient during line search is applied. The method successfully exits after 37.07s and 45 iterations, achieving the required relative improvement of $\mathfrak{J}^M$ by $3 \cdot 10^{-3}$. Results of the pre-shape gradient descent using the tangential component of the pre-shape derivative and the described methodology are shown in figure 5.4 (b) and figure 5.6.

Our second example uses the exact same parameters as in the first example. In particular, the starting mesh and its initial volume distribution g^M are the same as in the first example, and illustrated in figure 5.4 (a). To show the general applicability of parameterization tracking, we replace the uniform target f_φ from equation (5.92) by a more complicated non-uniform target

$$f_\varphi = \frac{\int_{[0,1]} \int_{[0,1]} g^M(x,y)\,\mathrm{d}x\,\mathrm{d}y}{\int_{[0,1]} \int_{[0,1]} 2 + \cos\Big(5 \cdot 2\pi \cdot \big((x-0.35)^2 + 2\cdot(y-0.4)^2\big)\Big)\,\mathrm{d}x\,\mathrm{d}y} \cdot \left(2 + \cos\Big(5 \cdot 2\pi \cdot \big((x-0.35)^2 + 2\cdot(y-0.4)^2\big)\Big)\right). \tag{5.94}$$

The pre-shape gradient descent for this non-uniform target achieves convergence after 38.12s and 46 iterations, achieving a relative improvement of $\mathfrak{J}^M$ by $3 \cdot 10^{-3}$. We visualize an intermediate mesh, and the final mesh in figure 5.4 (c) and (d). The target function values $\mathfrak{J}^M(\varphi_i)$ and pre-shape gradient norms are shown in figure 5.6. Interestingly, the intermediate mesh (c) looks like a superposition of the final and initial meshes (d) and (a). This is essentially an illustration of snapshots from a discretized flow in $\mathrm{Diff}(\overline{\mathbb{D}})$. We see in figure 5.4 (d), that the prescribed non-uniform cell volume distribution is achieved, even though the initial mesh in figure 5.4 (a) has degenerate cells distributed on vertical lines.

Our third example applies the parameterization tracking problem to a sphere in the hold-all domain $\overline{\mathbb{D}} = [0,1]^3 \subset \mathbb{R}^3$. It acts as the modeling manifold M, and its initial parameterization φ_0 is given by the identity embedding into the hold-all domain. The initial shape is a structured triangular surface mesh approximating a sphere centered in $(0.5, 0.5, 0.5)$ with radius 0.3 constructed via Gmsh. It consists of 6240 triangular cells and 3122 vertices on the surface. The sphere is embedded in a hold-all domain consisting of 21838 tetrahedric cells and 4059 nodes. For the third example, we prescribe a non-uniform surface cell volume distribution given by

$$f_\varphi \begin{pmatrix} x \\ y \\ z \end{pmatrix} = \frac{1}{\int_{\varphi(M)} 1 + \frac{1}{2}\cdot\sin(10\cdot 2\pi\cdot x)\,\mathrm{d}s} \cdot \big(1 + 0.5\cdot\sin(10\cdot 2\pi\cdot x)\big). \tag{5.95}$$

The target function is of the form (5.82), which permits use of the material derivative formula (5.84) to assemble the tangential component of pre-shape derivative. At the same time, it satisfies normalization condition (5.9). We set the initial vertex distribution to a constant

$$g^M = \frac{1}{\int_M 1\,\mathrm{d}s}. \tag{5.96}$$

In order to calculate covariant derivatives and associated Jacobian determinants, a Gram-Schmidt algorithm is applied to construct local tangential orthonormal bases. The condition $\tau_1 \times \tau_2 = n$ is enforced for all points of the shape to achieve a consistent orientation of tangential orthonormal frames. We choose weights $\alpha_{\mathrm{LE}} = 0.02$ and $\alpha_{L^2} = 1$, and Lamé parameters $\mu_{\max} = 30$ and $\mu_{\min} = 5$ for the gradient

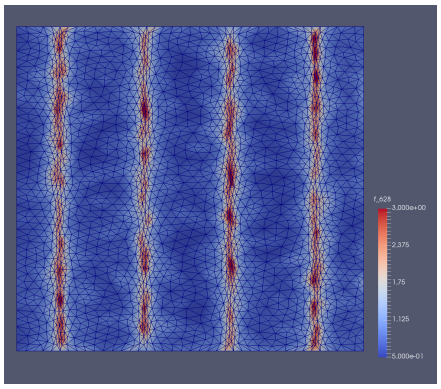

(a) Initial mesh $\varphi_0(M)$

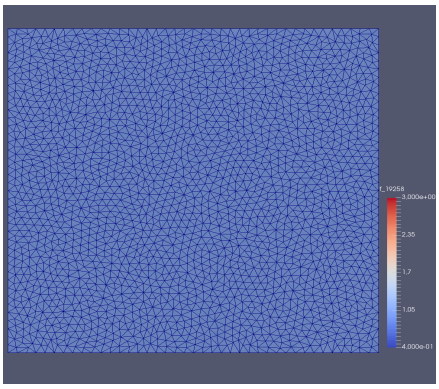

(b) Final mesh $\varphi_{45}(M)$ for uniform target

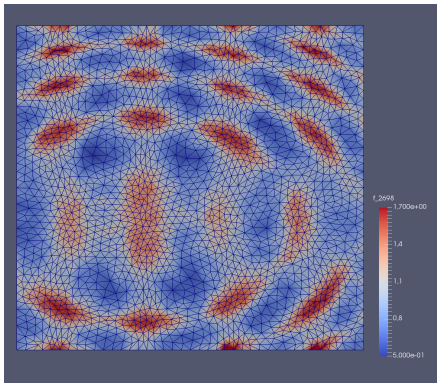

(c) Intermediate mesh $\varphi_6(M)$ for non-uniform target

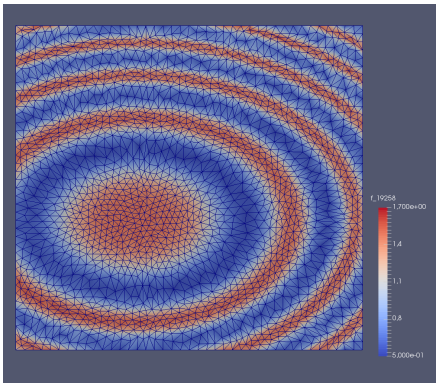

(d) Final mesh $\varphi_{46}(M)$ for non-uniform target

Figure 5.4: (a) Initial point distribution g^M depicted by color on the distorted initial mesh $\varphi_0(M)$. (b) Final mesh $\varphi_{45}(M)$ for the uniform target after 45 descent steps. (c) Intermediate mesh $\varphi_6(M)$ for the non-uniform target after 6 descent steps. (d) Final mesh $\varphi_{46}(M)$ for the non-uniform target after 46 descent steps. For (b) - (d), associated node densities $g^M \circ \varphi_i^{-1} \cdot \det D\varphi_i^{-1}$ at respective steps are shown in color.

representation. The line search employs an initial scaling factor $c = 0.001$ for the negative gradient. For this scenario, the gradient representation of the pre-shape derivative, and the resulting surface mesh with its associated vertex distribution are depicted in figure 5.5. The method successfully exits after 1256.78s and 48 iterations, with a required relative improvement of $\mathfrak{J}^M$ by $5 \cdot 10^{-2}$. Target function values $\mathfrak{J}^M(\varphi_i)$ and pre-shape gradient norms are shown in figure 5.6. In light of theorem 13, we see that the gradient norms and objective values $\mathfrak{J}^M(\varphi_i)$ both converge by using only the tangential component $g^{\mathcal{T}}$ of $\mathfrak{D}\mathfrak{J}^M$. Also, the shape of the sphere is left invariant, which is not the case if normal components or the full pre-shape derivative (cf. figure 5.3) are used.

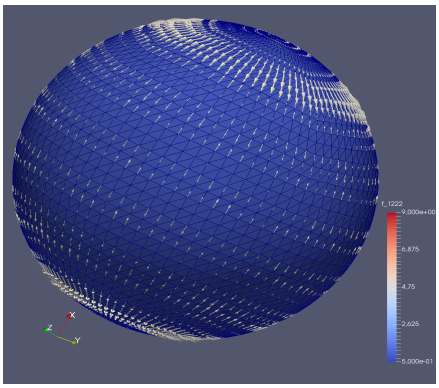

(a) g^M and $-U$ on $\varphi_0(M)$

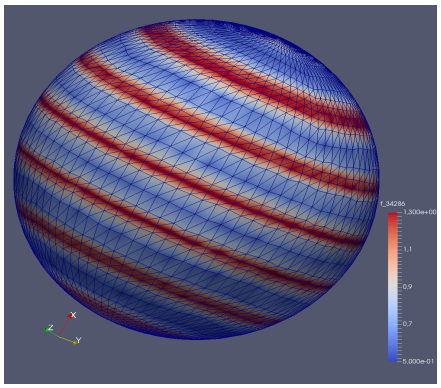

(b) $g^M \circ \varphi_{48}^{-1} \cdot \det D\varphi_{48}^{-1}$ on $\varphi_{48}(M)$

Figure 5.5: (a) Constant initial point distribution g^M and negative pre-shape gradient of the tangential component $g^{\mathcal{T}}$ represented via equation (5.89) on the initial surface mesh $\varphi_0(M)$ scaled by 0.03.
(b) Resulting surface mesh $\varphi_{48}(M)$ after 48 pre-shape gradient descent iterations with associated point distribution $g^M \circ \varphi_{48}^{-1} \cdot \det D\varphi_{48}^{-1}$ shown in color.

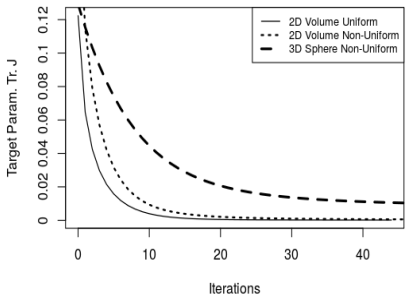

(a) $\mathfrak{J}^M(\varphi_i)$

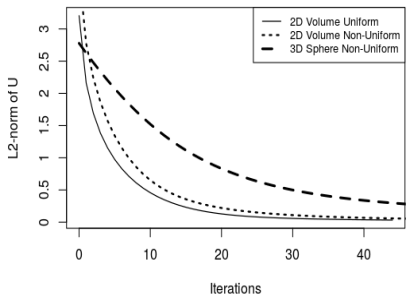

(b) $\|U_i\|_{L^2(\mathbb{D},\mathbb{R}^{n+1})}$

Figure 5.6: (a) Values for the parameterization tracking functional $\mathfrak{J}^M(\varphi_i)$ of iterates φ_i for the tangential pre-shape derivative component based steepest descent method. Values for the 3D sphere case are scaled by 3.
(b) L^2-norms $\|U_i\|_{L^2(\mathbb{D},\mathbb{R}^{n+1})}$ of the gradient representations U_i of pre-shape derivatives for each iterate φ_i. Gradient norms for the 3D sphere case are scaled by 25 to fit in the graph.

5.5 The Pre-Shape Hessian of Parameterization Tracking Problems

After our brief numerical intermezzo, we introduce pre-shape Hessians in this section. A closed formula for the pre-shape Hessian of the parameterization tracking problem is derived in theorem 14, and its features are discussed.

We want to have a pre-shape Hessian, which coincides with the shape Hessian when applied to shape functionals. Therefore, we use a formulation inspired by the shape Hessian definition of Delfour and Zolésio in [42, Ch. 9, Def. 6.1].

Definition 20 (Pre-Shape Hessian)**.** *Let* $\mathfrak{J}\colon \operatorname{Emb}(M,\mathbb{R}^{n+1}) \to \mathbb{R}$ *be pre-shape differentiable. Denote by* φ_t^W *the perturbation of identity for pre-shapes in direction* $W \in C^\infty(\mathbb{R}^{n+1},\mathbb{R}^{n+1})$*. Let* $\varphi \in \operatorname{Emb}(M,\mathbb{R}^{n+1})$*. If the limit*

$$\mathfrak{D}^2\mathfrak{J}(\varphi)[V][W] := \lim_{t\to 0} \frac{\mathfrak{D}\mathfrak{J}\big(\varphi_t^W\big)[V] - \mathfrak{D}\mathfrak{J}(\varphi)[V]}{t} = \frac{\mathrm{d}}{\mathrm{d}t}_{|t=0} \mathfrak{D}\mathfrak{J}\big(\varphi_t^W\big)[V] \tag{5.97}$$

exists for all $V, W \in C^\infty(\mathbb{R}^{n+1},\mathbb{R}^{n+1})$*, and it is bilinear and continuous in* V *and* W*, then we say* $\mathfrak{J}$ *is twice pre-shape differentiable in* φ *with* pre-shape Hessian $\mathfrak{D}^2\mathfrak{J}(\varphi)$*.*

The derivation of the following pre-shape Hessian formula for parameterization is slightly involved. However, it is still worthwhile to have a closed form pre-shape Hessian, since it can enable implementation of more powerful numerical solution methods for mesh quality optimization. In particular, we show that the closed form simplifies in solutions, giving the possible opportunity to use the resulting form as a preconditioner, e.g. for L-BFGS methods. We reaffirm previous findings by positive semidefiniteness of the pre-shape Hessian in solutions. Indefiniteness in solutions can be characterized via tangential f_φ-divergence free vector fields, which gives a connection to results from section 5.2.2.

Theorem 14 (Pre-Shape Hessian of the Parameterization Tracking Problem)**.** *Let the assumptions of theorem 12 hold. Suppose that second order pre-shape material derivatives for* f_φ *exist. Consider the outer unit normal vector field* n *on* $\varphi(M)$*. Then the pre-shape Hessian of the pre-shape parameterization tracking problem is given by*

$$\begin{aligned}
&\mathfrak{D}^2\mathfrak{J}^M(\varphi)[V][W] \\
&= \int_{\varphi(M)} \Big(f_\varphi \cdot \operatorname{div}_\Gamma(V) + \mathfrak{D}_m\big(f_\varphi\big)[V]\Big) \cdot \Big(f_\varphi \cdot \operatorname{div}_\Gamma(W) + \mathfrak{D}_m\big(f_\varphi\big)[W]\Big) \\
&\quad + \frac{1}{2} \cdot \Big(\big(g^M \circ \varphi^{-1} \cdot \det D^\tau \varphi^{-1}\big)^2 - f_\varphi^2\Big) \cdot \Bigg(\operatorname{div}_\Gamma(V) \cdot \operatorname{div}_\Gamma(W) - \operatorname{div}_\Gamma\big(DV \cdot W\big) \\
&\qquad\qquad - \Big\langle \big(DV + DV^T\big) \cdot n, \nabla_\Gamma \langle W, n\rangle_2 - D_\Gamma n \cdot W \Big\rangle_2 \Bigg) \\
&\quad - \Big(g^M \circ \varphi^{-1} \cdot \det D^\tau \varphi^{-1} - f_\varphi\Big) \cdot \mathfrak{D}_m\Big(\mathfrak{D}_m\big(f_\varphi\big)[V]\Big)[W] \,\mathrm{d}s.
\end{aligned} \tag{5.98}$$

Proof. Let us assume the setting of theorem 12, and f_φ to have second order pre-shape material derivatives. Fix $\varphi \in \operatorname{Emb}(M,\mathbb{R}^{n+1})$ and $V, W \in C^\infty(\mathbb{R}^{n+1},\mathbb{R}^{n+1})$.

We begin by applying corollary 2 to the first order pre-shape derivative (5.59)

$$\begin{aligned}
&\mathfrak{D}^2\mathfrak{J}^M(\varphi)[V][W] \\
&= \mathfrak{D}\Bigg(- \int_{\varphi(M)} \frac{1}{2} \cdot \Big(\big(g^M \circ \varphi^{-1} \cdot \det D^\tau \varphi^{-1}\big)^2 - f_\varphi^2 \Big) \cdot \operatorname{div}_\Gamma(V) \\
&\qquad\qquad + \Big(g^M \circ \varphi^{-1} \cdot \det D^\tau \varphi^{-1} - f_\varphi \Big) \cdot \mathfrak{D}_m\big(f_\varphi\big)[V] \, \mathrm{d}s \Bigg)[W] \\
&= - \int_{\varphi(M)} \mathfrak{D}_m \Bigg(\frac{1}{2} \cdot \Big(\big(g^M \circ \varphi^{-1} \cdot \det D^\tau \varphi^{-1}\big)^2 - f_\varphi^2 \Big) \cdot \operatorname{div}_\Gamma(V) \Bigg)[W] \\
&\qquad\qquad + \mathfrak{D}_m \Bigg(\Big(g^M \circ \varphi^{-1} \cdot \det D^\tau \varphi^{-1} - f_\varphi \Big) \cdot \mathfrak{D}_m\big(f_\varphi\big)[V] \Bigg)[W] \\
&\qquad\qquad + \frac{1}{2} \cdot \Big(\big(g^M \circ \varphi^{-1} \cdot \det D^\tau \varphi^{-1}\big)^2 - f_\varphi^2 \Big) \cdot \operatorname{div}_\Gamma(V) \cdot \operatorname{div}_\Gamma(W) \\
&\qquad\qquad + \Big(g^M \circ \varphi^{-1} \cdot \det D^\tau \varphi^{-1} - f_\varphi \Big) \cdot \mathfrak{D}_m\big(f_\varphi\big)[V] \cdot \operatorname{div}_\Gamma(W) \, \mathrm{d}s.
\end{aligned} \tag{5.99}$$

We proceed by finding closed expressions for the two occurring material derivatives. First, let us consider the term with the material derivative featuring $\operatorname{div}_\Gamma(V)$. Product and chain rules from corollary 2 lead to

$$\begin{aligned}
&\mathfrak{D}_m \Bigg(\frac{1}{2} \cdot \Big(\big(g^M \circ \varphi^{-1} \cdot \det D^\tau \varphi^{-1}\big)^2 - f_\varphi^2 \Big) \cdot \operatorname{div}_\Gamma(V) \Bigg)[W] \\
&= \Big(g^M \circ \varphi^{-1} \cdot \big(\det D^\tau \varphi^{-1}\big)^2 \Big) \cdot \mathfrak{D}_m\big(g^M \circ \varphi^{-1}\big)[W] \cdot \operatorname{div}_\Gamma(V) \\
&+ \Big(\big(g^M \circ \varphi^{-1}\big)^2 \cdot \det D^\tau \varphi^{-1} \Big) \cdot \mathfrak{D}_m\big(\det D^\tau \varphi^{-1}\big)[W] \cdot \operatorname{div}_\Gamma(V) \\
&- f_\varphi \cdot \mathfrak{D}_m\big(f_\varphi\big)[W] \cdot \operatorname{div}_\Gamma(V) \\
&+ \frac{1}{2} \cdot \Big(\big(g^M \circ \varphi^{-1} \cdot \det D^\tau \varphi^{-1}\big)^2 - f_\varphi^2 \Big) \cdot \mathfrak{D}_m\big(\operatorname{div}_\Gamma(V)\big)[W].
\end{aligned} \tag{5.100}$$

In the following, we tackle each component in this material derivative individually. By assumption, $g^M \colon M \to (0, \infty)$ is defined independent of φ. Thus equation (5.65) from the first pre-shape derivative proof can be applied. Hence the first term with $\mathfrak{D}_m(g^M \circ \varphi^{-1})[W]$ vanishes. We leave the third term involving the material derivative of f_φ as is, due to generality of f_φ.

Now we focus on the second term involving the tangential Jacobian expression. To apply arguments from the proof of theorem 12, we transform the Jacobian with the formula for inverse determinants

$$\begin{aligned}
\mathfrak{D}_m\big(\det D^\tau \varphi^{-1}\big)[W] &= \mathfrak{D}_m \left(\frac{1}{\det D^\tau \varphi} \circ \varphi^{-1} \right)[W] \\
&= - \frac{1}{(\det D^\tau \varphi)^2 \circ \varphi^{-1}} \circ \mathfrak{D}_m\big(\det D^\tau \varphi \circ \varphi^{-1}\big)[W] \\
&= - \frac{1}{(\det D^\tau \varphi)^2 \circ \varphi^{-1}} \cdot \big(\det D^\tau \varphi \circ \varphi^{-1}\big) \cdot \operatorname{div}_\Gamma(W) \\
&= - \det D^\tau \varphi^{-1} \cdot \operatorname{div}_\Gamma(W).
\end{aligned} \tag{5.101}$$

Here we combined several arguments from the proof of theorem 12, including equation (5.66) and equation (5.67), which we do not restate again to avoid redundancy.

Before we take care of the pre-shape material derivative of the tangential divergence $\mathfrak{D}_m(\operatorname{div}_\Gamma(V))[W]$, we introduce some necessary derivative identities. For

vector fields defined independently of φ, we can use the chain rule for the material derivative and remark 10 for material derivatives on moving boundaries, to see

$$\begin{aligned}\mathfrak{D}_m\left(\frac{\partial V}{\partial n}\right)[W](x_0) &= \frac{\mathrm{d}}{\mathrm{d}t}_{|t=0} DV(x_t)n_t(x_t) \\ &= \frac{\partial \nabla V^T W}{\partial n}(x_0) + \mathfrak{D}_m(n)[W](x_0).\end{aligned} \tag{5.102}$$

With arguments analogous to [44, Lem. 3.2], and remark 10, we have

$$\mathfrak{D}_m(n)[W] = -\nabla_\Gamma \langle W, n\rangle_2 + D_\Gamma n \cdot W. \tag{5.103}$$

Now we can derive the material derivative for the tangential divergence. We have to be careful during manipulation of terms involving the normal derivative, as objects participating might be not well defined in normal directions. In particular, the outer unit normal $n\colon \varphi(M) \to \mathbb{R}^{n+1}$ is defined solely on the parameterized shape, and not on an open neighborhood of it. Still, with the reasoning of remark 10, we can proceed while avoiding non-defined expressions

$$\begin{aligned}\mathfrak{D}_m\big(\operatorname{div}_\Gamma(V)\big)[W] &= \mathfrak{D}_m\big(\operatorname{div}(V)\big)[W] - \mathfrak{D}_m\Big(\Big\langle \frac{\partial V}{\partial n}, n\Big\rangle_2\Big)[W] \\ &= D\big(\operatorname{div}(V)\big)W - \Big\langle \mathfrak{D}_m\Big(\frac{\partial V}{\partial n}\Big)[W], n\Big\rangle_2 - \Big\langle \frac{\partial V}{\partial n}, \mathfrak{D}_m(n)[W]\Big\rangle_2 \\ &= \operatorname{div}(DV\cdot W) - \Big\langle \frac{\partial DV\cdot W}{\partial n}, n\Big\rangle_2 \\ &\quad - \Big\langle DV\cdot \mathfrak{D}_m(n)[W], n\Big\rangle_2 - \Big\langle \frac{\partial V}{\partial n}, \mathfrak{D}_m(n)[W]\Big\rangle_2 \\ &= \operatorname{div}_\Gamma(DV\cdot W) + \Big\langle \frac{\partial DV\cdot W}{\partial n}, n\Big\rangle_2 - \Big\langle \frac{\partial DV\cdot W}{\partial n}, n\Big\rangle_2 \\ &\quad - \Big\langle \big(DV + DV^T\big)n, \mathfrak{D}_m(n)[W]\Big\rangle_2 \\ &= \operatorname{div}_\Gamma(DV\cdot W) + \Big\langle \big(DV + DV^T\big)n, \nabla_\Gamma\langle W, n\rangle_2 - D_\Gamma n\cdot W\Big\rangle_2.\end{aligned} \tag{5.104}$$

Notice that we have used Schwarz's theorem in the third line, as well as the previously derived identities from equation (5.102) and equation (5.103) for terms involving the material derivative of normals.

Combined application of this formula, together with vanishing of $\mathfrak{D}_m(g^M\circ\varphi^{-1})[W]$, generality of $\mathfrak{D}_m(f_\varphi)[W]$, and equation (5.101), to equation (5.100) yields

$$\begin{aligned}&\mathfrak{D}_m\left(\frac{1}{2}\cdot\Big(\big(g^M\circ\varphi^{-1}\cdot\det D^\tau\varphi^{-1}\big)^2 - f_\varphi^2\Big)\cdot\operatorname{div}_\Gamma(V)\right)[W] \\ &= -\big(g^M\circ\varphi^{-1}\cdot\det D^\tau\varphi^{-1}\big)^2\cdot\operatorname{div}_\Gamma(V)\cdot\operatorname{div}_\Gamma(W) - f_\varphi\cdot\mathfrak{D}_m\big(f_\varphi\big)[W]\cdot\operatorname{div}_\Gamma(V) \\ &\quad + \frac{1}{2}\cdot\Big(\big(g^M\circ\varphi^{-1}\cdot\det D^\tau\varphi^{-1}\big)^2 - f_\varphi^2\Big)\cdot\Bigg(\operatorname{div}_\Gamma\big(DV\cdot W\big) \\ &\qquad\qquad + \Big\langle\big(DV+DV^T\big)\cdot n, \nabla_\Gamma\langle W,n\rangle_2 - D_\Gamma n\cdot W\Big\rangle_2\Bigg).\end{aligned} \tag{5.105}$$

We shift our attention to the second material derivative occurring in equation (5.99). But this one is easier, since we can use the same arguments applied to the previous

material derivative, and because we do not need to differentiate divergence terms. We apply assumed existence of the second order pre-shape material derivative of f_φ, and leave respective terms general, to get

$$\begin{aligned}
&\mathfrak{D}_m\Big(\Big(g^M\circ\varphi^{-1}\cdot\det D^\tau\varphi^{-1}-f_\varphi\Big)\cdot\mathfrak{D}_m\big(f_\varphi\big)[V]\Big)[W]\\
&=\Big(\mathfrak{D}_m\big(g^M\circ\varphi^{-1}\big)[W]\cdot\det D^\tau\varphi^{-1}+g^M\circ\varphi^{-1}\cdot\mathfrak{D}_m\big(\det D^\tau\varphi^{-1}\big)[W]\\
&\qquad\qquad-\mathfrak{D}_m\big(f_\varphi\big)[W]\Big)\cdot\mathfrak{D}_m\big(f_\varphi\big)[V]\\
&\quad+\Big(g^M\circ\varphi^{-1}\cdot\det D^\tau\varphi^{-1}-f_\varphi\Big)\cdot\mathfrak{D}_m\Big(\mathfrak{D}_m\big(f_\varphi\big)[V]\Big)[W]\\
&=-\big(g^M\circ\varphi^{-1}\cdot\det D^\tau\varphi^{-1}\big)\cdot\operatorname{div}_\Gamma(W)\cdot\mathfrak{D}_m\big(f_\varphi\big)[V]\\
&\quad-\mathfrak{D}_m\big(f_\varphi\big)[W]\cdot\mathfrak{D}_m\big(f_\varphi\big)[V]\\
&\quad+\Big(g^M\circ\varphi^{-1}\cdot\det D^\tau\varphi^{-1}-f_\varphi\Big)\cdot\mathfrak{D}_m\Big(\mathfrak{D}_m\big(f_\varphi\big)[V]\Big)[W].
\end{aligned}\tag{5.106}$$

Now that we computed the necessary material derivatives, we plug them into equation (5.99) to arrive at

$$\begin{aligned}
&\mathfrak{D}^2\mathfrak{J}^M(\varphi)[V][W]\\
&=-\int_{\varphi(M)}-\big(g^M\circ\varphi^{-1}\cdot\det D^\tau\varphi^{-1}\big)^2\cdot\operatorname{div}_\Gamma(V)\cdot\operatorname{div}_\Gamma(W)-f_\varphi\cdot\mathfrak{D}_m\big(f_\varphi\big)[W]\cdot\operatorname{div}_\Gamma(V)\\
&\qquad+\frac{1}{2}\cdot\Big(\big(g^M\circ\varphi^{-1}\cdot\det D^\tau\varphi^{-1}\big)^2-f_\varphi^2\Big)\cdot\Big(\operatorname{div}_\Gamma(DV\cdot W)\\
&\qquad\qquad+\Big\langle\big(DV+DV^T\big)\cdot n,\nabla_\Gamma\langle W,n\rangle_2-D_\Gamma n\cdot W\Big\rangle_2\Big)\\
&\qquad-\big(g^M\circ\varphi^{-1}\cdot\det D^\tau\varphi^{-1}\big)\cdot\operatorname{div}_\Gamma(W)\cdot\mathfrak{D}_m\big(f_\varphi\big)[V]\\
&\qquad-\mathfrak{D}_m\big(f_\varphi\big)[W]\cdot\mathfrak{D}_m\big(f_\varphi\big)[V]\\
&\qquad+\Big(g^M\circ\varphi^{-1}\cdot\det D^\tau\varphi^{-1}-f_\varphi\Big)\cdot\mathfrak{D}_m\Big(\mathfrak{D}_m\big(f_\varphi\big)[V]\Big)[W]\\
&\qquad+\frac{1}{2}\cdot\Big(\big(g^M\circ\varphi^{-1}\cdot\det D^\tau\varphi^{-1}\big)^2-f_\varphi^2\Big)\cdot\operatorname{div}_\Gamma(V)\cdot\operatorname{div}_\Gamma(W)\\
&\qquad+\Big(g^M\circ\varphi^{-1}\cdot\det D^\tau\varphi^{-1}-f_\varphi\Big)\cdot\mathfrak{D}_m\big(f_\varphi\big)[V]\cdot\operatorname{div}_\Gamma(W)\,\mathrm{d}s\\
&=-\int_{\varphi(M)}-\frac{1}{2}\cdot\Big(\big(g^M\circ\varphi^{-1}\cdot\det D^\tau\varphi^{-1}\big)^2+f_\varphi^2\Big)\cdot\operatorname{div}_\Gamma(V)\cdot\operatorname{div}_\Gamma(W)\\
&\qquad-f_\varphi\cdot\Big(\mathfrak{D}_m\big(f_\varphi\big)[V]\cdot\operatorname{div}_\Gamma(W)+\mathfrak{D}_m\big(f_\varphi\big)[W]\cdot\operatorname{div}_\Gamma(V)\Big)\\
&\qquad-\mathfrak{D}_m\big(f_\varphi\big)[W]\cdot\mathfrak{D}_m\big(f_\varphi\big)[V]\\
&\qquad+\frac{1}{2}\cdot\Big(\big(g^M\circ\varphi^{-1}\cdot\det D^\tau\varphi^{-1}\big)^2-f_\varphi^2\Big)\cdot\Big(\operatorname{div}_\Gamma(DV\cdot W)\\
&\qquad\qquad+\Big\langle\big(DV+DV^T\big)\cdot n,\nabla_\Gamma\langle W,n\rangle_2-D_\Gamma n\cdot W\Big\rangle_2\Big)\\
&\qquad+\Big(g^M\circ\varphi^{-1}\cdot\det D^\tau\varphi^{-1}-f_\varphi\Big)\cdot\mathfrak{D}_m\Big(\mathfrak{D}_m\big(f_\varphi\big)[V]\Big)[W]\,\mathrm{d}s
\end{aligned}$$

$$
\begin{aligned}
&= \int_{\varphi(M)} \Big(f_\varphi \cdot \operatorname{div}_\Gamma(V) + \mathfrak{D}_m\big(f_\varphi\big)[V] \Big) \cdot \Big(f_\varphi \cdot \operatorname{div}_\Gamma(W) + \mathfrak{D}_m\big(f_\varphi\big)[W] \Big) \\
&\qquad + \frac{1}{2} \cdot \Big(\big(g^M \circ \varphi^{-1} \cdot \det D^\tau \varphi^{-1} \big)^2 - f_\varphi^2 \Big) \cdot \Bigg(\operatorname{div}_\Gamma(V) \cdot \operatorname{div}_\Gamma(W) - \operatorname{div}_\Gamma(DV \cdot W) \\
&\qquad\qquad - \Big\langle \big(DV + DV^T \big) \cdot n, \nabla_\Gamma \langle W, n \rangle_2 - D_\Gamma n \cdot W \Big\rangle_2 \Bigg) \\
&\qquad - \Big(g^M \circ \varphi^{-1} \cdot \det D^\tau \varphi^{-1} - f_\varphi \Big) \cdot \mathfrak{D}_m \Big(\mathfrak{D}_m\big(f_\varphi\big)[V] \Big)[W] \, \mathrm{d}s,
\end{aligned}
$$

where we used a binomial expansion in the last equality, while paying attention to the minus sign in front of the integral, to get the final form of the pre-shape Hessian as in equation (5.98). Notice that no integration by parts or Stokes theorem was used, meaning no boundary integrals occur. □

By inspecting the pre-shape Hessian (5.98), we notice occurrence of non-symmetric terms. It is of course possible to symmetrize these terms and use a modified version of the Hessian. Such a symmetrized version might not necessarily give additional benefits if used in a higher order optimization method. This is because, with the next corollary, we see that the pre-shape Hessian is indeed symmetric in solutions to the parameterization tracking problem. So it could be argued, that removing non-symmetric terms in numerical applications to have a symmetric pre-shape Hessian has validity.

Remark 19 (Implementation of the Pre-Shape Hessian with First Order Elements)**.** *The pre-shape Hessian* (5.98) *of the parameterization tracking problem involves almost only terms featuring derivatives of order lower than 2. Only the two terms involving* $\operatorname{div}_\Gamma(DV \cdot W)$ *and* $\mathfrak{D}_m(\mathfrak{D}_m\big(f_\varphi\big)[V])[W]$ *potentially have second order derivatives with respect to* V *and* f_φ*. These two terms are part of the discussed asymmetric pre-shape Hessian terms. Nevertheless, we can use partial integrations to derive formulae only featuring first order derivatives. Taking the first term as an example, this boils down to*

$$
\begin{aligned}
&- \int_{\varphi(M)} \frac{1}{2} \cdot \Big(\big(g^M \circ \varphi^{-1} \cdot \det D^\tau \varphi^{-1} \big)^2 - f_\varphi^2 \Big) \cdot \operatorname{div}_\Gamma(DV \cdot W) \\
&= \int_{\varphi(M)} \Big(\big(g^M \circ \varphi^{-1} \cdot \det D^\tau \varphi^{-1} \big) \cdot \nabla_\Gamma \big(g^M \circ \varphi^{-1} \cdot \det D^\tau \varphi^{-1} \big) - f_\varphi \cdot \nabla_\Gamma f_\varphi \Big)^T (DV \cdot W) \\
&\quad - \int_{\partial\varphi(M)} \frac{1}{2} \cdot \Big(\big(g^M \circ \varphi^{-1} \cdot \det D^\tau \varphi^{-1} \big)^2 - f_\varphi^2 \Big) \cdot \big\langle DV \cdot W, n_{\varphi(M)} \big\rangle_2 \, \mathrm{d}s,
\end{aligned}
$$

where $n_{\varphi(M)}$ *is the outward pointing unit normal vector field on* $\partial\varphi(M)$*. This procedure enables implementation of the pre-shape Hessian in numerical routines by use of first order elements only.*

In the following, we denote by $\varphi \in \operatorname{Emb}(M, \mathbb{R}^{n+1})$ a fiber stationary point of the parameterization tracking problem, and omit the usual tilde notation for readability. We remind the reader that by theorem 13, such an embedding is a global solution.

Corollary 3 (Pre-Shape Hessian in Fiber Stationary Points)**.** *Let the assumptions from theorem 12 hold. Consider* f_φ *such, that it has second order pre-shape material derivatives. Let* $\varphi \in \operatorname{Emb}(M, \mathbb{R}^{n+1})$ *be a fiber stationary point of parameterization tracking problem* (5.10) *(cf. equation* (5.75)*), and let* n *be the outer unit normal vector field on* $\varphi(M)$*.*

Then, for all $V, W \in C^\infty(\mathbb{R}^{n+1}, \mathbb{R}^{n+1})$, the pre-shape Hessian to (5.10) *at φ has the form*

$$\mathfrak{D}^2\mathfrak{J}^M(\varphi)[V][W] = \int_{\varphi(M)} \Big(f_\varphi \cdot \operatorname{div}_\Gamma(V) + \mathfrak{D}_m\big(f_\varphi\big)[V]\Big) \cdot \Big(f_\varphi \cdot \operatorname{div}_\Gamma(W) + \mathfrak{D}_m\big(f_\varphi\big)[W]\Big)\, \mathrm{d}s. \tag{5.107}$$

In particular, the pre-shape Hessian is positive semidefinite at φ, i.e.

$$\mathfrak{D}^2\mathfrak{J}^M(\varphi)[V][V] \geq 0 \qquad \forall V \in C^\infty\big(\mathbb{R}^{n+1}, \mathbb{R}^{n+1}\big). \tag{5.108}$$

Additionally, for all directions V^τ tangential to $\varphi(M)$, not necessarily parallel to $\partial\varphi(M)$, the pre-shape Hessian at φ satisfies

$$\mathfrak{D}^2\mathfrak{J}^M(\varphi)\big[V^\tau\big]\big[W^\tau\big] = \int_{\varphi(M)} f_\varphi^2 \cdot \operatorname{div}_{f_\varphi,\Gamma}\left(V^\tau\right) \cdot \operatorname{div}_{f_\varphi,\Gamma}\left(W^\tau\right) \mathrm{d}s, \tag{5.109}$$

where $\operatorname{div}_{f_\varphi,\Gamma}$ is the tangential f_φ-divergence on $\varphi(M)$ (cf. equation (5.38)*). Further, it holds*

$$\mathfrak{D}^2\mathfrak{J}^M(\varphi)\big[V^\tau\big]\big[V^\tau\big] = 0 \tag{5.110}$$

for all tangential f_φ-divergence free vector fields V^τ. For other tangential vector fields on $\varphi(M)$, the pre-shape Hessian is strictly positive.

Proof. This corollary is a consequence of a combined application of the closed form pre-shape Hessian (5.98) and characterization of fiber stationary points as global minima from theorem 13. Let us assume the setting of theorem 12 and let f_φ have second order pre-shape material derivatives. Consider a fiber stationary point $\varphi \in \operatorname{Emb}(M, \mathbb{R}^{n+1})$. Existence of a fiber stationary point is guaranteed, since these are characterized exactly as global minimizers by theorem 13, for which we can apply the existence theorem 10.

Characterization of fiber stationary points φ in theorem 13 (ii) also gives relation (5.76). Using relation (5.76), and the resulting equality for their corresponding squares, in the closed formula for the pre-shape Hessian (5.98), we immediately get expression (5.107), as all integrands of the pre-shape Hessian (5.98) except for the first vanish. At this stage, positive semidefiniteness of $\mathfrak{D}^2\mathfrak{J}^M(\varphi)$ is seen directly by

$$\mathfrak{D}^2\mathfrak{J}^M(\varphi)[V][V] = \int_{\varphi(M)} \Big(f_\varphi \cdot \operatorname{div}_\Gamma(V) + \mathfrak{D}_m\big(f_\varphi\big)[V]\Big)^2 \mathrm{d}s \geq 0 \tag{5.111}$$

for all directions $V \in C^\infty(\mathbb{R}^{n+1}, \mathbb{R}^{n+1})$.

Next, we derive reformulation (5.109) of the pre-shape Hessian in tangential directions using the tangential f_φ-divergence. For this, we decompose the involved factors of the integrand in equation (5.107) by corollary 2 (i), which gives

$$f_\varphi \cdot \operatorname{div}_\Gamma(V) + \mathfrak{D}_m\big(f_\varphi\big)[V] = f_\varphi \cdot \operatorname{div}_\Gamma(V) + \mathfrak{D} f_\varphi[V] + \frac{\partial f_\varphi}{\partial n} \cdot \langle n, V\rangle_2 + \nabla_\Gamma f_\varphi^T V. \tag{5.112}$$

Let $V^\tau \in C^\infty(\mathbb{R}^{n+1}, \mathbb{R}^{n+1})$ be a direction tangential to $\varphi(M)$, but not necessarily parallel to $\partial\varphi(M)$. By assumption of theorem 10, we have that f_φ has shape functionality. Hence the structure theorem 9 (iii) for pre-shape derivatives guarantees, that the pre-shape derivative $\mathfrak{D} f_\varphi$ can be naturally restated as a shape derivative, and is supported only on normal directions. With this in mind, we insert a tangential direction V^τ into equation (5.112) to get

$$f_\varphi \cdot \operatorname{div}_\Gamma\left(V^\tau\right) + \mathfrak{D}_m\big(f_\varphi\big)\big[V^\tau\big] = f_\varphi \cdot \operatorname{div}_\Gamma\left(V^\tau\right) + \nabla_\Gamma f_\varphi^T V^\tau = \operatorname{div}_\Gamma\left(f_\varphi \cdot V^\tau\right). \tag{5.113}$$

With this, we get equation (5.109) by application of formula (5.38) for the tangential f_φ-divergence and strict positivity of f_φ. The last statement of corollary 3 concerning vanishing and strict positive definiteness of $\mathfrak{D}^2\mathfrak{J}^M(\varphi)[V^\tau][V^\tau]$ for tangential directions follows directly from equation (5.109). □

With formula (5.107), corollary 3 gives a vast simplification of the pre-shape Hessian (5.98) to the pre-shape parameterization tracking problem in solutions. We clearly see, that the resulting bilinear form is symmetric, which means that occurring non-symmetric terms of the pre-shape Hessian indeed vanish near solutions.

The pre-shape Hessian (5.107) in solutions can be used as a preconditioner for systems arising in algorithms for parameterization tracking in shape optimization. It is reasonable to focus on tangential directions in the preconditioning process, as the general interest for parameterization tracking is to find better mesh configurations, while still leaving the shape at hand invariant. For this task, formula (5.109) for the pre-shape Hessian in solutions for tangential directions is appropriate. To make it more practical for numerical implementations, we can substitute the tangential f_φ-divergence via its definition (5.38), to have terms featuring only tangential divergences. This gives the bilinear form

$$\langle V, W\rangle_{\varphi(M)} = \int_{\varphi(M)} \operatorname{div}_\Gamma(f_\varphi \cdot V) \cdot \operatorname{div}_\Gamma(f_\varphi \cdot W)\, \mathrm{d}s, \tag{5.114}$$

which equals the pre-shape Hessian in solutions for tangential directions. It can be used to precondition Newton-systems, for Hesse-approximations as used in L-BFGS algorithms, or as a bilinear form for enhanced gradient descent algorithms (cf. [161, 159]). For these applications, it is important to be aware of the semidefiniteness coming from tangential f_φ-divergence-free directions $V \in C^\infty(\mathbb{R}^{n+1}, \mathbb{R}^{n+1})$.

From theoretical perspective, the special form of the pre-shape Hessian for parameterization tracking in tangential directions seen in equation (5.109) fits to the results in section 5.2.2, which characterize equivalent solutions via Euler flows with tangential f_φ-divergence free initial velocities from L^2-metrics on fibers. The tangential f_φ-divergences weighted by the target f_φ are the major components of the Hessian in solutions. Characterization theorem 11 and its discussion show, that exactly the vector fields with vanishing tangential f_φ-divergence are in correspondence to the neighboring solutions leaving a shape invariant. Hence it is not surprising, that the last part of corollary 3 states semidefiniteness of the pre-shape Hessian in a solution exactly for these local solution generating directions. We remark that the results concerning equivalent solutions via tangential f_φ-divergence free vector fields and Euler flows do not rely on pre-shape calculus. At the same time, structures from this type of solution characterization are obviously apparent in the pre-shape Hessian.

Chapter 6

Regularizing Shape Optimization Problems by Parameterization Tracking

The main goal of this chapter is to introduce a theory for regularization of shape optimization problems by pre-shape parameterization tracking. This allows to simultaneously adapt shape and hold-all domain meshes to specified cell volume targets, while solving the underlying shape optimization problem. We reiterate, that techniques we develop do not involve changes in mesh topologies, and particularly avoid remeshing or mesh refinements. However, they can be combined with refinement and remeshing approaches.

For our endeavor, we rely on the key observation, that shape optimization problems can be extended to pre-shape spaces $\mathrm{Emb}(M, \mathbb{R}^{n+1})$. The fiber bundle structure offers an opportunity to modify the problem, such that the original shape solution is maintained, while at the same time an optimal parameterization from the solution fiber is selected. This gives rise to several different regularized shape optimization routines to achieve target mesh quality. Procedures and numerical implementations using our techniques are discussed in chapter 7, after we establish the theory for regularization by pre-shape parameterization problem tracking problems in this chapter.

Our approaches need to satisfy three properties. On the one hand, they must not interfere with the original shape optimization problem, i.e. leave the optimal shape or even intermediate shapes invariant. On the other hand, to be practically feasible, the mesh quality regularization approaches should not increase computational cost significantly. In particular, no additional solution of linear systems should be necessary if compared to standard shape gradient descent algorithms. And lastly, our approach should not depend on the form of gradient representations, such as linear elasticity or p-Laplacian ones, making it more versatile. We achieve all mentioned properties for the simultaneous shape and volume mesh quality regularizations of this work.

For their introduction, we proceed in multiple steps. First, in section 6.1, we analyze the case where quality of the mesh representing the shape is optimized. This amounts to increasing quality of the (hyper-)surface shape mesh $\varphi(M)$ embedded in the volume hold-all domain $\mathbb{D}$. We resituate shape optimization problems in pre-shape spaces, where they can be modified by parameterization tracking to yield regularized pre-shape optimization problems. Then, in section 6.2, we build on the surface mesh case by also demanding increased volume mesh quality of the hold-all domain $\mathbb{D}$. With this, we gain the opportunity to control both the volume and the

shape mesh quality at the same time. We provide sufficient spaces for pre-shapes ϕ representing volume meshes $\mathbb{D}$, in order to not interfere with shape optimization. With these spaces, the fully regularized problem can be formulated as a bilevel pre-shape optimization problem. We provide existence of solutions φ, such that an optimal pre-shape of the regularized shape optimization problem corresponds to its unregularized solution, while having optimal shape mesh quality with regard to the parameterization tracking problem. For this solution, existence of an optimal volume parameterization ϕ of the hold-all domain is guaranteed, which leaves the optimal shape $\varphi(M)$ invariant. Then, we provide modified pre-shape gradient systems, which permit simultaneous shape and mesh quality optimization by a single gradient system. In particular, we show consistency of this gradient system with the fully regularized problem. This serves as the foundation to formulate a simultaneous shape optimization and parameterization tracking algorithm. The discussion of this algorithm and results from numerical implementations using a model problem are given in the next chapter 7.

If not stated otherwise, we assume $M \subset \mathbb{R}^{n+1}$ to be an n-dimensional, oriented, connected and compact C^∞-manifold, perhaps with smooth boundary ∂M. To suit the context of numerical applications, we look at ambient spaces $\mathbb{D} \subset \mathbb{R}^{n+1}$, which are open, connected and oriented $n+1$-dimensional C^∞-submanifolds. Also, we assume the closures $\overline{\mathbb{D}}$ to have smooth boundaries $\partial\mathbb{D}$, in case the boundaries are nonempty. The according pre-shape space $\mathrm{Emb}(M, \mathbb{D})$ consists of all shapes embedded into the interior of $\mathbb{D}$. Previous statements about fiber-bundle structure, pre-shape calculus, and existence of solutions to parameterization tracking all remain valid. Also, the associated shape spaces B_e^n are well-defined, and are the base space of $\mathrm{Emb}(M, \mathbb{D})$ (cf. [61, Thm. 2.2]). Regularizations for the shape mesh discussed in section 6.1 do not rely on a bounded hold-all domain $\mathbb{D}$. However, regularization techniques for the hold-all domain $\mathbb{D}$ in section 6.2 indeed require its boundedness.

6.1 Simultaneous Shape Mesh Quality and Shape Optimization

In this section we formulate a regularized shape optimization problem to track for desired shape mesh quality using pre-shape calculus. Throughout chapter 6, we take a look at a general prototype shape optimization problem

$$\min_{\Gamma \in B_e^n} \mathcal{J}(\Gamma). \tag{6.1}$$

We only assume that the shape functional $\mathcal{J}\colon B_e^n \to \mathbb{R}$ is first order shape differentiable.

In the following, we reformulate problem (6.1) in the context of pre-shape optimization by use of the canonical projection $\pi\colon \mathrm{Emb}(M, \mathbb{D}) \to B_e^n$. We remind the reader, that the canonical projection π maps each pre-shape $\varphi \in \mathrm{Emb}(M, \mathbb{D})$ to an equivalence class $\pi(\varphi) = \Gamma \in B_e^n$, which consists of all parameterizations of the same shape $\varphi(M)$ in $\mathbb{D}$. Via the nonlinear Grassmannian (4.5), we can associate every $\pi(\varphi)$ with its set interpretation $\varphi(M) \subset \mathbb{D}$ of the shape. With proposition 2, the pre-shape formulation of problem (6.1) takes the form

$$\min_{\varphi \in \mathrm{Emb}(M,\mathbb{D})} (\mathcal{J} \circ \pi)(\varphi). \tag{6.2}$$

It is important to notice, that proposition 2 guarantees pre-shape differentiability of the extended target functional of problem (6.2), since we assumed $\mathcal{J}$ to be shape differentiable.

All necessary ingredients are laid out to formulate a regularized version of the general shape optimization problem (6.1). For $\alpha^\tau > 0$, we add the parameterization tracking functional in style of a regularizing term to pre-shape reformulation (6.2), which gives the *shape regularized problem*

$$\min_{\varphi \in \mathrm{Emb}(M,\mathbb{D})} (\mathcal{J} \circ \pi)(\varphi) + \alpha^\tau \cdot \mathfrak{J}^M(\varphi). \tag{6.3}$$

By proposition 2 and theorem 12, we know that the regularized objective of the initial shape optimization problem in (6.3) is pre-shape differentiable. This is foundational, because it means a pre-shape gradient system for the shape regularized problem (6.3) can be formulated.

The pre-shape derivative $\mathfrak{D}\mathfrak{J}^M(\varphi)[V]$ of the parameterization tracking problem is well-defined for weakly differentiable directions $V \in H^1(\overline{\mathbb{D}}, \mathbb{R}^{n+1})$ (cf. equation (5.59)). By assuming the same for the shape derivative $\mathcal{D}\mathcal{J}$ of the original problem (6.1), we can create a pre-shape gradient system for (6.3) using a weak formulation with H^1-functions. Given a symmetric and positive definite bilinear form $\mathfrak{a}(\cdot,\cdot)$, such a system takes the form

$$\mathfrak{a}(U^{\mathcal{J}+\mathfrak{J}^M}, V) = \mathcal{D}\mathcal{J}(\Gamma)[V] \;+\; \alpha^\tau \cdot \langle g_\varphi^{\mathcal{N}}, V\rangle \;+\; \alpha^\tau \cdot \langle g_\varphi^{\mathcal{T}}, V\rangle \qquad \forall V \in H_0^1\big(\mathbb{D}, \mathbb{R}^{n+1}\big). \tag{6.4}$$

Here, $g_\varphi^{\mathcal{N}}$ and $g_\varphi^{\mathcal{N}}$ are the components from the decomposition of $\mathfrak{D}\mathfrak{J}^M(\varphi)$ in equation (5.70). We use a fracture $\mathfrak{a}(\cdot,\cdot)$ to distinguish the form for the gradient representation from bilinear forms $a(\cdot,\cdot)$ arising in state equations of later chapters. With $\Gamma = \pi(\varphi)$, the right-hand side of equation (6.4) is indeed a full pre-shape gradient for the objective of problem (6.3). This stems from the fact, that the pre-shape extension $\mathcal{J} \circ \pi$ has shape functionality by construction, which makes the pre-shape derivative $\mathfrak{D}(\mathcal{J} \circ \pi)$ equal to the shape derivative $\mathcal{D}\mathcal{J}$ by application of structure theorem 9 (iii). Notice, that it is not necessary to have bilinearity or symmetry of $\mathfrak{a}(\cdot,\cdot)$. There are various approaches for shape gradient representations, which employ nonlinear equations with shape derivatives as right-hand sides. For example, the strong formulation of the quasilinear p-Laplacian equation as found in [135] can serve as a tool to represent shape gradients with beneficial properties for optimization.

The full pre-shape gradient system (6.4) can be used to achieve simultaneous solution of the shape optimization problem and parameterization tracking for the shape mesh. It is not required to solve an additional linear system to create a mesh quality regularized descent direction $U^{\mathcal{J}+\mathfrak{J}^M}$, since the original shape gradient system to problem (6.1) is modified by adding the two force terms $g^{\mathcal{N}}$ and $g^{\mathcal{T}}$. We also see, that calculation of a descent direction $U^{\mathcal{J}+\mathfrak{J}^M}$ via the single combined system (6.4) corresponds to a calculation with two separate steps. More specifically, the direction $U^{\mathcal{J}+\mathfrak{J}^M}$ equals the combined direction $U^{\mathcal{J}} + U^{\mathfrak{J}^M}$ of the shape gradient $U^{\mathcal{J}}$ and pre-shape gradient $U^{\mathfrak{J}^M}$, which solve the decoupled systems

$$\mathfrak{a}\big(U^{\mathcal{J}}, V\big) = \mathcal{D}\mathcal{J}(\Gamma)[V] \qquad \forall V \in H_0^1\big(\mathbb{D}, \mathbb{R}^{n+1}\big) \tag{6.5}$$

and

$$\mathfrak{a}\big(U^{\mathfrak{J}^M}, V\big) = \alpha^\tau \cdot \langle g_\varphi^{\mathcal{N}}, V\rangle + \alpha^\tau \cdot \langle g_\varphi^{\mathcal{T}}, V\rangle \qquad \forall V \in H_0^1\big(\mathbb{D}, \mathbb{R}^{n+1}\big). \tag{6.6}$$

However, gradient system (6.4) is not suitable for derivative based shape optimization. Application of $U^{\mathcal{J}+\mathfrak{J}^M}$ neither leaves intermediate nor optimal shapes of the underlying shape optimization problem invariant. This issue comes from involvement of the shape component $g_\varphi^{\mathcal{N}}$ of the pre-shape derivative to the parameterization tracking objective $\mathfrak{J}^M$ (cf. equation (5.71)). It acts solely in normal directions,

therefore altering shapes by interfering with the shape derivative $\mathcal{DJ}$ of the original problem. We numerically capture and examine this effect in section 7.3.

For this reason, we deviate from the full gradient system (6.4), and use a modified system

$$\mathfrak{a}\big(\tilde{U}, V\big) = \mathcal{DJ}(\Gamma)[V] + \alpha^\tau \cdot \big\langle g_\varphi^{\mathcal{T}}, V \big\rangle \qquad \forall V \in H_0^1\big(\mathbb{D}, \mathbb{R}^{n+1}\big). \tag{6.7}$$

We project the pre-shape derivative $\mathfrak{DJ}^M$ onto its tangential part, which is realized by simply removing the shape component $g^{\mathcal{N}}$ from the right-hand side of the gradient system. By this, we still have the numerical advantage of solving a single gradient system, while also achieving invariance of optimal and intermediate shapes. Of course, invariance is only guaranteed up to discretization errors. From a classical shape optimization perspective, this stems from considering equation (6.7) as a shape gradient system with additional force term $g^{\mathcal{T}}$, which acts on directions V in the kernel of the classical shape derivative $\mathcal{DJ}$. We recur, that Hadamard's theorem 7 and the structure theorem 9 for pre-shape derivatives identify directions tangential to shapes Γ to be in the kernel of $\mathcal{DJ}(\Gamma)$. In the pre-shape setting, we interpret these directions as vector fields corresponding to the fiber components of $\mathrm{Emb}(M, \mathbb{D})$.

We sum up and justify the use of the pre-shape regularized problem (6.3) and its modified gradient system (6.7), by providing existence of solutions and consistency of the modified gradients with the regularized problem.

Theorem 15 (Shape Regularized Problems)**.** *Let $\mathbb{D} \subset \mathbb{R}^{n+1}$ be an $n+1$-dimensional, open, connected and oriented C^∞-submanifold, such that its closure $\overline{\mathbb{D}}$ has a smooth boundary $\partial\mathbb{D}$. Assume $M \subset \mathbb{D}$ to be an n-dimensional, oriented, connected and compact C^∞-manifold, perhaps with smooth boundary. Let shape optimization problem* (6.1) *be shape differentiable and have a minimizer $\Gamma \in B_e^n$. For shape parameterization tracking, let us assume functions $g^M \colon M \to (0, \infty)$ and $f_\varphi \colon \varphi(M) \to (0, \infty)$ to be smooth, fulfill the normalization condition* (5.9)*, and f to have shape functionality.*

Then there exists a $\varphi \in \pi(\varphi) = \Gamma \subset \mathrm{Emb}(M, \mathbb{D})$ minimizing the shape regularized problem (6.3)*.*

The modified pre-shape gradient system (6.7) *is consistent with the full pre-shape gradient system* (6.4) *and the shape gradient system of the original problem* (6.5)*, in the sense that*

$$\tilde{U} = 0 \iff U^{\mathcal{J}+\mathfrak{J}^M} = 0 \text{ and } U^{\mathcal{J}} = 0. \tag{6.8}$$

In particular, if $U^{\mathcal{J}+\mathfrak{J}^M} = 0$ is satisfied, the necessary first order conditions for the shape regularized problem (6.3) *and the original problem* (6.1) *are satisfied as well.*

Proof. For the existence of solutions to the shape regularized problem (6.3), let us assume there exists a minimizer $\Gamma \in B_e^n$ to the original problem (6.1). By construction of the shape space B_e^n via equivalence relation (4.4), there exists a $\tilde{\varphi} \in \mathrm{Emb}(M, \mathbb{D})$, such that $\Gamma = \pi(\tilde{\varphi})$. So the set of pre-shapes $\pi(\tilde{\varphi})$ acts as a set of solution candidates for the shape regularized problem (6.3). Since we require shape functionality of f_φ and normalization condition (5.9), theorem 10 for solutions to parameterization tracking guarantees existence of a global minimizer for $\mathfrak{J}^M$ in every fiber of $\mathrm{Emb}(M, \mathbb{D})$. In particular, we can find such a φ in $\pi(\tilde{\varphi})$. From the last assertion of theorem 10, we also have $\mathfrak{J}^M(\varphi) = 0$. Additionally, since $\mathfrak{J}^M \geq 0$ due to the quadratic nature of the parameterization tracking objective, we have that φ is a solution to the shape regularized problem (6.3).

Next, we prove the non-trivial direction ' $\Longrightarrow$ ' for consistency of gradient systems in the sense of equivalence relation (6.8). Let us assume we have a pre-shape

gradient $\tilde{U} = 0$, which stems from the modified system (6.7). This immediately results in

$$\mathcal{D}\mathcal{J}(\Gamma)[V] + \alpha^\tau \cdot \left\langle g_\varphi^{\mathcal{T}}, V \right\rangle = 0 \qquad \forall V \in H_0^1\big(\mathbb{D}, \mathbb{R}^{n+1}\big). \tag{6.9}$$

However, due to the structure theorem 9 for pre-shape derivatives, we know that the supports of shape derivative $\mathcal{D}\mathcal{J}(\Gamma)$ and the pure pre-shape component $g_\varphi^{\mathcal{T}}$ are orthogonal. Hence

$$\mathcal{D}\mathcal{J}(\Gamma)[V] = 0 \quad \text{and} \quad \alpha^\tau \cdot \left\langle g_\varphi^{\mathcal{T}}, V \right\rangle = 0 \qquad \forall V \in H_0^1\big(\mathbb{D}, \mathbb{R}^{n+1}\big). \tag{6.10}$$

This is the first order condition for equation (6.1), in particular giving $U^{\mathcal{J}} = 0$.

It remains to show that the first order condition for the regularized problem (6.3) is satisfied, and that the complete gradient achieves $U^{\mathcal{J}+\mathfrak{J}^M} = 0$. Essentially, this is a special case of theorem 13, which characterizes global solutions of parameterization tracking by fiber stationarity. From the second equation (6.10) combined with structure theorem 9 (ii), we see that $\varphi \in \mathrm{Emb}(M, \mathbb{D})$ is a fiber stationary point. Hence theorem 13 states that φ is already a global minimizer of $\mathfrak{J}^M$, and satisfies the corresponding necessary first order condition. Even more, theorem 13 gives vanishing of $\mathfrak{D}\mathfrak{J}^M(\varphi)$ and $g_\varphi^{\mathcal{N}}$. Therefore, the right-hand side of the full gradient system equation (6.4) is zero, resulting in a vanishing full gradient $U^{\mathcal{J}+\mathfrak{J}^M} = 0$.

Implication '$\Leftarrow$' holds by the fiber stationarity characterization as well. Since vanishing of the shape gradient $U^{\mathcal{J}}$ gives $\mathcal{D}\mathcal{J}(\Gamma) = 0$, the full pre-shape derivative $\mathfrak{D}\mathfrak{J}^M(\varphi)$ must be zero if the full pre-shape gradient $U^{\mathcal{J}+\mathfrak{J}^M} = 0$. Then the fiber stationarity characterization theorem 13 tells us that both $g_\varphi^{\mathcal{T}}$ and $g_\varphi^{\mathcal{N}}$ vanish for φ, which proves the remaining direction of equivalence (6.8). □

With theorem 15 we can rest assured that optimization algorithms, which use the tangentially regularized gradient $\tilde{U}$ from equation (6.7) leave stationary points of the original problem invariant. Vanishing of the modified gradient $\tilde{U}$ indicates that we have a stationary shape $\Gamma = \pi(\varphi)$, whose pre-shape φ has desired cell volume allocation f_φ. Of course, this is only true up to discretization error. We also see that the modified gradient system (6.7) captures the same information as the shape gradient system (6.5) and full pre-shape gradient system (6.4) combined. This might seem counterintuitive at first, especially since necessary information is contained in one instead of two gradient systems. However, by application of pre-shape calculus to derive the fiber stationarity characterization theorem 13, we recognize this circumstance as a consequence of the special structure of regularizing functional $\mathfrak{J}^M$. The fact that pre-shape spaces are fiber spaces with locally orthogonal tangential bundles for parameterizations and shapes is a fundamental prerequisite to this. We discuss numerical results comparing optimization with standard shape gradients from equation (6.5) and gradients regularized by modified shape parameterization tracking from equation (6.7) in chapter 7.

Remark 20 (Equivalent Bilevel Formulation of the Regularized Problem)**.** *It is also possible to formulate the shape mesh regularization as a nonlinear bilevel problem*

$$\begin{aligned} &\min_{\varphi \in \mathrm{Emb}(M,\mathbb{D})} \mathfrak{J}^M(\varphi) \\ &\text{s.t. } \pi(\varphi) = \operatorname*{arg\,min}_{\Gamma \in B_e^n} \mathcal{J}(\Gamma). \end{aligned} \tag{6.11}$$

The lower level shape optimization problem restricts the set of feasible solution pre-shapes of the upper level problem. Intuitively, solving bilevel problem (6.11) *amounts to solving the lower level problem for a shape* Γ*, and then to select an optimal parameterization* $\varphi \in \Gamma = \pi(\varphi) \in B_e^n$ *in the fiber corresponding to the optimal shape. If a solution to the lower level shape optimization problem exists, a solution*

φ to the upper level problem exists as well, because global minimizers exist in every fiber of $\mathrm{Emb}(M,\mathbb{D})$ *by theorem 10.*

The bilevel formulation motivates the modified gradient system (6.7) *in a consistent manner. For this, we can take the perspective of nonlinear bilevel programming as in [151]. In finite dimensions, the authors of [151] propose a way to calculate a descent direction by solving a bilevel optimization problem derived from the original problem. We remind the reader, that we formulated our systems as gradient systems and not descent directions, hence a change of sign compared to systems for descent directions in [151] occurs. Also notice that the additional constraint $\pi(\varphi)=\Gamma$ for the feasible set of solutions has to be added to formulate our bilevel problem in the style of [151]. We can proceed with a symbolic and non-rigorous calculation following [151, Ch. 2] by using relations (ii) and (iii) from structure theorem 9 for pre-shape derivatives, the fact that $\mathfrak{J}^M$ does not explicitly depend on Γ of the subproblem, and that $\mathcal{J}$ does not explicitly depend on φ of the upper level problem. This yields a bilevel problem for the gradient U to bilevel problem* (6.11)

$$\begin{aligned} &\max_{U\in H_0^1(\mathbb{D},\mathbb{R}^{n+1}),\|U\|\leq 1} \mathfrak{D}\mathfrak{J}^M(\varphi)[U] \\ s.t.\ U^{\mathcal{N}} = &\operatorname*{arg\,max}_{W\in H_0^1(\mathbb{D},\mathbb{R}^{n+1}),\|W\|\leq 1} \mathcal{D}\mathcal{J}(\Gamma)[W], \end{aligned} \tag{6.12}$$

where $U^{\mathcal{N}}$ is the component of U normal to Γ. In [151, Ch. 3], a descent method is applied to problem (6.12) *by alternating computation of $U_k^{\mathcal{N}}$ and U_k.*

For our situation, a gradient $U_k^{\mathcal{N}}$ for the lower level problem of (6.12) *corresponds to $U^{\mathcal{J}}$ solving the shape gradient system* (6.5)*. With this, the lower level constraint fixes the normal component of U to be the shape derivative of the original problem* (6.1)*. By decomposing $U=U^{\mathcal{T}}+U^{\mathcal{N}}$ into tangential and normal directions, we see that the fixed normal component makes $\mathfrak{D}\mathfrak{J}^M(\varphi)[U^{\mathcal{N}}]=0$ a constant not relevant for the upper level problem. This lets us rewrite the system as*

$$\begin{aligned} &\min_{U^{\mathcal{T}}\in H_0^1(\mathbb{D},\mathbb{R}^{n+1}),\|U^{\mathcal{T}}\|\leq 1} \left\langle g_\varphi^{\mathcal{T}}, U^{\mathcal{T}}\right\rangle \\ &s.t.\ U^{\mathcal{N}} = U^{\mathcal{J}} \\ &\qquad U = U^{\mathcal{T}}+U^{\mathcal{N}}. \end{aligned} \tag{6.13}$$

We see that minimization of the tangential component $g_\varphi^{\mathcal{T}}$ in problem (6.13) *is not restricted by its constraints. Hence it can be decoupled. By considering an additional factor $\alpha^\tau>0$, this leads to a gradient system*

$$\mathfrak{a}\big(U^{\mathcal{T}},V\big)=\alpha^\tau\cdot\left\langle g_\varphi^{\mathcal{T}},V\right\rangle \qquad \forall V\in H_0^1\big(\mathbb{D},\mathbb{R}^{n+1}\big). \tag{6.14}$$

With the same orthogonality arguments made for systems (6.5) *and* (6.6)*, a separate computation of $U^{\mathcal{J}}$ and U^τ as in the general case found in [151] is not necessary. The gradient $U=U^{\mathcal{T}}+U^{\mathcal{N}}$ for the bilevel problem* (6.11) *can be calculated by a single system, which coincides exactly with the modified gradient $\tilde{U}$ from system* (6.7)*. With theorem 15, this means using the modified pre-shape gradient $\tilde{U}$ as a descent direction in fact solves the bilevel problem* (6.11)*, the regularized problem* (6.3)*, and the original shape problem* (6.1) *at the same time.*

6.2 Simultaneous Volume Mesh Quality and Shape Optimization

In this section, we introduce the necessary machinery for a regularization strategy of volume meshes representing the hold-all domain $\mathbb{D}$. We incorporate our previous results, which makes simultaneous optimization of shape and volume mesh quality possible. The regularization for the volume mesh representing the ambient space is designed, such that embedded shapes $\varphi(M) \subset \mathbb{D}$ are left invariant. As before, we show a way to calculate modified pre-shape gradients without need to solve additional (non-)linear systems compared to standard shape gradient calculations.

6.2.1 Volume Parameterization Tracking Problem with Invariant Shapes

In the previous sections we focused on tracking of the parameterization of shapes $\varphi(M)$, for which we regarded $\mathrm{Emb}(M, \mathbb{D})$ as a $\mathrm{Diff}(M)$-fiber bundle. This was necessary in order to distinguish the shape and parameterization aspects, and to show that, in some sense, they are naturally orthogonal and do not conflict each other. The pre-shape space $\mathrm{Emb}(M, \mathbb{D})$ is of course not suitable to model the hold-all domain, since it describes shapes $\varphi(M) \subset \mathbb{D}$ combined with their parameterization. Therefore we need a second, different pre-shape space to represent the hold-all domain $\mathbb{D}$. The situation is further complicated, since we have to account for optimization of shapes $\varphi(M)$ embedded in $\mathbb{D}$. Care must be taken, since we have to avoid that optimal hold-all pre-shapes deform embedded shapes. In particular, we need to pay attention to the topological situation regarding the complement of the shape $\mathbb{D} \setminus \varphi(M)$, which we make precise in this section. The ambient space does, except for the embedded shape, not explicitly influence the objective functional $\mathcal{J}$ of the underlying shape optimization problem. This is reflected by structure theorem 9, as the pre-shape derivative $\mathfrak{D}(\mathcal{J} \circ \pi)$ has no support on the ambient space, but solely on the shape $\varphi(M)$. Hence we can pose a volume parameterization tracking problem on the ambient space, and use the resulting pre-shape derivative to complement the derivatives of the shape optimization objective $\mathfrak{D}(\mathcal{J} \circ \pi)$ and the surface mesh pre-shape parameterization tracking target $\mathfrak{D}\mathfrak{J}^M$.

As in the previous section 6.1, we assume the ambient space to be a connected, open and oriented C^∞-manifold $\mathbb{D} \subset \mathbb{R}^{n+1}$, such that $\overline{\mathbb{D}}$ has a smooth boundary $\partial\mathbb{D}$. In addition, we demand boundedness of $\mathbb{D}$. We have trivial codimension of $\overline{\mathbb{D}}$ in $\mathbb{R}^{n+1}$ due to openness of $\mathbb{D}$. This means a suitable pre-shape space for the volume mesh parameterization tracking is $\mathrm{Emb}(\overline{\mathbb{D}}, \overline{\mathbb{D}}) = \mathrm{Diff}(\overline{\mathbb{D}})$, where regularity of diffeomorphisms corresponds to regularity of $\mathbb{D}$ and the boundary $\partial\mathbb{D}$. Note that $\mathrm{Diff}(\overline{\mathbb{D}})$ has trivial fiber bundle structure, which means that we are in the special case of optimization in a single fiber. With this, the existence theorem 10 for the pre-shape parameterization tracking problem holds, under the same assumptions, in the case of

$$\min_{\phi \in \mathrm{Diff}(\overline{\mathbb{D}})} \frac{1}{2} \int_{\mathbb{D}} \left(g^{\mathbb{D}} \circ \phi^{-1}(x) \cdot \det D\phi^{-1}(x) - f_\phi^{\mathbb{D}}(x) \right)^2 \mathrm{d}x =: \mathfrak{J}^{\mathbb{D}}(\phi). \tag{6.15}$$

Notice that Moser's theorem 4 also holds for manifolds with corners (cf. [28, Thm. 7]), and in particular on meshes modeled as simplices. Also, even though $\overline{\mathbb{D}}$ has a boundary, $\mathrm{Diff}(\overline{\mathbb{D}})$ is an ILH-Lie group (cf. [166, Thm. 3.19]). The functions $f_\phi^{\mathbb{D}} \colon \overline{\mathbb{D}} \to (0, \infty)$ and $g^{\mathbb{D}} \colon \overline{\mathbb{D}} \to (0, \infty)$ have the same interpretation as in the hypersurface case. Also, shape functionality of $f^{\mathbb{D}}$ is an empty condition, since optimization for the volume mesh takes place in a pre-shape space $\mathrm{Diff}(\overline{\mathbb{D}})$ with a single fiber.

It is natural to demand, that the shape of the hold-all domain should be left invariant. According directions for shape derivatives and gradient systems are therefore vanishing on $\partial\mathbb{D}$. Because diffeomorphisms map boundaries onto boundaries (cf. [111, Thm. 2.18]), the structure theorem 9 for pre-shape derivatives tells us that a pre-shape differentiable functional $\mathfrak{J}^{\mathbb{D}}\colon \operatorname{Diff}(\overline{\mathbb{D}}) \to \mathbb{R}$ always has trivial shape component $g^{\mathcal{N}} = 0$ of $\mathfrak{D}\mathfrak{J}^{\mathbb{D}}$ for such directions. In particular, this means ordinary shape calculus is not applicable for functionals of this type. Further, we mention that there is no need to use local orthonormal frames to represent the covariant derivative D^{τ}, which is the case for shapes that are embedded submanifolds.

We do not want the resulting hold-all pre-shape $\phi \in \operatorname{Diff}(\overline{\mathbb{D}})$ to interfere with the shape optimization or pre-shape parameterization tracking of the embedded shapes $\varphi(M) \subset \mathbb{D}$. This is not guaranteed for all $\phi \in \operatorname{Diff}(\overline{\mathbb{D}})$, since $\phi(\varphi(M)) \neq \varphi(M)$ in general. Hence, we have to restrict the space of possible pre-shapes for $\overline{\mathbb{D}}$. A suitable class of diffeomorphisms are those, which leave a given shape $\varphi(M) \subset \mathbb{D}$ and the hold-all boundary $\partial\mathbb{D}$ pointwise invariant, i.e.

$$\operatorname{Diff}_{\varphi(M)}\left(\overline{\mathbb{D}}\right) := \Big\{ \phi \in \operatorname{Diff}\left(\overline{\mathbb{D}}\right) : \ \phi(p) = p \quad \forall p \in \varphi(M) \cup \partial\mathbb{D} \Big\}. \tag{6.16}$$

If $\varphi(M)$ has empty boundary, then $\operatorname{Diff}_{\varphi(M)}(\overline{\mathbb{D}})$ is an ILH-Lie subgroup of $\operatorname{Diff}(\overline{\mathbb{D}})$, and the vector fields corresponding to its Lie-Algebra are vector fields vanishing on $\varphi(M) \cup \partial\mathbb{D}$ (cf. [166, Ch. 3.6]). Also notice, that $\operatorname{Diff}_{\varphi(M)}(\overline{\mathbb{D}})$ has volume invariant diffeomorphism as a subgroup, which leave a given shape $\varphi(M)$ fixed (cf. [166, Thm. 3.20, Thm. 3.21]). This means the decomposition in divergence and divergence-free components with regard to non-unique solutions to volume tracking problem (6.15) in analogy to equation (5.58) applies. Thus, results from section 5.2.2 carry over to the invariant submanifold case, under the modification that vector fields vanish on the invariant submanifold $\varphi(M) \subset \mathbb{D}$. The author is not aware of such a result for the case of $\varphi(M)$ with non-trivial boundary $\partial\varphi(M)$. Nevertheless, we can avoid reliance on the Lie group structure, and regard $\operatorname{Diff}_{\varphi(M)}(\overline{\mathbb{D}})$ simply as a feasible subset of $\operatorname{Diff}(\overline{\mathbb{D}})$. As the corresponding vector fields vanish on $\partial\mathbb{D}$ and $\varphi(M)$, we have an effect on the numerical techniques we develop in this section. More precisely, a projection of resulting vector fields using equation (6.15) becomes necessary to leave the boundary and shape invariant. The associated space of vector fields is given by

$$C^{\infty}_{0,\varphi(M)}\big(\mathbb{D}, \mathbb{R}^{n+1}\big) := \Big\{ V \in C^{\infty}_{0}\big(\mathbb{D}, \mathbb{R}^{n+1}\big) : \ \operatorname{Tr}_{|\varphi(M)}(V) = 0 \Big\}, \tag{6.17}$$

where $\operatorname{Tr}_{|\varphi(M)}(V)$ is the trace of V on $\varphi(M)$. We use an analogous definition for Sobolev functions $H^{1}_{0,\varphi(M)}\big(\mathbb{D}, \mathbb{R}^{n+1}\big)$, which is permissible via the Sobolev trace theorem (cf. [50, Ch. 5.5]).

Now we possess a pre-shape space suitable to model reparameterizations of the hold-all domain $\mathbb{D}$, which can leave a given shape $\varphi(M)$ invariant. Next, we formulate an analogue of parameterization tracking problem (6.3), which tracks for the volume parameterization of the hold-all domain. Let us fix a $\varphi \in \operatorname{Emb}(M, \mathbb{D})$ and the corresponding shape $\varphi(M) \subset \mathbb{D}$. In the following, we demand less restrictive regularity properties for volume parameterizations. Instead of smoothness on the entire domain $\overline{\mathbb{D}}$, we only demand smoothness on the interior $\mathbb{D} \setminus \varphi(M)$, excluding the invariant shape. Instead, only continuity and bijectivity are demanded on invariant shapes. In light of [39], we denote the associated space of pre-shapes by $\operatorname{Diff}(\mathbb{D} \setminus \varphi(M)) \cap \operatorname{Diff}_{\varphi(M)}(\overline{\mathbb{D}})$. In this case, the volume parameterization tracking problem takes the form

$$\min_{\phi \in \operatorname{Diff}(\mathbb{D}\setminus\varphi(M)) \cap \operatorname{Diff}_{\varphi(M)}(\overline{\mathbb{D}})} \frac{1}{2} \int_{\mathbb{D}} \Big(g^{\mathbb{D}} \circ \phi^{-1}(x) \cdot \det D\phi^{-1}(x) - f^{\mathbb{D}}_{\varphi(M)}(x) \Big)^2 \, \mathrm{d}x. \tag{6.18}$$

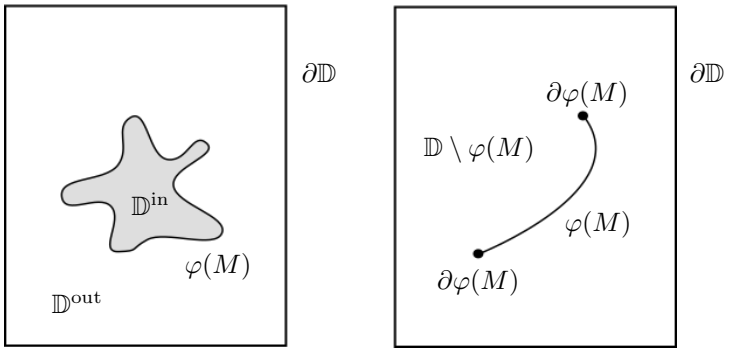

Figure 6.1: Example of a hold-all domain $\mathbb{D} \subset \mathbb{R}^2$. The left picture shows the case $\varphi \in \mathrm{Emb}(S^1, \mathbb{D})$, the right picture the case $\varphi \in \mathrm{Emb}([0,1], \mathbb{D})$. Notice that the set $\varphi(M)$ can be associated to a shape $\Gamma \in B_e^n$.

Notice that the objective functional is still well defined, since ϕ is bijective and differentiable up to a set of measure zero. There are several similarities and differences of volume parameterization tracking problem (6.18) and shape parameterization tracking problem (5.10). Both pre-shape functionals track for a parameterization dictated by a target f, and both feature a function g describing the initial parameterization. The volume tracking functional $\mathfrak{J}^{\mathbb{D}}$ differs from $\mathfrak{J}^M$ by featuring a volume integral, instead of a surface one. Also, the covariant derivative of the Jacobian determinant in $\mathfrak{J}^{\mathbb{D}}$ is just the Jacobian matrix of ϕ^{-1}.

The two most important differences concern their sets of feasible solutions and targets f. The volume target $f^{\mathbb{D}}_{\varphi(M)}$ does not depend on the pre-shape ϕ for the hold-all domain $\mathbb{D}$, but instead depends on the shape $\varphi(M)$, which is left to be invariant. Letting $f^{\mathbb{D}}$ depend on the shape of $\mathbb{D}$ does not make sense, since $\mathrm{Diff}(\mathbb{D} \setminus \varphi(M)) \cap \mathrm{Diff}_{\varphi(M)}(\overline{\mathbb{D}})$ consists only of one fiber, as the shape of $\overline{\mathbb{D}}$ remains invariant. Hence there is a dependence of both the feasible set of pre-shapes $\mathrm{Diff}(\mathbb{D} \setminus \varphi(M)) \cap \mathrm{Diff}_{\varphi(M)}(\overline{\mathbb{D}})$ and the target $f^{\mathbb{D}}_{\varphi(M)}$ on the shape $\varphi(M)$, because we desire $\varphi(M)$ to stay unaltered. For this reason, the shape invariant problem version (6.18) differs from volume parameterization tracking problem (6.15) to such an extent, that theorem 10 does not cover existence of solutions to problem (6.18), even under general conditions discussed in remark 13. This makes it necessary to formulate a result guaranteeing existence of solutions for volume parameterization tracking problem (6.18) with invariant shapes under appropriate conditions. In particular, we have to make distinctions depending on whether M has a nonempty boundary or not. The following theorem has two parts, where respective situations are illustrated in figure 6.1.

Theorem 16 (Existence of Solutions for the Volume Parameterization Tracking Problem with Invariant Shapes)**.** *Assume $\mathbb{D} \subset \mathbb{R}^{n+1}$ to a bounded, connected, open and oriented $n+1$-dimensional C^∞-manifold, such that $\overline{\mathbb{D}}$ has smooth boundary $\partial\mathbb{D}$. Let M be an n-dimensional, oriented, connected and compact C^∞-submanifold of $\mathbb{D}$. Fix a $\varphi \in \mathrm{Emb}(M, \mathbb{D})$ generating a shape $\varphi(M) \subset \mathbb{D}$. Let $g^{\mathbb{D}} \colon \overline{\mathbb{D}} \to (0, \infty)$ be a C^∞-function.*

(i) Let $M \subset \mathbb{D}$ be closed, i.e ∂M be empty. Denote by $\mathbb{D}^{in}_\varphi$ and $\mathbb{D}^{out}_\varphi$ the disjoint inner and outer components of $\mathbb{D}$ partitioned by $\varphi(M)$. Let $f^{\mathbb{D}}_{\varphi(M)} \colon \overline{\mathbb{D}} \to (0, \infty)$ be C^∞-regular on $\mathbb{D} \setminus \varphi(M)$. Further assume the normalization conditions

$$\int_{\mathbb{D}^{in}_\varphi} f^{\mathbb{D}}_{\varphi(M)} \, \mathrm{d}x = \int_{\mathbb{D}^{in}_\varphi} g^{\mathbb{D}} \, \mathrm{d}x \quad \text{and} \quad \int_{\mathbb{D}^{out}_\varphi} f^{\mathbb{D}}_{\varphi(M)} \, \mathrm{d}x = \int_{\mathbb{D}^{out}_\varphi} g^{\mathbb{D}} \, \mathrm{d}x. \tag{6.19}$$

Then there exists a C^∞-solution $\tilde{\phi} \in \mathrm{Diff}_{\varphi(M)}(\overline{\mathbb{D}})$ globally minimizing problem (6.18)*, with*

$$\left(g^{\mathbb{D}} \circ \tilde{\phi}^{-1}\right) \cdot \det D\tilde{\phi}^{-1} = f^{\mathbb{D}}_{\varphi(M)} \quad \text{on } \mathbb{D} \backslash \varphi(M) \qquad \text{and} \qquad \tilde{\phi}(p) = p \quad \forall p \in \partial\mathbb{D} \cup \varphi(M). \tag{6.20}$$

(ii) Let $M \subset \mathbb{D}$ have a non-trivial C^∞-boundary ∂M. Consider a target $f^{\mathbb{D}}_{\varphi(M)} \colon \overline{\mathbb{D}} \to (0, \infty)$, which is C^∞-regular on $\mathbb{D} \setminus \varphi(M)$ and continuous on $\overline{\mathbb{D}}$, such that

$$\mathrm{Tr}_{|\varphi(M)}\left(f^{\mathbb{D}}_{\varphi(M)}\right) = \mathrm{Tr}_{|\varphi(M)}\left(g^{\mathbb{D}}\right) \quad \text{and} \quad \mathrm{Tr}_{|\partial\mathbb{D}}\left(f^{\mathbb{D}}_{\varphi(M)}\right) = \mathrm{Tr}_{|\partial\mathbb{D}}\left(g^{\mathbb{D}}\right) \tag{6.21}$$

and the normalization condition

$$\int_{\mathbb{D}} f^{\mathbb{D}}_{\varphi(M)} \, \mathrm{d}x = \int_{\mathbb{D}} g^{\mathbb{D}} \, \mathrm{d}x \tag{6.22}$$

holds.

Then there exists a global minimizer $\tilde{\phi} \in \mathrm{Diff}(\mathbb{D} \setminus \varphi(M)) \cap \mathrm{Diff}_{\varphi(M)}(\overline{\mathbb{D}})$ for problem (6.18) *satisfying* (6.20)*, which in particular leaves $\varphi(M)$ invariant.*

Proof. Let the assumptions on $\mathbb{D} \subset \mathbb{R}^{n+1}$ and $M \subset \mathbb{D}$ be true. Let us start with the first scenario, and assume M to have empty boundary ∂M. The main idea for this case is to decompose $\mathbb{D}$ into interior and exterior, and to pose two uncoupled parameterization tracking problems, which can be tackled by the Dacorogna-Moser theorem separately.

We fix a $\varphi \in \mathrm{Emb}(M, \mathbb{D})$, and see that $\varphi(M) \subset \mathbb{D}$ is an n-dimensional, orientable, connected and compact C^∞-submanifold of $\mathbb{D}$ as well. With $\varphi(M)$ being a connected and compact submanifold of $\mathbb{D}$ with codimension 1, the celebrated Jordan-Brouwer theorem 6 guarantees existence of open and disjoint inner $\mathbb{D}^{\mathrm{in}}_\varphi$ and outer $\mathbb{D}^{\mathrm{out}}_\varphi$ of $\mathbb{D}$ separated by $\varphi(M)$. Next, let $g^{\mathbb{D}}$ and $f^{\mathbb{D}}_{\varphi(M)}$ be as described, in particular satisfying normalization conditions (6.19). With existence of a separated inner and outer, we can decouple volume tracking problem (6.18) into two independent subproblems

$$\min_{\phi_{\mathrm{in}} \in \mathrm{Diff}_{\partial\mathbb{D}^{\mathrm{in}}}(\overline{\mathbb{D}^{\mathrm{in}}})} \mathfrak{J}^{\mathbb{D}^{\mathrm{in}}}(\phi_{\mathrm{in}}) \quad \text{and} \quad \min_{\phi_{\mathrm{out}} \in \mathrm{Diff}_{\partial\mathbb{D}^{\mathrm{out}}}(\overline{\mathbb{D}^{\mathrm{out}}})} \mathfrak{J}^{\mathbb{D}^{\mathrm{out}}}(\phi_{\mathrm{out}}). \tag{6.23}$$

Both problems do not feature invariant submanifolds in the interior anymore, since $\partial\mathbb{D}^{\mathrm{in}}_\varphi = \varphi(M)$ and $\partial\mathbb{D}^{\mathrm{out}}_\varphi = \varphi(M) \cup \partial\mathbb{D}$. Thus interior and exterior are both C^∞-manifolds with C^∞-boundaries. With this, and the two required normalization conditions (6.19), we are in position to apply existence theorem 10 with regard to remark 13 for both independent subproblems (6.23). This gives us two C^∞-diffeomorphism $\tilde{\phi}_{\mathrm{in}} \in \mathrm{Diff}_{\partial\mathbb{D}^{\mathrm{in}}_\varphi}(\overline{\mathbb{D}^{\mathrm{in}}_\varphi})$ and $\tilde{\phi}_{\mathrm{out}} \in \mathrm{Diff}_{\partial\mathbb{D}^{\mathrm{out}}_\varphi}(\overline{\mathbb{D}^{\mathrm{out}}_\varphi})$, which globally solve the problems (6.23). In particular, they satisfy

$$\left(g^{\mathbb{D}} \circ \tilde{\phi}_{\mathrm{in}}^{-1}\right) \cdot \det D\tilde{\phi}_{\mathrm{in}}^{-1} = f^{\mathbb{D}}_{\varphi(M)} \ \text{ on } \mathbb{D}^{\mathrm{in}}_\varphi \quad \text{and} \quad \left(g^{\mathbb{D}} \circ \tilde{\phi}_{\mathrm{out}}^{-1}\right) \cdot \det D\tilde{\phi}_{\mathrm{out}}^{-1} = f^{\mathbb{D}}_{\varphi(M)} \ \text{ on } \mathbb{D}^{\mathrm{out}}_\varphi. \tag{6.24}$$

We define a global solution candidate for problem (6.18) by setting

$$\tilde{\phi} := \begin{cases} \tilde{\phi}_{\mathrm{out}}(x) & \text{for } x \in \overline{\mathbb{D}^{\mathrm{out}}} \\ \tilde{\phi}_{\mathrm{in}}(x) & \text{for } x \in \mathbb{D}^{\mathrm{in}}. \end{cases} \tag{6.25}$$

It is clear that $\tilde{\phi}$ is a bijection. Also, $\tilde{\phi}$ is the identity on $\partial\mathbb{D} \cup \varphi(M)$, which is the second property of (6.20). We know that $\tilde{\phi}_{\mathrm{in}}$ is C^∞-regular on $\overline{\mathbb{D}^{\mathrm{in}}_\varphi}$, and that $\tilde{\phi}_{\mathrm{out}}$ is C^∞-regular on $\overline{\mathbb{D}^{\mathrm{out}}_\varphi}$. With this, and $\tilde{\phi}_{\mathrm{in}} = \tilde{\phi}_{\mathrm{out}} = 0$ on $\varphi(M)$, we get that

$\tilde{\phi}$ has C^∞-regularity on the entire hold-all domain $\overline{\mathbb{D}}$. In combination, this means $\tilde{\phi} \in \mathrm{Diff}_{\varphi(M)}(\overline{\mathbb{D}})$. With equation (6.24), we also get the first assertion of (6.20). Finally, we can use equation (6.20) to see that $\mathfrak{J}^{\mathbb{D}}(\tilde{\phi}) = 0$, since $\varphi(M)$ is a set of measure zero. Due to quadratic nature of problem (6.18), we have $\mathfrak{J}^{\mathbb{D}} \geq 0$, which tells us that $\tilde{\phi}$ is a global solution. Since we did not use any special property of φ, the argumentation holds for all $\varphi \in \mathrm{Emb}(M, \mathbb{D})$ and gives part (i) of theorem 16.

Next, let us handle part (ii) of the theorem. For this, we assume a nonempty C^∞-boundary ∂M. Let an $f^{\mathbb{D}}_{\varphi(M)} \colon \overline{\mathbb{D}} \to (0, \infty)$ as describend in part (ii) of the theorem be given. Let us fix a $\varphi \in \mathrm{Emb}(M, \mathbb{D})$. The main idea is to apply the Dacorogna-Moser theorem 5 on general domains to the complement set $\mathbb{D} \setminus \varphi(M)$.

We see that $\varphi(M)$ inherits all properties demanded for M. In particular, it is an orientable, connected, compact and n-dimensional C^∞-submanifold of $\mathbb{D}$ with C^∞-boundary. Because $\mathbb{D}$ is an open manifold, and $\partial\varphi(M)$ is nonempty, and both $\mathbb{D}$ and $\varphi(M)$ are connected, we can use [86, p. 108] to see that $\mathbb{D} \setminus \varphi(M)$ is connected. Since $\varphi(M)$ is a closed set with respect to the Euclidean topology, we get that $\mathbb{D} \setminus \varphi(M)$ is connected and open. By assumption, we have continuity of $f^{\mathbb{D}}_{\varphi(M)}$ on $\overline{\mathbb{D}}$. Since $\overline{\mathbb{D}}$ is compact, the function $f^{\mathbb{D}}_{\varphi(M)}$ is bounded on $\overline{\mathbb{D}}$. In particular, it attains its minimum and maximum values in $(0, \infty)$. Therefore $f^{\mathbb{D}}_{\varphi(M)}$ and its reciprocal $1/f^{\mathbb{D}}_{\varphi(M)}$ are both bounded on $\mathbb{D} \setminus \varphi(M)$. The same argumentation holds for $g^{\mathbb{D}}$. Since we have C^∞-regularity of $\mathbb{D}$ and $\varphi(M)$ and their boundaries, and because we have assumed normalization condition (6.22), we can apply the Dacorogna-Moser theorem 5 for general domains to $\mathbb{D} \setminus \varphi(M)$. This guarantees existence of a $\phi \in \mathrm{Diff}(\mathbb{D} \setminus \varphi(M)) \cap \mathrm{Diff}_{\partial\mathbb{D}}(\overline{\mathbb{D}})$ solving the weak formulation (2.15). Further, because we have assumed consistency condition (6.21) of $f^{\mathbb{D}}_{\varphi(M)}$ and $g^{\mathbb{D}}$ on the shape and boundary, we have $\mathrm{supp}(f^{\mathbb{D}}_{\varphi(M)} - g^{\mathbb{D}}) \subset \mathbb{D} \setminus \varphi(M)$. In this case, theorem 5 gives $\mathrm{supp}(\phi - \mathrm{id}_{\overline{\mathbb{D}}}) \subset \mathbb{D} \setminus \varphi(M)$. This means ϕ is the identity on $\partial\mathbb{D} \cup \varphi(M)$, i.e. it leaves the hold-all boundary and the shape invariant. By setting $\tilde{\phi} := \phi^{-1}$, we verify that $\tilde{\phi} \in \mathrm{Diff}(\mathbb{D} \setminus \varphi(M)) \cap \mathrm{Diff}_{\varphi(M)}(\overline{\mathbb{D}})$. Also, the C^∞-regularity of $\tilde{\phi}$ on $\mathbb{D} \setminus \varphi(M)$, a transformation formula, and ϕ solving equation (2.15) give

$$\int_E \left(g^{\mathbb{D}} \circ \tilde{\phi}^{-1}\right) \cdot \det D\tilde{\phi}^{-1} \, \mathrm{d}x = \int_E f^{\mathbb{D}}_{\varphi(M)} \, \mathrm{d}x \tag{6.26}$$

for all open subsets $E \subset \mathbb{D} \setminus \varphi(M)$. Due to this, and because $\tilde{\phi}^{-1}$ is the identity on $\partial\mathbb{D}$ and $\varphi(M)$, the solution candidate $\tilde{\phi}$ achieves both relations in (6.20). Again, quadratic nature of $\mathfrak{J}^{\mathbb{D}}$ tells us that $\tilde{\phi}$ is a global solution to the volume parameterization tracking problem (6.18). Since we did not use any special property of φ, the argumentation holds for all $\varphi \in \mathrm{Emb}(M, \mathbb{D})$, and gives part (ii) of theorem 16. □

For guaranteed existence of optimal solutions $\phi \in \mathrm{Diff}(\mathbb{D} \setminus \varphi(M)) \cap \mathrm{Diff}_{\varphi(M)}(\overline{\mathbb{D}})$ to volume parameterization tracking with invariant shapes (6.18), it is necessary to assume normalization conditions (6.19) or (6.22), depending on the topological situation. To aid the reader, these are visualized in figure 6.1. A closed invariant shape $\varphi(M) \subset \mathbb{D}$ acts as a boundary, which partitions the hold-all domain into inner and outer. As we require solutions ϕ to leave $\varphi(M)$ pointwise invariant, the diffeomorphism ϕ is not allowed to transport volume from outside to inside and vice versa. Hence, in general, a single normalization condition on the entire hold-all domain $\mathbb{D}$ of type (5.9) is not sufficient for existence of solutions. A direct application of Dacorogna and Moser's theorem to (6.15) yields a $\phi \in \mathrm{Diff}(\overline{\mathbb{D}})$, which possibly transports volume across $\varphi(M)$, which we have to prohibit if $\varphi(M)$ is left to be invariant. As the total inner and outer volume change with varying $\varphi(M)$, we have to require normalization condition (6.19) for each $\varphi(M)$ separately.

If $\varphi(M)$ has a boundary, we have seen in the proof of theorem 16 (ii) that it does not separate $\mathbb{D}$. Hence volume can be transported in $\mathbb{D}$ without crossing $\varphi(M)$. This

is the reason that a single normalization condition (6.22) on $\mathbb{D}$ is necessary for the non-trivial boundary ∂M case. However, since the complement $\mathbb{D} \setminus \varphi(M)$ was left general, we need consistency assumption (6.21). Essentially, it lets the integrand of the parameterization tracking problem (6.18) vanish for the identity on $\varphi(M)$ and $\partial\mathbb{D}$, which guarantees the desired invariance of shapes and the outer boundary.

In both cases, the target $f^{\mathbb{D}}_{\varphi(M)}$ has to depend on $\varphi(M)$, even though the shape of $\mathbb{D}$ stays the same. This needs to be taken into account when designing targets $f^{\mathbb{D}}$ for numerical applications, which we discuss in section 7.1.2.

Remark 21 (Generality of Invariant Shapes)**.** *In existence theorem 16, we have required the invariant shape to have the formulation $\varphi(M)$ for some $\varphi \in \operatorname{Emb}(M, \mathbb{D})$. This is solely due to the context of optimization problem* (6.1) *posed for shape spaces B^n_e. It is absolutely possible to use any compact and connected submanifold $\Gamma \subset \mathbb{D}$ as an invariant shape for volume tracking problem* (6.18)*.*

In particular, we can also consider any shape in Euclidean space with codimension greater than one, as discussed at section 5.1. In this case, [90, Ch. IV, Thm. IV4 and Cor. 1] tells us that the complement of an embedded manifold $M \subset \mathbb{R}^{n+1}$ with $\dim(M) \leq n-1$ cannot separate $\mathbb{R}^{n+1}$ into an inside and outside. In fact, the complement $\mathbb{R}^{n+1} \setminus M$ has only a single connected component. Hence, for shapes with codimension greater equal two, either with or without boundaries, we are in the situation of theorem 16 (ii). In particular, no normalization on the inside and outside as in assumption (6.19) *is necessary. This means having two normalization conditions is special to the situation of codimension one shapes without boundaries.*

Even more general, any closed set $\Gamma \subset \mathbb{D}$ with respect to the Euclidean topology, such that its complement in $\mathbb{D}$ satisfies condition (H_k) from [39, p. 14, Appendix], can be left invariant during parameterization tracking for the volume mesh. This includes the case of non-connected sets without specific dimension, which can be locally described as the graph of a Lipschitz function, with isolated added or removed points. If they partition $\mathbb{D}$ into multiple connected components, necessary normalizations analogous to (6.19) *have to be taken into account. And if the invariant shape is irregular, consistency assumption* (6.21) *is needed. Then existence of $\phi \in \operatorname{Diff}(\mathbb{D} \setminus \Gamma) \cap \phi \in \operatorname{Diff}_\Gamma(\overline{\mathbb{D}})$ globally solving the volume parameterization tracking problem* (6.18)*, and leaving Γ invariant, is still guaranteed for such a general Γ.*

As we want to regularize shape optimization routines, we need to explicitly specify the pre-shape derivative to the volume parameterization tracking problem (6.18). This means that neither the formulation (6.18) in the context of classical shape optimization, nor the derivation of a derivative using classical shape calculus are possible. Since the form of $\mathfrak{J}^{\mathbb{D}}$ is similar to $\mathfrak{J}^M$, we can mimic the steps from theorem 12, which we do not restate to avoid redundancy. Then, the pre-shape derivative of $\mathfrak{DJ}^{\mathbb{D}}$ in decomposed form as in structure theorem 9 is given by

$$\mathfrak{DJ}^{\mathbb{D}}(\phi)[V] = \left\langle g^{\mathcal{N}}_\phi, V \right\rangle + \left\langle g^{\mathcal{T}}_\phi, V \right\rangle \qquad \forall V \in C^\infty_0\left(\mathbb{D}, \mathbb{R}^{n+1}\right), \tag{6.27}$$

with normal component

$$\left\langle g^{\mathcal{N}}_\phi, V \right\rangle = 0 \tag{6.28}$$

and tangential component

$$\begin{aligned}\left\langle g^{\mathcal{T}}_\phi, V \right\rangle = -\int_{\mathbb{D}} \frac{1}{2} \cdot \Big(\left(g^{\mathbb{D}} \circ \phi^{-1} \cdot \det D\phi^{-1}\right)^2 - {f^{\mathbb{D}}_{\varphi(M)}}^2 \Big) \cdot \operatorname{div}(V) \\ + \left(g^{\mathbb{D}} \circ \phi^{-1} \cdot \det D\phi^{-1} - f^{\mathbb{D}}_{\varphi(M)} \right) \cdot \mathfrak{D}_m\big(f^{\mathbb{D}}_{\varphi(M)}\big)[V] \, \mathrm{d}x.\end{aligned} \tag{6.29}$$

As previously mentioned, we signify a duality pairing by $\langle\cdot,\cdot\rangle$. It is also important to see that the restriction of $\mathrm{Diff}(\overline{\mathbb{D}})$ to $\mathrm{Diff}_{\varphi(M)}(\overline{\mathbb{D}})$ does not influence the form of pre-shape derivative $\mathfrak{D}\mathfrak{J}^{\mathbb{D}}$. Further restriction to $\mathrm{Diff}(\mathbb{D}\setminus\varphi(M))\cap\mathrm{Diff}_{\varphi(M)}(\overline{\mathbb{D}})$ leaves the integral still well defined, as non-defined areas are sets of measure zero. Instead, it influences the space of associated directions V by restricting $C^\infty(\mathbb{D},\mathbb{R}^{n+1})$ to $C^\infty_{0,\varphi(M)}(\mathbb{D},\mathbb{R}^{n+1})$. This stems from the relationship of tangential bundles of diffeomorphism groups with invariant submanifolds (cf. [166, Thm. 3.18]). There is also another subtle difference of $\mathfrak{D}\mathfrak{J}^{\mathbb{D}}$ and $\mathfrak{D}\mathfrak{J}^{M}$. Namely, the pre-shape material derivative $\mathfrak{D}_m\big(f^{\mathbb{D}}_{\varphi(M)}\big)$ featured in equation (6.29) depends on the invariant shape $\varphi(M)\subset\mathbb{D}$ instead of the volume pre-shape ϕ, which means equation (5.84) is not correct in this situation. We compute a correct material derivative for $f^{\mathbb{D}}_{\varphi(M)}$ in section 7.1.2. It is straightforward to formulate a pre-shape gradient system for $\mathfrak{D}\mathfrak{J}^{\mathbb{D}}$ from (6.18) in the style of section 6.1 using Sobolev functions. For a symmetric, positive-definite bilinear form $\mathfrak{a}(\cdot,\cdot)$, it takes the form

$$\mathfrak{a}\big(U^{\mathfrak{J}^{\mathbb{D}}},V\big)=\alpha^{\mathbb{D}}\cdot\mathfrak{D}\mathfrak{J}^{\mathbb{D}}(\phi)[V]\qquad\forall V\in H^1_{0,\varphi(M)}\big(\mathbb{D},\mathbb{R}^{n+1}\big). \tag{6.30}$$

6.2.2 Simultaneous Shape and Volume Mesh Regularization for Shape Optimization

At this point, we have a suitable pre-shape space to represent different parameterizations of hold-all domains $\mathbb{D}$, which leave a given shape $\varphi(M)\subset\mathbb{D}$ invariant. Also, we are able to guarantee existence for global minimizers to the volume version of parameterization tracking problem (6.18) for invariant shapes $\varphi(M)$. In this subsection, we incorporate the volume mesh quality regularization simultaneously with shape optimization and shape mesh quality regularization.

To formulate a regularized version of the original shape optimization problem (6.1), we have to keep the involvement of different types of pre-shapes in mind. We emphasize, that the pre-shapes $\varphi\in\mathrm{Emb}(M,\mathbb{D})$ and $\phi\in\mathrm{Diff}(\mathbb{D}\setminus\varphi(M))\cap\mathrm{Diff}_{\varphi(M)}(\overline{\mathbb{D}})$ correspond to the different shapes $\varphi(M)$ and $\mathbb{D}$. This is also illustrated by looking at the pre-shapes as maps

$$\varphi\colon M\to\mathbb{D}\quad\text{and}\quad\phi\colon\overline{\mathbb{D}}\to\overline{\mathbb{D}}. \tag{6.31}$$

For this reason, we cannot simply proceed by adding $\mathfrak{J}^{\mathbb{D}}$ in style of a regularizer to increase volume mesh quality. This signifies a main difference in application of shape mesh quality regularization via $\mathfrak{J}^{M}$ and volume mesh quality regularization via $\mathfrak{J}^{\mathbb{D}}$. To circumvent this issue, we formulate the shape and volume mesh regularized optimization problem with a bilevel approach. We have already seen in remark 20, that simultaneous shape parameterization tracking and shape optimization can be put into the bilevel framework. In fact, this turned out to be equivalent to the added regularizer approach from equation (6.3) with regard to resulting pre-shape gradient systems.

Let us consider weights $\alpha^{\mathbb{D}},\alpha^{\tau}>0$. We formulate the *simultaneous shape and volume mesh regularization of shape optimization problem* (6.1) as

$$\begin{aligned}\min_{\phi\in\mathrm{Diff}(\mathbb{D}\setminus\varphi(M))\cap\mathrm{Diff}_{\varphi(M)}(\overline{\mathbb{D}})}\ &\alpha^{\mathbb{D}}\cdot\mathfrak{J}^{\mathbb{D}}(\phi)\\ \text{s.t. }\varphi=\ &\operatorname*{arg\,min}_{\varphi\in\mathrm{Emb}(M,\mathbb{D})}\big(\mathcal{J}\circ\pi\big)(\varphi)+\alpha^{\tau}\cdot\mathfrak{J}^{M}(\varphi).\end{aligned} \tag{6.32}$$

Of course, the bilevel problem (6.32) can be formulated for $\alpha^{\mathbb{D}}=1$ without loss of generality. To stay coherent with section 6.1 in regard of pre-shape gradient systems, which feature weighted force terms, we prefer to formulate problem (6.32)

with a factor $\alpha^{\mathbb{D}} > 0$. In contrast to shape regularized problems (6.3) and (6.11), the simultaneous shape and volume mesh quality regularized problem (6.32) is not minimizing for one pre-shape, but for two different pre-shapes $\varphi \in \mathrm{Emb}(M, \mathbb{D})$ and $\phi \in \mathrm{Diff}(\mathbb{D} \setminus \varphi(M)) \cap \mathrm{Diff}_{\varphi(M)}(\overline{\mathbb{D}})$. The lower level problem is solved by a pre-shape φ, which corresponds to the actual parameterized shape solving the shape mesh regularized optimization problem (6.3). On the other hand, the upper level problem looks for a pre-shape ϕ, which corresponds to the parameterization of the hold-all domain $\overline{\mathbb{D}}$ with specified volume mesh quality. The set of feasible solutions $\mathrm{Diff}(\mathbb{D} \setminus \varphi(M)) \cap \mathrm{Diff}_{\varphi(M)}(\overline{\mathbb{D}})$ to the upper level problem depends on the lower level problem, because the optimal shape $\varphi(M)$ from the lower level problem is demanded to stay invariant.

In the remainder of this section, we propose a regularized pre-shape gradient system, which is suitable for simultaneous shape and volume mesh quality optimization during shape optimization. We prove a corresponding existence and consistency result for the fully regularized problem. As in section 6.1, we change the regularity of directions from C^∞ to H^1, as it is more suitable for numerical application. We remind the reader that the pre-shape derivative $\mathfrak{DJ}^{\mathbb{D}}(\phi)[V]$ is defined for directions $V \in H_0^1(\mathbb{D}, \mathbb{R}^{n+1})$ (cf. equation (6.27)). A criterion for successful application of volume mesh regularization for shape optimization routines has to leave optimal or intermediate shapes $\varphi(M)$ invariant. If $\mathfrak{DJ}^{\mathbb{D}}(\phi)[V]$ is used for regularizing the gradient in style of an added force term for general directions $V \in H_0^1(\mathbb{D}, \mathbb{R}^{n+1})$ as in equation (6.7), it could in general alter shapes and interfere with shape optimization. We display such unwanted effects in a numerical study in section 7.4, and compare them to the approach of this subsection. Also, it is not possible to put Dirichlet conditions on $\varphi(M)$, or to use a restricted space of test functions as in equation (6.30). Doing so would prohibit shape optimization itself, because the shape derivative $\mathcal{DJ}$ of the original problem has support exactly on the shapes $\varphi(M)$. Hence, we have to modify $\mathfrak{DJ}^{\mathbb{D}}$, such that general directions $V \in H_0^1(\mathbb{D}, \mathbb{R}^{n+1})$ are applicable as test functions, while the shape at hand is preserved. To resolve this problem, we introduce a projection

$$\mathrm{Pr}_{H^1_{0,\varphi(M)}} \colon H^1\big(\mathbb{D}, \mathbb{R}^{n+1}\big) \to H^1_{0,\varphi(M)}\big(\mathbb{D}, \mathbb{R}^{n+1}\big), \tag{6.33}$$

which is demanded to be the identity on $H^1_{0,\varphi(M)}(\mathbb{D}, \mathbb{R}^{n+1})$. We leave the operator projecting a given direction $V \in H^1(\mathbb{D}, \mathbb{R}^{n+1})$ onto $H^1_{0,\varphi(M)}(\mathbb{D}, \mathbb{R}^{n+1})$ general. Suitable options include the projection via solution of a least squares problem

$$\mathrm{Pr}_{H^1_{0,\varphi(M)}}(V) := \operatorname*{arg\,min}_{W \in H^1_{0,\varphi(M)}(\mathbb{D}, \mathbb{R}^{n+1})} \frac{1}{2} \|W - V\|^2_{H^1(\mathbb{D}, \mathbb{R}^{n+1})}. \tag{6.34}$$

In practice, it is feasible to construct a projection (6.33) by using a finite element representation of V, and setting degrees of freedom of basis functions on the discretization of $\varphi(M)$ to zero. With this projection operator, we can modify the pre-shape derivative $\mathfrak{DJ}^{\mathbb{D}}$ to suit directions $V \in H^1_{0,\varphi(M)}(\mathbb{D}, \mathbb{R}^{n+1})$ associated to the feasible hold-all pre-shape space $\mathrm{Diff}(\mathbb{D} \setminus \varphi(M)) \cap \mathrm{Diff}_{\varphi(M)}(\overline{\mathbb{D}})$.

Now we can formulate a fully regularized pre-shape gradient system suitable for simultaneous shape mesh quality, volume mesh quality, and shape optimization. We motivate the combined gradient system by the same formal calculations as in the bilevel formulation for shape quality regularization discussed in remark 20. Given a symmetric, positive-definite bilinear form $\mathfrak{a}(\cdot, \cdot)$, the pre-shape gradient system takes the form

$$\mathfrak{a}(U, V) = \mathcal{DJ}(\Gamma)[V] + \alpha^\tau \cdot \langle g_\varphi^{\mathcal{T}}, V \rangle + \alpha^{\mathbb{D}} \cdot \mathfrak{DJ}^{\mathbb{D}}(\phi)\big[\mathrm{Pr}_{H^1_{0,\varphi(M)}}(V)\big] \quad \forall V \in H_0^1\big(\mathbb{D}, \mathbb{R}^{n+1}\big), \tag{6.35}$$

where $g_\varphi^{\mathcal{T}}$ is the tangential pre-shape derivative component (5.72) for shape regularization, and $\mathcal{DJ}(\Gamma)$ is the shape derivative of the original shape objective with $\Gamma = \pi(\varphi)$. Notice that the fully regularized pre-shape gradient system (6.35) looks similar to the shape gradient system (6.5) of the original problem, differing only by two added force terms on the right-hand side. These forces can be thought of as regularizing terms to the original shape gradient. In practice, this means simultaneous shape and volume mesh quality improvement for shape optimization only needs adding of two terms on the right-hand side of the gradient system.

Theorem 17 (Shape and Volume Regularized Problems)**.** *Let shape optimization problem* (6.1) *be shape differentiable and have a minimizer* $\Gamma \in B_e^n$*. For shape and volume parameterization tracking, let the assumptions of both theorem 15 and theorem 16 be true.*

Then there exists a $\varphi \in \pi(\varphi) = \Gamma \subset \mathrm{Emb}(M, \mathbb{D})$*, and a* $\phi \in \mathrm{Diff}(\mathbb{D} \setminus \varphi(M)) \cap \mathrm{Diff}_{\varphi(M)}(\overline{\mathbb{D}})$*, minimizing the shape and volume regularized bilevel problem* (6.32)*.*

The fully regularized pre-shape gradient U *from system* (6.35) *is consistent with the modified shape regularized gradient* $\tilde{U}$ *from system* (6.7) *and volume tracking pre-shape gradient* $U^{\mathfrak{J}^{\mathbb{D}}}$ *from system* (6.30)*, in the sense that*

$$U = 0 \iff \tilde{U} = 0 \text{ and } U^{\mathfrak{J}^{\mathbb{D}}} = 0. \tag{6.36}$$

In particular, if $U = 0$ *is satisfied, the necessary first order conditions for the volume tracking problem* (6.18)*, the shape tracking regularized problem* (6.3)*, and the original problem* (6.1) *are all satisfied simultaneously.*

Proof. Let the assumptions of theorem 17 be given. This includes all assumptions made on M and $\mathbb{D}$, and functions $g^M, g^{\mathbb{D}}, f_\varphi, f^{\mathbb{D}}_{\varphi(M)}$ summarized in theorem 15 and theorem 16. Fix a solution $\Gamma \in B_e^n$ to the original problem (6.1). With theorem 15 for shape regularized problems, we have guaranteed existence of a solution $\varphi \in \pi(\varphi) = \Gamma \subset \mathrm{Emb}(M, \mathbb{D})$ to the lower level problem of (6.32), which coincides with the shape regularized problem (6.3). Let us select such a solution $\varphi \in \mathrm{Emb}(M, \mathbb{D})$. This fixes the set of solution candidates $\mathrm{Diff}(\mathbb{D} \setminus \varphi(M)) \cap \mathrm{Diff}_{\varphi(M)}(\overline{\mathbb{D}})$. Then, existence theorem 16 for volume tracking with invariant shapes provides a pre-shape $\phi \in \mathrm{Diff}(\mathbb{D} \setminus \varphi(M)) \cap \mathrm{Diff}_{\varphi(M)}(\overline{\mathbb{D}})$, which solves the upper level problem of (6.32) while leaving $\varphi(M)$ invariant. This proves existence of solutions to the shape and volume regularized bilevel problem (6.32).

For consistency relation (6.36) of pre-shape gradients, we first prove '$\Rightarrow$' by assuming $U = 0$. The right-hand side of the shape and volume regularized gradient system (6.35) consists of three added functionals $\mathcal{DJ}(\Gamma)$, $g_\varphi^{\mathcal{T}}$, and $\mathfrak{DJ}^{\mathbb{D}}(\phi)[\mathrm{Pr}_{H^1_{0,\varphi(M)}}(\cdot)]$. Since we have $U = 0$, the combined right-hand side of system (6.35) vanishes for all directions $V \in H^1_{0,\varphi(M)}(\mathbb{D}, \mathbb{R}^{n+1})$. By the structure theorem 9 for pre-shape derivatives, the functionals $\mathcal{DJ}(\Gamma)$ and $g_\varphi^{\mathcal{T}}$ are supported only on directions V not vanishing on $\varphi(M)$, because their underlying pre-shape space is $\mathrm{Emb}(M, \mathbb{D})$. This implies vanishing of $\mathfrak{DJ}^{\mathbb{D}}(\phi)[\mathrm{Pr}_{H^1_{0,\varphi(M)}}(\cdot)]$ for all $V \in H^1_0(\mathbb{D}, \mathbb{R}^{n+1})$. Therefore the right-hand side of the solo volume tracking system (6.30) vanishes as well, and thus we have $U^{\mathfrak{J}^{\mathbb{D}}} = 0$. Then, the remaining part $\mathcal{DJ}(\Gamma) + \alpha^\tau \cdot g_\varphi^{\mathcal{T}}$ vanishes for all $V \in H^1_0(\mathbb{D}, \mathbb{R}^{n+1})$ as well, which immediately yields $\tilde{U} = 0$ by the shape tracking regularized system (6.7).

For '$\Leftarrow$', let us assume $\tilde{U} = U^{\mathfrak{J}^{\mathbb{D}}} = 0$. Since $\tilde{U}$ vanishes, we see from shape tracking regularized system (6.7), that $\mathcal{DJ}(\Gamma) + \alpha^\tau \cdot g_\varphi^{\mathcal{T}}$ has to vanish for all $V \in H^1_0(\mathbb{D}, \mathbb{R}^{n+1})$. And because $U^{\mathfrak{J}^{\mathbb{D}}} = 0$, the volume tracking pre-shape derivative $\mathfrak{DJ}^{\mathbb{D}}$ vanishes for all $V \in H^1_{0,\varphi(M)}(\mathbb{D}, \mathbb{R}^{n+1})$. Considering the projection operator, this means $\mathfrak{DJ}^{\mathbb{D}}(\phi)[\mathrm{Pr}_{H^1_{0,\varphi(M)}}(\cdot)]$ vanishes for all $V \in H^1_0(\mathbb{D}, \mathbb{R}^{n+1})$. Together, the

complete right-hand side of the fully regularized system (6.35) vanishes, which gives $U = 0$, and establishes consistency relation (6.36).

The last assertion concerning necessary optimality conditions for volume tracking problem (6.18), shape tracking problem (6.3), and the original problem (6.1) is a consequence of consistency relation (6.36). If $U = 0$, we immediately get $U^{\mathfrak{J}^{\mathbb{D}}} = 0$, which implies the necessary first order condition for volume tracking via system (6.30). Consistency relation (6.36) and vanishing $U = 0$ also give $\tilde{U} = 0$. Therefore the last part of theorem 15 for shape regularized problems states that necessary first order conditions for shape tracking regularized problem (6.3) and the original problem (6.1) are satisfied as well. □

Theorem 17 for shape and volume regularized problems is of great importance for practical applications, since it guarantees the existence of solutions to the fully regularized problem (6.32) for a given shape optimization problem. It also tells us, that the shape Γ solving the original problem (6.1) remains unchanged by the shape and volume regularization. This is due to the two following properties. For one, it stems from guaranteed existence of a minimizing pre-shape φ in the fiber $\pi(\varphi)$ corresponding to the optimal shape Γ. And secondly, the optimal pre-shape ϕ representing the parameterization of the hold-all domain $\mathbb{D}$ comes from $\mathrm{Diff}(\mathbb{D}\setminus\varphi(M))\cap\mathrm{Diff}_{\varphi(M)}(\overline{\mathbb{D}})$, which means it leaves the optimal shape $\varphi(M)$ pointwise invariant. Furthermore, theorem 17 justifies the use of pre-shape gradient system (6.35) modified by force terms for shape and volume regularization. This gives a practical and straightforward applicability of shape and volume regularization strategies for shape optimization problems.

Remark 22 (Domains and Targets with Lower Regularity Assumptions)**.** *The setting of C^∞-smoothness is taken, because it is necessary to have a meaningful definition of a shape space B_e^n. However, results of theorem 15 and theorem 17 concerning existence of optimal parameterizations φ and ϕ for regularized problems* (6.3) *and* (6.32)*, their regularization strategies featuring the modified pre-shape gradient systems* (6.7) *and* (6.35)*, and consistency* (15) *remain valid for the case of open and bounded Lipschitz domains $\mathbb{D}$, and $f^{\mathbb{D}}$ and $g^{\mathbb{D}}$ with C^1-regularity in the interior $\mathbb{D}\setminus\varphi(M)$. Associated normalization and consistency conditions in respective existence theorems need to be verified nevertheless. In case $\mathbb{D}$ consists of multiple connected components, normalization conditions are necessary for each component. Of course, resulting optimal pre-shapes have lower regularity correspondingly (cf. theorem 5).*

Remark 23 (Numerical Feasibility)**.** *Our second criterion for a good regularization strategy, which demands low additional numerical cost for regularizations, is achieved. Calculation of a regularized gradient via* (6.35) *is numerically feasible, since it does not require additional solves of (non-)linear systems if compared to the standard shape gradient system* (6.5)*. In fact, the shape and volume regularized pre-shape gradient is a combination of three gradients*

$$U = U^{\mathcal{J}} + U^{\mathcal{T}} + U^{\mathfrak{J}^{\mathbb{D}}}, \tag{6.37}$$

coming from the original gradient system (6.5)*, modified solo shape tracking system* (6.14)*, and solo volume tracking system* (6.30)*. Instead of solving three systems separately, our approach permits a combined solution of only one system with the exact same size of the shape gradient system* (6.5) *to the original problem.*

Also, we see that our approach does not depend on the form $\mathfrak{a}(\cdot,\cdot)$ to represent gradients, because we solely modify the right-hand side of gradient system (6.35) *to achieve demanded mesh qualities. In particular, we numerically test our approach for different representations in chapter 7. To show the versatility of modified gradient systems, we use the weak formulation of linear elasticity motivated by [161],*

and a nonlinear p-Laplacian approach inspired by [135]. Together with invariance of the optimal and intermediary shapes, all three criteria for a satisfactory mesh regularization technique mentioned in the introduction of chapter 6 are achieved.

Remark 24 (Applicability of Shape and Volume Regularization for General Shape Optimization Problems)**.** *We emphasize, that we did not need any specific structure of the original shape optimization problem* (6.1) *to apply shape or volume mesh quality regularizations. The only assumptions are shape differentiability and existence of an optimal shape for $\mathcal{J}$. This means the shape and volume mesh regularization via parameterization tracking functionals $\mathfrak{J}^M$ and $\mathfrak{J}^{\mathbb{D}}$ are applicable for many meaningful shape optimization problems. In particular, PDE-constrained shape optimization problems can be regularized by this approach, which we discuss by an example in chapter 7. Even more, we apply extended volume regularization for shape optimization problems constrained by variational inequalities in chapter 9. The structure of modified gradient systems* (6.35) *stays the same for different shape optimization objectives $\mathcal{J}$ and their constraints. It is solely the shape derivative $\mathcal{D}\mathcal{J}$ on the right-hand side which changes depending on the shape problem objective. With regard to remark 23, this permits choice of various different left-hand sides to represent pre-shape gradients accustomed to the problem, in combination with regularization strategies presented in this chapter.*

Remark 25 (Volume Mesh Quality Regularization without Shape Regularization)**.** *It is of course possible to regularize a shape optimization problem* (6.1) *for volume mesh quality only, neglecting shape mesh parameterization tracking. In this scenario, the regularized problem takes the bilevel formulation*

$$\begin{aligned} \min_{\phi \in \mathrm{Diff}(\mathbb{D}\setminus\Gamma)\cap \mathrm{Diff}_\Gamma(\overline{\mathbb{D}})} \; & \alpha^{\mathbb{D}} \cdot \mathfrak{J}^{\mathbb{D}}(\phi) \\ s.t.\ \Gamma = \operatorname*{arg\,min}_{\Gamma \in B_e^n} & \mathcal{J}(\Gamma). \end{aligned} \tag{6.38}$$

In this case it is not necessary to use the pre-shape expansion (6.2) *of the original shape optimization problem. Instead, we associate $\Gamma \in B_e^n$ with its set interpretation via the nonlinear Grassmannian* (4.5)*.*

A result similar to theorem 17 can be formulated for the volume regularized problem (6.38) *by pursuing analogous arguments. In particular, the volume regularized pre-shape gradient system is of the form*

$$\mathfrak{a}\big(U^{\mathcal{J}+\mathfrak{J}^{\mathbb{D}}}, V\big) = \mathcal{D}\mathcal{J}(\Gamma)[V] \; + \; \alpha^{\mathbb{D}} \cdot \mathfrak{D}\mathfrak{J}^{\mathbb{D}}(\phi)\big[\mathrm{Pr}_{H^1_{0,\varphi(M)}}(V)\big] \qquad \forall V \in H_0^1\big(\mathbb{D}, \mathbb{R}^{n+1}\big). \tag{6.39}$$

Also, the according consistency of gradients is given by

$$U^{\mathcal{J}+\mathfrak{J}^{\mathbb{D}}} = 0 \iff U^{\mathcal{J}} = 0 \text{ and } U^{\mathfrak{J}^{\mathbb{D}}} = 0, \tag{6.40}$$

for shape gradient $U^{\mathcal{J}}$ of the original system (6.5) *and the pre-shape gradient $U^{\mathfrak{J}^{\mathbb{D}}}$ of solo volume tracking system* (6.30)*. If $U^{\mathcal{J}+\mathfrak{J}^{\mathbb{D}}} = 0$, the necessary first order conditions for the original problem* (6.1) *and volume regularized problem* (6.18) *are both satisfied.*

Chapter 7

Implementation of Shape and Volume Mesh Quality Regularizations

In this chapter, we put the different mesh quality regularization approaches to the test. For this, we conceive a shape optimization problem with an elliptic PDE-constraint, which is prone to mesh degeneration. The theoretical results of shape and volume regularization for shape optimization problems in chapter 6 are given in an abstract setting, where the involved objects remain general. In this chapter, systems and functionals are stated explicitly, so that the user can apply regularizations by referencing the exemplary problem as a guideline.

In section 7.1, we elaborate the process of regularizing a model problem. We also propose an additional modification for simultaneous shape and volume regularization, which allows for tangential movement of the boundary of the hold-all domain $\partial\mathbb{D}$ to increase mesh quality. Thereafter, we present numerical results in section 7.2, which compare several (un-)regularized optimization approaches. We test two different gradient representations and four regularizations of gradients by a standard gradient descent algorithm with a backtracking line search, totaling in 7 different approaches. The two gradient representations are given by the weak form of linear elasticity as found in [161], and a weak p-Laplacian representation inspired by [135] and studies found in [40]. The p-Laplacian approach discussed in [135] uses a strong formulation, which is solved using Picard iterations. We choose a different route, and employ a weak formulation with a regularization term, which is solved using Newton's method. The author of this work is not aware of such an approach in the current literature. Then, the different routines tested employ the unregularized, the shape regularized, the shape and volume regularized, and the shape and volume regularized gradient with varying outer boundary.

After this major study, we perform two minor studies to check for various possible mistakes a user can make while implementing pre-shape parameterization tracking as a regularizer. In section 7.3, we compare shape mesh regularizations near solutions of the shape optimization problem defined in section 7.1. The first method uses the full pre-shape gradient $\mathfrak{D}\mathfrak{J}^M$ found in equation (5.59). The second method uses our suggested approach, which only features its tangential component $g^{\mathcal{T}}$ found in equation (5.72). The second study in section 7.4 uses similar setup, but takes a focus on the volume mesh regularization. We examine the effect of a naive approach, which uses the direct volume reformulation of pre-shape parameterization tracking (6.15) over $\mathrm{Diff}(\overline{\mathbb{D}})$. This is compared to the approach, which uses the regularizing problem (6.18) stated over $\mathrm{Diff}(\mathbb{D} \setminus \varphi(M)) \cap \mathrm{Diff}_{\varphi(M)}(\overline{\mathbb{D}})$.

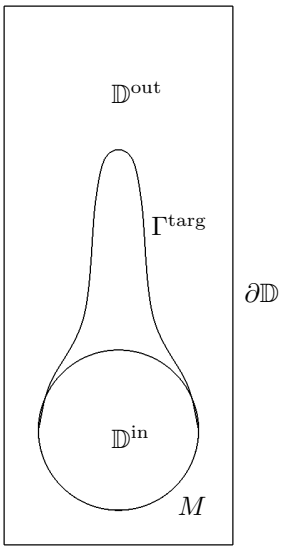

Figure 7.1: Hold-all domain $\mathbb{D} = \mathbb{D}^{\text{in}} \cup M \cup \mathbb{D}^{\text{out}}$ with initial circular shape M and target shape Γ^{targ}.

7.1 Model Problem and Application of Pre-Shape Mesh Quality Regularization

7.1.1 Model Problem Formulation and Regularization

In this subsection, we formulate a model problem to test our pre-shape regularization strategies. For this, we choose a tracking type shape optimization problem in two dimensions, constrained by a Poisson equation with varying source term. To highlight the difference of shape and pre-shape calculus techniques, we formulate the model problem in two ways. First, we use the classical shape space framework. The second reformulation uses the pre-shape setting, where pre-shape parameterization tracking regularizers can be added.

To start, we set the model manifold for shapes and the hold-all domain to

$$M = S^{0.35}_{(0.5,0.5)} \text{ and } \overline{\mathbb{D}} = [0,1] \times [0,2.35]. \tag{7.1}$$

The model manifold $M \subset \mathbb{D}$ is a sphere with radius 0.35 centered in $(0.5, 0.5)$, consisting of 63 surface nodes and 63 edges. It is embedded in the interior of the hold-all domain $\overline{\mathbb{D}}$, which is given by a rectangle $[0,1] \times [0,2.35]$ with non-trivial boundary $\partial\mathbb{D}$. The hold-all domain $\overline{\mathbb{D}}$ consists of 1402 nodes and has 741 volume cells. The situation is illustrated in figure 7.1. This problem is not easy for standard shape gradient descents, because solution requires a large deformation at a single local region of the initial shape. To make it even harder, the mesh is locally refined near the shape. Thus nearby cells are especially prone to degeneration by large deformations.

Notice that the manifold M acts as an initial shape for the optimization routines. This approach is always applicable, i.e. the manifold M for the pre-shape space $\text{Emb}(M, \mathbb{D})$ can always be picked as the initial shape (cf. remark 2). With this, the corresponding starting pre-shape is the identity $\text{id}_M \colon M \to \mathbb{D}$.

For the elliptic constraint of the shape optimization problem, we employ a piece-

wise constant source term varying dependent on the shape

$$r_{\varphi(M)}(x) = \begin{cases} r_1 \in \mathbb{R} & \text{for } x \in \overline{\mathbb{D}^{\text{out}}} \\ r_2 \in \mathbb{R} & \text{for } x \in \mathbb{D}^{\text{in}}. \end{cases} \tag{7.2}$$

A perimeter regularization with parameter $\nu > 0$ is added as well. Perimeter regularizations are frequently used to overcome ill-posedness of inverse problems. For example, [5] investigates the regularization and numerical solution of geometric inverse problems related to linear elasticity. Combining this, the model shape optimization problem takes the form

$$\begin{aligned} \min_{\Gamma \in B_e^n} \ & \frac{1}{2} \int_{\mathbb{D}} |y - \bar{y}|^2 \, \mathrm{d}x + \nu \int_{\Gamma} 1 \, \mathrm{d}s \\ \text{s.t.} \ & -\Delta y = r_\Gamma \quad \text{in } \mathbb{D} \\ & y = 0 \quad \text{on } \partial\mathbb{D}. \end{aligned} \tag{7.3}$$

Notice that we abuse notation, and associate $\Gamma \in B_e^n$ with its set valued interpretation via $\varphi(M)$ for $\Gamma \in \pi(\varphi) = \Gamma$. To calculate the target $\bar{y} \in H^1(\mathbb{D})$ of this problem, we use the source term (7.2) and solve the Poisson problem for the target shape pictured in figure 7.1. Problem (7.3) is formulated with the classical shape space approach, since the control variable Γ stems from the shape space B_e^n. It represents the abstract shape optimization problem (6.1) from the theoretical chapter 6.

Next, we reformulate problem (7.3) using pre-shapes, which permits addition of the regularizing term $\mathfrak{J}^M$ for shape mesh quality with parameter $\alpha^\tau > 0$, i.e.

$$\begin{aligned} \min_{\varphi \in \mathrm{Emb}(M,\mathbb{D})} \ & \frac{1}{2} \int_{\mathbb{D}} |y - \bar{y}|^2 \, \mathrm{d}x + \nu \int_{\varphi(M)} 1 \, \mathrm{d}s \\ & + \frac{\alpha^\tau}{2} \int_{\varphi(M)} \left(g^M \circ \varphi^{-1} \cdot \det D^\tau \varphi^{-1} - f_\varphi \right)^2 \mathrm{d}s \\ \text{s.t.} \ & -\Delta y = r_{\varphi(M)} \quad \text{in } \mathbb{D} \\ & y = 0 \quad \text{on } \partial\mathbb{D}. \end{aligned} \tag{7.4}$$

The combined shape and volume mesh quality regularized problem is given by formulating a bilevel problem with volume regularizing objective $\mathfrak{J}^{\mathbb{D}}$ as the upper level problem, and lower level problem (7.4), i.e.

$$\begin{aligned} \min_{\phi \in \mathrm{Diff}(\mathbb{D} \setminus \varphi(M)) \cap \mathrm{Diff}_{\varphi(M)}(\overline{\mathbb{D}})} \ & \frac{\alpha^{\mathbb{D}}}{2} \int_{\mathbb{D}} \left(g^{\mathbb{D}} \circ \phi^{-1} \cdot \det D\phi^{-1} - f^{\mathbb{D}}_{\varphi(M)} \right)^2 \mathrm{d}x \\ \text{s.t.} \ \varphi = \ & \operatorname*{arg\,min}_{\varphi \in \mathrm{Emb}(M,\mathbb{D})} \frac{1}{2} \int_{\mathbb{D}} |y - \bar{y}|^2 \, \mathrm{d}x + \nu \int_{\varphi(M)} 1 \, \mathrm{d}s \\ & + \frac{\alpha^\tau}{2} \int_{\varphi(M)} \left(g^M \circ \varphi^{-1} \cdot \det D^\tau \varphi^{-1} - f_\varphi \right)^2 \mathrm{d}s \\ & \text{s.t.} \ -\Delta y = r_{\varphi(M)} \quad \text{in } \mathbb{D} \\ & \quad y = 0 \quad \text{on } \partial\mathbb{D}. \end{aligned} \tag{7.5}$$

We remind the reader that, despite its intimidating form, bilevel problem (7.5) has guaranteed existence of solutions and simplified pre-shape gradient systems by theorem 17. The same is true for the shape regularized problem (7.4) by theorem 15.

7.1.2 Construction of Initial and Target Node Densities

To explicitly construct the regularizing terms, we need initial node densities $g^M \colon M \to (0, \infty)$ of the starting shape and $g^{\mathbb{D}} \colon \overline{\mathbb{D}} \to (0, \infty)$ of the initial hold-all

domain configuration. Also, we need to specify target node densities f_φ and $f^{\mathbb{D}}_{\varphi(M)}$, which describe the cell volume structure of optimal meshes representing $\varphi(M)$ and $\mathbb{D}$.

Our approach is to represent the initial point distributions g^M and $g^{\mathbb{D}}$ with a continuous Galerkin Ansatz featuring linear elements similar to the numerical study in section 5.4. Degrees of freedom are situated at the mesh vertices, and set to the average of inverses of surrounding cell volumes, i.e.

$$g(p) = \frac{1}{|\mathcal{C}|} \cdot \sum_{C \in \mathcal{C}} \frac{1}{\mathrm{vol}(C)}. \tag{7.6}$$

In the shape case $g = g^M$, a vertex p is part of the initial discretized shape M, and $\mathcal{C}$ is the set of its neighboring cells C in M. For 1-dimensional M, cells C correspond to edges, whereas for 2-dimensional M to faces. In the volume mesh case $g = g^{\mathbb{D}}$, p is a vertex of the initial discretized hold-all domain $\overline{\mathbb{D}}$, and $\mathcal{C}$ is the set of its neighboring volume cells C in $\overline{\mathbb{D}}$.

Next, we specify a way to construct target parameterizations f_φ and $f^{\mathbb{D}}_{\varphi(M)}$, together with their pre-shape material derivatives. We use our results from section 5.3, and define a target for shape parameterization tracking f_φ by a global target field $q \in H^2(\overline{\mathbb{D}}, (0,\infty))$. As argued in the last part of section 5.3, we can define

$$f_\varphi = \frac{\int_M g^M \,\mathrm{d}s}{\int_{\varphi(M)} q_{|\varphi(M)} \,\mathrm{d}s} \cdot q_{|\varphi(M)}. \tag{7.7}$$

With this construction, the target parameterization of $\varphi(M)$ depends on its location and shape in $\mathbb{D}$, as $q\colon \overline{\mathbb{D}} \to (0,\infty)$ is allowed to vary on the entire domain. Also, it satisfies the necessary normalization condition (5.9) for existence theorem 10.

The according material derivative is derived in equation (5.83). Because $\varphi(M)$ has empty boundary in our example, it has closed form

$$\begin{aligned}&\mathfrak{D}_m\big(f_\varphi\big)[V]\\ &= -\frac{\int_M g^M \,\mathrm{d}s}{\big(\int_{\varphi(M)} q \,\mathrm{d}s\big)^2} \cdot \int_{\varphi(M)} \Big(\frac{\partial q}{\partial n} + \dim(M)\cdot\kappa\cdot q\Big) \cdot \langle n, V\rangle_2 \,\mathrm{d}s \cdot q \;+\; \frac{\int_M g^M \,\mathrm{d}s}{\int_{\varphi(M)} q \,\mathrm{d}s} \cdot \nabla q^T V.\end{aligned} \tag{7.8}$$

Here, n is the outer unit normal vector field on $\varphi(M)$, and κ is the mean curvature as in equation (5.69). Notice that equation (7.8) includes both normal and tangential components. However, only its tangential component is needed if regularized gradient systems (6.7) and (6.35) are used. We explicitly state right-hand sides to gradient systems for our exemplary problem in section 7.1.3.

As we are dealing with closed shapes $\varphi(M)$ modeled by $M = S^{0.35}_{(0.5,0.5)}$, we are in the situation (i) of existence theorem 16 for volume regularization with invariant shapes. For a volume target $f^{\mathbb{D}}_{\varphi(M)}$, we therefore have to satisfy the separate normalization conditions (6.19) to guarantee existence of solutions.

We propose to use a field $q^{\mathbb{D}}\colon \overline{\mathbb{D}} \to (0,\infty)$ defined on the hold-all domain. Then an according target can be defined as

$$f^{\mathbb{D}}_{\varphi(M)} = \begin{cases} \frac{\int_{\mathbb{D}^{\mathrm{in}}_\varphi} g^{\mathbb{D}} \,\mathrm{d}x}{\int_{\mathbb{D}^{\mathrm{in}}_\varphi} q^{\mathbb{D}} \,\mathrm{d}x} \cdot q^{\mathbb{D}} & \text{for } x \in \mathbb{D}^{\mathrm{in}}_\varphi \\ \frac{\int_{\mathbb{D}^{\mathrm{out}}_\varphi} g^{\mathbb{D}} \,\mathrm{d}x}{\int_{\mathbb{D}^{\mathrm{out}}_\varphi} q^{\mathbb{D}} \,\mathrm{d}x} \cdot q^{\mathbb{D}} & \text{for } x \in \overline{\mathbb{D}^{\mathrm{out}}_\varphi}. \end{cases} \tag{7.9}$$

This is different to the construction of targets f_φ for embedded shapes, since the function $f^{\mathbb{D}}_{\varphi(M)}$ changes dependent on $\varphi(M)$, in order to guarantee normalization

condition (6.19) on the two disconnected components of the hold-all domain. It cannot vary due to change of the shape of $\mathbb{D}$, which remains fixed. This stays in contrast to the situation for $\varphi(M) \subset \mathbb{D}$, which can change its position in $\mathbb{D}$. Also notice that $f^{\mathbb{D}}_{\varphi(M)}$ as defined in equation (7.9) can be non-continuous on the shape $\varphi(M)$. However, in existence and consistency results theorem 16 (i) and theorem 17 for closed shapes, we have not demanded continuity or smoothness of $f^{\mathbb{D}}_{\varphi(M)}$ on the complete domain $\overline{\mathbb{D}}$. Smoothness of $f^{\mathbb{D}}_{\varphi(M)}$ is only demanded on the disconnected components of the complement $\mathbb{D} \setminus \varphi(M)$.

Now we derive the pre-shape material derivative $\mathfrak{D}_m(f^{\mathbb{D}}_{\varphi(M)})[V]$ for H^1_0-directions. These directions are not forced to vanish on the shape $\varphi(M)$, which is later needed to assemble combined gradients systems with V acting as test functions. This poses a difficulty for its derivation, because the partitioning depends on the pre-shape $\varphi \in \mathrm{Emb}(M, \mathbb{D})$, but not on $\phi \in \mathrm{Diff}_{\varphi(M)}(\overline{\mathbb{D}})$. The situation is depicted in figure 6.1. Let us fix a $\varphi \in \mathrm{Emb}(M, \mathbb{D})$ and compute on the outer domain $\mathbb{D}^{\mathrm{out}}_{\varphi}$ with pre-shape calculus rules from corollary 2. We write $\mathbb{D}^{\mathrm{out}}$ instead of $\mathbb{D}^{\mathrm{out}}_{\varphi}$ for slightly improved readability, having its pre-shape dependence in mind. Then

$$
\begin{aligned}
&\mathfrak{D}_m\big(f^{\mathbb{D}}_{\varphi(M)}\big)[V]_{|\mathbb{D}^{\mathrm{out}}} \\
&= \mathfrak{D}_m\left(\frac{\int_{\mathbb{D}^{\mathrm{out}}} g^{\mathbb{D}}\,\mathrm{d}x}{\int_{\mathbb{D}^{\mathrm{out}}} q^{\mathbb{D}}\,\mathrm{d}x} \cdot q^{\mathbb{D}}\right)[V] \\
&= \frac{1}{\int_{\mathbb{D}^{\mathrm{out}}} q^{\mathbb{D}}\,\mathrm{d}x} \cdot \int_{\mathbb{D}^{\mathrm{out}}} \Big(\mathfrak{D}\big(g^{\mathbb{D}}\big)[V] + \nabla\big(g^{\mathbb{D}}\big)^T V + \mathrm{div}(V) \cdot g^{\mathbb{D}}\Big)\,\mathrm{d}x \cdot q^{\mathbb{D}} \\
&\quad - \frac{\int_{\mathbb{D}^{\mathrm{out}}} g^{\mathbb{D}}\,\mathrm{d}x}{\big(\int_{\mathbb{D}^{\mathrm{out}}} q^{\mathbb{D}}\,\mathrm{d}x\big)^2} \cdot \int_{\mathbb{D}^{\mathrm{out}}} \Big(\mathfrak{D}\big(q^{\mathbb{D}}\big)[V] + \nabla\big(q^{\mathbb{D}}\big)^T V + \mathrm{div}(V) \cdot q^{\mathbb{D}}\Big)\,\mathrm{d}x \cdot q^{\mathbb{D}} \\
&\quad + \frac{\int_{\mathbb{D}^{\mathrm{out}}} g^{\mathbb{D}}\,\mathrm{d}x}{\int_{\mathbb{D}^{\mathrm{out}}} q^{\mathbb{D}}\,\mathrm{d}x} \cdot \Big(\mathfrak{D}\big(q^{\mathbb{D}}\big)[V] + \nabla\big(q^{\mathbb{D}}\big)^T V\Big) \\
&= \frac{1}{\int_{\mathbb{D}^{\mathrm{out}}} q^{\mathbb{D}}\,\mathrm{d}x} \cdot \int_{\mathbb{D}^{\mathrm{out}}} \mathrm{div}\left(g^{\mathbb{D}} \cdot V\right)\mathrm{d}x \cdot q^{\mathbb{D}} - \frac{\int_{\mathbb{D}^{\mathrm{out}}} g^{\mathbb{D}}\,\mathrm{d}x}{\big(\int_{\mathbb{D}^{\mathrm{out}}} q^{\mathbb{D}}\,\mathrm{d}x\big)^2} \cdot \int_{\mathbb{D}^{\mathrm{out}}} \mathrm{div}\left(q^{\mathbb{D}} \cdot V\right)\mathrm{d}x \cdot q^{\mathbb{D}} \\
&\quad + \frac{\int_{\mathbb{D}^{\mathrm{out}}} g^{\mathbb{D}}\,\mathrm{d}x}{\int_{\mathbb{D}^{\mathrm{out}}} q^{\mathbb{D}}\,\mathrm{d}x} \cdot \nabla\big(q^{\mathbb{D}}\big)^T V \\
&= \frac{1}{\int_{\mathbb{D}^{\mathrm{out}}} q^{\mathbb{D}}\,\mathrm{d}x} \cdot \int_{\partial\mathbb{D}\cup\varphi(M)} \Big(g^{\mathbb{D}} - \frac{\int_{\mathbb{D}^{\mathrm{out}}} g^{\mathbb{D}}\,\mathrm{d}x}{\int_{\mathbb{D}^{\mathrm{out}}} q^{\mathbb{D}}\,\mathrm{d}x} \cdot q^{\mathbb{D}}\Big) \cdot \big\langle n_{\mathbb{D}^{\mathrm{out}}}, V\big\rangle_2\,\mathrm{d}s \cdot q^{\mathbb{D}} \\
&\quad + \frac{\int_{\mathbb{D}^{\mathrm{out}}} g^{\mathbb{D}}\,\mathrm{d}x}{\int_{\mathbb{D}^{\mathrm{out}}} q^{\mathbb{D}}\,\mathrm{d}x} \cdot \nabla\big(q^{\mathbb{D}}\big)^T V \\
&= -\frac{1}{\int_{\mathbb{D}^{\mathrm{out}}} q^{\mathbb{D}}\,\mathrm{d}x} \cdot \int_{\varphi(M)} \Big(g^{\mathbb{D}} - \frac{\int_{\mathbb{D}^{\mathrm{out}}} g^{\mathbb{D}}\,\mathrm{d}x}{\int_{\mathbb{D}^{\mathrm{out}}} q^{\mathbb{D}}\,\mathrm{d}x} \cdot q^{\mathbb{D}}\Big) \cdot \big\langle n_{\varphi(M)}, V\big\rangle_2\,\mathrm{d}s \cdot q^{\mathbb{D}} \\
&\quad + \frac{\int_{\mathbb{D}^{\mathrm{out}}} g^{\mathbb{D}}\,\mathrm{d}x}{\int_{\mathbb{D}^{\mathrm{out}}} q^{\mathbb{D}}\,\mathrm{d}x} \cdot \nabla\big(q^{\mathbb{D}}\big)^T V.
\end{aligned}
\tag{7.10}
$$

Here, $n_{\mathbb{D}^{\mathrm{out}}}$ is the outer unit normal vector field on $\partial\mathbb{D}^{\mathrm{out}} = \partial\mathbb{D} \cup \varphi(M)$, and $n_{\varphi(M)}$ is the outer unit normal vector field on $\varphi(M)$. In particular, we used that $g^{\mathbb{D}}$ and $q^{\mathbb{D}}$ do neither explicitly depend on ϕ nor on φ, which lets their pre-shape derivatives vanish. Also, we applied the divergence theorem and used $V_{|\partial\mathbb{D}} = 0$. Notice the change of sign for the first summand of the last equality, due to $n_{\mathbb{D}^{\mathrm{out}}} = -n_{\varphi(M)}$ on $\varphi(M)$. Combined with an analogous computation on the interior $\mathbb{D}^{\mathrm{in}}$ with boundary

$\partial\mathbb{D}^{\text{in}} = \varphi(M)$, we get the pre-shape material derivative

$$\mathfrak{D}_m(f^{\mathbb{D}}_{\varphi(M)})[V] = \begin{cases} \frac{1}{\int_{\mathbb{D}^{\text{in}}} q^{\mathbb{D}}\,\mathrm{d}x} \cdot \int_{\varphi(M)} \left(g^{\mathbb{D}} - \frac{\int_{\mathbb{D}^{\text{in}}} g^{\mathbb{D}}\,\mathrm{d}x}{\int_{\mathbb{D}^{\text{in}}} q^{\mathbb{D}}\,\mathrm{d}x} \cdot q^{\mathbb{D}}\right) \cdot \left\langle n_{\varphi(M)}, V\right\rangle_2 \mathrm{d}s \cdot q^{\mathbb{D}} \\ \qquad\qquad + \frac{\int_{\mathbb{D}^{\text{in}}} g^{\mathbb{D}}\,\mathrm{d}x}{\int_{\mathbb{D}^{\text{in}}} q^{\mathbb{D}}\,\mathrm{d}x} \cdot \nabla(q^{\mathbb{D}})^T V \qquad \text{for } x \in \mathbb{D}^{\text{in}} \\ -\frac{1}{\int_{\mathbb{D}^{\text{out}}} q^{\mathbb{D}}\,\mathrm{d}x} \cdot \int_{\varphi(M)} \left(g^{\mathbb{D}} - \frac{\int_{\mathbb{D}^{\text{out}}} g^{\mathbb{D}}\,\mathrm{d}x}{\int_{\mathbb{D}^{\text{out}}} q^{\mathbb{D}}\,\mathrm{d}x} \cdot q^{\mathbb{D}}\right) \cdot \left\langle n_{\varphi(M)}, V\right\rangle_2 \mathrm{d}s \cdot q^{\mathbb{D}} \\ \qquad\qquad + \frac{\int_{\mathbb{D}^{\text{out}}} g^{\mathbb{D}}\,\mathrm{d}x}{\int_{\mathbb{D}^{\text{out}}} q^{\mathbb{D}}\,\mathrm{d}x} \cdot \nabla(q^{\mathbb{D}})^T V \qquad \text{for } x \in \overline{\mathbb{D}^{\text{out}}}. \end{cases} \tag{7.11}$$

This pre-shape material derivative is interesting from a theoretical perspective, since it is an example of a derivative depending on the shape of a submanifold $\varphi(M) \subset \mathbb{D}$, and not on the pre-shapes of the higher dimensional $\mathbb{D}$ on which $f^{\mathbb{D}}_{\varphi(M)}$ is defined. Also, we see that the sign of boundary integral on $\varphi(M)$ depends on whether the inside or outside of $\mathbb{D}$ is regarded. This nicely reflects that moving $\varphi(M)$ adds volume on one side, and takes it away from the other. We remind the reader, that normal directions $n_{\varphi(M)}$ are not normal directions associated to the shape of $\mathbb{D}$. They are supported on the interior of $\mathbb{D}$, and hence correspond to the vertical component of $\mathrm{Diff}(\overline{\mathbb{D}})$.

7.1.3 Pre-Shape Gradient Systems

In numerical shape optimization, raw shape derivatives are not ideally suited for performance of optimization steps, be it gradient or quasi-Newton or other types of routines. This owes to the distributional character of shape derivatives, which are linear, bounded functionals on the space of vector functions with certain regularity on the hold-all domain, or the shape itself, respectively. The same applies to pre-shape derivatives, including the ones for parameterization tracking functionals, as they are distributions as well. Hence, it is beneficial to transport these functionals into the primal space, which is the vector function space on which they operate. For shape derivatives, this type of gradient representation can for example be achieved by using Steklov-Poincraé metrics as discussed in chapter 3. Since the authors of [161] use them in the context of classical shape optimization, which exploits the representation of shape derivatives via use of outer normal vector fields on hypersurfaces of $\mathbb{R}^{n+1}$, we need to restate them to fit our use of normal, tangential and volume vector fields at the same time.

To compute pre-shape gradients U, we need suitable forms $\mathfrak{a}(\cdot,\cdot)$. The systems for our gradients are of prototypical formulation

$$\begin{aligned} \mathfrak{a}(U,V) &= \mathrm{RHS}(\varphi,\phi)[V] && \forall H^1_0(\mathbb{D},\mathbb{R}^{n+1}) \\ U &= \mathrm{BC} && \text{on } \partial\mathbb{D}. \end{aligned} \tag{7.12}$$

In our numerical implementations, we test two different forms $\mathfrak{a}(\cdot,\cdot)$ and four different right-hand sides. We abbreviate the right-hand sides by $\mathrm{RHS}(\varphi,\phi)[V]$ depending on pre-shapes $\varphi \in \mathrm{Emb}(M,\mathbb{D}), \phi \in \mathrm{Diff}(\mathbb{D}\setminus\varphi(M)) \cap \mathrm{Diff}_{\varphi(M)}(\overline{\mathbb{D}})$ and test functions V, and boundary conditions by BC. First, we consider the weak formulation of the linear elasticity equation with zero first Lamé parameter inspired by [159]

$$\begin{aligned} \int_{\mathbb{D}} \mu \cdot \epsilon(U) : \epsilon(V)\,\mathrm{d}x &= \mathrm{RHS}(\varphi,\phi)[V] && \forall V \in H^1_0(\mathbb{D},\mathbb{R}^{n+1}) \\ \epsilon(U) &= \frac{1}{2}\left(\nabla U + \nabla U^T\right) \\ \epsilon(V) &= \frac{1}{2}\left(\nabla V + \nabla V^T\right) \\ U &= 0 && \text{on } \partial\mathbb{D}. \end{aligned} \tag{7.13}$$

To give a physical interpretation, the choice of Lamé parameter μ enables control of the stiffness of the grid. Larger local values of μ lead to more stiffness of the mesh by locally decreasing the size of the gradient U, whereas lower local μ does the opposite.

As the second form for gradient representations, we consider the weak formulation of the vector valued p-Laplacian equation. In particular, the representation of the weak p-Laplacian is neither symmetric nor bilinear, but is rather of unsymmetric and quasilinear nature. Since systems stemming from the p-Laplacian have the issue to be indefinite, we employ a standard regularization by adding a parameter $\varepsilon > 0$. To make a comparison with the linear elasticity equation (7.13) viable, we use a local weighting $\mu \colon \mathbb{D} \to (0, \infty)$ in the quasilinear form, which is then given by

$$\begin{aligned} \int_{\mathbb{D}} \mu \cdot \Big(\varepsilon^2 + \nabla U : \nabla U\Big)^{\frac{p}{2}-1} \cdot \nabla U : \nabla V \, \mathrm{d}x = \mathrm{RHS}(\varphi, \phi)[V] \qquad & \forall V \in H_0^1(\mathbb{D}, \mathbb{R}^{n+1}) \\ U = 0 \qquad & \text{on } \partial\mathbb{D}. \end{aligned} \tag{7.14}$$

It is reported in [135], that the p-Laplacian gradient representation has particular advantages in resolution of sharp edges or kinks of optimal shapes. Illustration of this is not the goal of this work. We emphasize, that the p-Laplacian approach discussed in [135] uses a strong formulation, which is solved using Picard iterations. Since we use the weak formulation with a regularization term in equation (7.14), Newton's method is available for solution. This means we achieve higher order of convergence compared to the Picard iteration method found in [135]. The author of this work is not aware of such an approach in the current literature.

For our numerical examples, we choose the local weighting μ as the solution of Laplace problem

$$\begin{aligned} -\Delta \mu &= 0 && \text{in } \mathbb{D} \\ \mu &= \mu_{\max} && \text{on } \varphi(M) \\ \mu &= \mu_{\min} && \text{on } \partial\mathbb{D} \end{aligned} \tag{7.15}$$

for $\mu_{\max}, \mu_{\min} > 0$. In the context of linear elasticity equation (7.13), it can be interpreted as the so-called second Lamé parameter.

Remark 26 (Sufficiency of Linear Elements for Pre-Shape Regularization)**.** *To apply the pre-shape regularization approaches presented in this work, it is completely sufficient to use continuous linear elements to represent involved functions. As we can see in the pre-shape derivative formulas* (5.72) *and* (6.29)*, the highest order of featured derivatives is one. This is important for practical application, since shape and volume mesh quality regularization of shape gradient systems does not increase required order of elements. An exception is the unusual case, where zero order elements are used to represent shape gradients. All following systems are built using first order continuous Galerkin elements in FEniCS.*

Next, we need the shape derivative of the PDE-constrained tracking type shape optimization objective $\mathcal{J}$. It can be derived by a Lagrangian approach using standard shape or pre-shape calculus rules (cf. [160]), giving

$$\begin{aligned} \mathcal{D}\mathcal{J}\big(\pi(\varphi)\big)[V] = \int_{\mathbb{D}} & -(y - \bar{y}) \nabla \bar{y}^T V - \nabla y^T \big(\nabla V + \nabla V^T\big) \nabla p \\ & + \operatorname{div}(V) \Big(\frac{1}{2}(y - \bar{y})^2 + \nabla y^T \nabla p - r_{\varphi(M)} p\Big) \, \mathrm{d}x. \end{aligned} \tag{7.16}$$

Here, p is the adjoint solving the adjoint system

$$\begin{aligned} -\Delta p &= -(y - \bar{y}) && \text{in } \mathbb{D} \\ p &= 0 && \text{on } \partial\mathbb{D}. \end{aligned} \tag{7.17}$$

It is straightforward to derive the shape derivative of the perimeter regularization $\mathcal{J}^{\mathrm{Perim}}$, which takes the form

$$\mathcal{D}\mathcal{J}^{\mathrm{Perim}}\big(\pi(\varphi)\big)[V] = \int_{\varphi(M)} \mathrm{div}_\Gamma(V)\,\mathrm{d}s, \tag{7.18}$$

where $\mathrm{div}_\Gamma(V)$ is the tangential divergence of V on $\varphi(M)$.

In the following, we give four right-hand sides, which represent various regularization approaches to calculate pre-shape gradients. They correspond to the unregularized shape gradient, the shape regularized pre-shape gradient, the shape and volume regularized pre-shape gradient, and the shape and volume regularized pre-shape gradient with free tangential outer boundary $\partial\mathbb{D}$. We let $V \in H_0^1(\mathbb{D}, \mathbb{R}^{n+1})$.

For the *unregularized shape gradient*, the right-hand side of the gradient system (7.12) takes the standard form

$$\begin{aligned}\mathrm{RHS}(\varphi,\phi)[V] &= \mathcal{D}\mathcal{J}\big(\pi(\varphi)\big)[V] + \nu\cdot\mathcal{D}\mathcal{J}^{\mathrm{Perim}}\big(\pi(\varphi)\big)[V]\\ &= \int_{\mathbb{D}} -(y-\bar{y})\nabla\bar{y}^T V - \nabla y^T\big(\nabla V + \nabla V^T\big)\nabla p\\ &\qquad + \mathrm{div}(V)\Big(\frac{1}{2}(y-\bar{y})^2 + \nabla y^T\nabla p - r_{\varphi(M)}p\Big)\,\mathrm{d}x + \nu\cdot\int_{\varphi(M)}\mathrm{div}_\Gamma(V)\,\mathrm{d}s.\end{aligned} \tag{7.19}$$

In this case, the respective boundary condition for the gradient system is simply a Dirichlet zero condition $\mathrm{BC} = 0$.

Next, we give the right-hand side for the *shape regularized pre-shape gradient*. For shape parameterization tracking, we employ a target f_φ given by a globally defined function $q\colon \overline{\mathbb{D}} \to (0,\infty)$ (cf. equation (7.7)), which in combination yields

$$\begin{aligned}&\mathrm{RHS}(\varphi,\phi)[V]\\ &= \mathcal{D}\mathcal{J}\big(\pi(\varphi)\big)[V] + \nu\cdot\mathcal{D}\mathcal{J}^{\mathrm{Perim}}\big(\pi(\varphi)\big)[V] + \alpha^\tau\cdot\big\langle g_\varphi^{\mathcal{T}}, V\big\rangle\\ &= \int_{\mathbb{D}} -(y-\bar{y})\nabla\bar{y}^T V - \nabla y^T\big(\nabla V + \nabla V^T\big)\nabla p\\ &\qquad + \mathrm{div}(V)\Big(\frac{1}{2}(y-\bar{y})^2 + \nabla y^T\nabla p - r_{\varphi(M)}p\Big)\,\mathrm{d}x + \nu\cdot\int_{\varphi(M)}\mathrm{div}_\Gamma(V)\,\mathrm{d}s\\ &\quad -\alpha^\tau\cdot\int_{\varphi(M)}\frac{1}{2}\cdot\left(\big(g^M\circ\varphi^{-1}\cdot\det D^\tau\varphi^{-1}\big)^2 - \Big(\frac{\int_M g^M\,\mathrm{d}s}{\int_{\varphi(M)} q\,\mathrm{d}s}\cdot q\Big)^2\right)\cdot\mathrm{div}_\Gamma\left(V - \langle n, V\rangle_2\cdot n\right)\\ &\qquad + \Big(g^M\circ\varphi^{-1}\cdot\det D^\tau\varphi^{-1} - \frac{\int_M g^M\,\mathrm{d}s}{\int_{\varphi(M)} q\,\mathrm{d}s}\cdot q\Big)\cdot\frac{\int_M g^M\,\mathrm{d}s}{\int_{\varphi(M)} q\,\mathrm{d}s}\cdot\nabla_\Gamma q^T V\,\mathrm{d}s.\end{aligned} \tag{7.20}$$

The boundary condition is Dirichlet zero, i.e. $\mathrm{BC} = 0$. In order to assemble the shape regularization $\langle g_\varphi^{\mathcal{T}}, V\rangle$, it is necessary to compute the tangential Jacobian $\det D^\tau\varphi^{-1}$. In applications, this means storing the vertex coordinates of the initial shape is necessary. Then, φ^{-1} can be calculated simply as the difference of initial shape node coordinates to the current ones. Hence there is no need to invert matrices to calculate $D^\tau\varphi^{-1}$. We give a reminder that D^τ is the covariant derivative, and must not be confused with the tangential derivative (cf. equation (5.2)). In the case of an n-dimensional manifold $\varphi(M)$, the covariant derivative is a $n\times n$-matrix, whereas the tangential derivative is $(n+1)\times(n+1)$. The use of covariant derivatives requires to calculate local orthonormal frames, which can be done by standard or stabilized Gram-Schmidt algorithms. Knowing this, the computation of Jacobian determinants is inexpensive, since matrices from applications are of size smaller 3×3.

Building on equation (7.20), we can construct the right-hand side for the *shape and volume regularized pre-shape gradient*. For this, we use a volume tracking target $f^{\mathbb{D}}_{\varphi(M)}$ defined by a field $q^{\mathbb{D}}\colon \overline{\mathbb{D}} \to (0,\infty)$ as in equation (7.9). This gives

$$
\begin{aligned}
&\mathrm{RHS}(\varphi,\phi)[V]\\
&= \mathcal{DJ}\big(\pi(\varphi)\big)[V] + \nu\cdot\mathcal{DJ}^{\mathrm{Perim}}\big(\pi(\varphi)\big)[V] + \alpha^{\tau}\cdot\big\langle g^{\mathcal{T}}_{\varphi}, V\big\rangle + \alpha^{\mathbb{D}}\cdot\mathfrak{D}\mathfrak{J}^{\mathbb{D}}(\phi)[V]\\
&= \int_{\mathbb{D}} -(y-\bar{y})\nabla\bar{y}^T V - \nabla y^T\big(\nabla V + \nabla V^T\big)\nabla p\\
&\qquad\qquad + \operatorname{div}(V)\Big(\frac{1}{2}(y-\bar{y})^2 + \nabla y^T\nabla p - r_{\varphi(M)}p\Big)\,\mathrm{d}x + \nu\cdot\int_{\varphi(M)}\operatorname{div}_{\Gamma}(V)\,\mathrm{d}s\\
&\quad -\alpha^{\tau}\cdot\int_{\varphi(M)}\frac{1}{2}\cdot\left(\big(g^M\circ\varphi^{-1}\cdot\det D^{\tau}\varphi^{-1}\big)^2 - \Big(\frac{\int_M g^M\,\mathrm{d}s}{\int_{\varphi(M)} q\,\mathrm{d}s}\cdot q\Big)^2\right)\cdot\operatorname{div}_{\Gamma}\left(V - \langle n, V\rangle_2\cdot n\right)\\
&\qquad\qquad + \left(g^M\circ\varphi^{-1}\cdot\det D^{\tau}\varphi^{-1} - \frac{\int_M g^M\,\mathrm{d}s}{\int_{\varphi(M)} q\,\mathrm{d}s}\cdot q\right)\cdot\frac{\int_M g^M\,\mathrm{d}s}{\int_{\varphi(M)} q\,\mathrm{d}s}\cdot\nabla_{\Gamma}q^T V\,\mathrm{d}s\\
&\quad -\alpha^{\mathbb{D}}\cdot\int_{\mathbb{D}^{\mathrm{out}}}\frac{1}{2}\cdot\left(\big(g^{\mathbb{D}}\circ\phi^{-1}\cdot\det D\phi^{-1}\big)^2 - \Big(\frac{\int_{\mathbb{D}^{\mathrm{out}}} g^{\mathbb{D}}\circ\phi^{-1}\cdot\det D\phi^{-1}\,\mathrm{d}x}{\int_{\mathbb{D}^{\mathrm{out}}} q^{\mathbb{D}}\,\mathrm{d}x}\cdot q^{\mathbb{D}}\Big)^2\right)\cdot\operatorname{div}\left(\mathrm{Pr}_{H^1_{0,\varphi(M)}}(V)\right)\\
&\qquad\qquad + \left(g^{\mathbb{D}}\circ\phi^{-1}\cdot\det D\phi^{-1} - \frac{\int_{\mathbb{D}^{\mathrm{out}}} g^{\mathbb{D}}\circ\phi^{-1}\cdot\det D\phi^{-1}\,\mathrm{d}x}{\int_{\mathbb{D}^{\mathrm{out}}} q^{\mathbb{D}}\,\mathrm{d}x}\cdot q^{\mathbb{D}}\right)\\
&\qquad\qquad\qquad\cdot\frac{\int_{\mathbb{D}^{\mathrm{out}}} g^{\mathbb{D}}\circ\phi^{-1}\cdot\det D\phi^{-1}\,\mathrm{d}x}{\int_{\mathbb{D}^{\mathrm{out}}} q^{\mathbb{D}}\,\mathrm{d}x}\cdot\nabla\big(q^{\mathbb{D}}\big)^T\,\mathrm{Pr}_{H^1_{0,\varphi(M)}}(V)\,\mathrm{d}x\\
&\quad -\alpha^{\mathbb{D}}\cdot\int_{\mathbb{D}^{\mathrm{in}}}\frac{1}{2}\cdot\left(\big(g^{\mathbb{D}}\circ\phi^{-1}\cdot\det D\phi^{-1}\big)^2 - \Big(\frac{\int_{\mathbb{D}^{\mathrm{in}}} g^{\mathbb{D}}\circ\phi^{-1}\cdot\det D\phi^{-1}\,\mathrm{d}x}{\int_{\mathbb{D}^{\mathrm{in}}} q^{\mathbb{D}}\,\mathrm{d}x}\cdot q^{\mathbb{D}}\Big)^2\right)\cdot\operatorname{div}\left(\mathrm{Pr}_{H^1_{0,\varphi(M)}}(V)\right)\\
&\qquad\qquad + \left(g^{\mathbb{D}}\circ\phi^{-1}\cdot\det D\phi^{-1} - \frac{\int_{\mathbb{D}^{\mathrm{in}}} g^{\mathbb{D}}\circ\phi^{-1}\cdot\det D\phi^{-1}\,\mathrm{d}x}{\int_{\mathbb{D}^{\mathrm{in}}} q^{\mathbb{D}}\,\mathrm{d}x}\cdot q^{\mathbb{D}}\right)\\
&\qquad\qquad\qquad\cdot\frac{\int_{\mathbb{D}^{\mathrm{in}}} g^{\mathbb{D}}\circ\phi^{-1}\cdot\det D\phi^{-1}\,\mathrm{d}x}{\int_{\mathbb{D}^{\mathrm{in}}} q^{\mathbb{D}}\,\mathrm{d}x}\cdot\nabla\big(q^{\mathbb{D}}\big)^T\,\mathrm{Pr}_{H^1_{0,\varphi(M)}}(V)\,\mathrm{d}x.
\end{aligned}
\tag{7.21}
$$

The last two integrals correspond to the regularizer for volume parameterization tracking. As in previous cases, the corresponding Dirichlet condition is given by $\mathrm{BC} = 0$. All previous remarks on assembling the right-hand side are still valid. Additionally, it is necessary to store coordinates of the entire initial hold-all domain. With these, the volume pre-shape ϕ^{-1} can be calculated as the difference of initial to current coordinates of the volume mesh. For volume regularization, calculation of Jacobian determinants $\det D\phi^{-1}$ does not require local orthonormal frames via Gram-Schmidt algorithms, as no covariant derivatives are featured. It is very important to use a correct normalization for $q^{\mathbb{D}}$ to ensure existence of solutions. This is necessary, since in practical applications, an optimization step leads to change of the underlying shape, and thus also of inner and outer components of $\mathbb{D}$. Therefore, the upper level problem of the fully regularized bilevel formulation (7.5) changes after each mesh morphing step. Hence it is not enough to simply estimate $g^{\mathbb{D}}$ once in the beginning. Either, $g^{\mathbb{D}}$ needs to be estimated by equation (7.6) in every iteration for which the shape of $\varphi(M)$ changes. Or $g^{\mathbb{D}}$ is replaced by $g^{\mathbb{D}}\circ\phi^{-1}\cdot\det D\phi^{-1}$, which is motivated by the transformation rule. We have decided for the latter, which can be seen in the last two terms of equation (7.21). This also needs to be taken into account when calculating $\mathfrak{J}^{\mathbb{D}}$, e.g. for line search. As explained in section 6.2.2, it is necessary to use a projection $\mathrm{Pr}_{H^1_{0,\varphi(M)}}(V)$ for directions of the volume regularization, if shapes are enforced to stay invariant. The projection can be realized by setting the degrees of freedom of the finite element representation of V, which are located at the shape $\varphi(M)$, to zero. This leads to vanishing of the first term of

$\mathfrak{D}(f^{\mathbb{D}}_{\varphi(M)})[V]$ (cf. equation (7.11)), which does not occur in equation (7.21).

Lastly, the right-hand side for a *shape and volume regularized pre-shape gradient with free tangential outer boundary* is given by equation (7.21) as well. However, instead of employing Dirichlet zero boundary conditions, we permit the boundary $\partial\mathbb{D}$ to move tangentially. For this, we set

$$\mathrm{BC}_\phi = \alpha^{\partial\mathbb{D}} \cdot U_{L^2} \quad \text{on } \partial\mathbb{D}, \tag{7.22}$$

for a scaling factor $\alpha^{\partial\mathbb{D}} > 0$. Here, U_{L^2} is the L^2-representation of tangential components of $\mathfrak{D}\mathfrak{J}^{\mathbb{D}}(\phi)$. Notice that in practice, this does not require solution of an additional PDE, since the tangential values of $\mathfrak{D}\mathfrak{J}^{\mathbb{D}}(\phi)$ can be extracted directly from its finite element representation. We remind the reader that this is more of a heuristic approach, which leaves room for refinement and rigorous formulation in future works.

7.2 Numerical Results and Comparison of Algorithms

In this section we present computational results of unregularized and various pre-shape regularized gradient descents for the model shape optimization problem (7.3). We propose algorithm 7.1, which is a modified gradient descent method with a backtracking line search featuring regularized pre-shape gradients. We present 7 different implementations. The first 4 feature the linear elasticity representation from equation (7.13) with unregularized, shape regularized, shape and volume regularized, and shape and volume regularized free tangential outer boundary right-hand sides. The other 3 feature the regularized p-Laplacian representation from equation (7.14) with unregularized, shape regularized, and shape and volume regularized right-hand sides. For the p-Laplacian representation, we dismiss the free tangential outer boundary version, since solving it requires a modified Newton's method, and hence slight additional implementational effort. Both the linear elasticity equation (7.13) and the regularized p-Laplacian equation (7.14) involve a local weighting function μ stemming from Laplace equation (7.15) inspired by [159]. The two approaches for these metrics without any type of pre-shape regularization are denoted as their 'Vanilla' versions. For implementations, we use the open-source finite-element software FEniCS (cf. [117, 4]). Meshes are constructed via the free meshing software Gmsh (cf. [63]). We perform our calculations using a single Intel(R) Core(TM) i5-3210M CPU @ 2.50GHz featuring 6GB of RAM.

Algorithm 7.1 is essentially a steepest descent with a backtracking line search. The regularization procedures for shape and volume mesh quality take place by modifying the right-hand sides of gradient systems as described in section 7.1.3. However, we pinpoint some important differences of algorithm 7.1 compared to a standard gradient descent for shape optimization.

First, notice that the initial mesh coordinates are stored in order to calculate φ_k^{-1} and ϕ_k^{-1}. We have to store the surface mesh coordinates of M for shape regularization, or the complete initial volume mesh coordinates of $\mathbb{D}_0$ when volume regularization takes place. This corresponds to setting initial pre-shapes to $\varphi_0 = \mathrm{id}_M$ and $\phi_0 = \mathrm{id}_{\mathbb{D}_0}$. We emphasize, that in both cases, there is no need to store more information than initial vertex coordinates. In particular, this means mesh-connectivity and other topological data concerning the initial mesh do not contribute to storage cost. This owes to the fact, that pre-shape derivatives are evaluated in the current shape and volume mesh iterates due to use of retractions $g^M \circ \varphi_k^{-1} \cdot \det D^\tau \varphi_k^{-1}$ and $g^{\mathbb{D}} \circ \phi_k^{-1} \cdot \det D\phi_k^{-1}$ in the formulas. Since the current mesh coordinates are necessarily stored in a standard gradient descent, φ_k^{-1} and

ϕ_k^{-1} can be calculated as mesh coordinate differences. Calculating these inverse embeddings amounts to a matrix difference operation, and therefore is of negligible computational burden. Estimating initial vertex distributions g^M and $g^{\mathbb{D}}$ needs to be done only once at the beginning of our routine. Hence it does not contribute to computational cost in a significant way.

If shape regularization is partaking in the gradient system, it is necessary to compute and store local tangential orthonormal frames τ_0 of the initial shape M. Together with calculation of local tangential orthonormal frames τ_k for the current shape $\varphi_k(M)$, these are used to assemble the covariant Jacobian determinant for the regularized right-hand side of the gradient systems. Since this is done for each new iterate φ_k, it indeed increases computational cost. If required, this can be mitigated by parallel computing, since tangential orthonormal bases can be calculated simultaneously for all points $p \in \varphi_k(M)$. In higher dimensions, care must be taken to achieve a coherent orientation of local tangential orthonormal frames. For the example of surface meshes, this can be achieved by imposing $\langle \tau_{k,1} \times \tau_{k,2}, n \rangle_2 = 1$, where n is the outer unit normal vector field on the surface.

Another difference to standard steepest descent methods concerns the condition of convergence in line 6 of algorithm 7.1. It features two convergence conditions, namely sufficient decrease in either the absolute or relative norm of the pre-shape gradient, and sufficient decrease of relative values for the original shape objective $\mathcal{J}$. We use this approach, since several objective functionals participate simultaneously in formation of pre-shape gradients U_k. If shape or volume regularization take place, they influence the size of gradients depending on the mesh configuration. In order to compare different (un-)regularized gradient systems, we use this criterion to guarantee the same decrease of the original problem's objective for all strategies. The line search checks for a sufficient decrease of the combined objective functionals matching the gradient regularizations. This can be interpreted as a weighted descent for multi-criteria optimization, where the multiple objectives are $\mathcal{J}$ and the regularizations $\mathfrak{J}^M$ and $\mathfrak{J}^{\mathbb{D}}$.

Furthermore, we mention the difference of our two tested gradient representation forms $\mathfrak{a}(\cdot,\cdot)$ acting as left-hand sides. The weak linear elasticity representation from equation (7.13) leads to a linear system, which is solvable by use of standard techniques such as the CG-method. However, the weak p-Laplacian equation (7.14) is increasingly nonlinear for larger $p \geq 2$. This significantly increases computational cost and burden of implementation, since Newton's method requires multiple linear system solves. Also, systems are possibly indefinite if regularization parameter $\varepsilon > 0$ is too small. If chosen too large, we pay for positive definiteness by overregularizing the gradient systems. In order to achieve convergence of Newton's method for the p-Laplacian, we use gradients from the previous shape optimization step as an initial guess.

Remark 27 (Integrating Shape and Volume Regularization in Existing Solvers)**.** *Implementing shape and volume regularization with the pre-shape approach does not require a large overhead, if an existing solver for the shape optimization problem of concern is available. It solely requires accessibility of gradient systems* (7.12) *and mesh morphing to update meshes and shapes. With this, assembling and adding regularization terms in style of equation* (7.20) *or equation* (7.21) *to existing right-hand sides is all that needs to be done. This does not affect the user's choice of preferred metrics* $\mathfrak{a}(\cdot,\cdot)$ *to represent gradients. This is highlighted by our implementation and comparison of regularizations for the linear elasticity and the nonlinear p-Laplacian metrics. From this perspective, algorithm 7.1 is an in-depth explanation how right-hand side modifications of gradient systems are assembled.*

For a meaningful comparison of the 7 mentioned approaches, we use the same parameters for the problem throughout. Parameters for the source term $r_{\varphi(M)}$ of

Set starting domain $\mathbb{D}_0$ and shape $\varphi_0(M)$, save according vertex coordinates for future computations
Choose pre-shape regularizations by setting $\alpha^\tau, \alpha^{\mathbb{D}} \geq 0$
Set shape and volume targets $q, q^{\mathbb{D}} \colon \mathbb{D} \to (0, \infty)$
Estimate initial point distributions g^M for $\varphi_0(M)$ and $g^{\mathbb{D}}$ for $\mathbb{D}_0$ according to equation (7.6)
Calculate local orthonormal tangential bases τ_0 for each vertex of $\varphi_0(M)$ using Gram-Schmidt orthonormalization, save them for future iterations
while $\left(\|U_k\| > \varepsilon_{\text{abs}} \text{ and } \frac{\|U_k\|}{\|U_0\|} > \varepsilon_{\text{rel}} \right)$ or $\frac{\mathcal{J}\left(\pi(\varphi_k)\right)}{\mathcal{J}\left(\pi(\varphi_0)\right)} > \varepsilon_{\text{rel}}^{\mathcal{J}}$ **do:**
    Assemble right-hand side of pre-shape gradient system (7.12):
        Solve for state solution y_k via equation (7.3)
        Solve for adjoint solution p_k via equation (7.17)
        Calculate local orthonormal tangential bases τ^{φ_k} for each vertex of $\varphi_k(M)$ with same orientation as τ_0 using Gram-Schmidt orthonormalization
        if $\alpha^\tau = 0$ **and** $\alpha^{\mathbb{D}} = 0$**:** Assemble RHS(φ_k, ϕ_k) according to equation (7.19)
        elif $\alpha^\tau \neq 0$ **and** $\alpha^{\mathbb{D}} = 0$**:** Assemble RHS(φ_k, ϕ_k) according to equation (7.20)
        elif $\alpha^\tau \neq 0$ **and** $\alpha^{\mathbb{D}} \neq 0$**:** Assemble RHS$(\varphi_k, \phi_k)$ according to equation (7.21)
    Solve for pre-shape gradient U_k:
        Calculate local weighting parameters μ by solving equation (7.15)
        if linear elasticity:
            Assemble left-hand side $\mathfrak{a}(\cdot, \cdot)$ by equation (7.13) and solve by preconditioned CG-method
        elif p-Laplacian:
            Use preconditioned Newton's method to solve equation (7.12) with left-hand side $\mathfrak{a}(\cdot, \cdot)$ by equation (7.14)
    Perform a line search to get a sufficient descent direction $\tilde{U}_k$:
        $\tilde{U}_k \leftarrow \frac{1}{\|U_k\|} \cdot U_k$
        while
        $\mathcal{J}\left(\pi(\varphi_k + \tilde{U}_k \circ \varphi_k)\right) + \alpha^\tau \cdot \mathfrak{J}^M\left(\varphi_k + \tilde{U}_k \circ \varphi_k\right) + \alpha^{\mathbb{D}} \cdot \mathfrak{J}^{\mathbb{D}}\left(\phi_k + \tilde{U}_k \circ \phi_k\right)$
        $\geq \mathcal{J}\left(\pi(\varphi_k)\right) + \alpha^\tau \cdot \mathfrak{J}^M(\varphi_k) + \alpha^\tau \cdot \mathfrak{J}^{\mathbb{D}}(\phi_k)$ **do:**
            $\tilde{U}_k \leftarrow 0.5 \cdot \tilde{U}_k$
    Perform updates:
        $\varphi_{k+1} \leftarrow \varphi_k + \tilde{U}_k \circ \varphi_k$
        $\phi_{k+1} \leftarrow \phi_k + \tilde{U}_k \circ \phi_k$

Algorithm 7.1: Simultaneous shape and volume regularized shape optimization.

the PDE-constraint in equation (7.17) are chosen as $r_1 = -1000$ and $r_2 = 1000$. The scaling factor for perimeter regularization is $\nu = 0.00001$. Parameters to calculate local weightings μ via Laplace equation (7.15) are $\mu_{\max} = 1$ and $\mu_{\min} = 0.05$ for all approaches. The stopping criteria for all routines tested remain the same. Specifically, the tolerance for relative decrease of gradient norms is $\varepsilon_{\text{rel}} = 0.001$, absolute decrease of gradient norms $\varepsilon_{\text{abs}} = 0.00001$, and relative main objective decrease $\varepsilon_{\text{rel}}^{\mathcal{J}} = 0.0005$. If shape regularization is employed, it is weighted with $\alpha^{\tau} = 1000$ and uses a constant target $q = 1$. This enforces a uniform distribution of surface cell volumes of shapes. For volume regularization, the weighting is $\alpha^{\mathbb{D}} = 100$ with a constant $q^{\mathbb{D}} = 1$, which also enforces uniform volume cells of the hold-all domain. If we permit free tangential movement of the outer boundary via equation (7.22), we choose a weighting parameter $\alpha^{\partial\mathbb{D}} = 250$. In case of the p-Laplacian representation, we choose a parameter $p = 6$. Its regularization parameter is chosen as $\varepsilon = 8$ for the unregularized, and the shape and volume regularized routines. If solo shape regularization without volume regularization takes place, we have to increase the p-Laplacian regularization to $\varepsilon = 9.5$. This is necessary, since at some point lower values for ε result in indefinite systems during descent with p-Laplacian gradients.

We compare relative values of $\mathcal{J}$, $\mathfrak{J}^M$ and $\mathfrak{J}^{\mathbb{D}}$, which are illustrated in figure 7.3. Here, $\mathfrak{J}^M$ is interpretable as the deviation of the shape mesh from a surface mesh with equidistant edges. Similarly, $\mathfrak{J}^{\mathbb{D}}$ can be understood as the deviation of the volume mesh from a volume mesh with uniform cell volumes. Since a change of mesh coordinates leads to different qualities of finite element solutions to the PDE-constraint of model problem (7.3), the regularizations implicitly affect the original objective $\mathcal{J}$. Hence, we also measure distance of shapes $\varphi_k(M)$ to the target shape by a distance function

$$\operatorname{dist}\left(\varphi_k(M), \Gamma^{\text{targ}}\right) := \int_{\varphi_k(M)} \max_{p \in \Gamma^{\text{targ}}} \|s - p\|_2 \, \mathrm{d}s. \tag{7.23}$$

This gives us a geometric value for convergence of our algorithms in figure 7.3 (b), complementing the value of objective functionals for our results.

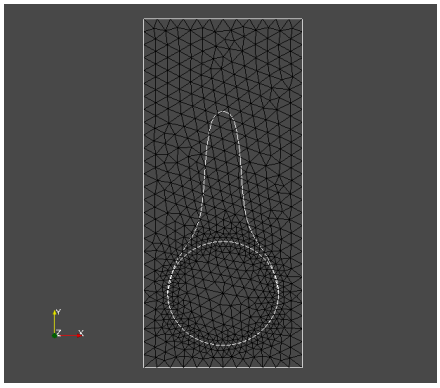

Figure 7.2: Initial mesh $\overline{\mathbb{D}}_0 = [0,1] \times [0,2.35]$ with embedded initial shape $M = S^{0.35}_{(0.5,0.5)}$. The mesh is locally refined near M, and the bottle like target shape Γ^{targ} is included as well.

The times for all optimization runs are presented in table 7.1. Final meshes with volume node densities are seen at the end of this section in figure 7.4, and with zoom in figure 7.5. Graphics with shape node densities are found in figure 7.6. Results for the objectives and distances to the target shape are found in figure 7.3.

From figure 7.3 (a) and (b), we see that all 7 methods converge. They all minimize the original shape objective $\mathcal{J}$, and the geometric mesh distance (7.23) to

	LE Vanilla	LE Tang	LE VolTang	LE VolTang Free	p-L Vanilla	p-L Tang	p-L VolTang
total time	49.0s	345.4s	199.9s	320.7s	135.4s	316.5s	325.8s
avg. time/step	1.2s	2.5s	2.6s	2.8s	2.4s	2.0s	4.6s
number steps	41	137	77	114	55	155	70

Table 7.1: Total times, averaged times per step and number of steps for all 7 methods.

the target shape (cf. figure 7.2). Seeing the geometrical mesh distance being minimized for all methods, we have confirmation that the optimal shape of original problem (7.3) is left invariant by our pre-shape regularizations. Also, convergence to the optimal shape is not affected by the choice of regularization and gradient representation via $\mathfrak{a}(\cdot,\cdot)$. Given a fixed $\mathfrak{a}(\cdot,\cdot)$, we see in figure 7.3 (a), that the shape objective values $\mathcal{J}$ for regularized routines vary only slightly from the unregularized one. This means intermediate shapes $\varphi_k(M)$ are left nearly invariant by all regularization approaches. We witness that the p-Laplacian representation (7.14) gives a pre-shape gradient descent with slightly slower convergence compared to the linear elasticity (7.13). However, one should keep in mind that the shapes considered here have rather smooth boundary, whereas the p-Laplacian approach is favorable to tackle shape optimization problems with non-smooth optimal shapes.

From table 7.1, we see that the fastest method in both time and step count is the unregularized approach with the linear elasticity representation. All regularized approaches need more steps for convergence, since the convergence condition features sufficient minimization of the gradient norms. As shape and volume tracking objectives $\mathfrak{J}^M$ and $\mathfrak{J}^{\mathbb{D}}$ participate in this condition, the optimization routine continues to optimize for mesh quality, despite a sufficient reduction of the original objective $\mathcal{J}$. This can be verified in figure 7.3. Notice that additional volume regularization did not considerably increase average computational time per step for the linear elasticity approach. The times for approaches featuring shape regularization can be improved by computing tangential orthonormal bases in parallel. We relied on rather inefficient but convenient implementations of these by solving several projection problems using FEniCS.

From table 7.1, we see that the unregularized p-Laplacian approach for $p = 6$ needs more steps to convergence compared to a linear elasticity based descent. Average time per step is higher too, since nonlinear gradient systems need to be solved. This approach needs careful selection of regularization parameter $\varepsilon > 0$ for equation (7.14), since the mesh quality degrades quickly for our problem. This makes calculation of gradients by Newton's method difficult, since conditioning of systems and indefiniteness are an issue at some point of the shape optimization routine. Computational times were slightly faster on average for the shape regularized p-Laplacian gradient compared to the unregularized p-Laplacian gradient. We amount this to faster convergence of the Newton method, since we needed to employ a higher regularization parameter $\varepsilon = 9.5$ for the shape regularized routine. This also explains longer computational times for the volume regularized p-Laplacian, since the same regularization parameter $\varepsilon = 8$ as in the unregularized approach is permissible, but more Newton iterations are necessary. Since the shape regularization takes place simultaneously with volume regularization, a lower permissible regularization ε indicates that volume regularization improves condition of linear systems.

Notice that the final shapes for all volume regularized routines, i.e. those seen in figure 7.6 (c), (d) and (g) are slightly non-symmetric, even though the initial and target shapes in figure 7.2 are symmetric. Because the volume mesh for the hold-all domain is generated in unstructured way by Gmsh, its cells are not mirror

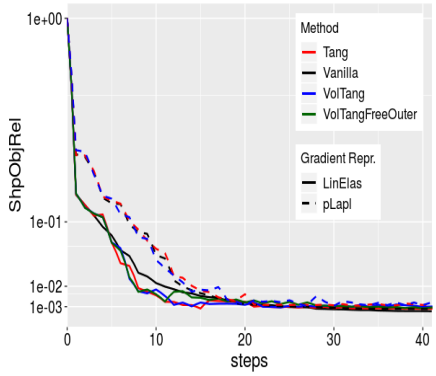

(a) Relative shape objective value $\frac{\mathcal{J}(\pi(\varphi_i))}{\mathcal{J}(\pi(\varphi_0))}$

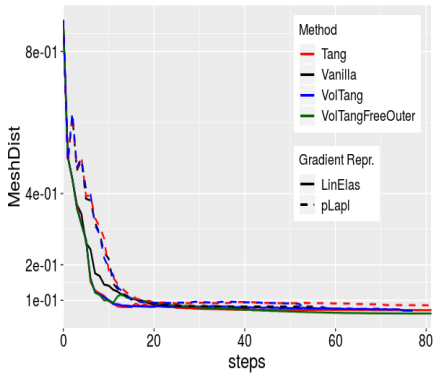

(b) Mesh distance of $\varphi_i(M)$ and target shape

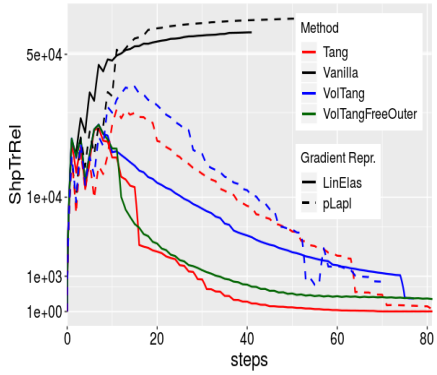

(c) Relative shape tracking value $\frac{\mathfrak{J}^M(\varphi_i)}{\mathfrak{J}^M(\varphi_0)}$

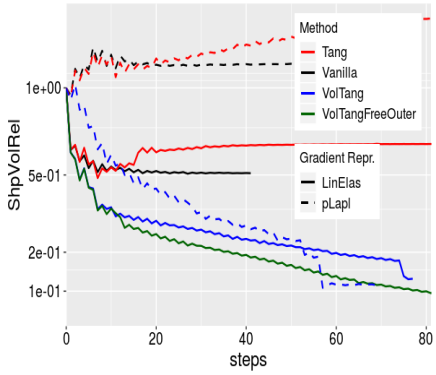

(d) Relative volume tracking value $\frac{\mathfrak{J}^{\mathbb{D}}(\phi_i)}{\mathfrak{J}^{\mathbb{D}}(\phi_0)}$

Figure 7.3: Relative values for three objective functionals $\mathcal{J}$, $\mathfrak{J}^M$ and $\mathfrak{J}^{\mathbb{D}}$, and mesh distance to the target shape for gradient descents using 7 different (un-)regularized pre-shape gradients and representations.

symmetric with respect to the $(0.5, y)$-axis. As all regularizations do not alter the node connectivity, while trying to achieve uniform cell volume distribution, a slight non-symmetry of final iterates is created due to the initial non-symmetry of the unstructured volume mesh topology.

To analyze quality of the shape mesh for all routines, we provide the relative value of the shape parameterization tracking target $\mathfrak{J}^M$ in figure 7.3 (c). It measures deviation of the current shape mesh $\varphi_k(M)$ from a uniform surface mesh. Also, the pushed forward surface node densities $g^M \circ \varphi_k^{-1} \cdot \det D^\tau \varphi_k^{-1}$ for final shapes of all routines are seen in figure 7.6. Their reciprocal values can be interpreted as the local surface cell volume, i.e. edge lengths. The colors in figure 7.6 highlight variation of node densities on the shape meshes, where a uniform color indicates approximately equidistant surface nodes. The starting mesh seen in figure 7.2 features an approximately uniform surface mesh. For both the unregularized linear elasticity and the unregularized p-Laplacian approach, we see in figure 7.3 (c), that $\mathfrak{J}^M$ increases during optimization. This means surface mesh quality deteriorates if no regularization takes place. For respective final shapes, this is visualized in figure 7.6 (a) and (e). There we clearly see an expansion of surface cell volumes at the top of final shapes. All other routines involve a shape regularization by $\mathfrak{J}^M$. In figure 7.3 (c), it is visible that for these routines, the deviation $\mathfrak{J}^M$ from uniform surface meshes increases initially. Once surface mesh quality becomes sufficiently bad, the shape parameterization takes effect and corrects quality until approximate uniformity is achieved. Convergence of $\mathfrak{J}^M$ is clearly visible for all shape regularized methods in

figure 7.3 (c). Also, we see an approximately uniform color of $g^M \circ \varphi_k^{-1} \cdot \det D^\tau \varphi_k^{-1}$ for respective final shapes in figure 7.6, which indicates a nearly equidistant surface mesh for the shape regularized routines. As a caveat, we see in figure 7.4 and figure 7.5 (b) and (f), that shape regularization without volume regularization decreases quality of the volume mesh surrounding the shape. This happens, since surface vertices are transported from areas with low edge length at the bottom to areas with high edge length at the top, while node connectivity remains unchanged. In case no volume regularization takes place, node coordinates from the hold-all domain are not corrected for this change. Nevertheless, if a remeshing strategy is employed for shape optimization including shape regularization, the improved surface mesh quality leads to a superior remeshed domain. Such routines are an interesting subject for further works.

In figure 7.3 (d), relative values of the volume parameterization tracking functional $\mathfrak{J}^{\mathbb{D}}$ are depicted for each routine. We interpret these values as a measure for non-uniformity of the volume mesh $\mathbb{D}$. The local node densities $g^{\mathbb{D}} \circ \phi^{-1} \cdot \det D\phi^{-1}$ for complete hold-all domains are depicted in figure 7.4, zoomed versions are found in figure 7.5. From figure 7.3 (d), we see that all non-volume regularized routines have significantly higher value of $\mathfrak{J}^{\mathbb{D}}$. Values even increase for the p-Laplacian representation, while there is a slight decrease for the linear elasticity. Notice that the initial mesh is locally refined near the shape M, which naturally increases the initial value of $\mathfrak{J}^{\mathbb{D}}$ for a uniform target. As already discussed, we see in figure 7.3 (d), that shape regularized approaches reduce quality of the volume mesh even further when compared to unregularized approaches. The decrease of mesh quality is especially visible in zoomed pictures figure 7.5 (a), (b), (e) and (f). We see that for these approaches, volume cells near the shape are compressed to such an extent, that their volumes nearly vanish. Also, the cell volume distribution for unregularized and shape regularized approaches varies largely, which can be seen in figure 7.4 (a), (b), (e) and (f). If volume regularization $\mathfrak{J}^{\mathbb{D}}$ is applied, we see in figure 7.3 (d), that convergence for $\mathfrak{J}^{\mathbb{D}}$ takes place independently of the specific gradient representation form $\mathfrak{a}(\cdot,\cdot)$. This is apparent when looking at the volume node densities in figure 7.4 (c), (d) and (g). Further, we see in the zoomed pictures from figure 7.5 (c), (d) and (g), that severe compression of cells neighboring the top of final shapes is resolved by volume regularization. Volume cells inside the neck of final shapes are still more or less compressed for all approaches. The interior cell volume cannot be transported through the shape, since it is forced to stay invariant. Since the mesh topology is not changed during the optimization routine, there is also limited possibility to redistribute the cell volumes inside the shape. This situation could be remedied by cell fusion, edge swapping, or remeshing strategies, which is beyond the scope of this work. Finally, we highlight the difference of volume regularizations with and without free tangential outer boundary $\partial\mathbb{D}$. If figure 7.4 (c) and (d) are compared, we see that the nodes on the outer boundary $\partial\mathbb{D}$ changed position for routine (d). Indeed, the cell volume distribution is more uniform for free outer boundary routine (d), which is visualized by less variation of color. This leads to even lower values of $\mathfrak{J}^{\mathbb{D}}$, which can be pinpointed in the graph of figure 7.3 (d).

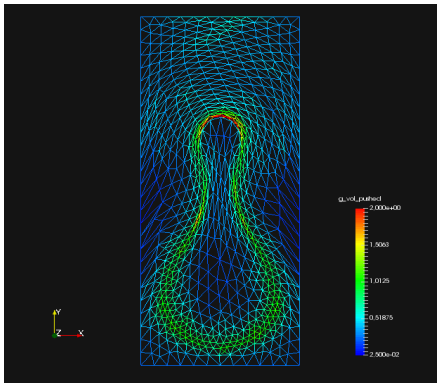

(a) LE Vanilla

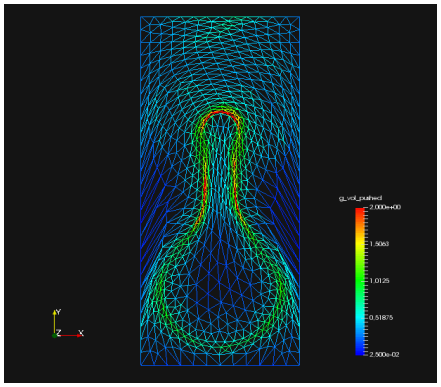

(b) LE Tang

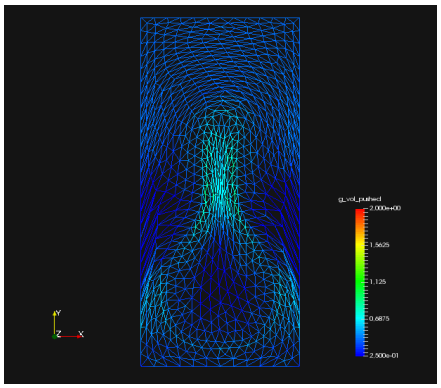

(c) LE VolTang

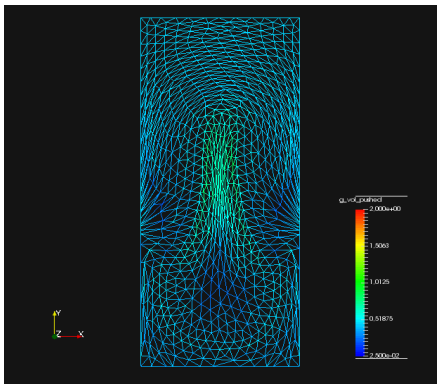

(d) LE VolTang Free

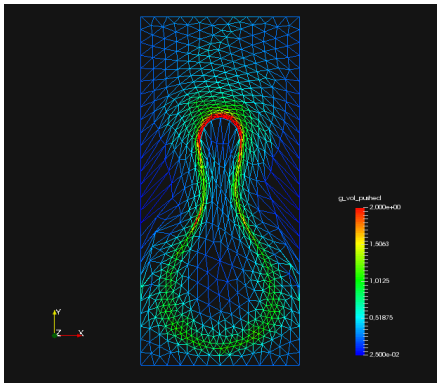

(e) p-L Vanilla

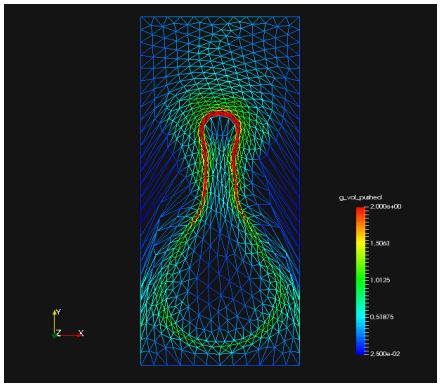

(f) p-L Tang

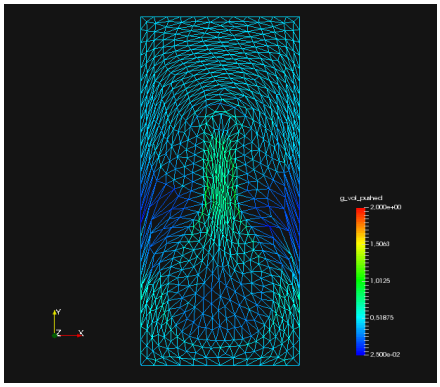

(g) p-L VolTang

Figure 7.4: Final meshes of linear elasticity (LE) and p-Laplacian (p-L) approaches. Color depicts the value of $g^{\mathbb{D}} \circ \phi^{-1} \cdot \det D\phi^{-1}$, which is interpretable as the density of allocated volume mesh vertices. More constant value corresponds to more uniform hold-all cell volumes.

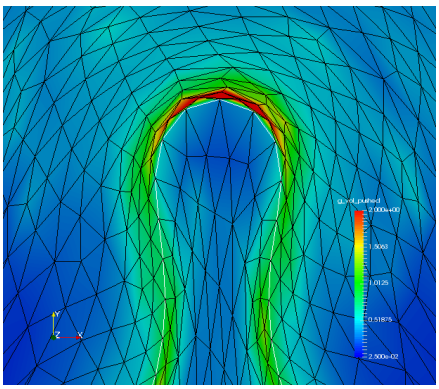

(a) LE Vanilla

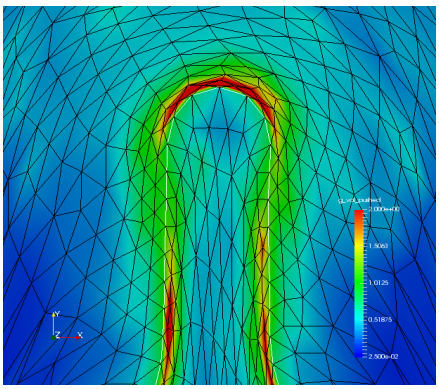

(b) LE Tang

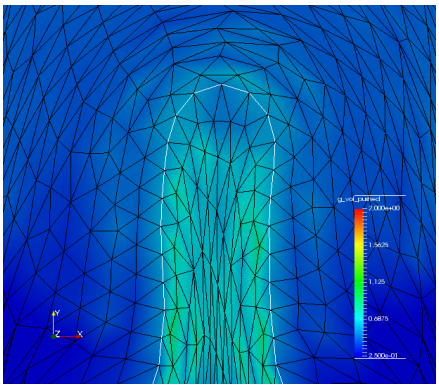

(c) LE VolTang

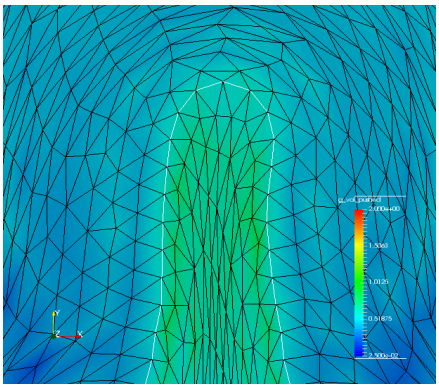

(d) LE VolTang Free

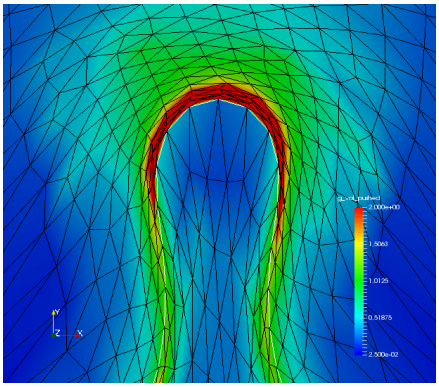

(e) p-L Vanilla

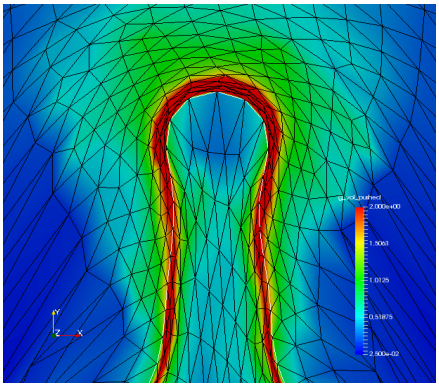

(f) p-L Tang

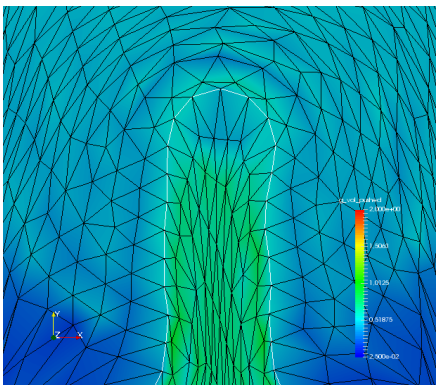

(g) p-L VolTang

Figure 7.5: Zoom of final meshes of linear elasticity (LE) and p-Laplacian (p-L) approaches at the top of the shape. Color depicts the value of $g^{\mathbb{D}} \circ \phi^{-1} \cdot \det D\phi^{-1}$, which is interpretable as the density of allocated volume mesh vertices. More constant value corresponds to more uniform hold-all cell volumes.

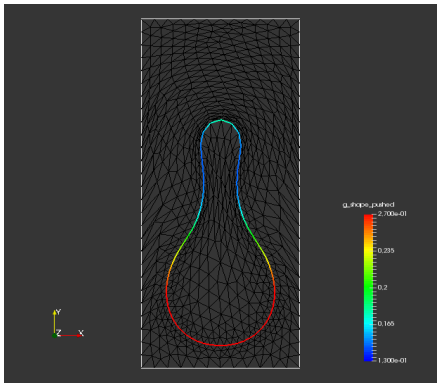

(a) LE Vanilla

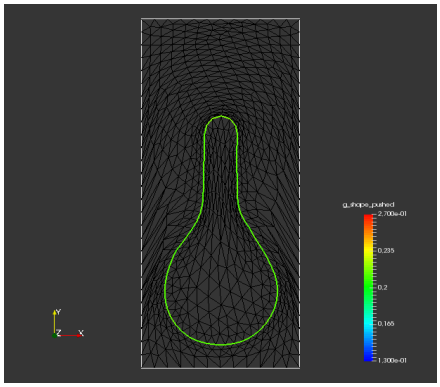

(b) LE Tang

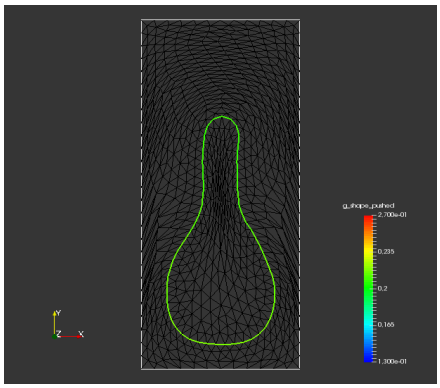

(c) LE VolTang

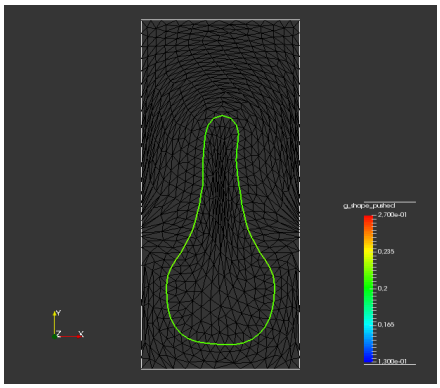

(d) LE VolTang Free

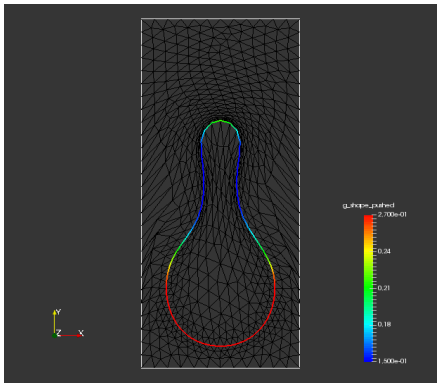

(e) p-L Vanilla

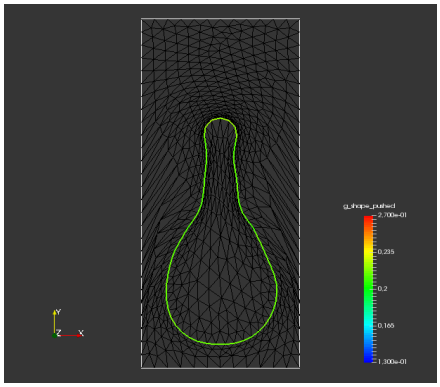

(f) p-L Tang

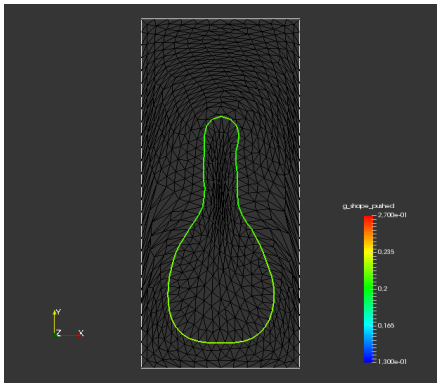

(g) p-L VolTang

Figure 7.6: Final meshes of linear elasticity (LE) and p-Laplacian (p-L) approaches. Color depicts the value of $g^M \circ \varphi^{-1} \cdot \det D^\tau \varphi^{-1}$, which is interpretable as the density of allocated shape mesh vertices. Its reciprocal gives the averaged local edge length. More constant value corresponds to more uniform shape mesh.

7.3 Shape Mesh Regularization via Full and Tangential Pre-Shape Derivatives

In this section, we compare numerical application of the full pre-shape derivative $\mathfrak{D}\mathfrak{J}^M$ of the parameterization tracking problem (5.10) for shape meshes with use of its tangential component $g^{\mathcal{T}}$. We derived the pre-shape derivative of $\mathfrak{J}^M$ in section 5.3, and explicitly decomposed it into shape and parameterization components in equation (5.70). For regularization of gradient systems in section 7.1.3, we solely used the tangential component $g^{\mathcal{T}}$ of the pre-shape derivative $\mathfrak{D}\mathfrak{J}^M$. This ensures invariance of optimal and intermediate shapes for the original shape optimization problem. We used theoretical arguments to justify this approach, which are formalized in theorem 15.

To further underpin this theoretical motivation, we numerically test gradient descents with the full pre-shape derivative $\mathfrak{D}\mathfrak{J}^M$ as found in equation (5.59), and its tangential component $g^{\mathcal{T}}$ as given in equation (5.72). Since these techniques serve as the basis of regularized shape optimization routines to achieve a target shape mesh quality, it is interesting to observe their behavior near solutions of an underlying original shape optimization problem. As an example, we make use of the previously studied PDE-constrained tracking type problem (7.3). We use an unregularized shape gradient descent for $\mathcal{J}$ to deform the shape and volume mesh. Once we see sufficient convergence, the shape and volume meshes of the last iterate near the solution are saved. The shape and volume meshes generated in this fashion are then used as the initial guess for a pre-shape gradient descent for $\mathfrak{J}^M$. In other words, we activate shape regularizations near the solution of the original shape optimization problem, without further optimizing the shape objective $\mathcal{J}$. The target f_φ is a uniform surface edge length distribution, i.e. we choose $q = 1$.

The pre-shape gradients are represented using the bilinear form of a weighted weak linear elasticity with zero order terms as in equation (5.89) from section 5.4, with weighting parameters $\alpha_{\mathrm{LE}} = 0.025$ and $\alpha_{L^2} = 1$. Bilinear forms featuring only higher order derivatives, such as weak linear elasticity, result in pre-shape gradients which are not perfectly tangential to the surface of shapes. This comes from the convolutive and smoothing effect of their corresponding solution operators. The numerical implementations described in section 7.1.3 and section 7.2 do not need zero order terms in the bilinear form for gradient representation, as parameterization tracking for the shape mesh is combined with the original shape optimization problem. Errors from not exactly tangential directions of the shape regularization are corrected in normal direction by the shape derivative $\mathcal{D}\mathcal{J}$ of the underlying shape optimization problem. Interestingly, uniqueness of shape solutions lets $\mathcal{D}\mathcal{J}$ act as a kind of penalty term, forcing discrete gradients of $g^{\mathcal{T}}$ solely to act in tangential directions. As we want to study the isolated effect of full pre-shape derivatives of shape parameterization tracking near solutions, we cannot include $\mathcal{D}\mathcal{J}$ as a force term. Hence zero order terms in the bilinear form are helpful, as these leave tangential and normal directions orthogonal. We use parameters $\mu_{\max} = 1$ and $\mu_{\min} = 0.05$ to calculate a local weighting μ via Laplace equation (7.15). A backtracking line search as found in algorithm 7.1 is employed. The gradients of each iteration are normed and initially rescaled by an initial factor of 0.01 for line search, which itself employs a rescaling parameter of 0.5 for the backtracking.

To capture the influence of parameterization tracking with full and tangential pre-shape derivatives on the original shape optimization problem, we look at two quantities. First, we examine the relative value $\mathcal{J}(\pi(\varphi_i))/\mathcal{J}(M)$ of the original shape objective. Secondly, we check for geometric influence on the shape by calculating the distance of intermediate shapes $\varphi_i(M)$ to the target shape with the distance function (7.23). Of course, we also track the relative shape parameteriza-

tion tracking values $\mathfrak{J}^M(\varphi_i)/\mathfrak{J}^M(\varphi_0)$, which should be minimized to give the desired uniform vertex distribution of the shape mesh. The results are shown in figure 7.7. Initial and target shapes, as well as the resulting shapes and meshes for the full pre-shape derivative $\mathfrak{D}\mathfrak{J}^M$ and its tangential component $g^{\mathcal{T}}$ are illustrated in figure 7.8.

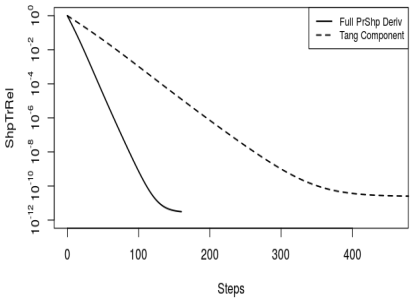

(a) Relative shape parameterization tracking objective $\frac{\mathfrak{J}^M(\varphi_i)}{\mathfrak{J}^M(\varphi_0)}$

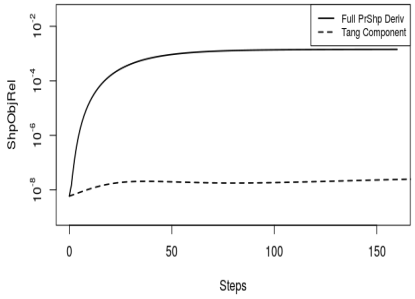

(b) Relative shape objective $\frac{\mathcal{J}(\pi(\varphi_i))}{\mathcal{J}(M)}$

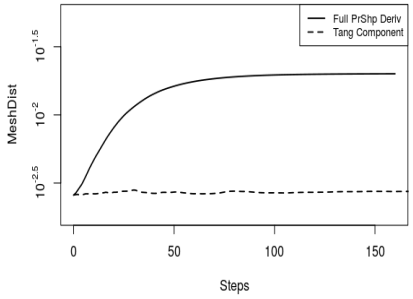

(c) Mesh distance of $\varphi_i(M)$ and target Γ^{targ}

Figure 7.7: (a) Relative objective values $\mathfrak{J}^M(\varphi_i)/\mathfrak{J}^M(\varphi_0)$ of shape parameterization tracking problem (5.10). The starting pre-shape φ_0 near the solution is constructed by a standard shape gradient descent for problem (7.3). (b) Relative objective values $\mathcal{J}(\pi(\varphi_i))/\mathcal{J}(M)$ with respect to starting shape $M = S^{0.35}_{(0.5,0.5)}$ of initial shape gradient descent. (c) Mesh distance of $\varphi_i(M)$ and target shape Γ^{targ} (cf. equation (7.23) and figure 7.8 (c)).

In figure 7.7 (a), we clearly see convergence of both pre-shape gradient descents, the first featuring the full pre-shape derivative $\mathfrak{D}\mathfrak{J}^M$, and the second using only its tangential component $g^{\mathcal{T}}$. This result reflects characterization theorem 13 of solutions to shape parameterization tracking by fiber stationarity, which states that vanishing full pre-shape derivative $\mathfrak{D}\mathfrak{J}^M$ and vanishing tangential component $g^{\mathcal{T}}$ are both equivalent sufficient criteria for a global minimizer of $\mathfrak{J}^M$. The full and tangential pre-shape derivatives generate descent directions, which are sufficient for convergence to approximately the same objective values. However, looking at figure 7.7 (b) and (c), we identify significant influence of the full pre-shape derivative $\mathfrak{D}\mathfrak{J}^M$ on the shapes and objective values of the underlying shape optimization problem. The shape seen in figure 7.8 (a) clearly differs from the shape near the op-

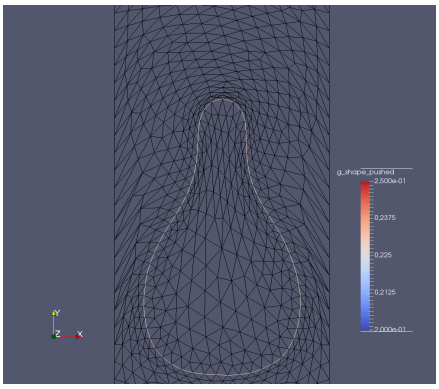

(a) Full pre-shape derivative $\mathfrak{D}\mathfrak{J}^M$

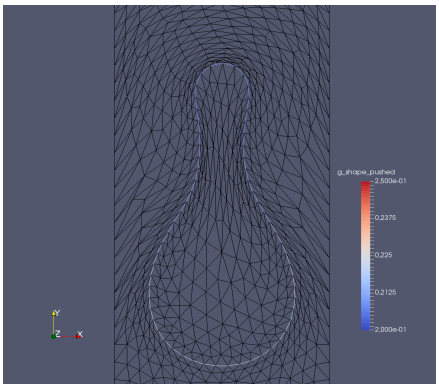

(b) Tangential pre-shape derivative $g^{\mathcal{T}}$

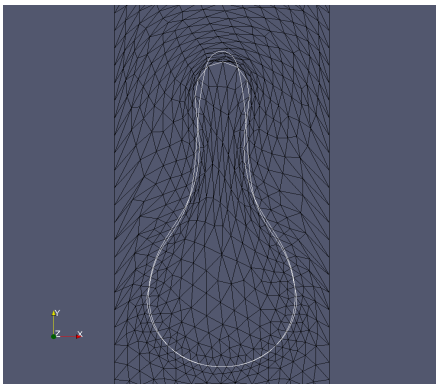

(c) Start and target shapes

Figure 7.8: Meshes of iteration 160 of pre-shape gradient descents for shape parameterization tracking problem (5.10). The starting mesh near the solution is constructed by using a standard shape gradient descent for problem (7.3).

timal solution depicted in figure 7.8 (c), but shows the desired uniform edge length distribution. This also confirms the behavior of the pre-shape derivatives normal component $g^{\mathcal{N}}$ described in section 5.3. The edge lengths at the upper tip of the starting shape are too long for uniformity, and due to positive local curvature κ at the top of the shape, the outer normal component of $\mathfrak{D}\mathfrak{J}^M$ acts by locally shrinking the shape in this area to compensate large edge length. On the other hand, edge lengths at the bottom of the shape are too small. Hence positive curvature κ leads to expansion of the shape in the outer normal direction by $g^{\mathcal{N}}$. This effect is visible by comparing shapes seen in figure 7.8 (a) and (c). Full pre-shape derivatives $\mathfrak{D}\mathfrak{J}^M$ of parameterization tracking are therefore not suitable for regularization in the context of shape optimization. On the other hand, as seen in figure 7.7 (b) and (c), the gradient descent with the tangential component $g^{\mathcal{T}}$ shows negligible change in both the relative shape objective value and distance to the optimal shape. This means the starting shape near the optimum of $\mathcal{J}$ is left approximately invariant by this approach.

The findings numerically substantiate our approaches for shape mesh quality regularization made in section 6.1 and section 7.1.3. Also, this highlights the importance of having a decomposition of pre-shape derivatives as guaranteed by structure theorem 9. Although it might seem counter-intuitive at first, users unfamiliar with pre-shape techniques need to be careful to not apply the full pre-shape derivative $\mathfrak{D}\mathfrak{J}^M$. Instead, it is critical to implement its tangential component $g^{\mathcal{T}}$ to successfully regularize shape optimization routines for desired shape mesh quality.

7.4 Comparing Direct and Shape Invariant Volume Parameterization Tracking

In this section, we examine two different approaches to volume mesh regularization. The first one is the 'naive' approach, which simply transfers the parameterization tracking problem formulation (5.10) to the volume case with pre-shapes from $\mathrm{Emb}(\overline{\mathbb{D}}, \overline{\mathbb{D}}) = \mathrm{Diff}(\overline{\mathbb{D}})$ seen in problem (6.15). We compare this approach to the one we proposed in section 6.2, which changes the volume parameterization tracking problem into formulation (6.18) to leave a given shape invariant. Contrasting the first formulation, the second one features the feasible set $\mathrm{Diff}(\mathbb{D} \setminus \varphi(M)) \cap \mathrm{Diff}_{\varphi(M)}(\overline{\mathbb{D}})$ of diffeomorphisms acting as the identity operator on a shape $\varphi(M) \subset \mathbb{D}$. Since this approach might seem overly technical at first, although it is justified theoretically in section 6.2, we underpin its correctness for shape optimization by numerical findings.

This comparison is approached by a setup similar to the shape regularization comparison study from section 7.3. We employ a shape gradient descent to compute a shape and volume mesh iterate near the solution of the underlying shape optimization problem (7.3). The shape created by this process is labeled Γ_{42}, since the shape gradient descent used 42 steps. Then we apply two pre-shape gradient descents starting in Γ_{42}. The first solves the volume tracking problem (6.15), and the second descent solves the volume tracking problem (6.18) with invariant shapes. By this we mimic the situation in practice, where volume mesh regularization is applied to shape optimization near solutions. The created starting mesh for volume parameterization tracking and the target shape are visualized in figure 7.10 (c). Readers should take special notice of the nearly complete degeneration of volume cells near the upper tip of the shape. As an invariant shape for the second approach, we choose the shape $\varphi_0(M) = \Gamma_{42}$ near the optimum seen in figure 7.10 (c). Of course, appropriate targets for cell volumes need to be chosen for each case. Here we choose a uniform cell volume target by setting $q^{\mathbb{D}} = 1$.

We emphasize, that due to the difference in feasible sets of both approaches, the corresponding targets $f_\phi^{\mathbb{D}}$ are different. For the first problem, the suitable target is of type (5.82), where objects for φ are of course substituted by those for ϕ. For the second approach, formulation (7.9) is correct. They inevitable differ, since different normalization conditions are necessary for existence of solutions. Respective conditions are given in equation (5.9) for the direct regularization, and in equation (6.19) for the shape invariant one. In particular, this leads to different pre-shape material derivatives of target volume distributions (cf. equation (5.84) and equation (7.11)), which in turn give different pre-shape derivatives $\mathfrak{D}\mathfrak{J}^{\mathbb{D}}$ for the two approaches.

The rest of the setup for our comparison study is similar to section 7.3, with the only difference that no zero order terms are used for the bilinear form $\mathfrak{a}(\cdot,\cdot)$ to represent pre-shape gradients. These are not necessary, since there is no need to enforce descent directions to be tangential on a shape. The featured bilinear form is given by the weighted weak formulation of the linear elasticity equation (7.13), and is used for both volume regularization approaches. For our analysis, we record the influence of both formulations on the underlying shape optimization objective $\mathcal{J}$, the difference of intermediate shapes to the target shape measured by the distance function (7.23), and the relative values for the volume parameterization objective $\mathfrak{J}^{\mathbb{D}}$ (cf. equation (6.18)). The results are portrayed in figure 7.9, whereas exemplary intermediate meshes and shapes are seen in figure 7.10 (a) and (b).

In figure 7.9 (a), we observe convergence of the volume parameterization objectives $\mathfrak{J}^{\mathbb{D}}$ for both approaches, which means volume meshes are becoming more uniform during the process. This is seen in figure 7.10 (a) and (b), where we emphasize the regeneration of cell quality near the upper tip of the shape. Notice,

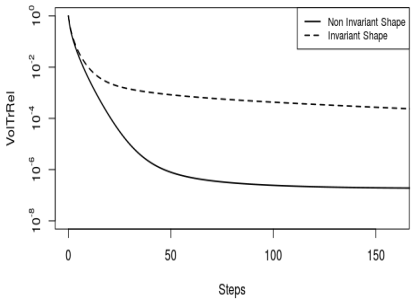

(a) Relative volume parameterization tracking objective $\frac{\mathfrak{J}^{\mathbb{D}}(\phi_i)}{\mathfrak{J}^{\mathbb{D}}(\phi_0)}$

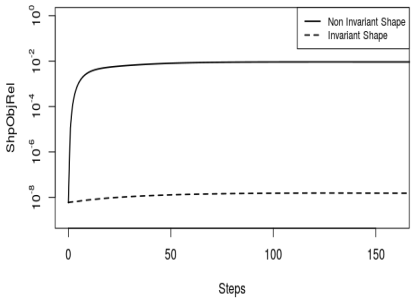

(b) Relative shape objective $\frac{\mathcal{J}(\phi_i(\Gamma_{42}))}{\mathcal{J}(M)}$

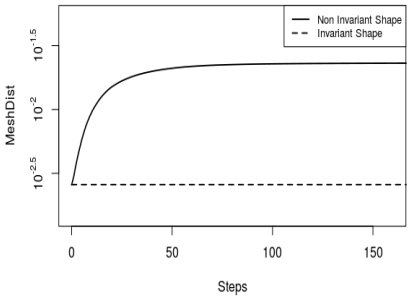

(c) Mesh distance of $\phi_i(\Gamma_{42})$ and target Γ^{targ}

Figure 7.9: (a) Relative objective values $\mathfrak{J}^{\mathbb{D}}(\phi_i)/\mathfrak{J}^{\mathbb{D}}(\phi_0)$ of volume parameterization tracking problems (6.15) and (6.18). The starting volume parameterization ϕ_0 and shape Γ_{42} near the solution are constructed by using a standard shape gradient descent for shape optimization problem (7.3). (b) Relative objective values $\mathcal{J}(\phi_i(\Gamma_{42}))/\mathcal{J}(M)$ with respect to starting shape $M = S^{0.35}_{(0.5,0.5)}$ of the initial shape gradient descent. (c) Mesh distance of $\phi_i(\Gamma_{42})$ and target shape Γ^{targ} (cf. equation (7.23) and figure 7.10 (c)).

that the relative objective value $\mathfrak{J}^{\mathbb{D}}(\phi_i)/\mathfrak{J}^{\mathbb{D}}(\phi_0)$ for the shape invariant approach is significantly higher than for the non-invariant approach. This stems from the mesh topology of the initial mesh seen in figure 7.10 (c). Due to the connectivity of vertices in the upper inside part of the shape, a shape invariant approach is only able to correct volume distributions up to a certain level. As this approach leaves the shape invariant, no expansion of cell volume in this area is possible. Otherwise the shape would blow up by expansion in the process. This is exactly what happens with the non-invariant approach, which is seen in figure 7.10 (a), explaining the lower volume tracking objective value. However, this is also the reason why we observe significant increase in both the relative shape objective value $\mathcal{J}(\phi_i(\Gamma_{42}))/\mathcal{J}(M)$ of the underlying shape problem and the distance to the target shape Γ^{targ}. This is seen in the graphs figure 7.9 (b) and (c). We also witness a change of shape in figure 7.10 (a), where the shape resulting by application of hold-all domain diffeomorphisms $\phi \in \text{Diff}(\overline{\mathbb{D}})$ is noticeably different to the nearly optimal starting shape seen in figure 7.10 (c). For the shape invariant approach with $\phi \in \text{Diff}(\mathbb{D} \setminus \varphi(M)) \cap \text{Diff}_{\varphi(M)}(\overline{\mathbb{D}})$, the distance of starting and target shapes is

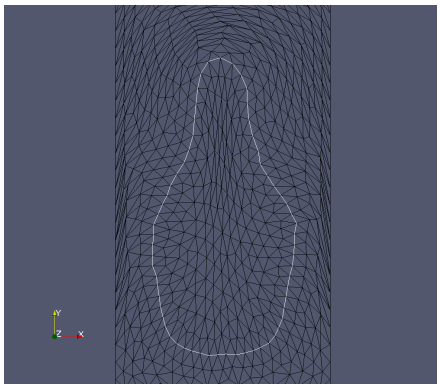

(a) Direct volume tracking

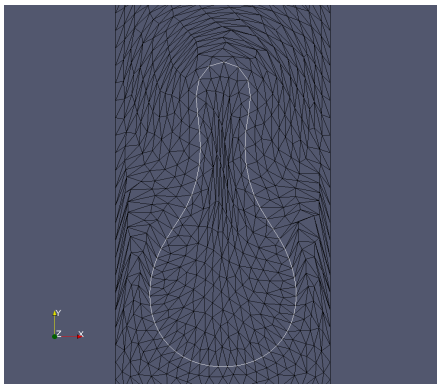

(b) Shape invariant volume tracking

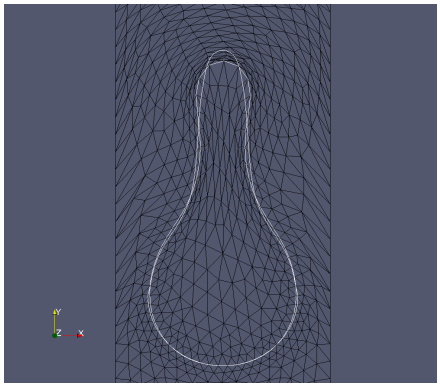

(c) Start and target shapes

Figure 7.10: Meshes of iteration 160 of pre-shape gradient descents for direct and shape invariant volume parameterization tracking problems (6.15) and (6.18). The starting mesh near the solution is constructed by using a standard shape gradient descent for problem (7.3).

left exactly unchanged. This differs from the tangential shape regularization case, which leaves the shape only approximately invariant due to numerical errors in tangential movement coming from the discretization. Nevertheless, we witness a subtle change of the relative shape objective in figure 7.9 (b). Because evaluation of the shape objective $\mathcal{J}$ is based on a finite element computation of its PDE-constraint, a change of the volume mesh also effects the values of the state solution y.

These findings confirm the necessity to use a shape invariant formulation for volume mesh regularization as proposed in section 6.2 and section 7.1.3. This is required in the context of shape optimization, since otherwise volume regularization can interact with the underlying shape optimization problem, and sabotage its convergence. If pre-shape techniques are applied outside the context of shape optimization, where invariance of subdomains is perhaps not mandatory, then it could of course be reasonable to use the non-invariant formulation to fully harness free movement of mesh vertices.

Chapter 8

Shape Optimization Problems Constrained by First Order Variational Inequalities

In this chapter, we stir away from the study of pre-shapes and mesh regularization to study a certain class of shape optimization problems. For this, examine a generalized version of model problem (7.3) from chapter 7, with a larger class of state equations. More specifically, we consider tracking type shape optimization problems constrained by variational inequalities (VI) of the first kind, so-called obstacle problems. Applications are manifold, and arise, whenever shape dependent state values are not allowed to exceed certain constraints. We can envision a heat equation depending on a shape, where the temperature is not allowed to surpass a certain threshold. This example corresponds to the model problem that we formulate in section 8.1. Applications of general VI's include contact problems in solid state mechanics, viscoplasticity and network equilibrium problems, and thus a wide range of industrial problems (cf. [102, 32, 36, 64]). For a literature review concerning variational inequality constrained shape optimization, we refer the reader to section 1.1. The results of this chapter are published in [122].

Constraints of shape optimization problem in the form of VIs are challenging, since classical constraint qualifications for deriving Lagrange multipliers generically fail. Therefore, not only the development of stable numerical solution schemes, but also derivation of suitable first order optimality conditions is an issue. The structure of this chapter is as follows. In section 8.1, we formulate the elliptic VI-constrained shape optimization model with general coefficients. Standard necessary optimality conditions cannot be formulated in a straightforward manner for semi-smooth shape optimization problems in general. We aim at optimality conditions in the flavor of those, which are concerned of VI-constrained optimal control problems found in [80, 81, 83]. Therefore, we regularize the VI-constraint, such that it results in a semilinear PDE. We remind the reader that, when we speak of regularization in this context, it has no connection with the mesh regularization methods of the previous chapters featuring pre-shapes. Under appropriate assumptions, we provide existence of adjoints resulting from the regularized variational inequalities, and prove their convergence in section 8.2. Then we show existence of shape derivatives to the fully regularized problem, and establish their convergence to a limiting object for vanishing regularization in section 8.3. In section 8.4, we formulate an algorithm to

solve the model problem based on our analytical results, and discuss results from the numerical implementation. The presented algorithm for VI-constraint shape optimization does no longer depend on the ad-hoc smoothing strategies found in [57]. The authors of [57] observe, that the performance of this algorithm strongly depends on the tightness of the obstacle. Such a problem does no longer arise with the strategy developed in the present chapter. On the contrary, our algorithm performs better for more degrees of freedom constrained by the obstacle.

8.1 First Order VI-Constrained Tracking Type Shape Optimization Problems

Let $\mathbb{D} \subset \mathbb{R}^{n+1}$ be a bounded and open domain, such that its closure $\overline{\mathbb{D}}$ has a smooth boundary $\partial\mathbb{D}$. As $n \in \mathbb{N}$ refers to the dimension of embedded shapes, we have $n = 1$ or $n = 2$ for typical applications. For the study in this chapter, we restrict ourselves to shapes modeled by closed and connected n-dimensional manifolds $M \subset \mathbb{D}$, i.e. we assume empty boundary ∂M. As argued in theorem 16 (i) with the Jordan-Brouwer theorem 6, the domain is partitioned into an outside and inside component. Because the results in this chapter are separate from the previously introduced pre-shape techniques, we abuse notation and write $\Gamma \in B_e^n$ instead of $\varphi(M)$, when we mean a shape in its set interpretation. As in previous chapters, we denote by $\mathbb{D}^{\text{out}} \subset \mathbb{D}$ the outer domain, and by $\mathbb{D}^{\text{in}} \subset \mathbb{D}$ the interior domain with boundary $\partial\mathbb{D}^{\text{in}} = \Gamma$. This means that we have a decomposition $\mathbb{D}^{\text{in}} \sqcup \mathbb{D}^{\text{out}} \sqcup \Gamma = \mathbb{D}$. We remind the reader, that when Γ changes, the subdomains $\mathbb{D}^{\text{in}}, \mathbb{D}^{\text{out}} \subset \mathbb{D}$ change accordingly. In the following, we also refer to the shape Γ as the interface, in contrast to the outer boundary $\partial\mathbb{D}$, which we assume to be fixed.

Let us recall the shape functional from the model problem (7.3). For $\nu > 0$, this tracking type objective can be written as

$$\mathcal{J}(y, \Gamma) + \mathcal{J}^{\text{Perim}}(\Gamma) := \frac{1}{2} \int_{\mathbb{D}} |y - \bar{y}|^2 \, \mathrm{d}x + \nu \int_{\Gamma} 1 \, \mathrm{d}s. \tag{8.1}$$

Instead of the Poisson equation, which acts as the PDE-constraint found in problem (7.3), we look at the more general *obstacle type variational inequality* constraint

$$a(y, v - y) \geq (r_\Gamma, v - y)_{L^2(\mathbb{D})} \quad \forall v \in K := \Big\{ v \in H_0^1(\mathbb{D}) \colon v(x) \leq \psi(x) \text{ in } \mathbb{D} \Big\}. \tag{8.2}$$

Here, $y \in K$ is the solution of the VI, $r_\Gamma \in L^2(\mathbb{D})$ is explicitly dependent on the shape. Moreover, $a(\cdot, \cdot)$ is a general strongly elliptic, i.e. coercive and symmetric bilinear form

$$\begin{aligned} a \colon H_0^1(\mathbb{D}) \times H_0^1(\mathbb{D}) &\to \mathbb{R} \\ (y, v) &\mapsto \int_{\mathbb{D}} \sum_{i,j} a_{i,j} \partial_i y \partial_j v + \sum_i d_i \big(\partial_i y v + y \partial_i v \big) + byv \, \mathrm{d}x, \end{aligned} \tag{8.3}$$

defined by coefficient functions $a_{i,j}, d_j, b \in L^\infty(\mathbb{D})$, fulfilling the weak maximum principle. Notice, that the results of this chapter still remain correct if symmetry of $a(\cdot, \cdot)$ is dropped as an assumption by modifications of proofs.

With the tracking-type objective $\mathcal{J}$, the shape Γ is fitted to data measurements $\bar{y} \in H^1(\mathbb{D})$ by its relation to the state solution y through the source term r_Γ. As in section 7.1, the second term $\mathcal{J}^{\text{Perim}}$ in the objective function is a perimeter regularization, which can serve as a regularization to ill-posedness of geometric inverse problems.

In variational inequality (8.2), ψ is denoted as the obstacle. It needs to be an element of $L^1_{\text{loc}}(\mathbb{D})$, such that the set of admissible functions K is nonempty

(cf. [168]). If additionally $\partial\mathbb{D}$ is Lipschitz, and $\psi \in H^1(\mathbb{D})$ with $\psi_{|\partial\mathbb{D}} \geq 0$, then there is a unique solution to variational inequality (8.2) satisfying $y \in H_0^1(\mathbb{D})$, given that the assumptions from above hold (cf. [93, 103, 176]). Further, variational inequality (8.2) can be equivalently expressed as

$$a(y,v) + (\lambda, v)_{L^2(\mathbb{D})} = (r_\Gamma, v)_{L^2(\mathbb{D})} \qquad \forall v \in H_0^1(\mathbb{D}) \tag{8.4}$$

$$\begin{aligned} \lambda &\geq 0 \qquad \text{in } \mathbb{D} \\ y &\leq \psi \qquad \text{in } \mathbb{D} \\ \lambda(y-\psi) &= 0 \qquad \text{in } \mathbb{D} \end{aligned} \tag{8.5}$$

for a $\lambda \in L^2(\mathbb{D})$.

An essential theoretical tool for the study of existence of solutions is the derivation of optimality conditions, which often rely on the formulation of an adjoint equation. For shape optimization problems constrained by VIs, this is an issue, since it is not guaranteed that an adjoint state can be introduced in general (cf. [168, Example in Ch. 1, Ch. 4]). Therefore we first investigate the model problem analytically in section 8.2, also in view of formulating a numerically applicable algorithm in section 8.4.

8.2 Regularized State and Adjoint Equations

We assume the situation of section 8.1, which is also found in [94], giving us $\lambda \in L^2(\mathbb{D})$. This in turn gives the possibility to summarize the complementarity conditions (8.5) equivalently into a single condition of the form

$$\lambda = \max\big(0, \lambda + c\cdot(y-\psi)\big) \qquad \text{for arbitrary } c > 0. \tag{8.6}$$

The direct handling of general obstacle-type variational inequalities formulated as in (8.4)-(8.5), with conditions (8.5) being equivalently substituted by equation (8.6), poses several challenges. One challenge to solve equation (8.4) is the occurrence of distributional numerical iterates for λ in $H^{-1}(\mathbb{D})$ when an augmented Lagrangian approach is applied to equation (8.4) constrained by equation (8.6), despite the analytical solution λ having L^2-regularity. For a more detailed discussion of this, see [94, p. 2]. In order to circumvent the occurrence of distributions in the solution scheme, the authors of [93, 94] introduce a relaxation for relation (8.6) with a given regularization parameter $\alpha \in (0,1)$

$$\lambda = \alpha\cdot\max\big(0, \lambda + \varrho\cdot(y-\psi)\big) \qquad \text{for arbitrary } \varrho > 0.$$

This in turn is equivalent to

$$\lambda = \max\big(0, \bar{\lambda} + c\cdot(y-\psi)\big),$$

if $\bar{\lambda} = 0$ and $c = \frac{\varrho\cdot\alpha}{1-\alpha} \in (0,\infty)$. Here, $\bar{\lambda} \in L^2(\mathbb{D})$ can be motivated by updates of the augmented Lagrangian. The result is equation

$$a\big(y_c, v\big) + \Big(\max\big(0, \bar{\lambda} + c\cdot(y_c-\psi)\big), v\Big)_{L^2(\mathbb{D})} = \big(r_\Gamma, v\big)_{L^2(\mathbb{D})} \qquad \forall v \in H_0^1(\mathbb{D}), \tag{8.7}$$

which in the following is called *regularized state equation*. Explicit dependence on λ is avoided, making the resulting semilinear elliptic equation tractable, for example by semi-smooth Newton methods (cf. [94]). Moreover, the authors of [94] prove L^2-convergence of the regularized multiplier $\max\big(0, \bar{\lambda} + c\cdot(y_c-\psi)\big)$ to the original λ for their proposed semi-smooth Newton method.

With problem (8.7), we are still left to solve a nonlinear semi-smooth problem. This still gives rise to problems concerning existence of adjoints for the shape optimization problem. Smoothing strategies can be applied to render this problem regular enough to show existence of adjoints. In light of [152] and [35], we pose the following assumptions on the smoothed max-function, which from now on is called $\max_\gamma\colon \mathbb{R} \to [0,\infty)$, with respect to the smoothing parameter $\gamma > 0$.

Assumption 1 (Smoothed max-Function)**.**

(i) $\max_\gamma \in C^1(\mathbb{R}, [0,\infty))$ *for all* $\gamma > 0$

(ii) *there exists a function* $g\colon (0,\infty) \to [0,\infty)$ *with* $g(\gamma) \to 0$ *as* $\gamma \to \infty$*, such that* $|\max_\gamma(x) - \max(0,x)| \leq g(\gamma)$ *for all* $x \in \mathbb{R}$ *and for all* $\gamma > 0$

(iii) $\max'_\gamma(x) \in [0,1]$ *and monotonically nondecreasing for all* $x \in \mathbb{R}$ *and all* $\gamma > 0$

(iv) $\max'_\gamma$ *converges uniformly to* 0 *on* $(-\infty, -\delta)$ *and to* 1 *on* (δ,∞) *for all* $\delta > 0$ *for* $\gamma \to \infty$*.*

To stay consistent with published literature [122], we denote by $\operatorname{sign}_\gamma$ the derivative of $\max_\gamma$ in the following. Notice that this is a slight misnomer, since the function $\operatorname{sign}_\gamma$ resembles the Heaviside function more than the actual sign function. An example satisfying assumptions (1) is given in equation (8.57) of the numerical section 8.4. Applying $\max_\gamma$ instead of max in equation (8.7) gives

$$a\big(y_{\gamma,c}, v\big) + \Big(\max\nolimits_\gamma\big(\bar\lambda + c\cdot(y_{\gamma,c} - \psi)\big), v\Big)_{L^2(\mathbb{D})} = \big(r_\Gamma, v\big)_{L^2(\mathbb{D})} \qquad \forall v \in H_0^1(\mathbb{D}), \tag{8.8}$$

which we call *fully regularized state equation* in the subsequent sections. Linearizing the corresponding Lagrangian with respect to $y_{\gamma,c}$ results in the typical adjoint equation (cf. [80, 152] in the context of optimal control)

$$\begin{aligned} &a\big(p_{\gamma,c}, v\big) + c\cdot\Big(\operatorname{sign}_\gamma(\bar\lambda + c\cdot(y_{\gamma,c} - \psi))\cdot p_{\gamma,c}, v\Big)_{L^2(\mathbb{D})} \\ &= -\big(y_{\gamma,c} - \bar y, v\big)_{L^2(\mathbb{D})} \qquad \forall v \in H_0^1(\mathbb{D}). \end{aligned} \tag{8.9}$$

As in [152], smoothness of the state equation (8.8) in $y_{\gamma,c}$ guarantees existence of solutions to the linearized equation (8.9) for a given $L^2(\mathbb{D})$-right-hand side, and thus existence of adjoints in the case of the considered tracking-type objective functional (8.1).

Next, we show that solutions of equation (8.8) converge strongly in H^1 to solutions of (8.4)-(8.5) for $\gamma, c \to \infty$. This is proven in [152] for stronger assumptions on the smoothed function $\max_\gamma$ and under $\gamma = c$. Since we rely on the general case $\gamma \neq c$ for the proofs in ongoing discussions, we state an according result. The first part of the following theorem is in analogy to [35, Lem. 4.2]. However, the difference is that we consider general elliptic bilinear forms and, more importantly, a modified argument in the maximum function resulting in different regularized state equations. These generalizations are necessary for our further analytical investigations leading to a limit of the adjoint equations.

Proposition 5 (Existence and H^1-Convergence of Regularized States)**.** *Consider a bounded and open domain* $\mathbb{D} \subset \mathbb{R}^{n+1}$ *with Lipschitz boundary. Assume* $a(\cdot,\cdot)$ *to be an elliptic bilinear form as in* (8.3)*. Let* $r_\Gamma \in L^2(\mathbb{D})$ *and* $\gamma, c > 0$*. Moreover, assume* $\psi \in H^1(\mathbb{D})$*,* $\bar\lambda \in L^2(\mathbb{D})$ *and let* $\max_\gamma\colon \mathbb{R} \to \mathbb{R}$ *satisfy assumption 1. Let* $y_{\gamma,c}$*,* y_c *and* y *be solutions to equation* (8.8)*, equation* (8.7) *and equation* (8.4)-(8.5)*, respectively.*

Then equation (8.8) *and equation* (8.7) *possess unique solutions, satisfying*

$$y_{\gamma,c} \to y_c \text{ in } H^1(\mathbb{D}) \quad \text{for } \gamma \to \infty \tag{8.10}$$

and

$$y_c \to y \text{ in } H^1(\mathbb{D}) \quad \text{for } c \to \infty. \tag{8.11}$$

Proof. We prove statement (8.10) of the theorem. For a proof of statement (8.11), we refer to [94, Thm. 3.1].

We start by ensuring the existence of solutions to equation (8.8) and equation (8.7). For this, we show that the Nemetskii-operator defined by

$$\Phi_\gamma \colon H^1(\mathbb{D}) \to L^2(\mathbb{D}), \;\; y \mapsto \max\nolimits_\gamma\big(\bar{\lambda} + c \cdot (y - \psi)\big) \tag{8.12}$$

is a monotone operator for all $\gamma, c > 0$. Due to assumption 1, it is clear that $\max_\gamma \colon \mathbb{R} \to \mathbb{R}$ is a point-wise monotone function, implying that $\max_\gamma \colon L^2(\mathbb{D}) \to L^2(\mathbb{D}), \;\; y \mapsto \max_\gamma(y)$ is a monotone operator (cf. definition 8). Since

$$\Psi_c \colon H^1(\mathbb{D}) \to L^2(\mathbb{D}), \;\; y \mapsto \bar{\lambda} + c \cdot (y - \psi)$$

is an affine linear operator, and thus monotone, the composition $\max_\gamma \circ \Psi_c = \Phi_\gamma$ is also monotone. The same argument holds for the non-smoothed operator

$$\Phi \colon H^1(\mathbb{D}) \to L^2(\mathbb{D}), \;\; y \mapsto \max\big(0, \bar{\lambda} + c \cdot (y - \psi)\big).$$

Since the bilinear form $a(\cdot,\cdot)$ is strongly elliptic by assumption, its corresponding operator mapping $H^1(\mathbb{D}) \to H^{-1}(\mathbb{D})$ is strictly monotone. Therefore, we can apply the Browder-Minty theorem 2, which yields the existence of unique solutions to equation (8.8) and equation (8.7) in $H^1(\mathbb{D})$ for all $r_\Gamma \in L^2(\mathbb{D})$.

Next, we prove the second convergence (8.10). For fixed $c > 0$, let $y_{\gamma,c}$ and y_c be solutions to equation (8.8) and equation (8.7), respectively. Assumption 1 (ii), together with the monotonicity of Φ, the coercivity of $a(\cdot,\cdot)$ with constant $K > 0$, and $y_{\gamma,c} - y_c \in H^1(\mathbb{D})$ acting as a test-function, yield

$$\begin{aligned}
0 &\leq K \cdot ||y_{\gamma,c} - y_c||^2_{H^1(\mathbb{D})} \\
&\leq a(y_{\gamma,c} - y_c, y_{\gamma,c} - y_c) \\
&\leq a(y_{\gamma,c} - y_c, y_{\gamma,c} - y_c) \\
&\quad + \Big(\max\big(0, \bar{\lambda} + c \cdot (y_{\gamma,c} - \psi)\big) - \max\big(0, \bar{\lambda} + c \cdot (y_c - \psi)\big), y_{\gamma,c} - y_c\Big)_{L^2(\mathbb{D})} \\
&= \Big(\max\big(0, \bar{\lambda} + c \cdot (y_{\gamma,c} - \psi)\big) - \max\nolimits_\gamma\big(\bar{\lambda} + c \cdot (y_{\gamma,c} - \psi)\big), y_{\gamma,c} - y_c\Big)_{L^2(\mathbb{D})} \\
&\leq \int_{\mathbb{D}} \Big|\max\big(0, \bar{\lambda} + c \cdot (y_{\gamma,c} - \psi)\big) - \max\nolimits_\gamma\big(\bar{\lambda} + c \cdot (y_{\gamma,c} - \psi)\big)\Big| \cdot |y_{\gamma,c} - y_c| \, \mathrm{d}x \\
&\leq g(\gamma) \cdot \mathrm{vol}(\mathbb{D})^{\frac{1}{2}} \cdot ||y_{\gamma,c} - y_c||_{H^1(\mathbb{D})},
\end{aligned}$$

which gives the desired convergence (8.10). □

After the following definition, we formulate the first main theorem of this chapter concerning the convergence of adjoints corresponding to the fully regularized problems. We also characterize the governing equation of the limit object.

Definition 21 (Regularly Decomposable Sets)**.** *Let $\mathbb{D} \subset \mathbb{R}^{n+1}$ be a bounded, open domain with Lipschitz boundary. A set $A \subseteq \mathbb{D}$ is called* regularly decomposable*, if there exists an $N \in \mathbb{N}$ and path-connected, bounded and open $A_i \subset \mathbb{D}$ with Lipschitz boundaries ∂A_i, such that $A = \bigsqcup_{i=1}^{N} \bar{A}_i$ is a disjoint union.*

Theorem 18 (Convergence of Adjoints)**.** *Let $\mathbb{D} \subset \mathbb{R}^{n+1}$ for $n \leq 3$ be a bounded and open domain with Lipschitz boundary. Moreover, let the following assumptions be satisfied:*

(i) We have $\psi \in H^1(\mathbb{D})$, $r_\Gamma \in L^2(\mathbb{D})$, $\bar{y} \in H^1(\mathbb{D})$ and coefficient functions $a_{i,j}, d_j, b \in L^\infty(\mathbb{D})$ for equation (8.4)-(8.5)

(ii) the active set $A = \{x \in \mathbb{D} : y - \psi \geq 0\}$ corresponding to equation (8.4)-(8.5) is regularly decomposable

(iii) the sets $A_c := \{x \in \mathbb{D} : \bar{\lambda} + c \cdot (y_c - \psi) \geq 0\}$ are regularly decomposable, and

$$A_c \subseteq A \qquad \forall c > 0, \tag{8.13}$$

where y_c solves the regularized state equation (8.7)

(iv) the following convergence holds:

$$\left\|\operatorname{sign}_\gamma\left(\bar{\lambda}+c\cdot(y_{\gamma,c}-\psi)\right)-\operatorname{sign}\left(\bar{\lambda}+c\cdot(y_c-\psi)\right)\right\|_{L^1(\mathbb{D})} \to 0 \quad \text{for } \gamma \to \infty. \tag{8.14}$$

Then the adjoints $p_{\gamma,c} \to p_c$ converge strongly in $H_0^1(\mathbb{D})$ for $\gamma \to \infty$ for all $c > 0$, where p_c is the solution to

$$a(p_c, v) + c \cdot \int_{\mathbb{D}} \mathbb{1}_{A_c} \cdot p_c \cdot v \, \mathrm{d}x = -\int_{\mathbb{D}} (y_c - \bar{y}) \cdot v \, \mathrm{d}x \qquad \forall v \in H_0^1(\mathbb{D}), \tag{8.15}$$

where $\mathbb{1}_{A_c}$ is the indicator function of A_c. Moreover, there exists $p \in H^{-1}(\mathbb{D})$, which is representable as an H_0^1-function given by the extension of $\tilde{p} \in H_0^1(\mathbb{D} \setminus A)$ to $\mathbb{D}$, i.e.

$$p = \begin{cases} \tilde{p} & \text{in } \mathbb{D} \setminus A \\ 0 & \text{in } A, \end{cases} \tag{8.16}$$

where $\tilde{p} \in H_0^1(\mathbb{D} \setminus A)$ is the solution of the elliptic problem

$$a_{\mathbb{D}\setminus A}(\tilde{p}, v) = -\int_{\mathbb{D}\setminus A} (y - \bar{y}) \cdot v \, \mathrm{d}x \qquad \forall v \in H_0^1(\mathbb{D} \setminus A), \tag{8.17}$$

with

$$\begin{aligned} a_{\mathbb{D}\setminus A} &\colon H_0^1(\mathbb{D} \setminus A) \times H_0^1(\mathbb{D} \setminus A) \to \mathbb{R} \\ &(\tilde{p}, v) \mapsto \int_{\mathbb{D}\setminus A} \sum_{i,j} a_{i,j} \partial_i \tilde{p} \partial_j v + \sum_i d_i (\partial_i \tilde{p} v + \tilde{p} \partial_i v) + b \tilde{p} v \, \mathrm{d}x \end{aligned} \tag{8.18}$$

being the restriction of bilinear form $a(\cdot, \cdot)$ to $\mathbb{D} \setminus A$. The solutions p_c of equation (8.15) converge strongly in $H_0^1(\mathbb{D})$ to the H_0^1-representation of p.

Proof. Let us consider the fully regularized state and adjoint equation (8.8) and (8.9) for $\gamma, c > 0$. Existence and uniqueness of smoothed states $y_{\gamma,c}$ are guaranteed by proposition 5. For the corresponding adjoints $p_{\gamma,c}$, existence and uniqueness are given by application of the Lax-Milgram theorem 1 to equation (8.9).

The proof consists of two main parts. First, we show the H^1-convergence of the smoothed to the non-smoothed regularized adjoint $p_{\gamma,c} \to p_c$ for $\gamma \to \infty$. Secondly, we analyze the limit of PDE (8.15) for $c \to \infty$, and prove that $p_c \to p$ in $H^1(\mathbb{D})$ for $c \to \infty$, where p is defined as in (8.16).

We start to show the H^1-convergence of the smoothed adjoints $p_{\gamma,c} \to p_c$ for $\gamma \to \infty$. The assumption (8.14) of L^1-convergence of $\operatorname{sign}_\gamma(\bar\lambda + c \cdot (y_{\gamma,c} - \psi))$ is equivalent to L^p-convergence for all $p \in [1, \infty)$ in our setting, since

$$\begin{aligned}
&\big\|\operatorname{sign}_\gamma\big(\bar\lambda + c \cdot (y_{\gamma,c} - \psi)\big) - \operatorname{sign}\big(\bar\lambda + c \cdot (y_c - \psi)\big)\big\|_{L^p(\mathbb{D})} \\
&\leq \big\|\operatorname{sign}_\gamma\big(\bar\lambda + c \cdot (y_{\gamma,c} - \psi)\big) - \operatorname{sign}\big(\bar\lambda + c \cdot (y_c - \psi)\big)\big\|^{1/p}_{L^1(\mathbb{D})} \to 0 \quad \text{for } \gamma \to \infty
\end{aligned}$$

by monotony of the integral and assumption 1 (ii)-(iv). Denote by $S_{\gamma,c}\colon H^1_0(\mathbb{D}) \to H^{-1}(\mathbb{D})$ the linear operator corresponding to the left-hand side of the smoothed adjoint equation (8.9), and $S_c\colon H^1(\mathbb{D}) \to H^{-1}(\mathbb{D})$ the one to equation (8.15). We establish convergence of $S_{\gamma,c}$ to S_c in the operator norm.

Since we are in the situation $\mathbb{D} \subset \mathbb{R}^{n+1}$ for $n \leq 3$, we have the following embedding with embedding constant $C > 0$ (cf. [1, Thm. 4.12 Part I, Case C])

$$H^1_0(\mathbb{D}) \hookrightarrow L^4(\mathbb{D}) \quad \text{for } n+1 \leq 4. \tag{8.19}$$

We also apply Hölder's inequality, and use L^p-convergence of $\operatorname{sign}_\gamma(\bar\lambda + c \cdot (y_{\gamma,c} - \psi))$ for $p = 2$, as well as boundedness of $\operatorname{sign}_\gamma$ and sign, which yield

$$\begin{aligned}
&\|S_{\gamma,c} - S_c\|_{\mathrm{op}} \\
&= \sup_{\substack{g \in H^1_0(\mathbb{D}) \\ \|g\|=1}} \sup_{\substack{h \in H^1_0(\mathbb{D}) \\ \|h\|=1}} c \cdot \Big| \Big(\big(\operatorname{sign}_\gamma\big(\bar\lambda + c \cdot (y_{\gamma,c} - \psi)\big) - \operatorname{sign}\big(\bar\lambda + c \cdot (y_c - \psi)\big)\big) \cdot g, h \Big)_{L^2(\mathbb{D})} \Big| \\
&\leq \sup_{\substack{g \in H^1_0(\mathbb{D}) \\ \|g\|=1}} \sup_{\substack{h \in H^1_0(\mathbb{D}) \\ \|h\|=1}} c \cdot \Big\|\operatorname{sign}_\gamma\big(\bar\lambda + c \cdot (y_{\gamma,c} - \psi)\big) - \operatorname{sign}\big(\bar\lambda + c \cdot (y_c - \psi)\big)\Big\|_{L^2(\mathbb{D})} \cdot \|g\|_{L^4(\mathbb{D})} \cdot \|h\|_{L^4(\mathbb{D})} \\
&\leq C^2 \cdot c \cdot \Big\|\operatorname{sign}_\gamma\big(\bar\lambda + c \cdot (y_{\gamma,c} - \psi)\big) - \operatorname{sign}\big(\bar\lambda + c \cdot (y_c - \psi)\big)\Big\|_{L^2(\mathbb{D})} \to 0 \quad \text{for } \gamma \to \infty.
\end{aligned}$$

This is the desired convergence in the operator norm. By continuity of the inversion $\mathcal{I}\colon S \mapsto S^{-1}$ in the domain of invertible and bounded linear operators over non-trivial Banach spaces (cf. [183, p. 237, Standard Example 9]), which is given in our setting, convergence of the solution operators $S^{-1}_{\gamma,c} \to S^{-1}_c$ in operator norm is implied immediately. Combining this with the convergence of $y_{\gamma,c} \to y_c$ in $H^1_0(\mathbb{D})$ established in proposition 5 gives

$$\begin{aligned}
&\|p_{\gamma,c} - p_c\|_{H^1_0(\mathbb{D})} \\
&= \big\| - S^{-1}_{\gamma,c}(y_{\gamma,c} - \bar y) + S^{-1}_c(y_c - \bar y)\big\|_{H^1_0(\mathbb{D})} \\
&\leq \big\|S^{-1}_{\gamma,c}(y_{\gamma,c} - \bar y) - S^{-1}_{\gamma,c}(y_c - \bar y)\big\|_{H^1_0(\mathbb{D})} + \big\|S^{-1}_{\gamma,c}(y_c - \bar y) - S^{-1}_c(y_c - \bar y)\big\|_{H^1_0(\mathbb{D})} \\
&\leq \big\|S^{-1}_{\gamma,c}\big\|_{\mathrm{op}} \big\|y_{\gamma,c} - y_c\big\|_{H^1_0(\mathbb{D})} + \big\|S^{-1}_{\gamma,c} - S^{-1}_c\big\|_{\mathrm{op}} \big\|y_c - \bar y\big\|_{H^1_0(\mathbb{D})} \to 0 \quad \text{for } \gamma \to \infty,
\end{aligned}$$

since $\|S^{-1}_{\gamma,c}\|_{\mathrm{op}}$ can be bounded due to the previously established convergence in operator norms.

Now we move to the second part of the proof, and analyze the limit of PDE (8.15) for $c \to \infty$. We show that $p_c \to p$ in $H^1(\mathbb{D})$ for $c \to \infty$, where p is defined as in (8.16). For this, we notice that our assumption concerning regular decomposability of $A = \{\, x \in \mathbb{D} :\ y - \psi \geq 0 \,\}$ ensures that $\partial A = \{\, x \in \mathbb{D} :\ y - \psi = 0 \,\}$ forms a $C^{0,1}$-manifold embedded in $\mathbb{D}$. This in turn leads to well-definedness of the restricted bilinear form $a_{\mathbb{D}\setminus A}(\cdot,\cdot)$, and the well-posedness of the variational problem (8.17). By application of the Lax-Milgram theorem 1, we have a unique $p \in H^1_0(\mathbb{D})$ as in (8.16). Our next step is to show

$$p_c \to p \quad \text{in } H^1(\mathbb{D}) \quad \text{for } c \to \infty. \tag{8.20}$$

For this, we artificially constrain problem (8.15) to $A \subseteq \mathbb{D}$. Denote by $a_A(\cdot,\cdot)$ the restriction of the bilinear form $a(\cdot,\cdot)$ to $A \subseteq \mathbb{D}$, defined in analogy to (8.18). The corresponding restricted problem becomes

$$a_A\big(p_{c_{|A}}, v\big) + c \cdot \int_A \mathbb{1}_{A_c} \cdot p_{c_{|A}} \cdot v \,\mathrm{d}x = -\int_A (y_c - \bar{y}) \cdot v \,\mathrm{d}x \qquad \forall v \in H_0^1(A), \tag{8.21}$$

with the Dirichlet condition $p_{c_{|A}} = p_c$ on ∂A. Dividing by $c > 0$ gives an equivalent equation, in the sense, that a solution $p_{c_{|A}} \in H^1(A)$ to equation (8.21) also solves

$$\frac{1}{c} \cdot a_A\big(p_{c_{|A}}, v\big) + \int_A \mathbb{1}_{A_c} \cdot p_{c_{|A}} \cdot v \,\mathrm{d}x = -\frac{1}{c} \cdot \int_A (y_c - \bar{y}) \cdot v \,\mathrm{d}x \qquad \forall v \in H_0^1(A). \tag{8.22}$$

The differential operator corresponding to the left-hand side of the equivalent equation (8.22) is given by

$$S_{A,c} \colon H^1(A) \to H^{-1}(A), \;\; p \mapsto \frac{1}{c} \cdot a_A(p, \cdot) + \big(\mathbb{1}_{A_c} \cdot p, \cdot\big)_{L^2(A)}. \tag{8.23}$$

Next, we show that the differential operators $S_{A,c}$ converge in the operator norm $\|\cdot\|_{\mathrm{op}}$ to the limit operator

$$S_A \colon H^1(A) \to H^{-1}(A), \;\; p \mapsto (p, \cdot)_{L^2(A)}. \tag{8.24}$$

Indeed, with assumption (8.13), we see

$$\begin{aligned}
&\|S_{A,c} - S_A\|_{\mathrm{op}} \\
&= \sup_{\substack{g \in H_0^1(A) \\ \|g\|=1}} \sup_{\substack{h \in H_0^1(A) \\ \|h\|=1}} \left| \frac{1}{c} \cdot a_A(g,h) - \int_{A \setminus A_c} g \cdot h \,\mathrm{d}x \right| \\
&\leq \sup_{\substack{g \in H_0^1(A) \\ \|g\|=1}} \sup_{\substack{h \in H_0^1(A) \\ \|h\|=1}} \left(\frac{1}{c} \cdot \Big(\sum_{i,j} \|a_{i,j}\|_{L^\infty(\mathbb{D})} + \sum_j \|d_j\|_{L^\infty(\mathbb{D})} + \|b\|_{L^\infty(\mathbb{D})} \Big) \right. \\
&\qquad\qquad \cdot \|g\|_{H_0^1(A)} \cdot \|h\|_{H_0^1(A)} \\
&\qquad\qquad \left. + \operatorname{vol}(A \setminus A_c)^{\frac{1}{2}} \cdot \|g\|_{L^4(A)} \cdot \|h\|_{L^4(A)} \right) \\
&\leq \frac{1}{c} \cdot \Big(\sum_{i,j} \|a_{i,j}\|_{L^\infty(\mathbb{D})} + \sum_j \|d_j\|_{L^\infty(\mathbb{D})} + \|b\|_{L^\infty(\mathbb{D})} \Big) + C^2 \cdot \operatorname{vol}(A \setminus A_c)^{\frac{1}{2}} \\
&\to 0 \quad \text{for } c \to \infty,
\end{aligned}$$

due to embedding (8.19) and since $\operatorname{vol}(A \setminus A_c) \to 0$ for $c \to \infty$, which would otherwise contradict $y_c \to y$ in $H_0^1(\mathbb{D})$. We can now apply a similar argument as in the first part of the proof, namely the continuity of the inversion operator $\mathcal{I} \colon S \mapsto S^{-1}$. This gives convergence of the solution operators $S_{A,c}^{-1} \to S_A^{-1}$ in $\|\cdot\|_{\mathrm{op}}$. Also notice that we can obtain the sequence of solutions $p_{c_{|A}}$ by solving equivalent equation (8.22) with the corresponding right-hand sides $-\frac{1}{c}(y_c - \bar{y})$, instead of solving the original equation (8.21). We also witness that the right-hand sides converge to 0 in $H^1(\mathbb{D})$ as $c \to \infty$, as y_c is H^1-convergent by proposition 5. We conclude

$$\begin{aligned}
0 \leq \|p_c\|_{H^1(A)} &= \Big\| S_{A,c}^{-1}\Big(-\frac{1}{c} \cdot (y_c - \bar{y}) \Big) \Big\|_{H^1(A)} \\
&\leq \frac{1}{c} \cdot \big\| (S_{A,c}^{-1} - S_A^{-1})(y_c - \bar{y}) \big\|_{H^1(A)} + \frac{1}{c} \cdot \big\| S_A^{-1}(y_c - \bar{y}) \big\|_{H^1(A)} \\
&\leq \frac{1}{c} \cdot \Big(\big\| S_{A,c}^{-1} - S_A^{-1} \big\|_{\mathrm{op}} + \big\| S_A^{-1} \big\|_{\mathrm{op}} \Big) \cdot \big(\|y_c - y\|_{H^1(A)} + \|\bar{y}\|_{H^1(A)} \big) \\
&\to 0 \quad \text{for } c \to \infty.
\end{aligned} \tag{8.25}$$

For the proof of convergence it remains to address the convergence of p_c on $\mathbb{D} \setminus A$. We can artificially restrict equation (8.15) to $\mathbb{D} \setminus A$ by imposing the Dirichlet boundary $p_{c|\mathbb{D}\setminus A} = 0$ on ∂A, since ∂A forms a $C^{0,1}$-submanifold of $\mathbb{D}$ by the assumed regular decomposability of the active set A (cf. definition 21). To distinguish the corresponding bilinear forms, we denote the restricted bilinear form by $a_{\mathbb{D}\setminus A}(\cdot,\cdot)$. Since the unrestricted bilinear form $a(\cdot,\cdot)$ is strongly elliptic, coercivity for some constant $K > 0$ also holds for $a_{\mathbb{D}\setminus A}(\cdot,\cdot)$. This, together with Hölder's inequality, assumption $A_c \subseteq A$ for all $c > 0$, and the fact that $p_c - \tilde{p} \in H_0^1(\mathbb{D} \setminus A)$ can act as a test function, gives

$$
\begin{aligned}
0 &\leq K \cdot \|p_c - \tilde{p}\|^2_{H^1(\mathbb{D}\setminus A)} \\
&\leq a_{\mathbb{D}\setminus A}(p_c - \tilde{p}, p_c - \tilde{p}) \\
&= a_{\mathbb{D}\setminus A}(p_c, p_c - \tilde{p}) - a_{\mathbb{D}\setminus A}(\tilde{p}, p_c - \tilde{p}) \\
&= -c \cdot \int_{\mathbb{D}\setminus A} \mathbb{1}_{A_c} \cdot p_c \cdot (p_c - \tilde{p}) \,\mathrm{d}x - \int_{\mathbb{D}\setminus A} (y_c - \bar{y})(p_c - \tilde{p}) \,\mathrm{d}x + \int_{\mathbb{D}\setminus A} (y - \bar{y})(p_c - \tilde{p}) \,\mathrm{d}x \\
&= \int_{\mathbb{D}\setminus A} (y - y_c)(p_c - \tilde{p}) \,\mathrm{d}x \\
&\leq \|y_c - y\|_{H^1(\mathbb{D})} \|p_c - \tilde{p}\|_{H^1(\mathbb{D}\setminus A)},
\end{aligned}
$$

where $\tilde{p} \in H^1(\mathbb{D} \setminus A)$ is defined as in equation (8.17). This results in

$$
p_c \to p \quad \text{in } H_0^1(\mathbb{D} \setminus A) \quad \text{for } c \to \infty \tag{8.26}
$$

due to our assumptions and $y_c \to y$ in $H^1(\mathbb{D})$ by proposition 5. Together with convergence (8.25), this gives the desired convergence $p_c \to p$ in $H_0^1(\mathbb{D})$. □

There are a few non-trivial assumptions in theorem 18, namely assumption (iii) and (iv). In the following, we formulate two remarks in which we address these assumptions (cf. remark 28 for (iii) and remark 29 for (iv)).

Remark 28 (Feasibility for Regularized VI)**.** *It is possible to fulfill assumption* (8.13) *on inclusion of the active sets $A_c \subset A$ by choosing a sufficient $\bar{\lambda} \in L^2(\mathbb{D})$. More precisely, if we assume $\psi \in H^2(\mathbb{D})$, we can choose $\bar{\lambda} := \max(0, r_\Gamma - S\psi)$ with S being the differential operator corresponding to the elliptic bilinear form $a(\cdot,\cdot)$ in (8.4). This guarantees feasibility $y_{c_1} \leq y_{c_2} \leq y \leq \psi$ for all $0 < c_1 \leq c_2$ (cf. [94, Sec. 3.2]).*

Remark 29 (L^1-convergence of sign_γ)**.** *Assumption* (8.14) *ensures that convergence of* sign_γ *is compatible with convergence of $y_{\gamma,c}$ for $\gamma \to \infty$. We verify this assumption in the numerical section 8.4 for several demonstrative cases. In general, this condition depends intimately on the concrete problem parameters of* (8.4)-(8.5)*, and the smoothing schemes employed to the max-function.*

Remark 30 (Exploiting the Regularized Adjoint Limit Structure)**.** *The limit object $p \in H_0^1(\mathbb{D})$ of the adjoints $p_{\gamma,c}$ as defined in* (8.16) *is the solution of an elliptic problem* (8.17) *on a domain $\mathbb{D}\setminus A$ with topological dimension greater than* 0*. This can be exploited in numerical computations, for instance by applying solvers harnessing sparsity, or a fat boundary method for finite elements on domains with holes as proposed in [126].*

Remark 31 (Regularized Adjoint Limit is not an Adjoint)**.** *We remind the reader, that p is not necessarily an adjoint to the original objective* (8.1) *constrained by* (8.4)-(8.5)*. It is merely a limiting object coming from the optimality conditions of the problem with fully regularized constraint* (8.8)*. For a discussion of a similar phenomenon in context of optimal control, we refer the interested reader to [35, Sec. 4.2].*

8.3 Shape Derivatives of Regularized VI-Constrained Problems

In this section, we utilize the established convergence for the regularized state and adjoint equations to derive results on shape derivatives of the shape optimization problem constrained by the fully regularized state equation (8.8). In general, shape derivatives of unregularized VI-constrained shape optimization problems do not exist (cf. [168, Ch. 1.1]). Nevertheless, we can show existence of shape derivatives for the shape optimization problem constrained by the fully regularized VI (8.8), and prove their convergence.

In the following, we split the main results into two theorems. The first theorem 19 discusses the existence and closed form of shape derivatives for the fully regularized problem. The second theorem 20 covers convergence their for $\gamma, c \to \infty$. Note that the objective functional and the shape derivative with respect to the regularized VI (8.8) depend on the parameters γ and c. To denote this dependency, we use the notation $\mathcal{J}_{\gamma,c}$ and $\mathcal{D}\mathcal{J}_{\gamma,c}(\Gamma)$ for the objective functional and its shape derivative, respectively.

Theorem 19 (Shape Derivative of Smoothed VI-Constrained Tracking Type Problems)**.** *Assume the setting of section 8.1. Let the assumptions of theorem 18 hold. Moreover, let* $M := (a_{i,j})_{i,j=1,2,\dots,n+1}$ *be the matrix of coefficient functions to the leading order terms of* $a(\cdot,\cdot)$ *in* (8.3)*. Assume* $y_{\gamma,c}, p_{\gamma,c} \in W^{1,4}(\mathbb{D})$*, and* $a_{ij}, b_i, d \in L^\infty(\mathbb{D}) \cap W^{1,4}(\mathbb{D})$ *and* $\bar{\lambda}, r_\Gamma \in H^1(\mathbb{D})$*. Furthermore, let* $\mathcal{D}_m(y_{\gamma,c}), \mathcal{D}_m(p_{\gamma,c}) \in H^1(\mathbb{D})$ *for all* $\gamma, c > 0$*.*

Then the shape derivative of $\mathcal{J}_{\gamma,c}$ *defined in* (8.1) *constrained by a fully regularized VI* (8.8) *in direction* $V \in H_0^1(\mathbb{D}, \mathbb{R}^{n+1})$ *exists, and is given by*

$$
\begin{aligned}
&\mathcal{D}\mathcal{J}_{\gamma,c}(\Gamma)[V] \\
&= \int_{\mathbb{D}} -\big(y_{\gamma,c} - \bar{y}\big) \cdot \nabla \bar{y}^T V - \nabla y_{\gamma,c}^T \Big(\nabla V \cdot M - \nabla M \cdot V + M \cdot \nabla V^T \Big) \nabla p_{\gamma,c} \\
&\quad + \big(\nabla b^T V\big) \cdot y_{\gamma,c} \cdot p_{\gamma,c} + y_{\gamma,c} \cdot \Big(\big(\nabla d^T V\big)^T \nabla p_{\gamma,c} - d^T \big(\nabla V \nabla p_{\gamma,c}\big) \Big) \\
&\quad + p_{\gamma,c} \cdot \Big(\big(\nabla d^T V\big)^T \nabla y_{\gamma,c} - d^T \big(\nabla V \nabla y_{\gamma,c}\big) \Big) \\
&\quad + \operatorname{sign}_\gamma\big(\bar{\lambda} + c \cdot (y_{\gamma,c} - \psi)\big) \cdot \big(\nabla \bar{\lambda} - c \cdot \nabla \psi\big)^T V \cdot p_{\gamma,c} - \big(\mathcal{D}(r_\Gamma)[V] + \nabla r_\Gamma^T V\big) \cdot p_{\gamma,c} \\
&\quad + \operatorname{div}(V) \cdot \Big(\frac{1}{2}\big(y_{\gamma,c} - \bar{y}\big)^2 + b y_{\gamma,c} p_{\gamma,c} + \sum_{i,j} a_{i,j} \partial_i y_{\gamma,c} \partial_j p_{\gamma,c} \\
&\qquad\qquad + \sum_i d_i \big(\partial_i y_{\gamma,c} p_{\gamma,c} + y_{\gamma,c} \partial_i p_{\gamma,c}\big) \\
&\qquad\qquad + \max\nolimits_\gamma \big(\bar{\lambda} + c \cdot (y_{\gamma,c} - \psi)\big) p_{\gamma,c} - r_\Gamma p_{\gamma,c} \Big) \, \mathrm{d}x \,.
\end{aligned}
\tag{8.27}
$$

Proof. Let us consider the shape optimization problem with objective $\mathcal{J}$ from equation (8.1) constrained by the fully regularized state equation with parameters $\gamma, c > 0$ as in equation (8.8). We fix a shape Γ to derive corresponding shape derivative. The first part of the proof consists of the existence of shape derivatives $\mathcal{D}\mathcal{J}_{\gamma,c}$ for all $\gamma, c > 0$. In the second part, we derive a closed formulation with a material derivative approach.

For the first part of proof, we employ the averaged adjoint theorem 8. Let $\gamma, c > 0$. To use the averaged adjoint approach, we first have to derive a closed form of the shape Lagrangian. By definition, the Lagrangian function corresponding to

our problem is given by

$$\begin{aligned}\mathcal{L}_{\gamma,c}\big(\Gamma, y_{\gamma,c}, p_{\gamma,c}\big) =& \frac{1}{2}\int_{\mathbb{D}} \big(y_{\gamma,c} - \bar{y}\big)^2 \,\mathrm{d}x + a\big(y_{\gamma,c}, p_{\gamma,c}\big) \\ &+ \Big(\max\nolimits_{\gamma}\big(\bar{\lambda} + c\cdot(y_{\gamma,c} - \psi)\big), p_{\gamma,c}\Big)_{L^2(\mathbb{D})} - \big(r_\Gamma, p_{\gamma,c}\big)_{L^2(\mathbb{D})}.\end{aligned} \tag{8.28}$$

Let us fix a deformation vector field V and denote the deformed domains by $\mathbb{D}_t := T_t(\mathbb{D})$ for deformation parameters $t \in [0,\tau]$ and some $\tau > 0$ small enough, such that the corresponding deformations T_t are bijective (cf. equation (3.9)). For the rest of the existence proof, we drop γ, c as the subscripts of $y_{\gamma,c}$ and $p_{\gamma,c}$ for readability purposes, still knowing we are in the fully regularized situation. The shape Lagrangian is given as

$$G\colon [0,\tau]\times H_0^1(\mathbb{D})\times H_0^1(\mathbb{D}) \to \mathbb{R},\ \ (t,y,p)\mapsto \mathcal{L}\big(\Gamma_t, y\circ T_t^{-1}, p\circ T_t^{-1}\big) \tag{8.29}$$

for the deformed domain $\mathbb{D}_t$ and shape Γ_t resulting from application of the deformation T_t in direction V parametrized by $t \in [0,\tau]$ (cf. equation (3.10)). We compute the retraction of the second order terms of the bilinear form $a(\cdot,\cdot)$. Computations for the other terms of the Lagrangian (8.28) follow in analogy. With the transformation formula and equation (3.18), we have

$$\begin{aligned}\int_{\mathbb{D}_t} \nabla\big(y\circ T_t^{-1}\big)^T M \nabla\big(p\circ T_t^{-1}\big)\,\mathrm{d}x &= \int_{\mathbb{D}} \Big(\nabla\big(y\circ T_t^{-1}\big)^T M \nabla\big(p\circ T_t^{-1}\big)\Big)\circ T_t \cdot \det(DT_t)\,\mathrm{d}x \\ &= \int_{\mathbb{D}} \big(DT_t^{-T}\nabla y\big)^T (M\circ T_t)\big(DT_t^{-T}\nabla p\big)\cdot\det(DT_t)\,\mathrm{d}x \\ &= \int_{\mathbb{D}} \nabla y^T \Big(DT_t^{-1}(M\circ T_t)DT_t^{-T}\Big)\nabla p\cdot\det(DT_t)\,\mathrm{d}x.\end{aligned} \tag{8.30}$$

In total, we have the shape Lagrangian

$$\begin{aligned}&G(t,y,p) \\ &= \frac{1}{2}\int_{\mathbb{D}} (y-\bar{y}\circ T_t)^2\cdot\det(DT_t)\,\mathrm{d}x + \int_{\mathbb{D}} \nabla y^T\Big(DT_t^{-1}(M\circ T_t)DT_t^{-T}\Big)\nabla p\cdot\det(DT_t)\,\mathrm{d}x \\ &+ \int_{\mathbb{D}} \Big(\big(DT_t^{-1}(d\circ T_t)\big)^T\nabla y\cdot p + y\cdot\big(DT_t^{-1}(d\circ T_t)\big)^T\nabla p\Big)\cdot\det(DT_t)\,\mathrm{d}x \\ &+ \int_{\mathbb{D}} (b\circ T_t)\cdot y\cdot p\cdot\det(DT_t)\,\mathrm{d}x + \int_{\mathbb{D}} \max\nolimits_{\gamma}\big(\bar{\lambda}\circ T_t + c\cdot(y-\psi\circ T_t)\big)\cdot p\cdot\det(DT_t)\,\mathrm{d}x \\ &- \int_{\mathbb{D}} (r_{\Gamma_t}\circ T_t)\cdot p\cdot\det(DT_t)\,\mathrm{d}x.\end{aligned} \tag{8.31}$$

In the following, we prove the assumptions (H0)-(H3) needed to apply the averaged adjoint theorem 8 to guarantee existence of shape derivatives. The first assumption (H0) concerns well-behavedness of the shape Lagrangian (8.31). First notice that the function in equation (8.31) is both differentiable in the state y and adjoint p. Thus for the set of state solutions $X(t)$ as defined in equation (3.11), we have

$$X(t) = \big\{y^t\big\} \subset H_0^1(\mathbb{D}) \qquad \forall t\in[0,\tau], \tag{8.32}$$

with $y^t := y_t\circ T_t$ being the retraction of the unique solution $y_t \subset H_0^1(\mathbb{D}_t)$ of the fully regularized state equation (8.8) on the deformed domain $\mathbb{D}_t$. The solution exists

and is unique by the use of Minty-Browder's theorem 2 as portrayed in the proof of proposition 5.

Further, the shape Lagrangian for direction V as a function of averaged states inserted

$$[0,1] \to \mathbb{R}, \;\; s \mapsto G\big(t, sy^t + (1-s)y^0, p\big) \tag{8.33}$$

is absolutely continuous in $s \in [0,1]$. For this, we make use of the fact that

$$L^q(\mathbb{D}) \hookrightarrow L^p(\mathbb{D}) \quad \text{for } 1 \le p < q \le \infty \tag{8.34}$$

for bounded $\mathbb{D} \subset \mathbb{R}^{n+1}$, with a constant depending on p and q, which comes by an application of Hölder's inequality. Absolute continuity is satisfied, because we have existing derivatives of the integrand due to assumption 1 (i), and integrability of the integrand due to

$$\begin{aligned}
&\big\|\max\nolimits_\gamma\big(\bar\lambda + c\cdot(z-\psi)\big)\big\|_{L^2(\mathbb{D})} \\
&\le \|\max\nolimits_\gamma\big(\bar\lambda + c\cdot(z-\psi)\big) - \max\big(0, \bar\lambda + c\cdot(z-\psi)\big)\big\|_{L^2(\mathbb{D})} \\
&\quad + \big\|\max\big(0, \bar\lambda + c\cdot(z-\psi)\big)\big\|_{L^2(\mathbb{D})} \\
&\le \mathrm{vol}(\mathbb{D})^{\frac{1}{2}} g(\gamma) + \big\|\bar\lambda\big\|_{L^2(\mathbb{D})} + c\cdot\big(\|z\|_{H_0^1(\mathbb{D})} + \|\psi\|_{H_0^1(\mathbb{D})}\big) < \infty
\end{aligned} \tag{8.35}$$

for all $\bar\lambda \in L^2(\mathbb{D})$ and all $z \in H_0^1(\mathbb{D})$ as by assumption 1 (ii), and $\mathbb{D}$ being bounded. Next, we use that the Jacobian determinants of Lipschitz transformations T_t are uniformly bounded in $t \in [0,\tau]$ by $0 < \bar j < \infty$ (cf. [172, Prop. 2.1]). The directional derivative mapping

$$[0,1] \to \mathbb{R}, \;\; s \mapsto \frac{\partial}{\partial y} G\big(t, sy^t + (1-s)y^0, p; \tilde y\big) \tag{8.36}$$

is therefore integrable for all $\tilde y \in H_0^1(\mathbb{D})$, since

$$\begin{aligned}
&\Big\|\frac{\partial}{\partial y} G\big(t, sy^t + (1-s)y^0, p; \tilde y\big)\Big\|_{L^1(0,1)} \\
&= \int_0^1 \Big| a_t(p,\tilde y) + c\cdot\Big(\mathrm{sign}_\gamma\big(\bar\lambda\circ T_t + c\cdot(sy^t + (1-s)y^0 - \psi\circ T_t)\big)\cdot p\cdot\det(DT_t), \tilde y\Big)_{L^2(\mathbb{D})} \\
&\qquad + \Big(\big(sy^t + (1-s)y^0 - \bar y\circ T_t\big)\cdot\det(DT_t), \tilde y\Big)_{L^2(\mathbb{D})}\Big| \,\mathrm{d}s \\
&\le \int_0^1 B_t\cdot\bar j\cdot\|p\|_{H_0^1(\mathbb{D})}\|\tilde y\|_{H_0^1(\mathbb{D})} + c\cdot\bar j\cdot\|p\|_{H_0^1(\mathbb{D})}\|\tilde y\|_{H_0^1(\mathbb{D})} \\
&\qquad + \bar j\cdot\Big(s\big\|y^t\big\|_{H_0^1(\mathbb{D})} + (1-s)\big\|y^0\big\|_{H_0^1(\mathbb{D})} + \|\bar y\|_{L^2(\mathbb{D})}\Big)\|\tilde y\|_{H_0^1(\mathbb{D})}\,\mathrm{d}s \\
&= \big(B_t + c\big)\cdot\bar j\cdot\|p\|_{H_0^1(\mathbb{D})}\|\tilde y\|_{H_0^1(\mathbb{D})} \\
&\qquad + \bar j\cdot\Big(\frac{1}{2}\big\|y^t\big\|_{H_0^1(\mathbb{D})} + \frac{1}{2}\big\|y^0\big\|_{H_0^1(\mathbb{D})} + \|\bar y\|_{L^2(\mathbb{D})}\Big)\|\tilde y\|_{H_0^1(\mathbb{D})} < \infty
\end{aligned}$$

by Hölder's inequality, assumption 1 (iii), and $a_t(\cdot,\cdot)$ being the bilinear form defined by retraction of $a(\cdot,\cdot)$ from $\mathbb{D}_t$ to $\mathbb{D}$ seen in equation (8.31), which is bound with constants $B_t > 0$. This, and the verification that G is an affine linear function in p, gives us (H0).

Next, we consider the set of averaged adjoints as defined in equation (3.12). We manipulate the averaged adjoint equation found in equation (3.12) by interchanging

integrals

$$
\begin{aligned}
0 &= \int_0^1 \frac{\partial}{\partial y} G\big(t, sy^t + (1-s)y^0, q; \tilde{y}\big)\, \mathrm{d}s \\
&= \int_0^1 a_t(q,\tilde{y}) + c \cdot \Big(\mathrm{sign}_\gamma\big(\bar{\lambda}\circ T_t + c\cdot(sy^t + (1-s)y^0 - \psi\circ T_t)\big)\cdot q \cdot \det(DT_t), \tilde{y}\Big)_{L^2(\mathbb{D})} \\
&\qquad + \Big(\big(sy^t + (1-s)y^0 - \bar{y}\circ T_t\big)\cdot\det(DT_t), \tilde{y}\Big)_{L^2(\mathbb{D})}\, \mathrm{d}s \\
&= a_t(q,\tilde{y}) + c\cdot\Big(\big(\int_0^1 \mathrm{sign}_\gamma\big(\bar{\lambda}\circ T_t + c\cdot(sy^t + (1-s)y^0 - \psi\circ T_t)\big)\,\mathrm{d}s\big)\cdot\det(DT_t)\cdot q, \tilde{y}\Big)_{L^2(\mathbb{D})} \\
&\qquad + \Big(\big(\frac{1}{2}y^t + \frac{1}{2}y^0 - \bar{y}\circ T_t\big)\cdot\det(DT_t), \tilde{y}\Big)_{L^2(\mathbb{D})},
\end{aligned}
\tag{8.37}
$$

which is an elliptic PDE with an additional positive $L^\infty(\mathbb{D})$-coefficient function for the zero'th order terms. By assumption 1 (iii), the additional coefficient term for the zero'th order terms in the averaged adjoint equation (8.37) satisfies

$$
0 \le \int_0^1 \mathrm{sign}_\gamma\big(\bar{\lambda}\circ T_t + c\cdot(sy^t + (1-s)y^0 - \psi\circ T_t)\big)\,\mathrm{d}s \le 1 \qquad \forall t\in[0,\tau], \tag{8.38}
$$

which results in coercivity and boundedness of the corresponding bilinear form of the averaged adjoint equation (8.37). This lets us apply the Lax-Milgram theorem 1, resulting in existence of a unique solution for the averaged adjoint equation, which we denote by $q^t \in H_0^1(\mathbb{D})$ for all $t\in[0,\tau]$. Thus we have the identity $Y(t,y^t,y^0) = \{q^t\} \subset H_0^1(\mathbb{D})$, which together with equation (8.32) ensures condition (H2). We also notice, that the derivatives $\frac{\partial}{\partial t}G$ exist, and can be explicitly calculated after application of the transformation theorem, giving us (H1).

To apply the averaged adjoint theorem 8, it remains to address (H3). We can satisfy this requirement by application of [171, Lem. 4.1]. For this, we mimic parts of the argumentation found in the proof of [171, Thm. 5.1] accustomed to our situation. Consider the solutions $y^0 \in X(0)$ and $q^0 \in Y(0,y^0,y^0)$, and a sequence $(t_n)_{n\in\mathbb{N}} \subset [0,\tau]$ converging to zero. First notice that we can use monotonicity (cf. definition 8) of the Nemetskii operator from equation (8.12) of the concerning semilinear state equation, to get

$$
\Big(\max_\gamma\big(\bar{\lambda}+c\cdot(z-\psi)\big), z\Big)_{L^2(\mathbb{D})} \ge \Big(\max_\gamma\big(\bar{\lambda}-c\cdot\psi\big), z\Big)_{L^2(\mathbb{D})} \qquad \forall z\in L^2(\mathbb{D}). \tag{8.39}
$$

This in turn, together with the coercivity of the retracted bilinearform $a_t(\cdot,\cdot)$ with constant $K_t > 0$, inequality (8.35), and choosing $y^t \in X(t) \subset H_0^1(\mathbb{D})$ as a test function, gives us

$$
\begin{aligned}
0 \le \big\|y^t\big\|^2_{H_0^1(\mathbb{D})} &\le K_t \cdot a_t\big(y^t, y^t\big) \\
&= K_t \cdot \int_{\mathbb{D}} \big(r_{\Gamma_t}\circ T_t\big)\cdot y^t - \max_\gamma\big(\bar{\lambda}\circ T_t + c\cdot(y^t - \psi\circ T_t)\big)\cdot y^t\,\mathrm{d}x \\
&\le K_t \cdot \int_{\mathbb{D}} \big(r_{\Gamma_t}\circ T_t\big)\cdot y^t - \max_\gamma\big(\bar{\lambda}\circ T_t - c\cdot\psi\circ T_t\big)\cdot y^t\,\mathrm{d}x \\
&\le K_t \cdot \Big(\big\|r_{\Gamma_t}\circ T_t\big\|_{L^2(\mathbb{D})} + \big\|\max_\gamma\big(\bar{\lambda}\circ T_t - c\cdot\psi\circ T_t\big)\big\|_{L^2(\mathbb{D})}\Big)\cdot\big\|y^t\big\|_{H_0^1(\mathbb{D})} \\
&\le K_t \cdot \frac{1}{\bar{\jmath}}\cdot\Big(\|r_{\Gamma_t}\|_{L^2(\mathbb{D})} + \big\|\max_\gamma\big(\bar{\lambda}-c\cdot\psi\big)\big\|_{L^2(\mathbb{D})}\Big)\cdot\big\|y^t\big\|_{H_0^1(\mathbb{D})} < \infty,
\end{aligned}
\tag{8.40}
$$

where we used the inversion rule for determinants in the last inequality. Dividing by $\|y^t\|_{H_0^1(\mathbb{D})}$, using the convergence T_t to the identity for $t \to 0$, and by taking a supremum, we achieve

$$\|y^t\|_{H_0^1(\mathbb{D})} \leq \sup_{t\in\{t_n\}} \left(\frac{1}{\bar{j}} \cdot K_t \cdot \left(\|r_{\Gamma_t}\|_{L^2(\mathbb{D})} + \|\max_\gamma(\bar{\lambda} - c\cdot\psi)\|_{L^2(\mathbb{D})} \right) \right) =: \bar{M} < \infty, \tag{8.41}$$

bounding the norms by a constant $0 < \bar{M} < \infty$ independent of $t \in [0,\tau]$, for $\tau > 0$ small enough. In the same line of argumentation we can confirm the boundedness of $\|q^t\|_{H_0^1(\mathbb{D})}$. For this, we apply the first inequality of (8.38) to get

$$\begin{aligned}
0 &\leq \|q^t\|^2_{H_0^1(\mathbb{D})} \leq K_t \cdot a_t(q^t, q^t) \\
&= -K_t \cdot \Bigg(c \cdot \Big(\int_0^1 \operatorname{sign}_\gamma(\bar{\lambda}\circ T_t + c\cdot(sy^t + (1-s)y^0 - \psi\circ T_t))\,\mathrm{d}s \cdot \det(DT_t)\cdot q^t, q^t \Big)_{L^2(\mathbb{D})} \\
&\qquad + \Big((\frac{1}{2}y^t + \frac{1}{2}y^0 - \bar{y}\circ T_t)\cdot\det(DT_t), q^t \Big)_{L^2(\mathbb{D})} \Bigg) \\
&\leq K_t \cdot \Big(\bar{j}\cdot\|y^t\|_{H_0^1(\mathbb{D})} + \bar{j}\cdot\|y^0\|_{H_0^1(\mathbb{D})} + \|\bar{y}\|_{L^2(\mathbb{D})} \Big) \cdot \|q^t\|_{H_0^1(\mathbb{D})}.
\end{aligned}$$

By finally using inequality (8.41), we arrive at

$$\|q^t\|_{H_0^1(\mathbb{D})} \leq \sup_{t\in\{t_n\}} \Big(K_t \cdot \big(\bar{j}\cdot\bar{M} + \bar{j}\cdot\|y^0\|_{H_0^1(\mathbb{D})} + \|\bar{y}\|_{L^2(\mathbb{D})} \big) \Big) < \infty. \tag{8.42}$$

As we have established bound (8.41), the Banach-Alaoglu and Eberlein-Smulian theorems permit us to choose a subsequence $(t_{n_k})_{k\in\mathbb{N}} \subseteq (t_n)_{n\in\mathbb{N}}$, such that $y^{t_{n_k}} \rightharpoonup z$ weakly in $H_0^1(\mathbb{D})$ for $k \to \infty$ and some $z \in H_0^1(\mathbb{D})$. Further, we can uniformly and independently of t_{n_k} bound

$$\begin{aligned}
&\|\max_\gamma(\bar{\lambda}\circ T_t + c\cdot(y^{t_{n_k}} - \psi\circ T_t))\|_{L^2(\mathbb{D})} \\
&\leq \frac{1}{\bar{j}}\cdot\mathrm{vol}(\mathbb{D})^{\frac{1}{2}} g(\gamma) + c\cdot\bar{M} + \frac{1}{\bar{j}}\cdot\|\bar{\lambda}\|_{L^2(\mathbb{D})} + \frac{1}{\bar{j}}\cdot c\cdot\|\psi\|_{L^2(\mathbb{D})} < \infty,
\end{aligned}$$

by using inequalities (8.35) and (8.41). By boundedness of the coercive bilinear forms $a_t(\cdot,\cdot)$, bound (8.41), and smoothness in $\max_\gamma$ by assumption 1 (i), we are able to apply Lebesgue's dominated convergence theorem to the retracted state equations, giving us $y_{t_{n_k}} \rightharpoonup y^0$ weakly in $H_0^1(\mathbb{D})$ due to the uniqueness of solutions in equation (8.32).

Applying the same routine due to bound (8.42), we can choose a subsequence of $\{t_{n_k}\}$, which we again call $\{t_{n_k}\}$ by abuse of notation, such that $q^{t_{n_k}} \rightharpoonup u$ weakly in $H_0^1(\mathbb{D})$ for some $u \in H_0^1(\mathbb{D})$. Then uniform boundedness (8.38), the previously established weak convergence $y_{t_{n_k}} \rightharpoonup y^0$, and bound (8.42), yield applicability of Lebegue's theorem for t_{n_k} inserted in the averaged adjoint equation (8.37). For $k \to \infty$, the limit equation of (8.37) is the fully regularized adjoint equation (8.9), which has a unique solution by Lax-Milgram's theorem 1. Hence $q^{t_{n_k}} \rightharpoonup q^0 = p_{\gamma,c} \in Y(0,y^0,y^0)$ weakly in $H_0^1(\mathbb{D})$ with the previously established weak convergence of $q^{t_{n_k}}$ and continuity of $\operatorname{sign}_\gamma$ by assumption 1 (i).

Now we have found a subsequence $\{t_{n_k}\} \subseteq \{t_n\}$, such that $q^{t_{n_k}} \rightharpoonup q^0$ weakly in $H_0^1(\mathbb{D})$. Using the transformation theorem, the shape Lagrangian $G(t, y^0, q^{t_{n_k}})$ from equation (8.29) can be stated as an integral in $\mathbb{D}$ with integrands that are differentiable in $t \in [0,\tau]$. The derivative $\frac{\partial}{\partial t}G(t, y^0, q^{t_{n_k}})$ is weakly continuous in its first and last argument, hence the weak convergence $q^{t_{n_k}} \rightharpoonup q^0$ implies condition

(H3) from theorem 8. All assumptions (H0)-(H3) for the averaged adjoint theorem 8 are satisfied, finally guaranteeing existence of shape derivatives $\mathcal{D}\mathcal{J}_{\gamma,c}$ for all $\gamma, c > 0$.

Now we move to the second part of the proof, where we derive the closed shape derivative expression. For this, we stay in the context of this work, and apply calculus rules established in chapter 4 (cf. remark 32). Note that equation (8.27) and following integrals are well defined due to our assumptions on integrability combined with (8.19) and dimension $n \leq 4$. By applying corollary 2 to the target functional part of the Lagrangian (8.28) we get

$$\begin{aligned}
&\mathcal{D}\Big(\frac{1}{2}\int_{\mathbb{D}} \big(y_{\gamma,c} - \bar{y}\big)^2 \mathrm{d}x\Big)[V] \\
&= \int_{\mathbb{D}} \big(y_{\gamma,c} - \bar{y}\big)\Big(\mathcal{D}_m\big(y_{\gamma,c}\big)[V] - \mathcal{D}_m(\bar{y})[V]\Big) + \frac{1}{2}\operatorname{div}(V)\big(y_{\gamma,c} - \bar{y}\big)^2 \,\mathrm{d}x \\
&= \int_{\mathbb{D}} \big(y_{\gamma,c} - \bar{y}\big)\mathcal{D}_m\big(y_{\gamma,c}\big)[V] \,\mathrm{d}x + \int_{\mathbb{D}} -\big(y_{\gamma,c} - \bar{y}\big)\nabla\bar{y}^T V + \frac{1}{2}\operatorname{div}(V)\big(y_{\gamma,c} - \bar{y}\big)^2 \,\mathrm{d}x,
\end{aligned} \tag{8.43}$$

since the target $\bar{y} \in L^2(\mathbb{D})$ does not depend on the shape. Next, as similarly found in [181], we calculate the shape derivative of the bilinear form $a(\cdot,\cdot)$. To avoid confusion with the active sets A and A_c, we call the coefficient matrix $(a_{i,j})_{i,j}$ of the leading order parts of the bilinear form M. As before, we have

$$\begin{aligned}
&\mathcal{D}\Big(a\big(y_{\gamma,c}, p_{\gamma,c}\big)\Big)[V] \\
&= \int_{\mathbb{D}} \mathcal{D}_m\Big(\sum_{i,j} a_{i,j}\partial_i y_{\gamma,c}\partial_j p_{\gamma,c} + \sum_i d_i\big(\partial_i y_{\gamma,c} p_{\gamma,c} + y_{\gamma,c}\partial_i p_{\gamma,c}\big) + b y_{\gamma,c} p_{\gamma,c}\Big)[V] \\
&\qquad + \operatorname{div}(V)\Big(\sum_{i,j} a_{i,j}\partial_i y_{\gamma,c}\partial_j p_{\gamma,c} + \sum_i d_i\big(\partial_i y_{\gamma,c} p_{\gamma,c} + y_{\gamma,c}\partial_i p_{\gamma,c}\big) + b y_{\gamma,c} p_{\gamma,c}\Big)\mathrm{d}x.
\end{aligned} \tag{8.44}$$

We use linearity, chain rules, product rules and gradient identities for the material derivative, as found in corollary 1 and corollary 2, to reformulate $\mathcal{D}_m\big(a(y_{\gamma,c}, p_{\gamma,c})\big)$. For readability, we analyze each term individually. We start with the leading order terms, where we in particular use corollary 2 (vi), and that M does not depend on shapes

$$\begin{aligned}
&\mathcal{D}_m\Big(\nabla y_{\gamma,c}^T M \nabla p_{\gamma,c}\Big)[V] \\
&= \nabla\Big(\mathcal{D}_m\big(y_{\gamma,c}\big)[V]\Big)^T M\nabla p_{\gamma,c} - \big(\nabla V^T \nabla y_{\gamma,c}\big)^T M\nabla p_{\gamma,c} + \nabla y_{\gamma,c}^T\big(\nabla M \cdot V\big)\nabla p_{\gamma,c} \\
&\quad + \nabla y_{\gamma,c}^T M \nabla\Big(\mathcal{D}_m\big(p_{\gamma,c}\big)[V]\Big) - \nabla y_{\gamma,c}^T M\big(\nabla V^T \nabla p_{\gamma,c}\big).
\end{aligned}$$

For the first order terms of $a(\cdot,\cdot)$, we only compute $y_{\gamma,c} d^T \nabla p_{\gamma,c}$, since calculations are analogous for the second term by switching the roles of $y_{\gamma,c}$ and $p_{\gamma,c}$. We get

$$\begin{aligned}
&\mathcal{D}_m\big(y_{\gamma,c} d^T \nabla p_{\gamma,c}\big)[V] \\
&= \mathcal{D}_m\big(y_{\gamma,c}\big)[V]\cdot d^T\nabla p_{\gamma,c} + y_{\gamma,c}\big(\nabla d^T V\big)^T\nabla p_{\gamma,c} + y_{\gamma,c} d^T \nabla\mathcal{D}_m\big(p_{\gamma,c}\big)[V] - y_{\gamma,c} d^T\big(\nabla V \nabla p\big),
\end{aligned}$$

where we again use shape independence of the coefficient functions of $a(\cdot,\cdot)$ together with corollary 2. For the term of order zero, we apply the product rule for material derivatives and shape independence of coefficient functions

$$\mathcal{D}_m\big(b y_{\gamma,c} p_{\gamma,c}\big)[V] = \big(\nabla b^T V\big) y_{\gamma,c} p_{\gamma,c} + b\cdot\mathcal{D}_m\big(y_{\gamma,c}\big)[V]\cdot p_{\gamma,c} + b y_{\gamma,c}\cdot\mathcal{D}_m\big(p_{\gamma,c}\big)[V].$$

Combining these formulas by plugging them into equation (8.44), and collecting all material derivatives of $y_{\gamma,c}$ and $p_{\gamma,c}$, result in the shape derivative of the bilinear form

$$
\begin{aligned}
&\mathcal{D}\Big(a\big(y_{\gamma,c}, p_{\gamma,c}\big)\Big)[V] \\
&= a\Big(\mathcal{D}_m\big(y_{\gamma,c}\big)[V], p_{\gamma,c}\Big) + a\Big(y_{\gamma,c}, \mathcal{D}_m\big(p_{\gamma,c}\big)[V]\Big) \\
&\quad - \int_{\mathbb{D}} \nabla y_{\gamma,c}^T \Big(\nabla V \cdot M - \nabla M \cdot V + M \cdot \nabla V^T\Big) \nabla p_{\gamma,c} \\
&\qquad + y_{\gamma,c} \cdot \Big(\big(\nabla d^T V\big)^T \nabla p_{\gamma,c} - d^T\big(\nabla V \nabla p_{\gamma,c}\big)\Big) \\
&\qquad + p_{\gamma,c} \cdot \Big(\big(\nabla d^T V\big)^T \nabla y_{\gamma,c} - d^T\big(\nabla V \nabla y_{\gamma,c}\big)\Big) + \big(\nabla b^T V\big) y_{\gamma,c} p_{\gamma,c} \\
&\qquad + \operatorname{div}(V)\Big(\sum_{i,j} a_{i,j} \partial_i y_{\gamma,c} \partial_j p_{\gamma,c} + \sum_i d_i\big(\partial_i y_{\gamma,c} p_{\gamma,c} + y_{\gamma,c} \partial_i p_{\gamma,c}\big) + b y_{\gamma,c} p_{\gamma,c}\Big) \mathrm{d}x.
\end{aligned}
$$

The shape derivative of the term including $\max_\gamma$ is calculated by chain rule, which is applicable since we have the assumption 1 (i) of a smooth $\max_\gamma$

$$
\begin{aligned}
&\mathcal{D}\Big(\int_{\mathbb{D}} \max\nolimits_\gamma\big(\bar{\lambda} + c \cdot (y_{\gamma,c} - \psi)\big) \cdot p_{\gamma,c} \,\mathrm{d}x\Big)[V] \\
&= \int_{\mathbb{D}} \mathcal{D}_m\Big(\max\nolimits_\gamma\big(\bar{\lambda} + c \cdot (y_{\gamma,c} - \psi)\big) \cdot p_{\gamma,c}\Big)[V] \\
&\qquad + \operatorname{div}(V) \cdot \max\nolimits_\gamma\big(\bar{\lambda} + c \cdot (y_{\gamma,c} - \psi)\big) \cdot p_{\gamma,c} \,\mathrm{d}x \\
&= \int_{\mathbb{D}} \operatorname{sign}_\gamma\big(\bar{\lambda} + c \cdot (y_{\gamma,c} - \psi)\big) \cdot \mathcal{D}_m\big(\bar{\lambda} + c \cdot (y_{\gamma,c} - \psi)\big)[V] \cdot p_{\gamma,c} \\
&\qquad + \max\nolimits_\gamma\big(\bar{\lambda} + c \cdot (y_{\gamma,c} - \psi)\big) \cdot \mathcal{D}_m\big(p_{\gamma,c}\big)[V] \\
&\qquad + \operatorname{div}(V) \cdot \max\nolimits_\gamma\big(\bar{\lambda} + c \cdot (y_{\gamma,c} - \psi)\big) \cdot p_{\gamma,c} \,\mathrm{d}x \\
&= \int_{\mathbb{D}} \operatorname{sign}_\gamma\big(\bar{\lambda} + c \cdot (y_{\gamma,c} - \psi)\big) \cdot \Big(\nabla \bar{\lambda}^T V + c \cdot \big(\mathcal{D}_m(y_{\gamma,c})[V] - \nabla \psi^T V\big)\Big) \cdot p_{\gamma,c} \\
&\qquad + \max\nolimits_\gamma\big(\bar{\lambda} + c \cdot (y_{\gamma,c} - \psi)\big) \cdot \mathcal{D}_m(p_{\gamma,c})[V] \\
&\qquad + \operatorname{div}(V) \cdot \max\nolimits_\gamma\big(\bar{\lambda} + c \cdot (y_{\gamma,c} - \psi)\big) \cdot p_{\gamma,c} \,\mathrm{d}x,
\end{aligned}
$$

where the last equality is due to $\mathcal{D}_m(\bar{\lambda})[V] = \nabla \bar{\lambda}^T V$ and $\mathcal{D}_m(\psi)[V] = \nabla \psi^T V$, as $\bar{\lambda}$ and ψ are invariant under perturbation of the domain by the problem definition. The shape derivative of the last term in the Lagrangian (8.28) is given by a simple product rule

$$
\mathcal{D}\Big(\int_{\mathbb{D}} r_\Gamma \cdot p_{\gamma,c} \,\mathrm{d}x\Big)[V] = \int_{\mathbb{D}} \mathcal{D}_m(r_\Gamma)[V] \cdot p_{\gamma,c} + r_\Gamma \cdot \mathcal{D}_m(p_{\gamma,c})[V] + \operatorname{div}(V) \cdot r_\Gamma \cdot p_{\gamma,c} \,\mathrm{d}x.
$$

We now use the assumptions $\mathcal{D}_m(y_{\gamma,c}), \mathcal{D}_m(p_{\gamma,c}) \in H_0^1(\mathbb{D})$. If we rearrange the terms with $\mathcal{D}_m(y_{\gamma,c})$ and $\mathcal{D}_m(p_{\gamma,c})$, we can let $\mathcal{D}_m(y_{\gamma,c})$ and $\mathcal{D}_m(p_{\gamma,c})$ act as test functions and apply the state equation (8.8) and adjoint equation (8.9). Therefore the terms involving $\mathcal{D}_m(y_{\gamma,c})$ and $\mathcal{D}_m(p_{\gamma,c})$ vanish. By adding the previously calculated shape derivative components of the Lagrangian, the shape derivative $\mathcal{D}\mathcal{J}_{\gamma,c}(\Gamma)[V]$ as in equation (8.27) is established. □

Remark 32 (Averaged Adjoint and Material Derivative Approaches)**.** *We proved the assumptions of the averaged adjoint theorem 8 in the first part of the proof to theorem 19 to have guaranteed existence of shape derivatives. Then we proceeded to calculate the shape derivative using the material derivative approach to stay coherent with the pre-shape calculus rules introduced in chapter 4. However, the averaged*

adjoint theorem 8 permits direct computation of the shape derivative via the shape Lagrangian equation (8.31) *and equation* (3.16)*. More specifically, product and chain rules, and* $\det(DT_0) = 1$*, yield*

$$
\begin{aligned}
&\mathcal{D}\mathcal{J}_{\gamma,c}(\Gamma)[V] \\
&= \frac{\partial}{\partial t} G(0, y_{\gamma,c}, p_{\gamma,c}) \\
&= -\int_{\mathbb{D}} (y_{\gamma,c} - \bar{y}) \cdot \Big(\frac{\partial}{\partial t}_{|t=0} \bar{y} \circ T_t \Big) \,\mathrm{d}x \\
&+ \int_{\mathbb{D}} \nabla y_{\gamma,c}^T \Big(\frac{\partial}{\partial t}_{|t=0} DT_t^{-1}(M \circ T_t) DT_t^{-T} \Big) \nabla p_{\gamma,c} \,\mathrm{d}x \\
&+ \int_{\mathbb{D}} \Big(\Big(\frac{\partial}{\partial t}_{|t=0} DT_t^{-1}(d \circ T_t) \Big)^T \nabla y_{\gamma,c} \cdot p_{\gamma,c} + y_{\gamma,c} \cdot \Big(\frac{\partial}{\partial t}_{|t=0} DT_t^{-1}(d \circ T_t) \Big)^T \nabla p_{\gamma,c} \Big) \,\mathrm{d}x \\
&+ \int_{\mathbb{D}} \Big(\frac{\partial}{\partial t}_{|t=0} b \circ T_t \Big) \cdot y_{\gamma,c} \cdot p_{\gamma,c} \,\mathrm{d}x \\
&+ \int_{\mathbb{D}} \Big(\frac{\partial}{\partial t}_{|t=0} \max\nolimits_\gamma \big(\bar{\lambda} \circ T_t + c \cdot (y_{\gamma,c} - \psi \circ T_t) \big) \Big) \cdot p_{\gamma,c} \,\mathrm{d}x \\
&- \int_{\mathbb{D}} \Big(\frac{\partial}{\partial t}_{|t=0} r_{\Gamma_t} \circ T_t \Big) \cdot p_{\gamma,c} \,\mathrm{d}x \\
&+ \int_{\mathbb{D}} \Big(\frac{\partial}{\partial t}_{|t=0} \det(DT_t) \Big) \cdot \Big(\frac{1}{2} \big(y_{\gamma,c} - \bar{y} \big)^2 + b y_{\gamma,c} p_{\gamma,c} + \sum_{i,j} a_{i,j} \partial_i y_{\gamma,c} \partial_j p_{\gamma,c} \\
&\qquad + \sum_i d_i \big(\partial_i y_{\gamma,c} p_{\gamma,c} + y_{\gamma,c} \partial_i p_{\gamma,c} \big) + \max\nolimits_\gamma \big(\bar{\lambda} + c \cdot (y_{\gamma,c} - \psi) \big) p_{\gamma,c} - r_\Gamma p_{\gamma,c} \Big) \,\mathrm{d}x.
\end{aligned}
\tag{8.45}
$$

By equation (3.9) *and [171, Lem. 2.14], we exemplary have*

$$
\frac{\partial}{\partial t}_{|t=0} DT_t^{-1}(M \circ T_t) DT_t^{-T} = -\nabla V \cdot M + \nabla M \cdot V - M \cdot \nabla V^T, \quad \frac{\partial}{\partial t}_{|t=0} \bar{y} \circ T_t = \nabla \bar{y}^T V.
$$

The other terms follow by analogous computations. Thus, after application of product and chain rules, and Jacobi's formula from proposition 1, equation (8.45) *coincides with the shape derivative* (8.27) *from the material derivative approach. This particularly shows, that the assumptions on material derivatives* $\mathcal{D}_m(y_{\gamma,c}), \mathcal{D}_m(p_{\gamma,c}) \in H_0^1(\mathbb{D})$ *for all* $\gamma, c > 0$ *in theorem 19 are not needed to have the closed shape derivative expression* (8.27)*.*

Remark 33 (H^1-Material Derivatives)**.** *The assumption* $\mathcal{D}_m(y_{\gamma,c}) \in H_0^1(\mathbb{D})$ *and* $\mathcal{D}_m(p_{\gamma,c}) \in H_0^1(\mathbb{D})$ *in theorem 19 are solely needed to apply the material derivative approach to achieve the closed form of the shape derivative.*

To fulfill $\mathcal{D}_m(y_{\gamma,c}) \in H_0^1(\mathbb{D})$*, it is sufficient that* $y_{\gamma,c} \in H_0^2(\mathbb{D})$*. For example, this regularity can be ensured by additionally assuming* $a_{i,j} \in C^1(\overline{\mathbb{D}})$*,* $d = 0$*,* $b = 0$ *for the coefficients of the strongly elliptic bilinear form* $a(\cdot,\cdot)$*, together with* $\psi > 0$ *and choosing* $\bar{\lambda} \in L^\infty(\mathbb{D})$*. The latter two assumptions imply that the maximal monotone Nemetskii-operator* (8.12) *is equal to* 0 *for* $y_{\gamma,c} = 0$ *and sufficiently large* $\gamma, c > 0$*. In combination with the former assumptions, [22, Thm. A.1.] can be applied to get* $y_{\gamma,c} \in H_0^2(\mathbb{D})$ *for all sufficiently large* $\gamma, c > 0$*.*

The assumption $\mathcal{D}_m(p_{\gamma,c}) \in H_0^1(\mathbb{D})$ *in theorem 19 can be fullfilled, e.g., by assuming additional regularity* $a_{i,j} \in C^1(\overline{\mathbb{D}})$ *of the leading coefficients of the bilinear form* $a(\cdot,\cdot)$ *and* C^2*-regularity of the boundary* $\partial\mathbb{D}$*. This, together with the fact that* $c \cdot \mathrm{sign}_\gamma(\bar{\lambda} + c \cdot (y_{\gamma,c} - \psi)) \in L^\infty(\mathbb{D})$ *acts as part of the coefficient function of the zero order terms, permits application of a regularity theorem for linear elliptic problems from [50, p. 317, Thm. 4], which gives* $p_{\gamma,c} \in H_0^2(\mathbb{D})$*. This in turn guarantees* $\mathcal{D}_m(p_{\gamma,c}) \in H_0^1(\mathbb{D})$*.*

Remark 34 (Approaches for Existence of Shape Derivatives)**.** *There are a multiple options to prove shape differentiability of shape functionals, and to derive the shape derivative of a PDE-constrained shape optimization problem. The min-max approach [42, Ch. 10.5] and the theorem of Correa and Seeger [37, Thm. 2.1], the chain rule approach [168], the Lagrange method of Céa [33], and the rearrangement method [95] can be mentioned in this context. To prove existence of shape derivatives $\mathcal{DJ}_{\gamma,c}$ in theorem 19, we relied on the averaged adjoint approach via theorem 8. For a more detailed discussion on this topic, we refer the reader to [171, Ch. 3, Ch. 4].*

Next, we formulate the second main theorem of this section, which states the convergence of the shape derivatives of the fully regularized problem.

Theorem 20 (Convergence of Shape Derivatives of Smoothed VI-Constrained Tracking Type Problems)**.** *Assume the setting of the shape optimization problem formulated in section 8.1. Let the assumptions of theorem 18 hold and let $\psi \in H^2(\mathbb{D})$. Moreover, denote by $M := (a_{i,j})_{i,j=1,2,\dots,n+1}$ be the matrix of coefficient functions to the leading order terms in (8.3).*

Then, for all $V \in H_0^1(\mathbb{D}, \mathbb{R}^{n+1})$, the shape derivatives $\mathcal{DJ}_{\gamma,c}(\mathbb{D})[V]$ from (8.27) *converge to $\mathcal{DJ}(\Gamma)[V]$ for $\gamma, c \to \infty$, where*

$$
\begin{aligned}
\mathcal{DJ}(\Gamma)[V] := \\
\int_{\mathbb{D}} & -\big(y-\bar{y}\big)\cdot\nabla\bar{y}^T V - \nabla y^T\big(\nabla V\cdot M - \nabla M\cdot V + M\cdot\nabla V^T\big)\nabla p \\
& + y\cdot\Big(\big(\nabla d^T V\big)^T\nabla p - d^T\big(\nabla V\nabla p\big)\Big) + p\cdot\Big(\big(\nabla d^T V\big)^T\nabla y - d^T\big(\nabla V\nabla y\big)\Big) \\
& + \big(\nabla b^T V\big)\cdot y\cdot p - \big(\mathcal{D}(r_\Gamma)[V] + \nabla r_\Gamma^T V\big)\cdot p \\
& + \operatorname{div}(V)\cdot\Big(\frac{1}{2}\big(y_{\gamma,c}-\bar{y}\big)^2 + \sum_{i,j} a_{i,j}\partial_i y\partial_j p \\
& + \sum_i d_i\big(\partial_i y p + y\partial_i p\big) + byp - r_\Gamma p\Big)\,\mathrm{d}x + \int_A \big(\psi-\bar{y}\big)\cdot\nabla\psi^T V\,\mathrm{d}x.
\end{aligned}
\tag{8.46}
$$

Proof. We see that (8.27) already resembles (8.46) except for the three terms

$$
T_0(V) := \int_{\mathbb{D}} \operatorname{sign}_\gamma\big(\bar{\lambda} + c\cdot(y_{\gamma,c}-\psi)\big)\cdot\nabla\bar{\lambda}^T V\cdot p_{\gamma,c}\,\mathrm{d}x, \tag{8.47}
$$

$$
T_1(V) := -c\cdot\int_{\mathbb{D}} \operatorname{sign}_\gamma\big(\bar{\lambda} + c\cdot(y_{\gamma,c}-\psi)\big)\cdot\nabla\psi^T V\cdot p_{\gamma,c}\,\mathrm{d}x \tag{8.48}
$$

$$
T_2(V) := \int_{\mathbb{D}} \operatorname{div}(V)\cdot\max_\gamma\big(\bar{\lambda} + c\cdot(y_{\gamma,c}-\psi)\big)\cdot p_{\gamma,c}\,\mathrm{d}x. \tag{8.49}
$$

This means that showing convergence of $\mathcal{DJ}_{\gamma,c}$ is equivalent to convergence of the functionals $T_0, T_1, T_2\colon H_0^1(\mathbb{D}, \mathbb{R}^{n+1}) \to \mathbb{R}$, since all the other terms featured in (8.27) converge due to $p_{\gamma,c} \to p$ and $y_{\gamma,c} \to y$ in $H_0^1(\mathbb{D})$ for $\gamma, c \to \infty$ by proposition 5 and theorem 18. First, we handle convergence of T_0 for $V \in H_0^1(\mathbb{D}, \mathbb{R}^{n+1})$. We have

$$
\begin{aligned}
&\int_{\mathbb{D}} \operatorname{sign}_\gamma\big(\bar{\lambda} + c\cdot(y_{\gamma,c}-\psi)\big)\cdot\nabla\bar{\lambda}^T V\cdot p_{\gamma,c}\,\mathrm{d}x \\
&\to \int_{\mathbb{D}} \operatorname{sign}(\bar{\lambda} + c\cdot(y_c-\psi))\cdot\nabla\bar{\lambda}^T V\cdot p_c\,\mathrm{d}x
\end{aligned}
\tag{8.50}
$$

for $\gamma \to \infty$ with assumption (iv) from theorem 18. With theorem 18 we also have $p_{\gamma,c} \to p$ in $H^1(\mathbb{D})$, and $A_c \subseteq A$ for all $c > 0$, and $p_{|A} = 0$. This, together with

Hölder's inequality, yields

$$\begin{aligned}
&\int_{\mathbb{D}} \left|\operatorname{sign}\big(\bar\lambda + c\cdot(y_c-\psi)\big)\cdot \nabla\bar\lambda^T V\cdot p_c\right| \,\mathrm{d}x\\
&\le \left\|\mathbb{1}_{A_c}\cdot p_c\right\|_{L^2(\mathbb{D})}\cdot\left\|\nabla\bar\lambda^T V\right\|_{L^2(\mathbb{D})}\\
&= \left\|\mathbb{1}_{A_c}\cdot (p_c-p)\right\|_{L^2(\mathbb{D})}\cdot\left\|\nabla\bar\lambda^T V\right\|_{L^2(\mathbb{D})}\\
&\le \left\|p_c-p\right\|_{L^2(\mathbb{D})}\cdot\left\|\nabla\bar\lambda^T V\right\|_{L^2(\mathbb{D})}\to 0 \quad \text{for } c\to\infty,
\end{aligned}$$

which is the convergence of T_0 to 0.

In order to tackle terms T_1 and T_2, we proceed in two steps. First, we show convergence for T_1 and T_2 as restricted operators on $C_0^\infty(\mathbb{D},\mathbb{R}^{n+1})$. Secondly, we show by a continuity argument that convergence can be extended to $H_0^1(\mathbb{D},\mathbb{R}^{n+1})$.

Let $V\in C_0^\infty(\mathbb{D},\mathbb{R}^{n+1})$. By this, and our assumption $\psi\in H^2(\mathbb{D})$, we have $\operatorname{div}(V)\cdot p_{\gamma,c}\in H_0^1(\mathbb{D})$ and $\nabla\psi^T V\in H_0^1(\mathbb{D})$ for all $\gamma,c>0$. This enables us to use these functions as test functions for the state and adjoint equations, which leads to

$$\begin{aligned}
T_1(V) &= -\,c\cdot\int_{\mathbb{D}}\operatorname{sign}_\gamma\big(\bar\lambda+c\cdot(y_{\gamma,c}-\psi)\big)\cdot\nabla\psi^T V\cdot p_{\gamma,c}\,\mathrm{d}x\\
&= a\big(p_{\gamma,c},\nabla\psi^T V\big)+\big(y_{\gamma,c}-\bar y,\nabla\psi^T V\big)_{L^2(\mathbb{D})}\\
&\to a\big(p,\nabla\psi^T V\big)+\big(y-\bar y,\nabla\psi^T V\big)_{L^2(\mathbb{D})} =: \tilde T_1(V)\quad \text{for } \gamma,c\to\infty
\end{aligned}$$

and

$$\begin{aligned}
T_2(V) &= \int_{\mathbb{D}}\operatorname{div}(V)\cdot\max_\gamma\left(\bar\lambda+c\cdot(y_{\gamma,c}-\psi)\right)\cdot p_{\gamma,c}\,\mathrm{d}x\\
&= -\,a\big(y_{\gamma,c},p_{\gamma,c}\cdot\operatorname{div}(V)\big)+\big(r_\Gamma,p_{\gamma,c}\cdot\operatorname{div}(V)\big)_{L^2(\mathbb{D})}\\
&\to -\,a\big(y,p\cdot\operatorname{div}(V)\big)+\big(r_\Gamma,p\cdot\operatorname{div}(V)\big)_{L^2(\mathbb{D})} =: \tilde T_2(V)\quad \text{for } \gamma,c\to\infty
\end{aligned}$$

due to theorem 18 and proposition 5.

Next, we lift the convergence from $V\in C_0^\infty(\mathbb{D},\mathbb{R}^{n+1})$ to $H_0^1(\mathbb{D},\mathbb{R}^{n+1})$ by continuous extension. Since $C_0^\infty(\mathbb{D},\mathbb{R}^{n+1})$ is a dense subspace of $H_0^1(\mathbb{D},\mathbb{R}^{n+1})$, and since the latter is the completion of the former by the $\|\cdot\|_{H_0^1(\mathbb{D},\mathbb{R}^{n+1})}$-norm, it is sufficient to show that the limits $\tilde T_1(V_n)$ and $\tilde T_2(V_n)$ form a Cauchy sequence for a given Cauchy sequence $(V_n)_{n\in\mathbb{N}}\subset C_0^\infty(\mathbb{D},\mathbb{R}^{n+1})$ under the $\|\cdot\|_{H_0^1(\mathbb{D},\mathbb{R}^{n+1})}$-norm. So let $(V_n)_{n\in\mathbb{N}}\subset C_0^\infty(\mathbb{D},\mathbb{R}^{n+1})$ with $\|V_n-V_m\|_{H_0^1(\mathbb{D},\mathbb{R}^{n+1})}\to 0$ for $m,n\to\infty$. For the

limit $\tilde{T}_1$ we have

$$
\begin{aligned}
&\big|\tilde{T}_1(V_n) - \tilde{T}_1(V_m)\big| \\
&\quad = \big|a\big(p, \nabla\psi^T(V_n - V_m)\big) + \big(y - \bar{y}, \nabla\psi^T(V_n - V_m)\big)_{L^2(\mathbb{D})}\big| \\
&\quad \le \Big(\sum_{i,j}\|a_{i,j}\|_{L^\infty(\mathbb{D})} + \sum_j \|d_j\|_{L^\infty(\mathbb{D})} + \|b\|_{L^\infty(\mathbb{D})}\Big) \\
&\qquad \cdot \Big| \int_{\mathbb{D}} \sum_{i,j} \partial_i p \cdot \partial_j\big(\nabla\psi^T(V_n - V_m)\big) \\
&\qquad\quad + \sum_i \Big(\partial_i p \cdot \nabla\psi^T(V_n - V_m) + p \cdot \partial_i\big(\nabla\psi^T(V_n - V_m)\big)\Big) \\
&\qquad\quad + p \cdot \nabla\psi^T(V_n - V_m)\,\mathrm{d}x\Big| + \int_{\mathbb{D}} \big|(y - \bar{y}) \cdot \nabla\psi^T(V_n - V_m)\big|\,\mathrm{d}x \\
&\quad = \Big(\sum_{i,j}\|a_{i,j}\|_{L^\infty(\mathbb{D})} + \sum_j \|d_j\|_{L^\infty(\mathbb{D})} + \|b\|_{L^\infty(\mathbb{D})}\Big) \\
&\qquad \cdot \Big| \int_{\mathbb{D}} \sum_{i,j} \Big(\partial_i p \cdot \big((\partial_j\nabla\psi)^T(V_n - V_m) + \nabla\psi^T\partial_j(V_n - V_m)\big)\Big) \\
&\qquad\quad + \sum_i \big(\partial_i p \cdot \nabla\psi^T(V_n - V_m) - \partial_i p \cdot \nabla\psi^T(V_n - V_m)\big) \\
&\qquad\quad + p \cdot \nabla\psi^T(V_n - V_m)\,\mathrm{d}x\Big| + \int_{\mathbb{D}} \big|(y - \bar{y}) \cdot \nabla\psi^T(V_n - V_m)\big|\,\mathrm{d}x \\
&\quad \le \Big(\sum_{i,j}\|a_{i,j}\|_{L^\infty(\mathbb{D})} + \sum_j \|d_j\|_{L^\infty(\mathbb{D})} + \|b\|_{L^\infty(\mathbb{D})}\Big) \\
&\qquad \cdot \|p\|_{H_0^1(\mathbb{D})} \cdot C \cdot \Big(\sum_{i,j}\big(\|(\partial_j\nabla\psi)^T(V_n - V_m)\|_{L^1(\mathbb{D})} + \big\|\nabla\psi^T\partial_j(V_n - V_m)\big\|_{L^1(\mathbb{D})}\big) \\
&\qquad\quad + \big\|\nabla\psi^T(V_n - V_m)\big\|_{L^1(\mathbb{D})}\Big) \\
&\qquad + C \cdot \|\psi\|_{H^1(\mathbb{D})} \cdot \|y - \bar{y}\|_{L^2(\mathbb{D})} \cdot \|V_n - V_m\|_{H_0^1(\mathbb{D},\mathbb{R}^{n+1})} \\
&\quad \le C \cdot \Big(\sum_{i,j}\|a_{i,j}\|_{L^\infty(\mathbb{D})} + \sum_j \|d_j\|_{L^\infty(\mathbb{D})} + \|b\|_{L^\infty(\mathbb{D})}\Big) \cdot \|p\|_{H_0^1(\mathbb{D})} \\
&\qquad \cdot \|\psi\|_{H^2(\mathbb{D})} \cdot 16^2 \cdot \|V_n - V_m\|_{H_0^1(\mathbb{D},\mathbb{R}^{n+1})} \\
&\qquad + C \cdot \|\psi\|_{H^1(\mathbb{D})} \cdot \|y - \bar{y}\|_{L^2(\mathbb{D})} \cdot \|V_n - V_m\|_{H_0^1(\mathbb{D},\mathbb{R}^{n+1})} \to 0 \quad \text{for } m, n \to \infty.
\end{aligned}
$$

Here, we used integration by parts together with $p_{|\partial\mathbb{D}} = 0$ and $(V_n - V_m)_{|\partial\mathbb{D}} = 0$. Also, we applied $L^2(\mathbb{D}) \hookrightarrow L^1(\mathbb{D})$ with constant $C > 0$ as in equation (8.34) due to bounded $\mathbb{D}$. Further, because $\mathbb{D} \subset \mathbb{R}^{n+1}$ for $n \le 3$ by assumption, the constant $16 = (n+1)^2$ is the maximal count of summands occuring in the sum over indices i and j. It should not be confused with the running index for V_n. Thus, $(\tilde{T}_1(V_n))_{n\in\mathbb{N}}$ forms a Cauchy sequence, and therefore gives a value for the continuous extension of $\tilde{T}_1$ for the limit of V_n in $H_0^1(\mathbb{D}, \mathbb{R}^{n+1})$.

For $\tilde{T}_2$, we use the same techniques, leading to

$$
\begin{aligned}
&\big|\tilde{T}_2(V_n) - \tilde{T}_2(V_m)\big| \\
&\quad = \big| - a\big(y, p \cdot \operatorname{div}(V_n - V_m)\big) + \big(r_\Gamma, p \cdot \operatorname{div}(V_n - V_m)\big)_{L^2(\mathbb{D})}\big| \\
&\quad \le \Big(\sum_{i,j}\|a_{i,j}\|_{L^\infty(\mathbb{D})} + \sum_j \|d_j\|_{L^\infty(\mathbb{D})} + \|b\|_{L^\infty(\mathbb{D})}\Big) \\
&\qquad \cdot 17 \cdot C \cdot \|y\|_{H_0^1(\mathbb{D})} \cdot \|p\|_{H_0^1(\mathbb{D})} \cdot \|V_n - V_m\|_{H_0^1(\mathbb{D},\mathbb{R}^{n+1})} \\
&\qquad + C \cdot \|r_\Gamma\|_{L^2(\mathbb{D})} \cdot \|p\|_{H_0^1(\mathbb{D})} \cdot \|V_n - V_m\|_{H_0^1(\mathbb{D},\mathbb{R}^{n+1})} \to 0 \quad \text{for } m, n \to \infty.
\end{aligned}
$$

Notice that the constant $17 = 16 + 1$ occurs, because the zero order terms of the bilinear form are added as well. With the established inequalities, we have convergence of T_1 and T_2 to the continuously extended limit objects, which we from now on denote by T_1 and T_2, for all $V \in H_0^1(\mathbb{D}, \mathbb{R}^{n+1})$. Next, we simplify the sum of these two limiting objects. Let $V \in C_0^\infty(\mathbb{D}, \mathbb{R}^{n+1})$. Then, by applying the state equation and test function property of $p \cdot \operatorname{div}(V)$ to get a term featuring $\lambda \in L^2(\mathbb{D})$, we achieve

$$\begin{aligned}
&T_1(V) + T_2(V) \\
&= a\big(p, \nabla\psi^T V\big) + \big(y - \bar{y}, \nabla\psi^T V\big)_{L^2(\mathbb{D})} \\
&\qquad - a\big(y, p \cdot \operatorname{div}(V)\big) + \big(r_\Gamma, p \cdot \operatorname{div}(V)\big)_{L^2(\mathbb{D})} \\
&= a_{\mathbb{D}\setminus A}\big(p, \nabla\psi^T V\big) + \big(y - \bar{y}, \nabla\psi^T V\big)_{L^2(\mathbb{D}\setminus A)} \\
&\qquad + a_A\big(p, \nabla\psi^T V\big) + \big(y - \bar{y}, \nabla\psi^T V\big)_{L^2(A)} + \big(\lambda, p \cdot \operatorname{div}(V)\big)_{L^2(\mathbb{D})} \\
&= \big(\psi - \bar{y}, \nabla\psi^T V\big)_{L^2(A)}.
\end{aligned} \tag{8.51}$$

In the second to last equation, the first two summands vanish by using test function properties of $\nabla\psi^T V$ and $p \cdot \operatorname{div}(V)$, and the defining equation of p from theorem 18. The third and fifth term in the second to last equation vanish by $p_{|A} = 0$ due to theorem 18, and complementary slackness of $\lambda \in L^2(\mathbb{D})$ and $p \in H^1(\mathbb{D})$. Again, we apply a continuity argument to gain this identity for all $V \in H_0^1(\mathbb{D}, \mathbb{R}^{n+1})$. We see that the limit object in (8.51) is exactly the missing term in the limit of the shape derivatives $\mathcal{DJ}_{\gamma,c}(\Gamma)[V]$ (cf. equation (8.46)). □

Remark 35 (Obstacle Explicitly Depending on Shapes and Jumping Source Terms)**.** *Theorem 19 is also valid when the obstacle $\psi_\Gamma \in H^1(\mathbb{D})$ depends explicitly on the shape Γ. For theorem 20, it is additionally needed to assume $\psi_\Gamma \in H^2(\mathbb{D})$ with shape derivatives $\mathcal{D}(\psi_\Gamma)[V] \in H_0^1(\mathbb{D})$. Weakly differentiable shape derivatives are needed solely for the limiting argument of theorem 20. Then the shape derivatives in equation* (8.27) *and equation* (8.46) *need to be modified accordingly by replacing terms with $\nabla\psi^T V$ by $\mathcal{D}(\psi_\Gamma)[V] + \nabla\psi_\Gamma^T V$. Further, theorem 19 and theorem 20 remain valid for piecewise constant $r_\Gamma \in L^\infty(\mathbb{D})$ depending on the shape $\mathbb{D}$. For this case, the proof can be adjusted by applying integral splitting techniques as found in [181, Rem. 4.21, Thm. 4.23].*

Remark 36 (Recovering Elliptic PDEs for Non-Binding Obstacles)**.** *By pushing the obstacle ψ to infinity, i.e. $\psi(x) \uparrow \infty$ for all $x \in \mathbb{D}$, the state equation representing the variational inequality* (8.4) *becomes a regular elliptic PDE. Its weak formulation is then given by*

$$a(y, v) = \big(r_\Gamma, v\big)_{L^2(\mathbb{D})} \qquad \forall v \in H_0^1(\mathbb{D})$$

due to (8.5)*. This means that we encounter shape optimization problems with elliptic PDE-constraints. Formula* (8.46) *remains valid by applying $A = \varnothing$, giving a shape derivative for a general elliptic problem. In particular, we recover the shape derivative found in equation* (7.16) *of section 7.1.3 as a special case.*

Remark 37 (Limit of Regularized Adjoints and Shape Derivatives as Optimality Systems)**.** *The limiting object* (8.46) *is in general not the shape derivative of the unregularized problem. It can be regarded as part of the limit system arising during convergence of the optimality systems of the fully regularized problem. For readers interested in a treatise on limiting systems of optimality systems in non-smooth optimal control, we recommend [35]. The limiting objects of the convergence results for adjoint variables and shape derivatives from theorem 18 and theorem 20 can*

be put into relation by conditions resembling C-stationarity, e.g., as found in [80, Thm. 2.1] and [81, Def. 4.1].

Using our terminology, C-stationarity-like conditions hold if there is a $\xi \in H^{-1}(\mathbb{D})$*, such that the adjoint equation can be formulated in the form*

$$a(p, v) + \langle \xi, v \rangle_{H^{-1}(\mathbb{D})} = -\big((y - \bar{y}), v\big)_{L^2(\mathbb{D})}. \tag{8.52}$$

We can define such a $\xi \in H^{-1}(\mathbb{D})$ *by emulating the definition of* p *in* (8.16)*, including enforcement of the Dirichlet condition* $p = 0$ *on* ∂A *with Nitsche's method using boundary terms (cf. [100]). The state equation, corresponding complementarity conditions, and the design equation, which in our setting can be viewed as the shape derivative analogue* (8.46)*, hold in analogy to the cited definition of C-stationarity. The remaining conditions*

$$\langle \xi, p \rangle_{H^{-1}(\mathbb{D})} \geq 0 \quad \textit{and} \quad p = 0 \ \textit{ a.e. in } \big\{\xi > 0\big\}, \tag{8.53}$$

by the definitions of ξ *and* p*, are satisfied as well. It is worth mentioning that—to knowledge of the author—no type of C-stationarity-like conditions for optimality of VI-constrained shape optimization problems have been investigated or defined before. Finding a framework for shape optimization to describe the type of these limiting objects and optimality systems can be part of further research, and is beyond the scope of this work.*

8.4 Algorithmic and Numerical Aspects of VI-Constrained Tracking Type Problems

In this section, we put the theoretical treatise from the previous sections into numerical practice. We employ a steepest descent algorithm with backtracking line search, in order to perform optimization procedures with various regularized and unregularized versions of an exemplary variational inequality constraint. Also, we propose a way to incorporate the unregularized approach in an algorithm, and compare it to the different regularizations.

For convenience, we assume $\mathbb{D} \subset \mathbb{R}^2$, and specialize the bilinear form $a(\cdot, \cdot)$ of the more general constraint (8.4) to a Laplacian version similar to chapter 7. The model problem of this section then reads

$$\min_{\Gamma \in B_e^n} \ \frac{1}{2} \int_{\mathbb{D}} |y - \bar{y}|^2 \ \mathrm{d}x + \nu \int_{\Gamma} 1 \ \mathrm{d}s \tag{8.54}$$

$$\begin{aligned} \text{s.t.} \quad \int_{\mathbb{D}} \nabla y^T \nabla v \ \mathrm{d}x + (\lambda, v)_{L^2(\mathbb{D})} &= \int_{\mathbb{D}} r_\Gamma v \ \mathrm{d}x \quad \forall v \in H_0^1(\mathbb{D}) \\ \lambda &\geq 0 \quad \text{in } \mathbb{D} \\ y &\leq \psi \quad \text{in } \mathbb{D} \\ \lambda(y - \psi) &= 0 \quad \text{in } \mathbb{D}. \end{aligned} \tag{8.55}$$

We use $\nu = 10^{-5}$ for all computations in this section. As the right-hand side of the state equation (8.55), we choose a piecewise constant source term $r_\Gamma \in L^\infty(\mathbb{D})$ defined by

$$r_\Gamma(x) = \begin{cases} -10 & \text{for } x \in \overline{\mathbb{D}_\Gamma^{\text{out}}} \\ 100 & \text{for } x \in \mathbb{D}_\Gamma^{\text{in}}. \end{cases} \tag{8.56}$$

In order to calculate the fully regularized state and adjoint, we have to specify a smoothed $\max_\gamma$, which satisfies assumption 1. For demonstrative purpose, we

choose a similar smoothing procedure as in [94, Sec. 2], which is given by

$$\max_\gamma(x) = \begin{cases} \max(0,x) & \text{for } x \in \mathbb{R} \setminus [-\frac{1}{\gamma}, \frac{1}{\gamma}] \\ \frac{\gamma}{4}x^2 + \frac{1}{2}x + \frac{1}{4\gamma} & \text{else.} \end{cases} \tag{8.57}$$

A different and more regular smoothing can be found in [152, Sec. 1]. Both mentioned smoothing techniques satisfy assumption 1. For the sake of completeness, we also give the first derivative formula

$$\operatorname{sign}_\gamma(x) = \begin{cases} 0 & \text{for } x \in (-\infty, -\frac{1}{\gamma}) \\ \frac{\gamma}{2}x + \frac{1}{2} & \text{for } x \in [-\frac{1}{\gamma}, \frac{1}{\gamma}] \\ 1 & \text{for } x \in (\frac{1}{\gamma}, \infty). \end{cases} \tag{8.58}$$

In this setting, the shape derivative limit (8.46) simplifies to

$$\begin{aligned} &\mathcal{D}\mathcal{J}(\Gamma)[V] \\ &= \int_{\mathbb{D}} -(y-\bar{y})\nabla\bar{y}^T V - \nabla y^T(\nabla V + \nabla V^T)\nabla p \\ &\qquad + \operatorname{div}(V)\Big(\frac{1}{2}(y-\bar{y})^2 + \nabla y^T \nabla p - r_\Gamma p\Big)\,\mathrm{d}x + \int_A (\psi - \bar{y})\nabla\psi^T V\,\mathrm{d}x. \end{aligned} \tag{8.59}$$

An analogous formula for the shape derivative (8.27) for the fully regularized equation holds as well. Notice that the shape derivative of the perimeter regularization is also included in our computations (cf. equation (7.18)). We emphasize the similarity of this shape derivative for the variational inequality constraint, and the shape derivative of the elliptic PDE without obstacle found in equation (7.16) of the previous chapter 7.

In the following numerical experiments, we consider two different obstacles

$$\psi_1(x) = 0.5 \quad \text{and} \quad \psi_2(x) = 5e^{-x_1-1}. \tag{8.60}$$

The calculations are performed in Python2.7 using the finite element package FEniCS (cf. [4, 117]). As in previous chapters, meshes are generated via the free meshing software Gmsh (cf. [63]). We choose a circle centered in $(0.5, 0.5)$ with radius 0.15 as the initial shape M. The computational mesh $\overline{\mathbb{D}} = [0,1]^2 \subset \mathbb{R}^2$ consists of 2 184 vertices with 4 206 cells, having a maximum cell diameter of 0.0359 and a minimum cell diameter of 0.018. This situation, including the kidney-like target shape Γ^{targ}, is sketched in figure 8.1. The target data $\bar{y} \in H^1(\mathbb{D})$ is computed by using the mesh of the target interface to calculate a corresponding state solution of equation (8.55) by the semi-smooth Newton method proposed in [94]. These are visualized in figure 8.2 for both obstacles ψ_1 and ψ_2. We apply the same semi-smooth Newton method from [94] to calculate state variables y in the unregularized optimization approach. The algorithm employed for the shape optimization is summarized in algorithm 8.2.

For the regularized and smoothed states $y_{\gamma,c}$ and y_c, we use a Newton and semi-smooth Newton method from the FEniCS library in order to solve the linear systems assembled by using first order continuous Galerkin elements on the computational meshes. All state calculations in our routines are performed with a stopping criterion of $\varepsilon_{\text{state}} = 0.0003$ for the error norms. In light of remark 28, we choose $\bar{\lambda} = \max(0, r_\Gamma + \Delta\psi)$, which is possible due to sufficient regularity of ψ_1 and ψ_2. To ensure assumptions of theorem 18, theorem 19 and theorem 20, it is necessary to fulfill

$$\big\|\operatorname{sign}_\gamma\big(\bar{\lambda} + c\cdot(y_{\gamma,c} - \psi)\big) - \operatorname{sign}\big(\bar{\lambda} + c\cdot(y_c - \psi)\big)\big\|_{L^1(\mathbb{D})} \to 0 \quad \text{for } \gamma \to \infty. \tag{8.61}$$

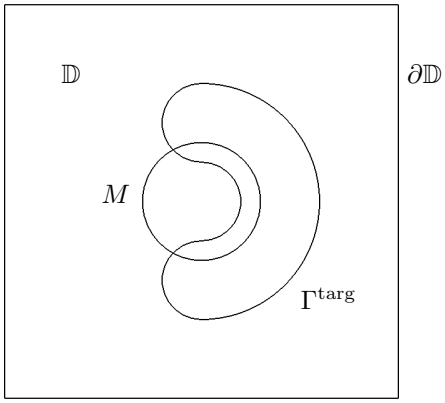

Figure 8.1: Hold-all domain $\mathbb{D} = (0,1)^2$ with boundary $\partial\mathbb{D}$, initial circular shape M and target shape Γ^{targ}.

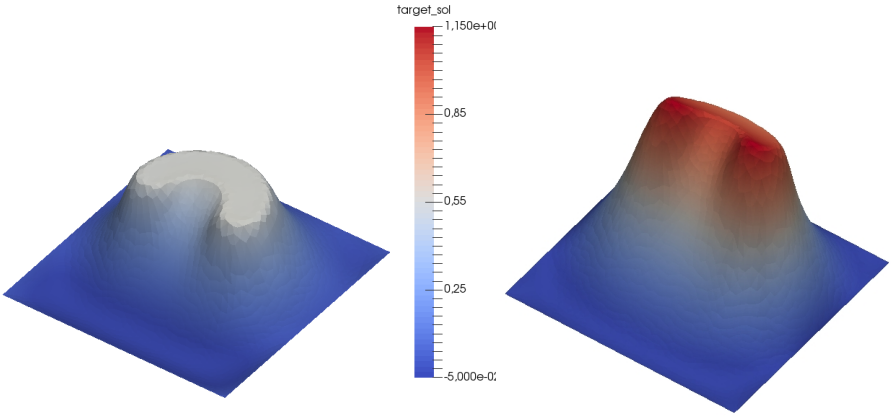

(a) $\bar{y}$ for $\psi_1 = 0.5$ (b) $\bar{y}$ for $\psi_2 = 5e^{-x_1-1}$

Figure 8.2: Solutions $\bar{y}$ to the VI in the target shape.

To numerically verify this assumption, we calculate the corresponding norm using various $c > 0$ for both obstacles ψ_1 and ψ_2, on refined meshes having 212 642 vertices and 423 682 cells, with maximum and minimum cell diameter of 0.0038 and 0.0015, respectively. The resulting convergence plot is found in figure 8.3. We point out that as $\gamma \to \infty$, the norm from (8.61) converges to an $\varepsilon > 0$ close to 0. This is due to numerical errors resulting from the state equation, because the state solution determines the active set, which is needed to calculate the values of sign and sign_γ. The functions, whose L^1-norms are of interest, are illustrated in figure 8.4 on a refined mesh. We observe that these functions, and hence the errors, go to zero for ever finer mesh widths and more precisely calculated states $y_{\gamma,c}$ and y. This is supported by a mesh study, which successively evaluates the mentioned L^1-norms in the circular start shape on meshes generated by adaptive refinement at the boundary of the active set for large $\gamma, c > 0$. The respective results are seen in figure 8.5.

The adjoints $p_{\gamma,c}$ and p_c are calculated by solving equation (8.9) and equation (8.15) with first order continuous elements by using the sparse LU method from PETSc as a FEniCS linear algebra back-end. Calculation of the limit p of the adjoints $p_{\gamma,c}$ as in equation (8.16) and equation (8.17) is performed in several steps.

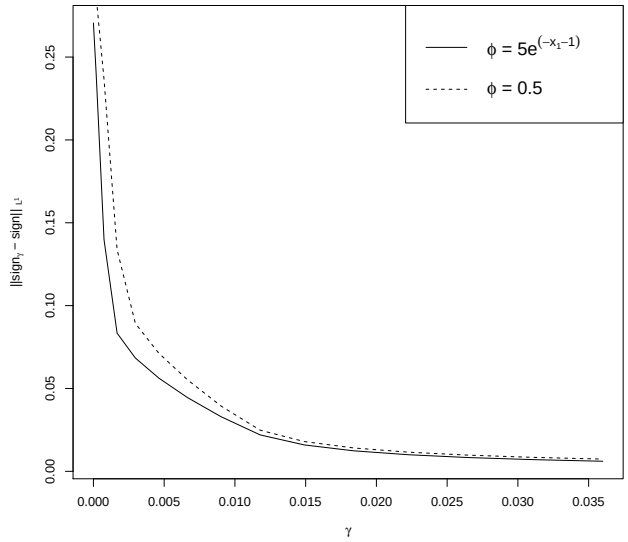

Figure 8.3: Convergence plots for $\|\mathrm{sign}_\gamma(\bar{\lambda}+c\cdot(y_{\gamma,c}-\psi))-\mathrm{sign}(\bar{\lambda}+c\cdot(y_c-\psi))\|_{L^1(\mathbb{D})}$ as a function of γ.

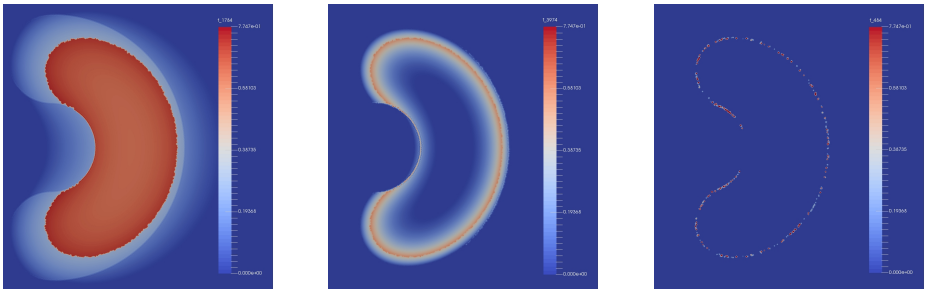

(a) $\gamma = 0.00075$ (b) $\gamma = 0.009$ (c) $\gamma = 10$

Figure 8.4: Graphs of $\mathrm{sign}_\gamma\big(\bar{\lambda} + c \cdot (y_{\gamma,c} - \psi)\big) - \mathrm{sign}\big(\bar{\lambda} + c \cdot (y_c - \psi)\big)$ as functions of $x \in \mathbb{D}$ calculated on the refined target mesh with $c = 1\,000$ and various $\gamma > 0$, indicating its convergence to zero for $\gamma \to \infty$.

First, a linear system corresponding to

$$\begin{aligned} -\Delta p &= -\,(y - \bar{y}) && \text{in } \mathbb{D} \\ p &= 0 && \text{on } \partial\mathbb{D} \end{aligned} \tag{8.62}$$

is assembled without incorporating information from the active set A. Then, the vertex indices corresponding to the points in the active set $A = \{x \in \mathbb{D} :\ y - \psi \geq 0\}$ are collected by checking the condition

$$y(x) - \psi(x) \geq -\varepsilon_{\mathrm{act}} \tag{8.63}$$

for some error tolerance $\varepsilon_{\mathrm{act}} > 0$. The one-sided error bound with $\varepsilon_{\mathrm{act}}$ can be incorporated due to our choice of $\bar{\lambda}$, since y is feasibly approximated by y_i via the semi-smooth Newton method from [94, Sec. 3.2], i.e. $y_i \leq \psi$ for all $i \in \mathbb{N}$ (cf. remark 28). After this, the collected vertex indices are used to incorporate the Dirichlet boundary condition $p = 0$ on the entire active set A into the linear system corresponding to (8.62). To solve the resulting system, we use the same procedures as to solve for $p_{\gamma,c}$ and p_c, i.e. a sparse LU method via PETSc as a linear algebra back-end. An exemplary solution p of the unregularized adjoint equation

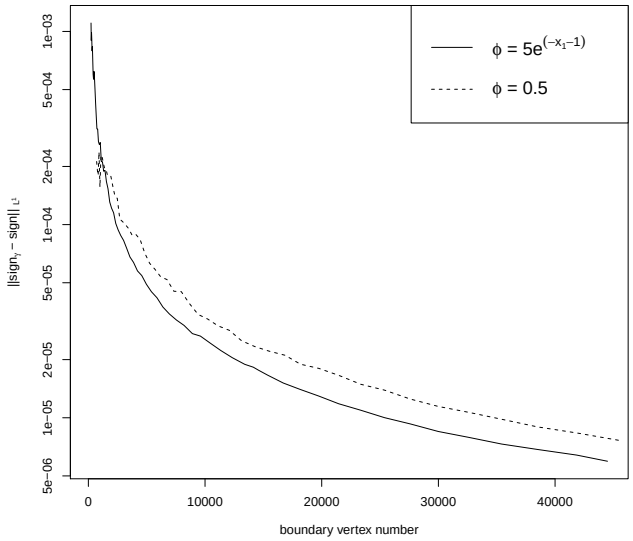

Figure 8.5: Graphs of $\|\mathrm{sign}_\gamma\big(\bar\lambda + c\cdot(y_{\gamma,c}-\psi)\big) - \mathrm{sign}\big(\bar\lambda + c\cdot(y_c-\psi)\big)\|_{L^1(\mathbb{D})}$ as functions of the number of mesh vertices at the boundary ∂A of the active set, calculated on refined meshes with $c = 10^5$, $\gamma = 10^8$.

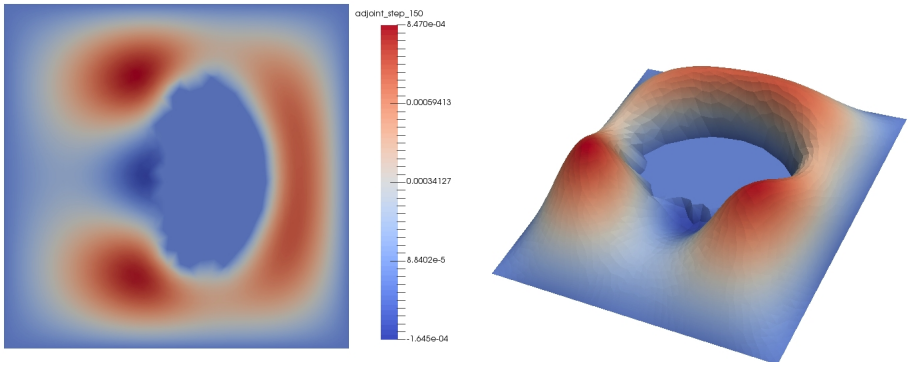

Figure 8.6: Solution of the adjoint p at step 150 for the unregularized equation (8.16) with obstacle $\psi_1 = 0.5$ and $\varepsilon_{\mathrm{act}} = 10^{-9}$.

is illustrated in figure 8.6. We point out that the active set, and consequently the zero level set resulting from the Dirichlet conditions, can be observed in figure 8.6.

To calculate gradients $U \in H_0^1(\mathbb{D},\mathbb{R}^2)$ for for the steepest descent method, we use a Steklov-Poincaré metric induced by the weak linear elasticity equation, as proposed in [161]. More specifically, we assemble the shape derivatives given in theorem 19 and theorem 20 as the right-hand side of the linear elasticity equation introduced in equation (7.13) of section 7.1.3. Here, we choose the Lamé parameters μ as the solution of the Laplace problem (7.15) for $\mu_{\max}, \mu_{\min} > 0$. The same physical interpretation of the Lamé parameter μ via stiffness of the mesh material described in section 7.1.3 applies in this context. For our calculations, we choose $\mu_{\min} = 0.0001$ and $\mu_{\max} = 25$ for ψ_1, and $\mu_{\min} = 0.0001$ and $\mu_{\max} = 55$ for ψ_2. Also, we set all right-hand side values of (7.13), which do not have a neighboring vertex on the shape, to 0. For a more detailed discussion of this stabilization procedure, we refer the reader to [161, 74].

We summarize our approach in algorithm 8.2 for the unregularized procedures, which itself use a simple backtracking line search with sufficient descent criterion

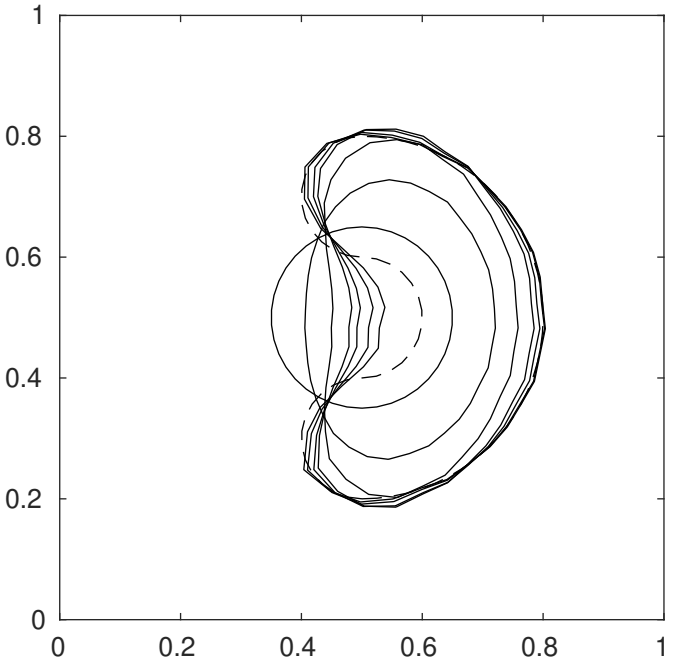

Figure 8.7: Shapes of steps 0, 50, 150, 320, 450, 750, 1200 of the unregularized optimization procedure using $\varepsilon_{\text{act}} = 10^{-3}$ and $\psi_2 = 5e^{-x_1-1}$. The target shape is represented by dotted lines, the starting shape is the centered circle.

$\tilde{U} \leftarrow U_k$
while $\mathcal{J}\big(y_{\tilde{U}}, T_{\tilde{U}}(\Gamma_k)\big) > 0.995 \cdot \mathcal{J}\big(y_k, \Gamma_k\big)$ **do:**
    $\tilde{U} \leftarrow 0.5 \cdot \tilde{U}$
$\mathbb{D}_{k+1} \leftarrow T_{\tilde{U}}(\mathbb{D}_k)$
$\Gamma_{k+1} \leftarrow T_{\tilde{U}}(\Gamma_k)$

Algorithm 8.1: Backtracking line search. U_k denotes the shape gradient calculated at the corresponding shape iterate Γ_k in step number k. $T_{\tilde{U}}(\Gamma_k) := \{y \in \mathbb{R}^2 : \ y = x + \tilde{U}(x) \text{ for some } x \in \Gamma_k\}$ is the deformation via $\tilde{U}$, and $y_{\tilde{U}}$ the state solution for $T_{\tilde{U}}(\Gamma_k)$.

seen in algorithm 8.1. The regularized and smoothed procedures work analogously by modifying the state, adjoint and shape derivative equations. The calculations of $p_{\gamma,c}$ and p_c are straightforward and do neither need the previously discussed additional steps, nor those outlined in algorithm 8.2, for the case of unregularized p. Notice that we employ a safeguarding technique in the design of algorithm 8.2. This stems from the fact, that the limit of shape derivatives $\mathcal{DJ}$ from equation (8.46) is in general not the true shape derivative of the initial problem, see remark 37. Hence, additional checks of the convergence criterion for the fully regularized shape derivative $\mathcal{DJ}_{\gamma,c}$ are performed after convergence by $\mathcal{DJ}$. If no convergence is detected by $\mathcal{DJ}$, the regularized shape derivative $\mathcal{DJ}_{\gamma,c}$ is used to calculate a further descent direction, as the latter is a true shape derivative for the smoothed problem by theorem 19. Further, the safeguarding acts as a safety, when the adjoint limit object p_k is flawed due to erroneous allocation of the active set A_k as discussed with condition (8.63). Since the smoothed model is not prone to this effect, it acts as a substitute model for further gradient calculations.

In our calculations, the safeguard was never activated by not finding a descent

direction during the line search procedure. This indicates that the shape derivative limit $\mathcal{DJ}$ acts as an appropriate shape derivative substitute for our examples, making the safeguard for this purpose obsolete. Still, the safeguarding is activated at convergence for coarse grids or imprecise calculations of the state y_k, indicating a non-neglectable difference in $\|\mathcal{DJ}_{\gamma,c}\|$ and $\|\mathcal{DJ}\|$. In these cases, we witness false allocation of the active set A_k as the cause, resulting in inaccurate p_k and $\|\mathcal{DJ}(\Gamma_k)\|$. However, for meshes with maximum cell diameter 0.01 or less, and error tolerance $\varepsilon_{\text{state}} < 10^{-7}$ for the state calculation, the errors in active set allocation are sufficiently small, which leads to inactiveness of the safeguarding at convergence with $\|\mathcal{DJ}(\Gamma_k)\| \approx \|\mathcal{DJ}_{\gamma,c}(\Gamma_k)\|$.

Set meshes $\mathbb{D}_0, \Gamma_0$ and parameters $\bar{\lambda}, \gamma, c$
while $\|\mathcal{DJ}(\Gamma_k)\| > \varepsilon_{shape}$ **or** $\|\mathcal{DJ}_{\gamma,c}(\Gamma_k)\| > \varepsilon_{shape}$ **do:**
    Calculate state y_k with tolerance $\varepsilon_{\text{state}}$
    Calculate adjoint limit p_k:
        Assemble adjoint system (8.62) neglecting the active set
        Collect vertex indices of the active set by (8.63)
        Implement Dirichlet conditions of the active set
        Solve modified adjoint linear system
    Calculate $\|\mathcal{DJ}(\Gamma_k)\|$ and shape gradient U_k:
        Assemble gradient system (7.13)
        Set $\mathcal{DJ}(\Gamma_k)[V] = 0$ on all vertices without support at interface Γ_k
        Solve for gradient U_k
    Perform backtracking line search algorithm 8.1 to get $\tilde{U}_k$
    if line search fails to give descent direction $\tilde{U}_k$ **or** $\|\mathcal{DJ}(\Gamma_k)\| \leq \varepsilon_{shape}$:
        Calculate fully regularized state $y_{\gamma,c}$
        Calculate fully regularized adjoint $p_{\gamma,c}$
        Calculate $\|\mathcal{DJ}_{\gamma,c}(\Gamma_k)\|$
        if $\|\mathcal{DJ}_{\gamma,c}(\Gamma_k)\| > \varepsilon_{shape}$:
            Calculate fully regularized gradient $U_{\gamma,c}$ by $\mathcal{DJ}_{\gamma,c}(\Gamma_k)$
            Perform backtracking line search algorithm 8.1 with $U_{\gamma,c}$ to get $\tilde{U}_k$
    $\mathbb{D}_{k+1} \leftarrow T_{\tilde{U}_k}(\mathbb{D}_k)$
    $\Gamma_{k+1} \leftarrow T_{\tilde{U}_k}(\Gamma_k)$

Algorithm 8.2: Shape optimization via limit systems for VI-constraints with safeguard strategy.

Our findings concerning convergence of unregularized approaches with various $\varepsilon_{\text{act}} > 0$, as well as regularized approaches with different parameters $\gamma > 0$ and $c > 0$, are displayed in figure 8.8 for obstacle $\psi_1 = 0.5$, and in figure 8.9 for $\psi_2 = 5e^{-x_1-1}$. Morphed shapes arising during the optimization procedure are plotted in figure 8.7 for the unregularized approach using $\varepsilon_{\text{act}} = 10^{-9}$. It can be seen in the plots, that there is a vanishing difference between approaches using fully regularized calculations with sufficiently large γ and c, regularized ones with large c, and the unregularized one. For smaller regularization parameters γ and c, the solved state and adjoint equations begin to differ from the original problem, and thus slow down convergence. For very small γ and c, there is no convergence at all, since regularized problems start to deviate from the original problem.

The convergence behavior of the unregularized method strongly depends on the selection of the active set. When the state solution y is not calculated with sufficient precision, the numerical errors lead to misclassification of vertex indices of the active set A. Hence, wrong Dirichlet conditions are incorporated in the adjoint limit

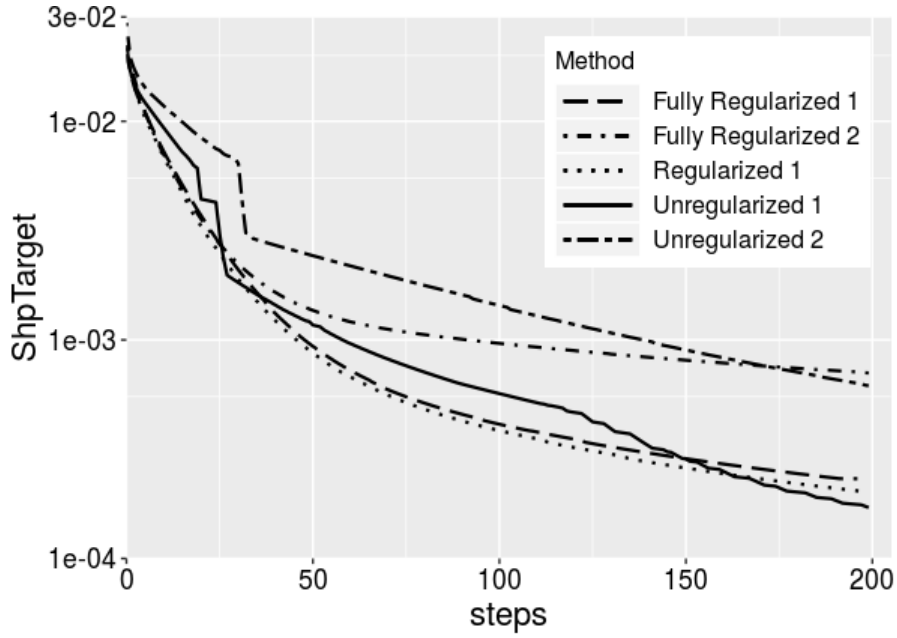

Figure 8.8: Convergence plots of shape objective values $\mathcal{J}(\Gamma_k)$ for different regularized and unregularized approaches for obstacle $\psi_1 = 0.5$ using steepest descents. Unregularized 1: $\varepsilon_{\text{act}} = 10^{-9}$. Unregularized 2: $\varepsilon_{\text{act}} = 10^{-2}$. Regularized 1: $c = 10^4$. Fully Regularized 1: $\gamma = 0.75$ and $c = 10^4$. Fully Regularized 2: $\gamma = 0.3$ and $c = 10^4$.

system, creating errors in the adjoint limit p. This makes the gradient sensitive to error for smaller ε_{act}, as can be seen by the slight roughness of the target graphs in figure 8.8 for $\varepsilon_{\text{act}} = 10^{-9}$. To compensate this, the condition to check for active set indices (8.63) can be relaxed by increasing $\varepsilon_{\text{act}} > 0$. This increases likelihood of correctly classifying the true active indices, while also increasing likelihood of misclassification of inactive indices. Therefore a relaxation can lead to errors in the adjoint increasing with ε_{act}, trading convergence levels for robustness. This is visible in figure 8.8 and figure 8.9. Of course, this strategy gets less feasible for highly oscillatory obstacles ψ with associated states y, as well as state solutions with large error tolerance $\varepsilon_{\text{state}}$. To circumvent this, it is sufficient to simply decrease error tolerance $\varepsilon_{\text{state}}$ of the state calculation. An exemplary result of this is seen in figure 8.9 under Unregularized 1*, where we decreased the error tolerance to $\varepsilon_{\text{state}} = 10^{-5}$. Nevertheless, additional decrease of $\varepsilon_{\text{state}}$ comes with more computational cost, whereas with increase of ε_{act} the robustness is paid by loss of convergence levels and speed.

It is worth to mention, that implementing the unregularized state and adjoint becomes especially numerically exploitable with higher resolution meshes and more strongly binding obstacles ψ, i.e. larger active sets A. This is possible by sparse solvers due to the proposed incorporation of Dirichlet conditions on the active set. An alternative to sparse solvers could be an application of the fat boundary method, as found in [126], to the limiting adjoint system for p from theorem 18. Both strategies are especially advantageous for large systems resulting from fine resolution meshes, as both sparsity of systems, and accuracy of our method increase at the same time. Such implementations could be envisioned as parts of future research.

So in contrast to the method proposed in [57], where performance slows down for more active obstacle ψ, we do not notice unusual slowdown in performance with the methods proposed in this chapter, and instead offer possibility of numerical benefit from more binding obstacle ψ.

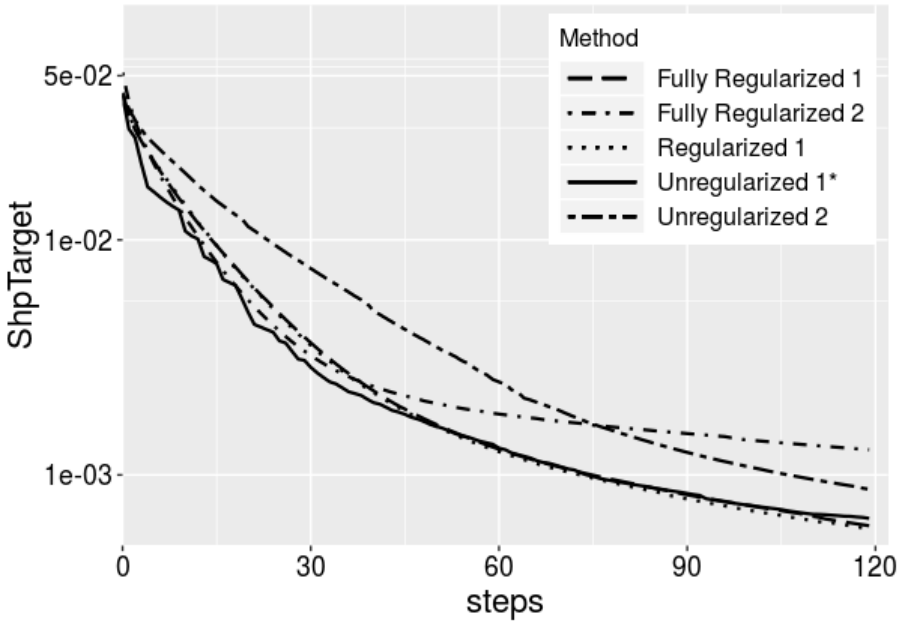

Figure 8.9: Convergence plots of shape objective values $\mathcal{J}(\Gamma_k)$ for different regularized and unregularized approaches for obstacle $\psi_2 = 5e^{-x_1-1}$ using steepest descents. Unregularized 1^*: $\varepsilon_{\text{act}} = 10^{-3}$. Unregularized 2: $\varepsilon_{\text{act}} = 10^{-2}$. Regularized 1: $c = 10^4$. Fully Regularized 1: $\gamma = 0.75$ and $c = 10^4$. Fully Regularized 2: $\gamma = 0.3$ and $c = 10^4$. Unregularized 1^* uses a lower tolerance $\varepsilon_{state} = 10^{-5}$ for the state calculation. Notice that regularized and fully regularized approaches for $\gamma = 0.75$ and $c = 10^4$ are almost indistinguishable.

Chapter 9

Custom Pre-Shape Regularization for VI-Constrained Shape Optimization

In this chapter, we blend and enhance techniques of previous chapters, and apply pre-shape parameterization tracking customized to shape optimization problems constrained by variational inequalities of first kind. In [25], mesh adaptivity strategies for tracking type optimal control problems constrained by elliptic variational inequalities are discussed. We are not aware of such a result in the context of VI-constrained shape optimization. Also, our approach does not build on remeshing or mesh refinement. Instead, we use the pre-shape regularizations from chapter 6 to adapt meshes to the VI solely by the mesh morphing routines during shape optimization. Rather, partial remeshing or refinement strategies can be incorporated in addition to the techniques we highlight in this chapter.

We focus on volume mesh regularization to illustrate the combined approach. Shape mesh quality optimization can be dealt with analogously by using appropriate terms as explained in section 7.1.3. So far, we defined a target cell volume $q^{\mathbb{D}}$ a priori, which gave us a regularization for shape optimization routines as studied in section 7.2. This includes the uniform mesh target as an important special case. However, this does not fully harness the capabilities of the pre-shape parameterization tracking objective $\mathfrak{J}^{\mathbb{D}}$. Its formulation offers the possibility to incorporate further information about desired cell volume allocation via its target $f^{\mathbb{D}}$, or $q^{\mathbb{D}}$ respectively. In particular, we can exploit the structure of underlying shape optimization problems to which mesh quality regularization is applied. We demonstrate this in section 9.1, by designing a target $f^{\mathbb{D}}$ tailored to the VI-constrained tracking type shape optimization problems, which we extensively discussed in chapter 8. Then, in section 9.2, we introduce a second method inspired by the alternating directions method (ADM). It permits us to exploit quasi-Newton methods for pre-shape regularization, and can be applied in addition to simultaneous pre-shape regularization strategies of chapter 6 and chapter 7. Finally, we compare this algorithm with the simultaneous mesh quality and shape optimization algorithm 7.1 from chapter 7.

9.1 Constructing a VI-Specific Cell Volume Target

There are several properties of variational inequalities, which can guide the design process of appropriate meshes for their solution. One such interesting feature is the boundary of the active set ∂A of the VI, as it captures the switching of the state regiment. The active set is of key interest for the case of obstacle problems, particularly for calculation of limiting objects of sensitivities for shape optimization (cf. theorem 18). It is also of interest outside the realm of tracking type objective functionals, e.g. when optimal designs depend on good resolution of the active region in contact problems. Hence we emphasize, that the techniques for mesh quality regularization in this section can be applied to different problem classes by slight modification. In particular, they are not limited to VI-constrained problems.

Following this train of thought, we design a target $f^{\mathbb{D}}$ for the parameterization tracking functional, which enforces a mesh adaptation for higher resolution of the active set boundary ∂A. We construct the target by application of a nonlinear transformation to a signed distance function associated to $\partial A \subset \mathbb{D}$. As we only change the target $f_{\mathbb{D}}$ by this, we can apply all techniques for regularization of gradient systems presented in section 7.1.3. Given an obstacle $\psi > 0$ of sufficient regularity, let us assume we have a solution y to the variational inequality (8.2) or its smoothly regularized problem (8.8). This automatically gives us the active set $A \subset \mathbb{D}$ by checking for the corresponding inequality constraint $y - \psi \geq 0$, or $\bar{\lambda} + c \cdot (y_{\gamma,c} - \psi) \geq 0$ respectively. Since we have numerical solutions for the VI, it is unavoidable to have error in the fulfillment of the constraint imposed by the obstacle. Therefore, we have to construct the numerical active set using a relaxed formulation such as by condition (8.63). The numerical active set is then used to infer the vertices of ∂A. With this, we can calculate a function ϑ, which approximates the signed distance function to the active set boundary ∂A. For some $\varepsilon_{\text{Eik}} > 0$ large enough, we do so by solving a *regularized or stabilized Eikonal equation*

$$\begin{aligned} -\varepsilon_{\text{Eik}} \cdot \Delta\vartheta + |\nabla\vartheta| &= 1 \quad \text{in } \mathbb{D} \\ \vartheta &= 0 \quad \text{on } \partial A. \end{aligned} \tag{9.1}$$

Of course, solving the unregularized Eikonal equation for $\varepsilon_{\text{Eik}} = 0$ is favorable. Several efficient numerical methods, such as the Fast Marching Algorithm, exist for this task, and are compared in [91]. However, we prefer to use the regularized version, since we can more easily integrate it into existing software structures. Existence and uniqueness of solutions $\vartheta \in H^2(\mathbb{D}) \cap H_0^1(\mathbb{D})$ to the regularized Eikonal equation (9.1) can be guaranteed by application of the Banach fix-point theorem for large enough $\varepsilon_{\text{Eik}} > 0$, since the absolute value is Lipschitz continuous (cf. [50, Ch. 9]). In our implementations, we solve the regularized Eikonal equation by using a semi-smooth Newton method. For this, the weak formulation of the regularized Eikonal equation (9.1) is given by

$$\varepsilon_{\text{Eik}} \cdot \int_{\mathbb{D}} \nabla\vartheta^T \nabla v \, \mathrm{d}x + \int_{\mathbb{D}} \sqrt{\nabla\vartheta^T \nabla\vartheta} \cdot v \, \mathrm{d}x = \int_{\mathbb{D}} v \, \mathrm{d}x \qquad \forall v \in H_0^1(\mathbb{D}). \tag{9.2}$$

The first variation of equation (9.2) in direction $\tilde{v} \in H^1(\mathbb{D})$ is given by

$$\varepsilon_{\text{Eik}} \cdot \int_{\mathbb{D}} \nabla\tilde{v}^T \nabla v \, \mathrm{d}x - \int_{\mathbb{D}} \frac{1}{\sqrt{\nabla\vartheta^T \nabla\vartheta}} \cdot \nabla\tilde{v}^T \nabla\vartheta \cdot v \, \mathrm{d}x = 0 \qquad \forall v \in H_0^1(\mathbb{D}). \tag{9.3}$$

As an initial guess for the Newton method, we solve the Poisson problem

$$\begin{aligned} -\varepsilon_{\text{Eik}} \cdot \Delta\vartheta &= 1 \quad \text{in } \mathbb{D} \\ \vartheta &= 0 \quad \text{on } \partial A. \end{aligned} \tag{9.4}$$

For the numerical implementations presented in this chapter, we use a relaxation parameter of 0.5 for the Newton method. Also, we choose the regularization parameter $\varepsilon_{\text{Eik}} = 10 \cdot h^{\mathbb{D}}_{\max}$, where $h^{\mathbb{D}}_{\max}$ is the maximum edge length of the current mesh iterate. An exemplary illustration of a solution to the stabilized Eikonal equation (9.1), featuring the active set boundary ∂A, is seen in figure 9.1 (b).

Next, we construct a target $f^{\mathbb{D}}$ by using the approximate signed distance function ϑ. The signed distance function itself lacks several properties to act as a target for the pre-shape parameterization tracking problem (6.18). In general, it does not fulfill necessary normalization conditions found in theorem 16 to guarantee existence of solutions to volume mesh regularization. Also, the signed distance function decreases in value with increasing proximity to ∂A. This results in a target, which decreases cell volume closer to ∂A. We reverse this, meaning that more mesh vertices should be allocated close to ∂A. And last but not least, the correspondence of discrete cell volume allocation and the values of our target $f^{\mathbb{D}}$ is non-trivial. Hence we apply a nonlinear transformation, which gives us the opportunity to model a desired variation in cell volume allocation.

We construct a nonlinear transformation with desired properties in the following. First, as $\mathbb{D}$ is bounded, we can normalize the values of ϑ to fit the reference interval $[0, 1]$, i.e. apply

$$L\colon \big[0, \max_{x \in \overline{\mathbb{D}}} \vartheta(x)\big] \to [0,1], \quad z \mapsto \frac{1}{\max\limits_{x \in \overline{\mathbb{D}}} \vartheta(x)} \cdot z. \tag{9.5}$$

At this point, there are multiple ways to transform the distances. Different transformations F result in different cell volume profiles. This means the user is free to model a volume allocation fitting his task. For illustrative purpose, and given a set of parameters $\mu \in \mathbb{R}$ and $\alpha, \beta, \gamma, \varepsilon_{\text{Transf}} > 0$, we choose a transformation inspired by the density function of the generalized normal distribution

$$F(x) = \alpha \cdot \frac{1}{e^{\left(\frac{|L(x)-\mu|}{\gamma}\right)^{\beta}}} + \varepsilon_{\text{Transf}}. \tag{9.6}$$

Notice that our transformed target is strictly positive, which is necessary for well-defined solutions to volume regularization (cf. theorem 16). The parameters serve to model the cell volume allocations. An exemplary illustration of equation (9.6) for a set of fixed parameters, for which volume mesh regularization results in a region with high node density near ∂A, is visualized in figure 9.1. With this, we can finally construct a meaningful cell volume target function. For the case of closed shapes $\varphi(M)$, i.e. empty ∂M, the associated target is given by

$$f^{\mathbb{D}}_{\varphi(M)} = \begin{cases} \frac{\int_{\mathbb{D}^{\text{in}}_{\varphi}} g^{\mathbb{D}}(x)\,\mathrm{d}x}{\int_{\mathbb{D}^{\text{in}}_{\varphi}} F(\vartheta(x))\,\mathrm{d}x} \cdot F \circ \vartheta & \text{for } x \in \mathbb{D}^{\text{in}}_{\varphi} \\ \frac{\int_{\mathbb{D}^{\text{out}}_{\varphi}} g^{\mathbb{D}}(x)\,\mathrm{d}x}{\int_{\mathbb{D}^{\text{out}}_{\varphi}} F(\vartheta(x))\,\mathrm{d}x} \cdot F \circ \vartheta & \text{for } x \in \overline{\mathbb{D}^{\text{out}}_{\varphi}}. \end{cases} \tag{9.7}$$

Just as in section 7.1.2, this type of definition guarantees necessary normalization conditions of $f^{\mathbb{D}}$ on the inside and outside of a shape iterate $\varphi(M) \subset \mathbb{D}$. For shapes with boundaries $\partial\varphi(M)$, the construct is adapted to suit the conditions found in theorem 16 (ii).

It is important to distinguish the shape $\varphi(M)$ and active set boundary ∂A, which obviously do not coincide in general. Also, we have discussed in remark 22, that lower regularity of objects participating in the volume parameterization tracking problem (6.18) is enough to guarantee existence of solutions. Hence, regularity of solutions ϑ to the stabilized Eikonal equation is not threatening applicability of volume mesh quality regularization with VI or shape specific targets.

From a technical perspective, the pre-shape material derivative $\mathfrak{D}_m(f^{\mathbb{D}}_{\varphi(M)})[V]$ seen in equation (7.11) is not correct for all directions $V \in H^1_0(\mathbb{D}, \mathbb{R}^{n+1})$ in case of the VI or shape specific target from equation (9.7) (cf. remark 39). However, it coincides for all directions V with vanishing normal component on $\varphi(M)$, which is in particular the case for all $V \in H^1_{0,\varphi(M)}(\mathbb{D}, \mathbb{R}^{n+1})$. We emphasize again, that directions normal to $\varphi(M)$ are in tangential or vertical component of $T\,\mathrm{Diff}(\overline{\mathbb{D}})$, as their support is a subset of the interior of $\mathbb{D}$. For volume parameterization tracking, the manifold of concern is $\mathbb{D}$. Thus only directions which change the shape of $\mathbb{D}$, i.e. directions normal to $\partial\mathbb{D}$, have components in the horizontal component of the fiber bundle $T\,\mathrm{Diff}(\overline{\mathbb{D}})$ (cf. equation (4.14)). The techniques presented in section 6.2.2, which implement volume parameterization tracking with invariant shapes, are therefore valid for the VI-specific target. The previous pre-shape material derivative is applicable in this scenario, since the employed modification projects the values of test directions V changing the shape of $\varphi(M)$ to zero on $\varphi(M)$ (cf. equation (6.35)). This means no extra care needs to be taken if VI or shape-specific targets are implemented via approaches highlighted in section 6.2 and chapter 7.

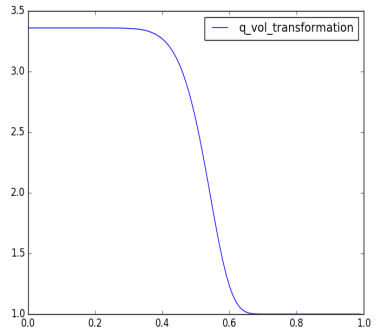

(a) Transformation F

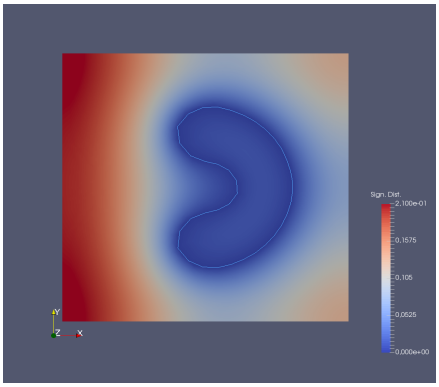

(b) Signed distance function ϑ

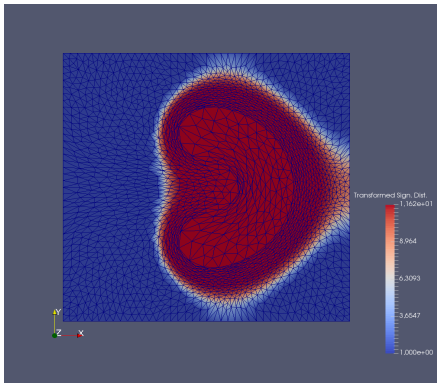

(c) Transformed signed distance $F(\vartheta)$ 2D

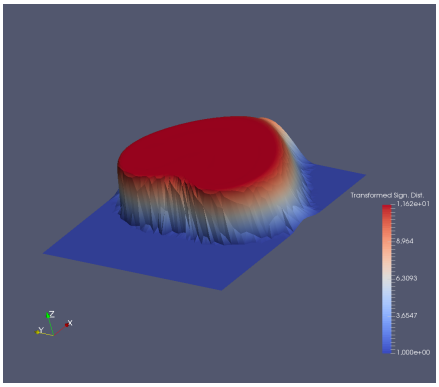

(d) Transformed signed distance $F(\vartheta)$ 3D

Figure 9.1: Objects to construct a VI-specific target $f^{\mathbb{D}}_{\varphi(M)}$. (a) Transformation F as in equation (9.6) for $\alpha = 5, \beta = 8, \varepsilon_{\text{Transf}} = 1, \mu = 0.1, \gamma = 0.25$. (b) Solution ϑ of the weak stabilized Eikonal equation (9.2) for step 130 of algorithm 7.1 with $\varepsilon_{\text{Eik}} = 10 \cdot h_{\max,130}$, and marked active set boundary ∂A for the fully regularized version of problem (8.54). (c) Transformed signed distance function $F(\vartheta)$ via equation (9.6) and parameters of (a) on the resulting mesh for simultaneous volume mesh regularization and shape optimization at step 130. For the initial mesh, see figure 9.2 (a). (d) 3D view of the transformed signed distance function $F(\vartheta)$.

Remark 38 (Local Mesh Adaption for General Hypersurfaces)**.** *Our method to construct customized cell volume targets for the active set boundary ∂A is also applicable for general n-dimensional submanifolds $N \subset \mathbb{D}$. By replacing ∂A with N, and following the previous approach, volume mesh regularization results in a mesh with specified cell volumes depending on the distance to $N \subset \mathbb{D}$. The submanifold N then acts as the boundary for the Dirichlet condition of the stabilized Eikonal equation* (9.1)*. In particular, choosing $N = \varphi(M)$ gives techniques, which adapt the mesh according to the shapes which arise during shape optimization.*

Remark 39 (Sensitivities for Pre-Shape Parameterization Tracking Constrained by Eikonal Equations)**.** *Although it is not necessary to have the complete pre-shape material derivative for target $f^{\mathbb{D}}$ from equation* (9.7)*, which captures effects in directions normal to $\varphi(M)$, it might still be calculated in closed form. This becomes clear, when the volume parameterization tracking problem is formulated for a shape specific target without shape optimization. For illustration, let $\Gamma \subset \mathbb{D}$ be a closed shape. Then such a formulation is given by*

$$\begin{aligned} \min_{\phi \in \mathrm{Diff}(\mathbb{D}\setminus\Gamma)\cap \mathrm{Diff}^0_\Gamma(\overline{\mathbb{D}})} \; & \frac{\alpha^{\mathbb{D}}}{2} \int_{\mathbb{D}} \left(g^{\mathbb{D}} \circ \phi^{-1}(x) \cdot \det D\phi^{-1}(x) - T(\vartheta)(x) \right)^2 \mathrm{d}x \\ s.t. \; & |\nabla \vartheta| = 1 \quad \text{in } \mathbb{D} \\ & \vartheta = 0 \quad \text{on } \Gamma. \end{aligned} \tag{9.8}$$

Here, the transformation T is defined as the operator which maps ϑ to $f^{\mathbb{D}}$ as in equation (9.7)*. We clearly see that the target $T(\vartheta)$ implicitly depends on the shape $\Gamma \subset \mathbb{D}$ via the boundary condition of the constraining Eikonal equation. Therefore formulation* (9.8) *shows, that volume parameterization tracking with a shape specific target can be regarded as a PDE-constrained pre-shape optimization problem. From such a point of view, a Lagrangian for problem* (9.8) *can be constructed. Such a Lagrangian can be used to produce an adjoint-like equation for the constraining Eikonal equation with respect to the target $\mathfrak{J}^{\mathbb{D}}$. The sensitivity can be used to calculate the pre-shape material derivative, which features influence of directions V normal to Γ. However, the fact that the absolute value is non-differentiable, and since it can lead to occurrence of singularities in the sensitivity system, creates additional difficulty. The situation becomes even more complex for volume parameterization tracking with shape specific targets that are coupled with shape optimization problems. If the shape optimization problem itself is constrained by a PDE or VI, then the sensitivity systems are in fact partially or even fully coupled. As previously explained, the full pre-shape material derivative is not needed for volume mesh regularization. Therefore it is not feasible to derive formulations for such sensitivities, let alone to numerically implement solution procedures for them. However, from theoretical perspective, a sensitivity analysis of equation* (9.8) *is an interesting example of a geometric problem, which can be stated and analyzed in the context of PDE-constrained pre-shape optimization.*

Before we implement volume mesh regularization with the presented VI-specific target, we introduce another method for mesh quality optimization during shape optimization. This method allows us to use quasi-Newton methods for mesh quality improvement, while avoiding, perhaps expensive, recomputations of targets $f^{\mathbb{D}}_{\varphi(M)}$.

9.2 A Quasi-Newton-ADM Approach for Mesh Quality and Shape Optimization

In chapter 7, we explored algorithms that simultaneously optimize shape and volume mesh quality, while solving a shape optimization problem. The simultaneous approach showed the advantage of saving additional computational cost by calculating a modified shape gradient. In this section, we illuminate a different approach inspired by the alternating directions method (ADM). We focus on volume mesh regularizations. In its most basic sense, such an approach uses an alternating optimization of the shape objective $\mathcal{J}$ and the pre-shape parameterization tracking functional $\mathfrak{J}^{\mathbb{D}}$. This would come with increased computational cost, which is why we use a different formulation to limit additional numerical burden, and to guarantee sufficient mesh quality.

We propose a modified ADM-inspired approach in the following. It does not exclude the use of simultaneous optimization strategies previously discussed, but can be either used in addition to, or instead of it. The full algorithm is depicted in algorithm 9.1. Instead of alternating optimization for the shape objective, or its simultaneous mesh quality regularized version, and the parameterization tracking functional for mesh quality in every step, we prioritize the simultaneous shape and mesh quality descent. In addition to the simultaneous shape and mesh quality descent as discussed in algorithm 7.1, we perform optimization steps solely for the parameterization tracking functional, if a condition for sufficient mesh quality is violated. Namely, we monitor the absolute and the relative values of $\mathfrak{J}^{\mathbb{D}}$ with respect to the initial mesh. If these values rise above a specified upper boundary $\overline{B} > 0$, then an optimization subroutine for $\mathfrak{J}^{\mathbb{D}}$ without the shape target $\mathcal{J}$ is triggered. Optimization in this subroutine takes place until the absolute or relative values of $\mathfrak{J}^{\mathbb{D}}$ drop below a specified baseline $\underline{B} > 0$, i.e. the mesh quality is sufficiently close to the specified target adaptation $f^{\mathbb{D}}$, or a maximum number of subroutine steps is reached. The descent direction for this is given via equation (6.30). With this procedure, a minimum mesh quality $\overline{B}$ with respect to the specified cell allocation $f^{\mathbb{D}}$ is ensured for the entire optimization procedure.

In an infinite dimensional framework, algorithm 9.1 is unlikely to be trapped in an infinite loop for this subroutine. This comes from theorem 13, which guarantees that the only stationary points for $\mathfrak{J}^{\mathbb{D}}$ are in fact globally optimal mesh parameterizations $\phi \in \mathrm{Diff}(\mathbb{D} \setminus \varphi(M)) \cap \mathrm{Diff}_{\varphi(M)}(\overline{\mathbb{D}})$ with $\mathfrak{J}^{\mathbb{D}}(\phi) = 0$. However, since we are dealing with discrete meshes, the mesh topology can in fact prohibit convergence to a globally optimal parameterization. This strongly depends on the connectivity of nodes, and is an interesting subject for future studies. Hence, care should be taken to not choose $\underline{B}$ too close to 0.

As was the case for simultaneous pre-shape regularization and shape optimization algorithm 7.1, pre-shape updates φ_{k+1} and ϕ_{k+1} are computed as the coordinate difference of mesh $k+1$ and the initial mesh. Mesh coordinate updates are performed by simple addition of a descent direction $\tilde{U}$, i.e. $x \leftarrow x + \tilde{U}(x)$. In algorithm 9.1, we have described the general case $\alpha^{\tau}, \alpha^{\mathbb{D}} > 0$ for simultaneous shape and volume mesh quality optimization, and shape optimization, complemented by conditional individual volume parameterization tracking. Of course, a simplified version of algorithm 9.1 for the case of shape optimization, which is complemented solely by conditional individual volume parameterization tracking, also applies. Further, it is not necessary to use VI-specific targets $f^{\mathbb{D}}$. If desired, a volume parameterization tracking target $f^{\mathbb{D}}$ based on independently prescribed cell volume allocation as described in section 7.1.2 can be used. In such cases, gathering of active set boundary nodes and/or solution of an Eikonal equation are not required for algorithm 9.1. If variational inequalities have tightly binding obstacles ψ, shape optimization featur-

Set starting domain $\mathbb{D}_0$ and shape $\varphi_0(M) = \Gamma_0$, and save according vertex coordinates for future computations
Set pre-shape and VI regularization parameters $\alpha^\tau, \alpha^{\mathbb{D}}, \gamma, c \geq 0$, and L-BFGS memory parameter $L \in \mathbb{N}$
Set shape tracking target $q\colon \mathbb{D} \to (0, \infty)$ and VI-specific volume target parameters
Estimate initial point distributions g^M for $\varphi_0(M)$ and $g^{\mathbb{D}}$ for $\mathbb{D}_0$ according to equation (7.6)
Calculate local orthonormal tangential bases τ_0 for each vertex of $\varphi_0(M)$ using Gram-Schmidt orthonormalization, and save them for future iterations
while $\left(\|U_k\| > \varepsilon_{\text{abs}} \text{ and } \frac{\|U_k\|}{\|U_0\|} > \varepsilon_{\text{rel}}\right)$ or $\frac{\mathcal{J}(\pi(\varphi_k))}{\mathcal{J}(\pi(\varphi_0))} > \varepsilon^{\mathcal{J}}_{\text{rel}}$ **do:**
    Solve for state solution y_k via equation (8.8)
    Collect vertices of active set boundary ∂A as in section 9.1
    Solve stabilized Eikonal equation (9.2) for ϑ using semi-smooth Newton method as described in section 9.1
    Calculate VI-specific target $f^{\mathbb{D}}_{\varphi_k(M)}$ using transformation equation (9.7)
    if $\frac{\mathfrak{J}^{\mathbb{D}}(\phi_k)}{\mathfrak{J}^{\mathbb{D}}(\phi_0)} > \overline{B}$:
        $\phi_{k,0} \leftarrow \phi_k$
        while $\frac{\mathfrak{J}^{\mathbb{D}}(\phi_k)}{\mathfrak{J}^{\mathbb{D}}(\phi_0)} > \underline{B}$ **do**:
            Calculate and store pre-shape gradient $U^{\mathbb{D}}_l$ via equation (6.30)
            Calculate shape L-BFGS direction $S^{\mathbb{D}}_l$ via algorithm 9.2
            Perform line search to get descent direction $\tilde{S}^{\mathbb{D}}_l$ for $\mathfrak{J}^{\mathbb{D}}$ and store it
            $\phi_{k,l+1} \leftarrow \phi_{k,l} + \tilde{S}^{\mathbb{D}}_l \circ \phi_{k,l}$
        $\phi_k \leftarrow \phi_{k,l+1}$
    Assemble right-hand side of pre-shape gradient system (7.12):
        Solve for adjoint p_k via equation (8.9)
        Calculate local orthonormal tangential bases τ^{φ_k} for each vertex of $\varphi_k(M)$ with same orientation as τ_0 using Gram-Schmidt orthonormalization
        Assemble RHS(φ_k, ϕ_k) according to equation (7.21) with $\mathcal{D}\mathcal{J}_{\gamma,c}$ from equation (8.27)
    Solve for pre-shape gradient U_k:
        Calculate local weighting parameters μ by solving equation (7.15)
        if linear elasticity:
            Assemble left-hand side $\mathfrak{a}(\cdot,\cdot)$ by equation (7.13) and solve by preconditioned CG-method
        elif p-Laplacian:
            Use preconditioned Newton's method to solve equation (7.12) with left-hand side $\mathfrak{a}(\cdot,\cdot)$ by equation (7.14)
    Perform a line search to get a sufficient descent direction $\tilde{U}_k$:
        $\tilde{U}_k \leftarrow \frac{1}{\|U_k\|} \cdot U_k$
        while
        $\mathcal{J}(\pi(\varphi_k + \tilde{U}_k \circ \varphi_k)) + \alpha^\tau \cdot \mathfrak{J}^M(\varphi_k + \tilde{U}_k \circ \varphi_k) + \alpha^{\mathbb{D}} \cdot \mathfrak{J}^{\mathbb{D}}(\phi_k + \tilde{U}_k \circ \phi_k)$
        $\geq \mathcal{J}(\pi(\varphi_k)) + \alpha^\tau \cdot \mathfrak{J}^M(\varphi_k) + \alpha^\tau \cdot \mathfrak{J}^{\mathbb{D}}(\phi_k)$ **do:**
            $\tilde{U}_k \leftarrow 0.5 \cdot \tilde{U}_k$
    Perform updates:
        $\varphi_{k+1} \leftarrow \varphi_k + \tilde{U}_k \circ \varphi_k$
        $\phi_{k+1} \leftarrow \phi_k + \tilde{U}_k \circ \phi_k$

Algorithm 9.1: VI-specific simultaneous shape and volume regularization with quasi-Newton-ADM subroutines for volume parameterization tracking.

ing limiting objects studied in chapter 8 can be of benefit. For such an approach, the adjoint limit p features increasing sparsity for larger active sets (cf. theorem 18). As a caveat, this also means the safeguarding strategy as described in algorithm 8.2 needs to be incorporated into algorithm 9.1, since the shape derivative limits from theorem 20 do not in general provide descent directions.

There are multiple potential benefits offered by application of the modified Quasi-Newton-ADM algorithm 9.1, which we list and discuss in the following.

Exactly Invariant Shapes A main benefit of a subroutine descent for volume mesh quality is a guaranteed exact shape invariance, meaning coordinates of shape mesh nodes remain unchanged. This opportunity comes from two requirements, which are achieved for ADM algorithm 9.1. First, the shape objective $\mathcal{J}$ is not participating in subroutines. And secondly, the subroutine optimizes $\mathfrak{J}^{\mathbb{D}}$ over the class of pre-shapes $\mathrm{Diff}(\mathbb{D} \setminus \varphi(M)) \cap \mathrm{Diff}_{\varphi(M)}(\overline{\mathbb{D}})$, which leave the shape $\varphi(M)$ invariant. Hence to these two properties, the right-hand side of pre-shape gradient systems of subroutines has no support on $\varphi(M)$. This offers the possibility to implement Dirichlet zero conditions on $\varphi(M) \subset \mathbb{D}$. Such a condition is not possible in a simultaneous approach, since we know from Hadamard's theorem 7 that the shape derivative $\mathcal{D}\mathcal{J}$ is supported in normal directions on $\varphi(M)$.

Sufficient Adaptation for Upcoming State Solutions Obviously, an ADM approach can adapt the mesh to the state equation of the current shape, which is then solved for the next shape optimization step. A simultaneous approach may not adapt the mesh sufficiently well for the upcoming state solution, since it only uses explicit information of the current mesh, and not of the upcoming mesh, where the next state is computed. In some sense the situation for our current formulation of simultaneous optimization resembles an explicit mesh adaptation algorithm. An implicit one would adapt the mesh to the next shape iterate to come. The ADM approach achieves this, but at the cost of not being able to simultaneously compute a descent direction for $\mathcal{J}$.

Reduced Cost for Expensive Target Constructions If targets $f^{\mathbb{D}}_{\varphi(M)}$ are expensive to construct, an extended optimization for the objective $\mathfrak{J}^{\mathbb{D}}$ without shape objective $\mathcal{J}$ does not need recomputation of $f^{\mathbb{D}}_{\varphi(M)}$, which saves costs. Additionally, computational cost is lower compared to a standard ADM approach, since volume mesh optimization is taking place only when mesh quality is sufficiently bad.

For the case of a target $f^{\mathbb{D}}$ varying with distance to the active set ∂A, or a shape Γ as in section 9.1, the main computational burden comes from solution of additional Eikonal equations. The invariant shape $\varphi(M)$ for the subroutine stays the same, which means solution of only one Eikonal equation is sufficient to compute a target $f^{\mathbb{D}}_{\varphi(M)}$. During simultaneous mesh quality and shape optimization, the shape $\varphi(M)$ changes in each iteration, because the shape derivative of the shape objective is participating in gradient systems. Thus, for each step of unregularized or simultaneous approaches, an Eikonal equation needs to be solved to adjust for the new shape iterate.

Large Deformations and Their Corrections are Possible Another benefit of an alternating approach comes from the scenario of large deformations of the shape with a highly varying target cell volume $f^{\mathbb{D}}_{\varphi(M)}$ at the same time. In such a case, the stand-alone simultaneous approach using gradient descents becomes increasingly difficult to apply, as descent directions are not always found.

The correction of mesh quality for large deformations and a highly varying cell volume target $f^{\mathbb{D}}$ becomes possible with the ADM algorithm 9.1. This comes from

applicability of Dirichlet zero conditions on $\varphi(M)$ for parameterization tracking descent directions, which we previously discussed in this section. This is difficult if volume regularized gradients are represented with forms $\mathfrak{a}(\cdot,\cdot)$ featuring higher order terms in the simultaneous approach. We suspect that the cause for this lies in the smoothing effect of the solution operator of higher order gradient representations. If the forces $\mathfrak{D}\mathfrak{J}^{\mathbb{D}}$ and $\mathcal{D}\mathcal{J}$ are strongly opposing near the shape $\varphi(M)$, then higher order representations $\mathfrak{a}(\cdot,\cdot)$ lead to cancellation by smoothing, whereas representations with lower order metrics lead to possible jumps of the gradient. In both cases, we witness stagnation of optimization routines during line search, as no permissible descent directions are computed. This cannot happen for the proposed ADM inspired approach.

For small steps, e.g. near a solution, the difference of consecutive meshes is not as large. Therefore an ADM approach is not favorable in this aspect when convergence is taking place, since the simultaneous approach leads to approximately the same benefits for mesh adaption at lower numerical cost.

Applicability of Quasi-Newton Methods Because the ADM algorithm 9.1 does not change the target $f^{\mathbb{D}}_{\varphi(M)}$ and objective functional $\mathfrak{J}^{\mathbb{D}}$ in subroutines, we can apply quasi-Newton approaches for mesh quality optimization. We propose to use a shape L-BFGS algorithm 9.2 instead of gradient descents in subroutines. Using L-BFGS updates for the simultaneous approach is not straightforward, since the objective $\mathfrak{J}^{\mathbb{D}}$ of the volume parameterization tracking problem changes every time the underlying shape $\varphi(M)$ is deformed. It is not immediately clear how to avoid this, because $\varphi(M)$ needs to stay invariant under volume mesh adaptation, which is ensured by suitable change of the target $f^{\mathbb{D}}_{\varphi(M)}$ and the problem formulation. In section 7.4, we presented a numerical study on the compromising effects of non-invariant formulations of the volume mesh parameterization tracking problem on shape optimization.

This difficulty does not occur for the subroutine case. Since the shape $\varphi(M)$ remains fixed, the parameterization tracking functional $\mathfrak{J}^{\mathbb{D}}$ also stays the same. This gives applicability of a shape L-BFGS routine, with a coherent gradient and descent history, without modifications. It requires storage of previous pre-shape gradients and descent directions of the subroutine for a memory length parameter $L \in \mathbb{N}$. Once the subroutine has sufficiently descended, the stored history can be deleted, as the shape L-BFGS routine starts fresh for every triggered subroutine. An algorithmic illustration of a shape version of the two loop L-BFGS recursion is seen in algorithm 9.2. To ensure positive definiteness of L-BFGS updates, we check for the so-called curvature condition. As we do not work in vector spaces, we resort to pre-shape calculus formulations of the curvature condition, which are given by

$$\mathfrak{D}\mathfrak{J}^{\mathbb{D}}\big(\phi_{k+1}\big)\big[S_k\big] - \mathfrak{D}\mathfrak{J}^{\mathbb{D}}\big(\phi_k\big)\big[S_k\big] = \mathfrak{a}\big(U_{k+1}, S_k\big) - \mathfrak{a}\big(U_k, S_k\big) > 0. \tag{9.9}$$

Here, U_k is the gradient given via equation (6.30), $\mathfrak{a}(\cdot,\cdot)$ is the sufficient form to represent the gradient, and S_k is the L-BFGS direction used for a descent in iteration k. We check for the curvature condition, whenever an L-BFGS step is applied. If the condition is not fulfilled, we resort to a gradient descent step, without update of the history. When we have a satisfied curvature condition (9.9), but the generated direction fails to give a descent during line search, we delete the history and proceed with a gradient descent. Then, for a successful gradient step, we begin a fresh L-BFGS history. If no gradient descent can be achieved via line search, we quit our optimization with a fail. In the context of pre-shape optimization, which performs optimization on infinite dimensional manifolds, the L-BFGS algorithm should use retractions to transport vector fields from one tangent space to another. Otherwise, meaningful algebraic operations with vector fields are not guaranteed in

general. However, as we are in the case of volume optimization, we have pre-shapes $\phi \in \mathrm{Diff}(\mathbb{D}\setminus\varphi(M))\cap\mathrm{Diff}_{\varphi(M)}(\overline{\mathbb{D}})$ from a pre-shape space consisting of a single fiber. This means the underlying shape $\mathbb{D}$ represented via pre-shapes ϕ is invariant. For simplicity of the numerical implementation, we therefore decide to use retractions $T_S(U)$, which initializes the degrees of freedom of $T_S(U)$ located in $x + S(x) \in \mathbb{D}$ with the values $U(x)$ previously located in $x \in \mathbb{D}$. Put in another way, we simply move the coordinates of DoFs corresponding to U in direction S to get $T_S(U)$.

$Z \leftarrow U_l^{\mathbb{D}}$
$Y_{l-1} \leftarrow U_l^{\mathbb{D}} - T_{S_{l-1}} U_{l-1}^{\mathbb{D}}$
for $k = l-2, \dots, l-L$:
    $Y_k \leftarrow T_{S_{l-1}} \dots T_{S_k} Y_k$
for $k = l-1, \dots, l-L$:
    $S_k \leftarrow T_{S_{l-1}} \dots T_{S_k} S_k$
    $\rho_k \leftarrow \mathfrak{a}(Y_k, S_k)^{-1}$
    $\alpha_k \leftarrow \rho_k \cdot \mathfrak{a}(S_k, Z)$
    $Z \leftarrow Z - \alpha_k \cdot Y_k$
$Z \leftarrow \frac{\mathfrak{a}(Y_{l-1}, S_{l-1})}{\mathfrak{a}(Y_{l-1}, Y_{l-1})} \cdot Z$
for $k = l-L, \dots, l-1$:
    $\beta_k \leftarrow \rho_k \cdot \mathfrak{a}(Y_k, Z)$
    $Z \leftarrow Z + (\alpha_k - \beta_k) \cdot S_k$
$S_l \leftarrow Z$

Algorithm 9.2: Shape optimization version of the two loop L-BFGS algorithm for volume parameterization tracking with memory length parameter $L \in \mathbb{N}$. We write $S_k := \tilde{S}_k^{\mathbb{D}}$ for readability, and remind the reader that these are the directions previously applied for descent.

9.3 Implementation and Results

In this section, we implement algorithm 9.1 for two different targets $f^{\mathbb{D}}$, and compare it to the unregularized and simultaneously regularized optimization algorithms. As our base model problem, we use the tracking type shape optimization problem (8.54) constrained by the obstacle problem (8.55) featuring the Laplace operator. For our comparison study, the parameters and solution method for the VI-constraint are the same for all approaches. The piecewise constant source term for the variational inequality depends on the shape $\varphi(M)$ embedded in $\overline{\mathbb{D}} = [0,1]^2$, and is given in equation (8.56). We choose a constant obstacle $\psi = 0.5$ and a $\bar{\lambda} = \max(0, r_{\varphi(M)} + \Delta\psi) = \max(0, r_{\varphi(M)})$ (cf. remark 28). The target $\bar{y}$ for the tracking type problem is set to the solution of unregularized variational inequality (8.55) at the target shape seen in figure 9.2 (a), i.e. we commit the so-called 'inverse crime'. It is initially computed via the semi-smooth Newton method proposed in [94], and is visualized in figure 8.2 (a). Further, we use the smoothly regularized state and adjoint equation (8.8) and equation (8.9), with a smoothed maximum function defined by equation (8.57), and its first derivative as in equation (8.58). In this scenario, all assumptions for the theory built in chapter 8 are fulfilled. Particularly, existence of smoothed states, adjoints and regularized shape derivatives $\mathcal{D}\mathcal{J}_{\gamma,c}$ are guaranteed. Corresponding regularizing parameters are chosen as $\gamma = 1$ and $c = 10$ throughout the entire study in this section. Also, the scaling parameter for the perimeter regularization is chosen as $\nu = 0.00001$ throughout the entire comparison study. Its associated shape derivative is given in equation (7.18).

As in section 7.2, calculations are performed in Python3.5 using the open-source finite-element software FEniCS (cf. [117, 4]). Calculations are performed by a single Intel(R) Core(TM) i5-3210M CPU @ 2.50GHz featuring 6GB of RAM. Our unstructured computational mesh is constructed via the free meshing software Gmsh (cf. [63]), and is visualized in figure 9.2 (a). The starting shape M is a circle $S^{0.15}_{(0.5,0.5)}$, i.e. it has radius 0.15 and is centered at $(0.5, 0.5)$. Our discretization of the hold-all domain $\overline{\mathbb{D}} = [0, 1]^2$ consists of 2 184 vertices and 4 206 triangular cells. For a consistent comparison, the exact same computational mesh and initial shape are used for all numerical approaches. The functions featured in all approaches are represented by continuous linear elements on the aforementioned computational mesh.

The regularized state equation features the smoothed $\max_\gamma$-function, which allows us to apply a Newton method. Here, we demand an absolute and a relative tolerance of 10^{-7} and 10^{-6} for residuals of occurring semilinear regularized state equations, at all steps for all (un-)regularized shape optimization approaches compared. Corresponding adjoint equations and subproblems of the Newton method for the state equation are solved using the PETSc linear algebra back-end in FEniCS. In particular, we employ a CG-method preconditioned by an incomplete Cholesky decomposition implemented in PETSc. Gradients, both for main- and subroutine optimizations, are of abstract form (7.12), and represented using a weakly formulated linear elasticity metric seen in equation (7.13). Corresponding Lamé parameters μ are generated by solution of Laplace problem (7.15) with parameters $\mu_{\min} = 0.05$ and $\mu_{\max} = 1$ for all routines. The gradient systems are solved via the CG-method from PETSc, which is preconditioned by an incomplete Cholesky decomposition. We remind the reader, that, as we use the fully regularized variational inequality of first kind and have met necessary conditions, the associated shape derivative $\mathcal{D}\mathcal{J}_{\gamma,c}$ always exists by theorem 19 and is given by the closed formulation in equation (8.27). This formulation of $\mathcal{D}\mathcal{J}_{\gamma,c}$ is utilized for all following optimization routines.

For our comparison, we track values similar to our study of the simultaneous approach featuring linear elasticity and p-Laplacian gradient representations from section 7.2. Namely, we collect the relative shape optimization objective values $\mathcal{J}(\Gamma_i)/\mathcal{J}(M)$, and the geometric distance of the shape iterates Γ_i to the target shape as defined in equation (7.23). As a convergence criterion, we require a relative value of $\varepsilon_{\text{rel}} = 0.0038$. This is the value at which the unregularized approach does not find a descent direction in the line search routine, and therefore quits the shape optimization. Moreover, we collect the relative values of the volume parameterization tracking objective $\mathfrak{J}^{\mathbb{D}}(\phi_i)/\mathfrak{J}^{\mathbb{D}}(\phi_0)$ for our two different targets $f^{\mathbb{D}}$. The values for the uniform target, and those of the VI-specific target, are depicted separately. Also notice that the relative values for the unregularized routine are included in each of the two graphs. Of course their values differ, as the corresponding targets in the pre-shape objective functionals are different.

The Different Routines In the following, seven approaches to solve the presented VI-constrained shape optimization problem, and their corresponding parameters, are described in detail. We do not incorporate shape mesh regularization techniques explored in section 6.1, as the number of methods to compare would become too large for a clear discussion. Of course, shape mesh regularization can be applied and compared in analogous fashion to volume mesh regularization implemented in this section. For this reason, the underlying shape optimization problem is formulated using shapes $\Gamma \in B_e^n$ instead of $\varphi \in \text{Emb}(M, \mathbb{D})$. Shapes $\varphi(M)$ occurring in referenced descriptions of the following methods can simply be replaced by Γ, and vice versa.

The first routine is the shape optimization approach using the variational in-

equality regularization techniques established in chapter 8. It is the basis for all other six methods, while also serving as a benchmark to which we compare the volume mesh quality enhancing routines. Throughout the rest of this section, we call this routine the unregularized approach (Unreg.), as it does not feature any kind of pre-shape regularization techniques. To avoid misconception, we remind the reader that the unregularized approach still features regularizations for the variational inequality constraints. As we use the fully regularized state equation (8.8), we do not have to rely on the safeguarding techniques proposed in algorithm 8.2. The shape derivative $\mathcal{DJ}_{\gamma,c}$ is the true shape derivative for the smoothed shape optimization problem featuring equation (8.8) as a constraint (cf. theorem 19), which therefore guarantees that shape gradients represented via linear elasticity metrics can serve as descent directions. However, this also means we cannot exploit sparsity of adjoint limit values induced by the obstacle (cf. theorem 18), which we do not necessarily need for a comparison study on pre-shape mesh regularization techniques. The unregularized approach features a simple shape gradient descent using a backtracking line search with rescaling parameter 0.5 and initial scaling of the normed shape gradient by 0.01. The mentioned line search parameters are applied for all main routines of forthcoming methods featuring the shape optimization objective, but not necessarily for the line search in ADM subroutines if stated otherwise. Such a small scaling is necessary, since initial shape gradients give descent directions deforming the hold-all domain near its boundary $\partial\mathbb{D}$ to such an extend, that reliable solution of the nonlinear state becomes impossible. Even for the rescaled approach, this effect is still visible for the unregularized routines at the upper, lower and right outer boundaries, and is pictured in figure 9.2 (b) and figure 9.3 (e).

The second routine involves volume mesh quality regularization using the simultaneous approach described in section 6.2 and section 7.1.3. In the following, we abbreviate this approach as 'Sim. uni.' when necessary. It has a uniform volume allocation target to correct degenerated cells coming from shape optimization. For this, the target $f^{\mathbb{D}}$ is constructed via equation (7.9) choosing $q^{\mathbb{D}} = 1$. Notice that such an a priori cell volume allocation does not require solution of an Eikonal equation, as it is not specific to the variational inequality of the current shape iteration Γ_i. The right-hand side of the corresponding pre-shape gradient system is given by equation (7.21) for $\alpha^\tau = 0$, and uses the pre-shape material derivative given in equation (7.11). The weighting of $\mathfrak{J}^{\mathbb{D}}$ is chosen as $\alpha^{\mathbb{D}} = 0.01$. Essentially, the simultaneous mesh quality optimization for uniform cell volumes and the unregularized routine differ by the additional force term $\alpha^{\mathbb{D}} \cdot \mathfrak{D}\mathfrak{J}^{\mathbb{D}}$ on the right-hand side of the pre-shape gradient system. Notice, that construction of this additional force term requires storage of the initial mesh node coordinates, which is not necessary for the unregularized approach.

The third routine implements the alternating direction approach to guarantee sufficiently uniform cell volume allocation. We identify it with the abbreviation 'Grad. ADM uni.' when necessary. The unregularized approach serves as a basis, while an additional subroutine for the volume version of pre-shape parameterization tracking problem (6.18) is included, as seen in algorithm 9.1. Subroutine optimization uses a pre-shape gradient descent, where the gradient is computed as the solution of equation (6.30) with $\alpha^{\mathbb{D}} = 1$. In particular, the shape iterate Γ_i of the current main routine is left invariant by implementing a Dirichlet zero boundary condition on $\Gamma_i \subset \mathbb{D}$. The line search parameters for the main routine are as explained before. For the subroutine line search, we choose an initial scaling of 10. We observed that this decreased time to convergence for the subroutine, whereas even larger initial scalings resulted in more line search steps, decreasing overall performance. For the main routine, the additional force term $\alpha^{\mathbb{D}} \cdot \mathfrak{D}\mathfrak{J}^{\mathbb{D}}$ in the gradient system is omitted, in order to purely evaluate performance of the ADM subroutine approach. As we do not use surface mesh quality optimization, i.e. we set $\alpha^\tau = 0$, there is no need

to calculate local tangential basis functions at shapes Γ_i in algorithm 9.1. Also, we use an a priori defined target $f^{\mathbb{D}}$ via $q^{\mathbb{D}} = 1$ in this routine, so there is no need to perform solution of a stabilized Eikonal equation in the optimization main- or subroutines. The initial volume mesh parameterization ϕ_0, as seen in figure 9.2 (a), has almost uniform cell volumes. Therefore we choose the upper bound of deviation from the starting cell volume distribution as $\overline{B} = 1.3$. When this tolerance level is exceeded, the subroutine is triggered, which performs mesh quality optimization until a decrease of $\mathfrak{J}^{\mathbb{D}}(\phi_i)/\mathfrak{J}^{\mathbb{D}}(\phi_0)$ below the level $\underline{B} = 0.3$ is achieved. We limit the amount of steps performed in each triggered subroutine to 25. If this number is reached, one main routine iteration is performed, and conditions are checked again.

The fourth routine is an alternating direction approach featuring an L-BFGS descent in the subroutine to achieve uniform cell volume allocation. It is abbreviated by 'L-BFGS ADM uni.' when appropriate. Instead of a gradient descent for $\mathfrak{J}^{\mathbb{D}}$, the L-BFGS method, as introduced in algorithm 9.2, is performed in the subroutine. We use a memory length of $L = 3$, and check for curvature conditions as described in section 9.2. The initial scaling of L-BFGS search directions is set to 0.9. All other parameters and settings of the fourth approach are identical to those of approach three.

Approaches five to seven do not target uniform meshes, but instead rely on VI-specific cell volume targets as derived in section 9.1. They all require solution of a stabilized Eikonal equation to construct the VI-specific target $f^{\mathbb{D}}$ via the approximate signed distance function ϑ. To set according Dirichlet boundary conditions, we solve the regularized variational inequality, and extract nodes participating in the active set boundary ∂A via criterion (8.63) adapted to the smoothed case with $\varepsilon_{\text{act}} = 0.025$. Then, we use a semi-smooth Newton method to solve its stabilized weak formulation (9.2) as described in section 9.1. For this, we choose the stabilizing parameter as $\varepsilon_{\text{Eik}} = 10 \cdot h_{\max}$, where $h_{\max}$ is the maximum edge length of the current mesh iterate ϕ_i. The required absolute and relative residual norms are 10^{-7} and 10^{-6} respectively, while maximum number of Newton iterations is limited to 70. Newton steps are damped by a scaling factor of 0.5. We solve corresponding subproblems by applying a GMRES method implemented in PETSc, which is preconditioned by an incomplete LU decomposition. Subsystem solution is required to achieve absolute and relative residual norms of 10^{-8} and 10^{-7}, with a maximum number of iterations set to 1000. With an approximate signed distance function ϑ, a VI-specific target $f^{\mathbb{D}}$ is constructed via equation (9.7) by using transformation F as in equation (9.6). The parameters for F are set to $\alpha = 2.5, \beta = 8, \varepsilon_{\text{Transf}} = 1, \mu = 0.1, \gamma = 0.45$ for routines five to seven.

The fifth approach features a simultaneous cell volume allocation specific to the constraining variational inequality of the current iteration. We abbreviate this approach by 'Sim. VI-sp.'. It is similar to approach two 'Sim. uni.', with the crucial difference that the target $f^{\mathbb{D}}$ for volume parameterization tracking is constructed in a VI-specific manner as previously discussed. The volume mesh regularization parameter is set to $\alpha^{\mathbb{D}} = 0.0025$. All other parameters not discussed are identical to those of approach two.

Approach six uses the modified ADM algorithm 9.1 with a VI-specific target and a gradient descent in the subroutine. Therefore we denote it by 'Grad. ADM VI-sp.'. Routine six is similar to routine three 'Grad. ADM uni.', differing by the VI-specific target and associated computations. Parameters of approach six are the same as in approach three, including initial line search scaling of 10 for pre-shape gradients in the subroutine, with the following exceptions. The permitted amount of rescales in each subroutine loop is set to 45. Also, the subroutine trigger is set to $\overline{B} = 0.5$, since the initial mesh is not adapted to the variational inequality. The corresponding lower threshold parameter is set to $\underline{B} = 0.03$, in order to permit sufficient adaption of the mesh to the active set boundary ∂A of the current main

	Unreg.	Sim. uni.	Grad. ADM uni.	L-BFGS ADM uni.	Sim. VI-sp.	Grad. ADM VI-sp.	L-BFGS ADM VI-sp.
total time	453.2s	680.3s	1226.1s	408.2s	2383.3s	1765.4s	1660.2s
avg. time/step	3.5s	4.7s	10.5s	3.7s	17.9s	15.0s	14.0s
number steps	130	144	117	110	133	118	119
number subr.	-	-	32	3	-	2	1
avg. time/subr.	-	-	26.3s	22.9s	-	24.3s	21.1s

Table 9.1: Total times, average times per step and number of steps for all 7 methods. For ADM approaches, the number of subroutines triggered, and their average times are included in total time and average time/step.

iteration.

Lastly, approach seven implements the full algorithm 9.1 with a VI-specific target and an L-BFGS method, as depicted in algorithm 9.2, for the subroutine. The L-BFGS memory length is $L = 3$, and the initial scaling of the subroutine line search is set to 0.25. All other parameter are the same as in routine six.

Results and Interpretation The results of the different routines concerning the shape objective $\mathcal{J}$, the volume parameterization tracking functional $\mathfrak{J}^{\mathbb{D}}$ for uniform and VI-specific $f^{\mathbb{D}}$, and the geometric mesh distance to the target shape are depicted in figure 9.4. Computational times of the main routines, and of subroutines if ADM approaches are incorporated, can be referenced in table 9.1. The number of subroutines triggered under an ADM regiment are found in table 9.1 as well. We want to emphasize, that total times and average times per step include the times of subroutines for the ADM case. Meshes of all routines at final iterations are illustrated in figure 9.2, while intermediate meshes are depicted in figure 9.3.

All routines do not disturb the underlying shape optimization approach, which is seen in figure 9.4 (a) by similarity of the graphs for the shape objective $\mathcal{J}$. In particular, they all achieve a decrease of the relative shape objective value to the level $\varepsilon_{\text{rel}} = 0.0038$, where the unregularized routine exits by finding no descent direction. Mesh quality regularization leaves the shape objective $\mathcal{J}$ approximately unchanged. Slight fluctuations can be explained by different mesh qualities, affecting the finite element solutions of the VI-constraint. This indicates that our approaches achieve the desired property of non-interference with the underlying problem by leaving shapes invariant. Also, the mesh distances to the target in figure 9.4 (b) look similar, with the possible exception of the L-BFGS based ADM approach with uniform target. The latter converges faster in geometric terms than the other routines, which we did not expect based on the theory. Possible reasons for this increased geometric convergence speed are still speculative, and part of further research.

Looking at the averaged times per step in table 9.1, we see that different volume mesh regularization techniques come with differing additional computational times. It is noticeable that the unregularized approach takes only the second place concerning total computational time, right after the L-BFGS based ADM approach with uniform target. The lower number of steps required to achieve the demanded relative shape objective value offers an explanation for this. We see that, if a scaled gradient descent for the ADM approach is applied, the total time compared to an L-BFGS approach is approximately tripled. This is reflected by the number of subroutines triggered. We have observed, that the first few shape optimization steps are fairly large, which resulted in deteriorating mesh quality. When looking at figure 9.4 (c), this deterioration of mesh uniformity is captured by the initial spike of $\mathfrak{J}^{\mathbb{D}}$ for the unregularized shape optimization routine. The simultaneous mesh quality and shape optimization routine continually decreases the non-uniformity, while the triggered ADM approaches prevent an extreme rise in non-uniformity. The gradient

based ADM approach needs significantly more subroutine steps to achieve the desired mesh uniformity. This means it exhausts the fixed maximum number of steps per subroutine, leading to more subroutines in total. This is seen in figure 9.4 (c) by the zig-zagging mesh quality for the gradient subroutine, whereas the L-BFGS based subroutine achieves jump-like decreases in mesh non-uniformity. Such fast decreases therefore require a lower number of subroutines, while the gradient based routine is not able to achieve the required mesh uniformity at once, explaining its significantly longer total computational times.

Average times for mesh quality ADM subroutines are overall lower for the L-BFGS subroutines compared to gradient ones. This is not a guaranteed finding, due to the computational overhead of two-loop L-BFGS routines. However, since the L-BFGS based methods converge significantly faster to demanded quality levels $\underline{B}$, while gradient methods need multiple full subroutines, the total amount of steps needed for L-BFGS subroutines is much lower than those of gradient based ones. Hence lower times for L-BFGS based mesh quality ADM routines stem from reduction of overall subroutine steps. If we take into account, that we have chosen initial line search scaling of the gradient subroutine to enhance their convergence speed, we recognize superiority of the L-BFGS based mesh quality approach compared to gradient based ones. Unscaled gradient descents performed noticeably worse, being the least effective type of algorithm. We also emphasize that the L-BFGS memory length for these results was chosen as $L = 3$, which means additional storage and computational costs of L-BFGS compared to gradient methods is limited. When looking at the average computational time per main routine step, we see that the unregularized method needs less time, which is expected. For the uniform case, the simultaneous approach performs slightly slower than the L-BFGS based ADM approach, but more than twice as fast as the gradient based ADM approach. This possibly comes from our construction of regularized gradient systems, which is based on multiple matrix and vector assemblations using UFL and FEniCS. We used these rather inefficient routines, since they were convenient regarding implementation and integration of our methods. Of course, multiple assemblations can be avoided by investing more manual labor in the code, which can increase effectiveness of the simultaneous approach even further. The possible decrease of its computational time could make the simultaneous approach more competitive with the L-BFGS base ADM approach.

In table 9.1, we observe that VI-specific routines need at least four times longer than the unregularized routine to achieve our convergence criterion for relative shape objective values $\varepsilon_{\text{rel}} = 0.0038$. This is not surprising, since a stabilized Eikonal equation is solved to construct the VI-specific target for every main optimization step. It is necessary for all three VI-specific mesh quality routines, either to calculate the simultaneous descent directions, or to evaluate the condition triggering an ADM subroutine. The ADM approach exploits that the shape Γ_k and target $f^{\mathbb{D}}_{\Gamma_k}$ stay the same during an entire subroutine, which reduces the number of Eikonal equations needed to match the simultaneous approach, as is explained in section 9.2. In table 9.1, we see that the ADM routines achieve even lower computational times per step than the simultaneous approach for the VI-specific target, with the L-BFGS based method slightly outperforming the scaled gradient method. This gives exemplary evidence, that an ADM based mesh quality approach performs potentially better than simultaneous approaches for targets which are expensive to compute. On the other hand, times found in table 9.1 suggest that the simultaneous approach could possibly compete with the L-BFGS ADM routine for targets that are simple to evaluate, such as the uniform target. We suspect that the simultaneous approach with the VI-specific target slightly suffered due to the line search criterion of the main routine. This criterion is seen in algorithm 7.1, and checks for the weighted sum of the main shape objective and the parameterization tracking objective. The

algorithm could benefit from advanced line search techniques from multi-objective optimization, which could be part of further research.

Relative values $\mathfrak{J}^{\mathbb{D}}(\phi_k)/\mathfrak{J}^{\mathbb{D}}(\phi_0)$ for VI-specific targets $f^{\mathbb{D}}$ are seen in figure 9.4 (d). For this target, $\mathfrak{J}^{\mathbb{D}}$ can be interpreted as a measure for deviation from the specified local adaptation of the mesh to the current active set boundary ∂A. As the initial cell volume distribution is uniform, and thus not adapted to the active set boundary of the initial shape, the first value $\mathfrak{J}^{\mathbb{D}}(\phi_0)$ is quite large. With this in mind, we observe that the values of $\mathfrak{J}^{\mathbb{D}}$ of the unregularized approach stay near its initial value. This can be interpreted as the mesh staying unadapted to the variational inequality throughout the first approach. The initial increase of adaptation can be regarded as a consequence of initial large deformations, which compress cells near the shape. As active set boundaries are close to the shape by nature of the jumping source terms (8.56) and the obstacle $\psi = 0.5$, this compression of cells leads to local adaptation to the active set boundary as a byproduct. For VI-specific mesh regularization approaches five to seven, we see significant decrease of $\mathfrak{J}^{\mathbb{D}}$ in figure 9.4 (d), which means the mesh is better adapted to the active set boundary. Both ADM methods adapt the uniform initial mesh to the VI, and are not triggered later during the main routines, because the mesh stays sufficiently adapted. Since the simultaneous approach incorporates an adaptation in every step, it also converges to zero, achieving lower values than the ADM approaches in figure 9.4 (d).

In figure 9.2, we depict the final meshes and shapes of the compared approaches. Also, we show intermediate meshes of the approaches for step 45 in figure 9.3. In figure 9.3, we do not show the intermediate meshes of gradient based ADM methods, as these are nearly identical to those of the L-BFGS based ADM approaches.

First, notice the almost uniform quality of the unstructured initial mesh depicted in figure 9.2 (a). The unregularized routine finishes after 130 steps without finding further descent directions, where the according final mesh is depicted in (b). Clearly, the initial uniform mesh quality is lost during unregularized shape optimization. We emphasize, that strong degradation of cell quality is visible at the upper, lower and right hold-all boundary $\partial\mathbb{D}$. This might be one reason that the unregularized routine quits at this point, since no reliable descent direction can be computed. Nevertheless, we see that all routines, including the unregularized one, manage to approximate the target shape depicted in figure 9.2 (a). For routines depicted in figure 9.2 (c), (d) and (e) with uniform cell volume targets, we witness an increase in mesh quality compared to the unregularized routine seen in (b). This is especially apparent at the hold-all boundary $\partial\mathbb{D}$. Unlike the unregularized approach, there is no cell degeneration detectable for approaches featuring uniform target. Although similar in their results, there is a small visible difference in final mesh quality of the simultaneous and ADM based uniformity approaches. The ADM approaches manage to redistribute more cells closer to the inner dent of the final shape, which the simultaneous approach does not achieve to the same extent. However, to accomplish this, the ADM approaches transport cells around the kidney shape, which comes at the price of cell compression near the upper and lower left hold-all boundary. We mention, that this could come from the difference in convergence speeds for $\mathfrak{J}^{\mathbb{D}}$ of the simultaneous and ADM methods. As seen in figure 9.4, the simultaneous approach does not converge as fast as the ADM methods. This is visible in figure 9.3, where the mesh at iteration 45 of the simultaneous approach in (a) has similar qualities as the unregularized approach seen in (e). The meshes associated to the ADM approaches differ from these two, as we see no area with strong associated cell degeneration in figure 9.3 (b). Such behavior is reflected in the formulation of the ADM algorithm 9.1. When a threshold of non-uniformity $\overline{B}$ is crossed, the ADM method is triggered to correct the mesh quality to a base level $\underline{B}$. Hence the mesh at step 45 seen in figure 9.3 (b) already shows uniform qualities, as large initial deformations were corrected immediately, as seen by the

graph of $\mathfrak{J}^{\mathbb{D}}(\phi_i)/\mathfrak{J}^{\mathbb{D}}(\phi_0)$ in figure 9.4 (c). When convergence for $\mathfrak{J}^{\mathbb{D}}$ with uniform target takes place, the resulting meshes exhibit the features of figure 9.2 (e). The mentioned compression resulting from cell redistribution is unavoidable with mesh deformation approaches, since they are essentially constrained by the mesh topology. To remedy this, future work could either incorporate techniques altering the mesh topology, such as cell fusions, edge swaps and partial refinement, or use connectivity information at the discrete level to modify the parameterization tracking approach.

For the VI-specific target routines five to seven, it does not make sense to examine the meshes solely for uniformity. Instead, we also look for local adaptation near the boundary of the active set ∂A, which in our examples is close or identical to the shapes Γ_i. In figure 9.2 (f), (g) and (h), we see higher node densities around the shapes at final steps. However, the final mesh for the simultaneous approach differs noticeably from those of the ADM approaches. In the simultaneous case (f), the mesh vertices are more uniformly distributed around the shape and right side of the hold-all domain. For the ADM approaches (g) and (h), the node densities are localized closer around the shape, creating a zone which envelops the shape with smaller sized cells. Also, this envelope is apparent during the entire optimization approach, as can be seen by the intermediate mesh in figure 9.3 (d). As for the uniform target, the ADM approach guarantees a sufficiently adapted mesh throughout the routine by checking for the subroutine trigger condition (cf. algorithm 9.1). The results show that the VI-specific target, as constructed in section 9.1, is indeed suitable for cell volume allocation depending on distances to a specified boundary. Notice that the VI-specific approaches also diminish the degeneration of cells close to the hold-all boundaries $\partial\mathbb{D}$. These are apparent for the unregularized approach figure 9.2 (b), but not in the same extent for figure 9.2 (f), (g) and (h).

The difference of resulting meshes concerning simultaneous and ADM approaches can be explained by the parameters of transformation F used to construct the VI-specific target via equation (9.6). As the variation of the target $f^{\mathbb{D}}$ determines the allocation of cell volumes, we can manipulate the aggressiveness of local adaptation. In fact, the mesh of the simultaneous approach seen in figure 9.2 (f) corresponds closer to the given target than those of the ADM approaches. This reflected by the lower relative values of $\mathfrak{J}^{\mathbb{D}}$ in figure 9.4 (d) for the simultaneous approach. However, we can change parameters of the target $f^{\mathbb{D}}$, such that the simultaneous approach yields optimal meshes similar to those of the ADM approaches in figure 9.2 (g) and (h). We have tested this by changing the scaling parameter of transformation equation (9.6) to $\alpha = 5$, leaving all other parameters fixed. The resulting target has higher variation than the one used for the study in this section, leading to the final mesh seen in figure 9.1 (c) for the simultaneous approach, with the other parameters identical to approach five. In particular, this shows that the user can achieve his desired node densities by choice of a sufficient target.

We notice that there is a stretching of cells taking place at the left of the kidney shape dent. The VI-specific target demands to allocate more mesh vertices closer to the shape boundary, which also includes the area at the outer domain close to the dent. Moving vertices close to this boundary requires relatively large translations. While this gives the enforced higher resolution of the active set boundary, it also leads to the stretching effect due to limitations posed by node connectivity. As was the case for the uniform approaches, these mesh topological phenomena occur at the discrete level, and are not naturally taken into account by the continuous optimization perspective. Incorporating information of mesh topology can be harnessed to upgrade our algorithms, and is part of further research.

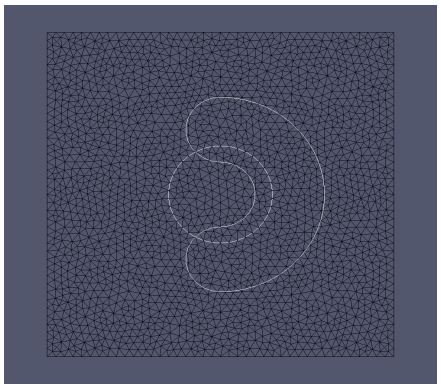

(a) Initial mesh with target shape

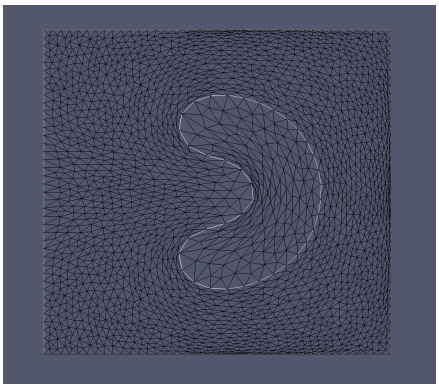

(b) Unregularized routine step 130

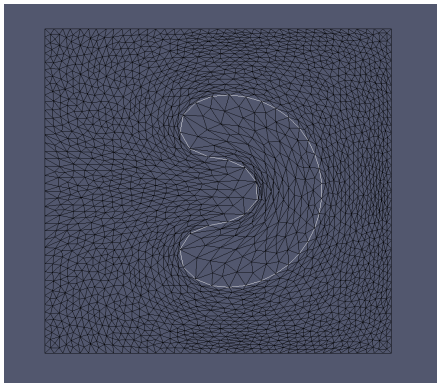

(c) Simultaneous VolOpt uniform step 144

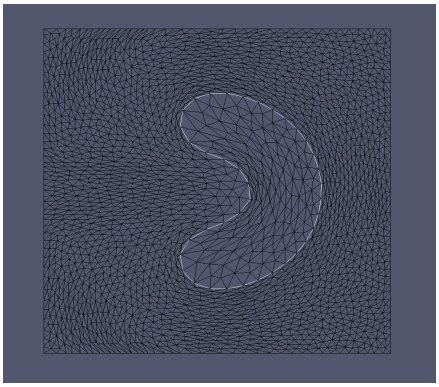

(d) Gradient ADM VolOpt uniform step 117

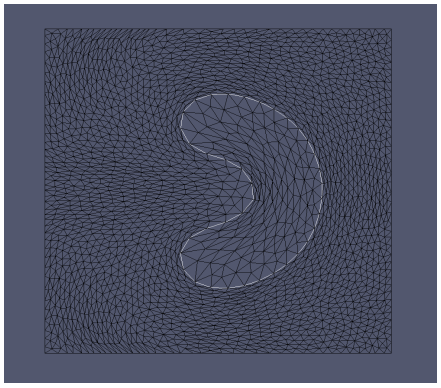

(e) L-BFGS ADM VolOpt uniform step 110

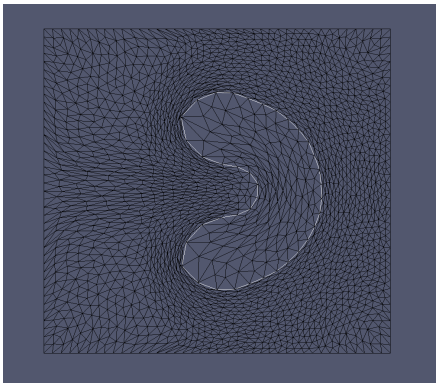

(f) Simultaneous VolOpt VI-sp. step 133

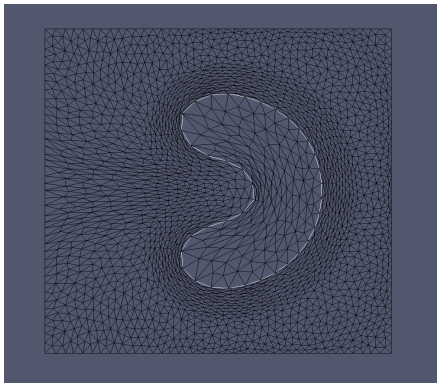

(g) Gradient ADM VolOpt VI-sp. step 118

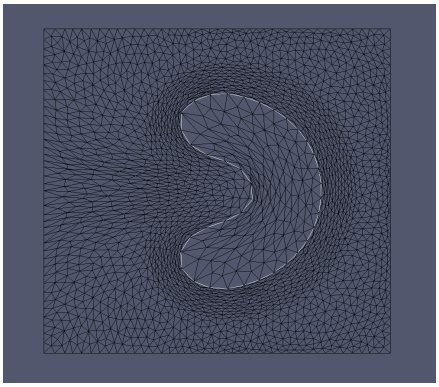

(h) L-BFGS ADM VI-sp. step 119

Figure 9.2: Final meshes of various (un-)regularized volume mesh quality optimization approaches for the VI-constrained problem.

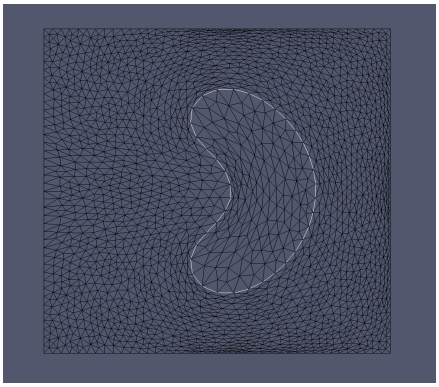

(a) Simultaneous VolOpt uniform

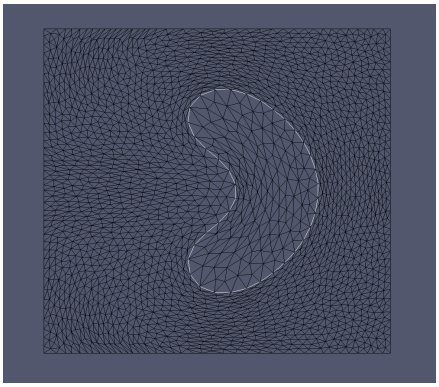

(b) L-BFGS ADM uniform

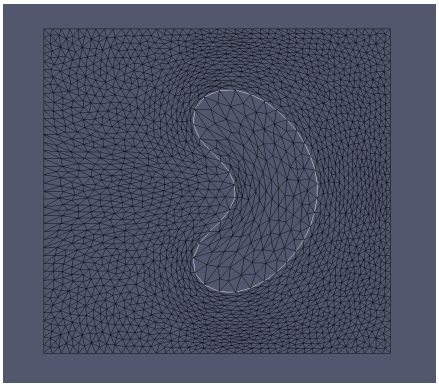

(c) Simultaneous VolOpt VI-sp.

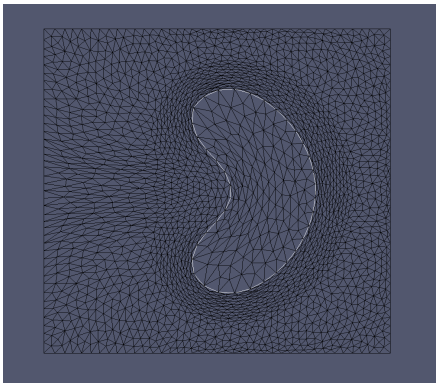

(d) L-BFGS ADM VI-sp.

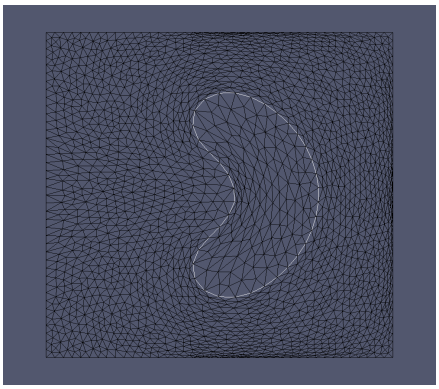

(e) Unregularized routine

Figure 9.3: Intermediate meshes at iteration 45 of various (un-)regularized volume mesh quality optimization approaches for the VI-constrained problem.

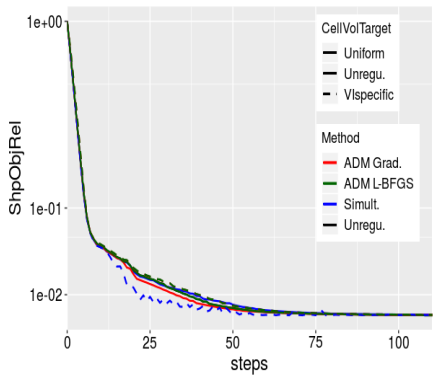

(a) Relative shape objective $\frac{\mathcal{J}(\Gamma_i)}{\mathcal{J}(\Gamma_i)}$

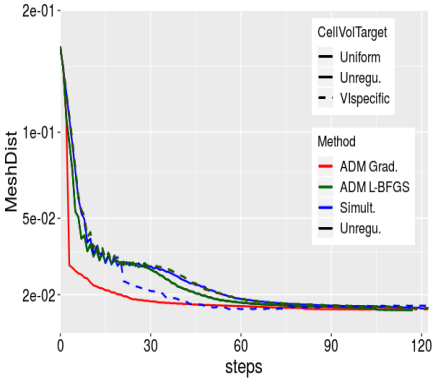

(b) Mesh distance of Γ_i and target shape

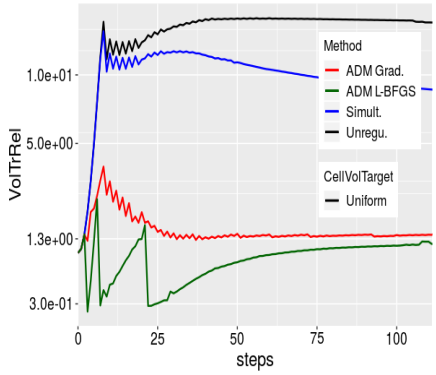

(c) $\frac{\mathfrak{J}^{\mathbb{D}}(\phi_i)}{\mathfrak{J}^{\mathbb{D}}(\phi_0)}$ for uniform target

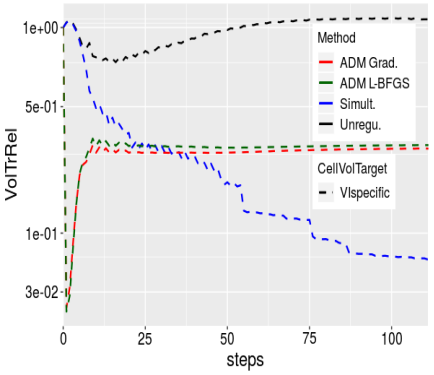

(d) $\frac{\mathfrak{J}^{\mathbb{D}}(\phi_i)}{\mathfrak{J}^{\mathbb{D}}(\phi_0)}$ for VI-sp. target

Figure 9.4: Results of the comparison study. (a) Relative values of the main shape optimization objective $\mathcal{J}$. (b) Mesh distance of shape iterates and target shape $\mathrm{dist}(\Gamma_k, \Gamma^{\mathrm{targ}})$ (cf. equation (7.23)). (c) Relative values of volume parameterization tracking objective $\mathfrak{J}^{\mathbb{D}}$ for the uniform target $f^{\mathbb{D}} = 1$. Here, $\overline{B} = 1.3$ and $\underline{B} = 0.3$ for volume mesh quality subroutines. (d) Relative values of volume parameterization tracking objective $\mathfrak{J}^{\mathbb{D}}$ for the VI-specific target $f^{\mathbb{D}}$ as in equation (9.7). Here, $\overline{B} = 0.5$ and $\underline{B} = 0.03$ for volume mesh quality subroutines.

Chapter 10

Conclusion and Outlook

Achievements of This Work In the following, we give a summary of the novel achievements in the field of shape optimization, which we derived throughout this work. We

- formulated a pre-shape optimization framework, enabling simultaneous formulation of shape optimization problems, and problems concerning parameterization of shapes. This formulation was flexible enough to pose problems for objects of different dimensions and with different boundary situations, including the case of ambient space/hold-all domain meshes.

- introduced the concept of pre-shape derivatives. We showed that shape differentiable functionals are pre-shape differentiable, derived pre-shape calculus rules extending shape calculus, and formulated a structure theorem extending the Hadamard-Zolésio theorem.

- defined the pre-shape parameterization tracking problem, provided existence of solutions in each fiber, analyzed its properties with respect to point sets, and gave a characterization of neighboring global solutions via L^2-metrics in fibers and Euler-Arnold-flows. We discussed its generalizations for pre-shapes of arbitrary codimension, perhaps with boundary, embedded in nonlinear ambient spaces, and implemented numerical examples generalizing the deformation method for mesh quality.

- derived the pre-shape derivative of the parameterization tracking problem, interpreted its components in light of the structure theorem for pre-shape derivatives, and used it to give a sufficient condition for global optimality via fiber stationarity.

- gave a closed expression for pre-shape Hessians to parameterization tracking, provided a simplified closed expression in solutions, and related its semidefinite directions to f-divergence free vector fields from the non-uniqueness characterization in fibers.

- showed how to use parameterization tracking to regularize shape optimization problems for desired shape mesh quality, proving existence of regularized solutions, leaving the original shape solution invariant. We provided sufficient spaces for parameterization tracking of hold-all domains with invariant embedded shapes, formulated simultaneous shape and volume regularized shape optimization problems as bilevel pre-shape optimization problems, and provided existence of regularized solutions coinciding with optimal shapes of the original problem.

- provided shape gradient regularizations for simultaneous optimization of shape and volume mesh quality, which did not depend on the structure of underlying shape optimization problems, and allowed for general choice of shape gradient representations. We proved consistency of regularized shape gradients from modified reduced systems with pre-shape gradients of the respective individual problems.

- gave an algorithm for simultaneous shape optimization and control of shape and volume mesh quality, without need for additional gradient solves, and invariance of intermediary and optimal shapes.

- implemented and compared various regularized routines for a PDE-constrained model problem, using linear elasticity and quasilinear p-Laplacian gradient representations. We also numerically analyzed the pitfalls of using full pre-shape gradients for parameterization tracking of shapes, and use of unsuitable spaces for parameterization tracking of hold-all domains.

- gave regularized formulations of tracking type shape optimization problems constrained by elliptic variational inequalities of first kind, showed convergence characterizations of states and adjoints under sufficient assumptions, proved existence of regularized shape derivatives, calculated closed formulations for them, and showed their convergence to a limiting object.

- provided an algorithm taking advantage of established convergence relations for fully regularized first order VI-constrained tracking type problems, and implemented numerical examples for two different obstacles.

- designed a parameterization tracking target customized for shape optimization under variational inequalities, which can also be applied to general shape optimization problems.

- introduced an ADM-inspired pre-shape regularization algorithm, featuring L-BFGS methods for mesh quality, which can be combined with all previous techniques, including simultaneous shape and volume regularization for general shape optimization problems. We implemented and compared previous algorithms for parameterization tracking using VI-specific and uniform targets for an exemplary VI-constrained shape optimization problem.

Further Research With the extensive coverage of pre-shape calculus and its application to mesh quality regularizations in shape optimization, we actually see this work as a starting point for further research in different directions. Pre-shape calculus could be extended to nonlinear ambient spaces, which are open manifolds of finite dimension themselves. This would require more differential geometric effort, and could be achieved by using perturbations of identities and associated pre-shape derivatives defined via retractions, or (weak) Riemannian or Lie group exponential maps. An exemplary application could be mitigation of coastal erosion on the world modeled by a spherical mesh. Even further, Whitney manifold germs as model manifolds are of interest, since they permit shapes with interesting features, such as corners and Lipschitz boundaries.

An immediate succession to the shape optimization regularizations via parameterization tracking is the design of targets f suited for the specific structure of underlying problems. We have shown how such a design process can work in the case of VI-constrained problems, but other problems coming from optimization in elastoplasticity, contact problems, and computational fluid dynamics could all be envisioned. A particularly interesting new case for pre-shape techniques could be

mesh quality adaption for time dependent problems. Design of targets suiting geometric quantities of shapes and hold-all domains, such as their curvature, could play a part in targets as well.

For VI-constrained shape optimization problems, better customized targets f for the parameterization tracking regularization would certainly be rewarding. These could incorporate the information on errors of the regularized and unregularized objective functionals, and mismatch in complementarity of primal variables and their multipliers, similar to refinement indicators found in [25].

Independent of pre-shape techniques, the question of convergence of optimal shapes of the fully regularized VI-constrained shape optimization problem of chapter 8 to an optimal shape of the unregularized problem remains an endeavor for the future. Further, the study of general variational inequality constrained shape optimization problems seems an area relatively unexplored. General objective functionals, as well as variational inequality constraints of second order, or even quasi-variational inequalities are certainly of interest. On a general note, a shape or pre-shape calculus for non- or semi-smooth problems would be beneficial. It could be used to carry over useful description of optimality conditions, e.g. by shape analogues of Clarke-, Bouligand- or Mordukhovich-stationarity, which have been fruitfully applied in the optimal control case.

The pre-shape parameterization tracking techniques and their gradient regularizations followed a first optimize, then discretize approach. They neglect discrete information, such as the connectivity and topology of the discretized mesh. Techniques based on the discrete setting could harness these properties, and be described in the context of pre-shape optimization. Also, their convergence to the continuous case, e.g. as hinted in section 5.2.1, could be explored. Our techniques do not change mesh topologies, which also permits beneficial combination with partial remeshing approaches in future applications.

Following this train of thought, exploring the relation of pre-shape parameterization tracking and hypersingular discrete Riesz-energy with external forces as in [23] could be of theoretical interest.

Numerical application of higher order parameterization tracking methods, such as Newton methods or customized pre-shape gradient representations, featuring its pre-shape Hessian from section 5.5, could also be an immediate next step.

On a more distant note, the connection of the abstract formulation of parameterization tracking in section 5.3 could be used to generate new regularization classes. In particular, studying its connection to optimal transport problems, and generalizations using L^p-Monge-Kantorovich and L^p-Monge-Ampère formulations in pre-shape spaces in light of [43, 72] could be interesting pursuits.

The pre-shape setting could also be used to pose regularization problems unrelated to the parameterization tracking problem. With the generality of pre-shape calculus developed in chapter 4, new regularizers for shape gradient systems in form of their tangential pre-shape derivative components can be constructed analogously.

List of Figures

3.1 Steklov-Poincaré and TRACE Shape Gradients for the T106A 23

4.1 The Shape Space B_e^n 28
4.2 The Pre-Shape Space $\mathrm{Emb}(M, \mathbb{R}^{n+1})$ 30
4.3 The Tangential Bundle TB_e^n 32
4.4 The Tangential Bundle $T\,\mathrm{Emb}(M, \mathbb{R}^{n+1})$ 33

5.1 Weak*-Convergence of Dirac Measures as Meshes 63
5.2 Tangential f-Divergence Free Vector Fields 67
5.3 Decomposition of the Parameteriztion Tracking Pre-Shape Gradient on a Sphere 81
5.4 2D Hold-All Parameteriztion Tracking Results without Shape Optimization 90
5.5 3D Shape Parameteriztion Tracking Results without Shape Optimization 91
5.6 Results of Pre-Shape Parameterization Tracking without Shape Optimization 91

6.1 Topological Situation for Shapes with and without Boundaries in Hold-All Domains 107

7.1 Shapes for the Numerical Study of Simultaneous Shape and Volume Tracking with Shape Optimization 117
7.2 Initial Mesh with Target Shape for the Numerical Study of Simultaneous Shape and Volume Tracking with Shape Optimization 128
7.3 Results of the Numerical Study of Simultaneous Shape and Volume Tracking with Shape Optimization 130
7.4 Final Meshes with $g^{\mathbb{D}} \circ \phi^{-1} \cdot \det D\phi^{-1}$ of the Numerical Study of Simultaneous Shape and Volume Tracking with Shape Optimization 132
7.5 Zoomed Top of Final Meshes with $g^{\mathbb{D}} \circ \phi^{-1} \cdot \det D\phi^{-1}$ of the Numerical Study of Simultaneous Shape and Volume Tracking with Shape Optimization 133
7.6 Final Shapes with $g^M \circ \varphi^{-1} \cdot \det D^\tau \varphi^{-1}$ of the Numerical Study of Simultaneous Shape and Volume Tracking with Shape Optimization 134
7.7 Results of the Comparison Study of Full and Tangential Pre-Shape Derivative for Shape Mesh Regularization 136
7.8 Initial and Final Meshes of the Comparison Study of Full and Tangential Pre-Shape Derivative for Shape Mesh Regularization 137
7.9 Results of the Comparison Study of Direct and Shape Invariant Volume Mesh Regularization 139
7.10 Initial and Final Meshes of the Comparison Study of Direct and Shape Invariant Volume Mesh Regularization 140

8.1 Shapes of the Numerical Study of VI-Constrained Shape Optimization 164
8.2 Solutions for Different Obstacle Problems 164
8.3 Convergence Plot for Derivatives of Smoothed max-Functions 165
8.4 Picture of $\operatorname{sign}_\gamma\big(\bar\lambda + c\cdot(y_{\gamma,c} - \psi)\big) - \operatorname{sign}\big(\bar\lambda + c\cdot(y_c - \psi)\big)$ for Different Regularization Parameters 165
8.5 Mesh Study Results for L^1-Convergence of $\operatorname{sign}_\gamma\big(\bar\lambda + c\cdot(y_{\gamma,c} - \psi)\big) - \operatorname{sign}\big(\bar\lambda + c\cdot(y_c - \psi)\big)$ 166
8.6 Regularized Adjoint Limit 166
8.7 Morphing Shapes of a VI-Constrained Shape Optimization Routine . 167
8.8 Results of the Comparison of VI-Constrained Shape Optimization Routines for Constant Obstacle 169
8.9 Results of the Comparison of VI-Constrained Shape Optimization Routines for Non-Constant Obstacle 170

9.1 Construction of VI-Specific Targets via Eikonal Equations 174
9.2 Initial and Final Meshes of Unregularized, Simultaneously Regularized and ADM-like Volume Mesh Qualtiy Routines for VI-Constrained Shape Optimization 188
9.3 Intermediate Meshes of Unregularized, Simultaneously Regularized and ADM-like Volume Mesh Qualtiy Routines for VI-Constrained Shape Optimization 189
9.4 Results for the Unregularized, Simultaneously Regularized and ADM-like Volume Mesh Qualtiy Routines for VI-Constrained Shape Optimization 190

List of Tables

7.1 Times of the Numerical Study of Simultaneous Shape and Volume Tracking with Shape Optimization 129

9.1 Times of the Unregularized, Simultaneously Regularized and ADM-like Volume Mesh Qualtiy Routines for VI-Constrained Shape Optimization 184

List of Algorithms

3.1 TRASOR Algorithm Using Steklov-Poincaré Metrics 22

7.1 Algorithm for Simultaneous Shape and Volume Regularized Shape Optimization 127

8.1 Backtracking Line Search 167
8.2 Algorithm with Safeguarding via Limit Systems for VI-Constrained Shape Optimization 168

9.1 Algorithm for VI-Specific Simultaneous Shape and Volume Regularization with Quasi-Newton-ADM Subroutines for Volume Parameterization Tracking 177
9.2 Two Loop Shape L-BFGS Algorithm 180

Bibliography

[1] R.A. Adams and J.J.F. Fournier. *Sobolev Spaces*, volume 140 of *Pure and Applied Mathematics*. Elsevier, 2003.

[2] M.E. Algorri and F. Schmitt. Mesh Simplification. In *Computer Graphics Forum*, volume 15, pages 77–86. Wiley Online Library, 1996.

[3] M.S. Alnæs. UFL: a Finite Element Form Language. In A. Logg, K.-A. Mardal, and G.N. Wells, editors, *Automated Solution of Differential Equations by the Finite Element Method*, volume 84 of *Lecture Notes in Computational Science and Engineering*, chapter 17. Springer, 2012.

[4] M.S. Alnæs, J. Blechta, J. Hake, A. Johansson, B. Kehlet, A. Logg, C. Richardson, J. Ring, M.E. Rognes, and G.N. Wells. The FEniCS Project Version 1.5. *Archive of Numerical Software*, 3(100), 2015.

[5] H.B. Ameur, M. Burger, and B. Hackl. Level Set Methods for Geometric Inverse Problems in Linear Elasticity. *Inverse Problems*, 20(3):673–696, 2004.

[6] V. Arnold. Sur la Géométrie Différentielle des Groupes de Lie de Dimension Infinie et ses Applications à l'Hydrodynamique des Fluides Parfaits. In *An-*

nales de l'Institut Fourier, volume 16, pages 319–361. Association des Annales de l'Institut Fourier, 1966.

[7] J. Backhaus, M. Bolten, O.T. Doganay, M. Ehrhardt, B. Engel, C. Frey, H. Gottschalk, M. Günther, C. Hahn, J. Jäschke, P. Jaksch, K. Klamroth, A. Liefke, and D. Luft et al. GivEn - Shape Optimization for Gas Turbines in Volatile Energy Networks. In *Mathematical Modeling, Simulation and Optimization for Power Engineering and Management*, pages 71–106. Springer, 2021.

[8] J. Backhaus, A. Schmitz, C. Frey, S. Mann, M. Nagel, M. Sagebaum, and N.R. Gauger. Application of an Algorithmically Differentiated Turbomachinery Flow Solver to the Optimization of a Fan Stage. In *AIAA-Paper 2017-3997*, 2017.

[9] S. Balay, S. Abhyankar, M. Adams, J. Brown, P. Brune, K. Buschelman, L. Dalcin, A. Dener, V. Eijkhout, W. Gropp, et al. *PETSc Users Manual*. Argonne National Laboratory, 2019.

[10] A. Banyaga. Formes-Volume sur les Variétés a Bord. *L'Enseignement Mathématique*, 20(2):127–131, 1974.

[11] M. Bauer, M. Bruveris, P. Harms, and P.W. Michor. Vanishing Geodesic Distance for the Riemannian Metric with Geodesic Equation the KdV-Equation. *Annals of Global Analysis and Geometry*, 41(4):461–472, 2012.

[12] M. Bauer, M. Bruveris, and P.W. Michor. Overview of the Geometries of Shape Spaces and Diffeomorphism Groups. *Journal of Mathematical Imaging and Vision*, 50(1-2):60–97, 2014.

[13] M. Bauer, P. Harms, and P.W. Michor. Almost Local Metrics on Shape Space of Hypersurfaces in n-Space. *SIAM Journal on Imaging Sciences*, 5(1):244–310, 2012.

[14] M. Bauer, P. Harms, and S.C. Preston. Vanishing Distance Phenomena and the Geometric Approach to SQG. *Archive for Rational Mechanics and Analysis*, 235:1445–1466, 2020.

[15] K. Becker, K. Heitkamp, and E. Kügeler. Recent Progress in a Hybrid-Grid CFD Solver for Turbomachinery Flows. *Proceedings Fifth European Conference on Computational Fluid Dynamics ECCOMAS CFD00 2010*, 2010.

[16] M.P. Bendsøe. Topology Optimization. *Encyclopedia of Optimization*, pages 3928–3929, 2009.

[17] M. Berggren. A Unified Discrete–Continuous Sensitivity Analysis Method for Shape Optimization. In *Applied and Numerical Partial Differential Equations*, volume 15 of *Computational Methods in Applied Sciences*, pages 25–39. Springer, 2010.

[18] L. Bittner and H. Gottschalk. Optimal Reliability for Components under Thermomechanical Cyclic Loading. *Control and Cybernetics*, 45:2–35, 2016.

[19] P. Bochev, G. Liao, and G. dela Pena. Analysis and Computation of Adaptive Moving Grids by Deformation. *Numerical Methods for Partial Differential Equations: An International Journal*, 12(4):489–506, 1996.

[20] M. Bolten, H. Gottschalk, C. Hahn, and M. Saadi. Numerical Shape Optimization to Decrease Failure Probability of Ceramic Structures. *Computing and Visualization in Science*, 21(1):1–10, 2019.

[21] M. Bolten, H. Gottschalk, and S. Schmitz. Minimal Failure Probability for Ceramic Design via Shape Control. *Journal of Optimization Theory and Applications*, 166(3):983–1001, 2015.

[22] J.F. Bonnans and D. Tiba. Pontryagin's Principle in the Control of Semilinear Elliptic Variational Inequalities. *Applied Mathematics and Optimization*, 23(1):299–312, 1991.

[23] S.V. Borodachov, D.P. Hardin, and E.B. Saff. *Discrete Energy on Rectifiable Sets*. Springer Monographs in Mathematics. Springer, 2019.

[24] V. Braibant and C. Fleury. Shape Optimal Design Using B-Splines. *Computer Methods in Applied Mechanics and Engineering*, 44(3):247–267, 1984.

[25] C. Brett, C.M. Elliott, M. Hintermüller, and C. Löbhard. Mesh Adaptivity in Optimal Control of Elliptic Variational Inequalities with Point-Tracking of the State. *Interfaces and Free Boundaries*, 17(1):21–53, 2015.

[26] H. Brézis. Monotonicity Methods in Hilbert Spaces and Some Applications to Nonlinear Partial Differential Equations. *Contributions to Nonlinear Functional Analysis*, pages 101–156, 1971.

[27] H. Brézis and G. Stampacchia. Sur la Regularité de la Solution d'Inéquations Elliptiques. *Bulletin de la Société Mathématique de France*, 96:153–180, 1968.

[28] M. Bruveris, P.W. Michor, A. Parusiński, and A. Rainer. Moser's Theorem on Manifolds with Corners. *Proceedings of the American Mathematical Society*, 146(11):4889–4897, 2018.

[29] X. Cai, B. Jiang, and G. Liao. Adaptive Grid Generation Based on the Least-Squares Finite-Element Method. *Computers & Mathematics with Applications*, 48(7-8):1077–1085, 2004.

[30] W. Cao, W. Huang, and R.D. Russell. A Study of Monitor Functions for Two-Dimensional Adaptive Mesh Generation. *SIAM Journal on Scientific Computing*, 20(6):1978–1994, 1999.

[31] W. Cao, W. Huang, and R.D. Russell. A Moving Mesh Method Based on the Geometric Conservation Law. *SIAM Journal on Scientific Computing*, 24(1):118–142, 2002.

[32] A. Capatina. *Variational Inequalities and Frictional Contact Problems*, volume 31 of *Advances in Mechanics and Mathematics*. Springer, 2014.

[33] J. Céa. Conception Optimale ou Identification de Formes, Calcul Rapide de la Dérivée Directionelle de la Fonction Coût. *ESAIM: Mathematical Modelling and Numerical Analysis*, 20(3):371–402, 1986.

[34] V. Cervera, F. Mascaro, and P.W. Michor. The Action of the Diffeomorphism Group on the Space of Immersions. *Differential Geometry and its Applications*, 1(4):391–401, 1991.

[35] C. Christof, C. Clason, C. Meyer, and S. Walther. Optimal Control of a Non-Smooth Semilinear Elliptic Equation. *Mathematical Control & Related Fields*, 8(1):247–276, 2018.

[36] M. Cocou. Existence of Solutions of a Dynamic Signorini's Problem with Nonlocal Friction in Viscoelasticity. *Zeitschrift für angewandte Mathematik und Physik ZAMP*, 53(6):1099–1109, 2002.

[37] R. Correa and A. Seeger. Directional Derivative of a Minimax Function. *Nonlinear Analysis: Theory, Methods & Applications*, 9(1):13–22, 1985.

[38] G. Csató, B. Dacorogna, and O. Kneuss. *The Pullback Equation for Differential Forms*, volume 83 of *Progress in Nonlinear Differential Equations and Their Applications*. Springer Science & Business Media, 2011.

[39] B. Dacorogna and J. Moser. On a Partial Differential Equation Involving the Jacobian Determinant. In *Annales de l'Institut Henri Poincaré (C), Non Linear Analysis*, volume 7, pages 1–26. Elsevier, 1990.

[40] K. Deckelnick, P.J. Herbert, and M. Hinze. A Novel $W^{1,\infty}$ Approach to Shape Optimisation with Lipschitz Domains. *arXiv preprint arXiv:2103.13857*, 2021.

[41] M.C. Delfour and J.-P. Zolésio. Shape Sensitivity Analysis via Min Max Differentiability. *SIAM Journal on Control and Optimization*, 26(4):834–862, 1988.

[42] M.C. Delfour and J.-P. Zolésio. *Shapes and Geometries: Metrics, Analysis, Differential Calculus, and Optimization*, volume 22 of *Advances in Design and Control*. SIAM, 2nd edition, 2001.

[43] G.L. Delzanno and J.M. Finn. The Fluid Dynamic Approach to Equidistribution Methods for Grid Adaptation. *Computer Physics Communications*, 182(2):330–346, 2011.

[44] F.R. Desaint and J.-P. Zolésio. Manifold Derivative in the Laplace–Beltrami Equation. *Journal of Functional Analysis*, 151(1):234–269, 1997.

[45] G. Dziuk. An Algorithm for Evolutionary Surfaces. *Numerische Mathematik*, 58(1):603–611, 1990.

[46] G. Dziuk and J. Hutchinson. The Discrete Plateau Problem: Algorithm and Numerics. *Mathematics of Computation*, 68(225):1–23, 1999.

[47] D.G. Ebin and J.E. Marsden. Groups of Diffeomorphisms and the Motion of an Incompressible Fluid. *Annals of Mathematics*, 92(1):102–163, 1970.

[48] K. Eppler and H. Harbrecht. A Regularized Newton Method in Electrical Impedance Tomography Using Shape Hessian Information. *Control and Cybernetics*, 34(1):203–225, 2005.

[49] T. Etling, R. Herzog, E. Loayza-Romero, and G. Wachsmuth. First and Second Order Shape Optimization Based on Restricted Mesh Deformations. *SIAM Journal on Scientific Computing*, 42(2):A1200–A1225, 2020.

[50] L.C. Evans. *Partial Differential Equations*, volume 19 of *Graduate Studies in Mathematics*. American Mathematical Society, 1993.

[51] B. Farb and D. Margalit. *A Primer on Mapping Class Groups*. Princeton University Press, 2012.

[52] B. Fedelich. A Stochastic Theory for the Problem of Multiple Surface Crack Coalescence. *International Journal of Fracture*, 91:23–45, 1998.

[53] D.A. Field. Laplacian Smoothing and Delaunay Triangulations. *Communications in Applied Numerical Methods*, 4(6):709–712, 1988.

[54] L.A. Freitag. On Combining Laplacian and Optimization-Based Mesh Smoothing Techniques. Technical report, Argonne National Lab., IL (United States), 1997.

[55] P.J. Frey and H. Borouchaki. Surface Mesh Quality Evaluation. *International Journal for Numerical Methods in Engineering*, 45(1):101–118, 1999.

[56] J. Friederich, G. Leugering, and P. Steinmann. Adaptive Finite Elements Based on Sensitivities for Topological Mesh Changes. *Control and Cybernetics*, 43, 2014.

[57] B. Führ, V. Schulz, and K. Welker. Shape Optimization for Interface Identification with Obstacle Problems. *Vietnam Journal of Mathematics*, 2018. DOI: 10.1007/s10013-018-0312-0.

[58] D. Gale. The Classification of 1-Manifolds: A Take-Home Exam. *The American Mathematical Monthly*, 94(2):170–175, 1987.

[59] P. Gangl, A. Laurain, H. Meftahi, and K. Sturm. Shape Optimization of an Electric Motor Subject to Nonlinear Magnetostatics. *SIAM Journal on Scientific Computing*, 37(6):B1002–B1025, 2015.

[60] R.V. Garimella, M.J. Shashkov, and P.M. Knupp. Triangular and Quadrilateral Surface Mesh Quality Optimization Using Local Parametrization. *Computer Methods in Applied Mechanics and Engineering*, 193(9-11):913–928, 2004.

[61] F. Gay-Balmaz and C. Vizman. Principal Bundles of Embeddings and Nonlinear Grassmannians. *Annals of Global Analysis and Geometry*, 46(3):293–312, 2014.

[62] German Aerospace Center. Variable Definitions Valid for TRACE SUITE 9.2. http://www.trace-portal.de/userguide/trace/variableNames.pdf, 2019.

[63] C. Geuzaine and J.-F. Remacle. Gmsh: A 3-D Finite Element Mesh Generator with Built-In Pre- and Post-Processing Facilities. *International Journal for Numerical Methods in Engineering*, 79(11):1309–1331, 2009.

[64] F. Giannessi and A. Maugeri, editors. *Variational Inequalities and Network Equilibrium Problems*. Proceedings of the International School of Mathematics "G. Stampacchia". Springer, 1995.

[65] H. Gottschalk, R. Krause, G. Rollmann, T. Seibel, and S. Schmitz. Probabilistic Schmid Factors and Scatter of LCF Life. *Materials Science & Engineering Technology*, 46:156–164, 2015.

[66] H. Gottschalk and S. Schmitz. Optimal Reliability in Design for Fatigue Life, Part I: Existence of Optimal Shapes. *SIAM Journal on Control and Optimization*, 52:2727–2752, 2014.

[67] H. Gottschalk, S. Schmitz, G. Rollmann, and R. Krause. A Probabilistic Approach to Low Cycle Fatigue. *Proceedings of ASME Turbo Expo 2013*, pages GT2013–94899, 2012.

[68] M. Grajewski, M. Köster, and S. Turek. Mathematical and Numerical Analysis of a Robust and Efficient Grid Deformation Method in the Finite Element Context. *SIAM Journal on Scientific Computing*, 31(2):1539–1557, 2009.

[69] M. Grajewski, M. Köster, and S. Turek. Numerical Analysis and Implementational Aspects of a New Multilevel Grid Deformation Method. *Applied Numerical Mathematics*, 60(8):767–781, 2010.

[70] V. Guillemin and A. Pollack. *Differential Topology*, volume 370. American Mathematical Society, 2010.

[71] H. Omori. *Infinite-Dimensional Lie Groups*, volume 158 of *Translations of Mathematical Monographs*. American Mathematical Society, 2017.

[72] S. Haker, L. Zhu, A. Tannenbaum, and S. Angenent. Optimal Mass Transport for Registration and Warping. *International Journal of Computer Vision*, 60(3):225–240, 2004.

[73] R.S. Hamilton. The Inverse Function Theorem of Nash and Moser. *Bulletin (New Series) of the American Mathematical Society*, 7(1):65–222, 1982.

[74] S. Hardesty, H. Antil, D. P. Kouri, and D. Ridzal. The Strip Method for Shape Derivatives. *Preprint available at http://dx.doi.org/10.13140/RG 2.32766.82246*, 2021.

[75] J. Haubner, M. Siebenborn, and M. Ulbrich. A Continuous Perspective on Shape Optimization via Domain Transformations. *SIAM Journal on Scientific Computing*, 43(3):A1997–A2018, 2021.

[76] C. Heinemann and K. Sturm. Shape Optimization for a Class of Semilinear Variational Inequalities with Applications to Damage Models. *SIAM Journal on Mathematical Analysis*, 48(5):3579–3617, 2016.

[77] A. Henrot and M. Pierre. *Shape Variation and Optimization*, volume 28 of *Tracts in Mathematics*. European Mathematical Society, 2018.

[78] R. Herzog and E. Loayza-Romero. A Manifold of Planar Triangular Meshes with Complete Riemannian Metric. *arXiv preprint arXiv:2012.05624*, 2020.

[79] M. Hintermüller. Inverse Coefficient Problems for Variational Inequalities: Optimality Conditions and Numerical Realization. *Mathematical Modelling and Numerical Analysis*, 35(1):129–152, 2001.

[80] M. Hintermüller. An Active-Set Equality Constrained Newton Solver with Feasibility Restoration for Inverse Coefficient Problems in Elliptic Variational Inequalities. *Inverse Problems*, 24(3):034017, 2008.

[81] M. Hintermüller and I. Kopacka. Mathematical Programs with Complementarity Constraints in Function Space: C- and Strong Stationarity and a Path-Following Algorithm. *SIAM Journal on Optimization*, 20(2):868–902, 2009.

[82] M. Hintermüller and L. Laurain. Optimal Shape Design Subject to Elliptic Variational Inequalities. *SIAM Journal on Control and Optimization*, 49(3):1015–1047, 2011.

[83] M. Hintermüller and T. Surowiec. First-Order Optimality Conditions for Elliptic Mathematical Programs with Equilibrium Constraints via Variational Analysis. *SIAM Journal on Optimization*, 21(4):1561–1593, 2011.

[84] R. Hiptmair and A. Paganini. Shape Optimization by Pursuing Diffeomorphisms. *Computational Methods in Applied Mathematics*, 15(3):291–305, 2015.

[85] R. Hiptmair, A. Paganini, and S. Sargheini. Comparison of Approximate Shape Gradients. *BIT Numerical Mathematics*, 55(2):459–485, 2015.

[86] M.W. Hirsch. *Differential Topology*, volume 33 of *Graduate Texts in Mathematics*. Springer Science & Business Media, 2012.

[87] E.O. Hjelle and A. Schmeding. Strong Topologies for Spaces of Smooth Maps with Infinite-Dimensional Target. *Expositiones Mathematicae*, 35(1):13–53, 2017.

[88] H. Hoheisel, R. Kiock, H.J. Lichtfuss, and L. Fottner. Influence of Free Stream Turbulence and Blade Pressure Gradient on Boundary Layer and Loss Behaviour of Turbine Cascades. In *ASME 1986 International Gas Turbine Conference and Exhibit*, pages V001T01A102–V001T01A102. American Society of Mechanical Engineers, 1986.

[89] L. Hörmander. *The Analysis of Linear Partial Differential Operators I: Distribution Theory and Fourier Analysis*. Classics in Mathematics. Springer, 2nd edition, 2015.

[90] W. Hurewicz and H. Wallman. *Dimension Theory (PMS-4)*, volume 4. Princeton University Press, 2015.

[91] S.-R. Hysing and S. Turek. The Eikonal Equation: Numerical Efficiency vs. Algorithmic Complexity on Quadrilateral Grids. In *Proceedings of ALGORITMY*, volume 22, 2005.

[92] S. Illman. The Very-Strong C^∞ Topology on $C^\infty(M, N)$ and K-Equivariant Maps. *Osaka Journal of Mathematics*, 40(2):409–428, 2003.

[93] K. Ito and K. Kunisch. Optimal Control of Elliptic Variational Inequalities. *Applied Mathematics and Optimization*, 41(3):343–364, 2000.

[94] K. Ito and K. Kunisch. Semi-Smooth Newton Methods for Variational Inequalities of the First Kind. *ESIAM: Mathematical Modelling and Numerical Analysis*, 37:41–62, 2003.

[95] K. Ito, K. Kunisch, and G.H. Peichl. Variational Approach to Shape Derivatives. *ESAIM: Control, Optimisation and Calculus of Variations*, 14(3):517–539, 2008.

[96] J. Haslinger and R.A.E. Mäkinen. *Introduction to Shape Optimization: Theory, Approximation, and Computation*, volume 7 of *Advances in Design and Control*. SIAM, 2003.

[97] A. Jameson. Aerodynamic Shape Optimization Using the Adjoint Method. *Lectures at the Von Karman Institute, Brussels*, 2003.

[98] B.P. Johnston, J.M. Sullivan Jr, and A. Kwasnik. Automatic Conversion of Triangular Finite Element Meshes to Quadrilateral Elements. *International Journal for Numerical Methods in Engineering*, 31(1):67–84, 1991.

[99] S.H. Joshi, E. Klassen, A. Srivastava, and I. Jermyn. Removing Shape-Preserving Transformations in Square-Root Elastic (SRE) Framework for Shape Analysis of Curves. In *International Workshop on Energy Minimization Methods in Computer Vision and Pattern Recognition*, pages 387–398. Springer, 2007.

[100] M. Juntunen and R. Stenberg. Nitsche's Method for General Boundary Conditions. *Mathematics of Computation*, 78(267):1353–1374, 2009.

[101] D.G. Kendall, D. Barden, T.K. Carne, and H. Le. *Shape and Shape Theory*, volume 500 of *Wiley Series in Probability and Statistics*. John Wiley & Sons, 2009.

[102] N. Kikuchi and J.T. Oden. *Contact Problems in Elasticity: A Study of Variational Inequalities and Finite Element Methods*, volume 8 of *Studies in Applied Mathematics*. SIAM, 1988.

[103] D. Kinderlehrer and G. Stampacchia. *An Introduction to Variational Inequalities and Their Applications*, volume 31 of *Classics in Applied Mathematics*. SIAM, 1980.

[104] M. Kocvara and J. Outrata. Shape Optimization of Elasto-Plastic Bodies Governed by Variational Inequalities. In J.-P. Zolésio, editor, *Boundary Control and Variation*, number 163 in Lecture Notes in Pure and Applied Mathematics, pages 261–271. Marcel Dekker, 1994.

[105] A. Kriegl and P.W. Michor. *The Convenient Setting of Global Analysis*, volume 53 of *Mathematical Surveys and Monographs*. American Mathematical Society, 1997.

[106] S. Lang. *Fundamentals in Differential Geometry*, volume 191 of *Graduate Texts in Mathematics*. Springer, 2nd edition, 2001.

[107] A. Laurain and K. Sturm. Domain Expression of the Shape Derivative and Application to Electrical Impedance Tomography. Technical Report No. 1863, Weierstraß-Institut für angewandte Analysis und Stochastik, Berlin, 2013.

[108] A. Laurain and S.W. Walker. Optimal Control of Volume-Preserving Mean Curvature Flow. *Journal of Computational Physics*, 438:110373, 2021.

[109] A. Laurain, M. Winckler, and I. Yousept. Shape Optimization for Superconductors Governed by H(curl)-elliptic Variational Inequalities. *SIAM Journal on Control and Optimization*, 59(3):2247–2272, 2021.

[110] J.M. Lee. *Manifolds and Differential Geometry*, volume 107 of *Graduate Studies in Mathematics*. American Mathematical Society, 2009.

[111] J.M. Lee. *Introduction to Smooth Manifolds*, volume 218 of *Graduate Texts in Mathematics*. Springer, 2nd edition, 2013.

[112] G. Liao and D. Anderson. A New Approach to Grid Generation. *Applicable Analysis*, 44(3-4):285–298, 1992.

[113] J.L. Lions and G. Stampacchia. Variational Inequalities. *Communications on Pure and Applied Mathematics*, 20(3):493–519, 1967.

[114] F. Liu, S. Ji, and G. Liao. An Adaptive Grid Method and its Application to Steady Euler Flow Calculations. *SIAM Journal on Scientific Computing*, 20(3):811–825, 1998.

[115] W.B. Liu and J.E. Rubio. Optimal Shape Design for Systems Governed by Variational Inequalities, Part 1: Existence Theory for the Elliptic Case. *Journal of Optimization Theory and Applications*, 69(2):351–371, 1991.

[116] W.B. Liu and J.E. Rubio. Optimal Shape Design for Systems Governed by Variational Inequalities, Part 2: Existence Theory for the Evolution Case. *Journal of Optimization Theory and Applications*, 69(2):373–396, 1991.

[117] A. Logg, K.-A. Mardal, G.N. Wells, et al. *Automated Solution of Differential Equations by the Finite Element Method*. Springer, 2012.

[118] A. Logg and G.N. Wells. DOLFIN: Automated Finite Element Computing. *ACM Transactions on Mathematical Software (TOMS)*, 37(2), April 2010.

[119] A. Logg, G.N. Wells, and J. Hake. DOLFIN: a C++/Python Finite Element Library. In A. Logg, K.-A. Mardal, and G.N. Wells, editors, *Automated Solution of Differential Equations by the Finite Element Method*, volume 84 of *Lecture Notes in Computational Science and Engineering*, chapter 10. Springer, 2012.

[120] D. Luft and V. Schulz. Pre-Shape Calculus: Foundations and Application to Mesh Quality Optimization. *Control and Cybernetics*, 50(3):263–301, 2021.

[121] D. Luft and V. Schulz. Simultaneous Shape and Mesh Quality Optimization Using Pre-Shape Calculus. *accepted for publication in Control and Cybernetics*, 2021.

[122] D. Luft, V. Schulz, and K. Welker. Efficient Techniques for Shape Optimization with Variational Inequalities Using Adjoints. *SIAM Journal on Optimization*, 30(3):1922–1953, 2020.

[123] M. Bucki, C. Lobos, Y. Payan and N. Hitschfeld. Jacobian-Based Repair Method for Finite Element Meshes after Registration. *Engineering with Computers*, 27(3):285–297, 2011.

[124] L. Mäde, S. Schmitz, H. Gottschalk, and T. Beck. Combined Motch and Size Effect Modeling in a Local Probabilistic Approach for LCF. *Computational Materials Science*, 142:377–388, 2018.

[125] J.E. Marsden and S. Shkoller. The Anisotropic Lagrangian Averaged Euler and Navier-Stokes Equations. *Archive for Rational Mechanics and Analysis*, 166(1):27–46, 2003.

[126] B. Maury. A Fat Boundary Method for the Poisson Problem in a Domain with Holes. *Journal of Scientific Computing*, 16(3):319–339, 2001.

[127] P.L. Meitner. Computer Code for Predicting Coolant Flow and Heat Transfer in Turbomachinery. *Technical Report*, 89-C-008, 1990.

[128] M. Micheli, P.W. Michor, and D. Mumford. Sobolev Metrics on Diffeomorphism Groups and the Derived Geometry of Spaces of Submanifolds. *Izvestiya: Mathematics*, 77(3):541, 2013.

[129] P.W. Michor. *Manifolds of Differentiable Mappings*, volume 3 of *Shiva Mathematics Series*. 1980.

[130] P.W. Michor. Manifolds of Mappings for Continuum Mechanics. In *Geometric Continuum Mechanics*, pages 3–75. Springer, 2020.

[131] P.W. Michor and D. Mumford. Vanishing Geodesic Distance on Spaces of Submanifolds and Diffeomorphisms. *Documenta Mathematica*, (10):217–245, 2005.

[132] P.W. Michor and D. Mumford. Overview of the Geometries of Shape Spaces and Diffeomorphism Groups. *Applied and Computational Harmonic Analysis*, 23(1):74–113, 2007.

[133] P.W. Michor and C. Vizman. N-Transitivity of Certain Diffeomorphism Groups. *Acta Mathematica Universitatis Comenianae*, 63(2):221–225, 1994.

[134] J. Moser. On the Volume Elements on a Manifold. *Transactions of the American Mathematical Society*, 120(2):286–294, 1965.

[135] P.M. Müller, N. Kühl, M. Siebenborn, K. Deckelnick, M. Hinze, and T. Rung. A Novel p-Harmonic Descent Approach Applied to Fluid Dynamic Shape Optimization. *arXiv preprint arXiv:2103.14735*, 2021.

[136] D. Müllner. Orientation Reversal of Manifolds. *Algebraic & Geometric Topology*, 9(4):2361–2390, 2009.

[137] J. Munkres. *Topology*. Pearson Education Limited, 2nd edition, 2014.

[138] A. Myśliński. Level Set Approach for Shape Optimization of Contact Problems. In P. Neittaanmäki, T. Rossi, K. Majava, O. Pironneau, and I. Lasiecka, editors, *European Congress on Computational Methods in Applied Sciences and Engineering ECCOMAS*, 2004.

[139] A. Myśliński. Level Set Method for Shape and Topology Optimization of Contact Problems. In *IFIP Conference on System Modeling and Optimization*, pages 397–410. Springer, 2007.

[140] A. Nägel, V. Schulz, M. Siebenborn, and G. Wittum. Scalable Shape Optimization Methods for Structured Inverse Modeling in 3D Diffusive Processes. *Computing and Visualization in Science*, 17(2):79–88, 2015.

[141] J. Olschewski, J. Ziebs, and B. Fedelich. Modellierung des Schädigungsverhaltens der Legierung in 738LC unter mehrachsiger thermischmechanischer Beanspruchung. *Abschlussbericht SFB 339*, Projekt C2:C21–63, 1997.

[142] H. Omori. On the Group of Diffeomorphisms on a Compact Manifold. In *Proceedings of Symposia in Pure Mathematics*, volume 15, pages 167–183. American Mathematical Society, 1970.

[143] H. Omori. Local Structures of Groups of Diffeomorphisms. *Journal of the Mathematical Society of Japan*, 24(1):60–88, 1972.

[144] H. Omori. On Banach-Lie Groups Acting on Finite Dimensional Manifolds. *Tôhoku Mathematical Journal, Second Series*, 30(2):223–250, 1978.

[145] S. Onyshkevych and M. Siebenborn. Mesh Quality Preserving Shape Optimization Using Nonlinear Extension Operators. *Journal of Optimization Theory and Applications*, 189(1):291–316, 2021.

[146] U. Pinkall and K. Polthier. Computing Discrete Minimal Surfaces and Their Conjugates. *Experimental Mathematics*, 2(1):15–36, 1993.

[147] W. Rudin. *Functional Analysis*. McGraw-Hill, Inc., 2nd edition, 1991.

[148] M. Růžička. *Nichtlineare Funktionalanalysis*. Springer, 2004.

[149] M. Sagebaum, E. Özkaya, N.R. Gauger, J. Backhaus, C. Frey, S. Mann, and M. Nagel. Efficient Algorithmic Differentiation Techniques for Turbomachinery Design. In *AIAA-Paper 2017-3998*, 2017.

[150] F. Santambrogio. Optimal Transport for Applied Mathematicians. *Birkäuser, NY*, 55(58-63):94, 2015.

[151] G. Savard and J. Gauvin. The Steepest Descent Direction for the Nonlinear Bilevel Programming Problem. *Operations Research Letters*, 15(5):265–272, 1994.

[152] A. Schiela and D. Wachsmuth. Convergence Analysis of Smoothing Methods for Optimal Control of Stationary Variational Inequalities. *ESAIM: Mathematical Modelling and Numerical Analysis*, 47(3):771–787, 2013.

[153] C. Schillings, S. Schmidt, and V. Schulz. Efficient Shape Optimization for Certain and Uncertain Aerodyamic Design. *Computers & Fluids*, 46(1):78–87, 2011.

[154] N. Schloe. Meshio - I/O for Mesh Files. https://github.com/nschloe/meshio, 2019.

[155] S. Schmidt. A Two Stage CVT/Eikonal Convection Mesh Deformation Approach for Large Nodal Deformations. *arXiv preprint arXiv:1411.7663*, 2014.

[156] S. Schmidt, C. Ilic, V. Schulz, and N.R. Gauger. Three-Dimensional Large-Scale Aerodynamic Shape Optimization Based on Shape Calculus. *AIAA Journal*, 51(11):2615–2627, 2013.

[157] S. Schmidt, E. Wadbro, and M. Berggren. Large-Scale Three-Dimensional Acoustic Horn Optimization. *SIAM Journal on Scientific Computing*, 38(6):B917–B940, 2016.

[158] V. Schulz. A Riemannian View on Shape Optimization. *Foundations of Computational Mathematics*, 14(3):483–501, 2014.

[159] V. Schulz and M. Siebenborn. Computational Comparison of Surface Metrics for PDE Constrained Shape Optimization. *Computational Methods in Applied Mathematics*, 16(3):485–496, 2016.

[160] V. Schulz, M. Siebenborn, and K. Welker. Towards a Lagrange-Newton Approach for PDE Constrained Shape Optimization. In A. Pratelli and G. Leugering, editors, *New Trends in Shape Optimization*, volume 166 of *International Series of Numerical Mathematics*, pages 229–249. Springer, 2015.

[161] V. Schulz, M. Siebenborn, and K. Welker. Efficient PDE Constrained Shape Optimization Based on Steklov-Poincaré Type Metrics. *SIAM Journal on Optimization*, 26(4):2800–2819, 2016.

[162] C. Scott. L^p Theory of Differential Forms on Manifolds. *Transactions of the American Mathematical Society*, 347(6):2075–2096, 1995.

[163] J.R. Shewchuk. What is a Good Linear Element? Interpolation, Conditioning, Anisotropy, and Quality Measures. *University of California, Berkeley, CA*, 2002.

[164] S.M. Shontz and S.A. Vavasis. A Mesh Warping Algorithm Based on Weighted Laplacian Smoothing. In *IMR*, pages 147–158, 2003.

[165] M. Siebenborn and K. Welker. Algorithmic Aspects of Multigrid Methods for Optimization in Shape Spaces. *SIAM Journal on Scientific Computing*, 39(6):B1156–B1177, 2017.

[166] N.K. Smolentsev. Diffeomorphism Groups of Compact Manifolds. *Journal of Mathematical Sciences*, 146(6):6213–6312, 2007.

[167] J. Sokolowski and A. Zochowski. Topological Derivative in Shape Optimization. *Encyclopedia of Optimization*, pages 3908–3918, 2009.

[168] J. Sokolowski and J.-P. Zolésio. *Introduction to Shape Optimization*, volume 16 of *Computational Mathematics*. Springer, 1992.

[169] D. Sornette, J.-P. Magnin, and Y. Brechet. The Physical Origin of the Coffin-Manson Law in Low-Cycle Fatigue. *EPL (Europhysics Letters)*, 20:433–438, 1992.

[170] A. Srivastava, E. Klassen, S. Joshi, and I.H. Jermyn. Shape Analysis of Elastic Curves in Euclidean Spaces. *IEEE Transactions on Pattern Analysis and Machine Intelligence*, 33(7):1415–1428, 2010.

[171] K. Sturm. *On Shape Optimization with Non-Linear Partial Differential Equations*. PhD thesis, Technische Universität Berlin, 2015.

[172] K. Sturm. Shape Differentiability Under Non-Linear PDE Constraints. In A. Pratelli and G. Leugering, editors, *New Trends in Shape Optimization*, volume 166 of *International Series of Numerical Mathematics*, pages 271–300. Springer, 2015.

[173] K. Sturm. A Structure Theorem for Shape Functions Defined on Submanifolds. *Interfaces and Free Boundaries*, 18(4):523–543, 2016.

[174] B. Sultanian. *Gas Turbines: Internal Flow Systems Modeling*, volume 44 of *Cambridge Aerospace Series*. Cambridge University Press, 2018.

[175] M. Taylor. *Partial Differential Equations I: Basic Theory*, volume 115 of *Applied Mathematical Sciences*. Springer Science & Business Media, 2nd edition, 2011.

[176] G.M. Troianiello. *Elliptic Differential Equations and Obstacle Problems*. The University Series in Mathematics. Plenum Press, 1987.

[177] C. Twining, S. Marsland, and C. Taylor. Metrics, Connections, and Correspondence: The Setting for Groupwise Shape Analysis. In *International Workshop on Energy Minimization Methods in Computer Vision and Pattern Recognition*, pages 399–412. Springer, 2011.

[178] C. Udrişte. *Convex Functions and Optimization Methods on Riemannian Manifolds*, volume 297 of *Mathematics and Its Applications*. Springer Netherlands, 1994.

[179] C. Voisin. *Hodge Theory and Complex Algebraic Geometry I*, volume 76 of *Cambridge Studies in Advanced Mathematics*. Cambridge University Press, 2002.

[180] D. Wan and S. Turek. Numerical Simulation of Coupled Fluid-Solid Systems by Fictitious Boundary and Grid Deformation Methods. In *Numerical Mathematics and Advanced Applications*, pages 906–914. Springer, 2006.

[181] K. Welker. *Efficient PDE Constrained Shape Optimization in Shape Spaces*. PhD thesis, Universität Trier, 2016.

[182] K. Welker. Suitable Spaces for Shape Optimization. *Applied Mathematics & Optimization*, 84:1–34, 2021.

[183] E. Zeidler. *Applied Functional Analysis: Main Principles and Their Applications*, volume 109 of *Applied Mathematical Sciences*. Springer Science & Business Media, 2012.

[184] Y. Zhang, C. Bajaj, and G. Xu. Surface Smoothing and Quality Improvement of Quadrilateral/Hexahedral Meshes with Geometric Flow. *Communications in Numerical Methods in Engineering*, 25(1):1–18, 2009.

[185] Z. Zhou, X. Chen, and G. Liao. A Novel Deformation Method for Higher Order Mesh Generation. *arXiv preprint arXiv:1710.00291*, 2017.

[186] J.-P. Zolésio. *Identification de Domaines par Déformations*. PhD thesis, Université de Nice, 1979.